ISSN 0015–5659
eISSN 1644–3284
Impact Factor: 1.2

POLISH ANATOMICAL SOCIETY

FOLIA MORPHOLOGICA

Vol. 82 2023 No. 4

VIA MEDICA

https://journals.viamedica.pl/folia_morphologica

FOLIA MORPHOLOGICA

An international multidisciplinary journal devoted to fundamental research in the morphological sciences
Official Journal of the Polish Anatomical Society
(a Constituent Member of European Federation for Experimental Morphology — EFEM)

https://journals.viamedica.pl/folia_morphologica

See our website for information on manuscript status, aims and scope, instructions for authors as well as editorial board.

Folia Morphologica

Publishing, Subscription and Advertising Office:
VM Media Group sp. z o.o., Grupa Via Medica
ul. Świętokrzyska 73, 80–180 Gdańsk, Poland
tel. (+48 58) 320 94 94, fax (+48 58) 320 94 60
Managing editor
Joanna Niezgoda
e-mail: fm.journals@viamedica.pl
Cover designer
Sylwia Scisłowska

The journal is published at: https://journals.viamedica.pl/folia_morphologica in one volume per year consisting of four numbers.

Subscription rates: Paper subscription, 4 issues incl. package and postage institutional — 210 euro. The above prices are inclusive of regular postage costs. Payment should be made to: VM Media Group sp. z o.o., Grupa Via Medica, BNP Paribas Bank Polska SA account number: 15 1600 1303 0004 1007 1035 9021; SWIFT: PPABPLPK. Single issues, subsriptions orders and requests for sample copies should be send to e-mail: prenumerata@viamedica.pl. Electronic orders option available at: https://journals.viamedica.pl/folia_morphologica. The publisher must be notified of a cancellation of access to electronic version not later then two months before the end of a calendar year. After that date electronic access will be automatically prolonged for another year.

Advertising. For details on media opportunities within this electronic version of journal please contact the advertising sales department, ul. Świętokrzyska 73, 80–180 Gdańsk, Poland, tel: (+48 58) 320 94 94, e-mail: viamedica@viamedica.pl
The editors accept no responsibility for advertisement contents.

Folia Morphologica is the official journal of the Polish Anatomical Society. For information about the Society, please contact: Prof. Janusz Moryś, Departent of Normal Anatomy, Pomeranian Medical University, Al. Powstańców Wielkopolskich 72, 70–111 Szczecin, Poland, tel. (+48 91) 466 15 43, e-mail: jmorys@pum.edu.pl

Editorial policies and author guidelines are published on journal website: https://journals.viamedica.pl/folia_morphologica

Legal note: https://journals.viamedica.pl/folia_morphologica/about/legalNote

Folia Morphologica is indexed by: Arianta, CAS, CINAHL, CrossRef, Dental Abstracts, EBSCO, Elsevier Biobase (CABS), EmBiology, FMJ, Google Scholar, Index Copernicus, Index Scholar, Medline, Polish Medical Bibliography, Polish Ministry of Education and Science, Proquest, Scopus, SJR (*Scimago Journal & Country Rank*), Ulrich's Periodicals Directory, Veterinary Bulletin, Web of Science (SCIE, *Science Citation Index Expanded*, Biological Abstracts, BIOSIS Previews, ESI, *Essential Science Indicators*, Zoological Record) and WorldCat.
Current Impact Factor of Folia Morphologica (2022) is 1.2.

www.viamedica.pl

ISSN 0015–5659
eISSN 1644–3284

22-6110.004.001

FOLIA MORPHOLOGICA

Editor-in-Chief
JANUSZ MORYŚ
Department of Normal Anatomy, Pomeranian Medical University
Al. Powstańców Wielkopolskich 72, 70–111 Szczecin, Poland
tel. (+48 91) 466 15 43, e-mail: jmorys@pum.edu.pl

EDITORIAL ADVISORY BOARD

VIA MEDICA

REVIEW ARTICLE

Folia Morphol.
Vol. 82, No. 4, pp. 745–757
DOI: 10.5603/FM.a2022.0102

ISSN 0015–5659
eISSN 1644–3284
journals.viamedica.pl

Nucleus pulposus cells degeneration model: a necessary way to study intervertebral disc degeneration

Y.-X. Li, X.-X. Ma, Ch.-L. Zhao, J.-H. Wei, A.-H. Mei, Y. Liu

Department of Spine Surgery, The Affiliated Hospital of Qingdao University, Qingdao, People's Republic of China

[Received: 17 October 2022; Accepted: 9 November 2022; Early publication date: 30 November 2022]

The availability of an appropriate and reliable research model is helpful for researchers to understand the occurrence and development of diseases. Historically, animal models have been beneficial in the study of intervertebral disc degenerative diseases, but intervertebral disc degeneration (IDD) is a precise and complex process that needs to appear and occur in a specific tissue microenvironment, and animal degeneration models cannot fully simulate these parameters. These challenges must be overcome, especially when animal models cannot fully generalise the complex pathology of humans. In the past few years, the research on the cell disease model has made important progress, and the construction of the nucleus pulposus cell (NPC) degeneration model has become an indispensable step in studying the occurrence and development of IDD. Here, several different methods of constructing NPC degeneration models and indicators for testing the effect of modelling are introduced. The practical applications of cell models constructed by different methods are enumerated to screen and evaluate effective methods of establishing degenerative cell models and explore the mechanism of IDD. (Folia Morphol 2023; 82, 4: 745–757)

Key words: human cell model, intervertebral disc degeneration, disease modelling, nucleus pulposus cell, methods

INTRODUCTION

Intervertebral disc degeneration (IDD) is a multifactorial pathological process associated with lower back pain, which can lead to severe neurological dysfunction and disability [3, 95]. The intervertebral disc (IVD), as the joint connecting the vertebral body, is the most critical part of the spine's load-bearing system, and it is also the earliest tissue in the human body to develop degenerative changes [83]. The nucleus pulposus, located in the centre of the annulus fibrosus and between the upper and lower endplate, is gelatinous, can carry a large number of water molecules, and has strong toughness, helping to buffer axial pressure and ensure the flexibility of the spine. The nucleus pulposus is essential to maintain the balance and steady state of the IVD [37]. The main pathological features of IDD are considered to be phenotypic changes, dysfunctions, decreases in the number of active cells, and decreases in the extracellular matrix (ECM) content of nucleus pulposus cells (NPCs). These lead to a cascade event, which begins with changes in the local cellular microenvironment and progresses to damage to the structure and function of IVD [110]. A series of factors such as mechanical changes, imbalance of mitochondrial quality control, inflammation, and oxidative stress are involved

Address for correspondence: Y. Liu, PhD, Department of Spine Surgery, The Affiliated Hospital of Qingdao University, No. 16 of Jiangsu Road, Shinan District, Qingdao, 266003, China, tel: +86 13953296687, e-mail: liuyongly8@126.com

in promoting the occurrence of NPC degeneration [16, 22, 87, 99]. The new pharmacological strategy focuses on eliminating or reversing the degenerative cells in the degenerative IVD to prevent and treat intervertebral disc degenerative disease (IVDD) [27, 125]. Therefore, it is urgent to establish a reliable disease model to study the molecular basis of IVDD to reproduce what happens in the human body *in vitro*. Historically, models built by non-upright walking animals cannot effectively simulate the changes experienced in human IDD [42]. Primate models are expensive and ethically burdensome, which causes this author to consider economic and technological conveniences and find compromises between larger animals and humans. In recent years, the public has called for minimizing the use of animals in research laboratories, also promoting the improvement of the *in vitro* model.

The traditional severe degenerative NPCs isolated from patients' tissues are difficult to apply in a monolayer cell expansion culture. Although normal or mildly degenerative cells can be further cultured, the experimental results are not significant. Therefore, it is urgently needed to build an effective degenerative cell model through different induction methods, which can not only enhance the credibility of the experiment and the persuasive power of the experimental data but also help society to have a clearer understanding of the occurrence and development of IVDD. In the past few years, there have been many methods to induce NPC degeneration, but the model establishment lacks unified standards and has no systematic summary. Therefore, this paper will introduce several methods and model-effect evaluation indicators for inducing NPC degeneration to provide a reference for future screening and evaluation of effective methods for establishing degenerative cell models and exploring the mechanisms of IVD degeneration.

NUCLEUS PULPOSUS CELLS DEGENERATION MODEL ESTABLISHED BY A PHYSICAL METHOD

The IVD comprises the nucleus pulposus, endplates, and annulus fibrosus. The nucleus pulposus in the central part is gelatinous, which can effectively retain moisture and has strong flexibility [53]. The osmosis of the upper and lower endplates is the main way NPCs metabolise nutrients. The outer fibrous annulus, composed of a staggered distribution of elastin and type I collagen, has strong tension [2, 19, 95].

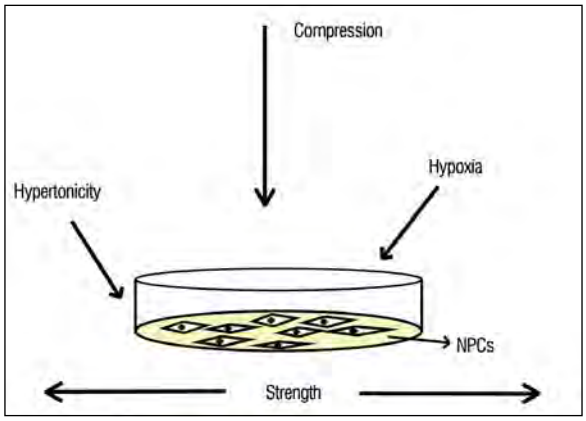

Figure 1. Simple schematic diagram of nucleus pulposus cells (NPCs) degeneration induced by commonly used physical methods.

These structures not only provide support for the IVD but also ensure the flexibility of the spine. However, this also exposes NPCs to various unfavourable environments, such as inadequate nutrient supply and long-term mechanical stress, including compression, shear stress, hydrostatic pressure, and tension [76, 78]. The long-term effects of these factors will cause changes in the structural and biochemical composition of the IVD, accompanied by a series of pathological changes, resulting in IVDD [32, 43]. It is particularly important to choose different modelling methods for different pathogeneses, according to which some researchers choose certain physical methods to induce NPC degeneration (axial compression, transverse stretching, hyperosmotic stress, hypoxia, etc., Fig. 1). In the axial compression method, NPCs are placed in a pressure device with good sealing to compress the air containing 5% carbon dioxide (CO_2) to provide different MPa pressure values and build NPC degeneration models [9, 44, 105]. In 2012, Ding et al. [15] used this method to construct a cell model and found that part of the pathological cause of IVDD induced by mechanical compression came from mitochondrial damage. Follow-up experiments showed that co-cultures with bone marrow mesenchymal stem cells could inhibit compression-induced NPC apoptosis [8]. The transverse periodic stretching method uses a transverse reciprocating stretching device to provide supracellular physiological tension for constructing a disease model [4, 14, 74, 100]. This method is also often used to build NPC degeneration models [115, 118]. In 2019, Yang et al. [107] used the Flexercell tension system to build an NPC degeneration model and found that abnormal mechanical stress promot-

ed NPC apoptosis and accelerated the occurrence of IDD, while autophagy helped to reverse apoptosis. When the biological stress exceeds the physiological expansion pressure of NPCs, whether the process is either axial compression or transverse stretching, the apoptosis pathway is activated, the expression of the polysaccharide-protein gene is down-regulated [12], and the osmotic and hydrostatic pressures increase. Some research teams have studied the effect of osmotic pressure on NPC biology because the change of osmotic pressure is a secondary change under biological stress. For example, in 2014, Dong et al. [18] established a rabbit NPC degeneration model by increasing the osmotic pressure of the culture medium and found that high osmotic pressure activated p38 mitogen-activated protein kinases (p38MAPK), mitogen-activated protein kinase 8/9 (JNK1/2), and mitogen-activated protein kinase 3/1 (ERK1/2) pathways in rabbit NPCs. The activated p38MAPK and JNK1/2 pathways induced NPC apoptosis, while the activated ERK1/2 pathway was beneficial to cell survival. The change in oxygen content is also closely related to NPC degeneration. In 2016, Choi et al. [10] successfully induced NPC degeneration by adjusting the oxygen concentration in an incubator from 21% to 1% (5% CO_2 and 94% nitrogen) in cultured cells for 24 h. In addition, reducing the pH value of the culture medium and creating an acidic environment can also be used to construct an NPC degeneration model [106].

NUCLEUS PULPOSUS CELLS DEGENERATION MODEL ESTABLISHED BY A CHEMICAL METHOD

Inflammatory reactions are important pathological mechanisms of IDD [84]. The overexpression of proinflammatory cytokines can destroy the ECM homeostasis of the IVD and induce degeneration and catabolism of the IVD [57, 71]. Neurotrophins are produced under the stimulation of inflammatory factors and promote nerve growth into the IVD, accelerating the IDD cascade [30]. In addition, inflammatory factors have a negative effect on reparative stem cells [55, 73, 89, 101]. The chemical method to construct the NPC degeneration model is to simulate the inflammatory environment in the early stage of lumbar pathology caused by chemical reagents and drugs to establish the cell model (Fig. 2). This type of cell model is highly important for promoting the research of IVDD. In 2006, Aota et al. [1] found that toll-like receptors in bovine NPCs are sensitive to the binding of bacterial lipopolysaccharides (LPSs) (a microbial component found in the outer membrane of Gram-negative bacteria). Toll-like receptors are important regulators of the nuclear factor kappa-B signalling pathway and are closely related to cellular inflammation and degeneration [75]. In 2013, Kim et al. [49] successfully established a degeneration model of bovine NPCs induced by LPS and used this cell model to prove that inhibition of the myeloid differentiation primary response 88 pathway can effectively inhibit inflammation and anti-catabolism. Since then, many scholars have chosen this modelling method [17, 60, 116, 121, 124], and the LPS induction method has since become the most used and popular modelling method. In addition, interleukin-1 beta and tumour necrosis factor-alpha are important pro-inflammatory factors involved in cell differentiation and apoptosis by regulating various pathways, so they are also often used to induce NPC degeneration [7, 31, 34, 47, 48, 117, 119, 123].

Some stressors can also be used to construct NPC degeneration models. These stressors strongly oxidize, which can destroy the normal redox state in cells, leading to the imbalance between the oxidation and antioxidant systems [81]. These stressors can also stimulate cells to produce harmful molecules, such as damaged nucleic acids, proteins, and lipids, which may lead to the occurrence and development of chronic degenerative disease [98]. Hydrogen peroxide (H_2O_2) is a commonly used induction reagent by researchers. As a type of reactive oxygen species, H_2O_2 can inhibit cell proliferation, cause oxidative damage to macromolecules in cells, and eventually lead to serious consequences, such as cell senescence, death, and mutation. Therefore, H_2O_2-induced oxidative stress cell models are widely used to explore the mechanism of free radical-mediated cell injury and the protection and repair mechanism of antioxidants on oxidative damage [35, 64, 72, 120]. In 2019, Tang et al. [93] used H_2O_2 to build a mouse NPC degeneration model to study the role of nuclear factor erythroid 2–related factor 2 (Nrf2) in NPC degeneration. It was found that Nrf2 can slow down NPC degeneration induced by oxidative stress by activating autophagy through feedback. Tert-butyl hydroperoxide (t-BHP) [70, 108, 122] can also be used to construct an NPC degeneration model. In 2016, Chen et al. [6] proved that metformin could inhibit the apoptosis and senescence of NPCs

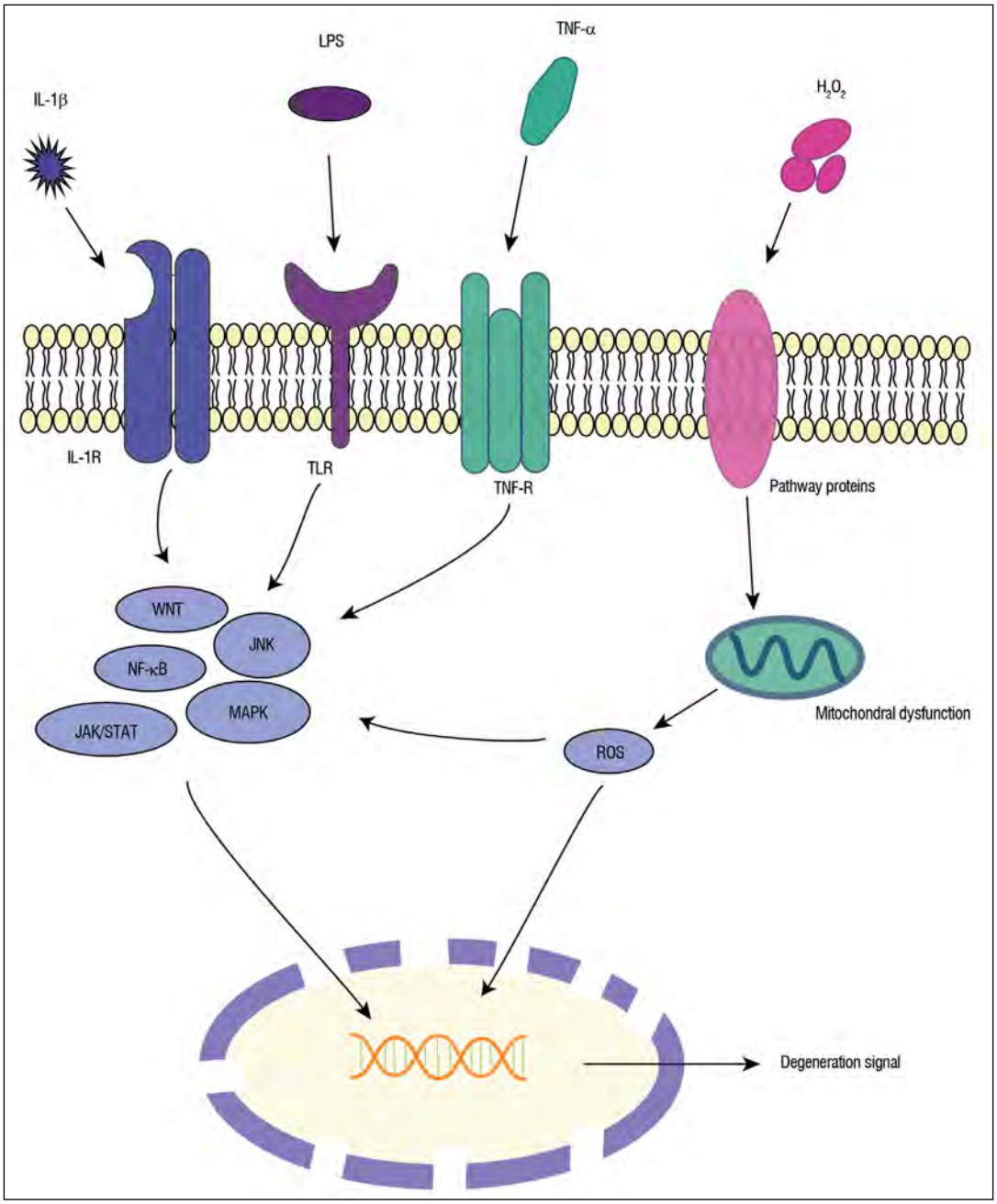

Figure 2. Simple schematic of nucleus pulposus cells degeneration induced by commonly used chemical methods; IL — interleukin; LPS — lipopolysaccharides; TNF — tumour necrosis factor; TLR — toll-like receptor; WNT — wingless-type MMTV integration site family; JNK — c-Jun N-terminal kinase; NF-κB — nuclear factor kappa-B; STAT — signal transducer and activator of transcription; MAPK — mitogen-activated protein kinases; ROS — reactive oxygen species.

induced by t-BHP by autophagy. In recent years, angiotensin II (AngII) has also been used to induce NPC degeneration [90]. The Ang II receptor type 1 (AT1) receptor (G protein-coupled receptor) is the main biological medium of AngII. The combination of AngII and AT1 can promote the production of reactive oxygen species and the accumulation of pro-inflammatory cytokines and classically activated macrophages, resulting in NPC degeneration [13, 88]. In addition, advanced oxidation protein products [104], stromal cell-derived factors [69], polymethyl methacrylate [24], nitroprusside [59], and cobalt chloride [23] can also be used to establish an NPC degeneration model.

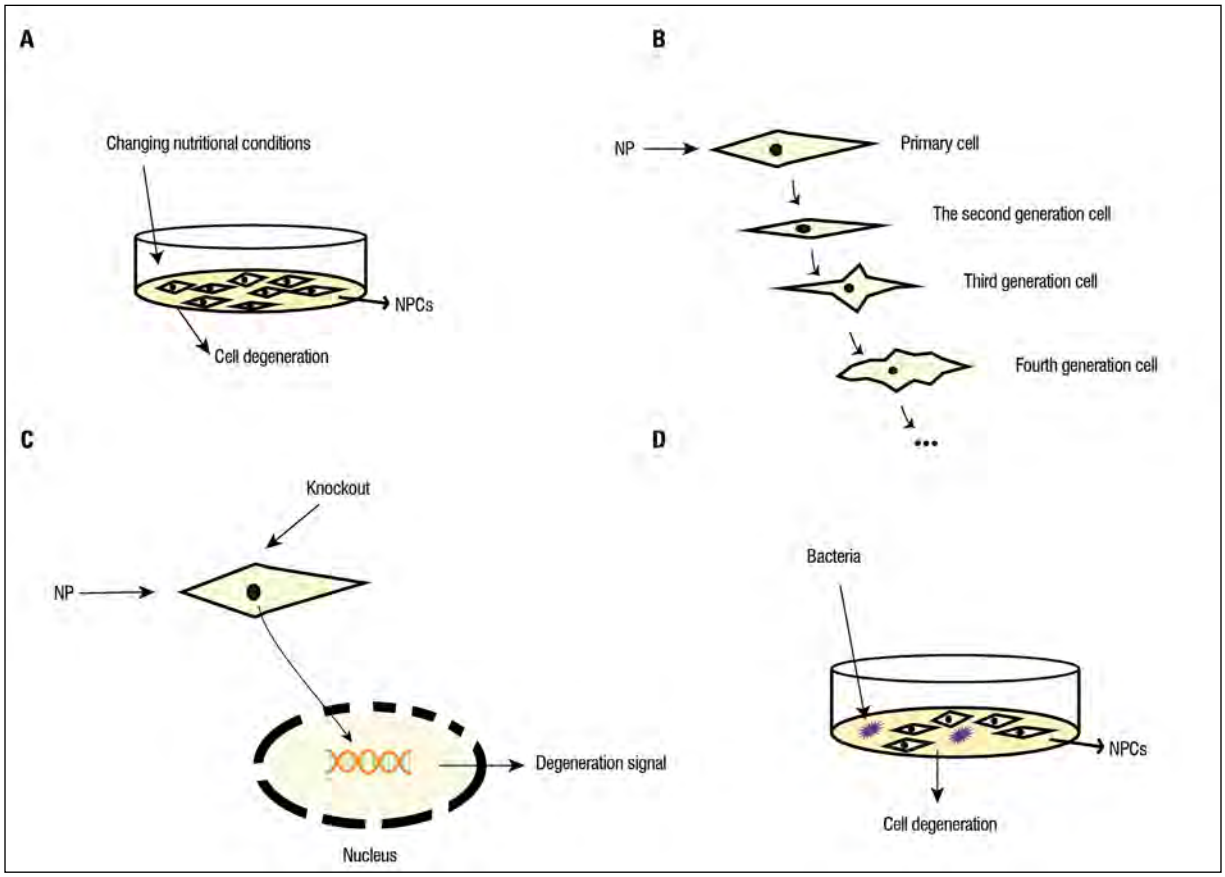

Figure 3. A–D. Simple schematic representation of biological or bioengineered methods for inducing nucleus pulposus (NP) cells (NPCs) degeneration.

NUCLEUS PULPOSUS CELL DEGENERATION MODEL ESTABLISHED BY BIOLOGICAL OR BIOENGINEERING METHODS

An NPC degeneration model can also be constructed by changing the nutritional environment, increasing replication algebra, gene knockout, microbial co-culture, etc. (Fig. 3). Nucleus pulposus cells exist in a unique environment regarding their nutritional supply. The IVD has no direct vascular supply, so nutrients are provided to NPCs by capillaries that penetrate the subchondral plate and terminate at the boundary of the cartilage endplate. The NPC microstructure changes, such as reduced capillary density [63, 113], endplate calcification [25, 112], and metabolic disorders [54], will cause the IVD to degenerate. In 2018, Wang et al. [97] successfully established an NPC degeneration model by incubating NPCs of normal mice in high glucose for 72 h. In 2017, Chang et al. [5] also successfully induced NPC degeneration by using a sugar-free medium. Amino acid and serum removal can also be used to construct an NPC degeneration model [61, 68]. The natural degeneration of NPCs is mostly related to age [51, 79]. In 2019, Gong et al. [28] constructed a degeneration model by repeated cell passage, which proved that bone morphogenetic protein 7 could reduce the senescence of human IVD NPCs induced by the passage of time by activating the phosphoinositide 3-kinase/protein kinase B pathway. Gene knockout and microbial co-culture are newer methods for NPC degeneration models. Kong et al. [52] constructed a degenerative cell model by down-regulating the hsa_circ_0059955 gene of normal mouse NPCs and inducing NPC apoptosis and cell cycle arrest. In 2020, He et al. [33] found that *Cutibacterium acnes* induce NPC degeneration by activating the NOD-like receptor thermal protein domain associated protein 3 (NLRP3)-dependent pathway.

MODEL EFFECT EVALUATION INDEX

After choosing different ways to construct the NPC degeneration model, it is necessary to further evaluate the success of the model, the state of cell activity, the degree of cell damage, etc. Morphological observation is a more intuitive way of detection

because degenerative cells will appear as swelling, flattening, with reduced nuclear volume, and have loose adhesion in the shape of a linear semi-adherent [15]. Transmission electron microscopes are used to observe the subcellular structure, nuclear shrinkage, a large number of apoptotic bodies, chromatin condensation, and cytoplasmic vesicles containing more dense vesicles [8]. However, there is no quantitative standard to judge the quality of cell morphology, so this method cannot be used as an evaluation index alone, and it is often necessary to use it alongside 3-(4,5-dimethylthiazol-2-yl)-2,5-diphenyltetrazolium bromide, cell counting Kit-8, or terminal deoxynucleotidyl transferase mediated nick end labelling assays, flow cytometry, etc. to further evaluate cell activity.

Type II collagen, polyproteoglycans, and cell matrix-degrading enzymes (matrix metalloproteinase [MMP] 3, MMP13, a disintegrin and metalloproteinase with thrombospondin motifs [ADAMTS] 4, and ADAMTS5) are often used as important indicators of NPC degeneration [58]. Type II collagen and polyproteoglycan are produced by NPCs and play an important role in maintaining the flexibility and compression function of the IVD. The decrease in its content is the initial factor of IDD because it changes the integrity of the biomechanical structure of the IVD and destroys the metabolic balance of the ECM. Under the stimulation of pathological conditions, inflammation-related pathways are activated, and matrix-degrading enzymes, whose main function is to degrade type II collagen and polyproteoglycans in NPCs, are promoted to secrete. In degenerative NPCs, the content of type II collagen and polyproteoglycan decreased, while the cell matrix-degrading enzyme content increased. The degree of change was related to the degree of cell degeneration.

In addition, the content of some apoptosis-related marker proteins can also be used to evaluate the degree of cell degeneration. Beta-galactosidase (β-galactosidase) (senescence-associated beta-galactosidase [SA-β-gal]) is found only in degenerative senescent cells and accumulates gradually with cell degeneration. Beta-galactosidase can hydrolyse β-galactosidase into monosaccharides. A blue stain precipitate will appear when β-galactosidase is present under acidic conditions. Cell degeneration can be further evaluated by observing the colour of the precipitate under a microscope [20]. There is a close relationship between caspase-3, B-cell lymphoma 2 (Bcl-2), Bcl-2-associated X protein (BAX), and apoptosis [109]. Caspase is a cysteine aspartic acid-specific protease in the cytoplasm, which is homologous to the suicide gene cell death protein 3 in nematodes and plays an important role in the process of cell senescence and degeneration [29]. B-cell lymphoma 2 contains two proteins: bcl-2 α and bcl-2 β. The bcl-2 α protein is an integrin of the mitochondrial membrane and plays a role in anti-apoptosis [85]. The BAX protein is inactive when it does not receive apoptosis stimulation. After it is activated, it can destroy the integrity of the mitochondrial membrane, antagonize the function of Bcl-2, and promote apoptosis [91]. The effect of establishing an NPC degeneration model can be evaluated by the content changes of the above indexes.

The cell oxidation ability can also be used to evaluate cell degeneration. Peroxidation often leads to cell dysfunction-induced degeneration, and malondialdehyde is one of the peroxidation products. The level of malondialdehyde content indicates the degree of cell damage and degeneration [38]. Superoxide dismutase and deacetylase are related to antioxidation [77, 114], and the level of these enzymes reflects the intracellular oxidation state and can be used as a detection index for the construction of an NPC degeneration model.

The key index to evaluating the modelling mode is to ensure the cell survival rate and successfully construct the degeneration model. The best way to induce degeneration is to have both the minimum cytotoxicity or damage and subsequently meet the needs of the experimental model. This makes it necessary to try different variables in the same way, such as intensity, concentration, time, etc., and use evaluation indicators to select the best treatment conditions. In this paper, different modelling methods are classified and summarised from the aspects of physics, chemistry, and biological engineering. The results of the same treatment methods and different treatment conditions are compared, and the best treatment conditions of the current research methods are selected (Table 1) [7, 9, 10, 17, 18, 28, 33–36, 39, 41, 44–46, 48, 50, 52, 56, 60, 62, 64–67, 70, 72, 80, 92, 102, 105, 107, 108, 111, 115–118, 120–122, 124].

CURRENT CHALLENGES

The physical modelling method is simple and controllable, causes less damage to cells, and is similar to the natural degeneration of NPCs, which is suitable for the pathological mechanism study. The modelling method is still not comprehensive, as treatments such

Table 1. Common methods of constructing nucleus pulposus cell degeneration model and optimal treatment conditions

Research style	Modelling approach	Optimum condition	References
Axial compression	The cells are placed in a pressurizing device that increases the pressure	Pressure value: 1 MPa; Treatment time was 36–48 h	[9, 36, 44, 45, 105]
Cyclic tension stretching	The cells are stimulated by periodic stretching	Tensile strength: 20%; Frequency: 1 Hz; Processing time: 4 to 6 h	[107, 115, 118]
Hypoxia-induce	Reduce the oxygen in the incubator	Oxygen content: 1%; The treatment time is 24 h	[10, 39, 50, 56]
Hypertonic-induce	Increase osmotic pressure of culture medium	Osmotic pressure: 550 mOsm/kg; Processing time: 3–7 days	[18, 41, 111]
LPS-induce	An appropriate amount of LPS was added to the culture medium	Concentration: 10 μg/mL; The processing time is 48 h	[17, 60, 62, 116, 121, 124]
IL-1β-induce	An appropriate amount of IL-1β was added to the culture medium	Concentration: 10 ng/mL; The treatment time is 24 h	[7, 34, 48, 80, 117]
H_2O_2-induce	An appropriate amount of H_2O_2 was added to the culture medium	Dose: 400 μmol; The treatment time is 24 h	[35, 64, 72, 102, 120]
TBHP-induce	An appropriate amount of TBHP was added to the culture medium	Dosage: 50 μmol; The treatment time is 24 h	[70, 46, 67, 108, 122]
Duplicator method	Cells were cultured by multiple passages	Passage times: 6 generations	[28]
Gene knockout	Knockdown of specific coding genes	Gene name: hsa_circ_0059955	[52]
Biological induction method	Co-culture with sustenance	Microorganism: P. acnes	[33, 65, 66, 92]

IL — interleukin; LPS — lipopolysaccharide; TBHP — tert-butyl hydrogen peroxide

as radiation, ultraviolet irradiation, current stimulation, low-temperature induction, and other cell modelling methods have not yet been applied. Chemical modelling has a variety of methods, short modelling times, and is practically simple. It is widely used to study the relationship between inflammation, oxidative stress, autophagy, and IDDs, but it causes varying degrees of damage to cells. A reasonable induction dose is particularly important for the success or failure of this modelling. The stability of the cell model constructed by a biological or bioengineering method is relatively poor, and it is not widely used at present. It is necessary to further explore the optimal conditions and optimize the induction method in the future.

Whether physical, chemical, biological, or bioengineering methods are used, the purpose of inducing cell degeneration can be achieved by simulating the changes in external stimulation conditions of NPCs. Some of the mechanisms of cell degeneration overlap; for example, hypoxia induction can cause cells to produce oxidative stress and degenerate, similar to using stressors to stimulate NPCs in chemical modelling methods. In the biological induction method, part of the reason for the construction of the NPC degeneration model with a microbial co-culture may be the inflammatory response of cells stimulated by microorganisms, which partially overlaps with the mechanism of the cell degeneration model constructed by inflammatory factors in chemical methods. Although there may be the same mechanisms in different induction methods, the occurrence and development of IDD involve multiple factors and stages. The *in vitro* model constructed by different methods can simulate the key sites or stages of specific lesions, which is conducive to a comprehensive and detailed study of IDD's aetiology and pathological mechanism.

Intervertebral disc degeneration resulting in pain and abnormal function of lower limbs, has become a serious problem in modern society, causing a huge economic burden [21]. Traditional surgery and drug therapy cannot satisfy the fundamental treatment goals. Changing IDD at the cellular, molecular, and genetic levels is the research goal for most researchers because *in vitro* experiments are controllable and accessible [26, 103]. The NPC degeneration model is an indispensable step in studying IDD's occurrence, so choosing a reliable, feasible, and appropriate modelling method is highly important to explore IDD's aetiology and pathogenesis.

CONCLUSIONS

Nucleus pulposus is located in the centre of annulus fibrosus and between the superior and inferior endplates. It has strong toughness and is an important part of maintaining the balance and stability of

IVD. The notochord cells originating from the mesoderm are wrapped in connective tissue derived from osteogenic knots and develop into nucleus pulposus tissue in the early stage of the embryo [82, 96]. Therefore, there are chordate cells with large shape and a large number of vesicles in the early nucleus pulposus. With the maturation of the IVD, the composition of the nucleus pulposus changed: the number of large vacuolar cells considered to be the origin of the notochord decreased and gradually transformed into small chondrocyte-like cells with smaller morphology and no vesicles [11, 86]. With the "disappearance" of notochord cells in human nucleus pulposus, some signs of early IDD, such as decreased water content of nucleus pulposus and microfissures of annulus fibrosus, began to appear. Based on this phenomenon, many scholars speculate that early IDD occurs with the disappearance or degeneration of notochord cells [94]. However, in some animals, such as rabbits, cattle and dogs, there are a large number of notochord cells in the nucleus pulposus, and there is almost no degeneration of the IVD [40]. Therefore, based on the fact that IVD cells are different from human IVD cells, there are some drawbacks when using animal models; they do not mimic the pathological changes of human degenerative IVD diseases.

Intervertebral disc degeneration is a multi-factor and complex process, and the changes in external stimuli and internal physical and chemical properties are the two core elements of IDD. A variety of provided animal and cell models assist greatly in in-depth studying and overcoming the mechanism of IDD. Compared with animal models, cell models have the advantages of short modelling cycles, economic factors, obvious effects, and a better ability to simulate the internal environment. In constructing an NPC degeneration model, the physical modelling method can be the most similar to the NPCs' natural degeneration, and the biological and chemical modelling methods can simulate the pathological environment to construct the model quickly. However, it is difficult to produce an *in vitro* model of NPCs induced by a single factor that meets the aetiology and pathogenesis of IVDD. Second, chemicals and microorganisms cause rapid degeneration through different degrees of cell damage. This is quite different from the degenerative cells in natural environments. Although the replicated model causes the least damage to the cells, the stability of the model is poor, and it is easy to generate apoptosis.

In summary, little is currently known about the cellular process of IDD's occurrence and development. Although the *in vitro* model cannot fully simulate the aetiology and pathological mechanism of IDD, researchers can choose a model reasonably according to the phenotype or pathogenic pathway due to the in-depth study of these *in vitro* models. To further optimise the construction mode and evaluation criteria of the cell model in the future, a suitable model can be constructed for pathological research or drug screening through differentiation analysis with natural degenerative cells to provide materials and basic data for exploring the mechanism and treatment strategy of IDD.

Acknowledgements

We are particularly grateful to all the people who have given us help on our article.

Funding

This study was supported by the "Clinical Medicine + X" scientific research project of the Affiliated Hospital of Qingdao University National Natural Science Foundation of China (81871804).

Conflict of interest: None declared

REFERENCES

1. Aota Y, An HS, Imai Y, et al. Comparison of cellular response in bovine intervertebral disc cells and articular chondrocytes: effects .of lipopolysaccharide on proteoglycan metabolism. Cell Tissue Res. 2006; 326(3): 787–793, doi: 10.1007/s00441-006-0225-1, indexed in Pubmed: 16788835.
2. Ashinsky B, Smith HE, Mauck RL, et al. Intervertebral disc degeneration and regeneration: a motion segment perspective. Eur Cell Mater. 2021; 41: 370–380, doi: 10.22203/eCM.v041a24, indexed in Pubmed: 33763848.
3. Bisson DG, Mannarino M, Racine R, et al. For whom the disc tolls: intervertebral disc degeneration, back pain and toll-like receptors. Eur Cell Mater. 2021; 41: 355–369, doi: 10.22203/eCM.v041a23, indexed in Pubmed: 33738788.
4. Campos LC, Ribeiro-Silva JC, Menegon AS, et al. Cyclic stretch-induced Crp3 sensitizes vascular smooth muscle cells to apoptosis during vein arterialization remodeling. Clin Sci (Lond). 2018; 132(4): 449–459, doi: 10.1042/CS20171601, indexed in Pubmed: 29437853.
5. Chang H, Cai F, Zhang Y, et al. Early-stage autophagy protects nucleus pulposus cells from glucose deprivation-induced degeneration via the p-eIF2α/ATF4 pathway. Biomed Pharmacother. 2017; 89: 529–535, doi: 10.1016/j.biopha.2017.02.074, indexed in Pubmed: 28254665.
6. Chen D, Xia D, Pan Z, et al. Metformin protects against apoptosis and senescence in nucleus pulposus cells and ameliorates disc degeneration in vivo. Cell Death Dis. 2016;

7(10): e2441, doi: 10.1038/cddis.2016.334, indexed in Pubmed: 27787519.
7. Chen F, Jiang G, Liu H, et al. Melatonin alleviates intervertebral disc degeneration by disrupting the IL-1β/NF-κB--NLRP3 inflammasome positive feedback loop. Bone Res. 2020; 8: 10, doi: 10.1038/s41413-020-0087-2, indexed in Pubmed: 32133213.
8. Chen S, Zhao L, Deng X, et al. Mesenchymal stem cells protect nucleus pulposus cells from compression-induced apoptosis by inhibiting the mitochondrial pathway. Stem Cells Int. 2017; 2017: 9843120, doi: 10.1155/2017/9843120, indexed in Pubmed: 29387092.
9. Chen S, Lv X, Hu B, et al. RIPK1/RIPK3/MLKL-mediated necroptosis contributes to compression-induced rat nucleus pulposus cells death. Apoptosis. 2017; 22(5): 626–638, doi: 10.1007/s10495-017-1358-2, indexed in Pubmed: 28289909.
10. Choi H, Merceron C, Mangiavini L, et al. Hypoxia promotes noncanonical autophagy in nucleus pulposus cells independent of MTOR and HIF1A signaling. Autophagy. 2016; 12(9): 1631–1646, doi: 10.1080/15548627.2016.1192753, indexed in Pubmed: 27314664.
11. Colombier P, Clouet J, Chariau C, et al. Generation of human nucleus pulposus cells from stem cells: First steps towards intervertebral disc regeneration. Osteoarthritis Cartilage. 2016; 24(Suppl. 1): S11–S12, doi: https://doi.org/10.1016/j.joca.2016.01.051.
12. Court C, Colliou OK, Chin JR, et al. The effect of static in vivo bending on the murine intervertebral disc. Spine J. 2001; 1(4): 239–245, doi: 10.1016/s1529-9430(01)00056-0, indexed in Pubmed: 14588327.
13. Dandona P, Dhindsa S, Ghanim H, et al. Angiotensin II and inflammation: the effect of angiotensin-converting enzyme inhibition and angiotensin II receptor blockade. J Hum Hypertens. 2007; 21(1): 20–27, doi: 10.1038/sj.jhh.1002101, indexed in Pubmed: 17096009.
14. Davidovich N, DiPaolo BC, Lawrence GG, et al. Cyclic stretch-induced oxidative stress increases pulmonary alveolar epithelial permeability. Am J Respir Cell Mol Biol. 2013; 49(1): 156–164, doi: 10.1165/rcmb.2012-0252OC, indexed in Pubmed: 23526210.
15. Ding F, Shao ZW, Yang SH, et al. Role of mitochondrial pathway in compression-induced apoptosis of nucleus pulposus cells. Apoptosis. 2012; 17(6): 579–590, doi: 10.1007/s10495-012-0708-3, indexed in Pubmed: 22392483.
16. Ding SL, Zhang TW, Zhang QC, et al. Excessive mechanical strain accelerates intervertebral disc degeneration by disrupting intrinsic circadian rhythm. Exp Mol Med. 2021; 53(12): 1911–1923, doi: 10.1038/s12276-021-00716-6, indexed in Pubmed: 34934193.
17. Dong Y, Liu L, Shan X, et al. Pilose antler peptide attenuates LPS-induced inflammatory reaction. Int J Biol Macromol. 2018; 108: 272–276, doi: 10.1016/j.ijbiomac.2017.11.176, indexed in Pubmed: 29208559.
18. Dong ZH, Wang DC, Liu TT, et al. The roles of MAPKs in rabbit nucleus pulposus cell apoptosis induced by high osmolality. Eur Rev Med Pharmacol Sci. 2014; 18(19): 2835–2845, doi: 10.1055/s-0034-1376584, indexed in Pubmed: 25339477.
19. Fearing BV, Hernandez PA, Setton LA, et al. Mechanotransduction and cell biomechanics of the intervertebral disc. JOR Spine. 2018; 1(3), doi: 10.1002/jsp2.1026, indexed in Pubmed: 30569032.
20. Feng C, Yang M, Zhang Y, et al. Cyclic mechanical tension reinforces DNA damage and activates the p53-p21-Rb pathway to induce premature senescence of nucleus pulposus cells. Int J Mol Med. 2018; 41(6): 3316–3326, doi: 10.3892/ijmm.2018.3522, indexed in Pubmed: 29512682.
21. Fiordalisi MF, Silva AJ, Barbosa M, et al. Intervertebral disc decellularisation: progress and challenges. Eur Cell Mater. 2021; 42: 196–219, doi: 10.22203/eCM.v042a15, indexed in Pubmed: 34613611.
22. Francisco V, Pino J, González-Gay MÁ, et al. A new immunometabolic perspective of intervertebral disc degeneration. Nat Rev Rheumatol. 2022; 18(1): 47–60, doi: 10.1038/s41584-021-00713-z, indexed in Pubmed: 34845360.
23. Gao XX, Liu CH, Hu ZL, et al. The biological effect of cobalt chloride mimetic-hypoxia on nucleus pulposus cells and the comparability with physical hypoxia . Front Biosci (Landmark Ed). 2021; 26(10): 799–812, doi: 10.52586/4989, indexed in Pubmed: 34719207.
24. Ge J, Yang H, Chen Y, et al. PMMA bone cement acts on the hippo/yap pathway to regulate CTGF and induce intervertebral disc degeneration. ACS Biomater Sci Eng. 2019; 5(7): 3293–3302, doi: 10.1021/acsbiomaterials.9b00146, indexed in Pubmed: 33405572.
25. Ge Q, Ying J, Shi Z, et al. Chlorogenic Acid retards cartilaginous endplate degeneration and ameliorates intervertebral disc degeneration via suppressing NF-κB signaling. Life Sci. 2021; 274: 119324, doi: 10.1016/j.lfs.2021.119324, indexed in Pubmed: 33711382.
26. Gianola S, Bargeri S, Del Castillo G, et al. Effectiveness of treatments for acute and subacute mechanical non-specific low back pain: a systematic review with network meta--analysis. Br J Sports Med. 2022; 56(1): 41–50, doi: 10.1136/bjsports-2020-103596, indexed in Pubmed: 33849907.
27. Gologorsky Y, Chi J. Bisphosphonate therapy for degenerative disc disease? Neurosurgery. 2013; 73(4): N12–N13, doi: 10.1227/01.neu.0000435113.33768.2d, indexed in Pubmed: 24051711.
28. Gong C, Pan W, Hu W, et al. Bone morphogenetic protein-7 retards cell subculture-induced senescence of human nucleus pulposus cells through activating the PI3K/Akt pathway. Biosci Rep. 2019; 39(3), doi: 10.1042/BSR20182312, indexed in Pubmed: 30787052.
29. Gröbner S, Adkins I, Schulz S, et al. Catalytically active Yersinia outer protein P induces cleavage of RIP and caspase-8 at the level of the DISC independently of death receptors in dendritic cells. Apoptosis. 2007; 12(10): 1813–1825, doi: 10.1007/s10495-007-0100-x, indexed in Pubmed: 17624595.
30. Gruber HE, Hoelscher GL, Ingram JA, et al. Genome-wide analysis of pain-, nerve- and neurotrophin-related gene expression in the degenerating human annulus. Mol Pain. 2012; 8: 63, doi: 10.1186/1744-8069-8-63, indexed in Pubmed: 22963171.
31. Guo Z, Gao WS, Wang YF, et al. MiR-502 suppresses tnf-alpha-induced nucleus pulposus cell apoptosis by tar-

geting TARF2. Biomed Res Int. 2021; 2021: 5558369, doi: 10.1155/2021/5558369, indexed in Pubmed: 33869626.
32. Haneder S, Ong MML, Budjan JM, et al. 23Na-magnetic resonance imaging of the human lumbar vertebral discs: in vivo measurements at 3.0 T in healthy volunteers and patients with low back pain. Spine J. 2014; 14(7): 1343–1350, doi: 10.1016/j.spinee.2014.01.031, indexed in Pubmed: 24472875.
33. He D, Zhou M, Bai Z, et al. Propionibacterium acnes induces intervertebral disc degeneration by promoting nucleus pulposus cell pyroptosis via NLRP3-dependent pathway. Biochem Biophys Res Commun. 2020; 526(3): 772–779, doi: 10.1016/j.bbrc.2020.03.161, indexed in Pubmed: 32265028.
34. He J, Yang J, Shen T, et al. Overexpression of long non-coding RNA XIST promotes IL-1β-induced degeneration of nucleus pulposus cells through targeting miR-499a-5p. Mol Cell Probes. 2021; 57: 101711, doi: 10.1016/j.mcp.2021.101711, indexed in Pubmed: 33722663.
35. He R, Cui M, Lin H, et al. Melatonin resists oxidative stress-induced apoptosis in nucleus pulposus cells. Life Sci. 2018; 199: 122–130, doi: 10.1016/j.lfs.2018.03.020, indexed in Pubmed: 29526797.
36. He R, Wang Z, Cui M, et al. HIF1A Alleviates compression-induced apoptosis of nucleus pulposus derived stem cells via upregulating autophagy. Autophagy. 2021; 17(11): 3338–3360, doi: 10.1080/15548627.2021.1872227, indexed in Pubmed: 33455530.
37. Hsieh AH, Twomey JD. Cellular mechanobiology of the intervertebral disc: new directions and approaches. J Biomech. 2010; 43(1): 137–145, doi: 10.1016/j.jbiomech.2009.09.019, indexed in Pubmed: 19828150.
38. Hu S, Zhang C, Qian T, et al. Promoting Nrf2/Sirt3-dependent mitophagy suppresses apoptosis in nucleus pulposus cells and protects against intervertebral disc degeneration. Oxid Med Cell Longev. 2021; 2021: 6694964, doi: 10.1155/2021/6694964, indexed in Pubmed: 34211633.
39. Huang Y, Wang Y, Wu C, et al. Elevated expression of hypoxia-inducible factor-2alpha regulated catabolic factors during intervertebral disc degeneration. Life Sci. 2019; 232: 116565, doi: 10.1016/j.lfs.2019.116565, indexed in Pubmed: 31251999.
40. Hunter CJ, Matyas JR, Duncan NA. The notochordal cell in the nucleus pulposus: a review in the context of tissue engineering. Tissue Eng. 2003; 9(4): 667–677, doi: 10.1089/107632703768247368, indexed in Pubmed: 13678445.
41. Jiao S, Li J, Liu B, et al. Nucleus pulposus cell apoptosis is attenuated by CDMP-2 through regulating oxidative damage under the hyperosmotic environment. Biosci Rep. 2018; 38(5), doi: 10.1042/BSR20181176, indexed in Pubmed: 30177520.
42. Jin L, Balian G, Li XJ. Animal models for disc degeneration: an update. Histology Histopathology. 2018; 33(6): 543–554, doi: 10.14670/HH-11-910, indexed in Pubmed: 28580566.
43. Johannessen W, Elliott DM. Effects of degeneration on the biphasic material properties of human nucleus pulposus in confined compression. Spine (Phila Pa 1976). 2005; 30(24): E724–E729, doi: 10.1097/01.brs.0000192236.92867.15, indexed in Pubmed: 16371889.
44. Kanda Y, Yurube T, Morita Y, et al. Delayed notochordal cell disappearance through integrin α5β1 mechanotransduction during ex-vivo dynamic loading-induced intervertebral disc degeneration. J Orthop Res. 2021; 39(9): 1933–1944, doi: 10.1002/jor.24883, indexed in Pubmed: 33049071.
45. Kang L, Liu S, Li J, et al. The mitochondria-targeted anti-oxidant MitoQ protects against intervertebral disc degeneration by ameliorating mitochondrial dysfunction and redox imbalance. Cell Prolif. 2020; 53(3): e12779, doi: 10.1111/cpr.12779, indexed in Pubmed: 32020711.
46. Kang L, Xiang Q, Zhan S, et al. Restoration of autophagic flux rescues oxidative damage and mitochondrial dysfunction to protect against intervertebral disc degeneration. Oxid Med Cell Longev. 2019; 2019: 7810320, doi: 10.1155/2019/7810320, indexed in Pubmed: 31976028.
47. Kang R, Li H, Rickers K, et al. Intervertebral disc degenerative changes after intradiscal injection of TNF-alpha in a porcine model. Eur Spine J. 2015; 24(9): 2010–2016, doi: 10.1007/s00586-015-3926-x, indexed in Pubmed: 25850392.
48. Kim H, Hong JY, Lee J, et al. IL-1β promotes disc degeneration and inflammation through direct injection of intervertebral disc in a rat lumbar disc herniation model. Spine J. 2021; 21(6): 1031–1041, doi: 10.1016/j.spinee.2021.01.014, indexed in Pubmed: 33460811.
49. Kim JS, Ellman MB, Yan D, et al. Lactoferricin mediates anti-inflammatory and anti-catabolic effects via inhibition of IL-1 and LPS activity in the intervertebral disc. J Cell Physiol. 2013; 228(9): 1884–1896, doi: 10.1002/jcp.24350, indexed in Pubmed: 23460134.
50. Kim JW, An HJ, Yeo H, et al. Activation of hypoxia-inducible factor-1α signaling pathway has the protective effect of intervertebral disc degeneration. Int J Mol Sci. 2021; 22(21), doi: 10.3390/ijms222111355, indexed in Pubmed: 34768786.
51. Kim YK, Kang D, Lee I, et al. Differences in the incidence of symptomatic cervical and lumbar disc herniation according to age, sex and national health insurance eligibility: a pilot study on the disease's association with work. Int J Environ Res Public Health. 2018; 15(10), doi: 10.3390/ijerph15102094, indexed in Pubmed: 30257414.
52. Kong D, Gu R, Zhang C, et al. Knockdown of hsa_circ_0059955 Induces Apoptosis and Cell Cycle Arrest in Nucleus Pulposus Cells via Inhibiting Itchy E3 Ubiquitin Protein Ligase. Drug Des Devel Ther. 2020; 14: 3951––3963, doi: 10.2147/DDDT.S253293, indexed in Pubmed: 33061300.
53. Kos N, Gradisnik L, Velnar T. A brief review of the degenerative intervertebral disc disease. Med Arch. 2019; 73(6): 421–424, doi: 10.5455/medarh.2019.73.421-424, indexed in Pubmed: 32082013.
54. Kritschil R, Scott M, Sowa G, et al. Role of autophagy in intervertebral disc degeneration. J Cell Physiol. 2022; 237(2): 1266–1284, doi: 10.1002/jcp.30631, indexed in Pubmed: 34787318.
55. Krock E, Rosenzweig DH, Haglund L. The inflammatory milieu of the degenerate disc: is mesenchymal stem cell-based therapy for intervertebral disc repair a feasible approach? Curr Stem Cell Res Ther. 2015; 10(4): 317–328, doi: 10.2174/1574888x10666150211161956, indexed in Pubmed: 25670061.

56. Kwon WK, Moon HJ, Kwon TH, et al. Influence of rabbit notochordal cells on symptomatic intervertebral disc degeneration: anti-angiogenic capacity on human endothelial cell proliferation under hypoxia. Osteoarthritis Cartilage. 2017; 25(10): 1738–1746, doi: 10.1016/j.joca.2017.06.003, indexed in Pubmed: 28647468.
57. Lee S, Moon CS, Sul D, et al. Comparison of growth factor and cytokine expression in patients with degenerated disc disease and herniated nucleus pulposus. Clin Biochem. 2009; 42(15): 1504–1511, doi: 10.1016/j.clinbiochem.2009.06.017, indexed in Pubmed: 19563795.
58. Li G, Song Yu, Liao Z, et al. Bone-derived mesenchymal stem cells alleviate compression-induced apoptosis of nucleus pulposus cells by N6 methyladenosine of autophagy. Cell Death Dis. 2020; 11(2): 103, doi: 10.1038/s41419-020-2284-8, indexed in Pubmed: 32029706.
59. Li K, Li Y, Mi J, et al. Resveratrol protects against sodium nitroprusside induced nucleus pulposus cell apoptosis by scavenging ROS. Int J Mol Med. 2018; 41(5): 2485–2492, doi: 10.3892/ijmm.2018.3461, indexed in Pubmed: 29436588.
60. Li Y, Li K, Mao Lu, et al. Cordycepin inhibits LPS-induced inflammatory and matrix degradation in the intervertebral disc. PeerJ. 2016; 4: e1992, doi: 10.7717/peerj.1992, indexed in Pubmed: 27190710.
61. Liang W, Ye D, Dai L, et al. Overexpression of hTERT extends replicative capacity of human nucleus pulposus cells, and protects against serum starvation-induced apoptosis and cell cycle arrest. J Cell Biochem. 2012; 113(6): 2112–2121, doi: 10.1002/jcb.24082, indexed in Pubmed: 22298321.
62. Liao Z, Li S, Liu R, et al. Autophagic degradation of gasdermin D protects against nucleus pulposus cell pyroptosis and retards intervertebral disc degeneration in vivo. Oxid Med Cell Longev. 2021; 2021: 5584447, doi: 10.1155/2021/5584447, indexed in Pubmed: 34239691.
63. Lin D, Alberton P, Delgado Caceres M, et al. Loss of tenomodulin expression is a risk factor for age-related intervertebral disc degeneration. Aging Cell. 2020; 19(3): e13091, doi: 10.1111/acel.13091, indexed in Pubmed: 32083813.
64. Lin J, Du J, Wu X, et al. SIRT3 mitigates intervertebral disc degeneration by delaying oxidative stress-induced senescence of nucleus pulposus cells. J Cell Physiol. 2021; 236(9): 6441–6456, doi: 10.1002/jcp.30319, indexed in Pubmed: 33565085.
65. Lin Y, Jiao Y, Yuan Y, et al. Propionibacterium acnes induces intervertebral disc degeneration by promoting nucleus pulposus cell apoptosis via the TLR2/JNK/mitochondrial-mediated pathway. Emerg Microbes Infect. 2018; 7(1): 1, doi: 10.1038/s41426-017-0002-0, indexed in Pubmed: 29323102.
66. Lin Y, Tang G, Jiao Y, et al. Induces intervertebral disc degeneration by promoting iNOS/NO and COX-2/PGE activation via the ROS-dependent NF-κB pathway. Oxid Med Cell Longev. 2018; 2018: 3692752, doi: 10.1155/2018/3692752, indexed in Pubmed: 30210652.
67. Liu J, Yu P, Dai F, et al. Tetrandrine reduces oxidative stress, apoptosis, and extracellular matrix degradation and improves intervertebral disc degeneration by inducing autophagy. Bioengineered. 2022; 13(2): 3944–3957, doi: 10.1080/21655979.2022.2031396, indexed in Pubmed: 35109761.
68. Liu J, Yuan C, Pu L, et al. Nutrient deprivation induces apoptosis of nucleus pulposus cells via activation of the BNIP3/AIF signalling pathway. Mol Med Rep. 2017; 16(5): 7253–7260, doi: 10.3892/mmr.2017.7550, indexed in Pubmed: 28944876.
69. Liu ZC, Wang ZL, Huang CY, et al. Duhuo Jisheng Decoction inhibits SDF-1-induced inflammation and matrix degradation in human degenerative nucleus pulposus cells in vitro through the CXCR4/NF-κB pathway. Acta Pharmacol Sin. 2018; 39(6): 912–922, doi: 10.1038/aps.2018.36, indexed in Pubmed: 29795361.
70. Luo L, Jian X, Sun H, et al. Cartilage endplate stem cells inhibit intervertebral disc degeneration by releasing exosomes to nucleus pulposus cells to activate Akt/autophagy. Stem Cells. 2021; 39(4): 467–481, doi: 10.1002/stem.3322.
71. Masuda K, Imai Y, Okuma M, et al. Osteogenic protein-1 injection into a degenerated disc induces the restoration of disc height and structural changes in the rabbit anular puncture model. Spine (Phila Pa 1976). 2006; 31(7): 742–754, doi: 10.1097/01.brs.0000206358.66412.7b, indexed in Pubmed: 16582847.
72. Mei L, Zheng Yi, Ma T, et al. (-)-Epigallocatechin-3-gallate ameliorates intervertebral disc degeneration through reprogramming of the circadian clock. Front Pharmacol. 2021; 12: 753548, doi: 10.3389/fphar.2021.753548, indexed in Pubmed: 34803694.
73. Mohanraj B, Huang AH, Yeger-McKeever MJ, et al. Chondrocyte and mesenchymal stem cell derived engineered cartilage exhibits differential sensitivity to pro-inflammatory cytokines. J Orthop Res. 2018; 36(11): 2901–2910, doi: 10.1002/jor.24061, indexed in Pubmed: 29809295.
74. Nagayama K, Fukuei T. Cyclic stretch-induced mechanical stress to the cell nucleus inhibits ultraviolet radiation-induced DNA damage. Biomech Model Mechanobiol. 2020; 19(2): 493–504, doi: 10.1007/s10237-019-01224-3, indexed in Pubmed: 31506862.
75. Narayanan KB, Park HHo. Toll/interleukin-1 receptor (TIR) domain-mediated cellular signaling pathways. Apoptosis. 2015; 20(2): 196–209, doi: 10.1007/s10495-014-1073-1, indexed in Pubmed: 25563856.
76. Nerurkar NL, Elliott DM, Mauck RL. Mechanical design criteria for intervertebral disc tissue engineering. J Biochem. 2010; 43(6): 1017–1030, doi: 10.1016/j.jbiomech.2009.12.001, indexed in Pubmed: 20080239.
77. Niu A, Bian WP, Feng SL, et al. Role of manganese superoxide dismutase (Mn-SOD) against Cr(III)-induced toxicity in bacteria. J Hazard Mater. 2021; 403: 123604, doi: 10.1016/j.jhazmat.2020.123604, indexed in Pubmed: 32781281.
78. O'Connell GD, Johannessen W, Vresilovic EJ, et al. Human internal disc strains in axial compression measured noninvasively using magnetic resonance imaging. Spine (Phila Pa 1976). 2007; 32(25): 2860–2868, doi: 10.1097/BRS.0b013e31815b75fb, indexed in Pubmed: 18246009.
79. Ohnishi T, Sudo H, Tsujimoto T, et al. Age-related spontaneous lumbar intervertebral disc degeneration in a mouse model. J Orthop Res. 2018; 36(1): 224–232, doi: 10.1002/jor.23634, indexed in Pubmed: 28631843.
80. Pei S, Ying J, Zhang Y, et al. RhTSG-6 inhibits IL-1β-induced extracellular matrix degradation and apoptosis by suppressing the p38, and JNK pathways in nucleus pulposus

cells. Folia Histochem Cytobiol. 2020; 58(3): 227–234, doi: 10.5603/FHC.a2020.0019, indexed in Pubmed: 32936927.
81. Pisoschi AM, Pop A. The role of antioxidants in the chemistry of oxidative stress: A review. Eur J Med Chem. 2015; 97: 55–74, doi: 10.1016/j.ejmech.2015.04.040, indexed in Pubmed: 25942353.
82. Pourquié O, Coltey M, Teillet MA, et al. Control of dorsoventral patterning of somitic derivatives by notochord and floor plate. Proc Natl Acad Sci USA. 1993; 90(11): 5242–5246, doi: 10.1073/pnas.90.11.5242, indexed in Pubmed: 8506372.
83. Rider SM, Mizuno S, Kang JD. Molecular mechanisms of intervertebral disc degeneration. Spine Surg Relat Res. 2019; 3(1): 1–11, doi: 10.22603/ssrr.2017-0095, indexed in Pubmed: 31435545.
84. Risbud MV, Shapiro IM. Role of cytokines in intervertebral disc degeneration: pain and disc content. Nat Rev Rheumatol. 2014; 10(1): 44–56, doi: 10.1038/nrrheum.2013.160, indexed in Pubmed: 24166242.
85. Roset R, Ortet L, Gil-Gomez G. Role of Bcl-2 family members on apoptosis: what we have learned from knock-out mice. Front Biosci. 2007; 12: 4722–4730, doi: 10.2741/2421, indexed in Pubmed: 17485408.
86. Sakai D, Nakamura Y, Nakai T, et al. Exhaustion of nucleus pulposus progenitor cells with ageing and degeneration of the intervertebral disc. Nature Communications. 2012; 3(1): 1264, doi: 10.1038/ncomms2226.
87. Song Yu, Lu S, Geng W, et al. Mitochondrial quality control in intervertebral disc degeneration. Exp Mol Med. 2021; 53(7): 1124–1133, doi: 10.1038/s12276-021-00650-7, indexed in Pubmed: 34272472.
88. Sparks MA, Crowley SD, Gurley SB, et al. Classical renin-angiotensin system in kidney physiology. Compr Physiol. 2014; 4(3): 1201–1228, doi: 10.1002/cphy.c130040, indexed in Pubmed: 24944035.
89. Sullivan CB, Porter RM, Evans CH, et al. TNFα and IL-1β influence the differentiation and migration of murine MSCs independently of the NF-κB pathway. Stem Cell Res Ther. 2014; 5(4): 104, doi: 10.1186/scrt492, indexed in Pubmed: 25163844.
90. Sun K, Sun X, Sun J, et al. Tissue renin-angiotensin system (tRAS) induce intervertebral disc degeneration by activating oxidative stress and inflammatory reaction. Oxid Med Cell Longev. 2021; 2021: 3225439, doi: 10.1155/2021/3225439, indexed in Pubmed: 34413926.
91. Tan KO, Fu NY, Sukumaran SK, et al. MAP-1 is a mitochondrial effector of Bax. Proc Natl Acad Sci USA. 2005; 102(41): 14623–14628, doi: 10.1073/pnas.0503524102, indexed in Pubmed: 16199525.
92. Tang G, Han X, Lin Z, et al. Propionibacterium acnes accelerates intervertebral disc degeneration by inducing pyroptosis of nucleus pulposus cells via the ROS-NLRP3 pathway. Oxid Med Cell Longev. 2021; 2021: 4657014, doi: 10.1155/2021/4657014, indexed in Pubmed: 33603947.
93. Tang Z, Hu Bo, Zang F, et al. Nrf2 drives oxidative stress-induced autophagy in nucleus pulposus cells via a Keap1/Nrf2/p62 feedback loop to protect intervertebral disc from degeneration. Cell Death Dis. 2019; 10(7): 510, doi: 10.1038/s41419-019-1701-3, indexed in Pubmed: 31263165.
94. Tessier S, Risbud MV. Understanding embryonic development for cell-based therapies of intervertebral disc degeneration: Toward an effort to treat disc degeneration subphenotypes. Dev Dyn. 2021; 250(3): 302–317, doi: 10.1002/dvdy.217, indexed in Pubmed: 32564440.
95. Vergroesen PPA, Kingma I, Emanuel KS, et al. Mechanics and biology in intervertebral disc degeneration: a vicious circle. Osteoarthritis Cartilage. 2015; 23(7): 1057–1070, doi: 10.1016/j.joca.2015.03.028, indexed in Pubmed: 25827971.
96. Wang W, Deng G, Qiu Y, et al. Transplantation of allogenic nucleus pulposus cells attenuates intervertebral disc degeneration by inhibiting apoptosis and increasing migration. Int J Mol Med. 2018; 41(5): 2553–2564, doi: 10.3892/ijmm.2018.3454, indexed in Pubmed: 29436582.
97. Wang W, Li P, Xu J, et al. Resveratrol attenuates high glucose-induced nucleus pulposus cell apoptosis and senescence through activating the ROS-mediated PI3K/Akt pathway. Biosci Rep. 2018; 38(2), doi: 10.1042/BSR20171454, indexed in Pubmed: 29273676.
98. Wang X, Wang W, Li Li, et al. Oxidative stress and mitochondrial dysfunction in Alzheimer's disease. Biochim Biophys Acta. 2014; 1842(8): 1240–1247, doi: 10.1016/j.bbadis.2013.10.015, indexed in Pubmed: 24189435.
99. Wang Y, Che M, Xin J, et al. The role of IL-1β and TNF-α in intervertebral disc degeneration. Biomed Pharmacother. 2020; 131: 110660, doi: 10.1016/j.biopha.2020.110660, indexed in Pubmed: 32853910.
100. Wang Y, Song Y, Zhong Q, et al. Suppressing ROS generation by apocynin inhibited cyclic stretch-induced inflammatory reaction in HPDLCs via a caspase-1 dependent pathway. Int Immunopharmacol. 2021; 90: 107129, doi: 10.1016/j.intimp.2020.107129, indexed in Pubmed: 33199234.
101. Wehling N, Palmer GD, Pilapil C, et al. Interleukin-1beta and tumor necrosis factor alpha inhibit chondrogenesis by human mesenchymal stem cells through NF-kappaB-dependent pathways. Arthritis Rheum. 2009; 60: 801–812, doi: 10.1002/art.24352, indexed in Pubmed: 19248089.
102. Xia C, Zeng Z, Fang B, et al. Mesenchymal stem cell-derived exosomes ameliorate intervertebral disc degeneration via anti-oxidant and anti-inflammatory effects. Free Radic Biol Med. 2019; 143: 1–15, doi: 10.1016/j.freeradbiomed.2019.07.026, indexed in Pubmed: 31351174.
103. Xia LM, Zhang AP, Zheng Q, et al. Quercetin-3-O-β-D-glucuronide inhibits mitochondria pathway-mediated platelet apoptosis via the phosphatidylinositol-3-kinase/AKT pathway in immunological bone marrow failure. World J Tradit Chin Med. 2022; 8(1): 115, doi: 10.4103/wjtcm.wjtcm_44_21.
104. Xiang Q, Cheng Z, Wang J, et al. Allicin attenuated advanced oxidation protein product-induced oxidative stress and mitochondrial apoptosis in human nucleus pulposus cells. Oxid Med Cell Longev. 2020; 2020: 6685043, doi: 10.1155/2020/6685043, indexed in Pubmed: 33381267.
105. Xiang Q, Kang L, Wang J, et al. CircRNA-CIDN mitigated compression loading-induced damage in human nucleus pulposus cells via miR-34a-5p/SIRT1 axis. EBioMedicine. 2020; 53: 102679, doi: 10.1016/j.ebiom.2020.102679, indexed in Pubmed: 32114390.
106. Xie ZY, Chen Lu, Wang F, et al. Endoplasmic reticulum stress is involved in nucleus pulposus degeneration and attenuates low pH-Induced apoptosis of rat nucleus

pulposus cells. DNA Cell Biol. 2017; 36(8): 627–637, doi: 10.1089/dna.2017.3736, indexed in Pubmed: 28622016.
107. Yang M, Feng C, Zhang Y, et al. Autophagy protects nucleus pulposus cells from cyclic mechanical tension-induced apoptosis. Int J Mol Med. 2019; 44(2): 750–758, doi: 10.3892/ijmm.2019.4212, indexed in Pubmed: 31173175.
108. Yang RZ, Xu WN, Zheng HL, et al. Involvement of oxidative stress-induced annulus fibrosus cell and nucleus pulposus cell ferroptosis in intervertebral disc degeneration pathogenesis. J Cell Physiol. 2021; 236(4): 2725–2739, doi: 10.1002/jcp.30039, indexed in Pubmed: 32892384.
109. Yang SD, Bai ZL, Zhang F, et al. Levofloxacin increases the effect of serum deprivation on anoikis of rat nucleus pulposus cells via Bax/Bcl-2/caspase-3 pathway. Toxicol Mech Methods. 2014; 24(9): 688–696, doi: 10.3109/15376516.2014.963772, indexed in Pubmed: 25224805.
110. Yang W, Yu XH, Wang C, et al. Interleukin-1β in intervertebral disk degeneration. Clin Chim Acta. 2015; 450: 262–272, doi: 10.1016/j.cca.2015.08.029, indexed in Pubmed: 26341894.
111. Yang Y, Wang X, Liu Z, et al. Osteogenic protein-1 attenuates nucleus pulposus cell apoptosis through activating the PI3K/Akt/mTOR pathway in a hyperosmotic culture. Biosci Rep. 2018; 38(6), doi: 10.1042/BSR20181708, indexed in Pubmed: 30459239.
112. Zehra U, Tryfonidou M, Iatridis JC, et al. Mechanisms and clinical implications of intervertebral disc calcification. Nat Rev Rheumatol. 2022; 18(6): 352–362, doi: 10.1038/s41584-022-00783-7, indexed in Pubmed: 35534553.
113. Zhan JW, Wang SQ, Feng MS, et al. Constant compression decreases vascular bud and VEGFA expression in a rabbit vertebral endplate ex vivo culture model. PLoS One. 2020; 15(6): e0234747, doi: 10.1371/journal.pone.0234747, indexed in Pubmed: 32584845.
114. Zhang GZ, Deng YJ, Xie QQ, et al. Sirtuins and intervertebral disc degeneration: Roles in inflammation, oxidative stress, and mitochondrial function. Clin Chim Acta. 2020; 508: 33–42, doi: 10.1016/j.cca.2020.04.016, indexed in Pubmed: 32348785.
115. Zhang K, Ding W, Sun W, et al. Beta1 integrin inhibits apoptosis induced by cyclic stretch in annulus fibrosus cells via ERK1/2 MAPK pathway. Apoptosis. 2016; 21(1): 13–24, doi: 10.1007/s10495-015-1180-7, indexed in Pubmed: 26467923.
116. Zhang Q, Weng Y, Jiang Y, et al. Overexpression of miR-140-5p inhibits lipopolysaccharide-induced human intervertebral disc inflammation and degeneration by downregulating toll-like receptor 4. Oncol Rep. 2018; 40(2): 793–802, doi: 10.3892/or.2018.6488, indexed in Pubmed: 29901170.
117. Zhang Y, He F, Chen Z, et al. Melatonin modulates IL-1β-induced extracellular matrix remodeling in human nucleus pulposus cells and attenuates rat intervertebral disc degeneration and inflammation. Aging (Albany NY). 2019; 11(22): 10499–10512, doi: 10.18632/aging.102472, indexed in Pubmed: 31772145.
118. Zhang YH, Shangguan WJ, Zhao ZJ, et al. Naringin inhibits apoptosis induced by cyclic stretch in rat annular cells and partially attenuates disc degeneration by inhibiting the ROS/NF-κB pathway. Oxid Med Cell Longev. 2022; 2022: 6179444, doi: 10.1155/2022/6179444, indexed in Pubmed: 35251479.
119. Zhao Y, Qiu C, Wang W, et al. Cortistatin protects against intervertebral disc degeneration through targeting mitochondrial ROS-dependent NLRP3 inflammasome activation. Theranostics. 2020; 10(15): 7015–7033, doi: 10.7150/thno.45359, indexed in Pubmed: 32550919.
120. Zheng J, Zhang J, Zhang X, et al. Reactive oxygen species mediate low back pain by upregulating substance P in intervertebral disc degeneration. Oxid Med Cell Longev. 2021; 2021: 6681815, doi: 10.1155/2021/6681815, indexed in Pubmed: 34093962.
121. Zhong H, Zhou Z, Guo L, et al. The miR-623/CXCL12 axis inhibits LPS-induced nucleus pulposus cell apoptosis and senescence. Mech Ageing Dev. 2021; 194: 111417, doi: 10.1016/j.mad.2020.111417, indexed in Pubmed: 33333129.
122. Zhou J, Liu Qi, Yang Z, et al. Rutin maintains redox balance to relieve oxidative stress induced by TBHP in nucleus pulposus cells. In Vitro Cell Dev Biol Anim. 2021; 57(4): 448–456, doi: 10.1007/s11626-021-00581-7, indexed in Pubmed: 33909255.
123. Zhu H, Sun B, Shen Q. TNF-α induces apoptosis of human nucleus pulposus cells via activating the TRIM14/NF-κB signalling pathway. Artif Cells Nanomed Biotechnol. 2019; 47(1): 3004–3012, doi: 10.1080/21691401.2019.1643733, indexed in Pubmed: 31322007.
124. Zhu J, Tang H, Zhang Z, et al. Kaempferol slows intervertebral disc degeneration by modifying LPS-induced osteogenesis/adipogenesis imbalance and inflammation response in BMSCs. Int Immunopharmacol. 2017; 43: 236–242, doi: 10.1016/j.intimp.2016.12.020, indexed in Pubmed: 28043032.
125. Zhu Y, Tchkonia T, Pirtskhalava T, et al. The Achilles' heel of senescent cells: from transcriptome to senolytic drugs. Aging Cell. 2015; 14(4): 644–658, doi: 10.1111/acel.12344.

VIA MEDICA

REVIEW ARTICLE

Folia Morphol.
Vol. 82, No. 4, pp. 758–765
DOI: 10.5603/FM.a2022.0086

ISSN 0015–5659
eISSN 1644–3284
journals.viamedica.pl

The cranio-orbital foramen: a meta-analysis with a review of the literature

P. Ostrowski[1], M. Bonczar[1], J. Iwanaga[2, 3], R. Canon[1], M. Dziedzic[1], B. Kołodziejczyk[1], A. Juszczak[1], J. Walocha[1], M. Koziej[1]

[1]*Department of Anatomy, Jagiellonian University Medical College, Krakow, Poland*
[2]*Department of Neurosurgery, Tulane University School of Medicine, New Orleans, United States*
[3]*Department of Oral and Maxillofacial Anatomy, Graduate School of Medical and Dental Sciences, Tokyo Medical and Dental University, Tokyo, Japan*

[Received: 14 August 2022; Accepted: 26 September 2022; Early publication date: 30 September 2022]

Background: *The goal of the present study was to provide accurate data on the prevalence and morphometrical aspects of the cranio-orbital foramen (COF), which can surely be of use by surgeons performing procedures on the lateral orbit. Furthermore, the embryology and the clinical significance of this osseous structure were thoroughly discussed.*

Materials and methods: *Major online medical databases such as PubMed, Scopus, Embase, Web of Science, and Google Scholar were searched to find all relevant studies regarding COF.*

Results: *Eventually, a total of 25 studies that matched the required criteria and contained complete and relevant data were included in this meta-analysis. The pooled prevalence of COF was found to be 48.37% (95% confidence interval [CI]: 41.67–55.10%). The occurrence of the COF unilaterally was set to be 71.92% (95% CI: 41.87–96.97%). The occurrence of the COF bilaterally was set at 26.08% (95% CI: 3.03–58.13%).*

Conclusions: *In conclusion, we believe that this is the most accurate and up-to--date study regarding the anatomy of the COF. The COF is prevalent in 48.37% of the cases, and it is most frequently unilateral (73.92%). Furthermore, the prevalence of accessory COFs was found to be 16.72%. The presence of these foramina may represent a source of haemorrhage that ophthalmic surgeons should be aware of when performing procedures in the lateral part of the orbit.*
(Folia Morphol 2023; 82, 4: 758–765)

Key words: cranio-orbital foramen, lateral orbit, whitnall tubercle, frontozygomatic suture

INTRODUCTION

The orbits are bilateral bony cavities in the facial skeleton housing numerous canals and foramina, which form connections with other neighbouring cavities of the skull. Oftentimes, these osteological structures are used as surgical landmarks by ophthalmic surgeons to define operating margins and locate nearby vulnerable neurovascular structures [28].

The cranio-orbital foramen (COF) is an ostial opening in the lateral wall of the orbit, adjacent to the superior orbital fissure. The COF is known by different names, such as the meningo-orbital foramen, lacri-

Address for correspondence: Dr. M. Koziej, Department of Anatomy, Jagiellonian University Medical College, ul. Mikołaja Kopernika 12, 33–332 Kraków, Poland, tel: +48 888 202 628, e-mail: mateusz.koziej@gmail.com

mal foramen, foramen of Hyrtl, spheno-frontal foramen, sinus canal foramen, and anastomotic foramen [9, 27, 30]. The foramen is said to contain an arterial anastomosis between the orbital branch of the middle meningeal artery and the lacrimal artery [31]. Its prevalence, which has been widely discussed in the available literature and across all studies, ranges from 28% to 82.9% [9]. Moreover, the morphometrical aspects of this osseous opening have also been a topic of discussion. These parameters include the distance between the supraorbital notch/foramen and the COF [1, 5, 21]. Furthermore, many studies have reported double or even triple accessory cranio-orbital foramina in cadaveric specimens [5, 21].

Knowledge about the prevalence and morphometrical aspects of the COF may be of great importance for ophthalmic surgeons involved in orbital reconstructions, anterior skull base procedures, orbital tumour resection, and decompression surgery for thyroid eye disease [1, 12]. During deep dissection of the lateral orbital wall, unexpected haemorrhage may complicate surgery if the COF is present.

Therefore, the goal of the present study was to provide accurate data on the prevalence and morphometrical aspects of the COF, which can surely be of use by surgeons performing procedures on the lateral orbit. Furthermore, the embryology and the clinical significance of this osseous structure were thoroughly discussed.

MATERIALS AND METHODS

Search strategy

Major online medical databases such as PubMed, Scopus, Embase, Web of Science, and Google Scholar were searched to find all relevant studies regarding COF. The search was conducted in July 2022. The following search terms were used: 'cranio-orbital' OR 'cranio orbital' OR 'meningo-orbital' OR 'meningo orbital' OR 'lacrimal foramen' OR 'Hyrtl foramen' OR 'spheno-frontal foramen' OR 'sinus canal foramen' OR 'anastomotic foramen'. The search terms were adjusted to each of the databases in order to maximise the number of results. No dates, language, article type, and/or text availability conditions were applied. Subsequently, an additional search was carried out for references from the screened studies. During this study, the Preferred Reporting Items for Systematic Reviews and Meta-Analyses (PRISMA) guidelines were followed. In addition, the Critical Assessment Tool for Anatomical Meta-analysis (CATAM) was used to provide the highest quality findings [7].

Eligibility assessment

The database search and the manual search identified a total of 3621 studies and were initially evaluated by two independent reviewers. After removing duplicates and irrelevant records, a total of 956 articles were qualified for full-text evaluation. To minimise potential bias and maintain an accurate statistical methodology, articles such as case reports, case series, conference reports, reviews, letters to the editors, and studies that provided incomplete or irrelevant data were excluded. The inclusion criteria involved original studies with extractable numerical data on the prevalence, morphology, and anatomical relations of the COF. Finally, a total of 25 studies were included in this meta-analysis. The AQUA Tool, which was specifically designed for anatomical meta-analyses, was used to minimise the potential bias of included studies [13]. The flow chart presenting the study inclusion process is shown in Figure 1.

Data extraction

Data from qualified studies were extracted by two independent reviewers. Qualitative data, such as year of publication, country, and continent, were gathered. Quantitative data, such as sample size, numerical data regarding the prevalence of the COF, its morphology, and the distances between the COF and other anatomical structures, were gathered. Studies containing mean results but without standard deviation or interquartile range or unclear or unspecified variations were excluded. Any discrepancies between the studies identified by the two reviewers were resolved by contacting the authors of the original studies wherever possible or by consensus with a third reviewer.

Statistical analysis

To perform statistical analysis, STATISTICA version 13.1 software (StatSoft Inc., Tulsa, OK, USA), MetaXL version 5.3 software (EpiGear International Pty Ltd, Wilston, Queensland, Australia), and Comprehensive Meta-analysis version 3.0 software (Biostat Inc., Englewood, NJ, USA) were used. A random-effects model was performed in all analyses. The chi-square test and I-square statistics were used to assess heterogeneity among the studies [14]. A p-value and confidence intervals were used to determine statistical significance between studies. A p-value less than 0.05 was considered statistically significant. In the case of overlapping confidence intervals, differences were considered statistically insignificant. The statistics of

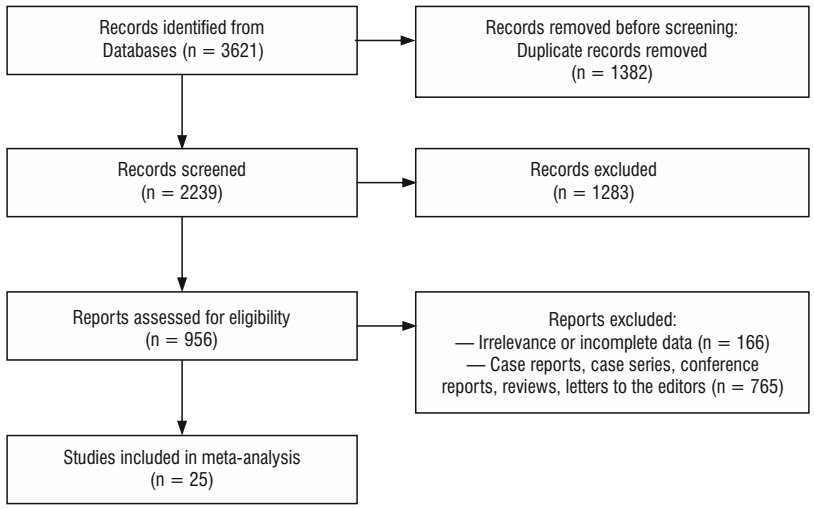

Figure 1. Flow-chart presenting the inclusion process in this meta-analysis.

squares were interpreted as follows: values of 0–40% were considered 'may not be important', values of 30–60% were considered 'may indicate moderate heterogeneity', values of 50–90% were considered 'may indicate substantial heterogeneity', and values of 75% to 100% were considered 'may indicate substantial heterogeneity'.

RESULTS

Eventually, a total of 25 studies that matched the required criteria and contained complete and relevant data were included in this meta-analysis [1–3, 5, 6, 9–11, 17–24, 26, 29, 31–33, 35, 37, 38, 40]. The characteristics of each study submitted are shown in Table 1.

The pooled prevalence of COF (n = 5649) was found to be 48.37% (95% confidence interval [CI]: 41.67–55.10%). The occurrence of the COF unilaterally (n = 926) was set to be 73.92% (95% CI: 41.87––96.97%). The occurrence of the COF bilaterally (n = 926) was set at 26.08% (95% CI: 3.03–58.13%).

The pooled prevalence of COF in men (n = 1061) was found to be 50.52% (95% CI: 40.38–60.64%). The pooled prevalence of COF in women (n = 1061) was 51.91% (95% CI 28.75–74.68%). Overall, there are no statistically significant differences in the occurrence of COF between men and women (p = 0.93).

The pooled prevalence of the COF on the left side (n = 773) was found to be 51.42% (95% CI: 34.85–67.83%), as on the right side (n = 773) it was established at 47.63% (95% CI: 28.11–67.51%).

The pooled prevalence of the accessory COF (n = 257) was set to 16.72% (95% CI: 11.09–23.22%).

Table 1. Characteristics of published studies

First author	Year	Continent	Country
Mahajan et al. [24]	2020	Asia	India
Simao-Parreira et al. [38]	2019	Europe	Portugal
Modasiya and Kanani [26]	2018	Asia	India
Silva et al. [37]	2017	South America	Chile
Garapati et al. [10]	2016	Asia	India
Macchi et al. [23]	2016	Europe	Italy
Pratha and Thenmozi [33]	2016	Asia	India
Agarwal et al. [2]	2015	Asia	India
Celik et al. [5]	2014	Asia	Turkey
Tomaszewska and Zelaźniewicz [40]	2014	Europe	Poland
Chauhan and Khanna [6]	2013	Asia	India
Krishna and Shenol [19]	2013	Asia	India
Pankaj et al. [32]	2013	Asia	India
Abed et al. [1]	2012	Europe	United Kingdom
Jadhav et al. [17]	2012	Asia	India
Babu et al. [3]	2011	Asia	India
Krishnamurthy et al. [20]	2008	Asia	India
O'Brien and McDonald [31]	2007	Europe	United Kingdom
Erturk et al. [9]	2005	Asia	India
Jovanovic et al. [18]	2003	Europe	Serbia
Kwiatkowski et al. [21]	2003	Europe	Poland
Lee and Chung [22]	2000	Asia	Korea
Georgiou and Cassell [11]	1991	North America	USA
Mysorekar and Nandedkar [29]	1987	Asia	India
Santo Neto et al. [35]	1984	South America	Brazil

Table 2. Statistical results of this meta-analysis regarding the prevalence of the cranio-orbital foramen (COF)

Category	Pooled prevalence	N	LCI	HCI	Q	I^2	P
Pooled prevalence of the COF	48.37%	5649	41.67%	55.10%	540.50	95.56	–
Pooled prevalence of occurrence of the COF in different locations							
COF in the sphenoid bone	26.28%	793	17.29%	36.37%	15.21	80.28	–
COF in the frontal bone	25.69%	793	14.21%	39.09%	26.51	88.68	
COF at the frontosphenoidal suture	15.06%	793	12.19%	18.17%	1.29	0.00	
COF at the ossified frontosphenoidal suture	18.87%	793	0.00%	57.32%	224.57	98.66	
COF at different locations	9.85%	793	0.00%	47.79%	282.18	98.94	
Occurrence of unilateral or bilateral COF							
Pooled prevalence of the unilateral COF	73.92%	926	41.87%	96.97%	25.74	92.23	0.36
Pooled prevalence of the bilateral COF	26.08%	926	3.03%	58.13%	25.74	92.23	
Occurrence of COF regarding sex							
Pooled prevalence of the COF in females	50.52%	1061	40.38%	60.64%	18.99	78.94	0.93
Pooled prevalence of the COF in males	51.91%	1061	28.75%	74.68%	105.24	96.20	
Occurrence of COF regarding patients' side							
Pooled prevalence of the COF on the left side	51.42%	773	34.85%	67.83%	50.97	90.19	0.82
Pooled prevalence of the COF on the right side	47.63%	773	28.11%	67.51%	72.64	93.12	
Occurrence of an additional COF							
Pooled prevalence of the aCOF	16.72%	257	11.09%	23.22%	3.10	35.56	–

LCI — lower confidence interval; HCI — higher confidence interval; Q — Cochran's Q

Table 3. Statistical results of this meta-analysis regarding the diameter of the cranio-orbital foramen (COF)

Category	N	Mean	SE	Var.	LCI	HCI	Z	P
Mean maximal diameter of the COF [mm]	944	0.969	0.140	0.019	0.695	1.242	6.943	0.00

SE — standard error; Var. — variance; LCI — lower confidence interval; HCI — higher confidence interval

All the results mentioned above and the more detailed ones can be found in Table 2.

The mean maximal diameter (n = 944) of the COF was set at 0.969 mm (standard error [SE] = 0.140). For more detailed results, see Table 3.

The mean distance between the COF and the frontozygomatic suture (n = 1347) was set to 26.89 mm (SE = 0.62). The mean distance between the COF and the supraorbital notch (n = 1347) was established at 34.95 mm (SE = 0.74). The mean distance between the COF and the Whitnall tubercle (n = 1347) was established to be 27.56 mm (SE = 0.62). The mean distance between the COF and the lateral angle (n = 1347) was established at 7.18 mm (SE = 0.76). For more detailed results and the analysis of distances on the sex and side of the patients, see Table 4.

DISCUSSION

Numerous anatomical studies have discussed the location, prevalence, and morphometric properties of the COF (Figs. 2–4) [1, 6, 17]. O'Brien and McDonald [31] conducted an anatomical study on the prevalence and the location of the COFs. In the study, the prevalence of this foramen was stated to be 73%. However, the location of the COF varied significantly, being found predominately where the frontosphenoidal suture had fused. This raised the question of whether the COF could create connections with the frontal rather than the middle cranial fossa. This communication was proved to exist in the aforementioned study, where 2 out of 16 specimens contained this connection. Pankaj et al. [32] reported a significantly lower prevalence of this structure (36.02%) in their cadaveric study. However, they also reported an orbit-anterior cranial fossa communication. Our results show that the COF is present in 48.37% of the cases and occurs more frequently unilaterally (73.92%), than bilaterally (26.08%). Furthermore, the location of the COF within the orbit was proven to be quite variable. The COF was located most frequently in the greater wing of the sphenoid bone (26.28%)

Table 4. Statistical results of this meta-analysis regarding the location of the cranio-orbital foramen (COF)

Category	N	Mean	SE	Var.	LCI	HCI	Z	P
Overall results								
Distance between COF and the frontozygomatic suture [mm]	1347	26.89	0.62	0.39	25.68	28.11	43.32	0.00
Distance between COF and the supraorbital notch [mm]	1347	34.95	0.74	0.54	33.50	36.39	47.37	0.00
Distance between COF and the Whitnall's tubercle [mm]	1347	27.56	0.62	0.39	26.34	28.78	44.19	0.00
Distance between COF and the lateral angle [mm]	1347	7.18	0.76	0.58	5.68	8.67	9.43	0.00
Results regarding sex								
Distance between COF and the frontozygomatic suture in females [mm]	248	25.92	0.93	0.87	24.09	27.75	27.72	0.00
Distance between COF and the frontozygomatic suture in males [mm]	248	26.03	0.36	0.13	25.32	26.73	72.24	0.00
Distance between COF and the supraorbital notch in females [mm]	248	34.52	0.66	0.44	33.22	35.82	52.06	0.00
Distance between COF and the supraorbital notch in males [mm]	248	34.33	0.41	0.17	33.52	35.14	83.09	0.00
Results regarding the patients' side								
Distance between COF and the frontozygomatic suture on the left side [mm]	192	24.78	1.92	3.69	21.01	28.54	12.90	0.00
Distance between COF and the frontozygomatic suture on the right side [mm]	176	25.62	2.30	5.27	21.12	30.12	11.16	0.00
Distance between COF and the supraorbital notch on the left side [mm]	192	35.19	1.58	2.50	32.09	38.29	22.24	0.00
Distance between COF and the supraorbital notch on the right side [mm]	176	35.12	1.83	3.37	31.53	38.72	19.14	0.00
Distance between COF and the superior orbital fissure on the left side [mm]	192	10.28	1.35	1.83	7.63	12.94	7.60	0.00
Distance between COF and the superior orbital fissure on the right side [mm]	176	11.10	2.29	5.25	6.61	15.59	4.84	0.00

SE — standard error; Var. — variance; LCI — lower confidence interval; HCI — higher confidence interval

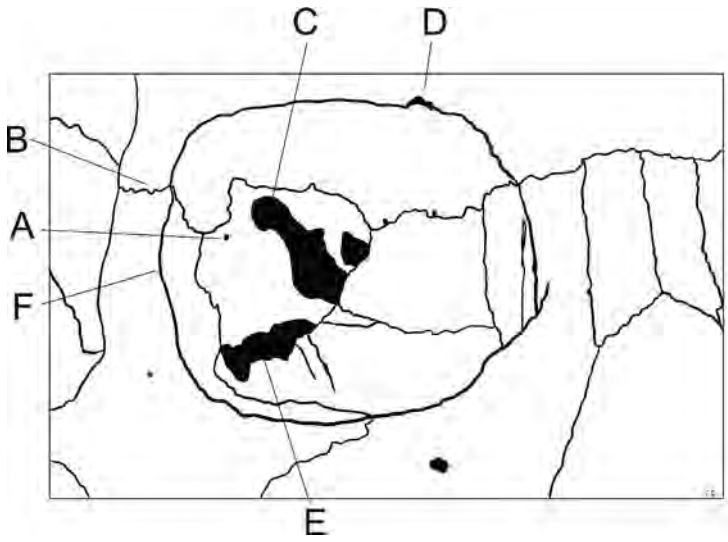

Figure 2. Scheme illustrating the cranio-orbital foramen and its anatomical area; A — cranio-orbital foramen; B — frontozygomatic suture; C — superior orbital fissure; D — supraorbital notch; E — inferior orbital fissure; F — Whitnall's tubercle.

and the orbital surface of the frontal bone (25.69%). Other intraorbital locations of the COF were within the frontosphenoidal suture (15.06%) and where the frontosphenoidal suture had fused (18.87%). Interestingly, no statistically significant differences in prevalence were observed with respect to the sex of the subject.

Many studies have also reported the presence of accessory COFs [9, 31, 32, 38]. The present study shows that the prevalence of any accessory COFs is 16.72%. However, Abed et al. [1] stated that these accessory cranio-orbital foramina are unlikely to be a source of significant haemorrhage because of their small calibre. However, bleeding at these locations can serve as a warning that a potential COF may be present, with a significantly larger vessel passing through it.

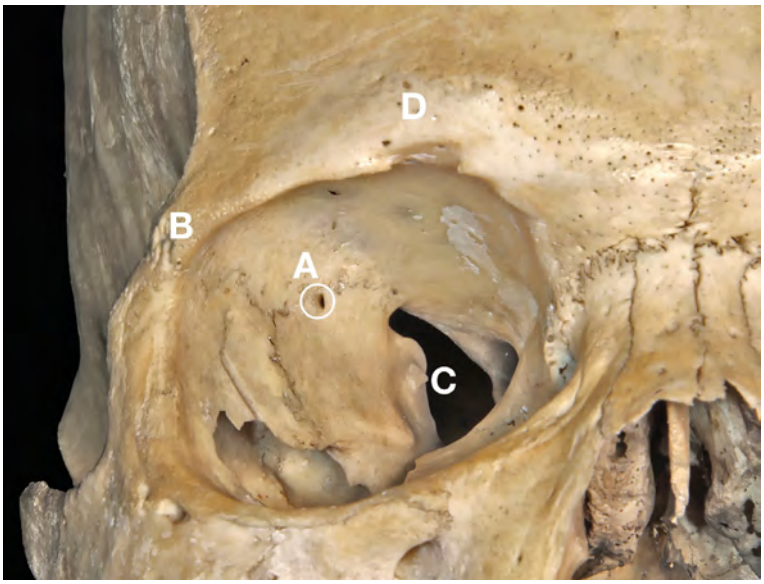

Figure 3. A photograph depicting the right orbit; A — cranio-orbital foramen; B — frontozygomatic suture; C — superior orbital fissure; D — supraorbital notch.

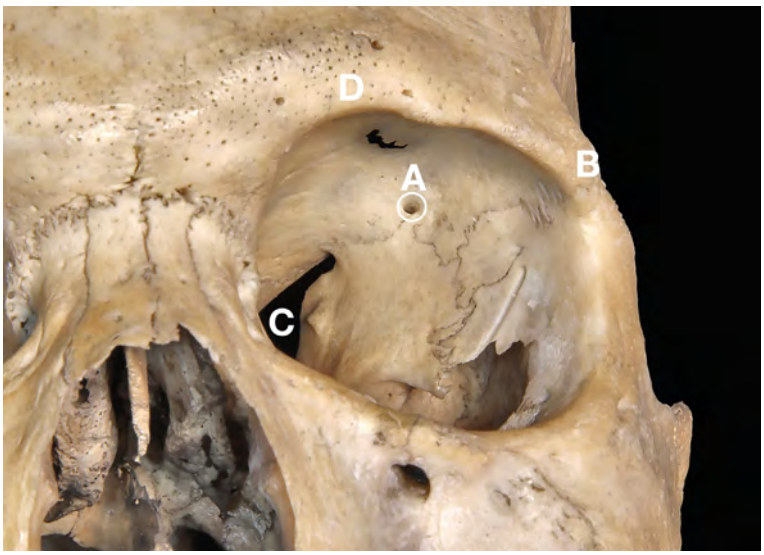

Figure 4. A photograph depicting the left orbit; A — cranio-orbital foramen; B — frontozygomatic suture; C — superior orbital fissure; D — supraorbital notch.

Georgiou and Cassell [11] presented a study about the relationship between the COF and the development of the ophthalmic artery. They described that the initial vascular supply of the orbit arises from the internal carotid artery and then by the supraorbital division of the stapedial artery, which is an embryonic artery that disappears during the 10th week in utero and is the precursor of some orbital, dural, and maxillary branches [4]. Furthermore, they describe the formation of an anastomosis between the ophthalmic artery and the supraorbital branch of the stapedial artery which forms a "ring" around the optic nerve. The stapedial artery is represented as the orbital branch of the middle meningeal artery in adulthood. It is thought that the COF represents the point at which the supraorbital division of the stapedial artery passes through the greater wing of the sphenoid bone which has not been ossified yet [1, 11].

The orbital branch of the middle meningeal artery (OB) enters the orbit through the superior orbital fissure or the COF and it forms an anastomosis with the lacrimal artery [8]. The anatomic features of the COF

and the course of the OB were thoroughly described by Erturk et al. [9] in a cadaveric study. In the study, the OB was most frequently observed to pass through the COF (43.2%). However, the vessel was also running through the superior orbital fissure in 16.2% of the cases. Shimada et al. [36] presented similar results, with the OB coursing most commonly through the COF rather than the superior orbital fissure. This vessel is said to contribute to the arterial supply of the anterior part of the dura of the middle cranial fossa and form anastomoses between the ophthalmic artery and middle meningeal artery. Furthermore, Stiernberg et al. [39] and Price et al. [34] showed that the aforementioned branch might provide accessory blood supply to the orbital contents. Therefore, great care has to be taken by the surgeon performing reconstructions of the anterior base of the skull and the orbit because the OB can get damaged and a large part of the blood supply to the orbital contents may be lost [9].

In order to provide an effective method for surgeons to localize the COF, morphometric values from the frontozygomatic suture and the supraorbital notch to the foramen have been measured and reported by previous studies [1, 15, 25]. The results of the present meta-analysis show that the average distance between the COF and the frontozygomatic suture and the supraorbital notch is 26.89 mm and 34.95 mm, respectively. McQueen et al. [25] presented a method of defining a safe operating zone with respect to the COF, where the shortest aforementioned measurements were subtracted by 5 mm. When using this method and taking advantage of the frontozygomatic suture and the supraorbital notch as surgical landmarks, operating beyond a distance of 29.95 mm and 21.89 mm from the COF, respectively, may increase the risk of damaging the contents of the foramen [1].

Other landmarks may also be used by the ophthalmic surgeon in order to establish a safe zone for the COF. These include the Whitnall's tubercle and the lateral angle, and the mean distance between these landmarks and the COF was set as 27.56 mm and 7.18 mm, respectively. All of the aforementioned measurements give the ophthalmic surgeon flexibility in choosing the technique of locating the COF in the orbit.

Limitations of the study

This study is not without limitations. It may be burdened with potential bias, as the results of this meta-analysis are limited by the accuracy of the studies submitted. The authors of the present study were unable to perform some of the morphological analyses due to the lack of consistent data in the literature. Additionally, most of the evaluated studies come from Asia, therefore, the results of this study may be burdened, as they may reflect the anatomical features of Asian people rather than the global population.

CONCLUSIONS

In conclusion, we believe that this is the most accurate and up-to-date study regarding the anatomy of the COF. The COF is prevalent in 48.37% of the cases, and it is most frequently unilateral (73.92%). Furthermore, the prevalence of accessory COFs was found to be 16.72%. The presence of these foramina may represent a source of haemorrhage that ophthalmic surgeons should be aware of when performing procedures in the lateral part of the orbit.

Acknowledgements

The authors are indebted to Mr. Jacenty Urbaniak for the technical support. "The authors sincerely thank those who donated their bodies to science so that anatomical research could be performed. Results from such research can potentially increase mankind's overall knowledge that can then improve patient care. Therefore, these donors and their families deserve our highest gratitude" [16].

Conflict of interest: None declared

REFERENCES

1. Abed SF, Shams P, Shen S, et al. A cadaveric study of the cranio-orbital foramen and its significance in orbital surgery. Plast Reconstr Surg. 2012; 129(2): 307e–311e, doi: 10.1097/PRS.0b013e31821b6382, indexed in Pubmed: 22286445.
2. Agarwal C, Garg R, Kumar S, et al. Foramen meningo-orbitale : its incidence and clinical significance in Indians. Ind J Basic Applied Med Res. 2015; 4(4): 127–132.
3. Babu Y, Sivanandan R, Saraswathy P. Inci-dence of Foramen Meningo - Orbitale in South Indian Population. Recent Res Sci Tech. 2011; 3(10): 43–44.
4. Bonasia S, Smajda S, Ciccio G, et al. Stapedial artery: from embryology to different possible adult configurations. Am J Neuroradiol. 2020; 41(10): 1768–1776, doi: 10.3174/ajnr.A6738, indexed in Pubmed: 32883664.
5. Celik S, Kazak Z, Ozer MA, et al. Navigational area of the cranio-orbital foramen and its significance in orbital surgery. Surg Radiol Anat. 2014; 36(10): 981–988, doi: 10.1007/s00276-014-1293-7, indexed in Pubmed: 24744137.
6. Chauhan R, Khanna J. Meningo-orbital foramen in the lateral orbital wall – topographical anatomy and clinical relevance. Int J Scien Res. 2012; 2(4): 268–270, doi: 10.15373/22778179/apr2013/95.

7. D'Antoni AV, Tubbs RS, Patti AC, et al. The critical appraisal tool for anatomical meta-analysis: a framework for critically appraising anatomical meta-analyses. Clin Anat. 2022; 35(3): 323–331, doi: 10.1002/ca.23833, indexed in Pubmed: 35015336.
8. Diamond MK. Homologies of the meningeal-orbital arteries of humans: a reappraisal. J Anat. 1991; 178: 223–241, indexed in Pubmed: 1810930.
9. Erturk M, Kayalioglu G, Govsa F, et al. The cranio-orbital foramen, the groove on the lateral wall of the human orbit, and the orbital branch of the middle meningeal artery. Clin Anat. 2005; 18(1): 10–14, doi: 10.1002/ca.20020, indexed in Pubmed: 15597374.
10. Garapati S, Santhi Ch, Bhanu P, et al. Incidence and clinical significance of cranio-orbital foramen in telangana region of south india. Int J Anat Res. 2016; 4(2.2): 2297–2300, doi: 10.16965/ijar.2016.199.
11. Georgiou C, Cassell MD. The foramen meningo-orbitale and its relationship to the development of the ophthalmic artery. J Anat. 1992; 180(Pt 1): 119–125, indexed in Pubmed: 1452466.
12. Ghosh S, Narayan R. Fractures involving bony orbit: a comprehensive review of relevant clinical anatomy. Trans Res Anat. 2021; 24: 100125, doi: 10.1016/j.tria.2021.100125.
13. Henry BM, Tomaszewski KA, Ramakrishnan PK, et al. Development of the anatomical quality assessment (AQUA) tool for the quality assessment of anatomical studies included in meta-analyses and systematic reviews. Clin Anat. 2017; 30(1): 6–13, doi: 10.1002/ca.22799, indexed in Pubmed: 27718281.
14. Higgins JPT, Thomas J, Chandler J. (eds.). Cochrane Handbook for Systematic Reviews of Interventions. Wiley 2019.
15. Huanmanop T, Agthong S, Chentanez V. Surgical anatomy of fissures and foramina in the orbits of Thai adults. J Med Assoc Thai. 2007; 90(11): 2383–2391, indexed in Pubmed: 18181324.
16. Iwanaga J, Singh V, Ohtsuka A, et al. Acknowledging the use of human cadaveric tissues in research papers: Recommendations from anatomical journal editors. Clin Anat. 2020; 34(1): 2–4, doi: 10.1002/ca.23671, indexed in Pubmed: 32808702.
17. Jadhav S, Roy P, Ambali M, et al. The foramen meningo-orbital in Indian dry skulls. Natl J Integr Res Med. 2012; 3(4): 46–49.
18. Jovanović IJ, Vasović L, Ugrenović S, et al. Variable foramen of hyrtl of the human skull. Arto Medica Medianae. 2003; 42(1): 1–5.
19. Krishna G, Shenol KA. study on position of Menngo orbital foramen in south Indian dissected skulls. Int J Innov Res Stud. 2013; 2(12): 2319–9725.
20. Krishnamurthy A, Nayak SR, Prabhu LV, et al. The morphology of meningo-orbital foramen in south Indian population. Bratisl Lek Listy. 2008; 109(11): 517–519, indexed in Pubmed: 19205564.
21. Kwiatkowski J, Wysocki J, Nitek S. The morphology and morphometry of the so-called "meningo-orbital foramen" in humans. Folia Morphol. 2003; 62(4): 323–325, indexed in Pubmed: 14655111.
22. Lee H, Chung I. Foramen meningo-orbit and its relationship with the middle meningeal artery. Anat. 2000; 33(1): 99–104.
23. Macchi V, Regoli M, Bracco S, et al. Clinical anatomy of the orbitomeningeal foramina: variational anatomy of the canals connecting the orbit with the cranial cavity. Surg Radiol Anat. 2016; 38(2): 165–177, doi: 10.1007/s00276-015-1530-8, indexed in Pubmed: 26233593.
24. Mahajan M, Anupriya A, Devi G, et al. Clinical implications in orbital and pterional flap surgeries as well as radioimaging studies to determine topographical prevalence and characterization of meningo-orbital foramen in orbits of the indian population. Int J Morphol. 2020; 38(6): 1810–1817, doi: 10.4067/s0717-95022020000601810.
25. McQueen CT, DiRuggiero DC, Campbell JP, et al. Orbital osteology: a study of the surgical landmarks. Laryngoscope. 1995; 105(8 Pt 1): 783–788, doi: 10.1288/00005537-199508000-00003, indexed in Pubmed: 7630287.
26. Modasiya UP, Kanani S. Meningo-orbital foramen in South Gujarat population. Nat J Clin Anat. 2018; 7(1): 12, doi: 10.4103/2277-4025.297642.
27. Moore KL, Dalley AF, Agur A. Clinically oriented anatomy (8th ed.). Lippincott Williams and Wilkins 2017.
28. Mpolokeng KS, Louw GJ. An unusual arrangement of the neurovascular structures in one ethmoidal foramen of the human orbit. Transl Res Anat. 2020; 18: 100058, doi: 10.1016/j.tria.2019.100058.
29. Mysorekar VR, Nandedkar AN. The groove in the lateral wall of the human orbit. J Anat. 1987; 151: 255–257, indexed in Pubmed: 3654356.
30. Narayan R, Ghosh S. Analysis of variations in morphological characteristics of orbito-meningeal foramen: An anatomical study with clinical implications. Transl Res Anat. 2021; 24: 100108, doi: 10.1016/j.tria.2020.100108.
31. O'Brien A, McDonald SW. The meningo-orbital foramen in a Scottish population. Clin Anat. 2007; 20(8): 880–885, doi: 10.1002/ca.20558, indexed in Pubmed: 17948295.
32. Pankaj AK, Kumar N, Verma RK. Incidence of meningo orbital foramen in dry skull and its clinical relevance. Ind J Basic Applied Med Res. 2013; 2(6): 514–517.
33. Pratha A, Thenmozhi MS. A study of occurrence and morphometric analysis on meningo orbital foramen. Res J Pharm Technol. 2016; 9(7): 880, doi: 10.5958/0974-360x.2016.00167.0.
34. Price JC, Loury M, Carson B, et al. The pericranial flap for reconstruction of anterior skull base defects. Laryngoscope. 1988; 98(11): 1159–1164, doi: 10.1288/00005537-198811000-00002, indexed in Pubmed: 3185068.
35. Santo Neto H, Penteado CV, de Carvalho VC. Presence of a groove in the lateral wall of the human orbit. J Anat. 1984; 138(Pt 4): 631–633.
36. Shimada K, Kaneko Y, Sato I, et al. Classification of the ophthalmic artery that arises from the middle meningeal artery in Japanese adults. Okajimas Folia Anat Jpn. 1995; 72(2-3): 163–176, doi: 10.2535/ofaj1936.72.2-3_163, indexed in Pubmed: 8559558.
37. Silva J, Araya C, Lagos E, et al. Foramen meningo orbitario. Int J Morphol. 2017; 35(2): 515–519, doi: 10.4067/s0717-95022017000200021.
38. Simão-Parreira B, Cunha-Cabral D, Alves H, et al. Morphology and navigational landmarks of the cranio-orbital foramen in a Portuguese population. Ophthalmic Plast Reconstr Surg. 2019; 35(2): 141–147, doi: 10.1097/IOP.0000000000001188, indexed in Pubmed: 30124605.
39. Stiernberg CM, Bailey BJ, Weiner RL, et al. Reconstruction of the anterior skull base following craniofacial resection. Arch Otolaryngol Head Neck Surg. 1987; 113(7): 710–712, doi: 10.1001/archotol.1987.01860070024009, indexed in Pubmed: 3580150.
40. Tomaszewska A, Zelaźniewicz A. Morphology and morphometry of the meningo-orbital foramen as a result of plastic responses to the ambient temperature and its clinical relevance. J Craniofac Surg. 2014; 25(3): 1033–1037, doi: 10.1097/SCS.0000000000000552, indexed in Pubmed: 24699100.

VIA MEDICA

REVIEW ARTICLE

Folia Morphol.
Vol. 82, No. 4, pp. 766–776
DOI: 10.5603/FM.a2022.0081

ISSN 0015–5659
eISSN 1644–3284
journals.viamedica.pl

Anatomical variations in the first dorsal compartment of the wrist: meta-analysis

M. Bonczar, J. Walocha, A. Pasternak, P. Depukat, M. Dziedzic, P. Ostrowski, T. Bonczar, Ł. Warchoł, M. Koziej

Department of Anatomy, Jagiellonian University Medical College, Krakow, Poland

[Received: 31 June 2022; Accepted: 9 September 2022; Early publication date: 27 September 2022]

Background: *The first dorsal compartment of the wrist includes tendons of abductor pollicis longus (APL) and extensor pollicis brevis (EPB). However, many studies have showed multiple anatomical variations including anomalies in the number of both APL and EPB tendons and presence of intercompartmental fibro-osseous septum. Unfortunately, studies describing those variations are not consistent, hence, the aim of this study was to provide most accurate data about these anatomical variations in the population, using systematic review and meta-analysis.*

Materials and methods: *For this purpose, PubMed, Scopus, Web of Science, Embase and a number of minor online libraries were searched. Articles which included exact data about the number of APL or EPB tendons or a presence of intercompartmental septum were qualified for a more precise evaluation. Therefore, out of 1629 studies initially evaluated, 68 were finally included in this meta-analysis. We followed the Preferred Reporting Items for Systematic Reviews and Meta-Analyses (PRISMA) guidelines.*

Results: *A total of 5229 studied wrists have been included in this study. Double APL and single EPB are the most common variations of tendons in the first dorsal compartment, both in cadavers and patients with de Quervain's disease, with no statistically significant differences between those two groups. Presence of intercompartmental fibro-osseus septum is much more common in patients with de Quervain's disease than in cadavers.*

Conclusions: *Our results should improve the awareness of anatomical variations in the first dorsal compartment, which in turn should have impact on treatment of de Quervain's disease in clinical practice.* (Folia Morphol 2023; 82, 4: 766–776)

Key words: de Quervain's disease, abductor pollicis longus, extensor pollicis brevis

INTRODUCTION

The first dorsal compartment of the wrist, also known as first extensor compartment of the wrist, includes tendons of abductor pollicis longus (APL) and of extensor pollicis brevis (EPB). APL tendon inserts into the radial side of the base of the first metacarpal bone but also into the trapezium bone, allowing abduction and extension in the carpometacarpal joint of the thumb. EPB tendon inserts into the base of the first phalanx of the thumb, allowing extension in the metacarpophalangeal join of the thumb. However, many studies have showed multiple anatomical variations in

Address for correspondence: Dr. M. Koziej, Department of Anatomy, Jagiellonian University Medical College, ul. Mikołaja Kopernika 12, 33–332 Kraków, Poland, tel: +48 888 202 628, e-mail: mateusz.koziej@gmail.com

the first dorsal compartment. Most frequently reported anomalies are multiple APL tendons, multiple EPB tendons and the presence of the intercompartmental fibro-osseus septum [3, 8, 25, 41, 48]. Unfortunately, studies describing those variations are not consistent. Awareness of anatomical anomalies in the first dorsal compartment is highly significant during both conservative and surgical treatment of de Quervain's disease. Usually, first method used in clinical treatment of de Quervain's disease are corticosteroid injections into the first dorsal compartment of the wrist [49]. Knowledge of anatomical conditions in the first dorsal compartment may increase chances of successful steroid treatment [49]. During surgical treatment of de Quervain's disease, anatomical orientation may prevent potential misinterpretations, which may lead to failure to decompress the compartment [16]. Therefore, the aim of this study was to provide most accurate data about these anatomical variations in the population, using systematic review and meta-analysis.

MATERIALS AND METHODS

Search strategy

Data collection was performed in January 2022 using either leading databases such as PubMed, Scopus, Web of Science and Embase but also number of minor online libraries. Search was made for publications referring to anatomical variations in the first dorsal compartment of the wrist, especially number of APL tendons, number of EPB tendons and presence of intercompartmental fibro-osseous septum. Search was ended in February 2022. Searched phrases were made according to Boolean search terms. In each database we used the following scheme: (first) AND ((dorsal) OR (extensor)) AND ((compartment) OR (slot)) AND ((anatomy) or (anatomic) or (anatomical) OR (variations) OR (variant) OR (anomalies)). We also used terms like "de Quervain's", "Quervain", "APL", "abductor pollicis longus", "EPB", "extensor pollicis brevis", "septum", "extensor retinaculum" in many variations. Neither date, language, article type or text availability conditions were applied. During our study we followed the Preferred Reporting Items for Systematic Reviews and Meta-Analyses (PRISMA) guidelines. Furthermore, the Critical Appraisal Tool for Anatomical Meta-analysis (CATAM) was used to provide the highest quality findings [13].

Eligibility criteria

A total of 1629 articles were initially evaluated including the main search and search through the references of the classified articles. After removing duplicates, 1248 publications were enrolled. Each article which included exact data about number of APL tendons or number of EPB tendons or a presence of intercompartmental septum was qualified for a more precise evaluation. Studies showing incomplete data, conference abstracts, letter to the editors or case reports were excluded. Subsequently, 101 articles were extracted, of which 33 were excluded due to its irrelevance or incomplete data. Finally, 68 articles were included in this meta-analysis. To minimise bias of included studies, we used the AQUA Tool which was specifically designed for anatomical meta-analyses. Process of collecting data is imaged in Figure 1.

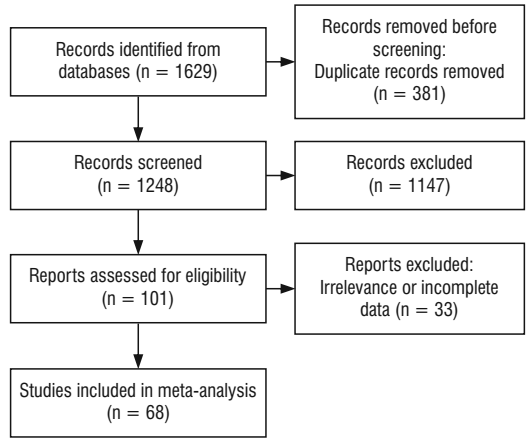

Figure 1. Flow diagram presenting process of collecting data included in this meta-analysis.

Data extraction

Data from qualified studies were extracted manually by two independent researchers. Numerical and categorical data including number of APL tendons, number of EPB tendons, presence of septum, number of individuals, number of wrists, sex of subjects and geographic location were extracted.

Statistical analysis

In order to perform those meta-analysis we used STATISTICA version 13.1 software (StatSoft Inc., Tulsa, OK, USA) and MetaXL version 5.3 (EpiGear International Pty Ltd, Wilston, Queensland, Australia) to calculate the pooled prevalence. We performed a random-effects model in all analyses. Heterogeneity among the studies was assessed, using both the Chi-squared test and I-squared statistic [23]. A p value less than 0.05 was considered to be statistically

significant. We interpretate the I-squared statistic as follows: 0–40% as "might not bed important"; 30–60% as "may represent moderate heterogeneity; 50–90% as "may represent substantial heterogeneity"; 75–100% as "may represent considerable heterogeneity". In order to determine statistically significant differences between studied groups, we used confidence intervals (CIs). If the CIs between groups overlapped, we considered the differences insignificant, while in the reverse situation, we considered the differences statistically significant.

RESULTS

Due to diversity of studied groups we decided to divide the extracted data into three categories — cadavers, patients with the de Quervain's disease and patients without the de Quervain's disease. Each category includes meta-analysis of data considering quantity of APL tendons, EPB tendons and presence of septum in the first dorsal compartment. Sets of characteristics from each study that has been included in this meta-analysis are presented in Table 1. Summarised geographic features of admitted articles can be found in Table 2.

Table 1. Characteristic of included studies

Author, year	Continent	Country	Affiliation*	Number of studied wrists
Roy et al., 2016	Asia	India	1	86
Gao et al., 2017	Asia	China	1	40
Aktan et al., 1998	Asia	Turkey	1, 2	69
Hazani et al., 2008	North America	USA	1	32
Sugiura et al., 2017	Asia	Japan	1	45
Nam et al., 2018	Asia	South Korea	1	40
Xu et al., 2018	Asia	China	1	2
Jackson et al., 1986	North America	USA	1, 2	340
Shiraishi and Matsumura, 2005	Asia	Japan	1	60
Takahashi et al., 1994	Asia	Japan	1, 2	267
Kutsumi et al., 2005	North America	USA	1	15
Bernstein et al., 2019	North America	Texas	1, 2	181
Mahakkanukrauh and Mahakkanukrauh, 2000	Asia	Thailand	1	200
Gurses et al., 2015	Asia	Turkey	1	50
Alemohammad et al., 2009	Asia	Iran	1, 2	233
Kang et al., 2017	Asia	South Korea	1	30
Nayak et al., 2009	Asia	India	1	156
Kulthanan and Chareonwat, 2007	Asia	Thailand	1, 2	148
Ravi et al., 2019	Asia	India	1	77
Mirzanli et al., 2012	Asia	Turkey	1	150
Rousset et al., 2010	Europe	Paris	1	40
Opreanu et al., 2010	North America	USA	1	50
Tripathy et al., 2015	Asia	India	1	50
Motoura et al., 2010	Asia	Japan	1	246
Minamikawa et al., 1991	North America	USA	1, 2	141
Sugiura et al., 2019	Asia	Japan	1	24
Leslie et al., 1990	North America	USA	1	100
Gonzalez et al., 1995	North America	USA	1	66
Leversedge et al., 2016	North America	USA	1	50
Kutsikovich and Merrell, 2018	North America	USA	1	43
Öztürk et al., 2021	Asia	Turkey	1	86
Güleç et al., 2016	Asia	Turkey	1	48

→

Table 1. cont. Characteristic of included studies

Author, year	Continent	Country	Affiliation*	Number of studied wrists
Suhani et al., 2012	Asia	India	1	73
Abdel-Hamid et al., 2013	Africa	Egypt	1	95
Leao, 1958	South America	Brazil	1	50
dos Remédios et al., 2005	Europe	France	1	31
Bharambe et al., 2017	Asia	India	1	100
Vollala, 2006	Asia	India	1	100
Giles, 1960	Europe	England	1	50
Oudenaarde, 1991	Europe	Netherlands	1	84
Schulz et al., 2002	Europe	Germany	1	73
Palatty et al., 2020	Asia	India	1	50
El-Beshbishy and Abdel-Hamid, 2013	Asia	Saudi Arabia	1	50
Brunelli and Brunelli, 1992	Europe	Italy	1	52
Kulshreshtha et al., 2007	Europe	England	1	44
Matzon et al., 2019	North America	USA	2	130
Choi et al., 2011	Asia	South Korea	2	15
Gousheh et al., 2009	Asia	Iran	2	50
Beutel et al., 2020	North America	USA	2, 3	102
Bahm et al., 1995	Europe	France	2	10
Lee et al., 2014	Asia	South Korea	2	60
Chang et al., 2017	North America	USA	2	94
Stahl et al., 2015	Europe	Germany	2	77
Kwon et al., 2010	Asia	South Korea	2	43
Sato et al., 2016	Asia	Japan	2	112
McDermott et al., 2012	North America	USA	2	42
Bing et al., 2018	Asia	South Korea	2	28
Kim et al., 2020	Asia	South Korea	2	29
López Mendoza et al., 2011	North America	Mexico	2	32
Shiroishi et al., 2002	Asia	Japan	2	158
Harvey et al., 1990	Australia	Australia	2	20
Yuasa and Kiyoshige, 1998	Asia	Japan	2	22
de Keating-Hart et al., 2016	Europe	France	2	41
Alexander et al., 2002	North America	USA	2	26
Witt et al., 1991	North America	USA	2	30
Weiss et al., 1994	North America	USA	2	45
Nagaoka et al., 2000	Asia	Japan	2	32
Hoch et al., 2004	Europe	Germany	3	14

*Affiliation of data to subcategory; 1 — cadaveric group; 2 — patients with de Quervain's disease group; 3 — patients without de Quervain's disease

APL

The quantity of APL tendons in the first dorsal compartment of the wrist was examined in 21 cadaveric studies [3, 8, 14, 16, 17, 22, 25, 26, 30, 32, 47, 51–53, 57, 59, 60, 65–68] including 1749 wrists. Number of APL tendons varied from zero to seven. For a single APL tendon, prevalence was 16.91% (95% CI: 8.96–26.63%). For a double APL tendon, prevalence was 46.04% (95% CI: 36.84–55.38%). For a triple APL tendon, prevalence was 19.19% (95% CI: 13.24–25.92%). Results mentioned above, are all gathered in Table 3.

Table 2. Summarized geographic featured of admitted articles

Continent	Number or studies	Number of wrists
Africa	1	95
Asia	36	3029
Australia	1	20
Europe	11	516
North America	18	1519
South America	1	50
Overall	68	5229

The quantity of APL tendons in the first dorsal compartment of the wrist in patients with de Quervain's disease was examined in 9 studies [3, 5, 12, 25, 30, 39, 41, 61, 66] including 608 wrists. Number of APL tendons varied from 1 to 6. For a single APL tendon, prevalence was 23.79% (95% CI: 15.12–33.68%). For a double APL tendon, prevalence was 45.33% (95% CI: 38.88–51.86%). For a triple APL tendon, prevalence was 22.69% (95% CI: 17.29–28.58%). Results mentioned above, are all gathered in Table 3.

Table 3. Statistical result of meta-analysis in each category

Category	Structure	Subcategory	Number of wrists	Prevalence	LCI	HCI	Cochran's Q	I^2 (95% CI)
Cadavers	APL	None APL	1749	0.27%	0.07%	0.58%	4.84	0.00 (0.00–0.00)
		Single APL	1749	16.91%	8.96%	26.63%	471.02	95.75 (94.53–96.70)
		Double APL	1749	46.04%	36.84%	55.38%	297.65	93.28 (91.01–94.98)
		Triple APL	1749	19.19%	13.24%	25.92%	219.99	90.91 (87.49–93.39)
		Quadruple APL	1749	5.91%	3.26%	9.24%	131.98	84.85 (78.07–89.53)
		Fivefold APL	1749	1.53%	0.61%	2.81%	62.56	68.03 (49.74–79.66)
		Sixfold APL	1749	0.65%	0.28%	1.16%	24.17	17.25 (0.00–51.02)
		Sevenfold APL	1749	0.33%	0.11%	0.66%	17.12	0.00 (0.00–38.13)
	EPB	None EPB	1814	1.18%	0.63%	1.89%	28.99	27.55 (0.00–57.00)
		Single EPB	1814	94.89%	92.54%	96.82%	81.45	74.22 (60.85–83.02)
		Double EPB	1814	3.47%	1.85%	5.55%	86.94	75.85 (63.59–83.98)
		Triple EPB	1814	0.49%	0.21%	0.87%	19.22	0.00 (0.00–41.21)
		Quadruple EPB	1814	0.27%	0.07%	0.57%	5.28	0.00 (0.00–0.00)
	Septum	Absent septum	2635	54.26%	47.25%	61.18%	383.58	91.92 (89.64–93.69)
		Single septum	2635	45.74%	38.82%	52.75%	383.58	91.92 (89.64–93.69)
Patients with de Quervain's disease	APL	Single APL	608	23.79%	15.12%	33.68%	54.01	85.19 (73.70–91.66)
		Double APL	608	45.33%	38.88%	51.86%	19.12	58.16 (12.40–80.02)
		Triple APL	608	22.69%	17.29%	28.58%	20.37	60.72 (18.49–81.07)
		Quadruple APL	608	5.37%	2.50%	9.16%	23.63	66.13 (31.32–83.31)
		Fivefold ALP	608	1.04%	0.35%	2.06%	8.27	3.24 (0.00–65.94)
		Sixfold APL	608	0.38%	0.02%	1.07%	2.53	0.00 (0.00–0.00)
	EPB	None EPB	608	2.38%	0.98%	4.33%	13.12	39.00 (0.00–71.93)
		Single EPB	608	92.04%	89.63%	94.16%	8.59	6.87 (0.00–67.22)
		Double EPB	608	4.65%	1.90%	8.44%	25.88	69.09 (38.21–84.54)
		Triple EPB	608	0.75%	0.19%	1.63%	3.01	0.00 (0.00–6.58)
	Septum	Absent septum	1592	36.37%	30.98%	41.94%	142.47	80.35 (72.47–85.97)
		Single septum	1592	63.30%	57.66%	68.76%	145.767	80.79 (73.15–86.26)
		Double septum	1592	0.69%	0.34%	1.17%	28.30	1.06 (0.00–41.95)
Patients without de Quervain's disease	APL	Single APL	14	90.26%	71.79%	100.00%	0.00	0.00 (0.00–0.00)
		Double APL	14	9.74%	0.00%	28.21%	0.00	0.00 (0.00–0.00)
	EPB	None EPB	56	3.58%	0.06%	10.47%	0.00	0.00 (0.00–0.00)
		Single EPB	56	96.42%	89.53%	99.94%	0.00	0.00 (0.00–0.00)
	Septum	Absent septum	164	69.89%	19.49%	100.00%	62.16	96.78 (93.42–98.43)
		Single septum	164	30.11%	0.00%	80.51%	62.16	96.78 (93.42–98.43)

→

Table 3. cont. Statistical result of meta-analysis in each category

Category	Structure	Subcategory	Number of wrists	Prevalence	LCI	HCI	Cochran's Q	I^2 (95% CI)
Overall results	APL	None APL	2371	0.29%	0.11%	0.55%	7.18	0.00 (0.00–0.00)
		Single APL	2371	22.26%	15.34%	30.04%	564.23	94.51 (93.15–95.59)
		Double APL	2371	43.45%	36.77%	50.26%	332.66	90.68 (87.93–92.81)
		Triple APL	2371	19.27%	14.73%	24.26%	258.75	88.02 (84.17–90.93)
		Quadruple APL	2371	5.67%	3.67%	8.06%	154.82	79.98 (72.37–85.49)
		Fivefold APL	2371	1.43%	0.75%	2.32%	70.64	56.12 (37.79–70.46)
		Sixfold APL	2371	0.56%	0.29%	0.90%	27.17	0.00 (0.00–31.20)
		Sevenfold APL	2371	0.34%	0.14%	0.63%	18.54	0.00 (0.00–0.00)
	EPB	None EPB	2478	1.57%	0.99%	2.28%	48.83	34.47 (0.00–57.20)
		Single EPB	2478	94.11%	92.28%	95.70%	95.46	66.48 (51.75–76.71)
		Double EPB	2478	3.78%	2.39%	5.46%	117.25	72.71 (61.46–80.67)
		Triple EPB	2478	0.57%	0.31%	0.91%	23.07	0.00 (0.00–15.69)
		Quadruple EPB	2478	0.29%	0.11%	0.55%	6.50	0.00 (0.00–0.00)
	Septum	Absent septum	4391	47.38%	42.24%	52.55%	751.84	91.35 (89.70–92.74)
		Single septum	4391	52.62%	47.45%	57.76%	751.84	91.35 (89.70–92.74)

APL — abductor pollicis longus; CI — confidence interval; EPB — extensor pollicis brevis; HCI — higher confidence interval; LCI — lower confidence interval; septum — intercompartmental fibro-osseus septum in the first dorsal compartment of the wrist

Overall, the number of APL tendons in the first dorsal compartment of the wrist was analysed in 2371 wrists. The number of APL tendons ranged from 0 to 7. The variation that occurs the most frequently was found to be a double APL tendon with a prevalence of 43.45% (95% CI: 36.77–50.26%). All the results mentioned above and the more detailed ones are gathered in Table 3.

EPB

The quantity of EPB tendons in the first dorsal compartment of the wrist was examined in 22 cadaveric studies [1, 3, 8, 10, 16, 17, 22, 25, 26, 29, 30, 47, 48, 52–54, 56, 57, 60, 63, 66, 71] including 1814 wrists. Number of EPB tendons varied from 0 to 4. For a single EPB tendon, prevalence was 94.89% (95% CI: 92.54–96.82%). Results mentioned above, are all gathered in Table 3.

The quantity of EPB tendons in the first dorsal compartment of the wrist in patients with de Quervain's disease was examined in 9 studies [3, 5, 12, 25, 30, 39, 41, 61, 66] including 608 wrists. Number of EPB tendons varied from 0 to 3. For a single EPB tendon, prevalence was 92.04% (95% CI: 89.63–94.16%). Results mentioned above, are all gathered in Table 3.

Overall, the number of EPB tendons in the first dorsal compartment of the wrist was analysed in 2478 wrists. The number of EPB tendons ranged from 0 to 4. The variation that occurs the most frequently was found to be a single EPB tendon with a prevalence of 94.11% (95% CI: 92.28–95.70%). All the results mentioned above and the more detailed ones are gathered in Table 3.

Septum

The presence of intercompartmental fibro-osseous septum in the first dorsal compartment of the wrist was examined in 32 cadaveric studies [2, 3, 6, 10, 15, 17, 19, 20, 22, 25, 26, 30–32, 34, 37, 38, 40, 43–45, 47, 48, 50, 54–57, 63, 64, 66, 71] including 2635 wrists. The septum was either present or not (there were no reports of double septum in this group, unlike in the patients with de Quervain's disease group). For absence of septum, prevalence was 54.26% (95% CI: 47.25–61.18%). For presence of septum, prevalence was 45.74% (95% CI: 38.82–52.75%). Results mentioned above, are all gathered in Table 3.

The presence of intercompartmental fibro-osseous septum in the first dorsal compartment of the wrist in patients with de Quervain's disease was examined in 29 studies [2–7, 9, 11, 12, 18, 21, 25, 27, 28, 30, 33, 35, 39, 41–43, 46, 58, 61, 62, 66, 69, 70, 72] including 1592 wrists. The septum was either absent, single our double. For absence of septum, prevalence was 36.37% (95% CI: 30.98–41.94%). For a single septum, prevalence was 63.30% (95% CI: 57.66–68.76%).

Table 4. P-values obtained after comparing cadavers and patients with de Quervain's disease groups

Compared variant	P
Single APL	0.3912
Double APL	0.9131
Triple APL	0.4754
Quadruple APL	0.8463
Fivefold APL	0.5955
Sixfold APL	0.5034
None EPB	0.2058
Single EPB	0.1016
Double EPB	0.6000
Triple EPB	0.6051
Absent septum	0.0002
Present septum	0.0007

APL — abductor pollicis longus; EPB — extensor pollicis brevis; septum — intercompartmental fibro-osseus septum in the first dorsal compartment of the wrist

For a double septum, prevalence was 0.69% (95% CI: 0.34–1.17%). Results mentioned above, are all gathered in Table 3.

The presence of intercompartmental fibro-osseous septum in the first dorsal compartment of the wrist in patients without de Quervain's disease was examined in 3 studies [7, 11, 24] including 164 wrists. The septum was either present or not (there were no reports of double septum in this group, unlike in the patients with de Quervain's disease group). For absence of septum, prevalence was 69.89% (95% CI: 19.49–100.00%). For presence of septum, prevalence was 30.11% (95% CI: 0.00–80.51%). Results mentioned above, are all gathered in Table 3.

Overall, the presence of the intercompartmental septum in the first dorsal compartment of the wrist was analysed in 4391 wrists. The septum occurred in 52.62% (95% CI: 47.45–57.76%). All the results mentioned above and the more detailed ones are gathered in Table 3.

Comparison between cadavers and patients with de Quervain's disease

Data regarding cadavers and patients with de Quervain's disease groups were compared and there are no statistically significant differences between cadavers and patients with de Quervain's disease when it comes to anatomical variations of APL and EPB tendons in the first dorsal compartment ($p > 0.05$). Moreover, there is statistically significant difference between cadavers and patients with de Quervain's disease when it comes to presence of septum in the first dorsal compartment ($p < 0.05$). Those p-values are gathered in Table 4.

DISCUSSION

Content of the first dorsal compartment of the wrist shows great anatomical variability. Many studies have described those anomalies, but overall results are inconsistent and some conclusions excludes one another. In clinical practice, anatomy of the first dorsal compartment is essential during treatment of de Quervain's disease, while its effectiveness may rely on awareness of the contents of patients compartment. Our goal was to provide surgeon's with the most comprehensive meta-analysis of anatomical variations of the first compartment of the wrist, regarding a total of 5229 studied hands. Our results differ from another systematic-review [36] showing, among others, higher prevalence of double APL variant, lower prevalence of single APL variant, higher prevalence of septum in both cadaveric and de Quervain's groups etc.

Our results differ from previous major studies regarding prevalence of all APL variations [3, 8, 25, 36, 41, 66]. Our results shows that mostly occurs the double-tendon APL variety with its 43.45% prevalence overall, 46.04% prevalence in cadavers and 45.33% prevalence in patients with de Quervain's disease. Comparing those and rest of the results in both groups, it may be accompted that there are no statistically significant differences between cadavers and patients with de Quervain's disease when it comes to anatomical variations of APL tendons in the first dorsal compartment ($p > 0.05$). Taking into consideration that data showing prevalence of the double APL tendon in cadavers may represent considerable heterogeneity ($I^2 = 93.28$; 95% CI: 91.01–94.98) and the fact that the lower CI value of prevalence of double APL is higher than any higher CI value of any other APL variety, we may acknowledge double APL as a most common variant in the population. In contrast of APL, EPB dominates with its single-tendon variety, both in cadavers and in patients with de Quervain's disease. Our results differ from previous major studies regarding prevalence of all EPB variations [3, 8, 25, 36, 41, 48, 66]. Comparing other varieties of EPB in both groups, it can also be accompted, that there are no statistically significant differences between cadavers and patients with de Quervain's disease, when it comes to anatomical variations of EPB in the first dorsal compartment ($p > 0.05$). Single EPB

tendon may be acknowledged as standard in the population because data showing its prevalence may represent substantial heterogeneity ($I^2 = 74.22$; 95% CI: 60.85–83.02) and its prevalence lower CI value is much higher than any other prevalence higher CI value in any other EPB variety in cadaveric studies. In case of the septum, there are statically significant differences between cadaveric and de Quervain's disease groups ($p < 0.05$). The presence of the septum is much more common in the de Quervain's disease group than in the cadaveric group, with its prevalence for a single septum being 63.30% and 45.74%, respectively. We decided not to compare the patients without de Quervain's disease with other groups due to small amount of studies and lack of data about first dorsal compartment in the no de Quervain's disease group. Results mentioned above may suggest that presence of the septum in the first dorsal compartment of the wrist may be one of the factors causing de Quervain's disease. Also it may be that presence of the septum originates this ailment more likely than multiple variations of APL or EPB tendon slips in the compartment. Those suggests can be considered in the further studies.

Clinical treatment of de Quervain's disease usually starts with a non-surgical approach. Most frequently the first used therapy technique is corticosteroids injection into the first dorsal compartment sheath. Unfortunately, patients experience treatment success after 1 injection only in 51.8% of cases, according to Oh et al. [49]. Anatomical knowledge and awareness of most common variations in the first dorsal compartment may increase chances of successful steroid treatment. We hope that by taking in consideration our results, surgeons will more often perform steroid treatment under the ultrasonography control so the awareness of patients anatomical variation may not be oversight. Especially important factors that may affect results of this treatment are number of APL tendons due to its great diversity in the population and presence of septum, because it creates either fully or partly closed two sub-compartments and injecting steroids into both sub-compartments results with increased chances for successful therapy [27, 42, 73]. During surgical release of the first dorsal compartment, comprehensive anatomical knowledge may prevent potential overlook of the supernumerary tendons, lying in the separate sub-compartment [66]. This knowledge is essential for surgeons while treating de Quervain's disease, as it may prevent inadequate recognition and in effect, failure to decompress the whole first dorsal compartment [36, 48]. Awareness of anatomical variations in the first dorsal compartment should also be helpful for radiologists who treat and examine wrists. Our results shows that arrangement of 3 tendons (double APL and single EPB) in the first dorsal compartment should be expected most often. This may help to accurately interpretate and describe imaging tests, which may be the base of further diagnostics. Additionally, obtaining an image of intercompartmental septum in the first dorsal compartment, should rise awareness, that this may be the factor causing de Quervain's disease in the future.

Taking in consideration geographical differences, especially in quantity of carried out research, authors are aware that results included in this meta-analysis might be burdened with a potential bias. Asia dominates with a number of studied wrists, while on the other side, researches realised in Africa, Australia or South America are singular. This may cause our results to reflect more of Asian than global population.

CONCLUSIONS

In conclusion, we believe that it is the most comprehensive analysis of the contents of the first dorsal compartment of the wrist. Double APL and single EPB are the most common variations of tendons in the first dorsal compartment overall and both in cadavers and patients with de Quervain's disease, with no statistically significant differences between those two groups. Presence of intercompartmental fibro-osseus septum is much more common in patients with de Quervain's disease than in cadavers, which may be one of the factors evoking de Quervain's disease. Our results should improve the awareness of anatomical variations in the first dorsal compartment, which in turn should have impact on treatment of de Quervain's disease in clinical practice.

Conflict of interest: None declared

REFERENCES

1. Abdel-Hamid GA, El-Beshbishy RA, Abdel Aal IH. Anatomical variations of the hand extensors. Folia Morphol. 2013; 72(3): 249–257, doi: 10.5603/fm.2013.0040, indexed in Pubmed: 24068687.
2. Aktan ZA, Oztürk L, Calli IH. An anatomical study of the first extensor compartment of the wrist. Kaibogaku Zasshi. 1998; 73(1): 49–54, indexed in Pubmed: 9538622.
3. Alemohammad AM, Yazaki N, Morris RP, et al. Thumb interphalangeal joint extension by the extensor pollicis

brevis: association with a subcompartment and de Quervain's disease. J Hand Surg Am. 2009; 34(4): 719–723, doi: 10.1016/j.jhsa.2008.12.015, indexed in Pubmed: 19345877.
4. Alexander RD, Catalano LW, Barron OA, et al. The extensor pollicis brevis entrapment test in the treatment of de Quervain's disease. J Hand Surg Am. 2002; 27(5): 813–816, doi: 10.1053/jhsu.2002.35309, indexed in Pubmed: 12239669.
5. Bahm J, Szabo Z, Foucher G. The anatomy of de Quervain's disease. A study of operative findings. Int Orthop. 1995; 19(4): 209–211, doi: 10.1007/BF00185223, indexed in Pubmed: 8557414.
6. Bernstein DT, Gonzalez MA, Hendrick RG, et al. Impact of septated first dorsal compartments on symptomatic de Quervain disease. Plast Reconstr Surg. 2019; 144(2): 389–393, doi: 10.1097/PRS.0000000000005827, indexed in Pubmed: 31348348.
7. Beutel BG, Doscher ME, Melone CP. Prevalence of a septated first dorsal compartment among patients with and without de Quervain tenosynovitis: an in vivo anatomical study. Hand (NY). 2020; 15(3): 348–352, doi: 10.1177/1558944718810864, indexed in Pubmed: 30428712.
8. Bharambe V, Patel D, Manvikar PR. A study of extensor pollicis longus and brevis and abductor pollicis longus from the perspective of evolution. J Med Res. 2017; 3(3): 146–150, doi: 10.31254/jmr.2017.3311.
9. Bing JH, Choi SJ, Jung SM, et al. Ultrasound-guided steroid injection for the treatment of de Quervain's disease: an anatomy-based approach. Skeletal Radiol. 2018; 47(11): 1483–1490, doi: 10.1007/s00256-018-2958-9, indexed in Pubmed: 29730702.
10. Brunelli GA, Brunelli GR. Anatomy of the extensor pollicis brevis muscle. J Hand Surg Br. 1992; 17(3): 267–269, doi: 10.1016/0266-7681(92)90112-f, indexed in Pubmed: 1624857.
11. Chang CY, Kheterpal AB, Vicentini JR, et al. Variations of anatomy on MRI of the first extensor compartment of the wrist and association with DeQuervain tenosynovitis. Skeletal Radiol. 2017; 46(8): 1047–1056, doi: 10.1007/s00256-017-2639-0, indexed in Pubmed: 28389821.
12. Choi SJ, Ahn JH, Lee YJ, et al. de Quervain disease: US identification of anatomic variations in the first extensor compartment with an emphasis on subcompartmentalization. Radiology. 2011; 260(2): 480–486, doi: 10.1148/radiol.11102458, indexed in Pubmed: 21613443.
13. D'Antoni AV, Tubbs RS, Patti AC, et al. The critical appraisal tool for anatomical meta-analysis: a framework for critically appraising anatomical meta-analyses. Clin Anat. 2022; 35(3): 323–331, doi: 10.1002/ca.23833, indexed in Pubmed: 35015336.
14. El-Beshbishy RA, Abdel-Hamid GA. Variations of the abductor pollicis longus tendon: an anatomic study. Folia Morphol. 2013; 72(2): 161–166, doi: 10.5603/fm.2013.0027, indexed in Pubmed: 23740505.
15. Gao ZY, Tao H, Xu H, et al. A novel classification of the anatomical variations of the first extensor compartment. Medicine. 2017; 96(35): e7875, doi: 10.1097/MD.0000000000007875, indexed in Pubmed: 28858099.
16. Giles KW. Anatomical variations affecting the surgery of de Quervain's disease. J Bone Joint Surg Br. 1960; 42-B: 352–355, doi: 10.1302/0301-620X.42B2.352, indexed in Pubmed: 13850049.
17. Gonzalez MH, Sohlberg R, Brown A, et al. The first dorsal extensor compartment: an anatomic study. J Hand Surg Am. 1995; 20(4): 657–660, doi: 10.1016/S0363-5023(05)80286-2, indexed in Pubmed: 7594297.
18. Gousheh J, Yavari M, Arasteh E. Division of the first dorsal compartment of the hand into two separated canals: rule or exception? Arch Iran Med. 2009; 12(1): 52–54, indexed in Pubmed: 19111030.
19. Güleç A, Türkmen F, Toker S, et al. Percutaneous release of the first dorsal extensor compartment: a cadaver study. Plast Reconstr Surg Glob Open. 2016; 4(10): e1022, doi: 10.1097/GOX.0000000000001022, indexed in Pubmed: 27826460.
20. Gurses IA, Coskun O, Gayretli O, et al. The anatomy of the fibrous and osseous components of the first extensor compartment of the wrist: a cadaveric study. Surg Radiol Anat. 2015; 37(7): 773–777, doi: 10.1007/s00276-015-1439-2, indexed in Pubmed: 25645546.
21. Harvey FJ, Harvey PM, Horsley MW. De Quervain's disease: surgical or nonsurgical treatment. J Hand Surg Am. 1990; 15(1): 83–87, doi: 10.1016/s0363-5023(09)91110-8, indexed in Pubmed: 2299173.
22. Hazani R, Engineer NJ, Cooney D, et al. Anatomic landmarks for the first dorsal compartment. Eplasty. 2008; 8: e53, indexed in Pubmed: 19092992.
23. Higgins JPT, Thomas J, Chandler J. (eds). Cochrane Handbook for Systematic Reviews of Interventions. Wiley 2019.
24. Hoch J, Fritsch H, Lewejohann S. Kongenitale oder erworbene Anlage des separaten Faches für die Sehne des M. extensor pollicis brevis bei der Tendovaginitis stenosans de Quervain? Makroanatomische und fetal-plastination-shistologische Untersuchungen zum 1. Strecksehnenfach. Ann Anat Anatomischer Anzeiger. 2004; 186(4): 305–310, doi: 10.1016/s0940-9602(04)80045-1.
25. Jackson WT, Viegas SF, Coon TM, et al. Anatomical variations in the first extensor compartment of the wrist. A clinical and anatomical study. J Bone Joint Surg. 1986; 68(6): 923–926, doi: 10.2106/00004623-198668060-00016.
26. Kang JW, Park JW, Lee SH, et al. Ultrasound-guided injection for De Quervain's disease: Accuracy and its influenceable anatomical variances in first extensor compartment of fresh cadaver wrists. J Orthop Sci. 2017; 22(2): 270–274, doi: 10.1016/j.jos.2016.11.013, indexed in Pubmed: 28209340.
27. de Keating-Hart E, Touchais S, Kerjean Y, et al. Presence of an intracompartmental septum detected by ultrasound is associated with the failure of ultrasound-guided steroid injection in de Quervain's syndrome. J Hand Surg Eur Vol. 2016; 41(2): 212–219, doi: 10.1177/1753193415611414, indexed in Pubmed: 26497593.
28. Kim SJ, Lee CH, Khil EK, et al. Can ultrasonography be useful in planning surgery for de quervain tenosynovitis?: a prospective study with emphasis on detection of the superficial radial nerve and dominant pathologic tendon. J Ultrasound Med. 2020; 39(8): 1553–1560, doi: 10.1002/jum.15244, indexed in Pubmed: 32045018.
29. Kulshreshtha R, Patel S, Arya AP, et al. Variations of the extensor pollicis brevis tendon and its insertion: a study of 44 cadaveric hands. J Hand Surg Eur Vol. 2007; 32(5):

550–553, doi: 10.1016/J.JHSE.2007.04.013, indexed in Pubmed: 17950220.
30. Kulthanan T, Chareonwat B. Variations in abductor pollicis longus and extensor pollicis brevis tendons in the Quervain syndrome: a surgical and anatomical study. Scand J Plast Reconstr Surg Hand Surg. 2007; 41(1): 36–38, doi: 10.1080/02844310600869720, indexed in Pubmed: 17484184.
31. Kutsikovich J, Merrell G. Accuracy of injection into the first dorsal compartment: a cadaveric ultrasound study. J Hand Surg Am. 2018; 43(8): 777.e1–777.e5, doi: 10.1016/j.jhsa.2018.01.020, indexed in Pubmed: 29478620.
32. Kutsumi K, Amadio PC, Zhao C, et al. Gliding resistance of the extensor pollicis brevis tendon and abductor pollicis longus tendon within the first dorsal compartment in fixed wrist positions. J Orthop Res. 2005; 23(2): 243–248, doi: 10.1016/j.orthres.2004.06.014, indexed in Pubmed: 15734232.
33. Kwon BC, Choi SJ, Koh SH, et al. Sonographic Identification of the intracompartmental septum in de Quervain's disease. Clin Orthop Relat Res. 2010; 468(8): 2129–2134, doi: 10.1007/s11999-009-1199-6, indexed in Pubmed: 20033358.
34. Leao L. De Quervain's disease; a clinical and anatomical study. J Bone Joint Surg Am. 1958; 40-A(5): 1063–1070, indexed in Pubmed: 13587574.
35. Lee KH, Kang CN, Lee BG, et al. Ultrasonographic evaluation of the first extensor compartment of the wrist in de Quervain's disease. J Orthop Sci. 2014; 19(1): 49–54, doi: 10.1007/s00776-013-0481-3, indexed in Pubmed: 24132793.
36. Lee ZH, Stranix JT, Anzai L, et al. Surgical anatomy of the first extensor compartment: a systematic review and comparison of normal cadavers vs. De Quervain syndrome patients. J Plast Reconstr Aesthet Surg. 2017; 70(1): 127–131, doi: 10.1016/j.bjps.2016.08.020, indexed in Pubmed: 27693273.
37. Leslie BM, Ericson WB, Morehead JR. Incidence of a septum within the first dorsal compartment of the wrist. J Hand Surg Am. 1990; 15(1): 88–91, doi: 10.1016/s0363-5023(09)91111-x, indexed in Pubmed: 2299174.
38. Leversedge F, Cotterell I, Nickel B, et al. Ultrasonography-guided de Quervain Injection. J Am Acad Ortho Surg. 2016; 24(6): 399–404, doi: 10.5435/jaaos-d-15-00753.
39. López Mendoza FJ, Barón Ramos CX, Gargollo Orvañanos A. Repercusión de la variabilidad anatómica del primer compartimento extensor de la mano en la enfermedad de De Quervain. Cirugía Plástica Ibero-Latinoamericana. 2011; 37(3): 289–293, doi: 10.4321/s0376-78922011000300010.
40. Mahakkanukrauh P, Mahakkanukrauh C. Incidence of a septum in the first dorsal compartment and its effects on therapy of de Quervain's disease. Clin Anat. 2000; 13(3): 195–198, doi: 10.1002/(sici)1098-2353(2000)13:3<195::aid-ca6>3.0.co;2-v.
41. Matzon JL, Graham JG, Lutsky KF, et al. A prospective evaluation of the anatomy of the first dorsal compartment in patients requiring surgery for de Quervain's tenosynovitis. J Wrist Surg. 2019; 8(5): 380–383, doi: 10.1055/s-0039-1688700, indexed in Pubmed: 31579546.
42. McDermott JD, Ilyas AM, Nazarian LN, et al. Ultrasound-guided injections for de Quervain's tenosynovitis. Clin Orthop Relat Res. 2012; 470(7): 1925–1931, doi: 10.1007/s11999-012-2369-5, indexed in Pubmed: 22552767.
43. Minamikawa Y, Peimer CA, Cox WL, et al. De Quervain's syndrome: surgical and anatomical studies of the fibroosseous canal. Orthopedics. 1991; 14(5): 545–549, doi: 10.3928/0147-7447-19910501-07, indexed in Pubmed: 2062731.
44. Mirzanli C, Ozturk K, Esenyel CZ, et al. Accuracy of intrasheath injection techniques for de Quervain's disease: a cadaveric study. J Hand Surg Eur Vol. 2012; 37(2): 155–160, doi: 10.1177/1753193411409126, indexed in Pubmed: 21593074.
45. Motoura H, Shiozaki K, Kawasaki K. Anatomical variations in the tendon sheath of the first compartment. Anat Sci Int. 2010; 85(3): 145–151, doi: 10.1007/s12565-009-0070-x, indexed in Pubmed: 20039153.
46. Nagaoka M, Matsuzaki H, Suzuki T. Ultrasonographic examination of de Quervain's disease. J Orthop Sci. 2000; 5(2): 96–99, doi: 10.1007/s007760050134, indexed in Pubmed: 10982641.
47. Nam YS, Doh G, Hong KiY, et al. Anatomical study of the first dorsal extensor compartment for the treatment of de Quervain's disease. Ann Anat. 2018; 218: 250–255, doi: 10.1016/j.aanat.2018.04.007, indexed in Pubmed: 29746921.
48. Nayak SR, Hussein M, Krishnamurthy A, et al. Variation and clinical significance of extensor pollicis brevis: a study in South Indian cadavers. Chang Gung Med J. 2009; 32(6): 600–604, indexed in Pubmed: 20035638.
49. Oh JK, Messing S, Hyrien O, et al. Effectiveness of corticosteroid injections for treatment of de quervain's tenosynovitis. Hand. 2017; 12(4): 357–361, doi: 10.1177/1558944716681976, indexed in Pubmed: 28644946.
50. Opreanu RC, Wechter J, Tabbaa H, et al. Anatomic variations of the first extensor compartment and abductor pollicis longus tendon in trapeziometacarpal arthritis. Hand. 2010; 5(2): 184–189, doi: 10.1007/s11552-009-9234-3, indexed in Pubmed: 19834771.
51. Oudenaarde van E. Structure and function of the abductor pollicis longus muscle. J Anat. 1991; 174: 221–227, indexed in Pubmed: 2032936.
52. Öztürk K, Dursun A, Kastamoni Y, et al. Anatomical variations of the extensor tendons of the fetal thumb. Surg Radiol Anat. 2021; 43(5): 755–762, doi: 10.1007/s00276-020-02611-7, indexed in Pubmed: 33170332.
53. Palatty B, Veeramani R, Manjunath KY. Variations in extensor tendons of the thumb: a cadaveric study. Indian J Clin Anat Physiol. 2020; 5(3): 383–388, doi: 10.18231/2394-2126.2018.0089.
54. Ravi PK, Tewari J, Mishra PR, et al. Variations of extensor pollicis brevis tendon in Indian population: a cadaveric study and review of literature. J Clin Orthop Trauma. 2019; 10(2): 278–281, doi: 10.1016/j.jcot.2018.02.008, indexed in Pubmed: 30828193.
55. dos Remédios C, Chapnikoff D, Wavreille G, et al. The abductor pollicis longus: relation between innervation, muscle bellies and number of tendinous slips. Surg Radiol Anat. 2005; 27(3): 243–248, doi: 10.1007/s00276-004-0286-3, indexed in Pubmed: 15549300.

56. Rousset P, Vuillemin-Bodaghi V, Laredo JD, et al. Anatomic variations in the first extensor compartment of the wrist: accuracy of US. Radiology. 2010; 257(2): 427–433, doi: 10.1148/radiol.10092265, indexed in Pubmed: 20829530.
57. Roy AJ, Roy AN, De C, et al. A cadaveric study of the first dorsal compartment of the wrist and its content tendons: anatomical variations in the Indian population. J Hand Microsurg. 2016; 4(2): 55–59, doi: 10.1007/s12593-012-0073-z, indexed in Pubmed: 24293951.
58. Sato J, Ishii Y, Noguchi H. Ultrasonographic evaluation of the prevalence of an intracompartmental septum in patients with de Quervain's disease. Orthopedics. 2016; 39(2): 112–116, doi: 10.3928/01477447-20160222-05, indexed in Pubmed: 26913767.
59. Schulz CU, Anetzberger H, Pfahler M, et al. The relation between primary osteoarthritis of the trapeziometacarpal joint and supernumerary slips of the abductor pollicis longus tendon. J Hand Surg Br. 2002; 27(3): 238–241, doi: 10.1054/jhsb.2002.0765, indexed in Pubmed: 12074609.
60. Shiraishi N, Matsumura G. Anatomical variations of the extensor pollicis brevis tendon and abductor pollicis longus tendon: relation to tenosynovectomy. Okajimas Folia Anat Jpn. 2005; 82(1): 25–29, doi: 10.2535/ofaj.82.25, indexed in Pubmed: 15934601.
61. Shiroishi T, Yasunaga H, Ohta K, et al. Clinical significance of first dorsal compartment in de quervain's disease. Orthop Traumatol. 2002; 51(3): 570–574, doi: 10.5035/nishiseisai.51.570.
62. Stahl S, Vida D, Meisner C, et al. Work related etiology of de Quervain's tenosynovitis: a case-control study with prospectively collected data. BMC Musculoskelet Disord. 2015; 16: 126, doi: 10.1186/s12891-015-0579-1, indexed in Pubmed: 26018034.
63. Sugiura S, Matsuura Y, Kuniyoshi K, et al. Anatomic study of the first extensor compartment and the relationship between the extensor tendon width and its distal insertion. Surg Radiol Anat. 2017; 39(11): 1223–1226, doi: 10.1007/s00276-017-1867-2, indexed in Pubmed: 28484860.
64. Sugiura S, Matsuura Y, Suzuki T, et al. Histological assessment of a septum in the first dorsal compartment: a fresh cadaver study. J Hand Surg Eur Vol. 2019; 44(8): 805–809, doi: 10.1177/1753193419838204, indexed in Pubmed: 30917737.
65. Suhani S, Narga N, Kumar N, et al. Multiple tendons for abductor pollicis longus in the first dorsal compartment and variation in their insertion pattern: Anatomical and clinical relevance. Res J Pharmaceutical. 2012; 3(4): 755–763.
66. Takahashi Y, Hashizume H, Inoue H, et al. Clinicopathological analysis of de Quervain's disease. Acta Med Okayama. 1994; 48(1): 7–15, doi: 10.18926/AMO/31135, indexed in Pubmed: 8191920.
67. Tripathy SK, Tewari J, Mishra PR. Anatomical variation of abductor pollicis longus in Indian population: a cadaveric study. Indian J Orthop. 2015; 49(5): 549–553, doi: 10.4103/0019-5413.164038, indexed in Pubmed: 26538762.
68. Vollala VR. Abductor Pollicis Longus: A Study of 50 South Indian Cadavers. Fırat Tıp Dergisi. 2006; 12(1): 17–19.
69. Weiss AP, Akelman E, Tabatabai M. Treatment of de Quervain's disease. J Hand Surg Am. 1994; 19(4): 595–598, doi: 10.1016/0363-5023(94)90262-3, indexed in Pubmed: 7963313.
70. Witt J, Pess G, Gelberman RH. Treatment of de Quervain tenosynovitis. A prospective study of the results of injection of steroids and immobilization in a splint. J Bone Joint Surg Am. 1991; 73(2): 219–222, indexed in Pubmed: 1993717.
71. Xu H, Wu JX, Wang Q, et al. Anatomical variations in the first extensor compartment: a cadaver study. ANZ J Surg. 2018; 88(9): 913–916, doi: 10.1111/ans.14808, indexed in Pubmed: 30117658.
72. Yuasa K, Kiyoshige Y. Limited surgical treatment of de Quervain's disease: decompression of only the extensor pollicis brevis subcompartment. J Hand Surg Am. 1998; 23(5): 840–843, doi: 10.1016/S0363-5023(98)80160-3, indexed in Pubmed: 9763259.
73. Zingas C, Failla JM, Van Holsbeeck M. Injection accuracy and clinical relief of de Quervain's tendinitis. J Hand Surg Am. 1998; 23(1): 89–96, doi: 10.1016/S0363-5023(98)80095-6, indexed in Pubmed: 9523961.

VIA MEDICA

REVIEW ARTICLE

Folia Morphol.
Vol. 82, No. 4, pp. 777–783
DOI: 10.5603/FM.a2022.0089

ISSN 0015–5659
eISSN 1644–3284
journals.viamedica.pl

Anatomical variations of the pelvis during abdominal hysterectomy for benign conditions

A. Matsas[1], T. Vavilis[2], D. Chrysikos[3], G. Komninos[4], V. Protogerou[3], T. Troupis[3]

[1]*Laboratory of Experimental Surgery and Surgical Research N.S. Christeas, Medical School, National and Kapodistrian University of Athens, Greece*
[2]*1st Laboratory of Medical Biology and Genetics, School of Medicine, Faculty of Health Sciences, Aristotle University of Thessaloniki, Greece*
[3]*Department of Anatomy, Medical School, National and Kapodistrian University of Athens, Greece*
[4]*Department of General Surgery, Hywel Dda University Health Board, SA31 2AF, Carmarthen, United Kingdom*

[Received: 25 April 2022; Accepted: 19 August 2022; Early publication date: 14 October 2022]

Background: *Anatomical variations are defined as atypical morphologic and positional presentations of anatomical entities. Pelvic anatomical variations encountered during abdominal hysterectomy can be of clinical interest, given that misidentification of certain structures can lead to iatrogenic injuries and postoperative sequelae. The aim of the present study was to detect and highlight the anatomical structures of interest and their variations to the surgeon performing abdominal hysterectomy for benign conditions.*

Materials and methods: *A narrative review of the literature was performed including reports of anatomical variations encountered in cadavers, by surgeons during abdominal hysterectomy and radiologists on computed tomography angiography, searching within a 10-year span on PubMed database. Studies regarding the treatment of malignant conditions requiring lymphadenectomy and different modes of surgical approach were reviewed with regards to the aspects relevant to benign conditions. The search was extended to the reference lists of all retrieved articles.*

Results: *Ureters and the uterine arteries, due to anatomical variations, are the anatomical structures most vulnerable during abdominal hysterectomy. Specifically, the ureters can present multiplications, retroiliac positionings and ureteric diverticula, whereas, the uterine arteries can present notable variability in their origins. Such variations can be detected preoperatively or intraoperatively.*

Conclusions: *Although rare, the presence of anatomical variations of the uterine arteries and ureters can increase the possibility of complications should they escape detection. Intraoperative misidentification could lead to improper dissection or ligation of the affected structures. Knowledge of these variations, coupled with extensive preoperative investigation and intraoperative vigilance can minimise the risk of complications.* (Folia Morphol 2023; 82, 4: 777–783)

Key words: anatomical variations, abdominal hysterectomy, benign gynaecological conditions, ureters, uterine arteries

Address for correspondence: Dr. T. Troupis, Department of Anatomy, Medical School, Faculty of Health and Sciences, National and Kapodistrian University of Athens, Mikras Asias str. 75, 11627 Athens, Greece, e-mail: ttroupis@med.uoa.gr

INTRODUCTION

Hysterectomy is considered to be the most frequent major gynaecological operation, with the open abdominal approach performed in over 50% of the reported cases, despite more recent advances in minimally invasive procedures [57]. Abdominal hysterectomy is performed for the surgical treatment of both benign and malignant gynaecological conditions. Amongst the common indications for abdominal hysterectomy are the benign conditions of large ovarian cysts and uterine fibroids, uterine bleeding, extensive adhesive conditions, myoma uteri, endometriosis, adenomyosis, benign adnexal masses, simple endometrial hyperplasia without atypia and pelvic pain, as well as the malignant conditions of endometrial, cervical and ovarian cancer [36, 48]. A differentiating feature of hysterectomy carried out for the treatment of a benign condition versus a malignant one is the extent to which the procedure is carried out: when treating a malignant condition, radical hysterectomy is usually performed, during which, apart from the uterus, the upper vagina, cervix, fallopian tubes, ovaries, parametrium tissue and pelvic lymph nodes are also removed in most cases [58]. As all surgical procedures, abdominal hysterectomy carries a risk of complications which can occur both intraoperatively and postoperatively. Complications include infections, injuries to anatomical structures and other pathological entities, such as thromboembolisms [44]. Infectious complications are the most common ones, accounting for 10% of all complications in abdominal hysterectomy followed by thromboembolisms which, depending on the sensitivity of the method of diagnosis, range from 1% to 12% [12, 26, 32, 33]. Anatomical complications, especially the most common ones of bladder and ureteric injuries, occur in about 1% to 8% of the cases, with the ureter remaining undetectable at the time of the surgery at a rate of 66% [13, 18, 51, 53]. It is to be expected that the more extensive the operation, the higher the risk of complications arising: for example, abdominal radical hysterectomy which includes pelvic lymphadenectomy, involves anatomical structures of the lymphatic system which can present complications, such as lymphocysts and lymphoceles [7, 10]. The above holds true even for anatomical entities which are of concern in the treatment of both benign and malignant pathologies, as ureteric injuries appear in 5% to 8% of the cases undergoing surgery for malignancies versus a 1% to 3% appearance in surgery for benign conditions [53]. Given the above, when employing abdominal hysterectomy specifically for benign conditions, the possibility of complications is generally expected to be lower.

Complications attributable to sustained injury to anatomical structures can be rendered more frequent in the presence of anatomical variations. In the case of abdominal hysterectomy the variations of interest pertain to the pelvic region including variations of the ureters, blood vessels, lymph vessels and lymph nodes [28]. Due to the less extensive nature of hysterectomy carried out for benign conditions, the surgeon's interest for relevant pelvic anatomical variations is restricted to those which concern the ureters, specifically their most caudal segment, as well as those which concern the uterine arteries. Anatomical variations can be described as non-pathological variations of human anatomy, where the morphology of an anatomical structure differs from the common descriptions in the literature [59]. Variations may include differences in the positioning and branching of blood vessels, alternative innervation of organs, differences in the orientation and attachment of ligaments, as well as morphological deviations of muscles and bones [2]. While such variations usually do not have a negative impact on the function of the organs, they can be clinically relevant, especially in surgery, where failure to acknowledge them could lead to injury to the unexpected surrounding structures and subsequent complications [8].

This narrative review focused on those pelvic anatomical variations that are of clinical significance when performing an abdominal hysterectomy for benign conditions only. A PubMed search was performed for literature published only during the last decade for reports of anatomical variations encountered in cadavers, by surgeons during abdominal hysterectomy and by radiologists on computed tomography angiography. Reports of malignant conditions requiring lymphadenectomy and different modes of surgical approach were reviewed with regards to the aspects relevant to benign conditions, given that such reports implicate additional anatomical structures and their respective variations. The keywords utilised for the search included "anatomical variations", "abdominal hysterectomy", "benign gynaecological conditions", "ureters", "uterine arteries" and relevant combinations. The search was also extended to include relevant material in the reference lists of all the articles retrieved.

Solid knowledge of anatomical variants of the ureters as well as the uterine vessels can reduce intraoperative complications associated with injury, should they be identified during the operation. Furthermore, the suspicion of presence of variations in other organs of common embryonic origin can prompt towards performing an extensive and targeted pre-operative investigation [28].

ANATOMICAL VARIATIONS OF THE URETER AND THEIR CLINICAL SIGNIFICANCE

Ureteric injuries of iatrogenic nature are a complication that might evade the surgeon's attention during the operation and give postoperative symptoms [45]. Ureteric injuries mostly occur in two distinct anatomical locations. The first is on the plane defined by the presence of the infundibulopelvic ligament. The second lies deeper in the pelvic area at the point where the ureter traverses sideways to the uterosacral ligament's peritoneum [28]. Early detection and subsequent treatment is considered of utmost importance if such intraoperative injuries are suspected, hence, knowing the symptoms is advised for any surgeon performing abdominal hysterectomies [39, 45]. Amongst the most common symptoms are pain, fever, abnormalities in urination, such as anuria or oliguria and urinary leakage [16, 25, 39, 56]. Presentation of some of those symptoms, especially pain, can be confounded with expected post-operative discomfort or side-effects, which calls for increased vigilance on the surgeon's part during patient's postoperative assessment [45].

While in half of the cases of ureteric damage no risk factor can be acknowledged, the remaining cases can be attributed to factors contributing to anatomical alterations of the ureter that are conducive to injury. Such conditions include large ovarian masses, previous pelvic surgery that might have deformed the area, endometriosis and the presence of ureteric variations [53].

Three main categories of ureteric variations are of interest to the surgeon performing an abdominal hysterectomy. Those are ureteric diverticula, retroiliac presence of the ureter and multiplications of the ureter.

Ureteric diverticulum is characterised as a rare variation, reported so far in only 50 cases in the international literature [35]. It is defined as a sac-like enlargement of the ureteric wall of unknown etiopathology [35]. Its presence might remain undetected since it can often be asymptomatic, although it has been reported to correlate with urinary tract infections, transient haematuria and pyuria [34]. While it can be an incidental finding during various medical imaging procedures, it can also be diagnosed utilising excretory urography [1, 15, 35, 55]. Ureteric diverticula are classified into three distinct categories according to their ontogenesis, which are true congenital diverticulum, abortive diverticulum and acquired diverticulum [22, 42]. Despite being a rare variation, surgical caution is advised since the presence of the diverticulum may be misidentified as vasculature or as a cyst-like formation and as such be ligated or incised by the surgeon [28].

Retroiliac ureters are another rare congenital variation that, as the term suggests, pertains to the trajectory of the ureters when they are located in a posterior position relative to the iliac arteries [14]. This variation has been reported to be both unilateral and bilateral [50]. Retroiliac ureter symptomatology encompasses pain in the flank area of the body as well as symptoms arising from ureteric obstruction. The diagnosis usually takes place intraoperatively. It should be noted that suspicion concerning the presence of this type of ureteric variation can be raised in the case of diagnosis of other anomalies of the urogenital system. Coexistence of hypoplastic or malrotated kidneys, urometrocolpos, vaginal atresia, urosacral agenesis along with this variation has been reported in the literature [19, 23, 27, 37, 46]. Given the ectopic nature of the retroiliac ureter, care should be taken not to be misidentified as a vascular structure during abdominal hysterectomy.

Finally, ureters may be duplicated or otherwise multiplied along their longitudinal axis, giving rise to two or more parallel anatomical entities. Duplicated ureters are by far the most commonly detected multiplication thought to occur in about 1% of the general population [4, 49]. Their high incidence combined with the fact that they are more common in females, renders the knowledge of their existence significant to the gynaecological surgeon since failure to acknowledge them can lead to their erroneous incision or ligation [6]. Ureteric duplication may be either complete, where the resulting ureters enter the urinary bladder in two distinct openings, or incomplete (bifid) where the ureters fuse before their common orifice in the bladder [21]. Bifid duplications tend to be detected unilaterally and they display

a preference towards the right side [17]. On the other hand, complete duplications display a tendency towards bilaterality [41]. Two kinds of ureteric injury can arise during hysterectomy. One of them pertains to direct injury sustained to the ureter itself, the ureter being mistaken for an artery. The other involves the interruption of the blood supply of the ureters by injury to the associated vessels, since duplicated ureters tend to be encapsulated in a common sheath [17]. Distinction of vasculature and ureters during surgery can take place by observing the structure in question: should ambiguity arise, the surgeon can differentiate between ureters and other structures by the tell-tale peristaltic movement of the former, given that the ureters vermiculate [28].

ANATOMICAL VARIATIONS OF THE UTERINE ARTERY AND THEIR CLINICAL SIGNIFICANCE

The main blood supply of the uterus derives from the uterine arteries. Therefore, the knowledge and identification of the location, origin and course of the uterine arteries are very important during abdominal hysterectomy for benign pathologies, given that high vascular ligation of these arteries is an integral part of the aforementioned operation. Nowadays, arterial embolisation, either as preoperative adjuvant treatment or as an alternative to surgery altogether, has also been increasingly used making the adequate knowledge of the uterine artery anatomy even more important.

The uterine artery is considered by tradition to arise from the anterior division of the internal iliac artery. It then continues medially along the inferior aspect of the broad ligament of the uterus and descends and bifurcates into ascending and descending branches at the level of the isthmus. The ascending branches follow a course along the uterus and anastomose with the ovarian artery, whereas the descending branches anastomose with the vaginal and inferior rectal arteries [5, 40]. The uterine artery follows a course anteriorly to the ureter in the pelvis crossing it laterally at the level of the uterine cervix below the isthmus [24].

However, several studies mainly in the last 10 years have demonstrated a significant spectrum of anatomical variations with regards to the origin of the uterine artery which differs from our traditional knowledge. In 2019, Chaudhuri et al. [11] published a study of a total of 31 Indian female cadavers that showed that the uterine artery originated from the anterior division of the internal iliac artery in all the cadavers without any variations whatsoever. In 2020, Orhan et al. [38] published a study where, after 756 retroperitoneal dissections in 378 female patients during laparoscopic hysterectomy for benign conditions, the uterine artery was the first branch of the anterior internal iliac artery in 80.9% of the cases, The uterine artery was also the second branch of the anterior trunk of the iliac artery in 4.9% of the cases, the first or second branch of the anterior trunk in 3.7% of the cases but in a trifurcation model with the posterior trunk and the other visceral branches, and lastly the first branch of the internal iliac artery but as a single trunk in 3.1% of the cases. However, in 7.4% of the cases the origin of the uterine artery could not be determined [38].

Nonetheless, several other studies, including Liapis et al. [30], have reported that the uterine artery can also originate from the umbilical artery or from the internal iliac artery as a common trunk along with the umbilical artery, the superior gluteal artery, the inferior gluteal artery, the superior vesical artery, the inferior vesical artery, the middle rectal artery, the internal pudental artery and the obturator artery. In 2014, Chantalat et al. [9] published a study of 218 uterine artery origins in 114 Caucasian females (60 cadaveric, 100 intraoperative and 58 post computed tomography angiography) that showed that in 80.7% of the cases the uterine artery originated from a common trunk with the umbilical artery, separately from the internal iliac artery in 13.16% of the cases, directly from the superior gluteal artery in 3.51% of the cases, from a common trunk with the internal pudendal artery in 1.75% of the cases and separately from the obturator artery in 0.88% of the cases. In 2018, Arfi et al. [3] published a radiological study where 86 origins of the uterine artery were visualised and in 62.4% of the cases the uterine artery was branch of a common trunk with the umbilical artery, in 9.3% of the cases it originated from the superior gluteal artery, in 2.3% it originated from the internal pudendal artery and only in 25.6% of the cases did the uterine artery originate from the internal iliac artery. All the above findings are of great significance given that the risk of intraoperative iatrogenic injury to the uterine artery is increased when the artery arises from the umbilical artery due to the fact that the uterine artery crosses the operative field in this case [28].

Equally interestingly, in 2019, Hao et al. [20] published a radiological study of 224 origins of the uterine artery which showed that in 64.3% of the cases the uterine artery originated from the inferior gluteal artery, in 22.8% of the cases from the internal iliac artery and in 12.9% of the cases as a trifurcation along with the inferior gluteal and the superior gluteal artery. In the same study, only in 60.7% of the cases the origin of the uterine artery was consistent between the right and left side [20]. Finally, the uterine artery has rarely been found to originate from the inferior vesical artery, the middle rectal, or the inferior epigastric artery, whereas, even the complete absence of it has been reported as well [29, 31, 47, 52, 54].

CONCLUSIONS AND COMMENTARY

Anatomical variations are akin to a change in a landmark during a hiker's expedition on a well-trodden path: it can be the root of confusion and unexpected sequelae. While the anatomical variations presented here tend to be rare, a surgeon should be aware of their existence, so as to modify the course of action should they present themselves during the operation. Preoperative preparedness in the form of extensive investigation, if suspicion of variations is present, as well as intraoperative vigilance can minimise complications attributed to iatrogenic damage to the unexpected anatomical findings.

The knowledge and identification of the location, origin and course of the ureters and the uterine arteries are very important during abdominal hysterectomy for benign pathologies. Ureters can show variations in morphology, such as ureteric diverticula or multiplications, as well as changes in positioning, such as following a retroiliac course. Those variations can be detected preoperatively with extensive investigation employing imaging techniques [15, 22, 55]. Such an approach is recommended in the presence of other variations detected in the urogenital system. Furthermore, the surgeon should employ both morphological and functional criteria to identify the ureters intraoperatively, in order to detect deviations from their typical presentation. High vascular ligation of the uterine arteries is an integral part of abdominal hysterectomy. Careful retroperitoneal dissection beginning at the iliac bifurcation down to the crossing of the uterine artery with the ureter, in order to ligate the uterine artery at its origin, can overcome obstacles due to anatomical variations and result in a safer operation [38, 43]. Additionally, computed tomography angiography, as an easily performed, non-invasive and financially efficient technique, can display the anatomical variations of the origin of the uterine artery and facilitate the performance of safer operations [20].

Conflict of interest: None declared

REFERENCES

1. Abdullatif V, Consolo M. Ureteral diverticulum in 65-year-old female. Cureus. 2021; 13(8): e17310, doi: 10.7759/cureus.17310, indexed in Pubmed: 34430187.
2. Alraddadi A. Literature review of anatomical variations: clinical significance, identification approach, and teaching strategies. Cureus. 2021; 13(4): e14451, doi: 10.7759/cureus.14451, indexed in Pubmed: 33996311.
3. Arfi A, Arfi-Rouche J, Barrau V, et al. Three-dimensional computed tomography angiography reconstruction of the origin of the uterine artery and its clinical significance. Surg Radiol Anat. 2018; 40(1): 85–90, doi: 10.1007/s00276-017-1941-9, indexed in Pubmed: 29124344.
4. Arumugam S, Subbiah NK, Mariappan Senthiappan A. Double ureter: incidence, types, and its applied significance-a cadaveric study. Cureus. 2020; 12(4): e7760, doi: 10.7759/cureus.7760, indexed in Pubmed: 32455077.
5. Barral JP, Croibier A. Uterine vessels. Visc Vasc Manip. 2011: 240–244, doi: 10.1016/b978-0-7020-4351-2.00032-6.
6. Bisset GS, Strife JL. The duplex collecting system in girls with urinary tract infection: prevalence and significance. AJR Am J Roentgenol. 1987; 148(3): 497–500, doi: 10.2214/ajr.148.3.497, indexed in Pubmed: 3492875.
7. Bourgioti C, Koutoulidis V, Chatoupis K, et al. MRI findings before and after abdominal radical trachelectomy (ART) for cervical cancer: a prospective study and review of the literature. Clin Radiol. 2014; 69(7): 678–686, doi: 10.1016/j.crad.2014.02.001, indexed in Pubmed: 24625691.
8. Cahill DR, Leonard RJ. Missteps and masquerade in American medical academe: clinical anatomists call for action. Clin Anat. 1999; 12(3): 220–222, doi: 10.1002/(SICI)1098-2353(1999)12:3<220::AID-CA14>3.0.CO;2-K, indexed in Pubmed: 10340461.
9. Chantalat E, Merigot O, Chaynes P, et al. Radiological anatomical study of the origin of the uterine artery. Surg Radiol Anat. 2014; 36(10): 1093–1099, doi: 10.1007/s00276-013-1207-0, indexed in Pubmed: 24052200.
10. Charoenkwan K, Kietpeerakool C. Retroperitoneal drainage versus no drainage after pelvic lymphadenectomy for the prevention of lymphocyst formation in women with gynaecological malignancies. Cochrane Database Syst Rev. 2017; 6(6): CD007387, doi: 10.1002/14651858.CD007387.pub4, indexed in Pubmed: 28660687.
11. Chaudhuri J, Lakshmi A, Mustafa VSK, et al. A detailed study of the course, branching pattern and dimensions of the uterine and vaginal arteries and their branches. MOJ Anat Physiology. 2019; 6(6), doi: 10.15406/mojap.2019.06.00276.
12. Clarke-Pearson DL, DeLong ER, Synan IS, et al. Variables associated with postoperative deep venous thrombosis: a prospective study of 411 gynecology patients and crea-

tion of a prognostic model. Obstet Gynecol. 1987; 69(2): 146–150, indexed in Pubmed: 3808500.
13. Clarke-Pearson DL, Geller EJ. Complications of hysterectomy. Obstet Gynecol. 2013; 121(3): 654–673, doi: 10.1097/AOG.0b013e3182841594, indexed in Pubmed: 23635631.
14. Cobellis G, Mastroianni L, Noviello C, et al. Retroiliac double ureters in duplex system: incidental retroperitoneoscopic diagnosis. J Laparoendosc Adv Surg Tech A. 2007; 17(4): 517–518, doi: 10.1089/lap.2006.0118, indexed in Pubmed: 17705740.
15. Emekli E, Gündoğdu E, Özen A, et al. A rare case of ureteral diverticulum incidentally detected during angiography. Curr Med Imaging. 2021; 17(4): 549–551, doi: 10.2174/1573405616999201029123851, indexed in Pubmed: 33135615.
16. Engelsgjerd JS, LaGrange CA. Ureteral Injury. StatPearls. StatPearls Publishing, Treasure Island (FL) 2022.
17. Foley CE, Mansuria S. Ureteral anomalies in gynecologic surgery. J Minim Invasive Gynecol. 2020; 27(3): 566–567, doi: 10.1016/j.jmig.2019.07.022, indexed in Pubmed: 31362116.
18. Gilmour DT, Das S, Flowerdew G. Rates of urinary tract injury from gynecologic surgery and the role of intraoperative cystoscopy. Obstet Gynecol. 2006; 107(6): 1366–1372, doi: 10.1097/01.AOG.0000220500.83528.6e, indexed in Pubmed: 16738165.
19. Gupta NP, Gill IS, Bhatia V. Retroiliac ureter with contralateral transverse malrotation of kidney: treated by crossed ureterocaliceal anastomosis. J Urol. 1987; 138(1): 118–119, doi: 10.1016/s0022-5347(17)43014-x, indexed in Pubmed: 3599191.
20. Hao YX, Wang KeF, Wang GR, et al. [Value of the CT angiography in displaying the anatomical variations of the origin of uterus artery]. Zhongguo Yi Xue Ke Xue Yuan Xue Bao. 2019; 41(2): 216–219, doi: 10.3881/j.issn.1000-503X.10596, indexed in Pubmed: 31060677.
21. Hawthorne AB. The embryological and clinical aspect of double ureter. Can Med Assoc J. 1936; 34(1): 21–26, indexed in Pubmed: 20320125.
22. Herndon CD, McKenna PH. Antenatally detected proximal ureteral diverticulum. Urology. 2000; 55(5): 774, doi: 10.1016/s0090-4295(00)00506-9, indexed in Pubmed: 10792106.
23. Iuchtman M, Assa J, Blatnoi I, et al. Urometrocolpos associated with retroiliac ureter. J Urol. 1980; 124(2): 283–285, doi: 10.1016/s0022-5347(17)55410-5, indexed in Pubmed: 7401250.
24. Jackson LA, Ramirez DMO, Carrick KS, et al. Gross and histologic anatomy of the pelvic ureter: clinical applications to pelvic surgery. Obstet Gynecol. 2019; 133(5): 896–904, doi: 10.1097/AOG.0000000000003221, indexed in Pubmed: 30969205.
25. Jacob GP, Vilos GA, Al Turki F, et al. Ureteric injury during gynaecological surgery: lessons from 20 cases in Canada. Facts Views Vis Obgyn. 2020; 12(1): 31–42, indexed in Pubmed: 32696022.
26. Jokinen E, Brummer T, Jalkanen J, et al. Hysterectomies in Finland in 1990-2012: comparison of outcomes between trainees and specialists. Acta Obstet Gynecol Scand. 2015; 94(7): 701–707, doi: 10.1111/aogs.12654, indexed in Pubmed: 25867490.
27. Katz G, Meirow D. An incompletely identified combined urogynecological malformation presenting as anuria. J Urol. 1993; 149(3): 610–612, doi: 10.1016/s0022-5347(17)36164-5, indexed in Pubmed: 8437277.
28. Kostov S, Kornovski Y, Slavchev S, et al. Pelvic lymphadenectomy in gynecologic oncology-significance of anatomical variations. Diagnostics (Basel). 2021; 11(1), doi: 10.3390/diagnostics11010089, indexed in Pubmed: 33430363.
29. Kozlov SV, Dvoretskii DD, Alekseenko LA, et al. Anatomical variants of uterine arteries. Ukr J Med Biol Sport. 2018; 3(4): 32–37, doi: 10.26693/jmbs03.04.032.
30. Liapis K, Tasis N, Tsouknidas I, et al. Anatomic variations of the Uterine Artery. Review of the literature and their clinical significance. Turk J Obstet Gynecol. 2020; 17(1): 58–62, doi: 10.4274/tjod.galenos.2020.33427, indexed in Pubmed: 32341832.
31. Maclaran KA, Edmonds DK, Tait P. Absence of uterine arteries discovered at fibroid embolisation. Br J Radiol. 2009; 82(983): e228–e230, doi: 10.1259/bjr/15564157, indexed in Pubmed: 19890116.
32. Mäkinen J, Brummer T, Jalkanen J, et al. Ten years of progress — improved hysterectomy outcomes in Finland 1996–2006: a longitudinal observation study. BMJ Open. 2013; 3(10): e003169, doi: 10.1136/bmjopen-2013-003169, indexed in Pubmed: 24165027.
33. Mäkinen J, Johansson J, Tomás C, et al. Morbidity of 10 110 hysterectomies by type of approach. Hum Reprod. 2001; 16(7): 1473–1478, doi: 10.1093/humrep/16.7.1473, indexed in Pubmed: 11425832.
34. McLoughlin LC, Davis NF, Dowling C, et al. Ureteral diverticulum: a review of the current literature. Can J Urol. 2013; 20(5): 6893–6896, indexed in Pubmed: 24128825.
35. Mejri R, Chaker K, Mokhtar B, et al. Ureteral diverticulum complicated by urinary lihiasis: about a case report. Urol Case Rep. 2021; 39: 101810, doi: 10.1016/j.eucr.2021.101810, indexed in Pubmed: 34485084.
36. Moen M. Hysterectomy for benign conditions of the uterus: total abdominal hysterectomy. Obstet Gynecol Clin North Am. 2016; 43(3): 431–440, doi: 10.1016/j.ogc.2016.04.003, indexed in Pubmed: 27521877.
37. Moscovici J, Juricic M, Galinier P, et al. [Retro-iliac ureter. Report of a case lumbosacral agenesis]. Bull Assoc Anat (Nancy). 1996; 80(249): 23–26, indexed in Pubmed: 9102054.
38. Orhan A, Ozerkan K, Kasapoglu I, et al. From where does the uterine artery originate? A prospective, observational laparoscopic anatomic study. J Minim Invasive Gynecol. 2020; 27(5): 1081–1086, doi: 10.1016/j.jmig.2019.07.031, indexed in Pubmed: 32294549.
39. Ouattara A, Pare AK, Kabore FA, et al. Iatrogenic ureteral injuries associated with gynecological and surgical procedures: our experience about 18 cases and literature review. Res Rep Urol. 2021; 13: 289–293, doi: 10.2147/RRU.S299590, indexed in Pubmed: 34079774.
40. Ouyang Z, Liu P, Yu Y, et al. Role of ovarian artery-to-uterine artery anastomoses in uterine artery embolization: initial anatomic and radiologic studies. Surg Radiol Anat. 2012; 34(8): 737–741, doi: 10.1007/s00276-011-0883-x, indexed in Pubmed: 22008785.
41. Papageorgiou D, Kyriazanos I, Zoulamoglou M, et al. Incomplete bilateral duplication of the ureters identified dur-

ing cytoreductive surgery for ovarian cancer: A case report. Int J Surg Case Rep. 2019; 60: 213–215, doi: 10.1016/j.ijscr.2019.06.015, indexed in Pubmed: 31238202.
42. Papin E, Eisendrath DN. Classification of renal and ureteral anomalies. Ann Surg. 1927; 85(5): 735–756, indexed in Pubmed: 17865673.
43. Peters A, Stuparich MA, Mansuria SM, et al. Anatomic vascular considerations in uterine artery ligation at its origin during laparoscopic hysterectomies. Am J Obstet Gynecol. 2016; 215(3): 393.e1–393.e3, doi: 10.1016/j.ajog.2016.06.004, indexed in Pubmed: 27287682.
44. Ramdhan RC, Loukas M, Tubbs RS. Anatomical complications of hysterectomy: a review. Clin Anat. 2017; 30(7): 946–952, doi: 10.1002/ca.22962, indexed in Pubmed: 28762535.
45. Ravlo M, Moen MH, Bukholm IR, et al. Ureteric injuries during hysterectomy-A Norwegian retrospective study of occurrence and claims for compensation over an 11-year period. Acta Obstet Gynecol Scand. 2022; 101(1): 68–76, doi: 10.1111/aogs.14293, indexed in Pubmed: 34766333.
46. Saalfeld J, Walsh PC, Goodwin WE. Ureterovaginoplasty for vaginal atresia (unique technique in treatment): a case report with description of associated arterial anomalies and retroiliac artery ureters. J Urol. 1973; 109(6): 1039––1045, doi: 10.1016/s0022-5347(17)60619-0, indexed in Pubmed: 4710672.
47. Saraiya PV, Chang TC, Pelage JP, et al. Uterine artery replacement by the round ligament artery: an anatomic variant discovered during uterine artery embolization for leiomyomata. J Vasc Interv Radiol. 2002; 13(9 Pt 1): 939–941, doi: 10.1016/s1051-0443(07)61779-5, indexed in Pubmed: 12354830.
48. Settnes A, Moeller C, Topsoee MF, et al. Complications after benign hysterectomy, according to procedure: a population-based prospective cohort study from the Danish hysterectomy database, 2004-2015. BJOG. 2020; 127(10): 1269–1279, doi: 10.1111/1471-0528.16200, indexed in Pubmed: 32145133.
49. Siomou E, Papadopoulou F, Kollios KD, et al. Duplex collecting system diagnosed during the first 6 years of life after a first urinary tract infection: a study of 63 children. J Urol. 2006; 175(2): 678–681, doi: 10.1016/S0022-5347(05)00184-9, indexed in Pubmed: 16407023.
50. Tawfik AM, Younis MH. Computed tomography imaging appearance of a unique variant of retroiliac ureter. Urology. 2016; 88: e7–e9, doi: 10.1016/j.urology.2015.11.021, indexed in Pubmed: 26627375.
51. Teeluckdharry B, Gilmour D, Flowerdew G. Urinary tract injury at benign gynecologic surgery and the role of cystoscopy: a systematic review and meta-analysis. Obstet Gynecol. 2015; 126(6): 1161–1169, doi: 10.1097/AOG.0000000000001096, indexed in Pubmed: 26551173.
52. Uflacker A, Sopata CE, Haskal ZJ. Inferior epigastric uterine artery. J Vasc Interv Radiol. 2017; 28(1): 23, doi: 10.1016/j.jvir.2016.04.035, indexed in Pubmed: 28007079.
53. Vellinga TT, Suzuki Y, Istre O, et al. Anatomic considerations in gynecologic surgery. Rev Obstet Gynecol. 2009; 2(3): 137–138, indexed in Pubmed: 19826570.
54. Wagner E, Soneji K, Semaan A, et al. Bilateral agenesis of the uterine arteries. Res Rep Gynaecol Obs. 2017; 1: 20–22.
55. Wan YL, Hsieh ML, Hsueh C, et al. Sonographic diagnosis of a ureteral diverticulum. J Ultrasound Med. 1996; 15(6): 483–485, doi: 10.7863/jum.1996.15.6.483, indexed in Pubmed: 8738995.
56. Wijaya T, Lo TS, Jaili S, et al. The diagnosis and management of ureteric injury after laparoscopy. Gynecol Minim Inv Therapy. 2015; 4(2): 29–32, doi: 10.1016/j.gmit.2015.02.003.
57. Wright JD, Herzog TJ, Tsui J, et al. Nationwide trends in the performance of inpatient hysterectomy in the United States. Obstet Gynecol. 2013; 122(2 Pt 1): 233–241, doi: 10.1097/AOG.0b013e318299a6cf, indexed in Pubmed: 23969789.
58. Yabuki Y. Twenty-first century radical hysterectomy: Journey from descriptive to practical anatomy. Gynecol Oncol Rep. 2020; 34: 100623, doi: 10.1016/j.gore.2020.100623, indexed in Pubmed: 32984492.
59. Żytkowski A, Tubbs R, Iwanaga J, et al. Anatomical normality and variability: Historical perspective and methodological considerations. Trans Res Anat. 2021; 23: 100105, doi: 10.1016/j.tria.2020.100105.

VIA MEDICA

ORIGINAL ARTICLE

Folia Morphol.
Vol. 82, No. 4, pp. 784–790
DOI: 10.5603/FM.a2022.0103

ISSN 0015–5659
eISSN 1644–3284
journals.viamedica.pl

Magnetic resonance based morphometric analysis of the tentorial notch

F.J. Arrambide-Garza[1]*, O. De-La-Garza-Castro[1]*, L.A. Alvarez-Lozada[1], E. Carranza-Rodriguez[2], A. Quiroga-Garza[1], A. Gomez-Sanchez[1], R. Pinales-Razo[2], R.E. Elizondo-Omaña[1], S. Guzman-Lopez[1]

[1]*Human Anatomy Department, School of Medicine, Universidad Autónoma de Nuevo León, Monterrey, Nuevo León, Mexico*
[2]*Radiology and Imaging Department, University Hospital "Dr. José Eleuterio González", Universidad Autónoma de Nuevo León, Monterrey, Nuevo León, Mexico*

[Received: 18 October 2022; Accepted: 14 November 2022; Early publication date: 30 November 2022]

Background: *The study of the tentorial notch can improve the understanding of brain injury mechanisms. Tentorial morphology has been analysed primarily in cadaveric studies. However, the postmortem effect can cause variability in the measurements. The objective was to evaluate the morphometry of the tentorial notch and the third cranial nerve on living subjects using magnetic resonance imaging (MRI).*

Materials and methods: *A retrospective cross-sectional study was performed. Using consecutive cases, 60 MRI scans were analysed for tentorial notch morphology. Maximum notch width (MNW), notch length (NL), interpeduncluclival (IC) distance, apicotectal (AT) distance, third cranial nerve (CN-III) distance, and inter-CN-III angle, were obtained. For the classification of the tentorial notch quartile distribution technique for MNW, NL, AT distance, and IC distance were used.*

Results: *According to the quartile of the MNW, patients were stratified into narrow, midrange, and wide groups. Using the NL quartile groups, they were also classified as short, midrange, and long. With these, the tentorial notch could be classified into eight types. Statistical differences between genders in the MNW and inter-CN-III angle were found, as well as a strong positive correlation between NL and AT distance, and between right and left CN-III distances.*

Conclusions: *There were differences between the cadaveric samples and living subjects in the CN-III distances. This difference could be explained by the dehydration of brain volume in the postmortem process which may cause nerve elongation. Morphometry of the tentorial notch and its neurovascular relations allows a better understanding of the mechanisms of brain herniation.* (Folia Morphol 2023; 82, 4: 784–790)

Key words: tentorial notch, third cranial nerve, brainstem, brain herniation

Address for correspondence: Dr. S. Guzman-Lopez and Dr. R.E. Elizondo-Omaña, Facultad de Medicina, Universidad Autónoma de Nuevo León, Av. Madero and Dr. Aguirre Pequeño S/N, Col. Mitras Centro, C.P. 64460, Monterrey, Nuevo León, México, tel: +52 1 81 8329 4171, fax: +521 81 8347 7790, e-mail: dr.santos.anato@gmail.com; rod_omana@yahoo.com

*Both authors participated equally in the study and are both in the position of first author.

INTRODUCTION

The cerebellar tentorium is a semilunar-shaped extension of the dura mater that separates the cerebellum from the cerebral hemispheres [17]. The triangular-shaped aperture located between the free edges of the tentorium cerebelli and the clivus is defined as the tentorial notch [18]. This space is involved in different brain injury processes due to the relation with midline structures and the rigidity of the dura mater [10].

Tentorial herniation is an upper or lower displacement of the temporal lobe through the tentorial notch, and is one of the most common herniation secondary result of an intracranial mass [15]. Different studies have published the possible influence of the morphometric analysis of this aperture in the understanding of the mechanism of different brain injuries [1, 5, 6]. The patterns of the tentorial herniation and differences in the clinical presentation could be partially influenced by the dimensions of the tentorial notch and the position of the brainstem, but this remains unclear [5].

The morphometric analysis of the tentorial notch has been analysed mainly in cadaveric studies [1, 6, 16, 23]. However, the tissue deterioration in the postmortem process, alterations due to dehydration from the absence of circulation, and the method of conservation used could have an impact on measurements, varying amongst themselves [7, 25, 27]. The objective of this study is to evaluate the morphometry of the tentorial notch and the third cranial nerve (CN-III) in living subjects by magnetic resonance imaging (MRI).

MATERIALS AND METHODS

A retrospective cross-sectional study was performed with 60 Fast Imaging Employing Steady/ /State Acquisition (FIESTA) MRI sequences. The study images were obtained from the database of the Radiology and Imaging Department. Screening was consecutive cases of patients between 18 and 60 years who underwent a brain FIESTA MRI sequence indicated by their treating physician. We excluded patients with posterior fossa diseases, central nervous system vascular disease, previous cranial surgery, or other central nervous system diseases that may alter anatomy. Studies with abnormalities or artifacts were eliminated. This study adheres to the STROBE guidelines for the report of observational studies [26].

Study technique

All patients underwent a head FIESTA MRI sequence (3 Tesla, Signa Twin HDx of General Electric-GE), Software 5.7.1, using the following parameters — temporal resolution: 1000 ms, echo time: 136 ms, flip angle: 110°, slice-thickness: 0.6 mm, slice oversampling: field of view: 200 × 200 mm, matrix: 320 × 320. All the imaging data was uploaded to the Carestream Vue PACS and analysed in coronal, axial, and sagittal planes. The images and measurements were assessed independently by two neuro-radiologists recorded in a database using millimetres with two decimal unit precision. All sets of inter-observer reliability analyses resulted in substantial reliability (interclass coefficient > 0.85 and Cohen's kappa > > 0.85).

Tentorial notch measurements

Definition and anatomical fundamentals for interpretation of the tentorial notch and CN-III variables, have been described mainly in human cadaveric samples. However, Adler et al. [1] reported a method to measure these variables using MRI. The following variables were measured: maximum notch width (MNW), notch length (NL), interpedunculoclival (IC) distance, and apicotectal (AT) distance. Although the anterior notch width, defined as the width of the tentorial notch in the dorsum sellae, is a variable described by other authors, this could not be reproduced with MRI. We propose a method for studying the CN-III with MRI with the following measures: CN-III distance, and inter-CN-III angle (Fig. 1). Although the measurement may be done by T2 RMI sequence

For the classification of the tentorial notch defined by Adler et al. [1] quartile distribution technique for MNW, NL, AT distance, and IC distance was used. Using the MNW quartile distribution the tentorial notch was divided into narrow, midrange, and long. The NL and AT distances quartile distribution were used to classify into short, midrange, and long. The position of the brainstem within the tentorial notch was labelled as pre-fixed, mid-position, and post-fixed applying the quartile distribution technique with the IC distance. According to the classification defined by Adler et al. [1] we used the MWN and NL to stratify tentorial notch into 8 types.

Ethical considerations

This study was previously reviewed and approved by the University's Ethics and Research Committees

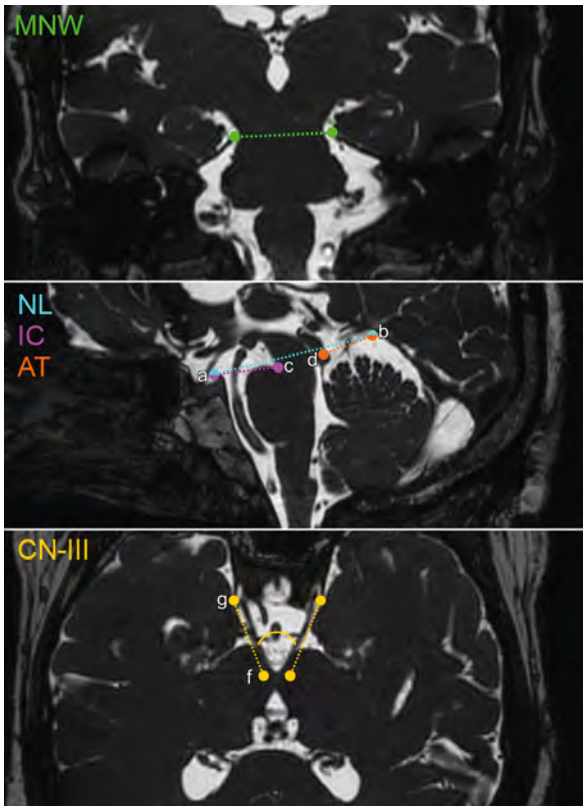

Figure 1. Measurements of the tentorial notch. Maximum notch width (MNW): using a coronal plane, the maximum width between the border of the tentorial notch in the coronal plane. Notch length (NL): using a sagittal plane, the length of the tentorial notch from the superior edge of the dorsum sellae (letter a) to the apex of the tentorial notch (letter b). Interpeduncloclival (IC) distance: using a sagittal plane, the distance between the superior edge of the dorsum sellae to the interpeduncular fossa (letter c). Apicotectal (AT) distance: using a sagittal plane, the distance from the tectum (letter d) to the apex of the tentorial notch. Left and right third cranial nerve (CN-III) distance: using a transverse plane, the distance between the origin of the CN-III (letter f) to the cavernous sinus (letter g). Inter-CN-III angle: using a transverse plane, the angle between the two third cranial nerves (curve line).

with the registration number AH21-00010, making sure it adheres to the Helsinki Declaration and national and international standards of research. The authors declare no financial or commercial gain for the realisation of this study. The authors declare no conflict of interest. None of the imaging studies were performed for the purposes of this study.

Statistical analysis

Sample size calculation was made with the formula for estimating a mean in an infinite population with a confidence of 95% and a margin of error of 5% resulting in a total of 60 studies. We obtained central tendency and dispersion data of the sample variables. We performed the Kolmogorov-Smirnov test for normality. Due to the normality distribution of sample data, the comparison between different sexes groups was made with a two-tailed Student t-test. Correlation tests were performed by Pearson correlation coefficients. The 95% confidence interval (CI) was obtained for the mean between-difference. A p-value of < 0.5 was considered statistically significant. For multiple comparisons, the Bonferroni correction was performed to adjust the p-value. The database was analysed using the SPSS Version 25.0 programme for Windows 10 (IBM, Armonk, NY, USA).

RESULTS

Descriptive statistics of the measurements stratified by sex are shown in Table 1. The mean age of the sample was 41.5 ± 12.1 years, of which 36 (60%) were women with a mean age of 42.08 ± 9.23 years and 24 (40%) men with a mean age of 41.11 ± 13.8 years. We found statistically differences between sexes in MNW distance and inter-CN-III angle. The MNW mean is 32.13 mm (range 28.1–39.8, 95% CI 30.95–33.31) for men and 30.72 mm (range 28.1–39.8, 95% CI 29.89–31.56) for women. The mean between-group difference is 1.4 mm (95% CI 0.038–2.77; $p = 0.04$). The inter-CN-III angle mean is 56.72 grades (range 45.72–70.56, 95% CI 53.98–59.46) for man and 53 grades (range 41.78–71.24, 95% CI 50.69–55.32). The mean between-group difference is of 3.71 grades (95% CI 0.20–7.22; $p = 0.04$).

Pearson's correlation coefficient between variables is shown in Table 2. We found a strong positive correlation coefficient between measurements between NL and AT distance ($r = 0.78$; $r^2 = 0.62$), and between right and left CN-III distances ($r = 0.93$; $r^2 = 0.86$).

Table 3 shows the ranges of the measurements used to classify the tentorial notch using MNW and NL quartiles and the percentages of the different types. The typical type that corresponds to the MNW and NL midrange was the most common. The mixed type was the least frequent in this sample.

DISCUSSION

Main findings

This study analysed the morphology of the tentorial notch and CN-III on living subjects in a healthy population. Our study demonstrates consistency with cadaveric studies, except for the variables of the CN-III. We obtained statistically significant differences between sexes in MNW and inter-CN-III angle; how-

Table 1. Comparison measurements of the tentorial notch between sexes

Measurement	General (n = 60)	Women (n = 36)	Men (n = 24)	P
Maximum notch width	31.28 ± 2.66	30.72 ± 2.46	32.13 ± 2.78	0.04*
Notch length	55.55 ± 4.82	55.94 ± 4.94	54.98 ± 4.66	0.45
Apicotectal distance	19.45 ± 3.81	19.8 ± 3.95	18.93 ± 3.6	0.39
Interpedunculoclival distance	21.03 ± 3.17	20.93 ± 3.32	21.17 ± 2.98	0.78
Right cisternal CN-III distance	22.81 ± 4.11	23.99 ± 3.81	22.03 ± 4.17	0.07
Left cisternal CN-III distance	22.02 ± 3.96	22.71 ± 3.76	21.56 ± 4.08	0.27
Inter-CN-III angle	54.49 ± 6.89	56.72 ± 6.49	53 ± 6.84	0.04*

Data are shown as mean ± standard deviation. Values are expressed in millimetres for distances and grades for angles. Independent-sample Student t-test was used for compared measurements between sexes; *statistically significant ($p < 0.05$); CN-III — third cranial nerve

Table 2. Pearson´s correlation coefficient between measurements of the tentorial notch

	MNW	NL	AT distance	IC distance	Right CN-III distance	Left CN-III distance
MNW		0.227	0.239	–0.056	0.456*	0.374*
NL			0.788*	0.482*	0.401	0.479*
AT distance				0.056	0.208	0.267
IC distance					0.286	0.297*
Right CN-III distance						0.935*
Left CN-III distance						

*Statistically significant with Bonferroni correction; AT — apicotectal; CN-III — third cranial nerve; IC — interpedunculoclival; MNW — maximum notch width; NL — notch length

Table 3. Types of tentorial notch

Type of notch	Dimension	Range [mm]	Percentage
Wide	MNW (wide)	32.5–39.8	15%
	NL (midrange)	55.6–58.9	
Narrow	MNW (narrow)	26.5–29.5	11.6%
	NL (midrange)	55.6–58.9	
Long	MNW (midrange)	29.6–32.4	10%
	NL (long)	59–64.9	
Short	MNW (midrange)	29.6–32.4	15%
	NL (short)	46.6–55.5	
Typical	MNW (midrange)	29.6–32.4	25%
	NL (midrange)	55.6–58.9	
Large	MNW (wide)	32.5–39.8	10%
	NL (long)	59–64.9	
Small	MNW (narrow)	26.5–29.5	10%
	NL (short)	46.6–55.5	
Mixed	MNW (narrow)	26.5–29.5	3%
	NL (long)	59–64.9	
	MNW (wide)	32.5–39.8	0%
	NL (short)	46.6–55.5	

MNW — maximum notch width; NL — notch length

ever, the absolute difference was small. Currently, a distinction between sexes in the understanding of brain injury has not been established. A strong positive correlation was found between NL and AT distance, and between the right and left cisternal CN-III distance.

Comparison with other studies

Most studies regarding tentorial notch analysis have used cadavers, which carries an important limitation (Table 4) [1, 6, 16, 23]. In the cadaveric conservation process, the deep brain is the last part conserved, as the fixation agent spread from the surface of the brain [7]. The conservation process depends mainly on the time of the initiation of the procedure after death [7, 9]. This allows macroscopic changes in the brain to set in, as the putrefaction phase of the postmortem process can be seen as early as 24 hours succeeding the death, which may impact on the measurements [14].

We obtained similar results in the MNW and NL measurements compared with other populations [1, 6, 16, 20, 22, 23]. Adler et al. [1] studied a larger population than other studies but the mean and standard deviation are similar among authors (Table 4). The variables that include dura matter appear to be less affected by the postmortem process than other structures inside the head [3].

Table 4. Measurement comparison of the tentorial notch between other populations

Author	Arrambide-Garza et al., 2022	Das et al., 2021 [6]	Staquet et al., 2020 [22]	Adler et al., 2002 [1]	Sunderland et al., 1984 [23]	Ono et al., 1984 [16]
Country	Mexico	USA	France	USA	Australia	USA
Sample	60 MRIs	40 cadavers	40 CTs	110 cadavers	30 cadavers	25 cadavers
Age	41.5 ± 12.1	20 to 65	–	42.5	–	–
ANW	–	26.92 ± 2.14	25.5 ± 3.5	26.6 ± 2.7	27.06 ± 3.5	
MNW	31.28 ± 2.66	29.77 ± 2.26	31.0 ± 2.5	29.6 ± 3.0	30.16 ± 3.21	29.6 (26–35)
NL	55.55 ± 4.82	57.98 ± 4.52	55.0 ± 5.3	57.7 ± 5.6	54.9 ± 6.93	52 (46–67)
IC distance	21.03 ± 3.17	21.21 ± 3.72	–	20.4 ± 3.2	–	12.1 (7.8–15.6)
AT distance	19.45 ± 3.81	25.81 ± 8.04	–	16.8 ± 5.4	–	19.8 (13–27)
Right CN-III distance	22.81 ± 4.11	–	–	26.1 ± 3.2	–	–
Left CN-III distance	22.02 ± 3.96	–	–	26.7 ± 2.9	–	–
Inter-CN-III angle	54.49 ± 6.89	–	–	57.3 ± 7.3	–	–

Data are shown as mean ± standard deviation and mean (range). Values are expressed in millimetres for distances and grades for angles. AMW — anterior notch width; AT — apicotectal; CN-III — third cranial nerve; CT — computed tomography; IC — interpedunculoclival; MRI — magnetic resonance imaging; MNW — maximum notch width; NL — notch length

The tentorial notch is divided into the anterior, middle, and posterior incisural spaces depending on the relation with the brainstem [4, 21]. The anterior and posterior incisural spaces are located anterior and posterior to the brainstem, respectively [18]. The anterior incisural space contains the internal carotid artery, basilar artery, optic nerves, and CN-III [23]. Despite the differences between the types of samples, we obtained similar results in the IC distance to Adler et al. (21.03 mm) [1] and Das et al. (21.21 mm) [6] but different results than Ono et al. (12.1 mm) [16]. The posterior incisura space lies posterior to the brainstem and contains the posterior cerebral artery, superior cerebellar artery, the internal and basal vein, and the fourth cranial nerve [18]. We found similar results to Adler et al. (16.8 mm) [1] and Ono et al. (19.8 mm) [16] but different data than to Das et al. (25.81 mm) [6]. These differences between cadaveric studies could be explained by the conservation method used and the population studied.

The CN-III exits from the midbrain and passes through the cavernous sinus, prior to entering the orbit through the supraorbital fissure [12]. We studied the distance of the CN-III from its origin to the cavernous sinus with differences in the length (right: 22.81 mm, left: 22.02 mm) compared to Adler et al. (right: 26.1 mm, left: 26.7 mm) [1]. However, results were similar in the inter CN-III (54.49 vs. 57.3 grades). The difference in the length of the CN-III could be explained by the dehydration of the brain in the postmortem process, causing an elongation of the nerve.

Brain herniation

Brain herniation is the most common secondary result of an intracranial mass. It is defined as a displacement of cerebral tissue from a compartment to another [19]. Clinical presentation varies according to the compartment and the brain structure affected. The tentorial herniation could cause pupillary dilatation, ophthalmoplegia, or ipsilateral hemiplegia due to the compression of the brainstem and CN-III [24]. Despite the actual comprehension of the mechanism of the tentorial herniation, the reason for the clinical variation among patients is still unclear. The severity of the disease is determined mainly by the volume of the mass lesion, the localization, or the velocity of the pathological process [11]. In addition, the dimensions of the tentorial notch could have an implication on the clinical and severity of the brain herniation in patients with the same type of lesion [5, 23].

The anterior incisura space is a site where the temporal lobe could move and compress the CN-III and cerebral peduncles during the tentorial herniation [6]. The length of the anterior incisural space could be estimated with the IC distance. Patients with wider and longer notches could have more exposition of the posterior cranial fossae and facilitate the displacement of the brain in the herniation process.

The superior aspect of the cerebellum is related to the posterior incisural space [18]. Although the cerebellar tissue exposed through the posterior incisural space could not be studied by MRI, it could be estimated by the AT distance [6]. The relation between large apertures and the total of the cerebellar tissue

exposed has been described in cadaveric studies. The cerebellar tissue has a higher exposition in a long and wide tentorial notch than in a short and narrow notch. These findings could influence the cerebellar herniation through the tentorial notch [1, 13, 23].

The length and course of the CN-III may be an explanation for the clinical differences among patients with this pathology. The tentorial herniation compresses mainly the brainstem and (CN-III) during the movement of the temporal lobe through the tentorial notch [2, 8].

The MWN and NL are used to stratify the tentorial notch into 8 types. Grille et al. [11] studied the characteristics of the tentorial notch in neurocritical patients. They described the "narrow," "short," and "small" as the most common types in neurocritical patients, which corresponded to wider and longer notch types [11]. Further studies comparing the characteristics in neurocritical patients are needed to determine the association between tentorial notch types and herniation patterns.

Limitations of the study

Our study has several limitations. Although the sample size was calculated to determine statistical difference, larger samples are needed to make a comparison between different populations. The measurements of the CN-III have not been validated by other studies or compared with other radiology techniques. The patients' anthropometric characteristics were not included in the analysis. The study was conducted using Hispanic patients; however further data is needed to compare results with other populations. Grille et al. [11] validated the MRI and computed tomography, but the brainstem and CN-III cannot be studied using computed tomography. Our study used MRI with FIESTA sequence, which is not broadly available.

CONCLUSIONS

Changes in cadaveric models in the tentorial notch could have an impact on the morphology of the tentorial notch and its neurovascular relations. There were differences between the cadaveric samples and living subjects in the cisternal third nerve distances. This difference could be explained by the dehydration of the brain in the postmortem process which may cause nerve elongation. The measurements of the tentorial notch may have implications for a better understanding of the mechanisms of brain herniation.

Conflict of interest: None declared

REFERENCES

1. Adler DE, Milhorat TH. The tentorial notch: anatomical variation, morphometric analysis, and classification in 100 human autopsy cases. J Neurosurg. 2002; 96(6): 1103–1112, doi: 10.3171/jns.2002.96.6.1103, indexed in Pubmed: 12066913.
2. Angulo Carvallo N, Patil P, Abello AL. Cerebral herniation. Crit Find Neuroradiol. 2016: 13–19, doi: 10.1007/978-3-319-27987-9_2.
3. Bliss LA, Sams MR, Deep-Soboslay A, et al. Use of postmortem human dura mater and scalp for deriving human fibroblast cultures. PLoS One. 2012; 7(9): e45282, doi: 10.1371/journal.pone.0045282, indexed in Pubmed: 23028905.
4. Bull JW. Tentorium cerebelli. Proc R Soc Med. 1969; 62(12): 1301–1310, doi: 10.1177/003591576906201242, indexed in Pubmed: 4983118.
5. Corsellis JA. Individual variation in the size of the tentorial opening. J Neurol Neurosurg Psychiatry. 1958; 21(4): 279–283, doi: 10.1136/jnnp.21.4.279, indexed in Pubmed: 13611569.
6. Das A, Chhabra S, Das S, et al. The tentorial notch: morphometric analysis and its clinical relevance to neurosurgery. J Clin Diagn Res. 2021, doi: 10.7860/jcdr/2021/47758.14545.
7. Dawe RJ, Bennett DA, Schneider JA, et al. Postmortem MRI of human brain hemispheres: T2 relaxation times during formaldehyde fixation. Magn Reson Med. 2009; 61(4): 810–818, doi: 10.1002/mrm.21909, indexed in Pubmed: 19189294.
8. Fisher CM. Brain herniation: a revision of classical concepts. Can J Neurol Sci. 1995; 22(2): 83–91, doi: 10.1017/s0317167100040142, indexed in Pubmed: 7627921.
9. Fountoulakis M, Hardmeier R, Höger H, et al. Postmortem changes in the level of brain proteins. Exp Neurol. 2001; 167(1): 86–94, doi: 10.1006/exnr.2000.7529, indexed in Pubmed: 11161596.
10. Glaister J, Carass A, Pham DL, et al. Automatic falx cerebri and tentorium cerebelli segmentation from magnetic resonance images. Proc SPIE Int Soc Opt Eng. 2017; 10137, doi: 10.1117/12.2255640, indexed in Pubmed: 28943701.
11. Grille P, Biestro A, Telis O, et al. Individual variation of tentorial notch morphometry in a series of neurocritical patients. Arq Neuropsiquiatr. 2021; 79(9): 781–788, doi: 10.1590/0004-282X-anp-2020-0335, indexed in Pubmed: 34669814.
12. Heiland Hogan MB, Subramanian S, Das JM. Neuroanatomy, Edinger–Westphal Nucleus (Accessory Oculomotor Nucleus). StatPearls Publishing, Treasure Island (FL) 2022.
13. Klintworth GK. The comparative anatomy and phylogeny of the tentorium cerebelli. Anat Rec. 1968; 160(3): 635–642, doi: 10.1002/ar.1091600312, indexed in Pubmed: 5664078.
14. Mann RW, Bass WM, Meadows L. Time since death and decomposition of the human body: variables and observations in case and experimental field studies. J Forensic Sci. 1990; 35(1): 103–111, indexed in Pubmed: 2313251.
15. Munakomi S, Das JM. Brain herniation. StatPearls Publishing, Treasure Island (FL) 2022.
16. Ono M, Ono M, Rhoton AL, et al. Microsurgical anatomy of the region of the tentorial incisura. J Neurosurg. 1984;

60(2): 365–399, doi: 10.3171/jns.1984.60.2.0365, indexed in Pubmed: 6693964.
17. Rai R, Iwanaga J, Shokouhi G, et al. The tentorium cerebelli: a comprehensive review including its anatomy, embryology, and surgical techniques. Cureus. 2018; 10(7): e3079, doi: 10.7759/cureus.3079, indexed in Pubmed: 30305987.
18. Rhoton AL. Tentorial incisura. Neurosurgery. 2000; 47(3 Suppl): S131–S153, doi: 10.1097/00006123-200009001-00015, indexed in Pubmed: 10983307.
19. Riveros Gilardi B, Muñoz López JI, Hernández Villegas AC, et al. Types of cerebral herniation and their imaging features. Radiographics. 2019; 39(6): 1598–1610, doi: 10.1148/rg.2019190018, indexed in Pubmed: 31589570.
20. Salinas-Alvarez Y, Arrambide-Garza F, Elizondo-Omaña R, et al. Morphometric analysis of the tentorial notch by magnetic resonance. FASEB J. 2022; 36(S1), doi: 10.1096/fasebj.2022.36.s1.r2423.
21. Samii M, Carvalho GA, Tatagiba M, et al. Meningiomas of the tentorial notch: surgical anatomy and management. J Neurosurg. 1996; 84(3): 375–381, doi: 10.3171/jns.1996.84.3.0375, indexed in Pubmed: 8609546.
22. Staquet H, Francois PM, Sandoz B, et al. Surface reconstruction from routine CT-scan shows large anatomical variations of falx cerebri and tentorium cerebelli. Acta Neurochir (Wien). 2021; 163(3): 607–613, doi: 10.1007/s00701-020-04256-2, indexed in Pubmed: 32034496.
23. Sunderland S. The tentorial notch and complications produced by herniations of the brain through that aperture. Br J Surg. 1958; 45(193): 422–438, doi: 10.1002/bjs.18004519306, indexed in Pubmed: 13536343.
24. Tadevosyan A, Kornbluth J. Brain herniation and intracranial hypertension. Neurol Clin. 2021; 39(2): 293–318, doi: 10.1016/j.ncl.2021.02.005, indexed in Pubmed: 33896520.
25. Tapia-Nañez M, Quiroga-Garza A, Guerrero-Mendivil F, et al. A review of the importance of research in Anatomy, an evidence-based science. Eur J Anat. 2022; 26(4), doi: 10.52083/EVZA1394.
26. von Elm E, Altman DG, Egger M, et al. STROBE Initiative. The Strengthening the Reporting of Observational Studies in Epidemiology (STROBE) statement: guidelines for reporting observational studies. Bull World Health Organ. 2007; 85(11): 867–872, doi: 10.2471/blt.07.045120, indexed in Pubmed: 18038077.
27. Weickenmeier J, Kurt M, Ozkaya E, et al. Brain stiffens post mortem. J Mech Behav Biomed Mater. 2018; 84: 88–98, doi: 10.1016/j.jmbbm.2018.04.009, indexed in Pubmed: 29754046.

VIA MEDICA

ORIGINAL ARTICLE

Folia Morphol.
Vol. 82, No. 4, pp. 791–797
DOI: 10.5603/FM.a2022.0088

ISSN 0015–5659
eISSN 1644–3284
journals.viamedica.pl

Morphology and variability of the facial nerve trunk depending on the branching pattern, gender, anthropometric type and side of the head in Moldovan population

A. Babuci[1], I. Catereniuc[1], Z. Zorina[1], A. Bendelic[1], T. Botnari[1], E. Stepco[2], S. Lehtman[3], S. Strisca[3], L. Nastas[3], G. Motelica[3], O. Procopenco[3]

[1]*Department of Anatomy and Clinical Anatomy, Nicolae Testemitanu State University of Medicine and Pharmacy, Chisinau, Republic of Moldova*
[2]*Department of Paediatric Oral and Maxillofacial Surgery and Paedodontics "Ion Lupan", Nicolae Testemitanu State University of Medicine and Pharmacy, Chisinau, Republic of Moldova*
[3]*Department of Oral and Maxillofacial Surgery and Oral Implantology "Arsenie Gutan", Nicolae Testemitanu State University of Medicine and Pharmacy, Chisinau, Republic of Moldova*

[Received: 27 August 2022; Accepted: 27 September 2022; Early publication date: 14 October 2022]

Background: *Knowledge concerning variability of the facial nerve trunk (FNT) direction after its exit through the stylomastoid foramen is of a great clinical significance for maxillofacial surgeons, otorhinolaryngologists, oncologists, specialists in plastic and aesthetic surgery. The aim of our study was to establish the variation of the FNT direction and its peculiarities depending on the branching pattern, gender, anthropometric type and side of the head.*

Materials and methods: *The direction of the FNT and its branching pattern were studied on 75 dissected hemifaces of adult formalised cadavers (59 male/ /16 female), and the morphometry of the FNT length, width and bifurcation angle was carried out.*

Results: *Seven branching patterns of the facial nerve were established: type I — 18.7%, type II — 14.7%, type III — 20%, type IV — 14.6%, type V — 5.3%, type VI — 18.7%, and type NI — 8% (bizarre types). The FNT had a descending direction in 73.3% of cases; ascending FNT — 9.3% (including 5.3% of very short diffuse branching trunks and 1.3% of arch-shaped FNT); horizontal FNT — 10.7%; number variants — 6.7%. The male/female ratio of the descending FNT was 69.5%/87.4%; ascending — 10.2%/6.3%; horizontal — 11.9%/6.3%; number variants — 8.4% (only in male). The right/left ratio of the descending FNT was 62.9%/82.5%; ascending — 11.4%/7.5%; horizontal — 11.4%/10%; number variants — 14.3% (only on the right side). The ratio of the descending FNT in mesocephalic type (MCT)/brachycephalic type (BCT)/dolichocephalic type (DCT) was respectively 70.6%/100%/66.7%; ascending — 12.1%/0%/0%; horizontal — 12.1/0%/11.1%. Numerical variants in MCT — 5.2%, in DCT — 22.2%. The mean number of FNT in MCT/BCT/DCT was respectively 1.07/1.0/1.22.*

Address for correspondence: Dr. A. Babuci, Department of Anatomy and Clinical Anatomy, Nicolae Testemitanu State University of Medicine and Pharmacy of the Republic of Moldova, Stefan cel Mare si Sfant Bd., 192, Chisinau, MD-2004, Republic of Moldova, tel: +373 79 667 409, +373 22 205 349, +373 22 205 235, fax: +373 22 242 411, e-mail: angela.babuci@usmf.md

Conclusions: *Three main directions are characteristic of the FNT: the descending, ascending and horizontal ones, which vary depending on the branching pattern, gender, shape and side of the head.* (Folia Morphol 2023; 82, 4: 791–797)

Key words: facial nerve, branching types, variation, peculiarities, morphometry

INTRODUCTION

The facial nerve morphology, its variability and specific features are subject of interest of many researchers all over the world. Nevertheless, the majority of the published papers describe only the variability of the facial nerve branching types, its connections and topography of the parotid plexus towards neighbouring anatomical structures [1–4, 6, 8, 10–12]. Non-articles were found on the variability of the facial nerve trunk (FNT) direction depending on the gender, anthropometric type and side of the head, or branching pattern.

Taking into consideration that the rate of the parotid tumours, polytrauma with involvement of the head and neck regions, as well as the demand for plastic surgery and rejuvenating procedures have increased lately, it is imperative to have a new approach towards the facial nerve morphology.

The purpose of our study was to establish the direction and morphological peculiarities of the FNT depending on the branching pattern, gender, anthropometric type and side of the head.

MATERIALS AND METHODS

The variability and morphological peculiarities of the FNT were studied on 75 hemifaces of adult formalised cadavers (59 male/16 female) in the period 2014–2022. The direction, length, width, bifurcation angle, number variation of the FNT and branching pattern of the facial nerve were analysed.

Each cadaver was carefully examined on presence of any deformities or damages of the soft tissues of the face and only the hemifaces with intact soft tissues were used for our study.

Ahead of dissection, the longitudinal and transverse dimensions of each head were measured. The longitudinal dimension was measured between the glabella and opisthocranion and the transverse one between the right and left euryons.

The anthropometric type of the head was established according to the formula:

$$\frac{Transverse\ diameter \times 100}{Longitudinal\ diameter}$$

The male specimens were represented by 59 (78.7%) hemifaces, and the female ones by 16 (21.3%) hemifaces. The right side hemifaces constituted 40 (53.3%) samples and the left ones — 35 (46.7%). The male/female ratio of the right specimens was 82.9%/17.1% and those of the left — 75%/25%. In male individuals the ratio of the right/left hemifaces was 49.2%/50.8% and in female it was 37.5%/62.5%.

The majority of the dissected samples, 58 (77.3%) hemifaces, belonged to the mesocephalic type (MCT). The brachycephalic type (BCT) was represented by 8 (10.7%) hemifaces and the dolichocephalic type (DCT) included 9 (12%) hemifaces. The ratio of the male/female hemifaces depending on the anthropometric type of the head for MCT was 81.3%/62.5%, for BCT — 6.8%/25% and for DCT — 11.9%/12.5%. The right/left ratio of samples in MCT was 77.2%/77.5%, in BCT — 11.4%/10% and in DCT — 11.4%/12.5%.

The branching patterns of the facial nerve were determined according to Davis classification [2]. In our study, each of those six classical patterns of branching had an atypical subtype, but type III had two atypical subtypes. For a relevant statistical analysis each atypical subtype was added to the corresponding classical type of branching and all the uncommon types were included into the "type NI" (non-identified in the specialised literature types).

The quantitative and qualitative variables were analysed using the Microsoft Excel 2016 processing programme and methods of descriptive and inferential statistics.

The indicators of variability were calculated using the following formulas:

1. Standard deviation (*s*): function STDEV

$$s = \sqrt{\frac{\sum(X_i - \bar{X})^2}{n-1}} \quad (1)$$

where: $\sum$ — sum; X_i — individual value of the X variable; $\bar{X}$ — arithmetic mean; n — number of cases.

2. Coefficient of variation (CV):

$$CV = \frac{s}{\bar{x}} \quad (2)$$

where: s — standard deviation; $\overline{X}$ — arithmetic mean; CV ≤ 10% homogenous population; 10% < CV ≤ 20% relatively homogenous population; 20% < CV ≤ 30% relatively heterogeneous population; 30% < CV heterogeneous population.

For the arithmetic mean of the quantitative variables the confidence interval (CI_{95}), with a safety level (p) of 0.95 and significance level (α) of 0.05 was calculated.

$$CI_{95} = \bar{X} \pm z \times SE \quad (3)$$

where: $\overline{X}$ — arithmetic mean; z — value for a confidence interval of 95% (equal to 1.96); SE — standard average error.

$$SE = \frac{s}{\sqrt{n}} \quad (4)$$

where: s — standard deviation; n — number of cases.

For that purpose the predefined Excel CONFIDENCE function was used, that determines the confidence interval $z \times SE$.

To compare the observed frequencies with the estimated frequencies the analysis of the qualitative variables frequency was performed using the non-parametric χ^2 test.

$$\chi^2 = \sum \frac{(f_o - f_e)^2}{f_e} \quad (5)$$

where: $\sum$ — sum; f_o — observed value; f_e — estimated value.

The measures of location were calculated using QUARTILE function: the first quartile (Q_1); the second quartile (Q_2); the third quartile (Q_3); the interquartile range (IQR): $Q_3 - Q_1$.

For distribution of the variables and symmetry measurement, the predefined Excel SKEW function was used.

$$\alpha = \frac{\sum_{i=1}^{n} \left(\frac{X_i - \bar{X}}{s}\right)^3}{n} \quad (6)$$

where: $\sum$ — sum; X_i — individual value of the X variable; $\overline{X}$ — arithmetic mean; s — standard deviation; n — number of cases; $\alpha = 0$ symmetric distribution; $\alpha < 0$ distribution with the tail to the right; $\alpha > 0$ distribution with the tail to the left.

In order to analyse the dispersion, the one-way ANOVA for comparing the means of three or more independent samples was used.

By the callipers were measured the length and width of the FNT and by a protractor was measured the degree of its bifurcation angle. All the measurement have been taken by the same observer.

Table 1. The mean values of the dimensions of the head depending on the gender

	Length of the head [mm]	Width of the head [mm]	Cephalic index
Male	195.5	150.3	76.9
Female	188.0	147.2	78.3
Difference	7.5	3.1	–1.4
P	0.000	0.001	0.004

Ethical consideration

The cadavers belonged to the Department of Anatomy and Clinical Anatomy of Nicolae Testemitanu State University of Medicine and Pharmacy of the Republic of Moldova.

The protocol for the research project has been approved by the Ethics Committee of Nicolae Testemitanu State University of Medicine and Pharmacy of the Republic of Moldova (minute No. 1 of 19.09.2014), and it was conducted at the Department of Anatomy and Clinical anatomy in full accordance with the Declaration of Helsinki.

RESULTS

The mean length (mm) of the heads for MCT was 194.21 ± 4.85, for BCT — 189.28 ± 4.42 and for DCT — 195.71 ± 4.01, statistically significant, p = 0.01.

In MCT the mean width (mm) of the heads was 149.91 ± 2.83, in BCT — 152.30 ± 3.22 and in DCT — 145.41 ± 3.00, highly statistically significant, p < 0.000.

The cephalic index in mesocephalic individuals had a mean value of 77.2097 ± 1.03, in brachycephalic people — 80.4674 ± 0.28 and in dolichocephalic ones — 74.3004 ± 0.53, and a very high statistical significance was established, p < 0.0000.

A significant difference in the mean values of the head dimensions depending on the gender was established for all the variables (Table 1).

Seven branching patterns of the facial nerve were established. Type I was determined in 18.7%, type II — 14.7%, type III — 20%, type IV — 14.6%, type V — 5.3%, type VI — 18.7%, and type NI — 8%. The male/female ratio of the branching pattern for type I was 20.3%/12.5%, type II — 10.2%/31.3%, type III — 23.7%/6.3%, type IV — 13.6%/18.8%, type V — 5.1%/6.3%, type VI — 16.9%/25.0% and type NI was present only in male with a rate of 10.2%, p = 0.48.

For our purpose, the extratemporal part of the facial nerve was divided into three segments: the premandibular (FNT and its primary divisions), intrap-

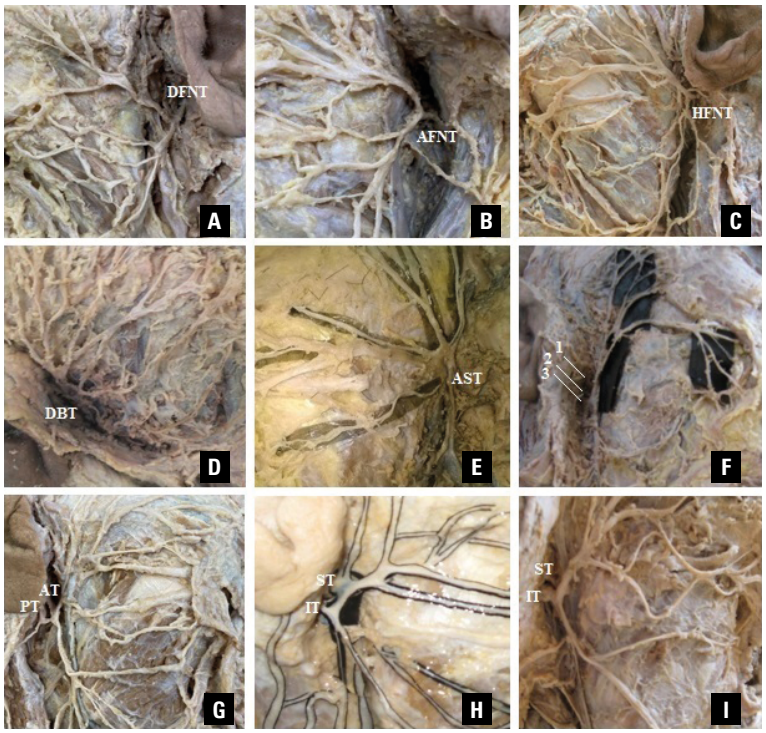

Figure 1. Morphological variability of the facial nerve trunk on the premandibular segment; **A.** Descending facial nerve trunk (DFNT); **B.** Ascending facial nerve trunk (AFNT); **C.** Horizontal facial nerve trunk (HFNT); **D.** Very short diffuse branching trunk (DBT); **E.** Arch-shaped trunk (AST); **F.** Triple trunk; 1 — superior trunk; 2 — middle trunk; 3 — inferior trunk; **G, H, I.** Double trunk; AT — anterior trunk; PT — posterior trunk; ST — superior trunk; IT — inferior trunk.

arotid (parotid plexus within the parotid gland) and postparotid (terminal divisions of the parotid plexus).

A range of peculiarities concerning FNT direction, number, length, width and angle of bifurcation were identified on the premandibular segment of the facial nerve.

Three main directions of the FNT were established: the descending, ascending and horizontal ones. The descending direction was marked out in 73.3%, the ascending one — in 9.3% and the horizontal — in 10.7%. Among the ascending FNT in 5.3% were determined very short diffuse branching trunks and in 1.3% an arch-shaped trunk was found (Fig. 1).

All the directions of the FNT were characteristic of both male and female. The descending FNT had a male/female ratio of 69.5%/87.4%, the ascending — 10.2%/6.3% and the horizontal one — 11.9%/6.3%. Number variants constituted 8.4% and were found only in male.

The right/left ratio of the descending FNT was 62.9%/82.5%; ascending — 11.4%/7.5%; horizontal — 11.4%/10%, and in 14.3%, only on the right hemifaces, were determined numerical variants.

Depending on the anthropometric type of the head, only in MCT were identified all the directions of the FNT. Thus, descending FNT was pointed out in 70.6%, and each of the ascending and horizontal positions were revealed in 12.1%. Numerical variants were found in 5.2% (Fig. 1).

In brachycephalic individuals only the descending direction of the FNT was established. In dolichocephalic individuals the descending FNT was present in 66.7% of cases, in 11.1% it had a horizontal position, and no ascending FNTs were found. Number variants were determined in 22.2%. The χ^2 test for FNT direction depending on the anthropometric type of the head was not statistically significant, $p = 0.25$.

The mean length of the FNT in male was 11.3 mm (5–21 mm) and in female — 10.4 mm (5–16 mm), $p = 0.289$. A similar mean length of 11.1 mm was determined for both right (5–18 mm) and left (5–21 mm) hemifaces, $p = 0.981$. In mesocephalic individuals the mean length (mm) of the FNT was 10.9 ± 2.87, in brachycephalic individuals — 12.3 ± 3.54 and in dolichocephalic ones — 10.9 ± 2.54, $p = 0.474$. The mean length (mm) of the FNT depending on the branching pattern for type I was 12.21 ± 3.33, type II — 11.00 ± 2.54, type III — 11.33 ± 2.93, type IV — 10.27 ± 3.85, type V — 11.50 ± 2.08, type VI — 10.07 ± 2.06 and type NI — 11.50 ± 3.11, $p = 0.578$.

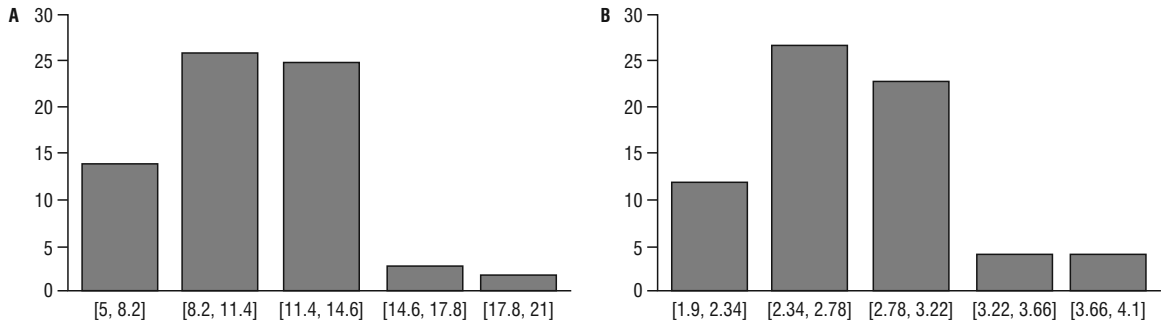

Figure 2. Curves of the central tendency and frequency distribution of the facial nerve trunk length (**A**) and width (**B**).

The mean width of the FNT was 2.7 mm for both male (1.9–4.1 mm) and female (1.9–3.8 mm) cadavers, p = 0.629. The same mean value of 2.7 mm of the FNT width was established for both right (1.9–4.0 mm) and left (1.9–4.1 mm) hemifaces, p = 0.868. The width of the FNT was variable depending on the anthropometric type of the head. In MCT the mean width (mm) was 2.75 ± 0.49, in BCT — 2.81 ± 0.42, and in DCT — 2.40 ± 0.24, p = 0.151. Depending on the branching pattern the mean width (mm) of the FNT varied as follows: type I — 2.71 ± 0.49, type II — 2.64 ± ± 0.37, type III — 2.70 ± 0.31, type IV — 2.82 ± 0.55, type V — 2.75 ± 0.34, type VI — 2.71 ± 0.57 and type NI — 2.95 ± 0.80, p = 0.950.

The curves of the central tendency and frequency of the FNT length and width distribution showed an asymmetry with the tail to the right (Fig. 2).

The mean value of the FNT bifurcation angle in male was 120.3° (40–180°) and in female — 142.7° (92–180°), statistically significant, p = 0.050. The right/left ratio of the mean bifurcation angle was 127.4° (40–180°)/121.2° (74–180°), p = 0.483. In MCT the bifurcation angle had a mean of 124.98° ± ± 34.17, in BCT — 119.14° ± 41.37, and in DCT — 123.89° ± 35.83, p = 0.919. The bifurcation angle was statistically significant depending on the branching pattern, p = 0.005 (Table 2).

The bifurcation of the FNT was determined in 84% of cases, the trifurcation in 6.6%, the quadrifurcation in 2.7%, the pentafurcation in 4%, and the hexafurcation in 2.7%. In all the cases of the FNT numerical variation, the trunks were connected to each other and then bifurcated.

The numerical variants of the FNT were represented by double trunk in 5.3% and triple trunk in 1.3% (Fig. 1). The mean value of the FNT number variation was 1.1 FNT, p = 0.261. On the right side the mean was 1.2 FNT, and on the left — 1.0 FNT, p = 0.019.

Table 2. Angle of the facial nerve trunk bifurcation depending on the facial nerve branching pattern

Type of branching	Mean value ± standard deviation [°]	Mean value ± 95% confidence interval [°]
Type I	103.7 ± 23.67	103.7 ± 13.39
Type II	156.8 ± 29.24	156.8 ± 17.28
Type III	125.4 ± 37.97	125.4 ± 21.49
Type IV	108.7 ± 25.78	108.7 ± 15.98
Type V	135.7 ± 22.50	135.7 ± 25.46
Type VI	118.5 ± 35.03	118.5 ± 20.70
Type NI	135.4 ± 36.16	135.4 ± 31.70

Depending on the anthropometrical type of the head the mean number of the FNT in MCT was 1.07 ± ± 0.32, in BCT — 1.00 ± 0.00, and in DCT — 1.22 ± ± 0.44, p = 0.311. Depending on the branching pattern the mean value of the FNT number for types I, IV, V and VI was 1.00 ± 0.00, and for the types II, III and type NI were established the following mean values: type II — 1.09 ± 0.30, type III — 1.20 ± 0.56, type NI — 1.33 ± 0.52, p = 0.192.

DISCUSSION

The majority of papers that concern the facial nerve branching pattern are based on 6 types reported by Davis et al. [2]. Nevertheless, the branching pattern of the facial nerve includes a wider range of variation, thus, Pitanguy et al. [14] and Stankevicius et al. [18] have identified 8 branching patterns, 11 types were described by Kopuz et al. [8] and 12 types were established by Martínez Pascual et al. [10]. In the current study 14 types were determined, including atypical ones, initially classified as intermediate types [1], but finally redistributed and reclassified into 7 types.

Three main directions of the FNT were established in the current study and according to our observation

they depended on variation of the mastoid segment of the facial canal, but it is not excluded, that those variants may even depend on variability of the stylomastoid foramen [5].

According to different sources, the length of the FNT is variable, thus, Wilhelmi et al. [20] reported a length between 5–15 mm, Kwak et al. [9] — 13.0 ± ± 2.8 mm, Khoa et al. [7] — 14.1 mm, Salame et al. [16] — 16.44 ± 3.2 mm, and the highest mean value of 17.0 ± 4.54 mm was established by Pacheco-Ojeda et al. [13]. In our study the mean length of the FNT was 11.1 ± 0.7 mm.

The width of the FNT is also variable. According to Martínez Pascual et al. [10] the width is 2.16 ± ± 0.49 mm, Khoa et al. [7] reported 2.5 mm and Salame et al. [16] 2.66 ± 0.55 mm. In the current study the mean width was 2.7 ± 0.1 mm.

Usually the FNT bifurcates into the temporofacial and the cervicofacial divisions [6, 10, 17]. Khoa et al. [7] obtained an angle of the FNT bifurcation of 91.2°. In our study the mean value in male was 120.3° and in female 142.7°, $p = 0.050$.

In some cases a trifurcation, or even multifurcation of the FNT is found [7–9, 12, 18, 19]. The reported incidence of the FNT bifurcation is about 80%, the trifurcation — 14% and numerical variants are found in 6% of cases [8, 18, 19]. In the current study the bifurcation of the FNT was established in 84% of cases (including 6.7% of number variation), trifurcation was established in 6.6% and multifurcation in 9.4% of cases. In cases of the facial canal dehiscence a double or triple FNT is present [8, 15, 19].

CONCLUSIONS

Three directions were characteristic of the FNT: descending, ascending and horizontal ones. The descending FNT prevailed in female with a male/female ratio of 0.79:1. The ascending and horizontal directions of the FNT were higher in male individuals. For the ascending FNT the male/female ratio was 1.62:1, and for the horizontal one — 1.89:1. The highest rate of the FNT direction variability was characteristic of MCT and the lowest one for BCT. The descending FNT prevailed in all the anthropometric types. The length of the FNT was variable on all the examined criteria. The width of the FNT was the same for both genders and both sides of the head, but variable depending on the anthropometric type of the head and branching pattern. The angle of bifurcation was higher in female cadavers; on the right hemifaces; in MCT and in individuals with type II branching pattern. The numerical variants were found only in male cadavers and only on the right hemifaces, but they were variable dependent on the anthropometric type of the head and pattern of branching.

Conflict of interest: None declared

REFERENCES

1. Babuci A. Types of extracranial branching of the facial nerve. Moldovan Med J. 2019; 62(1): 41–44, doi: 10.5281/zenodo.2590015.
2. Davis RA, Anson BJ, Budinger JM, et al. Surgical anatomy of the facial nerve and parotid gland based upon a study of 350 cervicofacial halves. Surg Gynecol Obstet. 1956; 102(4): 385–412, indexed in Pubmed: 13311719.
3. Farooq A, Muhammed EH, Riaz A, et al. Facial nerve; pattern of distribution in the parotid gland. Professional Med J. 2005; 12(1): 85–90.
4. Gataa IS, Faris BJ. Patterns and surgical significance of facial nerve branching within the parotid gland in 43 cases. Oral Maxillofac Surg. 2016; 20(2): 161–165, doi: 10.1007/s10006-015-0543-0, indexed in Pubmed: 26750137.
5. Ghosh SK, Narayan RK, et al. Variations in the morphology of stylomastoid foramen: a possible solution to the conundrum of unexplained cases of Bell's palsy. Folia Morphol. 2021; 80(1): 97–105, doi: 10.5603/FM.a2020.0019, indexed in Pubmed: 32073133.
6. Katz AD, Catalano P. The clinical significance of the various anastomotic branches of the facial nerve. Report of 100 patients. Arch Otolaryngol Head Neck Surg. 1987; 113(9): 959–962, doi: 10.1001/archotol.1987.01860090057019, indexed in Pubmed: 3606847.
7. Khoa TD, Bac ND, Luong HV, et al. Anatomical characteristics of facial nerve trunk in vietnamese adult cadavers. Open Access Maced J Med Sci. 2019; 7(24): 4230–4238, doi: 10.3889/oamjms.2019.366, indexed in Pubmed: 32215069.
8. Kopuz C, Turgut S, Yavuz S, et al. Distribution of facial nerve in parotid gland: analysis of 50 cases. Okajimas Folia Anat Jpn. 1994; 70(6): 295–299, doi: 10.2535/ofaj1936.70.6_295, indexed in Pubmed: 8041565.
9. Kwak HH, Park HD, Youn KH, et al. Branching patterns of the facial nerve and its communication with the auriculotemporal nerve. Surg Radiol Anat. 2004; 26(6): 494–500, doi: 10.1007/s00276-004-0259-6, indexed in Pubmed: 15368081.
10. Martínez Pascual P, Maranillo E, Vázquez T, et al. Extracranial course of the facial nerve revisited. Anat Rec (Hoboken). 2019; 302(4): 599–608, doi: 10.1002/ar.23825, indexed in Pubmed: 29659175.
11. Myint K, Azian AL, Khairul FA. The clinical significance of the branching pattern of the facial nerve in Malaysian subjects. Med J Malaysia. 1992; 47(2): 114–121, indexed in Pubmed: 1494331.
12. Naidu L, Rennie CO. The extracranial course of the facial nerve and bony anatomical landmarks for localization of the facial nerve trunk during parotidectomies. Eur J Anat. 2020; 24(1): 37–48.

13. Pacheco-Ojeda L, Moncayo-Young V, Merlo-Cifuentes F, et al. Anatomic patterns of the facial nerve in parotidectomized patients. Am J Otolaryngol Head Neck Surg. 2021; 4(6): 1143.
14. Pitanguy I, Ramos AS. The frontal branch of the facial nerve: the importance of its variations in face lifting. Plast Reconstr Surg. 1966; 38(4): 352–356, doi: 10.1097/00006534-196610000-00010, indexed in Pubmed: 5926990.
15. Rajeshwary A, Goutham MK, Somayaji KS. Dehiscent mastoid segment of the facial nerve. Arch Med Health Sci. 2018; 6: 187–188.
16. Salame K, Ouaknine GER, Arensburg B, et al. Microsurgical anatomy of the facial nerve trunk. Clin Anat. 2002; 15(2): 93–99, doi: 10.1002/ca.1102, indexed in Pubmed: 11877786.
17. Sargon MF, Ogretmenoglu O, Gunenc Beser C, et al. Quantitative analysis of the terminal branches of facial nerve in fresh frozen head and neck specimens. Folia Morphol. 2014; 73(1): 24–29, doi: 10.5603/FM.2014.0004, indexed in Pubmed: 24590519.
18. Stankevicius D, Suchomlinov A. Variations in facial nerve branches and anatomical landmarks for its trunk identification: a pilot cadaveric study in the lithuanian population. Cureus. 2019; 11(11): e6100, doi: 10.7759/cureus.6100, indexed in Pubmed: 31886041.
19. Thuku FM, Butt F, Guthua SW. An anatomic study of the facial nerve trunk and branching pattern in an African population. CMTR Open. 2018; 02(01): e31–e37, doi: 10.1055/s-0038-1669465.
20. Wilhelmi BJ, Mowlavi A, Neumeister MW. The safe face lift with bony anatomic landmarks to elevate the SMAS. Plast Reconstr Surg. 2003; 111(5): 1723–1726, doi: 10.1097/01.PRS.0000054237.81611.D8, indexed in Pubmed: 12655222.

VIA MEDICA

ORIGINAL ARTICLE

Folia Morphol.
Vol. 82, No. 4, pp. 798–804
DOI: 10.5603/FM.a2022.0099

ISSN 0015–5659
eISSN 1644–3284
journals.viamedica.pl

Different types of visual cells in the photoreceptor layer of the retinae of the treeshrew (Tupaia belangeri chinensis) as revealed by scanning microscopy

R.S.Y. Cheng[1], M.S.M. Wai[2], G.C.T. Leung[1, 3], T.C.H. Chow[1, 3], W.W. Sze-To[1], D.T. Yew[1, 2, 3]

[1]*School of Chinese Medicine, The Chinese University of Hong Kong, Shatin, Hong Kong*
[2]*School of Biomedical Science, The Chinese University of Hong Kong, Shatin, Hong Kong*
[3]*Hong Kong College of Technology, Shatin, Hong Kong*

[Received: 2 January 2022; Accepted: 3 May 2022; Early publication date: 29 November 2022]

Background: *The retinae of treeshrew have never been evaluated by scanning electron microscopic studies.*
Materials and methods: *This work described the visual cells in the photoreceptor layer of the retinae of treeshrew (Tupaia belangeri chinensis) living on the high plateau of Yunnan, China, via scanning electron microscopy.*
Results: *Results indicated five morphologically different types of cones, two of which contain oil droplets in their inner segments. To our knowledge, no prior studies have reported oil droplets in the visual cells of higher mammals, only in lower vertebrate and primitive mammals. In addition, this study revealed one type of degenerative visual cell without outer segments.*
Conclusions: *The findings signal the needs for additional studies to understand the physiological functions and phylogenetic relationships of the diversity of visual cells in this group of mammal.* (Folia Morphol 2023; 82, 4: 798–804)

Key words: retina, Tupaia belangeri, treeshrew, cones, rods, scanning electron microscopy

INTRODUCTION

Treeshrews are small mammals found widely across Southeast Asia, including Malaysia, Singapore, Thailand, Indonesia, and the Yunnan Province of China. The animal was first discovered in 1820 by two French zoologists, Diad and Duvancel. To date, scientists have classified the animal into two families (Tupaiinae and Ptilocercinae) under the order Scandentia. The genus *Tupaia* is the largest group of all and contains the highest number of species found. Two common species known in this group are *Tupaia glis* and *Tupaia belangeri*. Most of the discovered *Tupaia* treeshrews are diurnal animals with only the *Ptilocercus* species being nocturnal. Some treeshrews are arboreal [13], and they usually live on small trees that allow them to leap from one tree to another. Treeshrews, being omnivorous [5], obtain nutrients from juicy fruits, seeds, and insects. They have an average life-span of 12 years, just like pet dogs.

Treeshrews were initially classified as insectivores pre-1966, but they were later grouped under the order of primate, then under scandentia [19]. Hasler and Sorenson (1974) [5] conducted a behavioural study on *Tupaia chinensis* and reported high activities of these

Address for correspondence: Dr. D.T. Yew, Room 101, Li Wai Chun Building, Chung Chi College, The Chinese University of Hong Kong, Hong Kong; tel: (852) 39434140, e-mail: david-yew@cuhk.edu.hk

animals are found between 07:00 and 17:00 of the day. They spend most of their time on trees and move around by hopping. Tate (1947) [22] reported these animals usually stayed at altitudes of 1500–8000 ft., while spending half of their time searching for food in summer. In general, treeshrews rely on their vision more than olfaction [5].

The eyes of the treeshrews have been studied for almost half a century. The retinae of the *Tupaia* species have more cones with 4–5% rods [7], while the *Ptilocercus spp.,* being nocturnal animals, might have retinae consisted mainly of rods. Either way, documented by a study performing fundoscopy on *Tupaia glis* [19], no macula was found in the retinae of these animals.

Müller and Peichl (1993) [14] studied the retinae in whole mount and semi-thin sections, they later concluded that the cones in the treeshrew retinae were 2 to 10 times the numbers of rods in the retinae. Electron microscopic studies on the visual cells demonstrated that the cone cells had large and round groups of mitochondria at the apex of the inner segments (i.e. the apex of the ellipsoid region), which was termed as the "lens mitochondria" [9]. In fact, large number of mitochondria spread all the way downwards to the lower regions of the inner segments of cones, where they formed again dilated regions at the bases of these inner segments [9]. Recently, the treeshrews have been introduced as a model for myopic research [2].

Looking at other parts of the visual system in treeshrews, Campbell (1966) reported cross and uncross nerve fibres in the optic nerve of the *Tupaia spp.* [1]. In the lateral geniculate bodies, lamination was demonstrated in *Tupaia spp.* [1], while no lamination was observed in the nocturnal species of *Ptilocercus spp.* [20].

Despite the above findings, the different types of visual cells with different three-dimensional morphologies in the retinae of the treeshrews had never been recorded in the literature. Thus, we report here the different morphologies of various types of visual cells in the photoreceptor layer of the retinae of *Tupaia chinensis* observed under scanning electron microscopy.

MATERIALS AND METHODS

Animals and treatment

Five young adult treeshrews of the species *Tupaia chinensis* of an average of 4 inches in length (not including tails) were reared in the animal house of Yunnan Medical University. Unfortunately, these animals did not survive in long captivity and the brains and eyes were given to us in fixation upon death of the animals. The study was approved by the Research Coordination and Development Committee of the Hong Kong College of Technology, Shatin, New Territories, Hong Kong.

Tissue preparation for scanning electron microscopy

The retinae were fixed in 2.5% glutaraldehyde buffered at pH 7.4 in 0.1 M Sorensen's phosphate solution for 1 day. The eyes were bisected into anterior and posterior halves. The posterior halves with retinae were then washed in 0.1 M Sorensen's buffer at pH 7.4 for 3 times, 10 mins each. 1% aqueous osmium tetroxide was used to post-fix the tissues for 2 hours. The tissues were rinsed again with 0.1 M Sorensen's buffer (pH 7.4) for 3 times, 10 mins each. Afterwards, the tissues were dehydrated in graded ethanol for 5 mins of different concentration. Drying of the tissues was done with a Ladd critical point dryer (40°C, 1300 psi), using liquid CO_2 as the drying agent, and followed by cooling. The retinal layer with the pigment epithelium were mounted on a copper stub with double-sided sticky tape, followed by gold palladium coating in a sputter coater (Edwards S150B Sputter Coater). The retinae were ready for scanning under electron microscopic examination (JEOL JSM 6301F, Japan).

For semi-morphometry, the retinae of three animals were divided in to three equal sections, namely the central, the midperiphery, and the periphery regions. The central region was adjacent and nearest to the optic nerve as the retina had no macula. The periphery region was adjacent to the limbus. The region in between the central and periphery region was termed as midperiphery. After treatment of the retinae for scanning microscopy, three random areas of size 100 μm^2 were taken from each region of each animal; and the numbers of rod cells observed under the scanning electron microscopy were expressed as a percentage of the numbers of total photoreceptors in those areas for each region. Statistical analysis was conducted using Prism 6 (GraphPad Software, USA). Comparison of means was performed using one-way ANOVA and post-hoc Tukey's test. P-values of < 0.05 were considered statistically significant (Table 1).

Table 1. Measurement (ANOVA). Total percentage of rod cells in respective areas of the retina

ANOVA table	SS	DF	MS	F (DFn, DFd)	P value
Treatment (between columns)	1.540	2	0.7701	F (2, 24) = 209.2	< 0.0001
Residual (within columns)	0.08835	24	0.003681		
Total	1.629	26			

DF — degress of freedom; MS — mean squares; SS — sum-of-squares

RESULTS

General remarks

General morphological survey. The retinae of the treeshrews had closely aligned visual cells. Scanning electron microscopy indicated clusters of retinal pigment epithelial cells as well as clusters of phagosomes in the ventricular space amongst the visual cells of the photoreceptor layer (Fig. 1). There were more cone cells found in the central region of the retinae than rod cells (Fig. 2), with some of the cones tightly packed together (Fig. 2). From the midperiphery onwards to the periphery region, increasing rod cells was observed. Rods were not found to be in small quantity in the species of *Tupaia chinensis* studied by us.

Specific visual cells

The *Tupaia* treeshrews' retinae had slender and elongated rods with the outer and inner segments as roughly the same diameter under the coronal view (Fig. 3). The outer segment of the rods were of 1–1.5 μm in diameter and the inner segments were about 1 μm in diameter. In the dark-adapted retinae, the longest outer segment observed in rod cells was more than 10 μm. Sometimes, the tips of the outer segments of rods could be inclined at an angle (Fig. 3).

There were at least five morphologically different cone cells found in the treeshrews. The first type of cones (cone A) (Fig. 4A) had an inner segment of 4–5 μm in length; with a long ciliary stalk, reaching the length of 1–2 μm, and attaching to the outer segment. In rare cases, the ciliary stalk looked bifurcated (Fig. 4A). The outer segments of cone A were blade-shaped structures with average of 2.5–4 μm in length and diameter up to 1 μm (Fig. 4A).

The second type of cones (cone B) were of two types (B1 and B2). B2 outer segments were generally conical in shape and had short inner segments at an average of less than 4 μm in height with a short

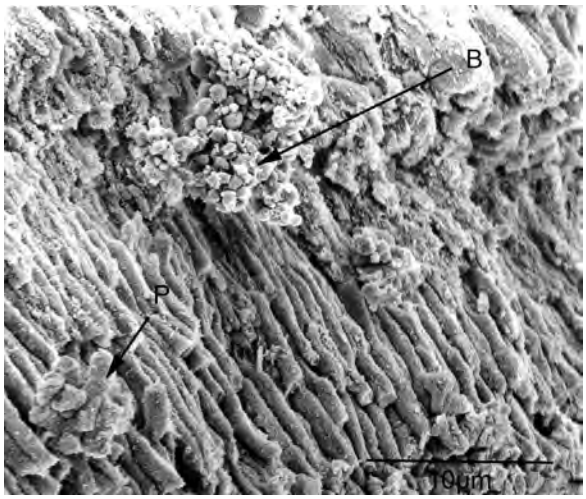

Figure 1. Central retinae of treeshrew. P denotes phagosome and B denotes a cluster of pigments. Scale bar is 10 μm.

Figure 2. Central areas of the retinae displayed many different cones (C1–C5). C2 was shorter in length. Rods (R) were few. Scale bar is 10 μm.

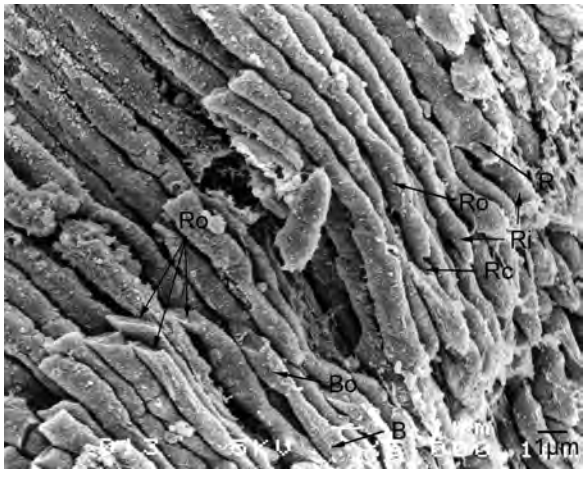

Figure 3. Treeshrews' retinae indicating a rod (R), rod outer segments (Ro), a rod inner segment (Ri). B denotes a type B1 cone and B0 denotes its conical outer segment. Very short cilium (if any) was seen between outer and inner segment of this type of cone. Scale bar is 1 μm.

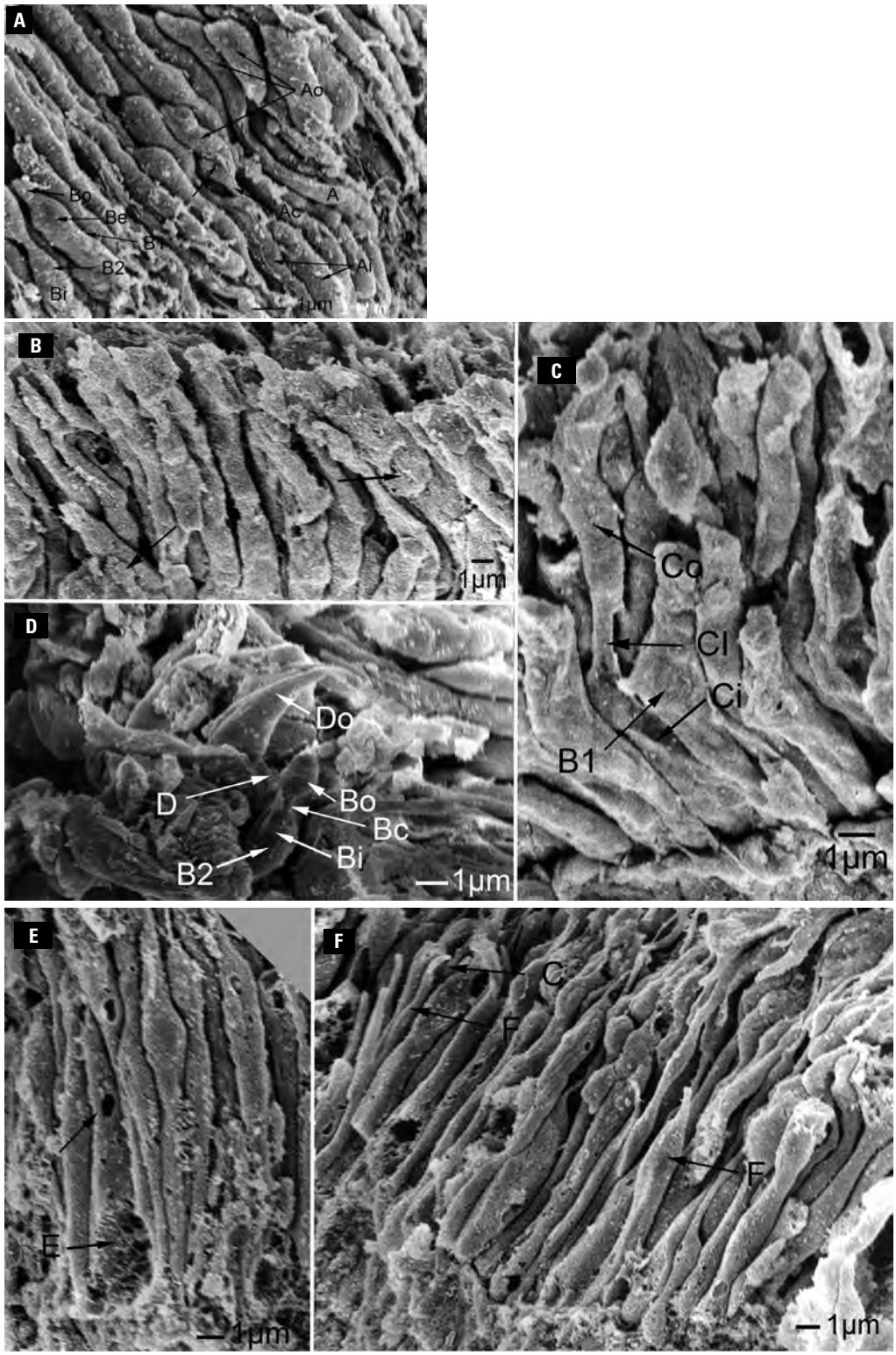

Figure 4. A. Cone types A and B. In cone A, Ao indicates blade-like outer segments, Ai denotes an inner segments and Ac denotes a cilium. An arrow shows possible bifurcation. Bo denotes outer segment tip of a B1 cone, and Be indicates ellipsoid region of the cone B1. Bi indicates thick inner segment of a cone B2. There were two types of B cones, namely B1 and B2. B1 contains unapparent cilia between outer and inner segments while B2 contains very short cilia. Scale bar 1 μm; **B.** Arrows indicate oil droplets in cone B. Scale bar 1 μm; **C.** Treeshrews' retinae showing an inner segment (Ci) and an outer segment (Co) of cone C. Cone Cs were usually longer and slender with a long cilium (Cl). B1 indicates B1 cones with large ellipsoid in inner segment. Scale bar 1 μm; **D.** B2 is a small cone with a short cilium (Bc). Bi denotes the inner segment and Bo indicates conical outer segment. D is a large hook-like outer segment of cone D, which contains a bulging and short inner segment. Scale bar 1 μm; **E.** A cone E with dilated inner segment at base and an oil droplet at top of inner segment (arrow). Scale bar 1 μm; **F.** A possibly degenerating cone F (F) with straight or hook like cilium (C) and no outer segment. Scale bar 1 μm.

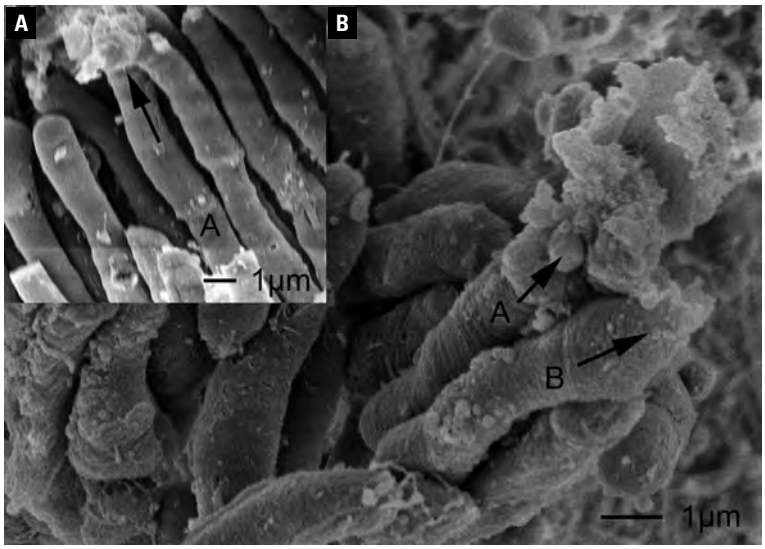

Figure 5. Outer segment shedding in rod A (**A**) and cone B (**B**). When plasma membrane ruptures, globular phagosomes (arrows) are generated. Scale bar 1 μm.

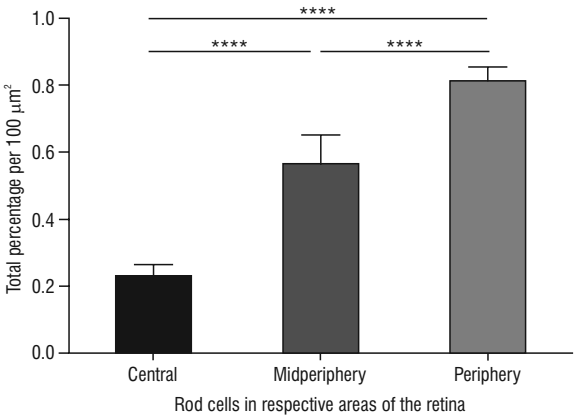

Figure 6. Relative proportion of rods (in density) in the three regions of the retinae; **** denotes $p \leq 0.0001$.

0.5 μm diameter (Fig. 4A). Cone B1 was slenderer (B1) (Fig. 4A) and had a relatively dilated distal tip (the ellipsoid) of the inner segments (Figs. 4A, C), while some B1 cones had oil droplets (Fig. 4B). All B1 cones had no significant cilia (Figs. 4A–C). The ellipsoids housing the oil droplets contained the lens' mitochondria below as described in the literature [15]. Cones B1 and B2 in many retinae were often seen in close proximity.

The third type of cones (cone C) had a long and strong cilium of 1.5–2 μm long in coronal view, extending from the 4 μm tall inner segment (Fig. 4E). Very few cone Cs had distally expanded inner segments (Fig. 4C).

Cone Ds had round bodies of inner segments averaged 4 μm in length with curved outer segments of 4 μm in length that appeared to be continuous (Fig. 4D). The outer segment, when magnified, appeared as a cutting curved blade of a farmer's knife (Fig. 4D). The base of the blade, at average, was about 2.5 μm in diameter with a tip of about 0.25 μm.

Apart from the forementioned types of cones, there was another type of cone with a broad and large proximal base of inner segment, which we named as cone E (Fig. 4E). These cones also had globular oil droplets (Fig. 4E).

Occasionally, long slender inner segments ending with cilia were also observed. As there was no obvious outer segment seen in this type of cone cell, we named it as immature or degenerative cones F (Fig. 4F). Although labelled as a cone, it was also possible that it was a degenerating rod. Shedding of the tips of normal rods and cones at the outer segments was observed, resulting in the globular phagosomes in both cases (Fig. 5A, B).

Our morphometric studies revealed fewer number of rod cells found in the central region than the midperiphery and the periphery regions. The amount of rod cells observed were, however, not as few as those reported earlier ($p < 0.05$; Fig. 6) [7, 11, 14]. A lot of the previous studies conducted their observations with transmission electron microscopy or with histology, thus the lack of three-dimensional morphology hampered the identification of visual cell types.

DISCUSSION

Samorajski et al. (1966) [19] studied retinae of *Tupaia glis*, using electron microscopy and histology. The team reported the absence of macula in *Tupaia glis*, and the presence of both large and small sized cones together with rods in the retinae, with the latter at the periphery. Van Dongen et al. (1976) [23] also reported a higher proportion of cone cells among visual cells observed in the retinae of treeshrews. Kuhne (1983) [11] concluded there were only 5 rod cells in the retinae among hundreds of cone cells. Later, Immel and Fisher (1985) [7] reported 5% of rod cells in the retinae. In our study, more rods are demonstrated compared to those previous findings in the literature, though the rods were mostly in the periphery, they were not so few in number [23].

We unveiled the various types of morphologically diversified cones in the treeshrews' retinae. Mosaic of cones were recognized in these animals by modern technique using optical coherence tomography [18]. Cone A were found to dominate the central retinae where rods were rarely seen. This cone type contains a blade-shaped outer segment, which connects to the inner segment with a long cilium. Cone B was with the classical conical-shaped outer segments, which appeared to coincide in shape with the red spectrum cones suggested by Müller and Peichl (1989) [15] in their transmission electron microscopy study. Two types of B cones were discovered, B2 had short cilia while B1 had no visible cilia between the outer and inner segments. B1 contained an oil droplet inside the ellipsoid of the inner segment. The other two types of cones (cone C and E) were different in shape, with cone C being slender and with a long cilium, while cone E had a broad-based inner segment. As cones A were found to be abundant in the treeshrews studied here and considering treeshrews being active under the sun in high plateau areas, these cone As may be related to the yellow spectrum of vision. The other three types of cones, B, C and E, were probably related to the two remaining light spectra of blue and green wavelengths documented in the literature [9, 15]. The oil droplet found in cone E and B1 might act as filters for certain wavelengths similar to those found in chickens [24]. Since the blue spectrum is near to the ultraviolet spectrum, it is likely that those cones are located in the peripheral retina. Cone D, with the presence of hook-like outer segments, had never been reported in vertebrates. Finally, cone F visual cells had a cilium and no outer segment, and were speculated to be vestigial or degenerating structures. Developmental defects in the retinae have been documented in cave animals and nocturnal animals, such as fish and serpent snake [6, 8, 12], or in degenerative cones that have lost their outer segments [25]. Considering the extrusion of cell bodies into the interreceptor matrix in the eyes of these animals (unpublished histological observation) and that the habitat of these animals is on the highland exposed to bright sunlight and ultraviolet radiation, some retinal degeneration is possible. Intense light causing retinal degeneration in addition to lens degeneration had been documented in the rodents [3]. One of the moves treeshrews took to protect themselves from light damage is the choice to live on short trees and branches rather than on the top of tall trees. The treeshrews, once were termed as a primitive "primate", deserved to be investigated further for its evolutionary and biological values.

The various cone cells reported in treeshrews in this study are similar to those found in lower vertebrates, e.g. fish, turtle [10, 17], birds [4, 24] and in primitive mammals like platypus [16] but not in monotremal anteaters [26], in that some of their cones displayed oil droplets. Oil droplets could act as microlens for spectral filtering [21]. As far as these were concern, retinae in treeshrews retained primitive features not found in most mammals.

CONCLUSIONS

In here, we were able to distinguish various novel types of cone cells by scanning electron microscopy in the photoreceptor layer of the treeshrews' retinae. The differences in physiology of each cone cell type should be taken into further studies and hopefully the phylogenetic position of the treeshrew could also be further evaluated.

Conflict of interest: None declared

REFERENCES

1. Campbell CB. Taxonomic status of tree shrews. Science. 1966; 153(3734): 436, doi: 10.1126/science.153.3734.436, indexed in Pubmed: 5943534.
2. Cao J, Yang EB, Su JJ, et al. The tree shrews: adjuncts and alternatives to primates as models for biomedical research. J Med Primatol. 2003; 32(3): 123–130, doi: 10.1034/j.1600-0684.2003.00022.x, indexed in Pubmed: 12823622.
3. Duncan JL, LaVail MM. Intense cyclic light-induced retinal degeneration in rats. Arch Ophthalmol. 2010; 128(2): 244–245, doi: 10.1001/archophthalmol.2009.399, indexed in Pubmed: 20142550.

4. Fang M, Li J, Wai SM, et al. Retinal twin cones or retinal double cones in fish: misnomer or different morphological forms? Int J Neurosci. 2009; 115(7): 981–987, doi: 10.1080/00207450590901422.
5. Hasler J, Sorenson MW. Behavior of the tree shrew, Tupaia chinensis, in captivity. Am Midland Naturalist. 1974; 91(2): 294, doi: 10.2307/2424324.
6. Hibbard E, Lavergne J. Morphology of the retina of the sea-snake, Pelamis platurus. J Anat. 1972; 112(Pt 1): 125–136, indexed in Pubmed: 4343745.
7. Immel JH, Fisher SK. Cone photoreceptor shedding in the tree shrew (Tupaia belangerii). Cell Tissue Res. 1985; 239(3): 667–675, doi: 10.1007/BF00219247, indexed in Pubmed: 3986885.
8. Jeffery WR. Cavefish as a model system in evolutionary developmental biology. Dev Biol. 2001; 231(1): 1–12, doi: 10.1006/dbio.2000.0121, indexed in Pubmed: 11180948.
9. Knabe W, Skatchkov S, Kuhn HJ. "Lens mitochondria" in the retinal cones of the tree-shrew Tupaia belangeri. Vision Res. 1997; 37(3): 267–271, doi: 10.1016/s0042-6989(96)00199-x, indexed in Pubmed: 9135860.
10. Kolb H, Jones J. The distinction by light and electron microscopy of two types of cone containing colorless oil droplets in the retina of the turtle. Vision Res. 1987; 27(9): 1445–1458, doi: 10.1016/0042-6989(87)90154-4, indexed in Pubmed: 3445479.
11. Kühne JH. Rod receptors in the retina of Tupaia belangeri. Anat Embryol (Berl). 1983; 167(1): 95–102, doi: 10.1007/BF00304603, indexed in Pubmed: 6881545.
12. Malonza PK, Granthon C, Williams DA. A new species of dwarf gecko in the genus Lygodactylus (squamata: Gekkonidae) from central Kenya. Zootaxa. 2016; 4061(4): 418–428, doi: 10.11646/zootaxa.4061.4.6, indexed in Pubmed: 27395510.
13. Martin RD. Primate origins and evolution. Chapman and Hall 1990.
14. Müller B, Peichl L. Horizontal cells in the cone-dominated tree shrew retina: morphology, photoreceptor contacts, and topographical distribution. J Neurosci. 1993; 13(8): 3628–3646, doi: 10.1523/JNEUROSCI.13-08-03628.1993, indexed in Pubmed: 7688042.
15. Müller B, Peichl L. Topography of cones and rods in the tree shrew retina. J Comp Neurol. 1989; 282(4): 581–594, doi: 10.1002/cne.902820409, indexed in Pubmed: 2723153.
16. O'Day K. The visual cells of the platypus (ornithorhyncus). Br J Ophthalmol. 1938; 22(6): 321–328, doi: 10.1136/bjo.22.6.321, indexed in Pubmed: 18169535.
17. Ohtsuka T. Relation of spectral types to oil droplets in cones of turtle retina. Science. 1985; 229(4716): 874–877, doi: 10.1126/science.4023716, indexed in Pubmed: 4023716.
18. Sajdak BS, Salmon AE, Cava JA, et al. Noninvasive imaging of the tree shrew eye: Wavefront analysis and retinal imaging with correlative histology. Exp Eye Res. 2019; 185: 107683, doi: 10.1016/j.exer.2019.05.023, indexed in Pubmed: 31158381.
19. Samorajski T, Ordy JM, Keefe JR. Structural organization of the retina in the tree shrew (Tupaia glis). J Cell Biol. 1966; 28(3): 489–504, doi: 10.1083/jcb.28.3.489, indexed in Pubmed: 5960809.
20. Simmons RM. "The diencephalon of Ptilocercus lowii (pen-tailed tree-shrew)". J Hirnforsch. 1979; 20(1): 69–92, indexed in Pubmed: 113455.
21. Stavenga DG, Wilts BD. Oil droplets of bird eyes: microlenses acting as spectral filters. Philos Trans R Soc Lond B Biol Sci. 2014; 369(1636): 20130041, doi: 10.1098/rstb.2013.0041, indexed in Pubmed: 24395968.
22. Tate GHH. Mammals of Eastern Asia. The Macmillan Company, New York, 1947, doi: 10.5962/bhl.title.6397.
23. Van Dongen PA, Ter Laak HJ, Thijssen JM, et al. Functional classification of cells in the optic tract of a tree shrew (Tupaia chinensis). Exp Brain Res. 1976; 24(4): 441–446, doi: 10.1007/BF00235010, indexed in Pubmed: 816664.
24. Wai MS, Lorke DE, Kung LS, et al. Morphogenesis of the different types of photoreceptors of the chicken (Gallus domesticus) retina and the effect of amblyopia in neonatal chicken. Microsc Res Tech. 2006; 69(2): 99–107, doi: 10.1002/jemt.20279, indexed in Pubmed: 16456833.
25. Yew DT, Li WW, Au C, et al. Retinal changes in a mutant form of goldfish with megalophthalmia. Scanning Microsc. 1991; 5(2): 585–594.
26. Young HM, Pettigrew JD. Cone photoreceptors lacking oil droplets in the retina of the echidna, Tachyglossus aculeatus (Monotremata). Vis Neurosci. 1991; 6(5): 409–420, doi: 10.1017/s0952523800001279, indexed in Pubmed: 2069895.

VIA MEDICA

ORIGINAL ARTICLE

Folia Morphol.
Vol. 82, No. 4, pp. 805–813
DOI: 10.5603/FM.a2022.0106

ISSN 0015–5659
eISSN 1644–3284
journals.viamedica.pl

Microsurgical anatomy of the cavernous sinus and limitations of surgical approaches: a cadaveric study

H. Kına[1], A. Ayran[2], İ. Demirtaş[2]

[1]*Department of Neurosurgery, Istinye University Medical Park Gaziosmanpasa Hospital, Gaziosmanpaşa, Istanbul, Turkey*
[2]*Department of Anatomy, School of Medicine, Istinye University, Zeytinburnu, Istanbul, Turkey*

[Received: 1 September 2022; Accepted: 16 October 2022; Early publication date: 22 December 2022]

Background: *The endoscopic endonasal approach is common in the treatment of pathologies in and around the cavernous sinus. This cadaveric study aims to examine the anatomy of the cavernous sinus to guide endoscopic studies and determine points to consider during surgical approaches.*

Materials and methods: *For this study, a total of 7 cadavers, 4 male and 3 female, were injected with coloured silicone and dissections were performed under the microscope. The characteristics of the surgical corridors encountered during the transsphenoidal, transsellar and transcavernous approaches were examined and their images were recorded.*

Results: *The stages and limitations of surgical approaches to the cavernous sinus in cadavers are presented. The anatomical features of the triangles defined in the cavernous sinus and the structures they contain are explained. It was determined that the surgical field formed by clinoidal and anteromedial triangles could be used effectively to reach cavernous sinus pathologies during endoscopic endonasal interventions. It was also observed that supratrochlear and infratrochlear triangles are dangerous for such surgical interventions.*

Conclusions: *The detailed anatomical features related to the cavernous sinus, revealed in our cadaveric study, are valuable in terms of preventing complications that may occur during surgical interventions.* (Folia Morphol 2023; 82, 4: 805–813)

Key words: cadaver, endoscopic endonasal, transcavernous approach, transsphenoidal surgery, cranial nerves, internal carotid artery

INTRODUCTION

The cavernous sinus (CS) has a complex anatomical structure and contains many important neurovascular structures. In addition to the venous vascular network, the internal carotid artery (ICA) and abducens nerve pass through the CS, which has four walls surrounded by the dura mater. Its lateral wall, from top to bottom, contains oculomotor, trochlear, ophthalmic and maxillary nerves [2]. Its medial wall is adjacent to the sella turcica and the sphenoidal sinus [30]. All these structures are at risk of being damaged during surgical procedures involving the CS and surrounding areas [19, 28].

Cavernous sinus was considered a "no man's land" for many years until Parkinson (1965) performed a microsurgical approach to this area in 1965 and explained its surgical anatomy [24]. Repeated surgical interventions over the years have demonstrated that

Address for correspondence: Assistant Professor İ. Demirtaş, İstinye Üniversitesi Topkapı Kampüsü, Maltepe Mah., Teyyareci Sami Sk., No. 3 Zeytinburnu, İstanbul, Turkey 34010, tel: +90 850 283 60 00, e-mail: ismetdemirtas21@gmail.com

the CS and its surroundings are surgically accessible. However, it has been reported that transcranial methods cause damage to important neurovascular structures. Since this method has a high morbidity rate, it has been avoided by surgeons over time [9].

Various endoscopic endonasal methods have been described in the last 30 years and these methods have begun to replace the open surgical approach [14]. The development of transsphenoidal and transmaxillary endoscopic techniques has made safe access to many parts of the CS possible. The identification of different surgical corridors in the studies [6, 8, 18, 27, 32] provided endoscopic access to CS and its surroundings.

Widespread application of the transcavernous approach by surgeons has facilitated access to tumours located in and around the CS [20, 32]. While midline interventions were frequently performed in previous years, the application of extended endoscopic endonasal approaches allowed surgical access to the lateral portions of the CS [21]. The triangular fields formed between the anatomical structures on the CS contributed to the understanding of the anatomical neighbourhoods observed in the endoscopic interventions [1]. However, neurovascular structures within these defined areas should be examined from different perspectives in order to safely perform minimally invasive surgical interventions.

This study explains in detail the anatomy of the CS and the complex neurovascular structures encountered during endoscopic endonasal surgical interventions, thus minimising the risk of complications that may occur during minimally invasive surgical procedures.

MATERIALS AND METHODS

This research was performed in line with the principles of the Declaration of Helsinki. Approval was granted by the Ethics Committee of Prof. Dr. Mazhar Osman Mental Health and Neurological Diseases Training and Research Hospital (Date: 06.09.2016/ /Ethics approval number: 571).

A total of 7 adult cadavers, 4 male and 3 female, were dissected and prepared for further examination. The cadavers of adults over the age of 18 who had not undergone previous craniofacial surgery were included in the study. Disruption of the integrity of the skull base anatomy and severe damage to the bone and mucosal tissue were determined as exclusion criteria. The study was carried out in the Microneurosurgery and Neuroanatomy Laboratory of Cerrahpaşa Medical Faculty between October and December 2016.

All cadavers were injected with silicone dye and preserved in 75% alcohol. During the preparation phase, the cadavers were positioned supine. A microscope unit was placed in front of the surgeon. After a surgical drill and aspirator were placed, the procedure was initiated. Dissections were performed using a microsurgery kit with a microscope (Zeiss OPMI Pico, Oberkochen, Germany) at 4× and 40× magnification. The high-speed surgical drill (Medtronic, USA) and an angled drill bit were used for the drilling process. The skull base images of the cadavers were obtained using a macro lens camera (Canon EOS 650 D, Tokyo, Japan).

The heads of the cadavers were fixed on the table using a 15-degree flexion position. The skin and subcutaneous tissue up to the orbicularis oculi muscle superiorly, the maxillary sinus inferiorly, and the malar eminence inferiorly and laterally were passed. The nasal septum was preserved, and the ala of the nose was removed. Then, the anterior wall of the maxillary sinus was drilled superiorly to the level of the maxillary nerve. The maxillary sinus mucosa and medial wall were removed, preserving the inferior nasal concha. The nasal septum was removed. The parts of the nasal conchae, except for the bone attachment areas, were excised to permit wider surgical exploration. The posterior wall of the maxillary sinus was removed with a drill and the pterygopalatine fossa was reached. An anterior sphenoidotomy was performed. The sinus mucosa and sphenoid septum were removed. Surgical margins were determined by imaging the base of the sella, sphenoidal plane, clivus, opticocarotid recess, optic protuberance and carotid protuberance. After the pterygoid process resection, the surgical anatomy of the sphenoidal sinus lateral wall, Meckel's cave, CS, ICA, and the pathways to the petrous apex were examined.

RESULTS

After the alae of the nose of the cadavers were removed, the medial nasal septum and the lateral middle and inferior nasal concha were detected. During endoscopic endonasal surgery, it's critical to stay oriented so as not to gravitate towards the anterior cranial fossa. One of the important anatomical structures for orientation is the choana; following choana localization, the inferior, middle, superior and, if present, supreme nasal concha should be defined.

Lateral to the middle nasal concha, the uncinate process anteriorly and ethmoidal bulla posteriorly

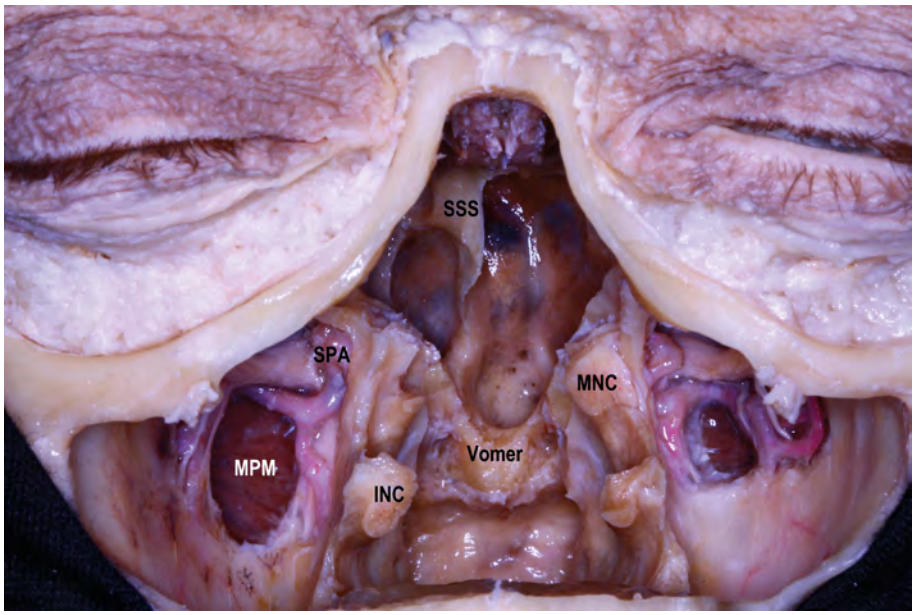

Figure 1. The anterior wall of the sphenoidal sinus was drilled to reach the sinus. Anterior sphenoidotomy was performed by drilling the inferior of the opening of the sphenoidal sinus to reveal the relationship between the opening of the sphenoidal sinus and the sella. It was observed that the opening of the sphenoidal sinus was at the same level as the base of the sella. After the sphenoidal sinus mucosa was removed, a septum directed towards the right carotid protuberance was seen; INC — inferior nasal concha; MNC — middle nasal concha; MPM — medial pterygoid muscle; SSS — septum of sphenoidal sinuses; SPA — sphenopalatine artery.

were exposed. Maxillary hiatus was observed in the middle or posterior 1/3 parts of the ethmoidal bulla. The choana was seen postero-inferior to the nasal cavity, posterior to the inferior nasal concha, and medial to the vomer.

One of the structures encountered in the first stage of surgery is the nasal septum, which consists of cartilage anteriorly and bone posteriorly. Most surgical approaches require a posterior nasal septectomy [23]. The sphenoethmoidal recess, where the sphenoidal sinus is opened, is one of the structures used to locate the sinus during surgery. If the sphenoethmoidal recess is followed superiorly to the choana, the opening of the sphenoidal sinus is reached [29].

Transsphenoidal approach

Without resection of the nasal septum, the middle and superior nasal concha was retracted laterally, and bilateral openings of sphenoidal sinuses were found. The opening of the sphenoidal sinus was detected just infero-medial to the superior nasal concha. As a result of the measurements, the opening of the sphenoidal sinus was determined approximately 15 mm superior to the choana or in the middle of the distance between the nasal septum and the superior nasal concha.

Conchae were resected bilaterally, and after the nasal septum mucosa was scraped subperiosteally, total nasal septectomy was performed. Both openings of sphenoidal sinuses were joined (Fig. 1). Intersphenoid septums were resected. During dissection of the inferolateral part of the sphenoidal sinus, care should be taken not to damage the vidian nerve and the sphenopalatine artery. The sphenopalatine artery was located in the inferolateral corner of the sphenoidal sinus and approximately 1 cm anterior to the posterior border of the middle nasal concha. The sphenoidal sinus was enlarged until the sphenoidal plane and anterior skull base in the superior, the sella in the postero-superior, the clival recess in the postero-inferior, and both paraclival carotid protuberances in the lateral appeared (Fig. 2). The opening of sphenoidal sinuses was seen just above and medial to the insertion site of the superior nasal concha in four of seven cadavers.

Transsellar approach

The sellar fossa was enlarged with a 3 mm drill and the sellar dura was exposed (Fig. 3). Maximum care should be taken not to damage the CS and pituitary gland during drilling. In standard approaches to the sellar region, it is sufficient to limit dural exposure

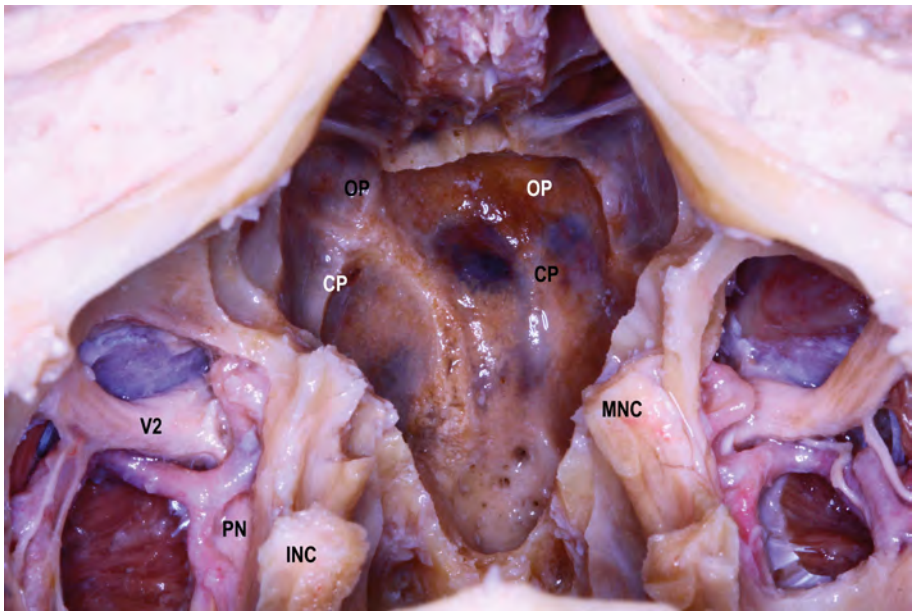

Figure 2. Some important points during the surgery were detected in the sellar type sphenoidal sinus. Carotid protuberance formed by the sellar prominence in the midline in the coronal plane and by the internal carotid artery in the antero-lateral of the sella was observed. Anterior to this prominence is the optic prominence. An opticocarotid recess was observed in the pit area between the optic protuberance and the carotid protuberance; CP — carotid protuberance; INC — inferior nasal concha; MNC — middle nasal concha; OP — optic protuberance; PN — palatine nerves; V2 — maxillary nerve.

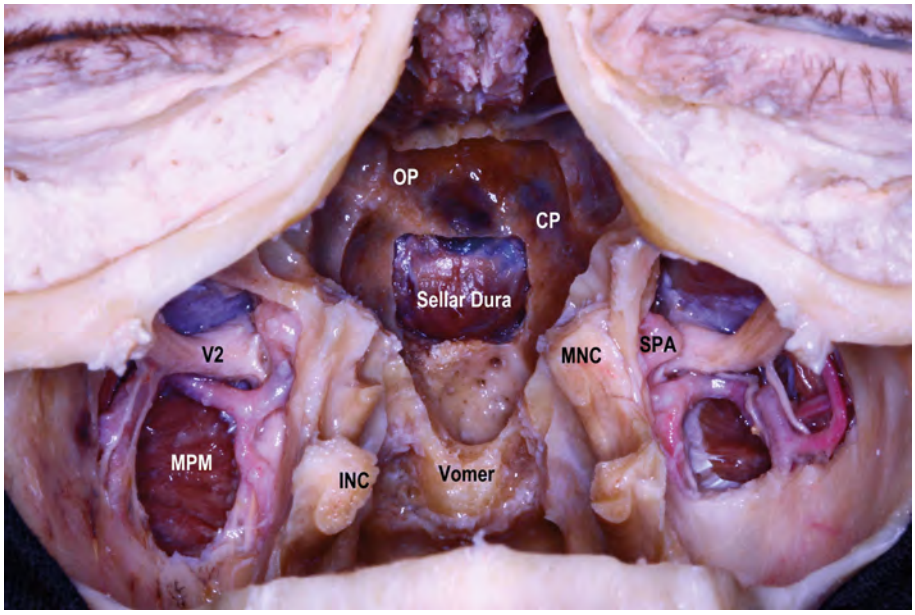

Figure 3. The anterior wall of the rectangular sella turcica was opened at the border of the anterior and inferior intercavernous sinuses. Medial opticocarotid recess (MOR) and lateral opticocarotid recess (LOR) were observed within the sinus. MOR was seen as a pit at the junction of the paraclinoid internal carotid artery, which was the optic nerve. LOR was observed lateral to the carotid protuberance and inferior to the optic canal. The clival recess starts from the dorsum sella at the posterior border of the sella turcica and extends to the inferior wall of the sphenoidal sinus. Laterally, it is surrounded by carotid protuberances; CP — carotid protuberance; INC — inferior nasal concha; MNC — middle nasal concha; MPM — medial pterygoid muscle; OP — optic protuberance; SPA — sphenopalatine artery; V2 — maxillary nerve.

between the anterior intercavernous sinus superiorly and the inferior intercavernous sinus inferiorly. The sellar dura was opened in a rectangular shape, preserving the cavernous portion of the ICA, and the pituitary gland was exposed (Fig. 4). The neurohypophysis was revealed by retracting the pituitary

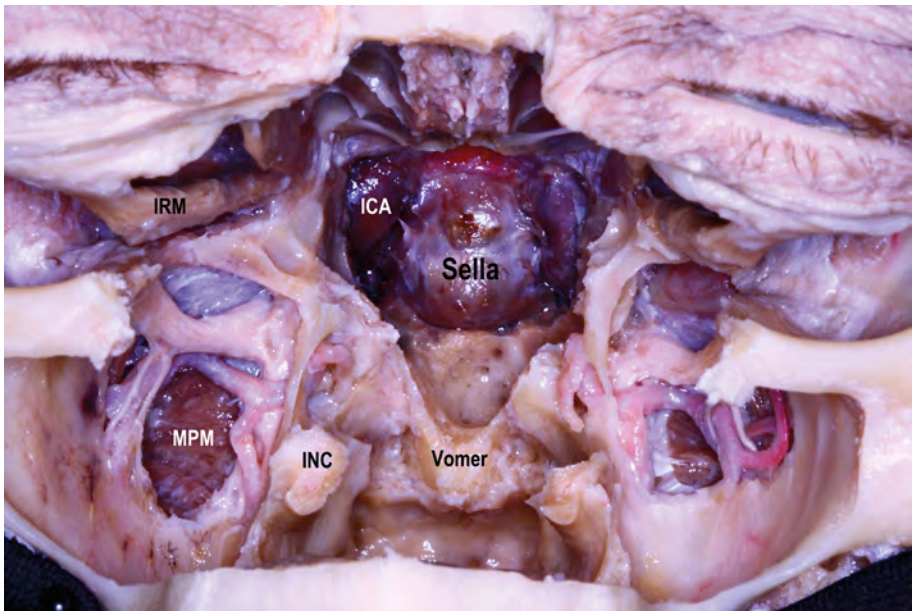

Figure 4. For extensive exploration, the hypophyseal fossa was opened lateral to both cavernous internal carotid arteries laterally and posterior to the level of the optic chiasm superiorly. Maximum care should be taken against internal carotid artery damage while the lateral border is being excised with the aid of a drill; ICA — internal carotid artery; INC — inferior nasal concha; IRM — inferior rectus muscle; MPM — medial pterygoid muscle.

gland superiorly. In addition, the pituitary gland was retracted medially, exposing the medial wall of the CS and the inferior hypophyseal artery. Then, the pituitary gland was resected and the sellar diaphragm was exposed.

Transcavernous approach

First of all, the conchae were resected to enlarge the surgical area. The medial and posterior walls of the maxillary sinus were removed. Sphenoidotomy was performed using the opening of the sphenoidal sinus as a landmark. Since the dura mater is thin and the nerves are just below this layer, particular care should be taken not to injure the abducens nerve at this stage. A periosteal incision was then made over the superior orbital fissure and the cavernous portion of the ICA (Fig. 5). After reaching the CS, the oculomotor, ophthalmic, and maxillary nerves were observed on the lateral wall. The abducens nerve and trigeminal ganglion were located on the medial wall. The trochlear nerve was not clearly seen from this angle.

The structures forming the borders of the triangles should be considered during the surgery and their course should be examined. The clinoidal triangle, which is defined as the region among the optic nerve, oculomotor nerve and ICA, was determined. Then, the anteromedial triangle located between the line connecting the ophthalmic nerve, maxillary nerve, foramen rotundum and superior orbital fissure was evaluated [4, 13].

When the dura on the CS was opened, the ophthalmic nerve was seen superiorly and the abducens nerve was observed just anteriorly to it. The maxillary nerve was traced backward from the foramen rotundum. It was observed that the V1 and V2 divisions of the trigeminal nerve merged in the trigeminal ganglion. After removing the bone and periosteum over the superior orbital fissure, the oculomotor nerve was exposed. The oculomotor, ophthalmic and abducens nerves entering the superior orbital fissure were seen. The trochlear nerve located posteriorly was observed after exclusion of the ophthalmic nerve.

The optic protuberance was drilled and traced up to the common tendinous ring, and the optic nerve was exposed. The supratrochlear triangle between the oculomotor nerve and the trochlear nerve was identified. Then, the infratrochlear triangle between the trochlear nerve and V1 division of the trigeminal nerve was exposed [13]. However, because it requires cranial nerve manipulation, this was not evaluated as a surgical corridor that could be used with endoscopic endonasal methods (Fig. 6).

In order to expose the posterior part of the CS, the superior nasal concha and posterior part of the ethmoidal sinus were resected. The uncinate process

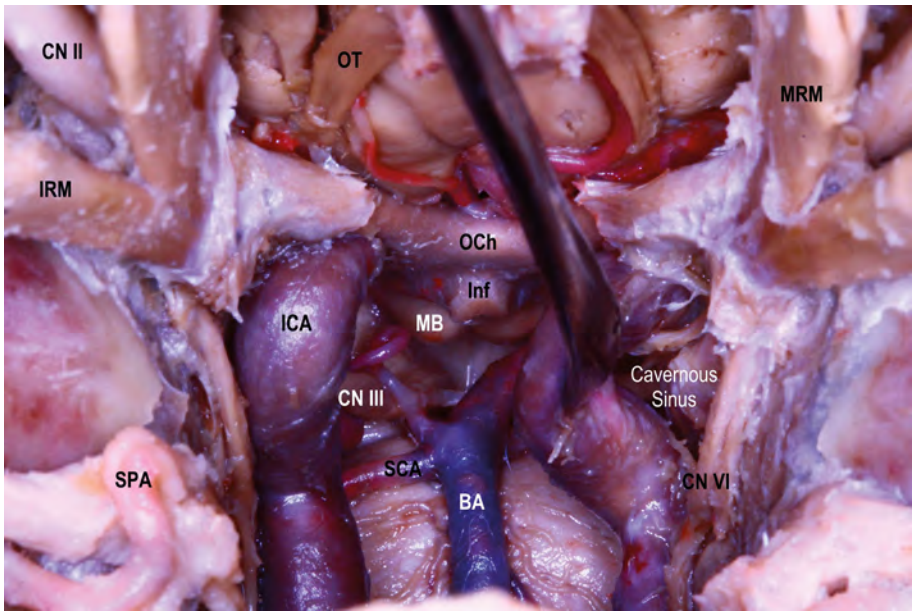

Figure 5. After the periosteum on the cavernous sinus was removed and the internal carotid artery was retracted medially, the inside of the sinus was reached. The oculomotor, ophthalmic and maxillary nerves are located on the lateral wall, while the abducens nerve and trigeminal ganglion are located on the medial wall. The trochlear nerve is not usually seen from this angle. In the region among the optic nerve, oculomotor nerve and internal carotid artery, the clinoidal triangle is detected. The anteromedial triangle is examined in the area between the line joining the ophthalmic nerve, maxillary nerve, foramen rotundum and superior orbital fissure; BA — basilar artery; CN II — optic nerve; CN III — oculomotor nerve; CN VI — abducens nerve; ICA — internal carotid artery; Inf — infundibulum; IRM — inferior rectus muscle; MB — mammillary body; MRM — medial rectus muscle; OCh — optic chiasm; OT — olfactory tract; SCA — superior cerebellar artery; SPA — sphenopalatine artery.

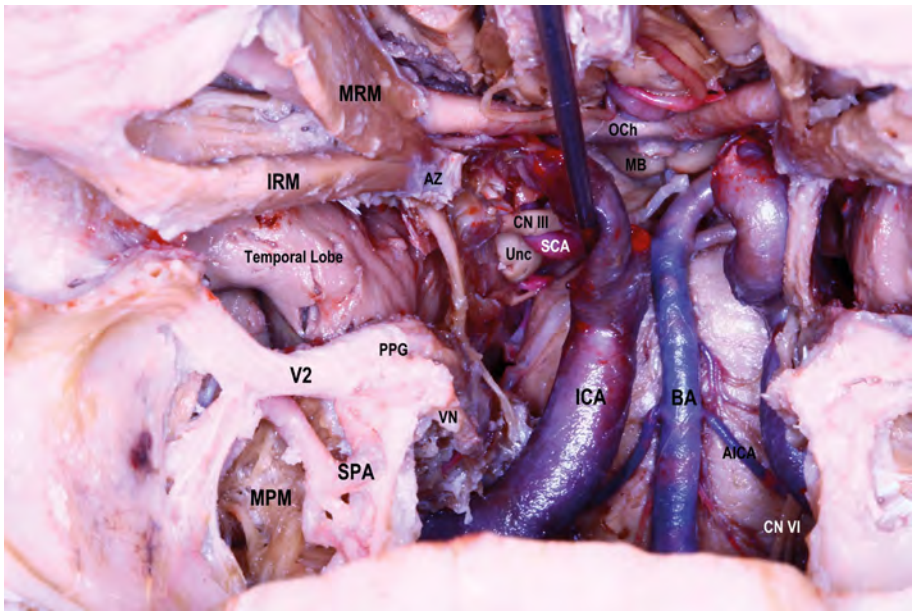

Figure 6. The oculomotor nerve, ophthalmic and abducens nerve in the cavernous sinus are seen. The trochlear nerve is not seen from the anterior view in the endoscopic endonasal approach. The most superficial region contains the abducens nerve. The ophthalmic nerve is located below the abducens nerve and the trochlear nerve is located posterior to these; therefore, the structure with the least risk of injury in lateral skull base approaches is the trochlear nerve. When the ophthalmic nerve is retracted to the inferior, there is the oculomotor nerve, the trochlear nerve, and the supratrochlear triangle located between the dura layers of these two nerves. When the ophthalmic nerve is pulled up, the infratrochlear triangle becomes visible; AICA — anterior inferior cerebellar artery; AZ — annulus of Zinn; BA — basilar artery; CN III — oculomotor nerve; CN VI — abducens nerve; ICA — internal carotid artery; IRM — inferior rectus muscle; MB — mammillary body; MPM — medial pterygoid muscle; MRM — medial rectus muscle; OCh — optic chiasm; PPG — pterygopalatine ganglion; SCA — superior cerebellar artery; SPA — sphenopalatine artery; Unc — uncus of the temporal lobe; V2 — Maxillary nerve; VN — vidian nerve.

was resected to expose its lateral wall. The base of the sella was resected towards the carotid prominence up to the pterygoid process, and the inferior of the CS was exposed. After exposure of the vidian nerve, a triangular region was detected lateral to the ICA. This triangle was formed inferiorly by the vidian nerve. The lateral edge of the triangle is formed by the medial plate of the pterygoid process, and the medial edge by the ICA. After the dura covering the triangle was opened, oculomotor, abducens and maxillary nerves were exposed. The described CS sections were examined in detail with ICA exclusion.

DISCUSSION

While the first endoscopic studies generally addressed pituitary adenomas, over the years the surgical field has been expanded from anterior to posterior. Endoscopic surgery's success encouraged surgeons to use it in approaching lateral and posterior skull base lesions as well. To reach these regions, it was necessary to apply extended endoscopic endonasal methods [3].

Surgery to the CS region is challenging because of the important neurovascular structures in the sinus. The CS is generally divided into four compartments that include medial, lateral, anteroinferior, and postero-superior. Transsphenoidal [12], transmaxillary [5], and transethmoidal [7] approaches have been described to safely reach different parts of the CS and adjacent structures. While endoscopic midline transsphenoidal surgery is sufficient to reach the medial part of the CS, extended approaches are often needed to reach the lateral part.

The primary pathologies of CS are meningiomas, neurogenic tumours and haemangiomas. These pathologies mostly tend to locate in the lateral part of the CS. Secondary tumours are pituitary adenomas, chordomas, chondrosarcomas, perineural spread of head and neck malignancies, and hematogenous spread of distant lesions. The localization of these pathologies can vary widely. Pituitary adenomas mostly involve the medial and postero-superior compartments, while chordomas and chondrosarcomas involve the antero-inferior compartment. The endonasal route is safer than other invasive procedures used to reach CS-invading lesions because of the intervention through the medial wall of the CS, which is devoid of cranial nerves [22].

There are some points to be considered during the endoscopic endonasal approach to CS. The meningeal wall of the CS has three weak points where tumours can invade more easily. These are the venous plexus around the superior orbital fissure, the medial wall adjacent to the pituitary gland, and the meningeal sheaths of the cranial nerves, where the dural layer is either very thin or absent [16]. Although there are two layers, meningeal and endosteal, on the lateral and superior walls of the CS, there is one layer on the medial wall [30]. In some cases, this layer is also absent or missing [10, 11]. Depending on the ICA localization, there are venous compartments of different shapes and sizes within the CS. These are called the superior, inferior, lateral, and medial compartments. While the venous space medial to the ICA is 48% dominant, the lateral venous space is 22% dominant [25]. In some cases, the pituitary gland may cover the intercavernous portion of the ICA with a protrusion [26].

Although the majority of nonfunctional pituitary adenomas are not aggressive or invasive, their spread into the CS can be explained by these features [31]. Due to the decompression of the sinuses after excision of the lesion, abundant venous bleeding may occur. These bleedings can be stopped by using suitable haemostatic materials. In addition, the risk of venous bleeding in endoscopic endonasal approaches is not different from the microscopic method [15]. Being away from the ICA and not damaging the cranial nerves below the dura is vital in removing the dura on the CS during the opening phase. The location of the tumour and the direction in which it displaces the ICA can be used to determine the opening of the dura.

In this study, first of all, the stages of transsphenoidal and transsellar approaches and points to be considered during the surgery were emphasized. Then, the surgical corridors encountered during the transcavernous stage were discussed. After opening the dura with the endoscopic endonasal method, the oculomotor nerve superiorly and the ophthalmic nerve inferiorly were identified. The abducens nerve was observed anterior and medial to the ophthalmic nerve, and the maxillary nerve was observed below it. The methods required for safe surgery were defined using the various sites and intervals in the CS.

Our study examined the clinoidal triangle, one of the smallest surgical fields defined in CS. Medial to the clinoidal triangle is the optic nerve, bounded by the optic canal, and lateral to it is a line drawn between the oculomotor nerve and the superior orbital fissure. The base of this triangle corresponds to the dura layer lying behind the medial and lateral border.

The clinoidal triangle is where the oculomotor nerve meets the lateral CS. The oculomotor nerve then enters the superior orbital fissure under the anterior clinoid process and lateral to the ICA. The contents of the clinoidal triangle can be reached after drilling the anterior clinoid process with supraorbital approaches. The morphology of the venous structure in this part of the ICA is highly variable. The anteromedial triangle (Mullan's triangle) is located between the first two branches of the trigeminal nerve. The ophthalmic nerve is located in the medial border of this triangle and the maxillary nerve is located in the lateral border of this triangle. The base of the anteromedial triangle is the line connecting the point where the ophthalmic nerve passes through the superior orbital fissure and the point where the maxillary nerve passes through the foramen rotundum [4, 13]. Although the ICA covers most of the CS, the opening formed by the clinoidal and anteromedial triangle allows access to other structures and pathological formations within the CS. It was stated that these potential sites facilitate endoscopic endonasal access to the middle cranial fossa [17].

On the lateral wall of the CS, a supratrochlear triangle is formed between the oculomotor nerve medially and the trochlear nerve laterally. At the base of this triangle is the dura layer, which lies between the entry points of these two cranial nerves. This triangle is suitable for examining the intracavernous portion of the ICA. However, great care should be taken because of the possibility of bleeding that can be caused by the meningohypophyseal trunk. This vein should be identified as a priority during interventions. The infratrochlear triangle (Parkinson's triangle) was defined by Parkinson in 1965 with the aim of safely reaching the lesions in the CS [24]. The medial border of this triangle is formed by the inferior surface of the trochlear nerve on the lateral wall of the CS from the sinus entrance to its exit. On the lateral border of the infratrochlear triangle is the superior surface of the ophthalmic nerve [4, 13]. Reaching the supratrochlear triangle and the infratrochlear triangle is seen as dangerous because they are narrowed by the cranial nerves. The anterior part of these two triangles is narrow and their posterior part is wide, but the abducens nerve limits the forward passage [17]. Similarly, during this cadaveric study, it was observed that the supratrochlear and infratrochlear triangles were not suitable for endoscopic endonasal approaches.

CONCLUSIONS

In this cadaveric study, the anatomy of the CS and the surgical sites encountered during endoscopic endonasal interventions in this region were examined. The limitations of surgical techniques and the points to be considered were described. Detailed information and recommendations needed to reduce complications that may occur during the treatment of various lesions encountered in CS were presented.

Acknowledgements

The authors sincerely thank those who donated their bodies to science so that anatomical research could be performed. Results from such research can potentially increase mankind's overall knowledge that can then improve patient care. Therefore, these donors and their families deserve our highest gratitude.

Conflict of interest: None declared

REFERENCES

1. Abuzayed B, Tanriover N, Gazioglu N, et al. Endoscopic anatomy and approaches of the cavernous sinus: cadaver study. Surg Radiol Anat. 2010; 32(5): 499–508, doi: 10.1007/s00276-010-0651-3, indexed in Pubmed: 20443000.
2. Campero A, Campero AA, Martins C, et al. Surgical anatomy of the dural walls of the cavernous sinus. J Clin Neurosci. 2010; 17(6): 746–750, doi: 10.1016/j.jocn.2009.10.015, indexed in Pubmed: 20378356.
3. Cavallo LM, Cappabianca P, Galzio R, et al. Endoscopic transnasal approach to the cavernous sinus versus transcranial route: anatomic study. Neurosurgery. 2005; 56(2 Suppl): 379–389, doi: 10.1227/01.neu.0000156548.30011.d4, indexed in Pubmed: 15794834.
4. Chung BS, Ahn YH, Park JS. Ten triangles around cavernous sinus for surgical approach, described by schematic diagram and three dimensional models with the sectioned images. J Korean Med Sci. 2016; 31(9): 1455–1463, doi: 10.3346/jkms.2016.31.9.1455, indexed in Pubmed: 27510391.
5. Couldwell WT, Sabit I, Weiss MH, et al. Transmaxillary approach to the anterior cavernous sinus: a microanatomic study. Neurosurgery. 1997; 40(6): 1307–1311, doi: 10.1097/00006123-199706000-00040, indexed in Pubmed: 9179908.
6. Dallan I, Di Somma A, Prats-Galino A, et al. Endoscopic transorbital route to the cavernous sinus through the meningo-orbital band: a descriptive anatomical study. J Neurosurg. 2017; 127(3): 622–629, doi: 10.3171/2016.8.JNS16465, indexed in Pubmed: 27858571.
7. Das K, Spencer W, Nwagwu CI, et al. Approaches to the sellar and parasellar region: anatomic comparison of endonasal-transsphenoidal, sublabial-transsphenoidal, and transethmoidal approaches. Neurol Res. 2001; 23(1):

51–54, doi: 10.1179/016164101101198280, indexed in Pubmed: 11210430.
8. de Lara D, Ditzel Filho LFS, Prevedello DM, et al. Endonasal endoscopic approaches to the paramedian skull base. World Neurosurg. 2014; 82(6 Suppl): S121–S129, doi: 10.1016/j.wneu.2014.07.036, indexed in Pubmed: 25496623.
9. DeMonte F, Smith HK, al-Mefty O. Outcome of aggressive removal of cavernous sinus meningiomas. J Neurosurg. 1994; 81(2): 245–251, doi: 10.3171/jns.1994.81.2.0245, indexed in Pubmed: 8027808.
10. Dietemann JL, Kehrli P, Maillot C, et al. Is there a dural wall between the cavernous sinus and the pituitary fossa? Anatomical and MRI findings. Neuroradiology. 1998; 40(10): 627–630, doi: 10.1007/s002340050653, indexed in Pubmed: 9833890.
11. Dolenc VV. Microsurgical anatomy and surgery of the central skull base. Springer, Vienna 2003.
12. Fahlbusch R, Buchfelder M. Transsphenoidal surgery of parasellar pituitary adenomas. Acta Neurochir (Wien). 1988; 92(1-4): 93–99, doi: 10.1007/BF01401978, indexed in Pubmed: 3407479.
13. Isolan GR, Krayenbühl N, de Oliveira E, et al. Microsurgical anatomy of the cavernous sinus: measurements of the triangles in and around it. Skull Base. 2007; 17(6): 357–367, doi: 10.1055/s-2007-985194, indexed in Pubmed: 18449336.
14. Jankowski R, Auque J, Simon C, et al. Endoscopic pituitary tumor surgery. Laryngoscope. 1992; 102(2): 198–202, doi: 10.1288/00005537-199202000-00016, indexed in Pubmed: 1738293.
15. Jho HD, Ha HG. Endoscopic endonasal skull base surgery: Part 2: The cavernous sinus. Minim Invasive Neurosurg. 2004; 47(1): 9–15, doi: 10.1055/s-2004-818346, indexed in Pubmed: 15100926.
16. Kawase T, van Loveren H, Keller JT, et al. Meningeal architecture of the cavernous sinus: clinical and surgical implications. Neurosurgery. 1996; 39(3): 527–534, doi: 10.1097/00006123-199609000-00019, indexed in Pubmed: 8875483.
17. Komatsu F, Oda S, Shimoda M, et al. Endoscopic endonasal approach to the middle cranial fossa through the cavernous sinus triangles: anatomical considerations. Neurol Med Chir (Tokyo). 2014; 54(12): 1004–1008, doi: 10.2176/nmc.oa.2014-0092, indexed in Pubmed: 25446385.
18. Komatsu F, Shimoda M, Oda S, et al. Identification of the internal carotid artery at the superior part of the cavernous sinus during endoscopic endonasal cavernous sinus tumor surgery. Acta Neurochir (Wien). 2014; 156(3): 475–479, doi: 10.1007/s00701-013-1986-4, indexed in Pubmed: 24413914.
19. Koutourousiou M, Vaz Guimaraes Filho F, Fernandez-Miranda JC, et al. Endoscopic endonasal surgery for tumors of the cavernous sinus: a series of 234 patients. World Neurosurg. 2017; 103: 713–732, doi: 10.1016/j.wneu.2017.04.096, indexed in Pubmed: 28450229.
20. Li H, Zhang B, Wang W, et al. Clinical features, intradural transcavernous surgical management, and outcomes of giant cavernous sinus hemangiomas: a single-institution experience. World Neurosurg. 2019; 125: e754–e763, doi: 10.1016/j.wneu.2019.01.165, indexed in Pubmed: 30735865.
21. Messerer M, Cossu G, Pasche P, et al. Extended endoscopic endonasal approach to clival and paraclival tumors: Indications and limits. Neurochirurgie. 2016; 62(3): 136–145, doi: 10.1016/j.neuchi.2015.12.003, indexed in Pubmed: 27179389.
22. Munawar K, Nayak G, Fatterpekar GM, et al. Cavernous sinus lesions. Clin Imaging. 2020; 68: 71–89, doi: 10.1016/j.clinimag.2020.06.029, indexed in Pubmed: 32574933.
23. Murchison AP, Rosen MR, Evans JJ, et al. Posterior nasal septectomy in endoscopic orbital apex surgery. Ophthalmic Plast Reconstr Surg. 2009; 25(6): 458–463, indexed in Pubmed: 19935249.
24. Parkinson D. A surgical approach to the cavernous portion of the carotid artery. Anatomical studies and case report. J Neurosurg. 1965; 23(5): 474–483, doi: 10.3171/jns.1965.23.5.0474, indexed in Pubmed: 5858438.
25. Rhoton AL, Hardy DG, Chambers SM. Microsurgical anatomy and dissection of the sphenoid bone, cavernous sinus and sellar region. Surg Neurol. 1979; 12(2): 63–104, indexed in Pubmed: 451866.
26. Rhoton AL, Harris FS, Renn WH. Microsurgical anatomy of the sellar region and cavernous sinus. Clin Neurosurg. 1977; 24: 54–85, doi: 10.1093/neurosurgery/24.cn_suppl_1.54, indexed in Pubmed: 583699.
27. Theodosopoulos PV, Cebula H, Kurbanov A, et al. The medial extra-sellar corridor to the cavernous sinus: anatomic description and clinical correlation. World Neurosurg. 2016; 96: 417–422, doi: 10.1016/j.wneu.2016.09.046, indexed in Pubmed: 27659813.
28. Valentine R, Wormald PJ. Carotid artery injury after endonasal surgery. Otolaryngol Clin North Am. 2011; 44(5): 1059–1079, doi: 10.1016/j.otc.2011.06.009, indexed in Pubmed: 21978896.
29. Yanagisawa E. Endoscopic view of sphenoethmoidal recess and superior meatus. Ear Nose Throat J. 1993; 72(5): 331–332, doi: 10.1177/014556139307200506.
30. Yasuda A, Campero A, Martins C, et al. The medial wall of the cavernous sinus: microsurgical anatomy. Neurosurgery. 2004; 55(1): 179–189, doi: 10.1227/01.neu.0000126953.59406.77, indexed in Pubmed: 15214988.
31. Yokoyama S, Hirano H, Moroki K, et al. Are nonfunctioning pituitary adenomas extending into the cavernous sinus aggressive and/or invasive? Neurosurgery. 2001; 49(4): 857–862, doi: 10.1097/00006123-200110000-00014, indexed in Pubmed: 11564246.
32. Zhang Q, Wang Z, Guo H, et al. Direct transcavernous sinus approach for endoscopic endonasal resection of intracavernous sinus tumors. World Neurosurg. 2019; 128: e478–e487, doi: 10.1016/j.wneu.2019.04.182, indexed in Pubmed: 31048053.

VIA MEDICA

ORIGINAL ARTICLE

Folia Morphol.
Vol. 82, No. 4, pp. 814–821
DOI: 10.5603/FM.a2022.0080

ISSN 0015–5659
eISSN 1644–3284
journals.viamedica.pl

Morphometrical features of left atrial appendage in the atrial fibrillation patients subjected to left atrial appendage closure

K.M. Słodowska[1], J. Batko[1], J.P. Hołda[1], D. Dudkiewicz[1], M. Koziej[1], R. Litwinowicz[2], K. Bartuś[2], M.K. Hołda[1, 3]

[1]*Heart Embryology and Anatomy Research Team (HEART), Department of Anatomy, Jagiellonian University Medical College, Krakow, Poland*
[2]*Department of Cardiovascular Surgery and Transplantology, Jagiellonian University Medical College, Krakow, Poland*
[3]*Division of Cardiovascular Sciences, The University of Manchester, United Kingdom*

[Received: 14 July 2022; Accepted: 19 August 2022; Early publication date: 25 August 2022]

Background: *This study aimed to evaluate the morphometrical features of left atrial appendage (LAA) in patients with atrial fibrillation, subjected to LAA percutaneous closure (LARIAT) for stroke prevention.*

Materials and methods: *Computed tomography (CT) scans of 51 patients with atrial fibrillation subjected to LARIAT procedure were comparatively evaluated with 50 patients with sinus rhythm (control group). Three-dimensional reconstructions were created using volume-rendering for evaluation.*

Results: *No differences were found in LAA types of distribution (cauliflower: 25.5 vs. 34.0%, chicken wing: 45.1 vs. 46.0%, arrowhead: 29.4 vs. 20.0%, all $p > 0.05$) between groups. However, the study group was characterized by LAAs with a lower number of lobes. The LAA orifice anteroposterior and transverse diameters (19.3 ± 4.12 vs. 17.2 ± 4.0 mm, $p = 0.01$ and 25.1 ± 5.1 vs. 20.5 ± ± 4.4 mm, $p = 0.001$), orifice area (387.2 ± 133.9 vs. 327.1 ± 128.3 mm^2, $p = 0.02$) and orifice perimeter (70.2 ± 12.5 vs. 61.2 ± 11.6 mm, $p = 0.04$) was significantly larger in atrial fibrillation patients. More oval LAA orifices was found in atrial fibrillation group (94.0 vs. 70.4%, $p = 0.001$). No statistically significant differences were found in LAA body length (47.4 ± 15.4 vs. 43.7 ± 10.9 mm, $p = 0.17$), body width (24.7 ± 5.6 vs. 24.4 ± 5.8 mm, $p = 0.81$), and chamber depth (17.7 ± 3.5 vs. 16.5 ± 3.8 mm, $p = 0.11$). Calculated LAA ejection fraction was significantly lower in study group compared to healthy patients (16.4 ± 14.9 vs. 48.2 ± 12.9%, $p = 0.001$).*

Conclusions: *Important morphometrical differences in LAA orifice have been found, which was significantly larger and more oval in patients with atrial fibrillation compared to healthy controls. Although no difference in LAA body type and size was observed; the LAA ejection fraction was significantly lower in atrial fibrillation rhythm patients.* (Folia Morphol 2023; 82, 4: 814–821)

Key words: left atrial appendage closure, left atrial appendage shape, atrial fibrillation, stroke

Address for correspondence: M.K. Hołda, MD, PhD, DSc, Heart Embryology and Anatomy Research Team (HEART), Department of Anatomy, Jagiellonian University Medical College, ul. Kopernika 12, 31–034 Kraków, Poland, tel/fax: +48 12 422 95 11, e-mail: mkh@onet.eu

INTRODUCTION

The left atrial appendage (LAA) is a small, irregular shape structure, outpouching from the left atrium (LA) of the heart [23]. LAA is a remnant of the primitive atrium developed in early gestation. It is proven that LAA takes part in the regulation of volume homeostasis through its mechanical function and neurohormonal secretion [12]. Moreover, the LAA is a well-established source of cardiac thrombogenesis and arrhythmogenesis [20]. For more than half of a century, the LAA is considered a primary source of cardioembolic events in patients with atrial tachycardia (atrial fibrillation [AF]) [28]. Numerous morphological features of the LAA, which include multilobular and trabeculated structure and small orifice with a narrow neck, predispose to turbulent blood flow and local blood stasis, thereby increasing the risk for thrombosis [20, 21]. Nevertheless, no consensus was reached as to which specific LAA morphometric features increased the risk of thrombogenicity.

Anticoagulation therapy is a standard of care to prevent cardioembolic stroke in patients with AF [14]. In patients with a high risk of bleeding, contraindications to anticoagulants, intolerance, or low patient compliance the LAA closure was proposed as an alternative approach to eliminate cardioembolic stroke risk [11]. This led to the development of several surgical and percutaneous approaches to close/exclude the LAA based on three concepts: plug, pacifier principle, and ligation [4]. Among the ligation techniques, the LARIAT (SentreHEART, Inc., Redwood City, CA, USA) procedure is a distinguished percutaneous adaptation of the surgical exclusion of LAA with a suture, used as an alternative to open-heart surgery [2]. Although the LARIAT procedure can be performed effectively with acceptably low complications, some short- and long-term complications of the intervention may occur [16]. The frequency of peri- and post-procedural complications can be lowered by adequate patients selection thanks to computed tomography (CT) evaluation of the LAA shape and size and detailed pre-procedural planning [26]. Morphology of the LAA can significantly affect pathophysiological properties of the LAA, choice of closure technique, the course of the procedure, its results, and complications [4, 23]. The present study aims to compare the LAA morphometrical features between patients with AF subjected to LAA percutaneous closure using LARIAT device and sinus rhythm patients using cardiac CT.

MATERIALS AND METHODS

The current study was conducted at the Department of Anatomy and the Department of Cardiovascular Surgery and Transplantology at the Jagiellonian University Medical College, Krakow, Poland. The study was conducted according to the principles expressed in the 1975 Declaration of Helsinki and was approved by the Bioethical Committee of the Jagiellonian University in Krakow, Poland (No. 1072.6120.4.2020).

Study population

The study evaluated 101 contrast-enhanced electrocardiograms (ECG) gated CT scans of hearts of which 51 were of consecutive adult patients with AF and who underwent percutaneous closure of the LAA with the LARIAT device (41.2% females, mean age of 61.0 ± 10.35 years) (study group). The CT scans were performed prior to the LARIAT procedure. The remaining 50 scans (control group) were of randomly selected adult patients subjected to non-invasive coronary arteries evaluation (50% females, mean age of 57.8 ± 14.45 years) of which inclusion criteria were: no history of ischaemic stroke, no AF, and absence of any significant structural heart defects. All sample patients gave written informed consent. The medical history of all included patients was reviewed, and the following data were extracted: sex, age, body mass index, existing comorbidities (i.e. hypertension, hyperlipidaemia, chronic heart failure, coronary artery disease, chronic obstructive pulmonary disease, diabetes mellitus, history of stroke, and history of myocardial infarction), heart rhythm status, and the medication's usage. The following scores were calculated: Canadian Cardiovascular Society (CCS) grading of angina pectoris and New York Heart Association (NYHA) Functional Classification and CHA_2DS_2-VASc Score for Atrial Fibrillation Stroke Risk.

Cardiac computed tomography

Every patient underwent a per-protocol contrast-enhanced ECG gated CT scan. All scans were performed in sinus rhythm. If the patient's heart rate was over 70 bpm before the cardiac CT examination, the patient was administered 10 or 40 mg of propranolol or 40 mg of verapamil, depending on the physician's recommendation. The examination was performed using a 64-row dual-source scanner (Siemens, Erlangen, Germany). The image acquisitions were collected during a deep inspiration breath-

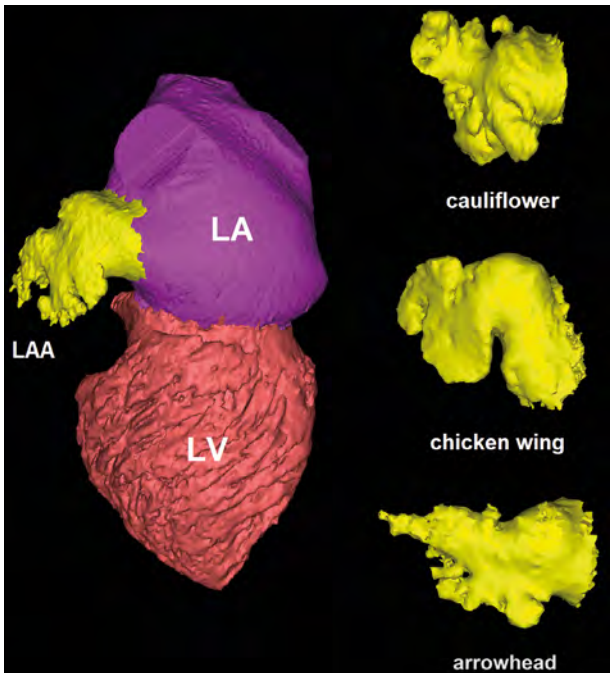

Figure 1. Representatives for three-dimensional reconstructions of each left atrial appendage (LAA) type (cauliflower, chicken wing, and arrowhead type), left atrium (LA) and left ventricle (LV) segmented from contrast-enhanced computed tomography of the heart (Mimics Innovation Suite 22, Materialise).

hold. The imaging parameters for dual-source CT were: a tube voltage of 100–120 kV and an effective tube current of 350–400 mA. The collimation and temporal resolution were 2 × 32 × 0.6 mm and 165 ms, respectively. The time of arrival of the contrast agent to the ascending aorta was determined at the level of the tracheal bifurcation and achieved with the test bolus method. Then, the 15 mL of contrast agent was infused, which was followed by 20 mL of saline. The contrast agent was injected at a dose of 1.0 mL/kg at a rate of 5.5 mL/s followed by a 40 mL saline chaser with the same infusion rate. In the test bolus, the acquisitions delay was the time of maximum density of the ascending aorta with an additional 6 s of delay. Images were reconstructed with a B26f and B46f kernel and an image matrix of 512 × 512 pixels. A multiphase reconstruction (from 10% to 100%) was done. Moreover, 30% (left ventricle end-systole) and 70% (left ventricle end-diastole) image reconstructions were evaluated. Then, the initial quality check was performed using multiplanar reconstructions.

Image postprocessing and analysis

Postprocessing analyses of CT scans were performed on dedicated workstations (Dell, USA). Three-dimensional (3D) reconstructions of the heart subcomponents (LAA, LA, and left ventricle) were created using volume-rendering and segmentation techniques using Innovation Suite 23 (Materialise, Belgium) software in both end-diastolic and end-systolic cardiac phases. Manual and semi-automatic methods of segmentation were used. Next, raw data and visualizations were subjected to multidirectional morphological and morphometrical analyses.

First, two independent, blinded to patients history investigators classified LAA based on its shape into one of the three groups: cauliflower, chicken wing, or arrowhead as discussed previously (Fig. 1) [23]. Additionally, some individual lobes have been established. The LAA orifice and body were measured on the 3D reconstructions in the end-diastolic phase of the heart using virtual callipers (Fig. 2). Orifice shape, dimensions, area, and perimeter were measured. In addition, the maximal LAA body length (from orifice to the most far point) and width (in the widest point at the LAA base) were obtained. Depth of the LAA chamber was measured as a distance from the orifice plane to the last perpendicular and the orifice plane. For the chicken wing type, the angle of the bend and lengths from orifice to bend and from the bend to the LAA apex were also evaluated. The main dimensions of the left ventricle and atrium were estimated. The volume of the LAA left atrium and the left ventricle was measured in end-diastolic and end-systolic cardiac phases. Then, ejection fractions of the above-mentioned chambers were calculated.

To reduce human bias, all measurements were recorded by two independent, blinded to patients history investigators. If results between the two re-

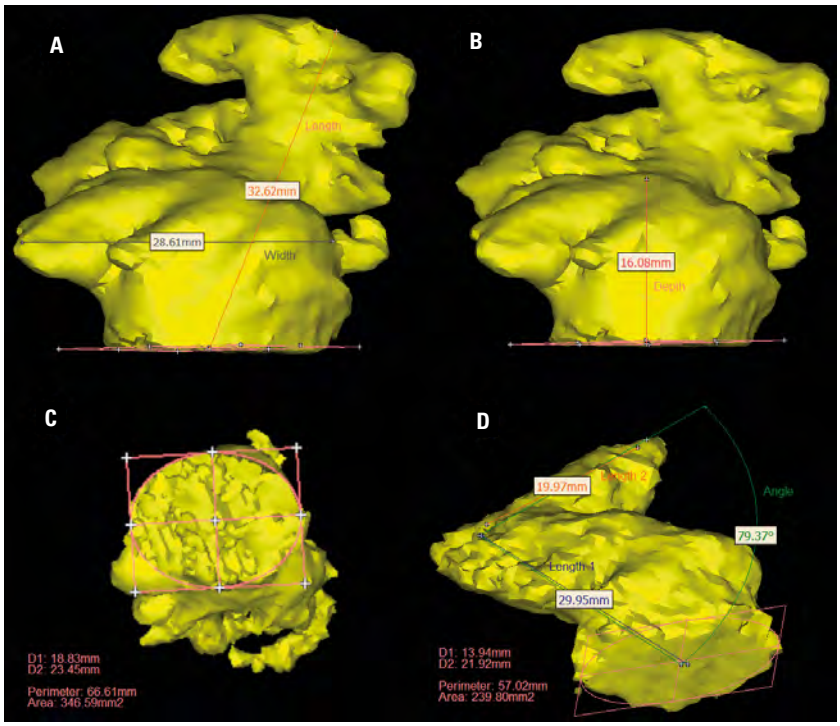

Figure 2. Three-dimensional visualisations of left atrial appendages (LAA) with marked measurements (Mimics Innovation Suite 22, Materialise); **A.** Body length and width; **B.** Depth of LAA chamber; **C.** Orifice dimensions (D1 and D2), area and perimeter; **D.** Angle of the bend and body lengths for chicken wing type.

searchers varied by more than 10%, both measurements were repeated. The mean of the two new values was calculated and reported as the final value.

Statistical analyses

Data are shown as mean values with corresponding standard deviations (± SD) or in percentages. The Shapiro–Wilk test was used to determine if the quantitative data were normally distributed, and Levene's test was performed to verify a relative homogeneity of variance. The Student t-tests, Wilcoxon signed-rank tests, and the Mann–Whitney U tests with Bonferroni corrections were used to conduct statistical comparisons. The non-parametric Kruskal–Walli's test was used to compare values between groups. Bonferroni correction was applied because of multiple comparisons. Correlation coefficients were calculated to assess whether there was a statistical dependence between the analysed parameters. A p-value lower than 0.05 was considered statistically significant. Statistical analyses were performed using StatSoft STATISTICA 13.3 software for Windows (StatSoft Inc., Tulsa, OK, USA).

RESULTS

Clinical characteristics of studied patients are presented in Table 1. Among the study group, 29.4% of patients had a history of ischaemic stroke. Arterial hypertension was more common in the study group than in control subjects (90.2 vs. 38.0%, $p < 0.001$). The clinical manifestation of chronic heart failure symptoms was significantly more severe in study group patients (NYHA scale, Table 1). Moreover, patients subjected to the LARIAT procedure have significantly higher thromboembolic risk than control patients (CHA_2DS_2-VASc, Table 1). No other significant differences in patients' demographic and clinical data were found.

The chicken wing shape was the most common type of LAA both in the study and control group (45.1 vs. 46.0%, $p = 0.93$), followed by arrowhead (29.4 vs. 20.0%, $p = 0.27$) and cauliflower (25.5 vs. 34.0%, $p = 0.35$) (Table 2). Although no statistically significant differences in LAA type distributions were found between groups, the study group was characterized by LAAs with a lower number of lobes (Table 2).

In both analysed groups, the LAA orifice was predominantly oval (study group: 94.0% vs. control group: 70.4%), and significantly fewer round orifices were found in the study group ($p = 0.001$, Table 2). Moreover, the size of the orifice was found to be significantly larger in LARIAT patients compared to the control group (higher diameters, orifice area, and orifice perimeter, Table 2).

Several major LAA morphometrical features were analysed (body length, body width, and chamber depth). However, no statistically significant differences

Table 1. Clinical characteristics of studied patients

Variable	Study group (n = 51)	Control group (n = 50)	P
Females (%)	41.2%	50.0%	0.09
Age [years]	61.04 (10.35)	57.80 (14.45)	0.20
Body mass index [kg/m^2]	28.8 (5.4)	28.6 (4.9)	0.83
Non-sinus tachycardia	51/100.0%	0/0.0%	< 0.001
Arterial hypertension	46/90.2%	19/38.0%	< 0.001
Hyperlipidaemia	3/5.9%	2/4.0%	0.67
Chronic heart failure	10/19.6%	6/12.0%	0.30
Coronary artery disease	11/21.6%	6/12.0%	0.20
Chronic obstructive pulmonary disease	2/3.9%	4/8.0%	0.39
Diabetes mellitus type II	6/11.8%	5/10.0%	0.78
History of myocardial infarction	1/2.0%	2/4.0%	0.55
History of ischaemic stroke	15/29.4%	0/0.0%	< 0.001
CCS:			
I	5/9.8%	3/6.0%	0.48
II	8/15.7%	4/8.0%	0.24
III	0/0.0%	1/2.0%	0.31
IV	0/0.0%	0/0.0%	–
NYHA:			
I	14/27.5%	6/12.0%	0.05
II	20/39.2%	8/16.0%	0.01
III	3/5.9%	0/0.0%	0.08
IV	0/0.0%	0/0.0%	–
CHA_2DS_2-VASc:			
0 (males) or 1 (females) — "low risk"	2/3.92%	22/44.0%	< 0.001
1 (males) — "low-moderate risk"	11/21.6%	5/10.0%	0.11
≥ 2 — "moderate-high risk"	38/74.5%	23/46.0%	0.01

Data are shown as number/% or mean (standard deviation). CCS — the Canadian Cardiovascular Society grading of angina pectoris; NYHA — New York Heart Association Classification of Heart Failure; CHA_2DS_2-VASc — risk stratification score for estimation of stroke risk for nonvalvular atrial fibrillation in adults

were found in those measured parameters between the two groups (all $p > 0.05$, Table 2). No differences between groups were noted in LAA end-systolic volumes, but a significant difference was observed in the end-diastolic cardiac phase (Table 2). The calculated LAA ejection fraction was significantly lower in the study group compared to healthy patients (16.4 ± 14.9 vs. 48.2 ± 12.9%, $p = 0.001$). For the chicken wing type, the angle of the bend was significantly smaller in LARIAT patients than in the control group (62.1 ± 10.4 vs. 68.5 ± 13.9°, $p = 0.011$). The LAA body lengths measured from orifice to bend and from bend to LAA apex showed no differences between analysed groups (to bend: 22.7 ± 3.8 vs. 18.4 ± 5.5 mm, $p = 0.103$; from bend: 28.1 ± 4.6 vs. 27.3 ± 5.8 mm, $p = 0.443$).

A significantly larger LA was observed in the study group compared to controls (larger anteroposterior diameter and volume) with reduced LA ejection fraction in LARIAT patients (13.9 ± 10.8 vs. 17.7 ± ± 6.5%, $p = 0.04$) (Table 2). No differences were found in measured left ventricle dimensions, volumes, and ejection fraction between investigated groups (all $p > 0.05$, Table 2). No other significant correlations and differences were found between all measured morphometric parameters.

DISCUSSION

The LAA morphology plays a significant role in the pathogenesis of ischaemic stroke. It was proven that complex LAA (non-chicken wing shape) is an independent risk factor for cryptogenic ischaemic stroke [6, 27]. However, little is known about the LAA anatomy that influences the course and results of the LAA closure procedures. Without a doubt,

Table 2. Comparison of corresponding parameters measured in both groups

Parameter	Study group (n = 51)	Control group (n = 50)	P
LAA shape (%):			
Cauliflower	25.5	34.0	0.35*
Chicken wing	45.1	46.0	0.93*
Arrowhead	29.4	20.0	0.27*
Number of LAA lobes (%):			
1	39.2	16.0	0.01**
2	33.3	20.0	0.13**
3	19.6	34.0	0.10**
≥ 4	7.8	30.0	0.01**
LAA orifice shape round/oval [%]	6.0/94.0	29.6/70.4	0.001
LAA orifice antero-posterior diameter [mm]	19.3 (4.12)	17.2 (4.0)	0.01
LAA orifice transverse diameter [mm]	25.1 (5.1)	20.5 (4.4)	0.001
LAA orifice area [mm^2]	387.2 (133.9)	327.1 (128.3)	0.02
LAA orifice perimeter [mm]	70.2 (12.5)	61.2 (11.6)	0.04
LAA body length [mm]	47.4 (15.4)	43.7 (10.9)	0.17
LAA width at the base [mm]	24.7 (5.6)	24.4 (5.8)	0.81
LAA chamber depth [mm]	17.7 (3.5)	16.5 (3.8)	0.11
LAA end-diastolic volume [mL]	9.0 (3.4)	5.4 (3.8)	0.001
LAA end-systolic volume [mL]	10.9 (3.6)	10.6 (4.3)	0.69
LAA ejection fraction [%]	16.4 (14.9)	48.2 (12.9)	0.001
Left atrial end-diastolic antero-posterior diameter [mm]	40.1 (6.9)	36.0 (7.1)	0.001
Left atrial end-diastolic volume [mL]	109.5 (38.9)	93.8 (30.8)	0.02
Left atrial end-systolic volume [mL]	129.5 (41.7)	112.5 (34.3)	0.04
Left atrial ejection fraction [%]	13.9 (10.8)	17.7 (6.5)	0.04
Left ventricular end-diastolic inner diameter [mm]	45.5 (6.8)	46.4 (6.3)	0.47
Left ventricular end-diastolic volume [mL]	124.5 (48.1)	133.5 (39.1)	0.15
Left ventricular end-systolic volume [mL]	68.7 (40.5)	65.7 (25.0)	0.56
Left ventricular ejection fraction [%]	46.7 (14.3)	50.7 (12.2)	0.14

Data are shown as % or mean (standard deviation). LAA — left atrial appendage; *Results are considered statistically significant at $p < 0.017$ to allow for a Bonferroni correction accounting for the multiple comparisons;**Results are considered statistically significant at $p < 0.013$ to allow for a Bonferroni correction accounting for the multiple comparisons

a significant morphologic remodelling of the LA occurs in patients with non-sinus rhythm [3, 25]. Nevertheless, a lack of consensus is observed regarding the LAA structural alterations related to rhythm and hemodynamical disturbances [3, 13]. Although it is hard to believe that the remodelling may concern the type (shape) of the LAA body, the changes in the LAA orifice shape and size, LAA body size, and LAA function may be substantial.

Regardless of the technique used, residual leaks after the LAA are commonly observed [9]. Our study shows that in AF patients, the biggest morphological changes are found in the LAA orifice, crucial for all LAA closure procedures. Left atria remodelling associated with enlargement in heart failure and arrhythmia patients changes the shape and size of the LAA opening. LAA orifices in diseased patients are significantly larger and more oval, which affects the risk of leakage [18]. An incomplete sealing may potentially occur in cases where an appropriately large device is used to close the LAA when implanted not in the round and when in oval or in irregular shape orifice [18]. Thus, operators should be aware of this change in LAA orifice morphology and choose the appropriate tool for the LAA closure to avoid danger to the health and life of patients' peri-device leaks. The observed reduced LAA ejection fraction in research group is another important observation emerging from the current work. The LAA ejection fraction was decreased even despite performing tomography scans during sinus

rhythm. This reduced contractile function of the LAA may be the indirect result of remodelling of the LA and altered atrial blood pressure, which influence structure of the LAA itself leading to impaired contractility of LAA. In paroxysmal AF remodelling of LA is most often negligible and reversable. The duration time of LA rhythm disturbances negatively affects the structure of the atrium. Persistent AF strongly promotes electrical remodelling and pressure/volume overload of LA promotes interstitial fibrosis leading to structural remodelling [23]. It follows that irreversible changes in LA morphology and consequently in LAA structure may start to develop in patients with AF lasting more than one week [1, 5]. On the other hand, the increased left atrial pressure may create to high resistance for the LAA to generate the effective force of its contraction. Previous studies showed that LAA ejection fraction may be an independent predictor of cardiac thrombo-embolization [8,22], which alters LAA emptying and predisposes to local blood stasis and its increased thrombogenicity [19].

Cardiac CT seems to be the preferable tool for pre-procedural imaging of the LAA as it provides the most faithful, 3D image of the LAA [24]. Moreover, it helps visualize other important heart cavities and main vessels (together with coronary vasculature), in which knowledge of morphology is crucial to avoid serious peri-procedural complications [7, 23]. Our study also indicates that LAA 3D visualization may provide useful information for the operator on the LAA morphology, thereby influencing the choice of the technique of its closure. The creation of a fully personalized virtual 3D model of the patient's LAA may be completed in less than an hour. This model can easily be subjected to multi-directional measurement or used to simulate procedures [10]. Moreover, the created model may be visualized using virtual or augmented reality techniques or using the 3D printed technique to better assist the clinicians [17]. Unfortunately, one of the obstacles to the use of this wonderful tool in all medical centres is the relatively low availability and high cost of software enabling the segmentation and visualization of the CT data, as well as the lack of experience of the staff in manufacturing the 3D models [15].

Some limitations to this study should be considered. First, this is a single-centre study with a relatively small sample size. A limited number of patients in both groups does not allow a comprehensive statistical analysis to determine which LAA morphometrical factors may contribute to the occurrence of a stroke or are associated with success rate or complications during the LARIAT procedure. Moreover, only Caucasian subjects were studied, and no inter-racial differences are studied. Despite these limitations, we believe that the current study has provided insight into the morphological characteristics of the LAA in different groups of patients.

CONCLUSIONS

Presented morphometrical data should be considered during planning and when performing procedures targeted to LAA closure, as significant differences in the anatomy of the LAA may be encountered in patients with AF. Substantial morphometrical differences in LAA orifice are found, which is significantly larger and more oval in patients with AF compared to healthy controls. Although no difference in LAA body type and size is observed, the LAA ejection fraction is significantly lower in AF patients.

Funding

This study was supported by the National Centre for Research and Development under the LIDER programme (LIDER/7/0027/L-10/18/NCBR/2019).

Conflict of interest: None declared

REFERENCES

1. Ausma J, Litjens N, Lenders MH, et al. Time course of atrial fibrillation-induced cellular structural remodeling in atria of the goat. J Mol Cell Cardiol. 2001; 33(12): 2083–2094, doi: 10.1006/jmcc.2001.1472, indexed in Pubmed: 11735256.
2. Bartus K, Podolec J, Lee RJ, et al. Atrial natriuretic peptide and brain natriuretic peptide changes after epicardial percutaneous left atrial appendage suture ligation using LARIAT device. J Physiol Pharmacol. 2017; 68(1): 117–123, indexed in Pubmed: 28456775.
3. Floria M, Radu S, Gosav EM, et al. Left atrial structural remodelling in non-valvular atrial fibrillation: what have we learnt from CMR? Diagnostics (Basel). 2020; 10(3), doi: 10.3390/diagnostics10030137, indexed in Pubmed: 32131455.
4. Glikson M, Wolff R, Hindricks G, et al. EHRA/EAPCI expert consensus statement on catheter-based left atrial appendage occlusion — an update. EuroIntervention. 2020; 15(13): 1133–1180, doi: 10.4244/EIJY19M08_01, indexed in Pubmed: 31474583.
5. Goette A, Honeycutt C, Langberg JJ. Electrical remodeling in atrial fibrillation. Time course and mechanisms. Circulation. 1996; 94(11): 2968–2974, doi: 10.1161/01.cir.94.11.2968, indexed in Pubmed: 8941128.
6. Gwak DS, Choi W, Kim YW, et al. Impact of left atrial appendage morphology on recurrence in embolic stroke of undetermined source and atrial cardiopathy. Front Neu-

rol. 2021; 12: 679320, doi: 10.3389/fneur.2021.679320, indexed in Pubmed: 34239496.
7. Hołda MK, Koziej M, Hołda J, et al. Anatomic characteristics of the mitral isthmus region: The left atrial appendage isthmus as a possible ablation target. Ann Anat. 2017; 210: 103–111, doi: 10.1016/j.aanat.2016.11.011, indexed in Pubmed: 27986642.
8. Iwama M, Kawasaki M, Tanaka R, et al. Left atrial appendage emptying fraction assessed by a feature-tracking echocardiographic method is a determinant of thrombus in patients with nonvalvular atrial fibrillation. J Cardiol. 2012; 59(3): 329–336, doi: 10.1016/j.jjcc.2012.01.002, indexed in Pubmed: 22342529.
9. Jang SJ, Wong SC, Mosadegh B. Leaks after left atrial appendage closure: ignored or neglected? Cardiology. 2021; 146(3): 384–391, doi: 10.1159/000513901, indexed in Pubmed: 33735867.
10. Jia D, Jeon B, Park HB, et al. Image-Based flow simulations of pre- and post-left atrial appendage closure in the left atrium. Cardiovasc Eng Technol. 2019; 10(2): 225–241, doi: 10.1007/s13239-019-00412-7, indexed in Pubmed: 30953246.
11. John Camm A, Colombo A, Corbucci G, et al. Left atrial appendage closure: a new technique for clinical practice. Heart Rhythm. 2014; 11(3): 514–521, doi: 10.1016/j.hrthm.2013.11.030, indexed in Pubmed: 24291776.
12. Karim N, Ho SY, Nicol E, et al. The left atrial appendage in humans: structure, physiology, and pathogenesis. Europace. 2020; 22(1): 5–18, doi: 10.1093/europace/euz212, indexed in Pubmed: 31578542.
13. Kishima H, Mine T, Takahashi S, et al. Morphologic remodeling of left atrial appendage in patients with atrial fibrillation. Heart Rhythm. 2016; 13(9): 1823–1828, doi: 10.1016/j.hrthm.2016.06.009, indexed in Pubmed: 27291510.
14. Kleindorfer D, Towfighi A, Chaturvedi S, et al. 2021 guideline for the prevention of stroke in patients with stroke and transient ischemic attack: a guideline from the American Heart Association/American Stroke Association. Stroke. 2021; 52(7): 364–467, doi: 10.1161/str.0000000000000375.
15. Lau I, Wong YH, Yeong CH, et al. Quantitative and qualitative comparison of low- and high-cost 3D-printed heart models. Quant Imaging Med Surg. 2019; 9(1): 107–114, doi: 10.21037/qims.2019.01.02, indexed in Pubmed: 30788252.
16. Litwinowicz R, Bartus M, Burysz M, et al. Long term outcomes after left atrial appendage closure with the LARIAT device-Stroke risk reduction over five years follow-up. PLoS One. 2018; 13(12): e0208710, doi: 10.1371/journal.pone.0208710, indexed in Pubmed: 30566961.
17. Litwinowicz R, Witowski J, Sitkowski M, et al. Applications of low-cost 3D printing in left atrial appendage closure using epicardial approaches — initial clinical experience. Polish J Cardio-Thoracic Surg. 2018; 15(2): 135–140, doi: 10.5114/kitp.2018.76481, indexed in Pubmed: 30069196.
18. Maan A, Heist EK. Left atrial appendage anatomy: implications for endocardial catheter-based device closure. J Innov Card Rhythm Manag. 2020; 11(7): 4179–4186, doi: 10.19102/icrm.2020.110704, indexed in Pubmed: 32724709.
19. Masci A, Barone L, Dedè L, et al. The impact of left atrium appendage morphology on stroke risk assessment in atrial fibrillation: a computational fluid dynamics study. Front Physiol. 2018; 9: 1938, doi: 10.3389/fphys.2018.01938, indexed in Pubmed: 30723422.
20. Naksuk N, Padmanabhan D, Yogeswaran V, et al. Left atrial appendage: embryology, anatomy, physiology, arrhythmia and therapeutic intervention. JACC Clin Electrophysiol. 2016; 2(4): 403–412, doi: 10.1016/j.jacep.2016.06.006, indexed in Pubmed: 29759858.
21. Patti G, Pengo V, Marcucci R, et al. The left atrial appendage: from embryology to prevention of thromboembolism. Eur Heart J. 2017; 38(12): 877–887, doi: 10.1093/eurheartj/ehw159, indexed in Pubmed: 27122600.
22. Shimizu T, Takada T, Shimode A, et al. Association between paroxysmal atrial fibrillation and the left atrial appendage ejection fraction during sinus rhythm in the acute stage of stroke: a transesophageal echocardiographic study. J Stroke Cerebrovasc Dis. 2013; 22(8): 1370–1376, doi: 10.1016/j.jstrokecerebrovasdis.2013.03.020, indexed in Pubmed: 23608370.
23. Słodowska K, Szczepanek E, Dudkiewicz D, et al. Morphology of the left atrial appendage: introduction of a new simplified shape-based classification system. Heart Lung Circ. 2021; 30(7): 1014–1022, doi: 10.1016/j.hlc.2020.12.006, indexed in Pubmed: 33582020.
24. Taina M, Korhonen M, Haataja M, et al. Morphological and volumetric analysis of left atrial appendage and left atrium: cardiac computed tomography-based reproducibility assessment. PLoS One. 2014; 9(7): e101580, doi: 10.1371/journal.pone.0101580, indexed in Pubmed: 24988467.
25. Thomas L, Abhayaratna WP. Left atrial reverse remodeling: mechanisms, evaluation, and clinical significance. JACC Cardiovasc Imaging. 2017; 10(1): 65–77, doi: 10.1016/j.jcmg.2016.11.003, indexed in Pubmed: 28057220.
26. Wilkins B, Fukutomi M, De Backer O, et al. Left atrial appendage closure: prevention and management of periprocedural and postprocedural complications. Card Electrophysiol Clin. 2020; 12(1): 67–75, doi: 10.1016/j.ccep.2019.10.003, indexed in Pubmed: 32067649.
27. Yamamoto M, Seo Y, Kawamatsu N, et al. Complex left atrial appendage morphology and left atrial appendage thrombus formation in patients with atrial fibrillation. Circ Cardiovasc Imaging. 2014; 7(2): 337–343, doi: 10.1161/CIRCIMAGING.113.001317, indexed in Pubmed: 24523417.
28. Zuo K, Sun L, Yang X, et al. Correlation between cardiac rhythm, left atrial appendage flow velocity, and CHA2DS2-VASc score: Study based on transesophageal echocardiography and 2-dimensional speckle tracking. Clin Cardiol. 2017; 40(2): 120–125, doi: 10.1002/clc.22639, indexed in Pubmed: 28075503.

VIA MEDICA

ORIGINAL ARTICLE

Folia Morphol.
Vol. 82, No. 4, pp. 822–829
DOI: 10.5603/FM.a2022.0100

ISSN 0015–5659
eISSN 1644–3284
journals.viamedica.pl

A coronary computed tomography angiography study on anatomical characteristics of the diagonal branch of anterior interventricular artery

D.-Q. Zhang[1, 2], Y.-F. Xu[2], Y.-P. Dong[2], S.-J. Yu[1, 2]

[1]*Hebei Medical University, Shijiazhuang, China*
[2]*Department of Diagnostic CT, Cangzhou Central Hospital, Cangzhou, China*

[Received: 22 September 2022; Accepted: 12 November 2022; Early publication date: 29 November 2022]

Background: *This study investigated the anatomical characteristics of the ramus intermedius (RI) and its correlation with the proximal diameter of the branch vessels of the left coronary artery (LCA) using coronary computed tomography angiography (CCTA).*

Materials and methods: *We screened patients who underwent CCTA from January to September 2021 and randomly enrolled 267 with RI (RI group) and 134 without RI (control group). We evaluated the anatomical features of RI (distribution, proximal diameter, length). We measured the proximal diameter of the anterior interventricular branch of the left coronary artery (LAD) and the circumflex branch of the left coronary artery (LCX). We compared the differences between groups in the proximal diameter of LAD and LCX and the correlation between gender and each parameter of the LCA (LAD, LCX, RI) within the RI group. In addition, we compared the correlation between the distribution characteristics of RI and the proximal diameter of LAD and LCX within the RI group.*

Results: *The LAD and LCX proximal diameters in the RI group were significantly smaller than those in the control group ($p < 0.05$). Comparisons within the RI group showed the following results: the RI distribution, RI diameter and length, and the LCX proximal diameter were not significantly different between male and female patients ($p > 0.05$), and the LAD proximal diameter was significantly larger in male than in female patients ($p < 0.05$). There were statistically significant differences in the LAD and LCX proximal diameters between the different RI distribution groups ($p < 0.05$). Based on the pairwise comparison, there were significant differences in the LAD (LCX) proximal diameter between the RI-beside--the-LAD (LCX) group and the RI-middle group, as well as between the RI-beside--the-LAD (LCX) group and the RI-beside-the-LCX (LAD) group ($p < 0.05$).*

Conclusions: *A CCTA accurately evaluated the anatomical characteristics of an RI, which has an impact on the proximal diameter of the branch vessels of the LCA (i.e. LAD and LCX), the degree of influence of which is correlated with the RI distribution.* (Folia Morphol 2023; 82, 4: 822–829)

Key words: ramus intermedius, bifurcation angle, coronary computed tomography angiography

Address for correspondence: S.-J. Yu, BM, Department of Diagnostic CT, Cangzhou Central Hospital, No.16 of Xinhua West Road, Canal District, Cangzhou 061000, China, tel: +86 18531705788, e-mail: 20204202@stu.hebmu.edu.cn

INTRODUCTION

The anatomical structure of the left main bifurcation area is an important factor impacting the haemodynamics of this condition, atherosclerosis, collateral damage, choice of interventional therapy, and clinical prognosis [4, 6, 12, 16]. Studies have shown that the size of the anterior interventricular branch of the left coronary artery (LAD)-circumflex branch of the left coronary artery (LCX) bifurcation angle is positively correlated with arteriosclerosis in the bifurcation area [2, 14]. The occurrence and development of coronary heart disease are subject to the proximal vessel diameter of the bifurcation part of the left coronary artery (LCA), and scholars have conducted the following corresponding mathematical modelling [8]. Liu et al. [11] measured the proximal diameter of left bifurcation in patients with a predominant right coronary artery and no ramus intermedius (RI). The results showed that the proximal diameter of the LAD was 3.48 ± 0.77 mm, and the proximal diameter of the LCX was 3.21 ± 1.07 mm. The RI is a coronary artery branch originating from the end of the left main coronary artery (LM) between the LAD and LCX. The emergence of an RI will change the anatomical structure of the original left main bifurcation area, splitting the bifurcation angle into two parts and dividing the LCA blood flow into three parts, which may cause changes in the diameter of the LAD and LCX and cause abnormal haemodynamics. No specific studies on RI were found as part of the current study's literature review. The purpose of this study was to explore the anatomical characteristics of an RI, and the correlation of its presence and location with the proximal diameter of the branch vessel of LCA using coronary computed tomography angiography (CCTA), and then provide guidance for the study of the influencing factors of atherosclerosis in the left main bifurcation area and the decision of interventional treatment.

MATERIALS AND METHODS

Participants

A total of 4,866 patients who underwent CCTA examinations in Cangzhou Central Hospital from January 1, 2021, to September 1, 2021, were selected as the study participants. Among them, 1,202 patients were identified as having an RI from the Picture Archiving and Communication System (PACS). After calculating the detection rate, 267 patients were included according to the exclusion criteria (outlined later in this section). These included 138 males with an average age of 54.05 ± 0.97 years and 129 females with an average age of 56.98 ± 0.87 years. In addition, 500 participants were randomly selected from the 3,664 patients without an RI using a computerized random number generator, and, among them, 134 patients were added to the control group according to the exclusion criteria (so that the sample size met the statistical requirements). This included 69 males with an average age of 50.14 ± 11.54 years and 69 females with an average age of 55.06 ± 9.67 years. The inclusion criteria comprised patients who underwent a CCTA examination in the authors' hospital and had complete clinical and imaging data. The exclusion criteria were as follows: 1) patients with metal implants (i.e. a stent or pacemaker); 2) patients with a history of coronary artery bypass surgery; 3) patients with organic heart disease (including heart valve implantations); 4) patients with a coronary artery anomaly (such as the abnormal origin of a coronary artery [coronary arteriovenous fistula]); 5) patients with poor CCTA image quality, or a missing image; 6) patients with a mural coronary artery (LAD, LCX, RI ≥ 1); 7) patients without a predominant right coronary artery; 8) patients with non-single RIs (excluding those without an RI); 9) patients with at least one diffuse plaque at the bifurcation part of the LCA.

Examination methods

All patients fasted for more than 4 h before the examination and were treated with an intravenous indwelling needle. All patients had their heart rate measured via an electrocardiogram and took part in breath-hold respiratory training; those with a higher heart rate were given beta-blockers to stabilise and control the heart rate within 74 bpm.

A Toshiba Aquiline ONE 320-slice computed tomography scanner was used to image and post-process all of the participants. Each patient was placed in a supine position with their feet entering the scanner first, and with their arms extended straight over their head. Three leads were placed at the bilateral subclavian region of the left ribs and lower margins to monitor heart rate changes in real-time. Scanning was performed on the patient in a single end-inspiratory hold.

The scanning range was determined to range from the lower tracheal bifurcation to the diaphragm according to anteroposterior and lateral images, which included the entire heart with a range of 140–160 mm. A non-ionic contrast medium (Iohexol, 60–65 mL)

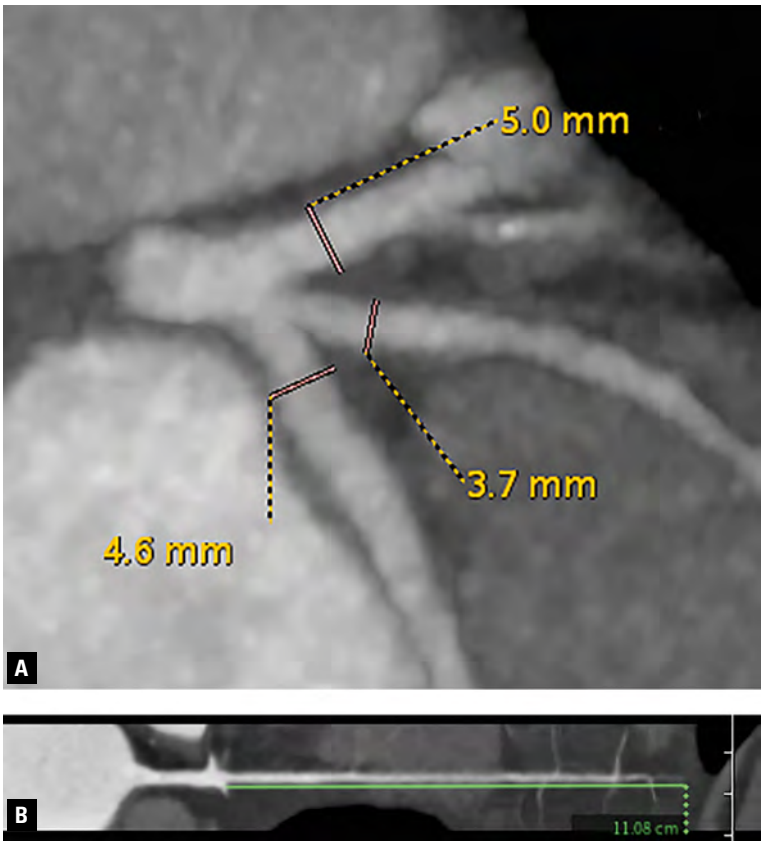

Figure 1. A. Diameter measurement; **B.** Ramus intermedius length measurement.

was injected at a flow rate of 4.5–5.0 mL/s with a Mallinckrodt dual-chamber high-pressure syringe, and the flow rate and volume were adjusted according to the body weight and vascular condition of the patient. Then, 40 mL of normal saline was injected at the same flow rate. Monitoring began 10 s after the injection of the contrast medium to observe the time-density curve.

The left ventricle was selected as the monitoring area for manual triggering with a trigger threshold of 150 Hounsfield Unit (HU). The scanning parameters were a tube voltage of 120 kV, a scanning slice thickness and incremental increase of 0.5 mm, and a scanning speed of 0.35 s. All the scans were performed in an intracardiac tube current using autoregulation mode to reduce the radiation dose.

Image post-processing and measurement

The optimal diastolic images were selected and uploaded to the Shukun CCTA image vascular stenosis analysis software and a General Electric AW4.6 workstation for post-processing to generate the two-dimensional (2D) and three-dimensional (3D) reconstruction images. The maximum diameters (including the tube wall) of the proximal LAD, LCX, and RI (1 cm from the bifurcation) were measured on the 2D oblique map (window level = 40 HU, window width = 400 HU, Fig. 1A). The 2D curved planar reconstruction was selected for length measurement (Fig. 1B), with the length of the RI measured from the initial part of the RI to the visible end.

The distribution judgment of the RI was conducted based on the 3D volume rendering (Fig. 2). The RI distribution was divided into three types according to the boundary of the line from the initial part to the cardiac apex: 1) the beside-the-LAD-group (Fig. 2A); 2) the middle group (Fig. 2B); 3) the beside-the-LCX--group (Fig. 2C).

Ethics approval and consent to participate

The study was conducted in accordance with the Declaration of Helsinki (as was revised in 2013). The study was approved by Ethics Committee of the Cangzhou Central Hospital. Written informed consent was obtained from all participants.

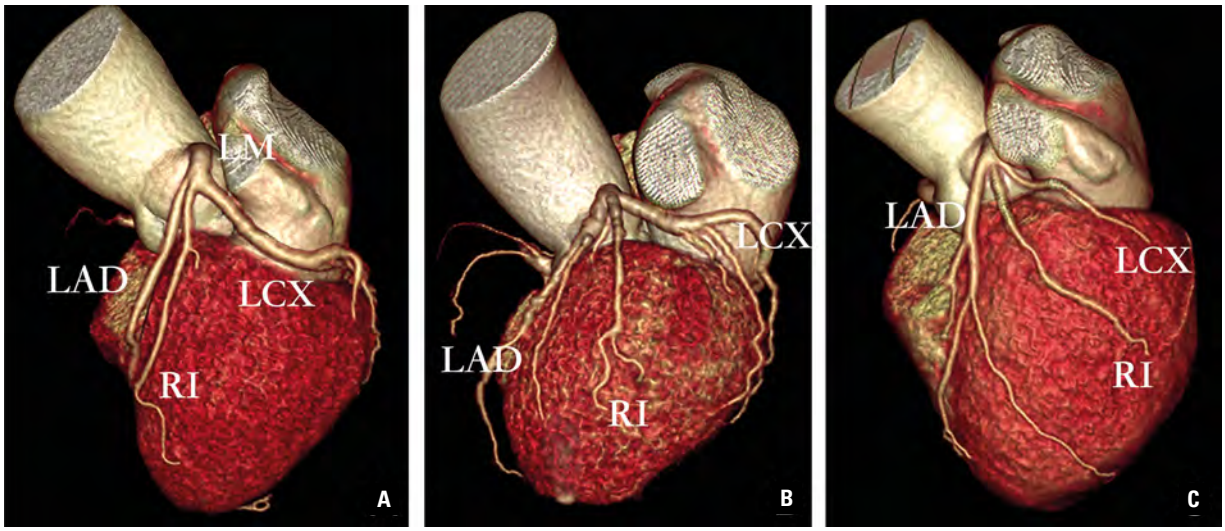

Figure 2. Distribution of ramus intermedius (RI); **A.** Ramus intermedius is close to the anterior interventricular branch of the left coronary artery (LAD); **B.** Ramus intermedius is located in the centre; **C.** Ramus intermedius is close to the circumflex branch of the left coronary artery (LCX); LM — left main coronary artery.

Statistical analysis

All data were statistically analysed using the SPSS Statistics 26.0 software programme. The measurement data were expressed as mean ± standard deviation (x ± SD). A t-test and one-way analysis of variance was conducted for data with a normal distribution and a homogeneity of variance, and the least significant difference method was used for pairwise comparison. In contrast, a nonparametric test was used for the data that did not have either a normal distribution or homogeneity of variance. The enumeration data were expressed as n/% and compared using a chi-square test. A p-value below 0.05 indicated that the difference was statistically significant (test α level = 0.05 for both sides).

RESULTS

The RI detection rate

Among the 4,866 patients that underwent a CCTA examination in Cangzhou Central Hospital from January 1, 2021, to September 1, 2021, 1,202 were found with an RI (detection rate, 24.7%).

Comparison of the left main coronary artery parameters in the RI group by gender

There were no statistically significant differences in the number of cases concerning the RI distribution by gender for any of the three types ($p > 0.05$, Table 1). There were no statistically significant differences in the RI diameter and length, RI distribution, or the LCX proximal diameter ($p > 0.05$, Table 1). The LAD proximal diameter in males was 4.09 ± 0.68 mm, while for females this was 3.86 ± 0.54 mm, indicating a significantly higher value in males than in females ($p < 0.05$, Table 1).

Comparison of the proximal diameters of the LAD and LCX among the RI distribution groups

There were no statistically significant differences in the RI distribution between males and females ($p > 0.05$, Table 2). The LAD proximal diameter was 3.75 ± 0.55, 4.04 ± 0.63, and 4.00 ± 0.64 mm in the beside-the-LAD-group, the beside-the-LCX-group, and the middle group, respectively, and the differences were statistically significant ($p < 0.05$, Table 2). The pairwise comparison showed that, in terms of measurements, the beside-the-LAD-group was significantly lower than the beside-the-LCX-group ($p < 0.05$, Fig. 3A); the beside-the-LAD-group was significantly lower than the middle group ($p < 0.05$, Fig. 3A), and the middle group was significantly lower than the beside-the-LCX-group ($p > 0.05$, Fig. 3A). The LCX proximal diameters were 3.74 ± 0.66, 3.35 ± 0.66, and 3.64 ± 0.69 mm in the beside-the-LAD-group, the beside-the-LCX--group, and the middle group, respectively, and the differences were statistically significant ($p < 0.05$, Table 2). The pairwise comparison showed that measurement-wise, the beside-the-LCX-group was

Table 1. Correlation between gender and left coronary artery parameters in the ramus intermedius (RI) group

	Male (n = 138)	Female (n = 129)	P
Age [years]	54.05 ± 11.44	56.98 ± 9.84	0.026
RI diameter [mm]	2.74 ± 0.63	2.60 ± 0.65	0.081
RI length [cm]	6.61 ± 2.63	6.30 ± 3.01	0.260
RI distribution (n/%):			
Beside LAD group	21/15.2%	22/17.1%	
Beside LCX group	72/52.2%	65/50.4%	0.913
Middle group	45/32.6%	42/32.6%	
LAD proximal diameter [mm]	4.09 ± 0.68	3.86 ± 0.54	0.002
LCX proximal diameter [mm]	3.57 ± 0.74	3.44 ± 0.63	0.135

LAD — anterior interventricular branch of the left coronary artery; LCX — circumflex branch of the left coronary artery

Table 2. Comparison of the anterior interventricular branch of the left coronary artery (LAD) and the circumflex branch of the left coronary artery (LCX) proximal diameter in each the ramus intermedius (RI) distribution group

	Beside LAD group (n = 43)	Beside LCX group (n = 137)	Middle group (n = 87)	χ^2 or F	P
Gender (n/%):					
Male	21/48.8%	72/52.6%	45/51.7%	0.181	0.913
Female	22/51.2%	65/47.4%	42/48.3%		
LAD proximal diameter [mm]	3.75 ± 0.55	4.04 ± 0.63	4.00 ± 0.64	3.519	0.031
LCX proximal diameter [mm]	3.74 ± 0.66	3.35 ± 0.66	3.64 ± 0.69	7.955	0.000

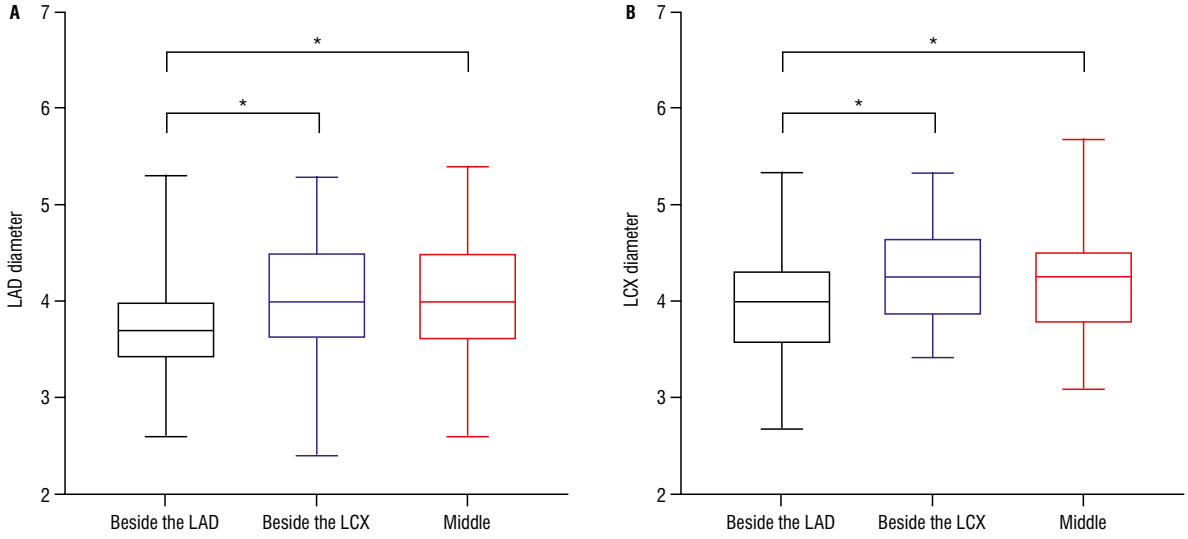

Figure 3. Pairwise comparison of anterior interventricular branch of the left coronary artery (LAD) (**A**) and the circumflex branch of the left coronary artery (LCX) (**B**) proximal diameter in each ramus intermedius distribution group; *The level of significance test for α is 0.05.

significantly lower than the beside-the-LAD-group ($p < 0.05$, Fig. 3B); the beside-the-LCX-group was significantly lower than the middle group ($p < 0.05$, Fig. 3B), and the middle group was significantly lower than the beside-the-LAD group ($p > 0.05$, Fig. 3B).

Comparison of the proximal diameters of the LAD and LCX between the RI group and the control group

There were no statistically significant gender differences between the LAD and LCX groups ($p > 0.05$, Table 3). The LAD proximal diameter was 3.98 ± 0.63 mm

Table 3. Comparison of the anterior interventricular branch of the left coronary artery (LAD) and the circumflex branch of the left coronary artery (LCX) proximal diameter between the ramus intermedius (RI) group and the control group

	With RI (n = 267)	Without RI (n = 134)	χ^2 or Z	P
Gender (n/%):				
Male	138/51.7%	69/51.5%	0.001	0.971
Female	129/48.3%	65/48.5%		
LAD proximal diameter [mm]	3.98 ± 0.63	4.57 ± 0.55	–8.327	0.000**
LCX proximal diameter [mm]	3.51 ± 0.69	4.08 ± 0.60	–7.645	0.000**

**The level of significance test for α is 0.001

in patients with an RI and 4.57 ± 0.55 mm in patients without an RI, indicating the diameter in patients with an RI was significantly smaller than in patients without an RI ($p < 0.05$, Table 3). The LCX proximal diameter was 3.51 ± 0.69 mm in patients with an RI and 4.08 ± 0.60 mm in patients without an RI, indicating that the diameter in patients with an RI was significantly smaller than in patients without an RI ($p < 0.05$, Table 3).

DISCUSSION

Ajayi et al. [1] reported an RI incidence of 21.8%, while Liu et al. [11] reported a detection rate of 25.6% for RIs in Xinjiang. In the present study, the detection rate of RIs in the current authors' hospital was similar at 24.7%.

The present study compared the RI length and diameter, the RI distribution, and the LAD and LCX diameters between males and females for the first time and found no statistically significant differences concerning RI length, diameter, or distribution. The LAD diameter was significantly higher in males than in females (4.09 ± 0.68 vs. 3.86 ± 0.54 mm, $p < 0.05$), but there were no statistically significant differences in the LCX diameter ($p > 0.05$). The differences in the LAD and LCX diameters between males and females in the population without RIs have been compared in domestic and foreign studies. Verim et al. [15] measured the lumen area at the proximal segments of the branch vessels of the LCA in 108 patients and found that the LAD lumen area in males was significantly larger than in females; no gender difference was observed in the LCX lumen area. Liu et al. [11] compared the lumen intraluminal diameter of proximal vessels between males and females at the left main bifurcation area of patients with predominant right coronary arteries and without RIs and found significant differences in the LAD and LCX intraluminal diameters (larger in males than in females). The mean intraluminal diameter was smaller than the data in the present study because the tube wall was included in the measurement process in the current paper. Gong [5] found that the LAD diameter in males was significantly larger than in females in a school-age group (i.e. ≥ 6 and < 9 years old). The findings of the current study are consistent with the research results of domestic and foreign scholars on the non-RI population, suggesting that individuals with and without RIs follow the same gender rules. Ren [13] found that the LAD diameter in males was significantly larger than in females in a non-normalised condition. Still, no statistically significant differences were observed after normalising height, weight, and body surface area parameters, indicating that the differences above had been the result of body surface area. This study was not normalised due to data collection.

The current study found that the diameters of the LAD and LCX in patients with an RI were significantly smaller than those in patients without an RI ($p < 0.05$). The reason for this was because the RI, an additional branching vessel, undertakes delivering part of the blood supply to the myocardium. Compared to patients without RIs, the blood flow of the LCA experienced additional shunting, and the blood flow of each branch vessel was reduced. Furthermore, the diameter of blood vessels may become thinner in a compensatory manner during the development of the human body.

The RI distribution was also divided into the beside-the-LAD-group, the beside-the-LCX-group, and the middle group. There were statistically significant differences in the LAD and LCX proximal diameters between the three groups ($p < 0.05$), i.e. the closer the RI was to the coronary artery, the more significant the effect on the decrease of the LAD and LCX proximal diameters. When the RI was in the middle, it had little effect on the diameter of the LCA on either side. This indicated that the closer the RI was to the coronary

artery, the higher the blood supply proportion of the original coronary artery was, with more obvious blood redistribution. Galbraith et al. [3] posited that the RI, a shunt vessel, would lead to a greater blood flow disturbance in the proximal segment of the LAD, and these blood flow disturbances may cause focal atherosclerosis. Meanwhile, studies [7, 9, 10] have indicated that 8.9%-19% of branch vessels were occluded following main branch stent implantation, with the severity associated with the diameters and lengths of the branch vessels. It is generally believed to be caused by the displacement of the bifurcation crest and plaque, as well as the suspension of the bifurcation opening stent. Compared to the population without an RI, those with an RI should be carefully monitored to observe whether the RI (a new branch of the LM) will be occluded after an LM and/or LAD proximal stent implantation, which will increase the incidence of myocardial infarction in the blood supply area. Further study of the anatomical structure and haemodynamics of the RI and the left main bifurcation area thus has great clinical significance.

CONCLUSIONS

Coronary computed tomography angiography could accurately evaluate the anatomical characteristics of RI, which can influence the proximal diameter of the branch vessels of the LCA (i.e. LAD and LCX), with the degree of influence correlated with the RI distribution. The limitations of this study are as follows: 1) the present study was a single-centre retrospective observational study with a low level of evidence; 2) the included cases were patients who had been admitted to the hospital due to illness; accordingly, a degree of bias may have been included; 3) the distribution type of the coronary artery could affect its anatomical data. To ensure research objectivity, only the population with predominance in the right coronary area was included in this study. Other factors that could have affected the measurement data were excluded, which may also have caused a degree of bias to be included.

Acknowledgements

We are particularly grateful to all the people who have given us help on our article.

Conflict of interest: None declared

REFERENCES

1. Ajayi NO, Lazarus L, Vanker EA, et al. The prevalence and clinical importance of an "additional" terminal branch of the left coronary artery. Folia Morphol. 2013; 72(2): 128–131, doi: 10.5603/fm.2013.0021, indexed in Pubmed: 23740499.
2. Cui Y, Zeng W, Yu J, et al. Quantification of left coronary bifurcation angles and plaques by coronary computed tomography angiography for prediction of significant coronary stenosis: A preliminary study with dual-source CT. PLoS One. 2017; 12(3): e0174352, doi: 10.1371/journal.pone.0174352, indexed in Pubmed: 28346530.
3. Galbraith EM, McDaniel MC, Jeroudi AM, et al. Comparison of location of "culprit lesions" in left anterior descending coronary artery among patients with anterior wall ST-segment elevation myocardial infarction having ramus intermedius coronary arteries versus patients not having such arteries. Am J Cardiol. 2010; 106(2): 162–166, doi: 10.1016/j.amjcard.2010.02.027, indexed in Pubmed: 20598997.
4. Genuardi L, Chatzizisis YS, Chiastra C, et al. Local fluid dynamics in patients with bifurcated coronary lesions undergoing percutaneous coronary interventions. Cardiol J. 2021; 28(2): 321–329, doi: 10.5603/CJ.a2020.0024, indexed in Pubmed: 32052855.
5. Gong T. Regression equations of z-scores of aorta and coronary arteries in healthy minors in Chongqing, China. Journal of Chongqing Medical University. 2020.
6. Gwon HC. Understanding the coronary bifurcation stenting. Korean Circ J. 2018; 48(6): 481–491, doi: 10.4070/kcj.2018.0088, indexed in Pubmed: 29856142.
7. Hahn JY, Chun WJ, Kim JH, et al. Predictors and outcomes of side branch occlusion after main vessel stenting in coronary bifurcation lesions: results from the COBIS II Registry (COronary BIfurcation Stenting). J Am Coll Cardiol. 2013; 62(18): 1654–1659, doi: 10.1016/j.jacc.2013.07.041, indexed in Pubmed: 23954335.
8. Huo Y, Finet G, Lefevre T, et al. Which diameter and angle rule provides optimal flow patterns in a coronary bifurcation? J Biomech. 2012; 45(7): 1273–1279, doi: 10.1016/j.jbiomech.2012.01.033, indexed in Pubmed: 22365499.
9. Kim HY, Doh JH, Lim HS, et al. Identification of coronary artery side branch supplying myocardial mass that may benefit from revascularization. JACC Cardiovasc Interv. 2017; 10(6): 571–581, doi: 10.1016/j.jcin.2016.11.033, indexed in Pubmed: 28259665.
10. Kralev S, Poerner TC, Basorth D, et al. Side branch occlusion after coronary stent implantation in patients presenting with ST-elevation myocardial infarction: clinical impact and angiographic predictors. Am Heart J. 2006; 151(1): 153–157, doi: 10.1016/j.ahj.2005.01.034, indexed in Pubmed: 16368309.
11. Liu XB. Atherosclerosis in the lumen of a bifurcated left coronary artery and the proximal segment. J Xinjiang Medical University. 2019.
12. Redfors B, Généreux P, Witzenbichler B, et al. Percutaneous coronary intervention for bifurcation lesions. Interv Cardiol Clin. 2016; 5(2): 153–175, doi: 10.1016/j.iccl.2015.12.011, indexed in Pubmed: 28582201.

13. Ren XJ. Quantification of left coronary artery branch angle and coronary artery diameter lines by 256iCT. J Hebei Medical University. 2014.
14. Sun Z, Chaichana T. An investigation of correlation between left coronary bifurcation angle and hemodynamic changes in coronary stenosis by coronary computed tomography angiography-derived computational fluid dynamics. Quant Imaging Med Surg. 2017; 7(5): 537–548, doi: 10.21037/qims.2017.10.03, indexed in Pubmed: 29184766.
15. Verim S, Öztürk E, Küçük U, et al. Cross-sectional area measurement of the coronary arteries using CT angiography at the level of the bifurcation: is there a relationship? Diagn Interv Radiol. 2015; 21(6): 454–458, doi: 10.5152/dir.2015.15108, indexed in Pubmed: 26359878.
16. Zhang D, Dou K. Coronary bifurcation intervention: what role do bifurcation angles play? J Interv Cardiol. 2015; 28(3): 236–248, doi: 10.1111/joic.12203, indexed in Pubmed: 26065486.

VIA MEDICA

ORIGINAL ARTICLE

Folia Morphol.
Vol. 82, No. 4, pp. 830–840
DOI: 10.5603/FM.a2022.0084

ISSN 0015–5659
eISSN 1644–3284
journals.viamedica.pl

Sex differences in adrenal cortex beta-catenin immunolocalisation of the Saharan gerbil, Libyan jird (*Meriones libycus*, Lichtenstein, 1823)

N. Aknoun-Sail[1, 2], Y. Zatra[1, 2, 3], I. Sahut-Barnola[4], A. Benmouloud[1, 2, 5], A. Kheddache[1, 2, 6], M. Khaldoun[1, 2], S. Charallah[1, 2], F. Khammar[1, 2], A. Martinez[4], Z. Amirat[1, 2]

[1]*Arid Zones Research Laboratory (LRZA), Faculty of Biological Sciences, University of Sciences and Technology Houari Boumediene (USTHB), Algiers, Algeria*
[2]*Faculty of Sciences, University of Algiers I Benyoucef Benkhedda, Algiers, Algeria*
[3]*Nature and Life Sciences Faculty, Saad Dahlab University of Blida (USDB 1), Blida, Algeria*
[4]*Génétique, Reproduction et Développement (GReD), Centre National de La Recherche Scientifique CNRS, Institut National de La Santé and de La Recherche Médicale (INSERM), Université Clermont-Auvergne (UCA), France*
[5]*Department of Biology, Faculty of Sciences, M'Hamed Bougara University of Boumerdes (UMBB), Algeria*
[6]*Department of Biological and Agricultural, University Mouloud Mammeri Tizi Ouzou (UMMTO), Tizi Ouzou, Algeria*

[Received: 4 August 2022; Accepted: 10 September 2022; Early publication date: 27 September 2022]

Background: *The adrenal cortex provides adequate steroidogenic responses to environmental changes. However, in desert rodents, the adrenocortical activity varies according to several factors especially sex, age, and seasonal variations. Herein, we examined the sex differences in the adrenal cortex activity and explored the involvement of sex hormones in the regulation of this function in Libyan jird Meriones libycus.*

Materials and methods: *Twenty-four adult male and female animals weighing 109–110 g were captured in the breeding season and equally assigned into control and gonadectomised groups. Animal euthanasia was performed 50 days after the gonadectomy. Adrenal gland was processed for structural and immunohistochemistry study of β-catenin, whereas plasma was used for cortisol assay.*

Results: *The results showed that female adrenal gland weight was heavier than male and gonadectomy reduced this dimorphism. The adrenal cortex thickness was greater in the female than in the male, mainly due to significant development of the zona fasciculata. Females presented higher cell density in fasciculata and reticularis zones. The plasma cortisol was higher in females than in males. The immunolocalisation of β-catenin showed that the expression was particularly glomerular in both sexes. However, in the female, the immunostaining was present in the zona reticularis while it was absent in the control male. Orchiectomy reduced zona glomerulosa cell density and induced hypertrophy of zona reticularis characterised by strong β-catenin immunoreactivity. However, ovariectomy leads to hyperplastic expansion and high β-catenin expression in the zona glomerulosa associated with zona fasciculata and reticularis hypoplasia distinguished by weak β-catenin immunostaining.*

Address for correspondence: Dr. N. Aknoun-Sail, Arid Zones Research Laboratory (LRZA), Faculty of Biology, University of Sciences and Technology Houari Boumediene (USTHB), BP 32, 16111, Algiers, Algeria, tel: 00 213 560 900451, fax: 00 213 21 24 72 17, e-mail: naouel.aknoun_fsb@usthb.edu.dz

Conclusions: *Results indicated that sex hormones had a major role in the regulation of the Saharan gerbil's adrenal homeostasis by modulating β-catenin signalling. Androgens seem to inhibit the Wnt-β-catenin pathway and oestrogens are activators of the adrenal inner zones.* (Folia Morphol 2023; 82, 4: 830–840)

Key words: adrenal cortex, gonadectomy, sex differences, structure, β-catenin, *Meriones libycus*

INTRODUCTION

The adrenal cortex is an essential endocrine tissue that produces steroid hormones controlling numerous physiological parameters that maintain body homeostasis. It is organized into three distinct zones each controlled by numerous hormones and paracrine factors. Mineralocorticoids that are involved in blood pressure and hydroelectrolytic homeostasis control are produced in the outermost zona glomerulosa (ZG), glucocorticoids that are important in stress and immune response are synthesized in the zona fasciculata (ZF), and androgens that induce adrenarche in primates are produced in the innermost zona reticularis (ZR) [7]. To achieve a rapid and adequate response to intrinsic and extrinsic factors, the adrenocortical cells have developed mechanisms to ensure proper functioning throughout life. Wnt signalling is an essential paracrine pathway involved in adrenocortical homeostasis, zonation, development, and regeneration [18]. β-catenin, the main intracellular effector of canonical Wnt signalling, is highly expressed in the ZG in mice which regulates both the proliferation and steroidogenic activity of ZG cells to maintain the progenitor cell population and activates the expression of CYP11B2 in cells producing aldosterone that eventually replenish the ZF [6, 8]. Moreover, the activity of this gland is sexually dimorphic and has been shown in several animal species [17, 19]. Androgens cause the disappearance of the X-zone in male mice [9] while it persists in females; this zone reappears after male gonadectomy [7]. Recent cellular and molecular studies on the determinism of this dimorphism reveal that sex hormones are directly involved in the homeostasis and the remodelling of the adrenal cortex [10]. Indeed, studies have shown that the renewal of adrenal gland tissues in female mice shows a renewal rate 6.3-fold higher than in males, especially in the outer ZF [12].

Desert rodents are important models for understanding the cellular and molecular mechanisms that are involved in the development and homeostasis of the adrenal gland due to their adaptation in the extreme conditions of the biotope, which requires increased steroidogenic activity in order to respond to the needs of the environmental conditions. Previous studies reveal that the environment plays a major role in the modulation of adrenal responses; indeed, the activity of the cortex is correlated either positively or negatively with the season and reproductive cycle [2, 16]. Circulating sex hormones are also factors that control this steroidogenic and homeostatic function. In desert rodents, the zone reticularis produces androgens, likely to participate synergistically with glucocorticoids to provide an anabolic effect and contribute to reproductive success [22].

In order to elucidate the role of sex hormones in the regulation of adrenocortical homeostasis, we compared the structure of the adrenal cortex in male and female *Meriones libycus* captured during the breeding season and analysed the effects of gonadectomy on the remodelling and homeostasis of the adrenal cortex by exploring the weight parameters, structural changes, and the identification, by immunohistochemistry of a main mediator of Wnt/β-catenin signalling.

MATERIALS AND METHODS

Animals and sample collection

Animal experiments were carried out according to the guidelines of the Federation of European Laboratory Animal Science Associations (FELASA), following approval by the Institutional Animal Care Committee of the Algerian Higher Education and Scientific Research. The permits and ethical rules were achieved according to the Executive Decree n°10–90 completing the Executive Decree n°04–82 of the Algerian Government, establishing the terms and approval modalities of animal welfare in animal facilities. Furthermore, it was recently supported by the local university ethical committee "Algerian Association of Experimental Animal Sciences" AASEA (Agreement Number 45/DGLPAG/DVA.SDA.14).

Twenty-four adult male and female gerbils (*Meriones libycus*, Lichtenstein, 1823), weighing 109 ± ± 3 g, were captured early morning in the field in the region of Béni-Abbès (30°07'N 2°10'W, altitude 492 m) during the breeding season (February–March) [4]. The adult reproductive condition was evaluated according to body weight (80–140 g) and genital status was assessed during the breeding season. They were housed in individual cages (50 cm in length, 35 cm in width, and 30 cm in height) in a temperature-controlled room (20–22°C) and a light/dark cycle respecting the natural circadian L/D cycle (11/13 in February–March) and were fed with barley, bread, dates, some carrots, and some vegetables. The animals were divided into four groups: control male (CM, n = 6), orchiectomised (ORX, n = 6), control female (CF, n = 6), and ovariectomised (OVX = 6).

Orchiectomy and ovariectomy

Six male and six female jirds were gonadectomised bilaterally under anaesthesia induced by intraperitoneal injection of hydrochloride ketamine (Ketalar, Pfizer, NY, Toronto, Canada, 10 mg/kg administered *i.p.*) and xylazine (Xylamax, Bimeda-MTC; 10 mg/kg *i.p.*). The animals were then held supervised until they woke up, for 50 days. At the end of the experiments, all animals were euthanized between 9:00 and 11:00 a.m. The testes, ovaries of control groups; the seminal vesicles, and uterine horns of all animals were removed, weighed, and conserved for further studies. Adrenal glands were quickly removed, cleaned from their surrounding fat, and weighed separately. Adrenal glands were fixed in 10% neutral buffered formalin solution for 24 h for histological and immunohistochemical studies.

Histology

Adrenals gland were dehydrated through successive exposure to increasing concentrations of ethanol (70%, 95%, and 100%), cleaned in the toluene, and after 24 h of impregnation in paraffin in an incubator at 60°C, adrenals were embedded in paraffin. Samples were then sectioned at 5 μm using a Leitz 1512 rotatory microtome (Marshall Scientific, Hampton, VA, USA). The resulting slices were placed in Superfrost® glass slides (Thermo Scientific, Menzel-Gläser, Brausschweig, Germany). Following rehydration in decreased concentrations of ethanol (100%, 95%, 70%), parts of the serial slices were stained with Masson's trichrome while the others were subjected to immunohistochemistry.

Morphometric study

A comparison of adrenal cortex zones was performed by serially sectioning the whole adrenal at 5 μm. To account for the shape of the adrenal and allow for consistent measurements, counts were performed on 20 slides randomly chosen in the middle of the gland of all jirds. Zone depth was measured from the boundaries of each zone with 4 measurements per slide. The cell density was measured in ten slides randomly chosen on the grid area of 1713 μm^2. The zone depth and cell density were measured using ZEN Blue Software (ZEN 2.3 Blue edition Carl Zeiss Microscopy GmbH).

Hormone assays

Plasma cortisol level was analysed by electro-chemiluminescence immunoassay ECLIA (Roche Diagnostics, Meylan, France), using an automated hormone analyser Elecsys 1010. Intra- and inter-assay coefficients of variation were 1.3/1.6%.

Immunohistochemistry

To detect the presence of β-catenin in the adrenal tissue, immunohistochemistry was performed using specific primary monoclonal antibodies (mouse) on tissues embedded in paraffin, after unmasking with sodium citrate 10 mM, Tween 0.05%. They were then incubated overnight with β-catenin antibody (BD610153) used at 1/500 dilution. The primary antibodies were detected with Signal Stain Boost HRP-Polymer solution (#8114S or #8125P, Cell Signalling). The quantitative evaluation of the immuno-reactivity was performed using the ImageJ software (http://mirror.imagej.net/docs/examples/stained-sections/index.html). Quantification is based on a subtraction operation of the light intensity between the positive and negative signal areas. To make comparisons, an Image Type conversion to RGB mode stack, the saturation threshold, and the standardisation of the measured area are required.

Statistical analysis

All numerical data are expressed as means ± standard error of the mean. Data were normally distributed, Values were analysed by a two-tailed unpaired t-test (if comparing two groups) or a one-way ANOVA with Tukey's post-hoc test (if comparing multiples groups and variables) and it was considered significant when $p < 0.05$. Statistical analyses were performed by using GraphPad Prism (version 7; GraphPad Software Inc., San Diego, CA, USA).

Table 1. Characteristics of some weight parameters in male and female Libyan jird *Meriones libycus* during the breeding season. Sex-dependent difference and effect of gonadectomy

Animal groups		Body weight [g]	Adrenals [mg/100 BW]			Reproductive tracts [mg/100 BW]	
			Right adrenal	Left adrenal	Adrenals	Seminal vesicle	Uterine horns
Male	CM	106.77 ± 4.71	12.99 ± 0.31	13.58 ± 0.55	26.57 ± 0.39	397 ± 62	–
	ORX	104.53 ± 4.09	13.14 ± 0.65	15.64 ± 0.61	28.77 ± 0.98	113 ± 5***	–
Female	CF	97.70 ± 2.26	15.42 ± 1.01	16.99 ± 0.66	32.41 ± 1.15*	–	230 ± 118
	OVX	99.53 ± 4.25	13.47 ± 0.61	15.60 ± 0.73	29.07 ± 1.26	–	215 ± 34

Data is reported as mean ± standard error of the mean, n = 6 animals/group; BW — body weight; CF — control female; CM — control male; ORX — orchidectomised; OVX — ovariectomised; *CF vs. CM: $p < 0.05$; ***ORX vs. CM: $p < 0.001$

RESULTS

Sex differences and effect of sex hormones on weight parameters

Data for weight parameters were summarised in Table 1. It can be seen that body mass does not show a significant gender difference even if it is non-significant lower in females (–9%, p = 0.1). Gonadectomy caused no effect on body mass both in male and female jirds (–2%, p = 0.7; –2%, p = 0.8), respectively (Table 1).

However, the weight of the relative adrenal is significantly higher in female compared to male (+22%, p = 0.004) and gonadectomy reduced this dimorphism (+1%, p = 0.8) due to a little effect on adrenals weight in the male (+8%, p = 0.07) and a potential regression in the female (–10%, p = 0.06) (Table 1).

The relative weight of the seminal vesicles and uterine horns were used as a reference to confirm the sex hormone reduction following gonadectomy. Indeed, the vesicles weight drastically reduced 50 days after orchiectomy (–76% of relative vesicle weight in ORX vs. CM, p = 0.04) when uterine horns were also reduced in ovariectomised but none significantly (Table 1).

Gender differences in the jird adrenal structure

The adrenal gland in the male and female jird has a structure like all other mammals, with an elongated shape allowing the distinction between two parts, an external peripheral adrenal cortex and a central internal area, adrenal medulla, bounded all around by thick connective tissue. The gland is surrounded by a connective capsule made up of collagen fibres, fibroblasts, and blood capillaries (Fig. 1A, B). The adrenal cortex is subdivided into three zones oriented from the outside to the inside: zona glomerulosa (ZG), zona fasciculata (ZF), and zona reticularis (ZR) (Fig. 1A, B). Morphometric measurements of the adrenal cortex revealed that the female has a larger adrenal cortex with a higher depth than those of the male (16%, p = 0.0003) (Fig. 2).

The ZG is the outermost and thinnest zone of the cortex and appears as cell clusters forming arcing cords separated from each other by connective tissue containing blood capillaries (Fig. 3A, G). The depth of glomerulosa shows non-significant gender changes (Fig. 2A, B), but the zona is covered with a well-defined connective capsule in the male with many cells of small size and elongated in shape while in the female (Fig. 3A, G), the cells number is reduced compared to the male (–16%, p = 0.02) (Fig. 4A).

The ZF is the thickest area of the adrenal cortex (Fig. 1A, B). The cells are organized in long, narrow parallel cords, perpendicular to the capsule and directed towards the medulla (Fig. 3B, H). The cells appear less acidophilic than other adrenal cortex cells due to the lipid droplets within these cells also called spongiocytes. The comparison between the male and the female ZF shows that the depth of the zona is greater in the female (26%, p = 0.001) (Fig. 2) with the presence of a higher number of cells per area unit (Fig. 4B).

The ZR is the innermost layer is separated from the medulla by a connective tissue that seems developed in *Meriones libycus* (Fig. 1A, B); it is thinner than the ZF and is formed by an irregular network of anastomosed cords and cell clusters separated by bulky capillaries (Fig. 3C, I). Although the ZR presents numerous small cells which are more abundant in female (Fig. 4C), it remains similar in depth within genders (Fig. 2D).

Gonadectomy alters the adrenal structure both in male and female jird

Histological sections of the adrenal gland in gonadectomised animals show significant remodelling and

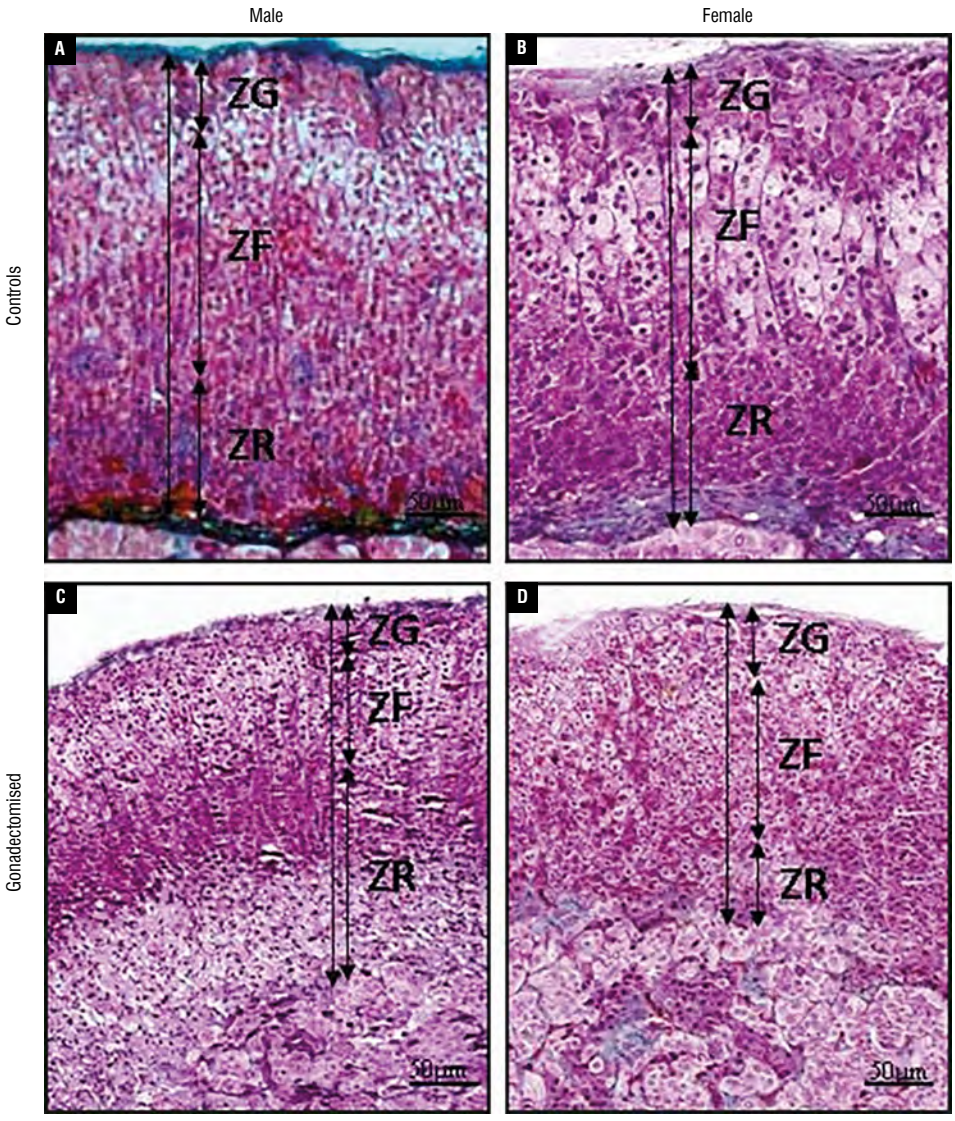

Figure 1. A–D. Gender differences in the structure of the adrenal gland in the Libyan jird *Meriones libycus* during breeding season and effect of gonadectomy. Scale bar: 50 μm; ZF — zona fasciculata; ZG — zona glomerulosa; ZR — zona reticularis.

structural changes in the cortex (Fig. 1C, D). Indeed, castration in the male induces the development of the cortex (+9%, $p = 0.05$) (Fig. 2) associated with hypertrophy of ZR (+45%, $p < 0.0001$) (Fig. 1A, C). In the ovariectomized female, the adrenal gland appears withered (Fig. 1B, D), and the cortex thickness decreases due to the decrease of the ZF and ZR (Fig. 2A, C, D).

The ZG displays a change in the structure and organization since it loses organization in rounded cords, especially in the male (Fig. 3A, D) with a decrease of cell density (–40%, $p < 0.0001$) (Fig. 4A), whereas in the female, ZG presents numerous smaller cells than those of the control (+25%, $p < 0.0001$) (Figs. 3G, J; 4A).

The ZF appears disorganized in the male after orchiectomy, the parallel cord appearance of the cells disappears, they become small and of various shapes separated by thin connective tissue tracts containing blood capillaries (Fig. 3B, E); depth and cell density measurements show no significant variations (Figs. 2C; 4B). After ovariectomy, this area is also disorganized, the arrangement of cells in parallel cords is no longer visible (Fig. 3H, K), and it undergoes a significant reduction in the depth (–16%; $p = 0.05$) (Fig. 2C) without changes in cell density number (Fig. 4B).

The ZR is significantly hypertrophied in the orchiectomized (Fig. 1C) and infiltrated by connective tissue (Fig. 3C, F) with an increase in depth zona (Fig. 2D) and a reduction of cell number per unit

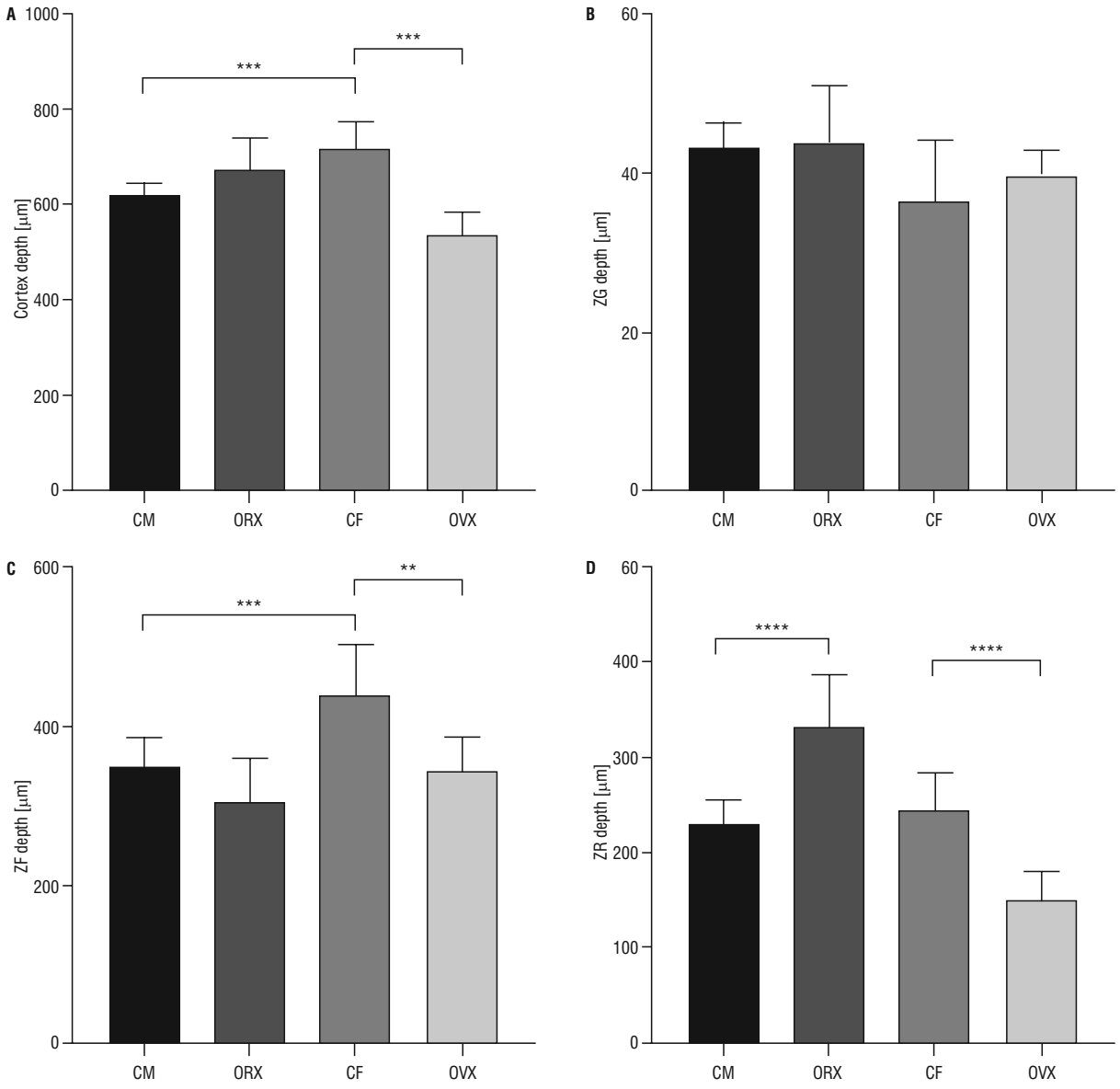

Figure 2. A–D. Gender differences and effect of gonadectomy on the morphometric measure of the depth of adrenocortical zone in *Meriones libycus* during the breeding season; CF — control female; CM — control male; ORX — orchidectomised; OVX — ovariectomised; ZF — zona fasciculata; ZG — zona glomerulosa; ZR — zona reticularis; **p < 0.01; ***p < 0.001; ****p < 0.0001.

(Fig. 4C) while it decreases in the female ovariectomized (Fig. 3I, L) both in depth and cell density (Fig. 2D; 4C).

Hormonal effects

The mean concentration of plasma cortisol was higher in the female control vs. male control values (+139%, p = 0.002), after 50 days of gonadectomy, plasma cortisol was significantly elevated in male gerbils and reduced in the female compared with control values (respectively, +121%, p = 0.02; –55%, p = 0.04) (Fig. 5).

Immunolocalisation of β-catenin in the adrenal cortex of the Libyan jird

Semiquantitative evaluation of the adrenal β-catenin immunoreactivity was summarised in Table 2. β-catenin is present in the adrenal cortex both in male and female as well as after gonadectomy (Fig. 6); however, its distribution varies in both sexes. It is immunolocalised particularly at the ZG in both male and female (Fig. 6A, B) with less important staining as well as at the innermost zones, in particular, ZR in the female (Fig. 6A, B), while in the male, the β-catenin is also found at the ZG but more intensively compared

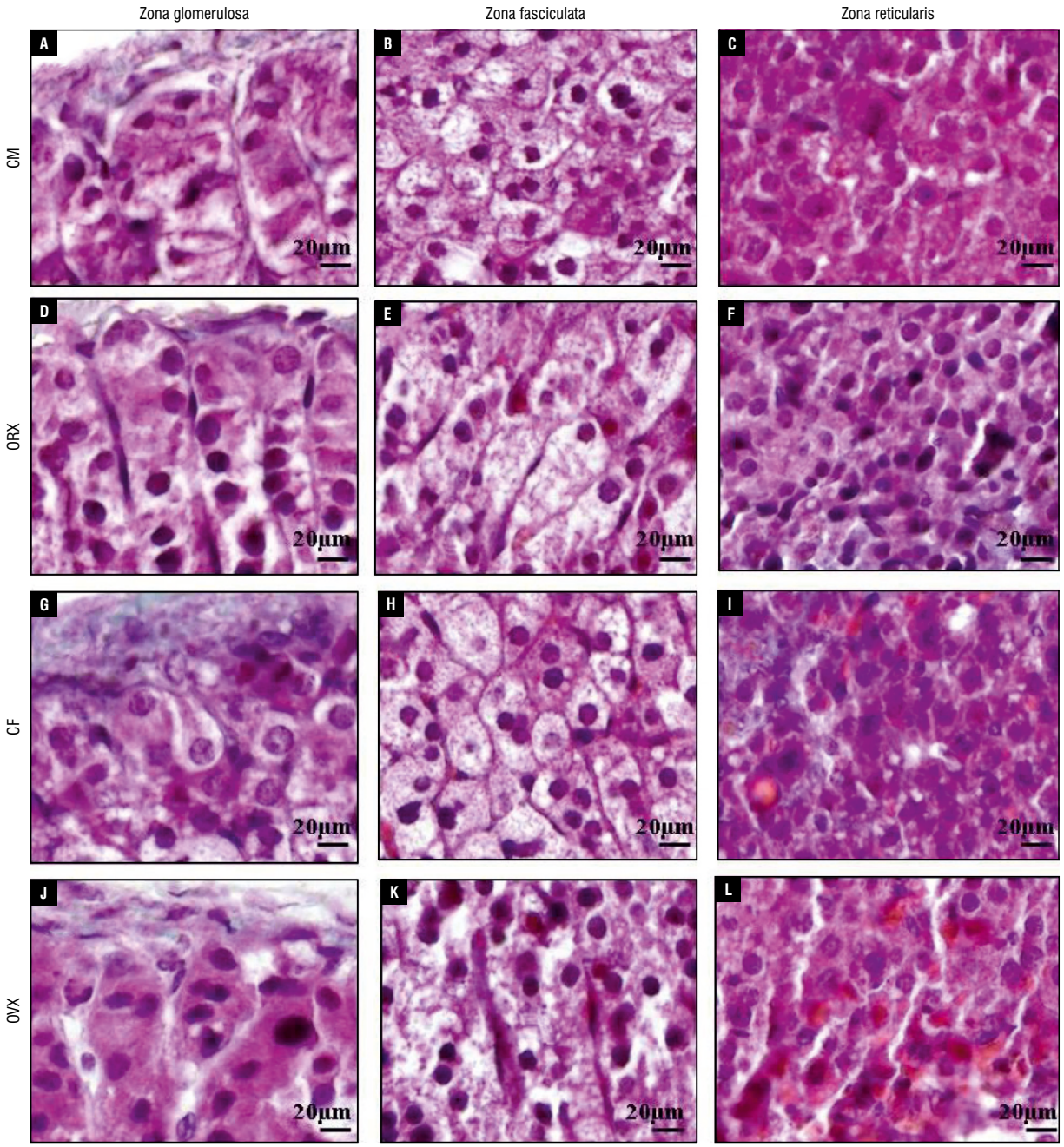

Figure 3. A–L. Gender differences in the structure of adrenocortical zone and effect of gonadectomy on this structure in *Meriones libycus* during breeding season. Scale bar: 20 μm; CF — control female; CM — control male; ORX — orchidectomised; OVX — ovariectomised.

to the female and lack fully in the innermost zones of the adrenal cortex (Fig. 6A, B).

Gonadectomy induces a marked change in the distribution of β-catenin in the adrenal cortex. Indeed, it becomes internal in the male after castration where it forms a weakly immunolabeled trail in the ZF which appears more intensive in the ZR (Fig. 6A, C). In the ovariectomised female, β-catenin is more immunostained in the ZG with more numerous cell layers (Fig. 6B, D); on the other hand, the distribution of β-catenin in the inner adrenal cortex zones is reduced and less intense than in the control (Table 2).

DISCUSSION

Our results clearly showed that the adrenal cortex is more active in female than in male of *Meriones libycus*; this has been seen in the weight, structural and hormonal level. In male, the ZG is more developed than in female with a higher number of cells per unit area suggesting a greater mitotic activity. However,

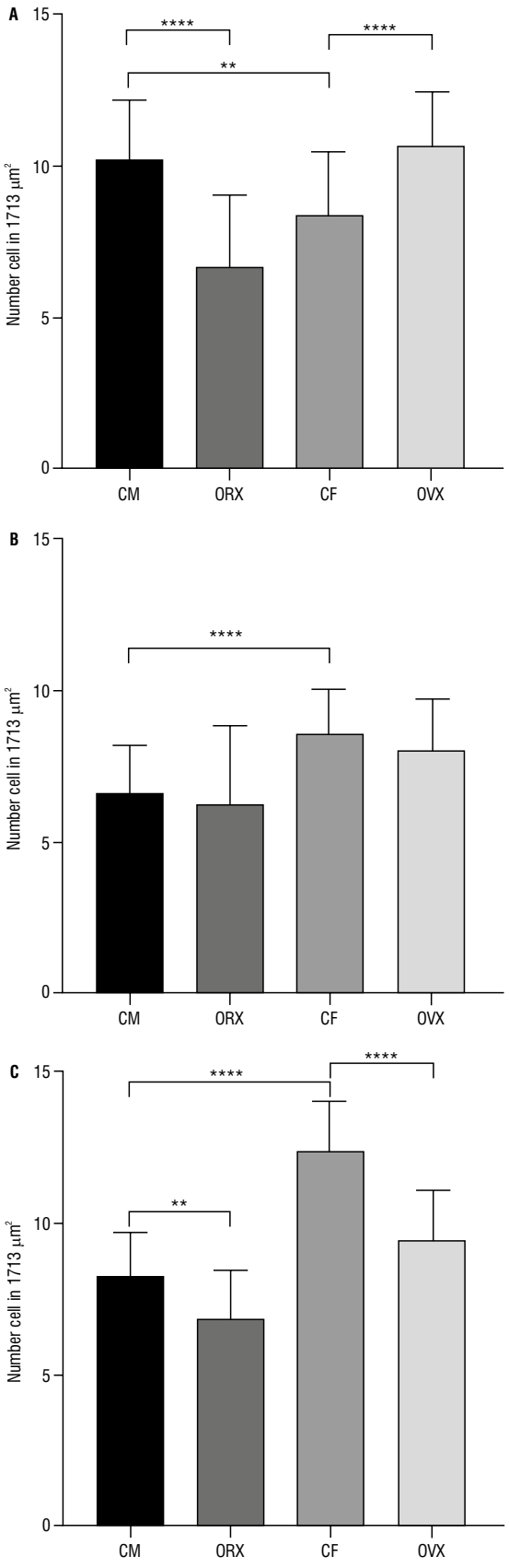

Figure 4. A–C. Gender differences in the cell density of the adrenocortical zone and the effect of gonadectomy in *Meriones libycus* during breeding season; CF — control female; CM — control male; ORX — orchidectomised; OVX — ovariectomised; **p < 0.01; ****p < 0.0001.

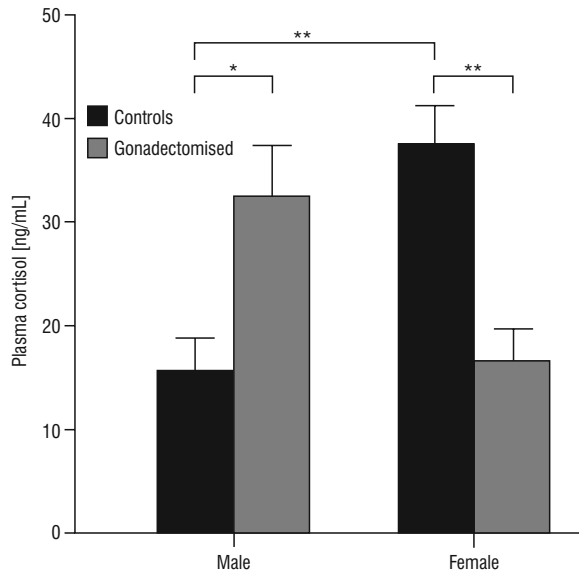

Figure 5. Sex differences in plasma cortisol concentrations and gonadectomy effects in male and female *Meriones libycus* during breeding season. Data is reported as mean ± standard error of the mean, n = 6 animals/group; **Control female (CF) vs. Control male (CM), Gonadectomised female vs. CF: **p < 0.01; *Orchidectomised vs. CM: *p < 0.05.

Table 2. Quantification of β-catenin immunoreactivity in the adrenal cortex of *Meriones libycus* male and female during the breeding season. Effect of gonadectomy

Groups		β-catenin immunoreactivity (%)		
		ZG	ZF	ZR
Male	CM	62.39 ± 0.7	7.11 ± 0.7	12.38 ± 0.6
	ORX	40.93 ± 0.9***	14.59 ± 1.7**	46.21 ± 2.1***
Female	CF	59.23 ± 0.6	12.14 ± 0.9*	37.38 ± 0.6***
	OVX	57.11 ± 1.2	10.77 ± 0.3	14.71 ± 0.8###

CF — control female; CM — control male; ORX — orchidectomised; OVX — ovariectomised; ZF — zona fasciculata; ZG — zona glomerulosa; ZR — zona reticularis;
CF vs. CM: *p < 0.05; ***p < 0.001; ORX vs. CM: **p < 0.01; ***p < 0.001;
OVX vs. CF: ###p < 0.001

in female, the innermost zones especially the ZF and ZR show a large thickness associated with many cells per unit area, suggesting a remarkable proliferative activity. This finding corroborates with the cortisol plasma level which is higher in female than in male.

Immunohistochemical analyses of β-catenin showed that this protein is mainly immunolocalised at the ZG in both sexes. Previous work has shown that it is responsible for the acquisition of the identity of ZG by the Wnt4 ligand [14]. However, in females, this protein is also found in innermost zona of the cortex forming a centripetal immunostaining gradient that is not observed in controls males. This distribution of β-catenin in the inner zona suggests that the Wnt-β-

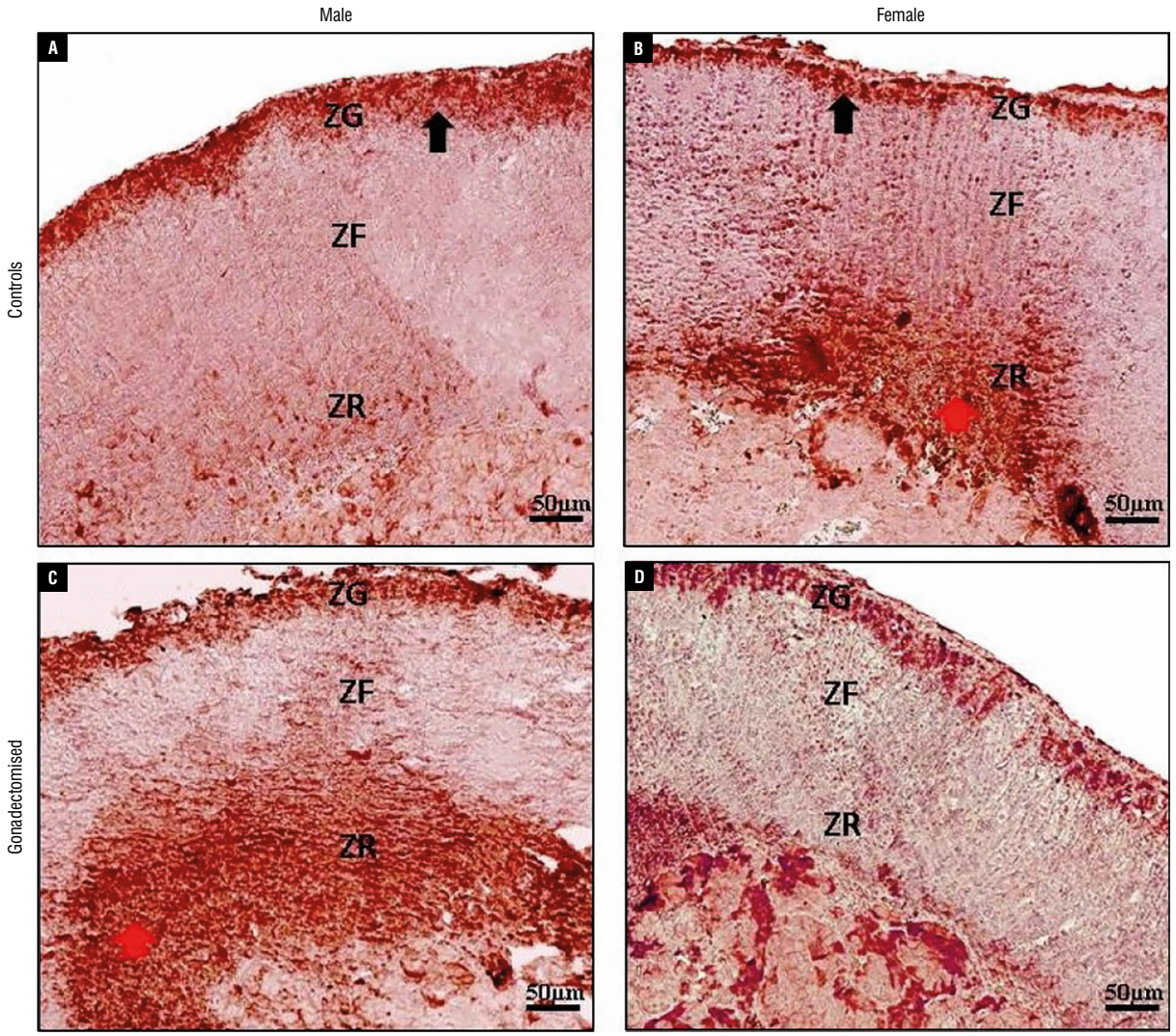

Figure 6. A–D. Immureactive β-catenin in the adrenal cortex of *Meriones libycus* male and female and the effect of gonadectomy; ZF — zona fasciculata; ZG — zona glomerulosa; ZR — zona reticularis.

-catenin signalling pathway is also taken especially in the ZR probably participating in the zonation process, which once again explains the intense development of the cortex in the female compared to the male. Recent studies have also revealed the presence of a centripetal decreasing gradient of β-catenin regulated by other paracrine factors including zinc and ring finger 3 (ZNRF3) [3].

The literature has reported the existence of sex differences in the structure and the function of the adrenal cortex, in rat models, the activity is in favour of the female [20]; however, it has been reported in the Hamster that the cortex is more active in male than in female [11, 19]. These differences are reported at several levels of adrenal function, in fact, the development of the adrenal glands is different since the fetal cortex or X-zone disappears in the male after puberty and persists in the female and does not disappear until the time of pregnancy [15]. The female cortex of the mouse is 6-fold more active due to a high proliferative activity especially in the outer ZF and the increased recruitment of GLI1+ capsular stem cells, resulting in their higher differentiated ability [12]. Another study also demonstrated that the sex-related gene was more abundantly expressed in female rats compared to male rats [25]. Furthermore, the hypothalamic-pituitary adrenal axis is more active in female than in male [13, 26].

Experiments of sex hormones deprivation confirmed the gender differences. Indeed, orchiectomy in *Meriones* led to a reduction in the number of glomerular cells as well as hypertrophy of the ZR; in the female, the ZG cells are more abundant and more β-catenin immunoreactive with hypoplasia of

the innermost zones. These findings were supported by the distribution of β-catenin which is found in hypertrophied reticularis zona of the male and by the disappearance of immunostaining in the female which is shown in the control. On one hand, this suggests that the Wnt/-β-catenin pathway is necessarily involved in the process of adrenal cortex zonation, especially the recruitment and increased renewal of steroidogenic cells. On the other hand, this pathway is regulated by gonadal hormones with probably a stimulating action of oestrogen and an inhibitory action of androgens on the inner areas. The sex hormones mediate pituitary adrenal axis responsiveness to stress since the oestrogen increased adrenocorticotrophin hormone (ACTH) and corticosterone secretion in rats [28] while the androgen decreased the corticotropin releasing hormone (CRH), ACTH, and corticosterone concentrations both in the laboratory animals [23, 27] and the non-laboratory animals such as *Psammomys obesus* [5], *Meriones libycus* [1] and *Gerbillus tarabuli* [29]. Sex hormones also act on adrenal androgens with, in particular, a stimulatory effect of oestrogens in humans on the secretion of dehydroepiandrosterone (DHEA) [21] and an indirect inhibitory effect by inhibiting the expression of 3β-HSD in the mouse [24]. Few studies report the effects of gonadectomy on the distribution of β-catenin; however, it has been shown that testicular androgens increase Wnt signalling that antagonizes PKA, leading to slower adrenocortical cell turnover and delayed phenotype whereas gonadectomy sensitizes males to hypercorticism and reticularis-like formation [7]. Investigations using immunoblotting of β-catenin throughout the adrenal gland and the assay of androstenedione should provide more knowledge about the action of testicular androgens in modulating adrenal activity.

CONCLUSIONS

The female *Meriones* adrenal gland is more active than the one of the male, characterised by the significant development of the ZF and reticularis leading to high plasma cortisol. Sex hormones participate in the modulation of this activity; androgens inhibit the activity of the steroidogenic cells in the innermost zone whereas oestrogens are stimulators reducing the pool of progenitor cells located in ZG. These actions of sex hormones seem to occur via the regulation of the Wnt-β-catenin pathway which appears involved in the zonation of the innermost zone of the adrenal. Androgens seem to inhibit the Wnt-β-catenin pathway in the inner zones and oestrogens are stimulators of the Wnt-β-catenin pathway in the inner zones.

Acknowledgements

We are grateful to the staff of Research station of Béni Abbès, in the Algerian Sahara Desert, for their help in trapping jirds. We want also to thank R. Mehaoudi and K. Hemila for their help in statistical analysis. The financial support of the Algerian Ministry of Higher Education and Scientific Research and the University of Clermont-Ferrand (France) are strongly acknowledged for immunohistochemistry technical.

Conflict of interest: None declared

REFERENCES

1. Aknoun-Sail N, Zatra Y, Kheddache A, et al. Pituitary adrenal axis activity in the male libyan jird, *meriones libycus*: seasonal effects and androgen mediated regulation. Folia Biologica. 2017; 65(2): 95–105, doi: 10.3409/fb65_2.95.
2. Amirat Z, Khammar F, Brudieux R. Seasonal changes in plasma and adrenal concentrations of cortisol, corticosterone, aldosterone, and electrolytes in the adult male sand rat (Psammomys obesus). Gen Comp Endocrinol. 1980; 40(1): 36–43, doi: 10.1016/0016-6480(80)90093-3, indexed in Pubmed: 6986323.
3. Basham KJ, Rodriguez S, Turcu AF, et al. A ZNRF3-dependent Wnt/β-catenin signaling gradient is required for adrenal homeostasis. Genes Dev. 2019; 33(3-4): 209–220, doi: 10.1101/gad.317412.118, indexed in Pubmed: 30692207.
4. Belhocine M, Gernigon-Spychalowicz T, Robert AM, et al. Ecophysiological responses of the seminal vesicle of Libyan jird (Meriones libycus) to the Saharan conditions: histological, morphometric and immunohistochemical analysis. Histol Histopathol. 2007; 22(6): 603–615, doi: 10.14670/HH-22.603, indexed in Pubmed: 17357090.
5. Benmouloud A, Amirat Z, Khammar F, et al. Androgen receptor-mediated regulation of adrenocortical activity in the sand rat, Psammomys obesus. J Comp Physiol B. 2014; 184(8): 1055–1063, doi: 10.1007/s00360-014-0859-3, indexed in Pubmed: 25179180.
6. Berthon A, Drelon C, Ragazzon B, et al. WNT/β-catenin signalling is activated in aldosterone-producing adenomas and controls aldosterone production. Hum Mol Genet. 2014; 23(4): 889–905, doi: 10.1093/hmg/ddt484, indexed in Pubmed: 24087794.
7. Dumontet T, Sahut-Barnola I, Septier A, et al. PKA signaling drives reticularis differentiation and sexually dimorphic adrenal cortex renewal. JCI Insight. 2018; 3(2), doi: 10.1172/jci.insight.98394, indexed in Pubmed: 29367455.
8. Freedman BD, Kempna PB, Carlone DL, et al. Adrenocortical zonation results from lineage conversion of differentiated zona glomerulosa cells. Dev Cell. 2013; 26(6): 666–673, doi: 10.1016/j.devcel.2013.07.016, indexed in Pubmed: 24035414.
9. Gannon AL, O'Hara L, Mason JI, et al. Androgen receptor signalling in the male adrenal facilitates X-zone regression,

cell turnover and protects against adrenal degeneration during ageing. Sci Rep. 2019; 9(1): 10457, doi: 10.1038/s41598-019-46049-3, indexed in Pubmed: 31320667.
10. Gao X, Yamazaki Y, Tezuka Y, et al. Gender differences in human adrenal cortex and its disorders. Mol Cell Endocrinol. 2021; 526: 111177, doi: 10.1016/j.mce.2021.111177, indexed in Pubmed: 33582213.
11. Gaskin JH, Kitay JI. Adrenocortical function in the hamster. Sex differences and effects of gonadal hormones. Endocrinology. 1970; 87(4): 779–786, doi: 10.1210/endo-87-4-779, indexed in Pubmed: 4318198.
12. Grabek A, Dolfi B, Klein B. The adult adrenal cortex undergoes rapid tissue renewal in a sex-specific manner. Cell Stem Cell. 2019; 25(2): 290–296.e2, doi: 10.1016/j.stem.2019.04.012, indexed in Pubmed: 31104943.
13. Handa RJ, Burgess LH, Kerr JE, et al. Gonadal steroid hormone receptors and sex differences in the hypothalamo-pituitary-adrenal axis. Horm Behav. 1994; 28(4): 464–476, doi: 10.1006/hbeh.1994.1044, indexed in Pubmed: 7729815.
14. Heikkilä M, Peltoketo H, Leppäluoto J, et al. Wnt-4 deficiency alters mouse adrenal cortex function, reducing aldosterone production. Endocrinology. 2002; 143(11): 4358–4365, doi: 10.1210/en.2002-220275, indexed in Pubmed: 12399432.
15. Huang CCJ, Kang Y. The transient cortical zone in the adrenal gland: the mystery of the adrenal X-zone. J Endocrinol. 2019; 241(1): R51–R63, doi: 10.1530/JOE-18-0632, indexed in Pubmed: 30817316.
16. Khammar F, Brudieux R. Seasonal changes in testicular contents and plasma concentrations of androgens in the desert gerbil (Gerbillus gerbillus). J Reprod Fertil. 1987; 80(2): 589–594, doi: 10.1530/jrf.0.0800589, indexed in Pubmed: 3656287.
17. Leśniewska B, Miśkowiak B, Nowak M, et al. Sex differences in adrenocortical structure and function. XXVII. The effect of ether stress on ACTH and corticosterone in intact, gonadectomized, and testosterone- or estradiol-replaced rats. Res Exp Med (Berl). 1990; 190(2): 95–103, doi: 10.1007/pl00020011, indexed in Pubmed: 2161554.
18. Little DW, Dumontet T, LaPensee CR, et al. β-catenin in adrenal zonation and disease. Mol Cell Endocrinol. 2021; 522: 111120, doi: 10.1016/j.mce.2020.111120, indexed in Pubmed: 33338548.
19. Malendowicz LK, Nussdorfer GG. Sex differences in adrenocortical structure and function: 29. Morphometric and functional studies on the effects of gonadectomy and gonadal-hormone replacement on the hamster adrenal cortex. Acta Anat (Basel). 1992; 145(1): 68–72, doi: 10.1159/000147344, indexed in Pubmed: 1329427.
20. Malendowicz LK. Sex differences in adrenocortical structure and function. V. The effects of postpubertal gonadectomy and gonadal hormone replacement on nuclear-cytoplasmic ratio, morphology and histochemistry of rat adrenal cortex. Folia Histochem Cytochem (Krakow). 1979; 17(3): 195–214, indexed in Pubmed: 488856.
21. Mesiano S, Jaffe RB. Interaction of insulin-like growth factor-II and estradiol directs steroidogenesis in the human fetal adrenal toward dehydroepiandrosterone sulfate production. J Clin Endocrinol Metab. 1993; 77(3): 754–758, doi: 10.1210/jcem.77.3.8396578, indexed in Pubmed: 8396578.
22. Romero LM. Seasonal changes in plasma glucocorticoid concentrations in free-living vertebrates. Gen Comp Endocrinol. 2002; 128(1): 1–24, doi: 10.1016/s0016-6480(02)00064-3, indexed in Pubmed: 12270784.
23. Seale JV, Wood SA, Atkinson HC, et al. Gonadal steroid replacement reverses gonadectomy-induced changes in the corticosterone pulse profile and stress-induced hypothalamic-pituitary-adrenal axis activity of male and female rats. J Neuroendocrinol. 2004; 16(12): 989–998, doi: 10.1111/j.1365-2826.2004.01258.x, indexed in Pubmed: 15667454.
24. Stalvey JRD. Inhibition of 3beta-hydroxysteroid dehydrogenase-isomerase in mouse adrenal cells: a direct effect of testosterone. Steroids. 2002; 67(8): 721–731, doi: 10.1016/s0039-128x(02)00023-5, indexed in Pubmed: 12117620.
25. Trejter M, Hochol A, Tyczewska M, et al. Sex-related gene expression profiles in the adrenal cortex in the mature rat: microarray analysis with emphasis on genes involved in steroidogenesis. Int J Mol Med. 2015; 35(3): 702–714, doi: 10.3892/ijmm.2015.2064, indexed in Pubmed: 25572386.
26. Viau V, Bingham B, Davis J, et al. Gender and puberty interact on the stress-induced activation of parvocellular neurosecretory neurons and corticotropin-releasing hormone messenger ribonucleic acid expression in the rat. Endocrinology. 2005; 146(1): 137–146, doi: 10.1210/en.2004-0846, indexed in Pubmed: 15375029.
27. Viau V, Meaney MJ. The inhibitory effect of testosterone on hypothalamic-pituitary-adrenal responses to stress is mediated by the medial preoptic area. J Neurosci. 1996; 16(5): 1866–1876, doi: 10.1523/JNEUROSCI.16-05-01866.1996, indexed in Pubmed: 8774455.
28. Viau V, Meaney MJ. Variations in the hypothalamic-pituitary-adrenal response to stress during the estrous cycle in the rat. Endocrinology. 1991; 129(5): 2503–2511, doi: 10.1210/endo-129-5-2503, indexed in Pubmed: 1657578.
29. Zatra Y, Aknoun-Sail N, Kheddache A, et al. Seasonal changes in plasma testosterone and cortisol suggest an androgen mediated regulation of the pituitary adrenal axis in the Tarabul's gerbil Gerbillus tarabuli (Thomas, 1902). Gen Comp Endocrinol. 2018; 258: 173–183, doi: 10.1016/j.ygcen.2017.08.012, indexed in Pubmed: 28811197.

VIA MEDICA

ORIGINAL ARTICLE

Folia Morphol.
Vol. 82, No. 4, pp. 841–853
DOI: 10.5603/FM.a2022.0097

ISSN 0015–5659
eISSN 1644–3284
journals.viamedica.pl

Transplantation of bone marrow-derived mesenchymal stem cells ameliorated dopamine system impairment in a D-galactose-induced brain ageing in rats

G. El-Akabawy[1, 2, 3], S.O.F. El-Kersh[4], L.A. Rashed[5], S.N. Amin[6, 7], A.A.K. El-Sheikh[8]

[1]*Department of Basic Medical Sciences, College of Medicine, Ajman University, Ajman, United Arab Emirates*
[2]*Centre of Medical and Bio-allied Health Sciences Research, Ajman University, Ajman, United Arab Emirates*
[3]*Department of Anatomy and Embryology, Faculty of Medicine, Menoufia University, Menoufia, Egypt*
[4]*Faculty of Medicine, Galala University, Suez, Egypt*
[5]*Department of Medical Biochemistry, Faculty of Medicine, Cairo University, Cairo, Egypt*
[6]*Department of Anatomy, Physiology, and Biochemistry, Faculty of Medicine, The Hashemite University, Zarqa, Jordan*
[7]*Department of Medical Physiology, Faculty of Medicine, Cairo University, Cairo, Egypt*
[8]*Basic Health Sciences Department, College of Medicine, Princess Nourah Bint Abdulrahman University, Riyadh, Saudi Arabia*

[Received: 17 September 2022; Accepted: 3 November 2022; Early publication date: 29 November 2022]

Background: *Ageing is the primary risk factor for Parkinson's disease. Progressive motor and coordination decline that occurs with ageing has been linked to nigrostriatal dysfunction. Few studies have investigated the efficacy of mesenchymal stem cells in ameliorating the structural and functional alterations in the ageing nigrostriatal system. This study is the first to evaluate the effects of intravenous injection of bone marrow-derived mesenchymal stem cells (BMMSCs) in a D-galactose-induced rat model of nigrostriatal ageing.*

Materials and methods: *BMMSCs were intravenously injected once every 2 weeks for 8 weeks. The transplanted cells survived, migrated to the brain, and differentiated into dopaminergic neurones and astrocytes.*

Results: *BMMSC transplantation improved locomotor activity, restored dopaminergic system function, preserved atrophic dopaminergic neurones in the substantia nigra, exerted antioxidative effects, and restored neurotrophic factors.*

Conclusions: *Our findings demonstrate the efficacy of BMMSC injection in a nigrostriatal ageing rat model, and suggest that these cells may provide an effective therapeutic approach for the ageing nigrostriatal system.* (Folia Morphol 2023; 82, 4: 841–853)

Key words: bone marrow-mesenchymal stem cells, D-galactose, rat, nigrostriatal dysfunction

INTRODUCTION

Ageing is associated with several biochemical and molecular changes that eventually lead to cognitive and somatosensory impairments. This can be considered a primary risk factor for the development of neurodegenerative diseases such as Parkinson's dis-

Address for correspondence: G.F.A. El-Akabawy, PhD, Department of Basic Medical Sciences, College of Medicine, Ajman University, Ajman, United Arab Emirates, tel: 00971554200803, e-mail: g.elakabawy@ajman.ac.ae; Gehanakabawy@gmail.com

ease (PD) [8, 23, 54, 72]. Dopaminergic (DA) neurones are among the most vulnerable cells of the central nervous system to the deleterious consequences of ageing. The most obvious indication of DA neurone susceptibility to ageing is the degradation of nigrostriatal DA neurones [35, 56].

Ageing has also been associated with structural alterations of the nigrostriatal system. Several reports have shown that pathogenic alterations associated with PD are identical to age-related changes in DA neurones. The loss of DA neurones in the substantia nigra (SN), which reduces the amount of dopamine released and the number of DA receptors in the striatum and causes bradykinesia, muscular stiffness, and shaking, is a notable neuropathological aspect of PD [21, 35, 44, 56, 63]. These characteristics are mostly related to ageing (also known as late-onset PD) and are dependent on environmental and hereditary variables [19]. A substantial body of evidence suggests that brain-derived neurotrophic factor (BDNF) is essential for the survival of SN DA neurones. BDNF helps SN neurones survive in vitro and is protective against a variety of neurotoxic injuries both in vitro and in vivo [6, 40, 46]. Another neurotrophic factor, glial cell line-derived neurotrophic factor (GDNF), supports the survival of DA cells in the midbrain, increases the function of the remaining DA neurones in the SN, and inhibits degeneration and DA neuronal death [38, 41, 42]. In addition, oxidative stress appears to be a crucial risk factor for ageing-mediated neuronal and neurotransmitter changes [25, 62].

The morphological and functional alterations associated with ageing are exacerbated in age-related diseases; therefore, therapies that attenuate primary and/or secondary ageing are the main focus of ageing research [10, 32, 33]. Both preclinical and clinical trials of stem cell treatment have demonstrated its effectiveness in the treatment of Alzheimer's disease (AD) and PD. Mesenchymal stem cells (MSCs) are the most promising type of stem cells owing to their ability to differentiate into the neuronal phenotype, secrete neurotrophic cytokines, and promote endogenous brain repair. In addition, they have immunomodulatory, neuroprotective, and angiogenic capabilities [5, 9, 26]. In rodent PD models, bone marrow-derived MSC (BMMSC) transplantation has been demonstrated to improve behavioural performance, ameliorate DA system degeneration in the SN and striatum, attenuate histopathological alterations, reduce the inflammatory response, and induce the release of neurotrophic factors [2, 20, 37, 39, 64, 67, 69]. Based on a study in 2021, a single-centre, open-label phase 1 clinical study was conducted to assess the safety and feasibility of intravenous injection of allogeneic BMMSCs delivered in escalating doses to patients with idiopathic PD [55].

Most of the research on the effectiveness of stem cells has been conducted on preclinical animal models or on patients with AD and PD, whose structural and functional brain capabilities have significantly deteriorated. It is possible that early intervention to address neuropathological changes during primary ageing will stop or at least delay the pathological processes leading to secondary ageing, thus lowering the prevalence of age-related disorders [3, 10, 32, 33, 48, 59]. Few studies have evaluated the efficacy of MSC transplantation in animal models of ageing [13, 15, 18, 29, 47, 57, 68]. Therefore, we aimed to evaluate, for the first time, the potential beneficial effects of systemic transplantation of BMMSCs on the nigrostriatal system in a D-galactose (D-gal)-induced rat model of brain ageing to evaluate their potential as a protective approach for age-related neurodegeneration.

MATERIALS AND METHODS

Animal

Thirty male Sprague Dawley rats (8 weeks old, 180–200 g) were obtained from the Theodor Bilharz Research Institute, Imbaba, Egypt, and housed in the animal facility of the Faculty of Medicine, Menoufia University, Egypt. The rats were housed in standard polycarbonate cages with 2 rats in each cage under standard laboratory settings (22 ± 5°C, 60 ± 5% humidity, and a 12-h/12-h light/dark cycle). Standard laboratory chow and tap water were provided ad libitum. All experimental procedures involving animals were approved by the Institutional Review Board of Ajman University, UAE (IRB# M-F-A-14-Mar), and the Institutional Review Board of Menoufia University, Faculty of Medicine, Egypt (IRB# 191219ANAT), and were conducted in accordance with the guidelines on the ethical use of animals in the European Community Council Directive 2010/63/EU.

BMMSC isolation and culture

Bone marrow-derived MSC were obtained from 6–8-week-old male Sprague Dawley rats, as previously reported [49]. Briefly, bone marrow plugs were harvested from the femurs and tibias of rats using

a 23-gauge needle and centrifuged for 5 min at room temperature at 1800 rpm. The cell pellets were then resuspended in Dulbecco's modified Eagle's medium (Gibco, Carlsbad, CA, USA) containing 10% fetal bovine serum (FBS) (Gibco) and 1% penicillin-streptomycin (Gibco) and seeded at a density of 1×10^6 cells/cm in 25 cm^2 cell culture flasks. Cells were incubated at 37°C in a humidified atmosphere containing 5% CO_2. The culture medium was changed every 3–4 d to eliminate non-adherent haematopoietic cells. When the cells reached 70% confluence, they were harvested for 2–5 min using 0.25% Trypsin–EDTA (Sigma-Aldrich, St. Louis, MO, USA), neutralised with a complete medium, and centrifuged at 500 × g for 5 min. Cell pellets were resuspended in a complete medium. Cell viability was examined by adding equal volumes of the cell suspension and 0.4% trypan blue (Gibco) and loading 10 μL of the stained suspension into each chamber of a haemocytometer. Viable and dead cells were counted within 5 min of the sample preparation. Cells with greater than 90% viability were subcultured at a 1:3 ratio (passage 1). The cells were used at passage 4.

Flow cytometry

Cells were resuspended in staining buffer (2% FBS/ /phosphate buffer solution [PBS]) and surface-stained with fluorescein isothiocyanate-conjugated mouse anti-rat CD44 (BioLegend, UK), FITCH-conjugated mouse anti-rat CD90 (BD Pharmingen, USA), or PE-conjugated rabbit anti-rat CD34 (Abcam, UK) at 4°C for 30 min. Isotype-matched antibodies served as controls. Cells were analysed using an EPICS XL flow cytometer (Beckman Coulter).

Experimental design

The rats were randomly divided into three groups: control, D-gal-treated, and D-gal + BMMSC-treated (n = 10 in each group). The sample size was calculated using G Power software. D-gal (300 mg/kg; Sigma-Aldrich, St. Louis, MO, USA) was administered subcutaneously to rats in the D-gal and D-gal + + BMMSCs treatment groups daily for 8 weeks. Once every 2 weeks, 1×10^6 BMMSCs labelled with the membrane-bound fluorescent marker PKH26 (Sigma-Aldrich) were intravenously delivered to rats in the D-gal + BMMSCs group.

Behavioural tests

All animals were acclimatised for 1 week after arrival to behavioural testing. Tests were conducted 1 week after the last transplantation. The test sessions were conducted between 2 PM and 5 PM. Two observers were present throughout each session and blinded to the experimental conditions.

Open-field test. The open-field test allows the simultaneous evaluation of exploration and locomotion. A box 1 m × 1 m × 50 cm in height was made of wood. The floor of the box was divided into equal areas. Each rat was positioned in the centre of the open-field arena, and the rearing frequency and number of crossings (with both forepaws) were recorded using a video camera installed 2.5 m above the box for 5 min. The box was then placed in a noiseless room under controlled illumination.

Beam walking test. Beam walking is a test of motor coordination [22]. The rats had to traverse a beam (100 cm long wooden beam, 4 cm wide, and 3 cm tall), which was hung between a start stage at one end and their home cage at the other end at a height of 80 cm, was suspended by two pillars. Foam padding was placed underneath the beam to protect the animals from injury during a fall. A line (20 cm) was drawn at the start of the beam. During the test, the rat was placed within this starting area facing its home cage, and a stopwatch was started upon release of the animal. The timer was halted when all four paws were fully placed on the finishing platform at the other end of the beam. The numbers of footsteps and faults were also recorded.

Measurement of body weight and the brain index

The general appearance of the rats, including behavioural activity, shininess, and hair coat colour, was observed daily. Body weights were assessed weekly. At the end of the experiment, the rats were anaesthetised by intraperitoneal injection of ketamine (90 mg/ /kg) and xylazine (15 mg/kg), and decapitated. Brains were immediately collected from all rats and weighed. Brain indices were calculated using the following formula: brain tissue weight (mg)/final body weight (g).

Assessment of oxidative stress and antioxidants indices

A spectrophotometer was used to assess the levels of malondialdehyde (MDA) and glutathione (GSH) in brain tissues. To assess the extent of lipid peroxidation, rat striata (100 mg) were homogenised in 1 mL of PBS (pH 7.0), and the MDA concentration was measured [65]. The homogenates were centrifuged after mixing with trichloroacetic acid (20%) at 5000 rpm

for 15 min. The supernatants were treated with a 5% thiobarbituric acid solution before boiling in a water bath for 10 min. The absorbance at 532 nm was measured, and the MDA concentration was estimated using a standard curve. The results are expressed in nmol per mg of protein. Ellman's method [16] was used to assess the GSH levels. A solution of dithiobis nitrobenzoate was added to the striatal tissue homogenate and incubated for 1 h. The absorbance was measured at 412 nm. A standard curve was used to measure the GSH concentration. The findings are expressed in mmol per mg of protein.

Table 1. List of primers used in reverse-transcription-quantitative polymerase chain reaction

Gene name	Gene accession	Primer sequence forward/ /Reverse 5'→3'
TH	NM_012740.3	TCGGAAGCTGATTGCAGAGA TTCCGCTGTGTATTCCACATG
DAT	NM_012694.2	CCAGCAATTCAGTGATGACATCA CAGCATAGCCGCCAGTACAG
VMAT2	NM_013031	CGC AAA CTG ATC CTG TTC AT 5-AGA AGA TGC TTT CGC AGG TG
D1R	NM_012546.2	GGAGGACACCGAGGATGA ATGAGGGACGATGAAATGG
D2R	NM_012547.1	TGGGTCAGAAGGGAAGG GATGATAAAGATGAGGAGGGT
BDNF	NM_012842	TGTCCGAGGTGGTAGTACTTCATC CATGCAACCGAAGTATGAAATAACC
VEGF	AF062644	GAGGAAAGGGAAAGGGTCAAAA CACAGTGAACGCTCCAGGATT
GDNF	NM_019139.1	CCAGAGAATTCCAGAGGGAA CTTCACAGGAACCGCTACAA
BETA ACTIN	NM_031144	ATTTGGCACCACACTTTCTACA TCACGCACGATTTCCCTCTCAG

Abbreviations — see text

Quantitative reverse-transcription polymerase chain reaction

Total RNA was extracted from homogenised striata of rats in each group using RNeasy Purification Reagent (Qiagen, Valencia, CA, USA), according to the manufacturer's protocol. RNA purity was assessed with a spectrophotometer; the wavelength absorption ratio (260/280 nm) was between 1.8 and 2.0 for all preparations. RNA was reverse-transcribed into cDNA using Superscript II (Gibco Life Technologies, Grand Island, NY, USA). Quantitative polymerase chain reactions were run and analysed using a StepOneTM instrument with software version 3.1 (Applied Biosystems, Foster City, CA, USA). The reaction mixtures contained SYBR Green Master Mix (Applied Biosystems), gene-specific primer pair (Table 1), cDNA, and nuclease-free water. The cycling conditions were as follows:10 min at 95°C, followed by 40 cycles of 15 s at 95°C, and 60 s at 60°C.

The ABI Prism sequence detection system software was used to analyse the data, and quantification was performed using Sequence Detection Software v1.7 (PE Biosystems, Foster City, CA). Relative target gene expression was calculated using the comparative cycle threshold method [34]. All values were normalised to β-actin mRNA levels.

Immunofluorescence analysis

For immunofluorescence staining, brains were dissected and fixed at 4°C for 24 h, then cryoprotected in 30% sucrose at 4°C. Serial sections (40 μm) were cut by a cryostat and stored at –20°C until use. The sections were incubated in 10% blocking solution (10% normal goat serum in 0.3% Triton X-100 in PBS) at room temperature (RT) for 1 h, then incubated at 4°C overnight in the primary antibodies rabbit anti-glial fibrillary acidic protein (GFAP) (1:1000, Abcam, Cat. #ab7260), or rabbit anti-tyrosine hydroxylase (TH) (1:500, Abcam, Cat. #ab112). The sections were then rinsed in PBS and a secondary antibody was applied (1:500, Alexa-488, Cat. #A-11034, Molecular Probes) at RT for 1 h. Finally, the sections were rinsed in PBS and mounted in Fluoroshield mounting medium with 4',6-diamidino-2phenylindole (DAPI) (Abcam, Cat. #ab104139).

Quantitative histological assessments

Four non-overlapping images per section were randomly captured from the striatum and SN and analysed for each brain section for each marker. Immunofluorescence images were captured using a Leica DM5500 B/11888817/12 microscope equipped with a Leica DFC450C camera, using a Leica HI PLAN 10/0.25 objective. For each image, the region of interest was the field of view at a magnification of 10x. From at least three sections/rat, immunopositive cells were counted using ImageJ software (National Institutes of Health, Bethesda, Maryland, US) by a manual approach using the plugin/cell counter tool [53] and then averaged per field for each rat. The calculated numbers for the 10 animals/experimental group were used for comparison and statistical analyses. Concerning TH

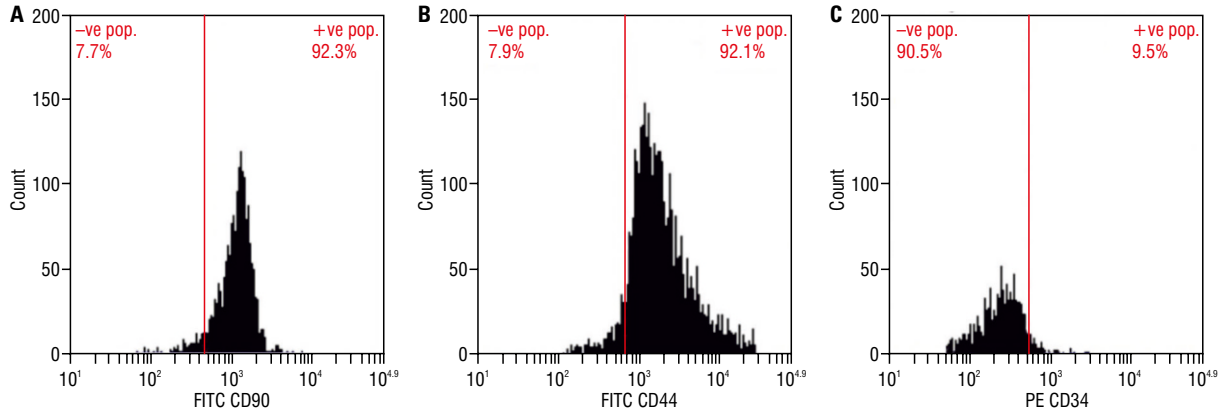

Figure 1. Characterisation of the bone marrow-derived mesenchymal stem cells (BMMSCs) population. The cell-surface phenotype of the BMMSCs was assessed by flow cytometry using antibodies against CD90 (**A**), CD44 (**B**), and CD34 (**C**). In total, 92.3%, and 92.1% of the cells expressed CD90 and CD44, respectively, whereas only 9.5% expressed CD34; –ve — negative; +ve — positive; pop. — population; FITC — fluorescein isothiocyante; PE — phycoerythrin.

immunoreactive striatal fibres, the immunoreactivity of TH fibres in the striatum was measured by densitometry as described by Febbraro et al. [17]. Photos were converted to grayscale using Image J programme (1.51 version; National Institute of Health, Bethesda, MD, USA) and analysed for grey intensity after calibrating the Image J programme by assessing the optical density. Optical density values for the treatment groups are presented as a percentage of the control groups.

Statistical analysis

Data are expressed as the mean ± standard error of the mean. Normal distributions were evaluated using the D'Argostino and Pearson normality tests, and data were analysed using one-way or two-way analysis of variance followed by a post hoc Bonferroni test. Statistical significance was set at $p < 0.05$. Statistical analyses were performed using the GraphPad software.

RESULTS

Characterization of BMMSCs

Mesenchymal stem cells derived from the bone marrow of Sprague-Dawley rats were spindle-shaped, fibroblast-like cells after 10 days of culture. At passage 4, cells were evaluated by flow cytometry for the expression of CD90, CD44 (mesenchymal cell marker), and CD34 (haematopoietic lineage marker). More than 90% of the cells were CD90+ and CD44+, and less than 10% were CD34+ (Fig. 1). These results indicated that the cells were mostly non-haematopoietic MSCs.

BMMSC transplantation improved the physical characteristics and brain indices

Rats in the D-gal group showed physical signs of general ageing, such as reduced activity and rough, dull, yellow hair coat with hair loss, whereas rats in the transplanted group exhibited signs of normal activity and smooth, glossy, brightly coloured hair coat, indicating that BMMSC treatment had beneficial effects on D-gal-induced ageing. In the current study, the body weights of rats in the control, D-gal, and transplanted groups were not significantly different (Fig. 2A). However, the brain index was significantly reduced in D-gal-treated rats compared with that in the control rats, whereas the brain index of the BMMSC-treated group was significantly improved compared with that in the aged rats (Fig. 2B), demonstrating that transplanted cells reversed D-gal-induced brain atrophy.

BMMSCs recovered locomotion and motor coordination in D-gal ageing rats

Aged rats showed significantly decreased locomotor activity, as indicated by a significant decline in the number of line crossings compared with those in the control group. This was significantly improved by BMMSC injection, as indicated by the significant increase in the number of line crossings compared to the values in the ageing group (Fig. 3A). In addition, aged rats showed increased rearing, which was significantly reversed in the BMMSC-injected group (Fig. 3B). In aged rats, beam walking tests exhibited a significant increase in crossing time (Fig. 4A), foot fault number (Fig. 4B), and footstep number (Fig. 4C),

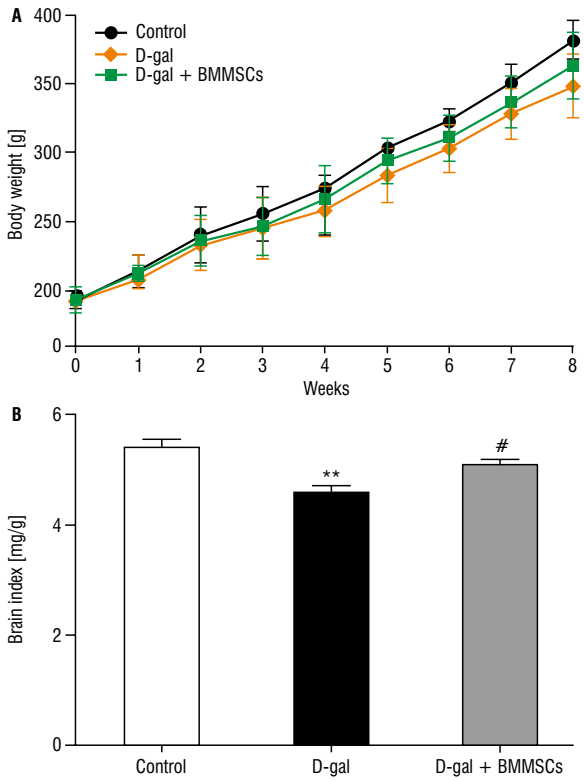

Figure 2. Body weight (**A**) and brain index (**B**) were evaluated in the control, aged (D-gal), and transplanted (D-gal + BMMSCs) rats; **p < 0.01 vs. control rats; #p < 0.01 vs. aged rats. Data are expressed as mean ± standard error of the means; n = 10/ /group; BMMSCs — bone marrow-derived mesenchymal stem cells.

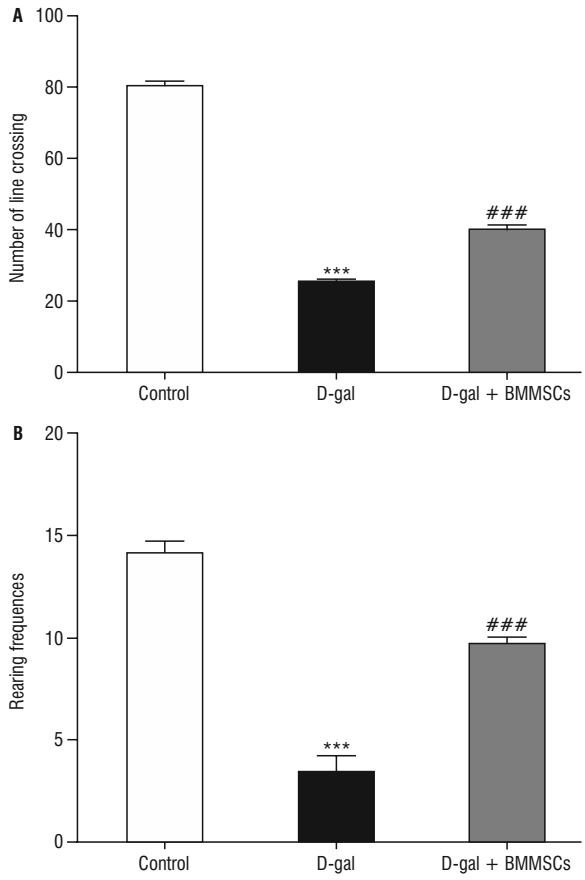

Figure 3. Locomotion was evaluated in control, aged (D-gal), and transplanted (D-gal + BMMSCs) rats. Locomotion (horizontal locomotion and vertical rearing) were assessed for 5 min in an open--field test; **A.** Number of line crossing; **B.** Rearing frequences; ***p < 0.001 vs. control rats; ###p < 0.001 vs. aged rats. Data are expressed as means ± standard error of the means; n = 10/group; BMMSCs — bone marrow-derived mesenchymal stem cells.

with a marked reduction in velocity (Fig. 4D), when compared to control rats. These observations demonstrate marked changes in motor coordination during ageing. Interestingly, D-gal + BMMSC-treated rats showed significant improvement in these parameters.

BMMSCs restored DA system function

The impact of age on several DA targets, including receptors, transporters, and relevant enzymes in the striatum, has been reported [4, 12, 21, 27, 28]. Gene expression of the main functional components of DA neurones was assessed in the different groups. Gene expression of TH for dopamine synthesis, vesicular monoamine transporter-2 (VMAT2) for dopamine transport into the vesicle, presynaptic dopamine transporter (DAT), and main postsynaptic receptors, D1 and D2, were downregulated in the striatum of aged rats compared to control rats (Fig. 5). These declines in DA markers' expression were significantly prevented in the striatum of the D-gal + BMMSCs group.

BMMSCs differentiated into TH-positive cells and astrocytes, and protected DA neurones in the D-gal ageing brain

To examine the underlying mechanisms by which BMMSCs improve motor deficits and restore functional DA system alterations, we first examined whether systemically administered BMMSCs homed to and survived in the brains of transplanted rats. PKH labelled BMMSCs were extensively found in all brain regions in the transplanted group. Studies have shown that age-related changes in DA neurones are comparable to the pathogenic changes observed in PD. A decline in the number of TH-positive cells has been reported in the SN of healthy aged subjects. TH staining demonstrated a significant decrease in TH-positive cells in the SN and TH fibre density in the striatum of aged rats compared to that in the controls (Fig. 6). Transplantation of BMMSCs significantly increased

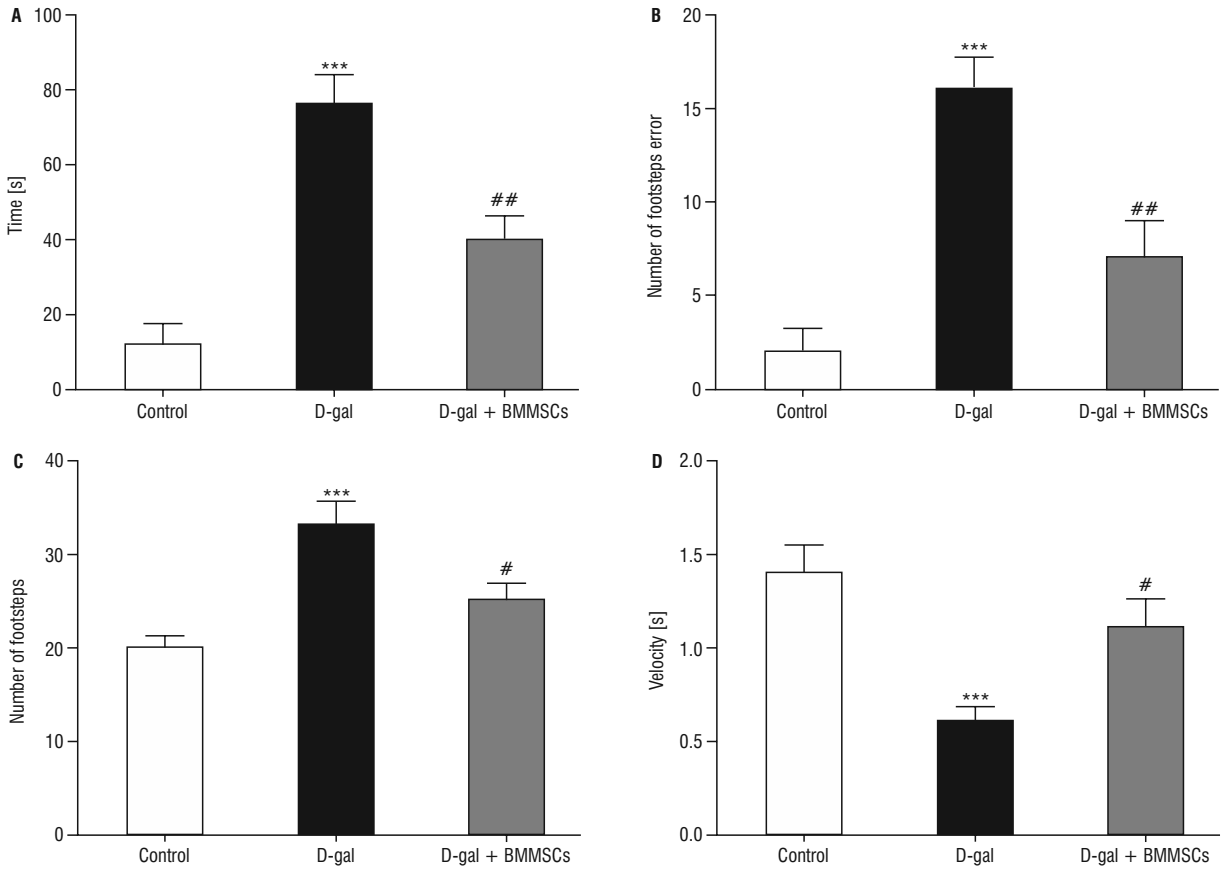

Figure 4. A–D. Motor coordination was evaluated using a beam walking test in control, aged (D-gal), and transplanted (D-gal + BMMSCs) rats; ***p < 0.001 vs. control rats; #p < 0.05 and ##p < 0.01 vs. aged rats. Data are expressed as means ± standard error of the means; n = 10/group; BMMSCs — bone marrow-derived mesenchymal stem cells.

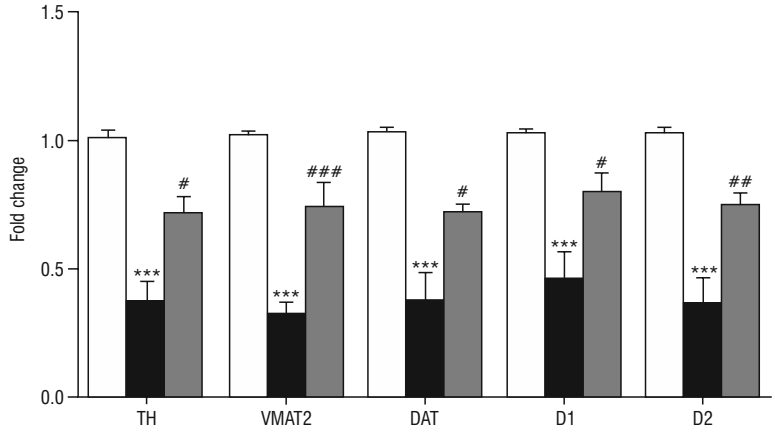

Figure 5. Gene expression of dopaminergic system markers in the striatum in control, aged (D-gal), and transplanted (D-gal + BMMSCs) rats as measured by reverse-transcription-quantitative polymerase chain reaction; ***p < 0.001 vs. control rats; #p < 0.05, ##p < 0.01, and ###p < 0.001 vs. aged rats. Data are expressed as means ± standard error of the means; n = 10/group; BMMSCs — bone marrow-derived mesenchymal stem cells; TH — tyrosine hydroxylase; VMAT2 — vesicular monoamine transporter-2; DAT — dopamine transporter.

the number of TH neurones in the SN and TH fibre density in the striatum compared to that in aged rats. Interestingly, some of the PKH-labelled BMMSCs co-expressed TH in SN, indicating their differentiation into DA neurones. Furthermore, in the striatum, approximately 20% of the PKH-labelled BMMSCs co-expressed GFAP, indicating their differentiation into astrocytes (Fig. 7).

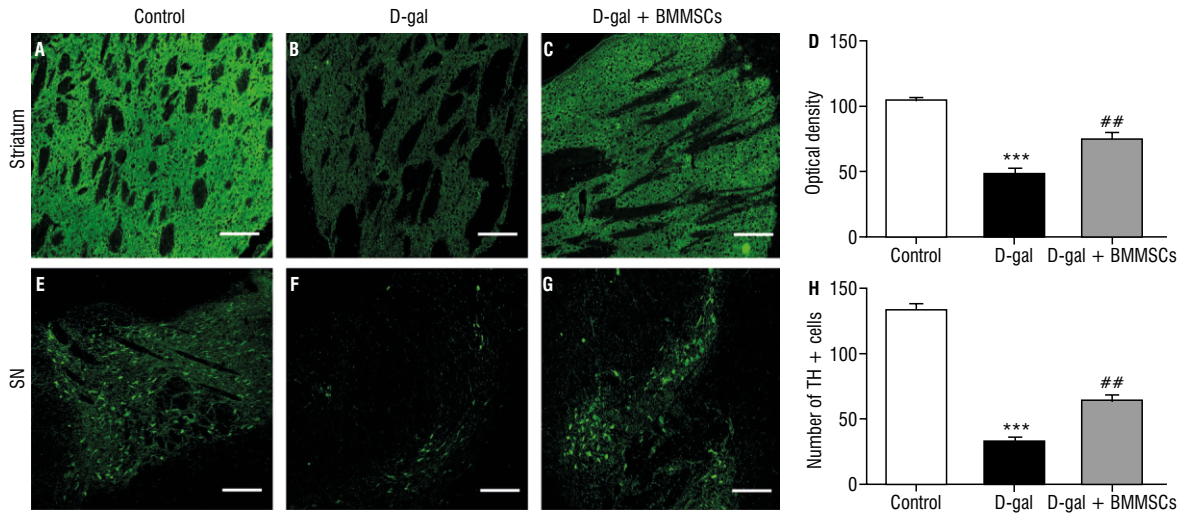

Figure 6. A–H. Number of tyrosine hydroxylase (TH) positive neurones in the substantia nigra (SN) and the density of the TH fibres in the striatum in control, aged (D-gal), and transplanted (D-gal + BMMSCs) rats. Scale bar = 500 μm; ***p < 0.001 vs. control rats; ##p < 0.01 vs. aged rats. Data are expressed as means ± standard error of the means; n = 10/group; BMMSCs — bone marrow-derived mesenchymal stem cells.

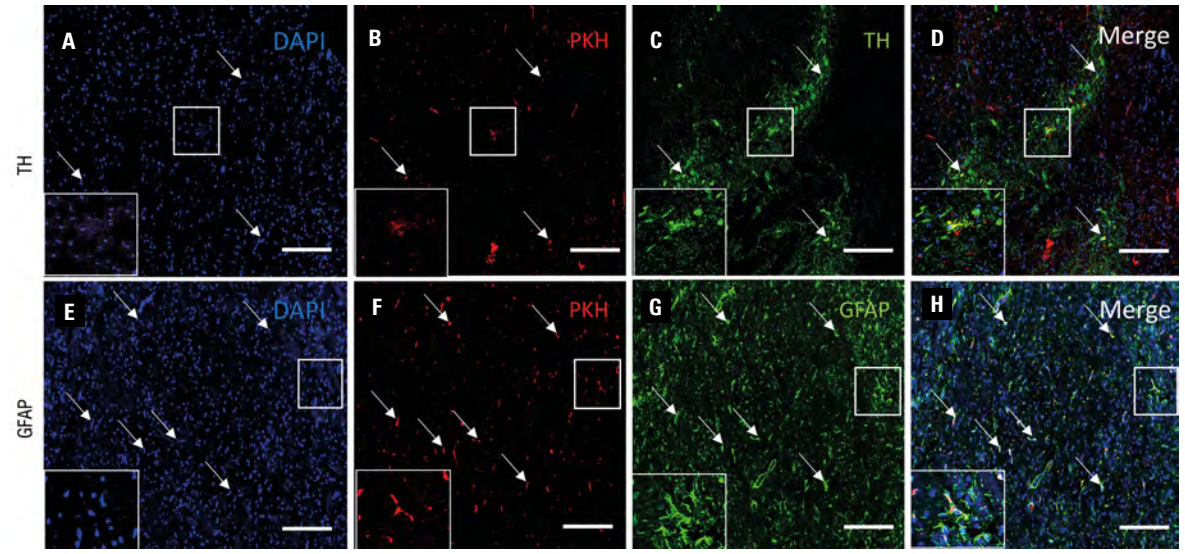

Figure 7. Survival and differentiation of transplanted bone marrow-derived mesenchymal stem cells (BMMSCs) into tyrosine hydroxylase (TH) positive neurones in the substantia nigra (**A–D**) and astrocytes in the striatum (**E–H**) in the transplanted (D-gal + BMMSCs) group. A number of PKH-labelled BMMSCs (red) (**B**, **F**) co-expressed TH (green) (**C**) and anti-glial fibrillary acidic protein (GFAP) (green) (**G**). The insets display the boxed area at a higher magnification. PKH-labelled cells (red) (**B**, **F**), TH-positive cells (green) (**C**), GFAP-positive cells (green) (**G**), 4′,6-diamidino-2phenylindole (DAPI)-stained nuclei (blue) (**A**, **E**), and merged images (**D**, **H**). Scale bar = 500 μm.

BMMSCs induced antioxidative effects and restored neurotrophic factors

The modification of neuronal and neurotransmitter functions that accompanies ageing seems to be linked to oxidative stress. The specific susceptibility of SN neurones to ageing accumulated reactive oxygen species that may be the cause of the age-associated reduction in DA and motor function in elderly rats [25, 62]. Aged rats had higher levels of MDA, an index of lipid peroxidation, in the striatum than control rats. Furthermore, GSH levels were significantly downregulated in aged rats compared with those in control rats. In D-gal + BMMSC-treated rats, MDA levels significantly declined, whereas GSH levels were upregulated when compared with the levels in aged rats (Fig. 8A, B). Neurotrophic factors, such as BDNF

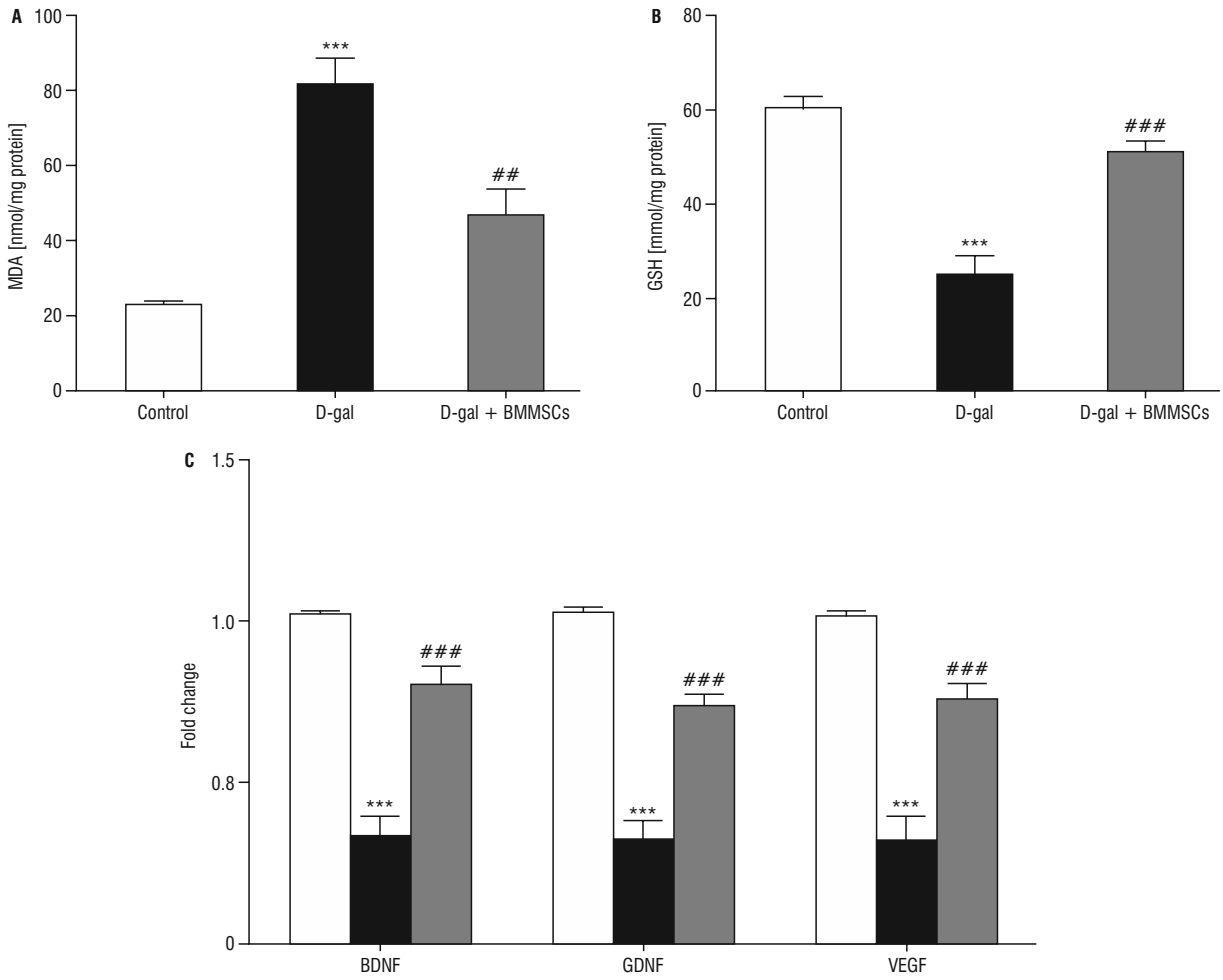

Figure 8. Status of malondialdehyde (MDA) (**A**) and glutathione (GSH) (**B**) and gene expression of brain-derived neurotrophic factor (BDNF), glial cell line-derived neurotrophic factor (GDNF), and vascular endothelial growth factor (VEGF) (**C**) in the striatum of control, aged (D-gal), and transplanted (D-gal + BMMSCs) rats; ***$p < 0.001$ vs. control rats; ##$p < 0.01$ and ###$p < 0.001$ vs. aged rats. Data are expressed as means ± standard error of the means; n = 10/group; BMMSCs — bone marrow-derived mesenchymal stem cells.

and GDNF, are crucial for the synaptic activity, survival, and function of DA neurones, and their decline has been linked to motor deficits associated with aged animals [7, 11, 14, 24, 38, 43, 52, 71]. In the striatum of aged rats, the expression of BDNF, GDNF, and vascular endothelial growth factor (VEGF) was remarkably reduced when compared with the expression in control rats, and these declines were reversed by BMMSC transplantation (Fig. 8C).

DISCUSSION

The most important risk factor for PD is ageing, and progressive motor and coordination deterioration associated with normal ageing has been linked to nigrostriatal degeneration. Several studies have shown that the DA system, both structurally and functionally, is affected during normal ageing [8, 23, 35, 44, 54, 56, 63, 72]. The capability of stem cells to replace lost or malfunctioning cells has been the focus of recent research [13, 15, 18, 29, 47, 57, 68]. This study is the first to examine the potential beneficial effects of systemic transplantation of BMMSCs on the DA system in a D-gal-induced rat model of brain ageing. In this study, we demonstrated that intravenous transplantation of BMMSCs into D-gal-aged rats ameliorated behavioural deficits, restored DA dysfunction, differentiated into TH-positive cells in the SN, protected TH immunoreactivity in the aged striatum, and induced antioxidative and neurotrophic effects. These data demonstrate the therapeutic effectiveness of BMMSCS in the aged brain.

Ageing is characterised by a gradual decline in locomotion and motor coordination. In our study, BMMSCs improved motor alterations in D-gal + + BMMSCs. Our results are consistent with those of previous studies. Implantation of BMMCs into the stri-

atum of naturally aged rats increased the functional recovery of swimming performance as measured by the Marshall scale for vigour and success, as well as motor coordination as measured by the transverse bridge test [18]. In various animal models of PD, BMMSCs implantation improved motor impairments [20, 31, 37, 45, 64, 67]. The beam walk test, which examines limb movements, such as accurate stepping, coordination, and precise positioning of the paw, is particularly susceptible to DA depletion [37, 51, 61]. In our study, the detected decrease in striatal DA levels resulted in significant motor incoordination in D-gal rats, as indicated by an increased number of footsteps and foot slips and a significant decline in velocity. Intravenous injection of BMMSCs decreased the number of footsteps and foot faults with an increase in velocity. The observed motor improvements were associated with increased DA and TH levels in the striatum, suggesting that BMMC transplantation improved motor dysfunction in aged rats, possibly through DA upregulation in the striatum.

Several studies have demonstrated the significance of DA signalling in the maintenance of motor function, and that declines in dopamine functional component availability might be responsible for age-related behavioural deficits [4, 12, 21, 27, 28]. In the treated group, the gene expression of DA markers demonstrated an overall increase compared to that in aged rats. A study evaluating the striatal implantation of rat adult bone marrow MSCs in a 6-hydroxydopamine rat model of PD reported a partial albeit significant recovery of DA presynaptic markers such as D1, D2, DAT, and VMAT2 in treated animals compared to non-treated ones [12]. Therefore, it can be concluded that the detected improvements in motor and coordination activities might be due to the recovery of the DA system.

The survival, migration, and differentiation capacity of the injected BMMSCs in D-gal-aged rats were investigated to explain the mechanism behind the behavioural and DA functional improvements observed following BMMSC transplantation. Repeated intravenous BMMSC injection resulted in significant cell migration across all brain areas studied. These findings corroborate prior findings. Ageing has been associated with increased blood-brain barrier permeability in both animals and humans, which might be caused by numerous ageing-related processes, including increased oxidative stress and greater microglial activation [50, 60]. In our study, a few transplanted cells differentiated into TH+ cells in SN. Substantial evidence suggests that BMMSCs can differentiate into neurones, particularly DA neurones, both in vitro and in vivo [1, 30, 58, 66, 70]. Moreover, the nigrostriatal pathway is known to be involved in ageing and PD progression, and the striatum is well established to be the target brain structure for DA projections from the SN. We further assessed whether the DA fibres of the striatum were re-innervated in the transplanted group. Our results revealed that transplantation of BMMSCs significantly increased the number of endogenous TH neurones in the SN and TH fibre density in the striatum compared to that in aged rats. These results suggest endogenous restoration of the host DA system in the SN of transplanted rats. Therefore, we next sought to investigate the potential paracrine mechanisms mediated by transplanted BMMSCs that could contribute to the endogenous revival of the host DA system.

Mesenchymal stem cells can be considered as mini-bioreactors capable of secreting a wide range of cytokines and neurotrophic factors that are crucial in the treatment of neurodegenerative disorders. There is a substantial body of evidence that MSCs express a variety of neurotrophic factors, including nerve growth factor, GDNF, BDNF, insulin-like growth factor-1, and basic fibroblast growth factor at both the mRNA and protein levels [24, 52, 71]. Synaptic plasticity, as well as the survival and function of midbrain dopamine neurones, are dependent on BDNF. By comparing BDNF (+/–) with wild-type mice at various ages, the effects of a partial genetic deletion of BDNF on motor activities and DA level measurements were studied. With age, a decrease in BDNF expression becomes more important for DA circuits and associated behavioural performance [11]. Depletion of BDNF leads to declined TH expression in the SN [14]. GDNF is a secretory protein that protects DA neurones both in vitro and in vivo. GDNF treatment increases striatal dopamine levels and potentiates striatal DA fibre regeneration in preclinical animals [38]. As a result, intracranial ectopic administration of GDNF has been attempted in multiple PD clinical studies with promising but equivocal outcomes [7]. We observed decreased BDNF and GDNF expression in D-gal aged rats, and these decreases were remarkably restored in BMMSC-transplanted rats. GDNF is primarily produced by astrocytes in the brain. GDNF expression is increased in astrocytes in the striatal region of PD animal models with DA innervation, reflecting a process

of endogenous regeneration [43]. Interestingly, in the present study, 20% of transplanted cells differentiated into astrocytes in the striatum. The biological features of BMMSC production of neurotrophic factors such as GDNF, as well as the ability of these cells to differentiate into astrocytes, indicate their potential for treating age-related neurodegenerative diseases.

CONCLUSIONS

This study demonstrated that intravenous transplantation of BMMSCs prevented locomotion and coordination deficits in a D-gal ageing rat model by restoring DA system function, protecting atrophic DA neurones in the SN, inducing antioxidative effects, and secreting neurotrophic factors. Our study provides proof of principle that the systemic transplantation of BMMSCs is a potential therapeutic approach for the protection of nigrostriatal changes associated with ageing.

Funding

This research project was funded by the Deanship of Research and Graduate Studies, Ajman University, UAE (grant no. GL5211642).

Conflict of interest: None declared

REFERENCES

1. Ababneh NA, Al-Kurdi B, Jamali F, et al. A comparative study of the capability of MSCs isolated from different human tissue sources to differentiate into neuronal stem cells and dopaminergic-like cells. PeerJ. 2022; 10: e13003, doi: 10.7717/peerj.13003, indexed in Pubmed: 35341051.
2. Abdelwahab SA, Elsebay SA, Ibrahim MF, et al. Cerebral and cerebellar histological changes in the rat animal model of rotenone induced parkinsonism can be ameliorated by bone marrow derived stem cell conditioned media. J Chem Neuroanat. 2021; 111: 101892, doi: 10.1016/j.jchemneu.2020.101892, indexed in Pubmed: 33220428.
3. Artegiani B, Calegari F. Age-related cognitive decline: can neural stem cells help us? Aging (Albany NY). 2012; 4(3): 176–186, doi: 10.18632/aging.100446, indexed in Pubmed: 22466406.
4. Bäckman L, Nyberg L, Lindenberger U, et al. The correlative triad among aging, dopamine, and cognition: current status and future prospects. Neurosci Biobehav Rev. 2006; 30(6): 791–807, doi: 10.1016/j.neubiorev.2006.06.005, indexed in Pubmed: 16901542.
5. Badyra B, Sułkowski M, Milczarek O, et al. Mesenchymal stem cells as a multimodal treatment for nervous system diseases. Stem Cells Transl Med. 2020; 9(10): 1174–1189, doi: 10.1002/sctm.19-0430, indexed in Pubmed: 32573961.
6. Baquet ZC, Bickford PC, Jones KR. Brain-derived neurotrophic factor is required for the establishment of the proper number of dopaminergic neurons in the substantia nigra pars compacta. J Neurosci. 2005; 25(26): 6251–6259, doi: 10.1523/JNEUROSCI.4601-04.2005, indexed in Pubmed: 15987955.
7. Barker RA, Björklund A, Gash DM, et al. GDNF and Parkinson's disease: where next? A summary from a recent workshop. J Parkinsons Dis. 2020; 10(3): 875–891, doi: 10.3233/JPD-202004, indexed in Pubmed: 32508331.
8. Behfar Q, Ramirez Zuniga A, Martino-Adami PV. Aging, Senescence, and Dementia. J Prev Alzheimers Dis. 2022; 9(3): 523–531, doi: 10.14283/jpad.2022.42, indexed in Pubmed: 35841253.
9. Berebichez-Fridman R, Montero-Olvera PR. Sources and clinical applications of mesenchymal stem cells: state-of--the-art review. Sultan Qaboos Univ Med J. 2018; 18(3): e264–e277, doi: 10.18295/squmj.2018.18.03.002, indexed in Pubmed: 30607265.
10. Blinkouskaya Y, Caçoilo A, Gollamudi T, et al. Brain aging mechanisms with mechanical manifestations. Mech Ageing Dev. 2021; 200: 111575, doi: 10.1016/j.mad.2021.111575, indexed in Pubmed: 34600936.
11. Boger HA, Mannangatti P, Samuvel DJ, et al. Effects of brain-derived neurotrophic factor on dopaminergic function and motor behavior during aging. Genes Brain Behav. 2011; 10(2): 186–198, doi: 10.1111/j.1601-183X.2010.00654.x, indexed in Pubmed: 20860702.
12. Bouchez G, Sensebé L, Vourc'h P, et al. Partial recovery of dopaminergic pathway after graft of adult mesenchymal stem cells in a rat model of Parkinson's disease. Neurochem Int. 2008; 52(7): 1332–1342, doi: 10.1016/j.neuint.2008.02.003, indexed in Pubmed: 18372079.
13. Cao N, Liao T, Liu J, et al. Clinical-grade human umbilical cord-derived mesenchymal stem cells reverse cognitive aging via improving synaptic plasticity and endogenous neurogenesis. Cell Death Dis. 2017; 8(8): e2996, doi: 10.1038/cddis.2017.316, indexed in Pubmed: 28796260.
14. Dluzen DE, McDermott JL, Anderson LI, et al. Age-related changes in nigrostriatal dopaminergic function are accentuated in +/- brain-derived neurotrophic factor mice. Neuroscience. 2004; 128(1): 201–208, doi: 10.1016/j.neuroscience.2004.06.032, indexed in Pubmed: 15450367.
15. El-Akabawy G, Aabed K, Rashed LA, et al. Preventive effects of bone marrow-derived mesenchymal stem cell transplantation in a D-galactose-induced brain aging in rats. Folia Morphol. 2022; 81(3): 632–649, doi: 10.5603/FM.a2021.0073, indexed in Pubmed: 34355788.
16. Ellman GL. Tissue sulfhydryl groups. Arch Biochem Biophys. 1959; 82(1): 70–77, doi: 10.1016/0003-9861(59)90090-6, indexed in Pubmed: 13650640.
17. Febbraro F, Andersen KJ, Sanchez-Guajardo V, et al. Chronic intranasal deferoxamine ameliorates motor defects and pathology in the α-synuclein rAAV Parkinson's model. Exp Neurol. 2013; 247: 45–58, doi: 10.1016/j.expneurol.2013.03.017, indexed in Pubmed: 23531432.
18. Fernández CI, Alberti E, Mendoza Y, et al. Motor and cognitive recovery induced by bone marrow stem cells grafted to striatum and hippocampus of impaired aged rats: functional and therapeutic considerations. Ann NY Acad Sci. 2004; 1019: 48–52, doi: 10.1196/annals.1297.011, indexed in Pubmed: 15246993.
19. Foltynie T, Sawcer S, Brayne C, et al. The genetic basis of Parkinson's disease. J Neurol Neurosurg Psychiatry. 2002;

73(4): 363–370, doi: 10.1136/jnnp.73.4.363, indexed in Pubmed: 12235301.
20. Ghahari L, Safari M, Rahimi Jaberi K, et al. Mesenchymal stem cells with granulocyte colony-stimulating factor reduce stress oxidative factors in Parkinson's disease. Iran Biomed J. 2020; 24(2): 89–98, doi: 10.29252/ibj.24.2.89, indexed in Pubmed: 31677610.
21. Giacobbo BL, Özalay Ö, Mediavilla T, et al. The aged striatum: evidence of molecular and structural changes using a longitudinal multimodal approach in mice. Front Aging Neurosci. 2022; 14: 795132, doi: 10.3389/fnagi.2022.795132, indexed in Pubmed: 35140600.
22. Goldstein LB. Rapid reliable measurement of lesion parameters for studies of motor recovery after sensorimotor cortex injury in the rat. J Neurosci Methods. 1993; 48(1-2): 35–42, doi: 10.1016/s0165-0270(05)80005-6, indexed in Pubmed: 8377521.
23. Hou Y, Dan X, Babbar M, et al. Ageing as a risk factor for neurodegenerative disease. Nat Rev Neurol. 2019; 15(10): 565–581, doi: 10.1038/s41582-019-0244-7, indexed in Pubmed: 31501588.
24. Inden M, Takata K, Nishimura K, et al. Therapeutic effects of human mesenchymal and hematopoietic stem cells on rotenone-treated parkinsonian mice. J Neurosci Res. 2013; 91(1): 62–72, doi: 10.1002/jnr.23128, indexed in Pubmed: 23073839.
25. Ionescu-Tucker A, Cotman CW. Emerging roles of oxidative stress in brain aging and Alzheimer's disease. Neurobiol Aging. 2021; 107: 86–95, doi: 10.1016/j.neurobiolaging.2021.07.014, indexed in Pubmed: 34416493.
26. Jiménez-Acosta MA, Hernández LJ, Cristerna ML, et al. Mesenchymal stem cells: new alternatives for nervous system disorders. Curr Stem Cell Res Ther. 2023; 18(3): 299–321, doi: 10.2174/1574888X17666220511153133, indexed in Pubmed: 35546750.
27. Juarez EJ, Castrellon JJ, Green MA, et al. Reproducibility of the correlative triad among aging, dopamine receptor availability, and cognition. Psychol Aging. 2019; 34(7): 921–932, doi: 10.1037/pag0000403, indexed in Pubmed: 31589058.
28. Karalija N, Papenberg G, Wåhlin A, et al. Sex differences in dopamine integrity and brain structure among healthy older adults: Relationships to episodic memory. Neurobiol Aging. 2021; 105: 272–279, doi: 10.1016/j.neurobiolaging.2021.04.022, indexed in Pubmed: 34134056.
29. Kim D, Kyung J, Park D, et al. Health span-extending activity of human amniotic membrane- and adipose tissue-derived stem cells in F344 rats. Stem Cells Transl Med. 2015; 4(10): 1144–1154, doi: 10.5966/sctm.2015-0011, indexed in Pubmed: 26315571.
30. Li M, Yang J, Cheng O, et al. Effect of TO901317 on GF to promote the differentiation of human bone marrow mesenchymal stem cells into dopamine neurons on Parkinson's disease. Ther Adv Chronic Dis. 2021; 12: 2040622321998139, doi: 10.1177/2040622321998139, indexed in Pubmed: 33796244.
31. Li Y, Li Z, Gu J, et al. Exosomes isolated during dopaminergic neuron differentiation suppressed neuronal inflammation in a rodent model of Parkinson's disease. Neurosci Lett. 2022; 771: 136414, doi: 10.1016/j.neulet.2021.136414, indexed in Pubmed: 34954117.
32. Li Z, Zhang Z, Ren Y, et al. Aging and age-related diseases: from mechanisms to therapeutic strategies. Biogerontology. 2021; 22(2): 165–187, doi: 10.1007/s10522-021-09910-5, indexed in Pubmed: 33502634.
33. Limke TL, Rao MS. Neural stem cells in aging and disease. J Cell Mol Med. 2002; 6(4): 475–496, doi: 10.1111/j.1582-4934.2002.tb00451.x, indexed in Pubmed: 12611637.
34. Livak KJ, Schmittgen TD. Analysis of relative gene expression data using real-time quantitative PCR and the 2(-Delta Delta C(T)) Method. Methods. 2001; 25(4): 402–408, doi: 10.1006/meth.2001.1262, indexed in Pubmed: 11846609.
35. Lopez-Leon M, Reggiani PC, Claudia B, et al. Regenerative medicine for the aging brain. Enliven: J Stem Cell Res Regen Med. 2014; 01(01), doi: 10.18650/2379-5751.11001.
36. Lövdén M, Karalija N, Andersson M, et al. Latent-Profile analysis reveals behavioral and brain correlates of dopamine-cognition associations. Cereb Cortex. 2018; 28(11): 3894–3907, doi: 10.1093/cercor/bhx253, indexed in Pubmed: 29028935.
37. Mahendru D, Jain A, Bansal S, et al. Neuroprotective effect of bone marrow-derived mesenchymal stem cell secretome in 6-OHDA-induced Parkinson's disease. Regen Med. 2021; 16(10): 915–930, doi: 10.2217/rme-2021-0018, indexed in Pubmed: 34553608.
38. Manfredsson FP, Polinski NK, Subramanian T, et al. The future of GDNF in Parkinson's disease. Front Aging Neurosci. 2020; 12: 593572, doi: 10.3389/fnagi.2020.593572, indexed in Pubmed: 33364933.
39. Mendes-Pinheiro B, Anjo SI, Manadas B, et al. Bone marrow mesenchymal stem cells' secretome exerts neuroprotective effects in a Parkinson's disease rat model. Front Bioeng Biotechnol. 2019; 7: 294, doi: 10.3389/fbioe.2019.00294, indexed in Pubmed: 31737616.
40. Mercado NM, Collier TJ, Sortwell CE, et al. BDNF in the Aged Brain: Translational Implications for Parkinson's Disease. Austin Neurol Neurosci. 2017; 2(2), indexed in Pubmed: 29726549.
41. Mickiewicz AL, Kordower JH. GDNF family ligands: a potential future for Parkinson's disease therapy. CNS Neurol Disord Drug Targets. 2011; 10(6): 703–711, doi: 10.2174/187152711797247876, indexed in Pubmed: 21838676.
42. Mitra S, Turconi G, Darreh-Shori T, et al. Increased endogenous GDNF in mice protects against age-related decline in neuronal cholinergic markers. Front Aging Neurosci. 2021; 13: 714186, doi: 10.3389/fnagi.2021.714186, indexed in Pubmed: 34475820.
43. Nakagawa T, Yabe T, Schwartz JP. Gene expression profiles of reactive astrocytes cultured from dopamine-depleted striatum. Neurobiol Dis. 2005; 20(2): 275–282, doi: 10.1016/j.nbd.2005.03.009, indexed in Pubmed: 16242635.
44. Naoi M, Maruyama W. Cell death of dopamine neurons in aging and Parkinson's disease. Mech Ageing Dev. 1999; 111(2-3): 175–188, doi: 10.1016/s0047-6374(99)00064-0, indexed in Pubmed: 10656535.
45. Nicaise AM, Willis CM, Crocker SJ, et al. Stem cells of the aging brain. Front Aging Neurosci. 2020; 12: 247, doi: 10.3389/fnagi.2020.00247, indexed in Pubmed: 32848716.
46. Palasz E, Wysocka A, Gasiorowska A, et al. BDNF as a promising therapeutic agent in parkinson's disease. Int J Mol Sci. 2020; 21(3), doi: 10.3390/ijms21031170, indexed in Pubmed: 32050617.
47. Park D, Yang G, Bae DK, et al. Human adipose tissue-derived mesenchymal stem cells improve cognitive func-

tion and physical activity in ageing mice. J Neurosci Res. 2013; 91(5): 660–670, doi: 10.1002/jnr.23182, indexed in Pubmed: 23404260.
48. Piccardi L, Curcio G, Palermo L, et al. Ageing and neurodegenerative disorders. Behav Neurol. 2015; 2015: 149532, doi: 10.1155/2015/149532, indexed in Pubmed: 26185358.
49. Polisetti N, Chaitanya VG, Babu PP, et al. Isolation, characterization and differentiation potential of rat bone marrow stromal cells. Neurol India. 2010; 58(2): 201–208, doi: 10.4103/0028-3886.63789, indexed in Pubmed: 20508336.
50. Popescu BO, Toescu EC, Popescu LM, et al. Blood-brain barrier alterations in ageing and dementia. J Neurol Sci. 2009; 283(1-2): 99–106, doi: 10.1016/j.jns.2009.02.321, indexed in Pubmed: 19264328.
51. Quinn LP, Perren MJ, Brackenborough KT, et al. A beam-walking apparatus to assess behavioural impairments in MPTP-treated mice: pharmacological validation with R-(-)-deprenyl. J Neurosci Methods. 2007; 164(1): 43–49, doi: 10.1016/j.jneumeth.2007.03.021, indexed in Pubmed: 17498809.
52. Rahbaran M, Zekiy AO, Bahramali M, et al. Therapeutic utility of mesenchymal stromal cell (MSC)-based approaches in chronic neurodegeneration: a glimpse into underlying mechanisms, current status, and prospects. Cell Mol Biol Lett. 2022; 27(1): 56, doi: 10.1186/s11658-022-00359-z, indexed in Pubmed: 35842587.
53. Rangan GK, Tesch GH. Quantification of renal pathology by image analysis. Nephrology (Carlton). 2007; 12(6): 553–558, doi: 10.1111/j.1440-1797.2007.00855.x, indexed in Pubmed: 17995580.
54. Reeve A, Simcox E, Turnbull D. Ageing and Parkinson's disease: why is advancing age the biggest risk factor? Ageing Res Rev. 2014; 14(100): 19–30, doi: 10.1016/j.arr.2014.01.004, indexed in Pubmed: 24503004.
55. Schiess M, Suescun J, Doursout MF, et al. Allogeneic bone marrow-derived mesenchymal stem cell safety in idiopathic Parkinson's disease. Mov Disord. 2021; 36(8): 1825–1834, doi: 10.1002/mds.28582, indexed in Pubmed: 33772873.
56. Seo JP, Koo DK. Aging of the nigrostriatal tract in the human brain: a diffusion tensor imaging study. Medicina (Kaunas). 2021; 57(9), doi: 10.3390/medicina57090994, indexed in Pubmed: 34577917.
57. Shen J, Tsai YT, Dimarco NM, et al. Transplantation of mesenchymal stem cells from young donors delays aging in mice. Sci Rep. 2011; 1: 67, doi: 10.1038/srep00067, indexed in Pubmed: 22355586.
58. Shetty P, Ravindran G, Sarang S, et al. Clinical grade mesenchymal stem cells transdifferentiated under xenofree conditions alleviates motor deficiencies in a rat model of Parkinson's disease. Cell Biol Int. 2009; 33(8): 830–838, doi: 10.1016/j.cellbi.2009.05.002, indexed in Pubmed: 19465139.
59. Sikora E, Bielak-Zmijewska A, Dudkowska M, et al. Cellular senescence in brain aging. Front Aging Neurosci. 2021; 13: 646924, doi: 10.3389/fnagi.2021.646924, indexed in Pubmed: 33732142.
60. Simpson JE, Wharton SB, Cooper J, et al. Alterations of the blood-brain barrier in cerebral white matter lesions in the ageing brain. Neurosci Lett. 2010; 486(3): 246–251, doi: 10.1016/j.neulet.2010.09.063, indexed in Pubmed: 20887772.
61. Strome EM, Cepeda IL, Sossi V, et al. Evaluation of the integrity of the dopamine system in a rodent model of Parkinson's disease: small animal positron emission tomography compared to behavioral assessment and autoradiography. Mol Imaging Biol. 2006; 8(5): 292–299, doi: 10.1007/s11307-006-0051-6, indexed in Pubmed: 16897319.
62. Trist BG, Hare DJ, Double KL. Oxidative stress in the aging substantia nigra and the etiology of Parkinson's disease. Aging Cell. 2019; 18(6): e13031, doi: 10.1111/acel.13031, indexed in Pubmed: 31432604.
63. Umegaki H, Roth GS, Ingram DK. Aging of the striatum: mechanisms and interventions. Age (Dordr). 2008; 30(4): 251–261, doi: 10.1007/s11357-008-9066-z, indexed in Pubmed: 19424849.
64. Wang X, Zhuang W, Fu W, et al. The lentiviral-mediated Nurr1 genetic engineering mesenchymal stem cells protect dopaminergic neurons in a rat model of Parkinson's disease. Am J Transl Res. 2018; 10(6): 1583–1599, indexed in Pubmed: 30018702.
65. Wills ED. Evaluation of lipid peroxidation in lipids and biologicalmembranes. In: Snell K, Mullock B (eds.), Biochemical Toxicology: A PracticalApproach. Oxford, London 1987.
66. Xiong N, Yang H, Liu L, et al. bFGF promotes the differentiation and effectiveness of human bone marrow mesenchymal stem cells in a rotenone model for Parkinson's disease. Environ Toxicol Pharmacol. 2013; 36(2): 411–422, doi: 10.1016/j.etap.2013.05.005, indexed in Pubmed: 23770451.
67. Xue J, Liu Y, Darabi MA, et al. An injectable conductive Gelatin-PANI hydrogel system serves as a promising carrier to deliver BMSCs for Parkinson's disease treatment. Mater Sci Eng C Mater Biol Appl. 2019; 100: 584–597, doi: 10.1016/j.msec.2019.03.024, indexed in Pubmed: 30948095.
68. Zappa Villar MF, Lehmann M, García MG, et al. Mesenchymal stem cell therapy improves spatial memory and hippocampal structure in aging rats. Behav Brain Res. 2019; 374: 111887, doi: 10.1016/j.bbr.2019.04.001, indexed in Pubmed: 30951751.
69. Zarbakhsh S, Safari M, Aldaghi MR, et al. Irisin protects the substantia nigra dopaminergic neurons in the rat model of Parkinson's disease. Iran J Basic Med Sci. 2019; 22(7): 722–728, doi: 10.22038/ijbms.2019.33444.7987, indexed in Pubmed: 32373292.
70. Zhang J, Yang Bo, Luo L, et al. Effect of NTN and Lmx1 on the notch signaling pathway during the differentiation of human bone marrow mesenchymal stem cells into dopaminergic neuron-like cells. Parkinsons Dis. 2021; 2021: 6676709, doi: 10.1155/2021/6676709, indexed in Pubmed: 34373779.
71. Zheng W, Honmou O, Miyata K, et al. Therapeutic benefits of human mesenchymal stem cells derived from bone marrow after global cerebral ischemia. Brain Res. 2010; 1310: 8–16, doi: 10.1016/j.brainres.2009.11.012, indexed in Pubmed: 19913518.
72. Zia A, Pourbagher-Shahri AM, Farkhondeh T, et al. Molecular and cellular pathways contributing to brain aging. Behav Brain Funct. 2021; 17(1): 6, doi: 10.1186/s12993-021-00179-9, indexed in Pubmed: 34118939.

VIA MEDICA

ORIGINAL ARTICLE

Folia Morphol.
Vol. 82, No. 4, pp. 854–861
DOI: 10.5603/FM.a2022.0095

ISSN 0015–5659
eISSN 1644–3284
journals.viamedica.pl

The greater omentum and similar serous formations of testis in male white rats

V. Hryn, Y. Kostylenko, O. Maksymenko

Department of Human Anatomy, Poltava State Medical University, Poltava, Ukraine

[Received: 14 August 2022; Accepted: 28 October 2022; Early publication date: 28 November 2022]

Background: *The greater omentum of white rats appears, in basic morphological features (in miniature), to be homologous to the greater omentum of humans. We study of the greater omentum reaction to the catgut implant. After implantation of the catgut thread, it turned out that not only the greater omentum, but also serous formations similar to it, related to the testicles, are involved in the covering of the implant. The aim of the study was to study the general plan of the structure and the principles of morphometric analysis of serous formations of testis in white male rats.*

Materials and methods: *The experiment involved 15 white male rats of reproductive age, weighing from 284 to 334 grams.*

Results: *It has been established that each testicle of white rats has serous (peritoneal derivatives) formations of two types. One of them is a typical mesentery, with which each testicle is separately fixed to the posterior wall of the pelvic cavity, and the other formation is a free regrowth of a duplication of the serous membrane. It was called the epididymal omentum. According to the algorithm for studying the greater omentum in our previous works, it is noteworthy that the area of the greater omentum is noticeably inferior to the area of the epididymal omentums ($F = 0.239$; $p = 0.006$). So, if the average value of the area of the greater omentum is 2766.51 ± 388.12 mm^2, then the same indicator of the epididymal omentum reaches 4383.36 ± 793.56 mm^2, with their approximately the same thickness ($F = 1.35$; $p = 0.291$).*

Conclusions: *It has been established that the greater omentum has two, homeomorphic to it, derivatives of the peritoneum, associated with the epididymis, which were justifiably called epididymal omentums and were fully described in the literature for the first time.* (Folia Morphol 2023; 82, 4: 854–861)

Key words: greater omentum, epididymal omentum, vascular-fatty arcades, radial vascular-fatty tracts, serous-reticular membrane, adipocytes, aseptic inflammation, serous membrane

INTRODUCTION

Information on the features of the anatomical structure of the internal organs of white rats can be obtained from the works of many authors who are engaged in experimental modelling of various pathological conditions, and according to these authors, some organs of humans and white rats have more similarities than differences [12–14, 26, 29].

The greater omentum of white rats appears, in basic morphological features (in miniature), to be

Address for correspondence: Dr. O. Maksymenko, Department of Human Anatomy, Poltava State Medical University, Shevchenko str. 73, 173, Poltava city, Poltava region, Ukraine, 36039, tel: +380951290969, e-mail: dr.aleksmaksymenko@gmail.com

homologous to the greater omentum of humans [20, 27, 30].

The data obtained in previous works indicate that the greater omentum of white male rats can be in a latent form, being mostly located among the loops of the small intestine and in its usual state — located on the loops of the small and large intestine and consists of two component formations. They are represented by arcuate prostrate and anastomosing between themselves vascular-fatty arcades, which are linked by areas of the thinnest duplication of the serous membrane, called serous-reticular membranes. Each of them can be represented as a finely perforated thinnest duplication of the peritoneum. Its reticular structure can be distinguished relatively wide looped strands, surrounded by mesothelium, and narrow, variable in configuration membranes, which transversely connect them [18].

These data were obtained in order to conduct further experimental studies – the study of the greater omentum reaction to the catgut implant. After implantation of the catgut thread, it turned out that not only the greater omentum, but also serous formations similar to it, related to the testicles, are involved in the covering of the implant. It should be noted that these formations appear in the literature under such different names as: "gonadal depot of visceral white adipose tissue", "epididymal white adipose tissue", "gonadal fat", "epididymal fat", "epididymal fat pad" [1, 5, 9, 16, 17]. Gonadal white adipose tissue in female rats surrounds the uterus and ovaries and is called ovarian or parametrial white adipose tissue. In male rats, it's connected with the epididymis and with the testicle itself and is called epididymal white adipose tissue [8, 23]. According to the literature, the cytoarchitectonics of epididymal fat is represented by several types of cells, such as preadipocytes, mature adipocytes, immune and endothelial cells [3, 7]. But a sufficiently intelligible description of the structure of these formations, no matter what they are called, was not found in any source of literature. It forces us to conduct a thorough study in the same algorithm that we were guided by when studying the greater omentum, in determining the most accessible and indicative for them metric analysis of morphological dimensions, which will serve as control criteria in evaluating the results of planned experimental investigation.

The aim of the study was to study the general plan of the structure and the principles of morphometric analysis of serous formations of testis in white male rats.

MATERIALS AND METHODS

The experiment involved 15 white male rats of reproductive age, weighing from 284 to 334 grams. All animals were kept under standard conditions of the experimental biological clinic (vivarium) of the Poltava State Medical University, in accordance with the rules for keeping experimental animals established by the Directive 2010/63/EU of the European Parliament and of the Council, by Order of the Ministry of Education, Science, Youth and Sports of Ukraine No. 249 of 01.03.2012 "On Approval of the Procedure for Carrying out Experiments, Experiments on Animals by Scientific Institutions" and "General Ethical Principles of Animal Experiments", adopted by the Fifth National Congress on Bioethics (Kyiv, 2013), (Report No. 198 of 21.10.2021 from the meeting of the Commission on Biomedical Ethics of the Poltava State Medical University) [10, 21].

Vivisection was carried out in accordance with all the norms and requirements for conducting acute experiments on animals. The abdominal cavity was opened in all animals one-by-one (on a dissecting device in position of the animals on the back). It created a complete overview of the internal organs in their natural proportions [11].

Before further manipulations, at first, the entire content of the peritoneal cavity was subjected to gentle washing with warm 0.9% saline NaCl solution, and then irrigated from a syringe with 10% neutral formalin solution. Some total preparations of omentums were stained in a solution of haematoxylin and eosin and Van Gieson. Only after that overview photographs were taken with a digital camera directly in the body of a laboratory animal on laminated graph paper and matte glass.

At the same time, in such a straightened form of preparations, it was possible to carry out their metric measurements, which were carried out using the electronic calliper "Miol". Initially, the length and width of the omentums were measured. The length was measured from the point of the proximal-fixed side to the farthest point of its free-distal edge. The width was measured within its lateral dimensions. And if these two opposite sides are supplemented with two lateral lines, then the all omentum fits into a rectangle of a definite area. The area, of course, will be the derivative of two mutually perpendicular linear

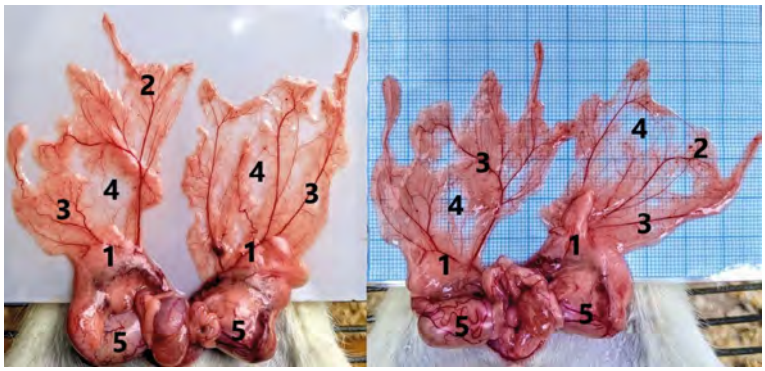

Figure 1. General view of the total preparation of the epididymal omentums of a sexually mature male rat; 1 — the base of the omentum; 2 — free edges of the omentum; 3 — radial vascular-fatty tracts; 4 — serous-reticular membranes; 5 — testicles.

distances. Finally, using the methods of variational statistics, we obtained the mean metric parameters of the epididymal omentum area and the greater omentum area of white rats. The second general morphometric parameter of the omentums was their thickness. But, due to the fact that it is variable over its entire area, this parameter can be obtained indirectly, based on its thickest irregularities. First, the thickness of the two slides was measured, then the fixed and free edges of the omentum were alternately placed on the first slide, covered with the second slide, and the thickness of the received "sandwiches" was measured. The desired index of the thickness of the two edges of the omentum was obtained by subtracting the known thickness of both slides from the total obtained value. Thus, the arithmetic mean of the two found indicators served as the general thickness of the epididymal omentum and the greater omentum of white rats. Only after that overview photographs were taken and it was proceeded to the direct study of the objects, followed by statistical processing of the obtained mathematical data.

Statistical analysis of the results was carried out on a personal computer using the Prism 5 (version 5/03) and Microsoft Excel 2010 software packages, descriptive statistics and statistical analysis methods. The description statistics are presented for the mean ± standard deviation. Quantitative values were presented in terms of median and interquartile (25%–75%) range (Q1–Q3).

The study was carried out in a Konus light microscope equipped with a Sigeta DCM-900 9.0MP digital microphotographic attachment with the Biorex 3 programme adapted for these studies (serial number 5604). Morphometric characteristics of the tissue structures of the corresponding preparations were obtained using a system for visual analysis of histological preparations, as well as using a Sigeta X 1 mm/100 Div. x0.01 mm object micrometer, the scale of which (equal to 1 mm, where the small division corresponds to 10 μm) was applied on the corresponding micrograph were obtained at an equivalent magnification.

RESULTS

With a sufficiently wide opening of the peritoneal cavity of animals and a comprehensive examination of its content, one can easily determine the location of the desired formations, which in intact animals are located in different positions. Thus, in some cases, they occupy a superficial location accessible for direct observation; in other animals, they are hidden (like the greater omentum) among the loops of the small intestine, and sometimes they can be found within the pelvic cavity and even immersed in scrotum [18]. But in all cases, they can be extracted together with the testicles, followed by the manufacture of visual total preparations, which were placed on thin frosted glass or laminated graph paper (Fig. 1).

It has been established that each testicle of white rats has serous (peritoneal derivatives) formations of two types. One of them is a typical mesentery, with which each testicle is separately fixed to the posterior wall of the pelvic cavity, and the other formation is a free regrowth of a duplication of the serous membrane. It was called the epididymal omentum (this name will be fully justified below). Actually, these serous formations belong to the sphere of our interests. Attention is drawn to the great diversity of their shape, which refers not only to individual differences, but also to bilateral asymmetry. But, along with this, there are fan-shaped forms, as well as resembling peculiar lobes or a petal, which has

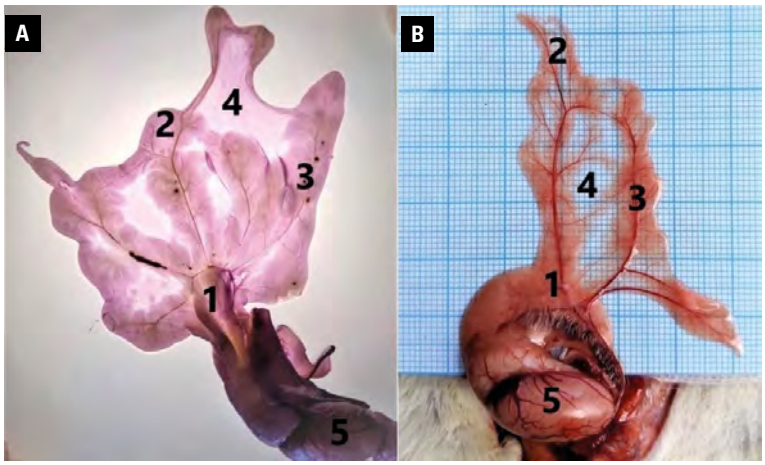

Figure 2. Various forms of epididymal omentums in male white rats. Total preparations; **A.** Stained with haematoxylin and eosin; **B.** Intact, unstained preparation; 1 — the base of the omentum; 2 — free edge of the omentum; 3 — radial vascular-fatty tracts; 4 — serous-reticular membranes; 5 — testicle.

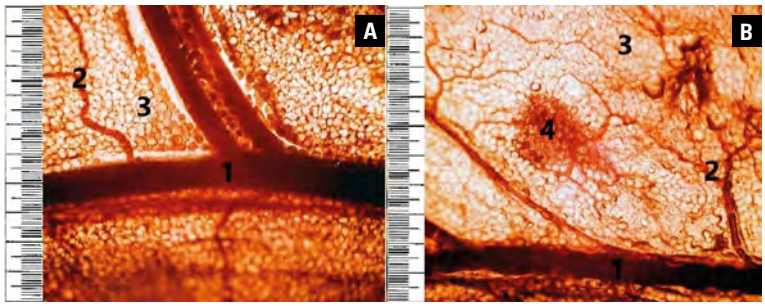

Figure 3. A, B. Areas of preparations of the epididymal omentum of a white male rat, totally stained with haematoxylin and eosin; 4× objective lens; small division of the metric scale: 10 microns; 1 — axial blood vessels; 2 — blood microvessels; 3 — fat cells; 4 — milky spot.

a narrow and short base, which starts from the head of the epididymis (Figs. 1, 2).

Starting from the head of the epididymis, blood vessels, which branch radially in the duplication of this serous lobe, penetrate through the narrow base of the epididymal omentum, which can be called a stem or pedicle. At the same time, in each radially oriented blood tract, there is an arterial vessel closely accompanied by a venous vessel (Fig. 3A). It should be noted that, in the greater omentum, the origins of the vascular-fatty arcades originate along the width of its base from the duodenum, greater curvature of the stomach and spleen.

It is quite remarkable that each radially oriented vascular tract occupies an axial position in the limbic adipose tissue, which has a lobular distribution. At the same time, along the length, they gradually become thinner to terminal microvessels. This picture exactly corresponds to the structural organization of the vascular-fatty arcades of the greater omentum, with the only difference being that anastomosing occurs between their terminal sections in the area of the free edge of the greater omentum [18]. But unlike the greater omentum in the serous lobes of the testicles, similar formations are not arcade, but radial in shape, which gives reason to call them radial vascular-fatty tracts. Basically, they are homeomorphic formations. This is also confirmed by the fact that in the fatty lobules of the radial vascular-fatty tracts of the serous lobes of the testicles, there are separate milk spots (Fig. 3B). However, compared to the greater omentum, they are much less common.

An expressive similarity between the structure of the greater omentum and the serous lobes of the rat testis lie in the presence of a reticular structure of intermediate zones between their radial vascular-fatty tracts, which were called serous-reticular membranes. They clearly coincide with each other in their architectonics (Fig. 2). In support of this, we present only some micrographs of the intermediate zones of the

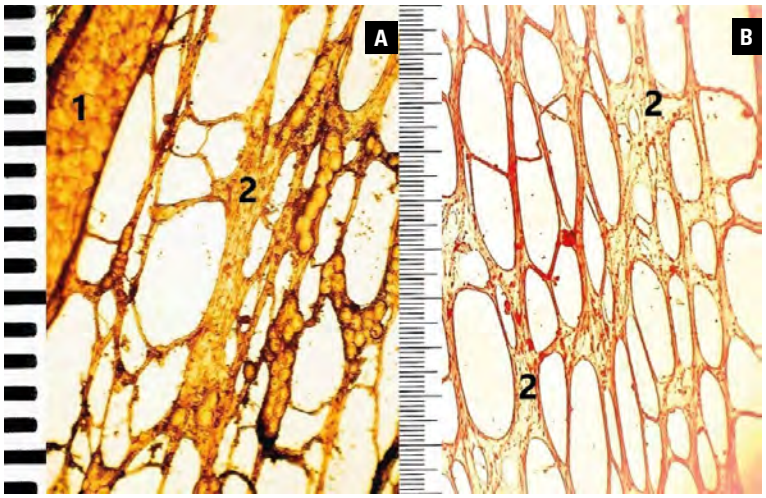

Figure 4. Areas of the serous intermediate zones of the epididymal omentum (**A**) and greater omentum (**B**) of a white male rat; **A.** 40× objective lens, stained with haematoxylin and eosin; **B.** 10× objective, Van Gieson staining; small division of the metric scale: 10 microns; 1 — tissue structures of the radial vascular-fatty tracts on the border with serous-reticular membranes; 2 — looped strands of serous-reticular membranes.

Table 1. Metric parameters of the epididymal omentum of white rats at the macroscopic level (n = 15)

	Min	Q1	Median	Q3	Max
Length [mm]	43.52	57.96	62.62	68.77	87.92
Width [mm]	52.88	63.94	69	75.14	90.01
Area [mm^2]	3222.43	3928.48	4348.74	4838.24	6245.84
Thickness [mm]	0.49	0.54	0.57	0.61	0.69
The lateral width of the radial vascular-fatty tracts of the epididymal omentum [mm]	2.7	3.65	3.81	4.2	5.02
The medial width of the radial vascular-fatty tracts of the epididymal omentum [mm]	3.56	5.03	5.22	6.16	7.08

Min, Max — minimal and maximal value; Q1 — first quartile; Q3 — third quartile

serous lobes of the testicles, which are comparable to those of the greater omentum (Fig. 4).

According to the algorithm for studying the greater omentum in our previous works, it has the following dimensions (on average, length 43.61 ± 3.50 mm; width 63.22 ± 5.69 mm; area 2766.51 ± 388.12 mm^2; thickness 0.52 ± 0.07 mm), its vascular-fatty arcades had the following width (duodenal arcade 3.58 ± ± 0.99 mm; gastric arcade 2.28 ± 0.35 mm and splenic arcade 3.82 ± 1.16 mm). A morphometric analysis of the epididymal omentum was carried out. It was found that they differ in great variability in their size, that is, in the area of contact with the peritoneal fluid, in which they are located in a rather arbitrary arrangement and have the following dimensions (on average, length 63.36 ± 9.43 mm; width 69.54 ± 9.77 mm; area 4383.36 ± 793.56 mm^2; thickness 0.58 ± 0.06 mm), the width of the radial vascular-fatty tracts of the epididymal omentum was also measured (lateral tract 3.92 ± 0.52 mm and medial tract 5.59 ± 0.99 mm)

Table 1 shows the main numerical data reflecting the metric characteristic of one of the two epididymal omentums. In Table 2 is presents metric parameters of the greater omentum.

Despite the relativity of these metric parameters, they make it possible to judge the dimensional relationships between the serous formations and the greater omentum. First of all, it is noteworthy that, according to the obtained planimetric data, the area of the greater omentum is noticeably inferior to the area of the epididymal omentums ($F = 0.239$; $p = 0.006$). So, if the average value of the area of the greater omentum is 2766.51 ± 388.12 mm^2, then the same indicator of the epididymal omentum reaches 4383.36 ± 793.56 mm^2, with their approximately the same thickness ($F = 1.35$; $p = 0.291$).

The area of epididymal omentums has a large individual variation ranging from 3222.43 to 6245.84 mm^2. Noteworthy is the fact that this range of individual variability depends mainly on the length ($r = 0.669$;

Table 2. Metric parameters of the greater omentum of white rats at the macroscopic level (n = 15)

	Min	Q1	Median	Q3	Max
Length [mm]	35.65	41.61	43.27	45.62	48.68
Width [mm]	50.64	59.96	63.55	66.49	72.60
Area [mm^2]	1805.31	2544.03	2804.89	2988.99	3354.98
Thickness [mm]	0.40	0.48	0.52	0.56	0.69
The duodenal width of the vascular-fatty arcades of the greater omentum [mm]	2.03	3.01	3.45	4.15	5.88
The gastric width of the vascular-fatty arcades of the greater omentum [mm]	1.85	2.07	2.19	2.48	3.01
The splenic width of the vascular-fatty arcades of the greater omentum [mm]	1.97	3.16	3.99	4.49	5.80

Min, Max — minimal and maximal value; Q1 — first quartile; Q3 — third quartile

$p = 0.006$), while the area of the greater omentum varies individually mainly due to its width ($r = 0.873$; $p < 0.0001$).

Additional morphometric information was obtained by measuring the width of the radial vascular--fatty tracts of the epididymal omentum (Table 1). They differ from the vascular-fatty arcades of the greater omentum only in shape, but not in their internal structure, except that in the epididymal omentums, they are, according to average statistics, somewhat wider ($F = 28.08$; $p < 0.0001$) due to a greater deposition of adipose tissue in them on the sides of the axial blood vessels.

DISCUSSION

According to the world literature, visceral white adipose tissue plays an important role in the accumulation and release of energy, maintaining homeostasis, thermoregulation, secretion of adipokines in order to regulate metabolism, immune reactions, and maintaining the body's energy balance. Visceral adipocytes surround vital organs and are contained in the gonadal, perirenal, retroperitoneal, omentum, and pericardial depots. According to research by Bagchi and MacDougald [1] epididymal white adipose tissue is connected to the epididymis and blood vessels, which is also confirmed by our research. In turn, there may be several visible blood vessels and they are oriented and branched radially, occupying an axial position — that is why we call them radial vascular-fatty tracts, about which there are no data in the literature.

In the conducted literature search, no attention is paid to determining the shape of epididymal serous formations of the testicles. In our work, we drew attention to the variety of forms and bilateral asymmetry of epididymal omentums, which, starting with a narrow and short leg and can have a petal-like or fan-like shape.

In the process of research, we didn't find comparative literary data of the greater omentum with epididymal fat; therefore, we made an attempt to compare these formations and as a result of the research, the undeniable similarity of the structural elements of their morphological structure was revealed. Based on the obtained results, we think it is more correct than the existing terms in the literature to call these serous formations of the testicles epididymal omentums.

During the anatomical study of epididymal fat, some authors distinguish the proximal and distal part of the epididymal fat pad [15, 17].

While studying the external structure of the epididymal omentums, a short base that starts from the head of the epididymis and a free edge where it ends were identified. This fact was investigated and confirmed by Berry et al. [2, 22].

We also single out the mesentery, which fixes the testicle directly to the back wall of the pelvic cavity, and the actual free growth of the duplication of the serous membrane with adipose tissue.

During the morphometric analysis, it was established that the area of the epididymal omentum exceeds the area of the greater omentum — mainly due to the length, which is confirmed by the studies of other authors [5, 24], who recognise epididymal fat as the largest representative of white visceral fat in rodents.

According to Cleary et al. [7] and, Billon and Dani [3], epididymal fat is composed of several cell types, including mature adipocytes of various sizes, immune cells, endothelial cells, and preadipocytes. At the microscopic examination, milky spots, endothelial cells, and adipocytes were found, but we did not differentiate the maturity of adipocytes or their precursors. The number of milky spots in the epididymal omentum, according to the observation, is significantly less than

in the greater omentum, which coincides with the data of the literature about milky spots of the greater omentum and the gonadal fat [19, 25, 28].

At present, the function of epididymal fat is not clearly identified. According to Chu et al. [6], surgical removal of epididymal fat causes cessation of spermatogenesis in the testis. It is suggested that secretory molecules derived from epididymal fat, such as leptin, resistin, and adiponectin, may influence the regulation of testicular function. A group of other authors believes that gonadal white adipose tissue may regulate gametogenesis by modulating neuroendocrine signalling [16, 17, 31].

We, in turn, without delving into molecular research, noted the active participation of the epididymal omentum in acute inflammatory processes of the abdominal cavity, namely, the prevention of the spread of the peritoneal inflammation (peritonitis, both septic and aseptic), which is the perspective of our further research.

Also, the epididymal omentum deserves attention, especially when conducting experimental studies on laboratory animals, as it is absent in humans, which was also noted by some authors [4].

Thus, when comparing the anatomical structure of the structural components of the greater omentum with the epididymal omentum, we consider it appropriate to call the vascular ways of the greater omentum — vascular-fatty arcades, and the epididymal omentum — radial vascular-fatty tracts; intermediate avascular areas of omentums — serous-reticulate membranes, which are similar in their structure. This is also confirmed by the fact that in the fatty lobes of the radial vascular-fatty tracts of the testicles there are individual milky spots located along the blood vessels [18].

Therefore, the conducted brief comparative analysis between the structure of the greater omentum and the serous formations of the testicles of white rats shows that, due to their combination of similar tissue components, they can be considered as homologous derivatives of the peritoneum. Based on this thesis, we consider it is more correct than the existing terms in the literature to call these serous testicular formations epididymal omentums, as mentioned above, since they begin with short stems (or pedicles) from the head of the epididymis of the corresponding testicle.

CONCLUSIONS

We established that the greater omentum has two, homeomorphic to it, derivatives of the peritoneum, associated with the epididymis, which were justifiably called epididymal omentums and were fully described in the literature for the first time.

Thus, in the peritoneal cavity of white male rats, in contrast to humans, according to our data, there are not one but three omentums. Because, according to the structure and topology in the peritoneal cavity, the small and large omentums cannot be considered identical formations, since the small one belongs to the category of ligaments.

Conflict of interest: None declared

REFERENCES

1. Bagchi DP, MacDougald OA. Identification and dissection of diverse mouse adipose depots. J Vis Exp. 2019(149), doi: 10.3791/59499, indexed in Pubmed: 31355801.
2. Berry DC, Stenesen D, Zeve D, et al. The developmental origins of adipose tissue. Development. 2013; 140(19): 3939–3949, doi: 10.1242/dev.080549, indexed in Pubmed: 24046315.
3. Billon N, Dani C. Developmental origins of the adipocyte lineage: new insights from genetics and genomics studies. Stem Cell Rev Rep. 2012; 8(1): 55–66, doi: 10.1007/s12015-011-9242-x, indexed in Pubmed: 21365256.
4. Bjørndal B, Burri L, Staalesen V, et al. Different adipose depots: their role in the development of metabolic syndrome and mitochondrial response to hypolipidemic agents. J Obes. 2011; 2011: 490650, doi: 10.1155/2011/490650, indexed in Pubmed: 21403826.
5. Chusyd DE, Wang D, Huffman DM, et al. Relationships between rodent white adipose fat pads and human white adipose fat depots. Front Nutr. 2016; 3: 10, doi: 10.3389/fnut.2016.00010, indexed in Pubmed: 27148535.
6. Chu Ye, Huddleston GG, Clancy AN, et al. Epididymal fat is necessary for spermatogenesis, but not testosterone production or copulatory behavior. Endocrinology. 2010; 151(12): 5669–5679, doi: 10.1210/en.2010-0772, indexed in Pubmed: 20881242.
7. Cleary MP, Greenwood MR, Brasel JA. A multifactor analysis of growth in the rat epididymal fat pad. J Nutr. 1977; 107(11): 1969–1974, doi: 10.1093/jn/107.11.1969, indexed in Pubmed: 908953.
8. Cinti S. The adipose organ at a glance. Dis Model Mech. 2012; 5(5): 588–594, doi: 10.1242/dmm.009662, indexed in Pubmed: 22915020.
9. Dai Y, Ren Ke, Kurosawa K, et al. The distribution of nerves supplying the testis, epididymis and accessory sex glands of Suncus murinus. Anat Sci Int. 2019; 94(1): 128–135, doi: 10.1007/s12565-018-0459-5, indexed in Pubmed: 30206773.
10. Directive, 2010/63/EU (sept. 22, 2010). European Parliament and of the Council. On the protection of animals used for scientific purposes. 2010:276:0033:0079:EN:PDF. https://docplayer.ru/49033909-Direktiva-2010-63-eu-evropeyskogo-parlamenta-i-soveta-evropeyskogo-soyuza.html.
11. Hryn VH, Brovarnyk YAO, Vynakhidnyky; Ukrayinska medychna stomatolohichna akademiya, patentov-

lasnyk. Operatsiyno-preparuvalnyy stolyk z fiksatoramy dlya laboratornykh shchuriv. Patent Ukrayiny No. 142955. 2020 lyp. 10. http://repository.pdmu.edu.ua/bitstream/123456789/13459/1/H_B_patent_2020.pdf.
12. Hryn VH, Kostylenko YP, Bilash VP, et al. Microscopic structure of albino rats' small intestine. Wiad Lek. 2019; 72(5 cz. 1): 733–738, indexed in Pubmed: 31175762.
13. Hryn VH, Kostylenko YP, Yushchenko YP, et al. Comparative histological structure of the gastrointestinal mucosa in human and white rat: a bibliographic analysis. Wiad Lek. 2018; 71(7): 1398–1403, indexed in Pubmed: 30448817.
14. Hryn VH, Kostylenko YP, Yushchenko YP, et al. Comparative histological structure of the gastrointestinal mucosa in human and white rat: a bibliographic analysis. Wiad Lek. 2018; 71(7): 1398–1403, indexed in Pubmed: 30448817.
15. Johnson PR, Hirsch J. Cellularity of adipose depots in six strains of genetically obese mice. J Lipid Res. 1972; 13(1): 2–11, indexed in Pubmed: 5059196.
16. Lee KH. Expression of adipocyte-associated genes in the mouse tail epididymal fat at different postnatal ages. Dev Reprod. 2020; 24(3): 167–176, doi: 10.12717/DR.2020.24.3.167, indexed in Pubmed: 33110948.
17. Lee KH. Postnatal expressional patterns of adipose-associated molecules in the mouse proximal epididymal fat. Dev Reprod. 2019; 23(4): 313–322, doi: 10.12717/DR.2019.23.4.313, indexed in Pubmed: 31993537.
18. Maksymenko OS, Hryn VH, Kostylenko Y. General structure and principles of morphometric analysis of greater omentum in white rats. APMM. 2022; 22(1): 105–110, doi: 10.31718/2077-1096.22.1.105.
19. Martinez-Santibañez G, Cho KW, Lumeng CN. Imaging white adipose tissue with confocal microscopy. Methods Enzymol. 2014; 537: 17–30, doi: 10.1016/B978-0-12-411619-1.00002-1, indexed in Pubmed: 24480339.
20. Meza-Perez S, Randall TD. Immunological functions of the omentum. Trends Immunol. 2017; 38(7): 526–536, doi: 10.1016/j.it.2017.03.002, indexed in Pubmed: 28579319.
21. Nakaz Ministerstva osvity i nauky, molodi ta sportu Ukrayiny No. 249 vid 01.03.2012 r. «Pro zatverdzhennya poryadku provedennya naukovymy ustanovamy doslidiv, eksperymentiv na tvarynakh» [About approval of the procedure of carrying out scientific experiments, experiments on animals]. Ofitsiynyy visnyk Ukrayiny. 2012 Apr 06;24:82. https://zakon.rada.gov.ua/laws/show/z0416-12.
22. Niemalä S, Miettinen S, Sarkanen JR, et al. Adipose tissue and adipocyte differentiation: molecular and cellular aspects and tissue engineering applications. Top Tissue Eng. 2008; 4: 1–26.
23. Rosen ED, Spiegelman BM. What we talk about when we talk about fat. Cell. 2014; 156(1-2): 20–44, doi: 10.1016/j.cell.2013.12.012, indexed in Pubmed: 24439368.
24. Sakata N, Yoshimatsu G, Kodama S. White adipose tissue as a site for islet transplantation. Transplantology. 2020; 1(2): 55–70, doi: 10.3390/transplantology1020006.
25. Schurink B, Cleypool CGJ, Bleys RL. A rapid and simple method for visualizing milky spots in large fixed tissue samples of the human greater omentum. Biotech Histochem. 2019; 94(6): 429–434, doi: 10.1080/10520295.2019.1583375, indexed in Pubmed: 30896309.
26. Starchenko II, Dyachenko LV, Prylutskyi OK, et al. The observation of congenital retroperitoneal large size neuroblastoma. Exp Oncol. 2019; 41(2): 179–181, doi: 10.32471/exp-oncology.2312-8852.vol-41-no-2.13321, indexed in Pubmed: 31262150.
27. Suzuki D, Kim JiH, Shibata S, et al. Topographical anatomy of the greater omentum and transverse mesocolon: a study using human fetuses. Anat Cell Biol. 2019; 52(4): 443–454, doi: 10.5115/acb.19.112, indexed in Pubmed: 31949984.
28. Takemori N. Omental milky spots are splenoid in nature. Hirosaki Medical. 2007; 59: 288–291.
29. Tarasenko LM, Neporada KS, Klusha V. Stress-protective effect of glutapyrone belonging to a new type of amino acid-containing 1,4-dihydropyridines on periodontal tissues and stomach in rats with different resistance to stress. Bull Exp Biol Med. 2002; 133(4): 369–371, doi: 10.1023/a:1016250121896, indexed in Pubmed: 12124648.
30. Wilkosz S, Ireland G, Khwaja N, et al. A comparative study of the structure of human and murine greater omentum. Anat Embryol (Berl). 2005; 209(3): 251–261, doi: 10.1007/s00429-004-0446-6, indexed in Pubmed: 15662530.
31. Yang CF, Liu WW, Wang HQ, et al. Gonadal white adipose tissue is important for gametogenesis in mice through maintenance of local metabolic and immune niches. J Biol Chem. 2022; 298(5): 101818, doi: 10.1016/j.jbc.2022.101818, indexed in Pubmed: 35278432.

VIA MEDICA

ORIGINAL ARTICLE

Folia Morphol.
Vol. 82, No. 4, pp. 862–868
DOI: 10.5603/FM.a2022.0110

ISSN 0015–5659
eISSN 1644–3284
journals.viamedica.pl

Quantitative anatomy of the growing supraspinatus muscle in the human fetus

M. Biernacki, M. Badura, M. Grzonkowska, M. Szpinda, M. Dąbrowska, M. Paruszewska-Achtel, M. Wiśniewski, M. Baumgart

Department of Normal Anatomy, the Ludwik Rydygier Collegium Medicum in Bydgoszcz, the Nicolaus Copernicus University in Torun, Poland

[Received: 6 October 2022; Accepted: 1 December 2022; Early publication date: 23 December 2022]

Background: *The supraspinatus muscle, one of the four rotator cuff muscles, initiates abduction of the arm, simultaneously stretching the articular capsule at the glenohumeral joint, and also contributes to exorotation of the arm. In the present study we aimed to evaluate the age-specific normative values for morphometric parameters of the supraspinatus muscle in human fetuses at varying ages and to elaborate their growth models.*

Materials and methods: *Using anatomical dissection, digital image analysis (NIS Elements AR 3.0) and statistics (Student's t-test, regression analysis), the length, width, circumference and projection surface area of the supraspinatus muscle were measured in 34 human fetuses of both sexes (16 males, 18 females) aged 18–30 weeks of gestation.*

Results: *Neither sex nor laterality differences were found in numerical data of the supraspinatus muscle. In the supraspinatus muscle its length and projection surface area increased logarithmically, while its width and circumference grew proportionately to gestational age. The following growth models of the supraspinatus muscle were established: $y = -71.382 + 30.972 \times \ln(Age) \pm 0.565$ for length, $y = -2.988 + 0.386 \times Age \pm 0.168$ for greatest width (perpendicular to superior angle of scapula), $y = -1.899 + 0.240 \times Age \pm 0.078$ for width perpendicular to the scapular notch, $y = -19.7016 + 3.381 \times Age \pm 2.036$ for circumference, and $y = -721.769 + 266.141 \times \ln(Age) \pm 6.170$ for projection surface area.*

Conclusions: *The supraspinatus muscle reveals neither sex nor laterality differences in its size. The supraspinatus muscle grows logarithmically with reference to its length and projection surface area, and proportionately with respect to its width and circumference.* (Folia Morphol 2023; 82, 4: 862–868)

Key words: supraspinatus muscle, growth dynamics, fetal development

INTRODUCTION

Morphometric data referring to skeletal muscles in man may provide a great amount of conducive information for a precise assessment of the musculoskeletal systems and may be of relevance in surgery [16]. Developmental disturbances at the embryonic period may result in congenital defects of skeletal muscles, thus being responsible for their dysfunction, reduced joint mobility, joint stiffness and consecutive muscle atrophy.

Address for correspondence: Dr. M. Biernacki, Department of Normal Anatomy, the Ludwik Rydygier Collegium Medicum in Bydgoszcz, ul. Łukasiewicza 1, 85–821 Bydgoszcz, Poland, tel: +48 52 585 37 05, e-mail: kizanat@cm.umk.pl

The supraspinatus muscle is triangular in shape, tapers laterally and occupies the osteofibrous supraspinous compartment on the posterior surface of the scapula, bounded inferiorly by the supraspinous fossa, which is sealed superiorly by the supraspinatus fascia. The supraspinatus muscle fibres end in a strong short tendon, which inserts onto both the superior posterior one-third surface of the greater tubercle of humerus and the shoulder joint capsule. Along with the three other tendons of the infraspinatus, teres minor and subscapularis muscles, the supraspinatus tendon contributes to the formation of the so called musculotendinous cuff or rotator cuff. The function of the supraspinatus muscle is to abduct the arm with stretching the articular capsule at the glenohumeral joint, as well as to rotate the arm laterally (exorotation) with minimum flexion, working in conjunction with the deltoid muscle [9]. The supraspinatus muscle alone initiates abduction at the glenohumeral joint until first 30 degrees, and then continues this action with the deltoid muscle [17].

Compression of the supraspinatus tendon may first lead to its haemorrhage and oedema, occurring in its critical section. This is followed by degeneration and ultimately by mechanical partial damage to the rotator cuff, resulting in both a weakening and a pain of the shoulder joint. The partial or complete damage to the rotator cuff muscles, especially to the supraspinatus muscle, may necessitate surgery [11].

Despite the use of different modern imaging methods, including ultrasound, magnetic resonance imaging, computed tomography and autopsy studies in adults, we still failed to find any numerical data about the supraspinatus muscle in human fetuses. Therefore, according to our best knowledge, the present study constitutes the first report in the professional literature to morphometrically analyse the size of the growing supraspinatus muscle in the human fetus.

The three aims of the present study were:

— to perform morphometric analysis of the fetal supraspinatus muscle (linear and planar parameters), so as to determine their age-specific normative values;
— to examine possible sex and laterality differences for all analysed morphometric parameters; and finally
— to compute growth dynamics for all the analysed morphometric parameters, expressed by best-matched mathematical models.

MATERIALS AND METHODS

The study material comprised 34 human fetuses (16 males and 18 females) aged 18–30 weeks of gestational age, which originated from spontaneous abortions and preterm deliveries. The fetuses were acquired before the year 2000 and constitute part of the specimen collection of the Department of Normal Anatomy in the Ludwik Rydygier Collegium Medicum in Bydgoszcz of the Nicolaus Copernicus University in Torun. This experiment was approved by the Bioethics Committee of our University (KB 275/2011). The gestational ages were based on the crown-rump length. Table 1 lists the characteristics of the study group, including the ages, number and sex of the fetuses studied.

With the use of anatomical dissection, the supraspinatus muscle was bilaterally visualised and excised, then imaged due to a Canon EOS 70D(W) digital camera and finally subjected to morphometric analysis with a digital image system (NIS Elements AR 3.0). For every supraspinatus muscle examined, the following five parameters on the dorsal projection of the scapula were precisely defined and measured (Fig. 1):

— its length based on the determined distance between its origin and insertion;
— its greatest width based on the determined distance between its superior and inferior borderlines, just perpendicular to the superior angle of scapula;
— its width based on the determined distance between the superior and inferior borderlines, just perpendicular to the scapular notch;
— its circumference, based on the contour of the entire supraspinatus muscle;
— its projection surface area bounded by the contour of the supraspinatus muscle.

The obtained numerical data was statistically analysed in such a manner that distribution of variables was checked using the Shapiro-Wilk (W) test, while homogeneity of variance was checked using Fisher's test. The results were expressed as arithmetic means with standard deviations. To compare the means, Student's t-test for independent variables and one-way analysis of variance were used. Tukey's test was used for post-hoc analysis. If no similarity of variance occurred, the non-parametric Kruskal-Wallis test was used. The description of growth dynamics of the analysed parameters was based on linear and nonlinear regression analysis. The match between the numerical data and computed regression curves was evaluated based on the coefficient of determination (R^2).

Table 1. Age, number and sex of the fetuses studied

Gestational age	Crown-rump length [mm]				Number of fetuses	Sex	
	Mean	Standard deviation	Minimum	Maximum		Male	Female
18	135.17	130.00	142.00	4.22	6	3	3
19	151.00	148.00	154.00	4.24	2	1	1
20	166.00	165.00	167.00	1.41	2	1	1
21	172.67	169.00	176.00	3.51	3	2	1
22	182.00	182.00	182.00	–	1	1	0
23	198.00	194.00	202.00	5.66	2	1	1
24	208.00	205.00	212.00	3.61	3	1	2
25	217.00	214.00	221.00	3.16	4	1	3
26	229.33	225.00	232.00	3.79	3	1	2
27	237.00	235.00	240.00	2.16	4	1	3
28	246.00	245.00	247.00	1.41	2	1	1
29	257.00	255.00	260.00	2.65	3	2	1
30	265.00	265.00	265.00		1	1	1
Total					36	16	18

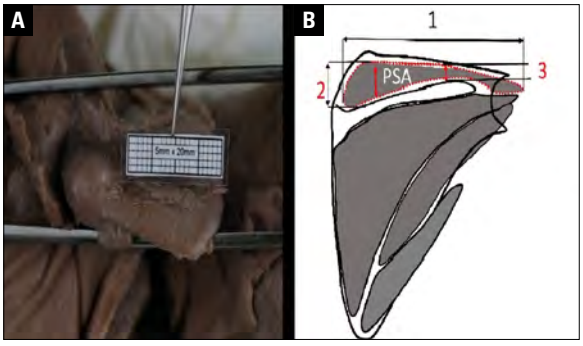

Figure 1. The supraspinatus muscle (**A**) in a male fetus at 27 weeks showing the measured parameters (**B**); 1 — length; 2, 3 — widths; PSA — projection surface area.

RESULTS

No anatomical variability of the supraspinatus muscle was found. Of note, the statistical analysis revealed neither sex nor laterality differences for all the analysed parameters ($p > 0.05$). The mean numerical data, including the length, widths, circumference and projection surface area of the supraspinatus muscle have been presented in Tables 2 and 3. Thus, we evaluated the growth dynamics of all parameters without taking the sex or age into account. The growth dynamics of the widths and circumference of the supraspinatus muscle followed linear functions, while those of the length and projection surface area of the supraspinatus muscle revealed natural logarithmic models (Fig. 2).

The mean length of the supraspinatus muscle in the gestational age range of 18–30 weeks increased from 17.79 ± 0.68 to 33.17 mm on the right side, and from 17.76 ± 0.70 to 33.21 mm on the left side, following the natural logarithmic function: $y = -71.382 + 30.972 \times \ln(\text{Age}) \pm 0.565$ ($R^2 = 0.98$) (Fig. 2A).

The mean greatest width of the supraspinatus muscle ranged from 3.93 ± 0.34 mm at 18 weeks of gestation to 8.40 mm at 30 weeks of gestation on the right side, and from 3.91 ± 0.32 to 8.41 mm on the left side, in accordance with the linear function: $y = -2.988 + 0.386 \times \text{Age} \pm 0.168$ ($R^2 = 0.99$) (Fig. 2B). The mean width of the supraspinatus muscle at the gestational ages of 18–30 weeks grew from 2.38 ± 0.12 to 5.26 mm on the right side, and from 2.38 ± 0.13 to 5.28 mm on the left side, following the linear function: $y = -1.899 + 0.240 \times \text{Age} \pm 0.078$ ($R^2 = 0.98$) (Fig. 2C).

In the analysed gestational age range the supraspinatus muscle revealed an increase in mean circumference from 39.10 ± 1.91 to 81.32 mm on the right side, and from 38.99 ± 1.96 to 81.54 mm on the left side, following the linear function: $y = -19.7016 + 3.381 \times \text{Age} \pm 2.036$ ($R^2 = 0.97$) (Fig. 2D).

At the age of 18–30 weeks the mean projection surface area of the supraspinatus muscle oscillated from 46.89 ± 7.23 to 179.29 mm^2 on the right side, and from 48.44 ± 5.06 to 179.41 mm^2 on the left side, following the natural logarithmic function: $y = -721.769 + 266.141 \times \ln(\text{Age}) \pm 6.170$ ($R^2 = 0.98$) (Fig. 2E).

Table 2. Statistical analysis of numerical data (mean ± standard deviation [SD]) of the right supraspinatus muscle

Gestational age [weeks]	N	Right supraspinatus muscle									
		Width 1 [mm]		Width 2 [mm]		Length [mm]		Circumference [mm]		Projection surface area [mm^2]	
		Mean	SD	Mean	SD	Mean	SD	Mean	SD	Mean	SD
18	6	3.93	0.34	2.38	0.12	17.79	0.68	39.10	1.91	46.89	7.23
19	2	4.46	0.06	2.65	0.02	19.09	0.03	45.64	0.49	62.53	2.14
20	2	4.89	0.04	2.95	0.01	22.15	0.05	49.95	0.04	75.85	1.41
21	3	5.08	0.18	3.11	0.11	22.51	0.40	53.59	5.46	79.65	2.60
22	1	5.31		3.32		23.64		53.67		89.82	
23	2	5.71	0.14	3.62	0.21	26.20	1.56	57.63	2.96	10.77	9.72
24	3	5.94	0.19	3.80	0.02	27.77	0.59	61.98	2.44	127.06	14.28
25	4	6.59	0.29	4.20	0.15	28.64	0.15	66.35	1.92	144.67	1.63
26	3	7.13	0.18	4.42	0.05	29.69	0.45	69.45	0.90	147.70	1.04
27	4	7.55	0.13	4.56	0.06	30.67	0.41	70.74	0.28	150.58	0.95
28	2	7.74	0.06	4.71	0.00	31.16	0.01	71.87	0.21	157.08	0.48
29	3	8.12	0.08	4.93	0.10	31.83	0.44	76.61	2.89	172.11	2.09
30	1	8.40		5.26		33.17		81.32		179.29	

Table 3. Statistical analysis of numerical data (mean ± standard deviation [SD]) of the left supraspinatus muscle

Gestational age [weeks]	N	Left supraspinatus muscle									
		Width 1 [mm]		Width 2 [mm]		Length [mm]		Circumference [mm]		Projection surface area [mm^2]	
		Mean	SD	Mean	SD	Mean	SD	Mean	SD	Mean	SD
18	6	3.91	0.32	2.38	0.13	17.76	0.70	38.99	1.96	48.44	5.06
19	2	4.53	0.05	2.67	0.04	19.29	0.08	45.95	0.54	62.81	2.10
20	2	4.89	0.03	2.97	0.02	22.08	0.09	49.85	0.10	75.76	1.38
21	3	5.09	0.15	3.10	0.10	22.52	0.40	50.36	0.32	79.95	2.93
22	1	5.34		3.33		23.62		53.59		89.71	
23	2	5.70	0.18	3.62	0.19	26.21	1.52	57.73	3.00	105.83	9.45
24	3	5.92	0.09	3.82	0.07	27.81	0.51	61.75	1.97	127.08	13.69
25	4	6.55	0.26	4.18	0.16	28.62	0.12	66.33	1.72	144.55	1.23
26	3	7.15	0.18	4.43	0.04	29.69	0.49	69.43	0.93	147.63	1.12
27	4	7.54	0.16	4.56	0.08	30.66	0.46	70.57	0.33	150.82	1.12
28	2	7.72	0.01	4.70	0.01	31.13	0.03	71.77	0.18	156.79	0.61
29	3	8.13	0.11	4.93	0.12	31.86	0.43	75.65	1.23	172.21	2.11
30	1	8.41		5.28		33.21		81.54		179.41	

DISCUSSION

The supraspinatus tendon is the most frequently injured structure within the musculotendinous (rotator) cuff. The incidence of supraspinatus tendinopathy is approximately 61.9% in men and 38.1% in women [12]. According to some authors [6, 10], supraspinatus tendinopathy is associated with an extremely complex structure of the supraspinatus tendon, which is not typical of fusiform muscles. In fact, in the supraspinatus tendon two disparately anterior and posterior subregions are distinguished. It is noteworthy that the anterior subregion of supraspinatus tendon is thicker and more cylindrical, when compared to the posterior subregion of supraspinatus tendon, which is thinner and belt-like. Furthermore, unlike the posterior subregion, the anterior subregion of supraspinatus tendon extends further medially from its insertion on the greater tubercle of humerus and form a ramified fibrous structure [1]. Therefore, it is important to understand the development and

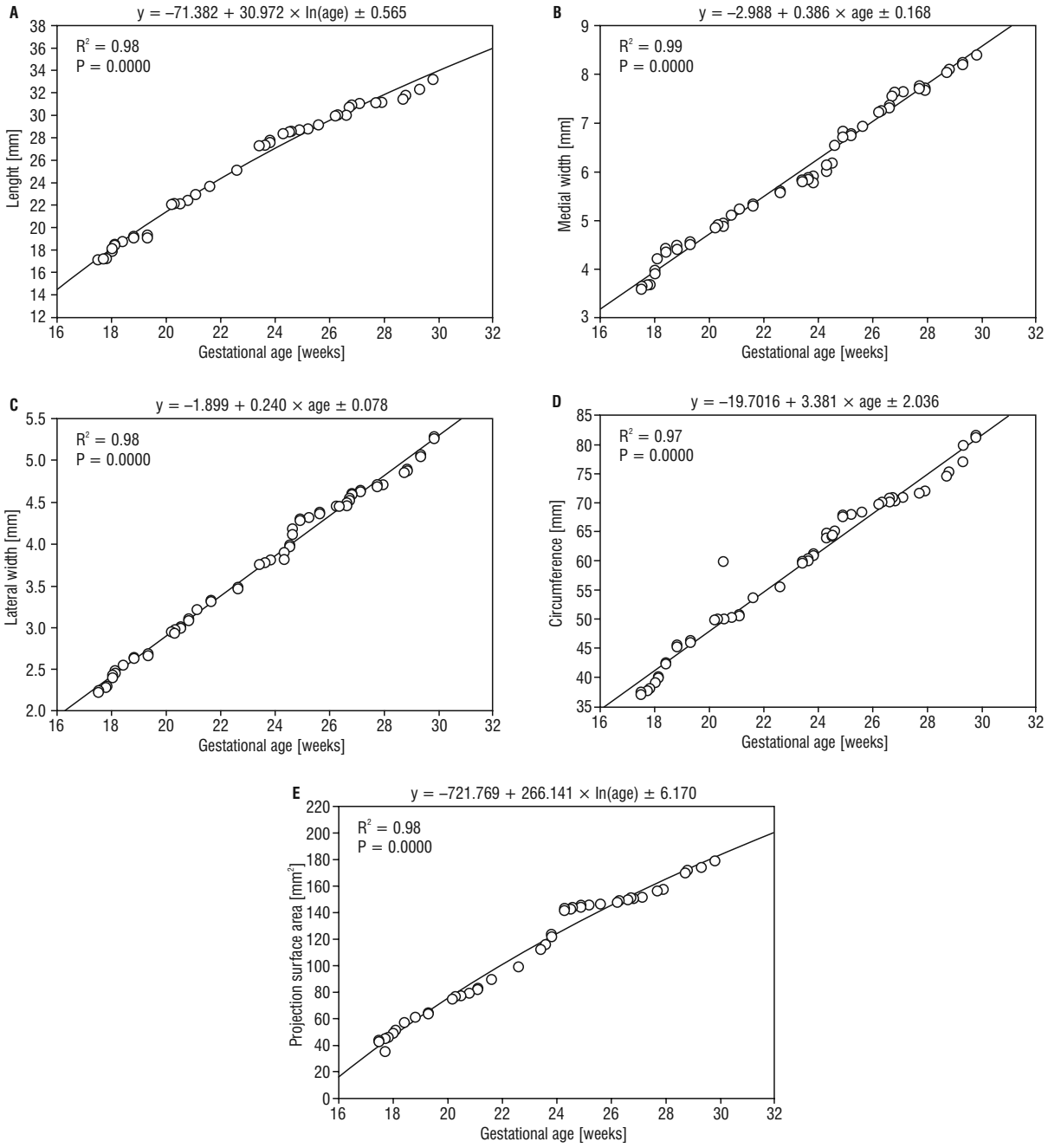

Figure 2. Regression lines for the length (**A**), widths (**B**, **C**), circumference (**D**) and projection surface area (**E**) of the supraspinatus muscle.

growth dynamics of the parameters of the supraspinatus muscle evaluated in the present study.

Abe et al. [1] found the supraspinatus tendon together with the tendons of the infraspinatus and subscapularis muscles to be separated from the articular cavity of the shoulder joint by the glenohumeral ligaments in week 9 of gestation, without explicit insertion to the humerus. Their connection to the anatomical neck of humerus occurred as late as week 12 of gestation. The authors concluded the superficial part of the supraspinatus tendon to be formed near the infraspinatus tendon until week 12 of gestation; the latter along with the coracohumeral ligament appear to compress the insertion of the supraspinatus tendon. Therefore, the authors suggested that the supraspinatus and infraspinatus tendons develop very close to each other and form one anatomical element.

Fealy et al. [5], who mostly focused on the shoulder joint in terms of its articular cavity and the glenohumeral ligaments described the ossification of

the scapula that clearly affects the origin of the supraspinatus muscle and the force exerted by it. The authors concluded such an incorrect structure of the supraspinatus muscle to result in reduced muscle work and an inappropriate pull exerted on the humerus. This may produce the instability at the shoulder joint from an early fetal age.

There are no reports in the professional literature concerning the size and dimensions of the supraspinatus muscle in human fetuses, which precludes a more comprehensive discussion on this topic.

In this study we found the supraspinatus muscle to demonstrate neither sex nor laterality differences in its morphometric parameters. Similar findings were emphasized by some authors, who deal with the development of other skeletal muscles in human fetuses, i.e. triceps brachii muscle [7] biceps brachii muscle [14], biceps femoris muscle [15], trapezius muscle [2], deltoid muscle [13], semitendinosus muscle [4], semimembranosus muscle [3] and quadratus lumborum muscle [8].

To our best knowledge the present study is the first one in the professional literature to evaluate mathematical growth dynamics of the supraspinatus muscle as a function of gestational age in weeks. Morphometric parameters of the supraspinatus muscle increased either logarithmically or linearly in accordance with the following functions: $y = -71.382 + 30.972 \times \ln(\text{Age}) \pm 0.565$ for length, $y = -2.988 + 0.386 \times \text{Age} \pm 0.168$ for greatest width, $y = -1.899 + 0.240 \times \text{Age} \pm 0.078$ for width perpendicular to the scapular notch, $y = -19.7016 + 3.381 \times \text{Age} \pm 2.036$ for circumference, and $y = -721.769 + 266.141 \times \ln(\text{Age}) \pm 6.170$ for projection surface area.

Numerical data for the supraspinatus muscle may be conducive in the assessment of the development of both the musculoskeletal systems and the fetus, with a potential relevance in surgery. We believe that the age-specific normative values for the growing supraspinatus muscle in human fetuses at varying gestational weeks obtained in this study will provide an introductory basis for future autopsy studies.

The main limitation of this study is a relatively narrow gestational age range from 18 to 30 weeks, and a small number of cases, including 34 human fetuses.

CONCLUSIONS

Neither sex nor laterality differences are found for all studied morphometric parameters of the supraspinatus muscle.

The growth dynamics of the length and projection surface area of the supraspinatus muscle increase logarithmically, while its widths and circumference increase proportionately to gestational age.

Conflict of interest: None declared

REFERENCES

1. Abe S, Nakamura T, Rodriguez-Vazquez JF, et al. Early fetal development of the rotator interval region of the shoulder with special reference to topographical relationships among related tendons and ligaments. Surg Radiol Anat. 2011; 33(7): 609–615, doi: 10.1007/s00276-011-0780-3, indexed in Pubmed: 21249362.
2. Badura M, Grzonkowska M, Baumgart M, et al. Quantitative anatomy of the trapezius muscle in the human fetus. Adv Clin Exp Med. 2016; 25(4): 605–609, doi: 10.17219/acem/61899, indexed in Pubmed: 27629832.
3. Badura M, Wiśniewski M, Szpinda M, et al. Developmental dynamics of the semimembranosus muscle in human foetuses. Med Biol Sci. 2011; 25: 13–16.
4. Badura M, Wiśniewski M, Szpinda M, et al. The growth of the semitendinosus muscle in human foetuses. Med Biol Sci. 2011; 25: 17–21.
5. Fealy S, Rodeo SA, Dicarlo EF, et al. The developmental anatomy of the neonatal glenohumeral joint. J Shoulder Elbow Surg. 2000; 9(3): 217–222, indexed in Pubmed: 10888166.
6. Gates JJ, Gilliland J, McGarry MH, et al. Influence of distinct anatomic subregions of the supraspinatus on humeral rotation. J Orthop Res. 2010; 28(1): 12–17, doi: 10.1002/jor.20947, indexed in Pubmed: 19621422.
7. Grzonkowska M, Badura M, Lisiecki J, et al. Growth dynamics of the triceps brachii muscle in the human fetus. Adv Clin Exp Med. 2014; 23(2): 177–184, doi: 10.17219/acem/37045, indexed in Pubmed: 24913107.
8. Grzonkowska M, Baumgart M, Badura M, et al. Quantitative anatomy of the growing quadratus lumborum in the human foetus. Surg Radiol Anat. 2018; 40(1): 91–98, doi: 10.1007/s00276-017-1901-4, indexed in Pubmed: 28756538.
9. Jeka S, Dura M, Waszczak-Jeka M. Ultrasonografia najczęstszych zespołów bólowych kończyny górnej w ambulatoryjnej praktyce reumatologicznej. Forum Reumatol. 2016; 2(3): 111–117.
10. Karas V, Cole BJ, Wang VM, et al. Biomechanical factors in rotator cuff pathology. Sports Med Arthrosc Rev. 2011; 19(3): 202–206, doi: 10.1097/JSA.0b013e318225cc99, indexed in Pubmed: 21822102.
11. Neer CS. Anterior acromioplasty for the chronic impingement syndrome in the shoulder: a preliminary report. J Bone Joint Surg Am. 1972; 54(1): 41–50, indexed in Pubmed: 5054450.
12. Redondo-Alonso L, Chamorro-Moriana G, Jiménez-Rejano JJ, et al. Relationship between chronic pathologies of the supraspinatus tendon and the long head of the biceps tendon: systematic review. BMC Musculoskelet Disord. 2014; 15: 377, doi: 10.1186/1471-2474-15-377, indexed in Pubmed: 25408141.
13. Szpinda M, Paruszewska-Achtel M, Baumgart M, et al. Quantitative growth of the human deltoid muscle in human foetuses. Med Biol Sci. 2011; 25: 59–64.

14. Szpinda M, Paruszewska-Achtel M, Dąbrowska M, et al. The normal growth of the biceps brachii muscle in human fetuses. Adv Clin Exp Med. 2013; 22(1): 17–26, indexed in Pubmed: 23468258.
15. Szpinda M, Wiśniewski M, Rolka Ł. The biceps femoris muscle in human foetuses: a morphometric, digital and statistical study. Adv Clin Exp Med. 2011; 20: 575–582.
16. Ward WT, Fleisch ID, Ganz R. Anatomy of the iliocapsularis muscle. Relevance to surgery of the hip. Clin Orthop Relat Res. 2000(374): 278–285, doi: 10.1097/00003086-200005000-00025, indexed in Pubmed: 10818987.
17. You T, Frostick S, Zhang WT, et al. Os acromiale: reviews and current perspectives. Orthop Surg. 2019; 11(5): 738–744, doi: 10.1111/os.12518, indexed in Pubmed: 31486589.

VIA MEDICA

ORIGINAL ARTICLE

Folia Morphol.
Vol. 82, No. 4, pp. 869–874
DOI: 10.5603/FM.a2022.0090

ISSN 0015–5659
eISSN 1644–3284
journals.viamedica.pl

Morphological evaluation and clinical significance of the supracondylar process and supratrochlear foramen: an anatomic and radiological study

Z.K. Coşkun[1], A. Erkaya[2], T. Kuçlu[3], T.V. Peker[1], F.N. Baran Aksakal[3]

[1]*Department of Anatomy, Faculty of Medicine, Gazi University, Ankara, Turkey*
[2]*Department of Anatomy, Faculty of Medicine, Lokman Hekim University, Ankara, Turkey*
[3]*Department of Public Health, Faculty of Medicine, Gazi University, Ankara, Turkey*

[Received: 5 September 2022; Accepted: 21 October 2022; Early publication date: 28 October 2022]

Background: *In our literature review, we did not encounter any study examining the supracondylar process (SP) and the supratrochlear foramen (STF) with a three-dimensional (3D) reconstruction method. The present study aimed to evaluate SP and STF morphologically by employing the 3D reconstruction method and emphasize their clinical significance.*

Materials and methods: *The research was carried out on dried human humeri of unknown sex and without pathological alterations. A total of 81 humeri (42 right, 39 left) were obtained from the Departments of Anatomy of Gazi University Faculty of Medicine and Lokman Hekim University Faculty of Medicine. The morphometric measurements of SP and STF were made with a digital vernier calliper. The computed tomography images acquired for radiological evaluation were analysed with the 3D reconstruction method.*

Results: *The narrower distal medullary canal widths of humeri with STF were found to be statistically significant. No statistically significant difference was found between the transverse diameters (TD), vertical diameters (VD), the distance of the medial edge to the medial epicondyle, and the distance of the lateral edge to the lateral epicondyle of the supratrochlear foramen of the right and left humeri.*

Conclusions: *The supracondylar process is often evaluated by mistake as a pathological condition of the bone, not as a normal anatomical variation. Knowing different shapes and dimensions, e.g. the TD and VD distance in which STF emerges, can assist in avoiding the misinterpretation of radiographs.* (Folia Morphol 2023; 82, 4: 869–874)

Key words: supracondylar process, supratrochlear foramen, three-dimensional reconstruction

Address for correspondence: Z.K. Coşkun, PhD, Department of Anatomy, Gazi University Faculty of Medicine, 06500 Besevler, Ankara, Turkey, tel: +90 532 467 8501, fax: +90 312 212 4647, e-mail: zcoskun@gazi.edu.tr

INTRODUCTION

The supracondylar process (SP) of the humerus, also known as the epicondylar, supra-epitrochlear, or a supratrochlear spur, represents a hook-like, bony spine with varied dimensions, which may project distally from the anteromedial surface of the humerus [10]. The process is usually located 4 to 8 cm proximal to the medial epicondyle (ME) [5]. The SP is often evaluated by mistake as a pathological condition of the bone, not as a normal anatomical variation [24]. It can sometimes induce symptoms by compressing the brachial artery or median nerve, or both of them [26].

The olecranon and the coronoid fossa are separated by a thin bone plate, which can sometimes be perforated, causing a foramen named supratrochlear foramen (STF). STF represents a significant and comparatively frequent anatomic variation in the lower end of the humerus in people [12]. Orthopaedic surgical experience has demonstrated an association between STF and a narrow intramedullary cavity [20]. The treatment for supracondylar fractures is intramedullary nailing, which can be compromised by the mentioned aperture. While the humerus is being evaluated radiologically, the presence of STF can be misjudged as a pathological lesion or cyst [17].

MATERIALS AND METHODS

The present research was conducted on a total of 81 (42 right, 39 left) dried humeri obtained from the Departments of Anatomy of Gazi University and Lokman Hekim University, Ankara, Turkey. Only adult bones were utilized in the current study. A digital vernier calliper was used to measure the transverse (TD) and vertical (VD) diameters of STF, the distance of the lateral edge of STF to the lateral epicondyle (LE), and the distance of the medial edge of STF to the ME. The presence of an STF was detected, and its shape was observed and separated into three types (oval, round, and triangular) (Fig. 1). In bones without the foramen, the translucency of the supratrochlear septum was noted with the help of transmitted light posterior to anterior. The length of the protrusion from the surface of SP, the length and width of the base of SP, the distance of the root of SP to the upper end of the ME, and the distance of SP to the nutrient foramen were measured with a digital vernier calliper. Computed tomography (CT) was taken on humeri with STF and SP and four control humeri. Three-dimensional (3D) scientific modelling and morphometric measurements of the humeri with CT were performed from sequential serial images in the DICOM format, using a 3D reconstruction programme (Materialize Mimics 17, Leuven, Belgium) used for scientific purposes. To better evaluate the medullary canals in the acquired models in comparison with normal CT images, solid humerus models were made transparent in the digital environment. For this purpose, Cinema 4D (R25, Friedrichsdorf, Germany) 3D modelling and animation programme was used. With the help of Materialize Mimics, the proximal medullary canal width of humeri with STF and SP and four control humeri was measured 25% proximally of the humerus, the midshaft medullary canal width was measured from 50% midshaft of the humerus, and the distal medullary canal width was measured 25% distally of the humerus (Fig. 2). Furthermore, Materialize Mimics was used to measure the distance between the end of the medullary canal and STF, and the distance between the lower point of STF and the lower end of the humerus. Ethics committee approval was granted for our study by Lokman Hekim University Non-Interventional Clinical Research Ethics Committee.

Figure 1. Different shapes of the supratrochlear foramen.

Figure 2. Transparentised image of the three-dimensional reconstructed humeri with computed tomography; **A.** Control humerus; **B.** Supracondylar process; **C.** Supratrochlear foramen (red line: proximal medullary canal width, green line: midshaft medullary canal width, blue line: distal medullary canal width, orange arrow head: supratrochlear foramen).

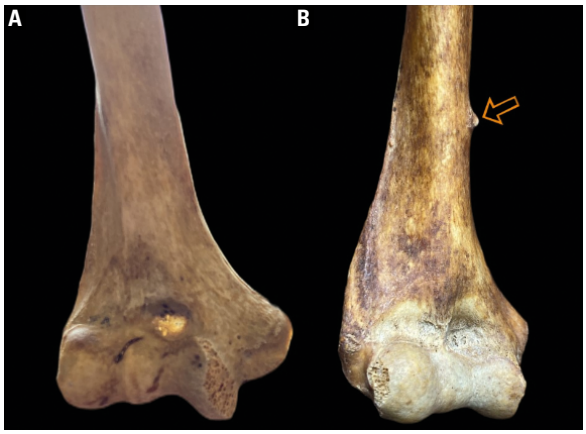

Figure 3. Translucent septum (**A**) and supracondylar process (**B**); arrow: supracondylar process.

Table 1. Incidence of different shapes of the supratrochlear foramen

Variables	Right side	Left side	Total
Oval shape	3 (23.07%*)	7 (53.84%*)	10 (76.92%*)
Round shape	1 (7.69%*)	1 (7.69%*)	2 (15.38%*)
Triangular shape	–	1 (7.69%*)	1 (7.69%*)

*The percentage in bones with supratrochlear foramen

Statistical analysis

Statistical Package for the Social Sciences v23.0 (SPSS Inc, Chicago, IL) was used for statistical analysis. The normality distribution of continuous variables was assessed with the Kolmogorov-Smirnov, histogram and Q–Q plot tests. Categorical variables are presented with numbers and percentages, while continuous variables are shown in tables with mean and standard deviation, median and minimum–maximum values. The Mann-Whitney U test was conducted to compare continuous variables that were not normally distributed. $P < 0.05$ was considered statistically significant.

RESULTS

Of the 81 humeri we examined, only 1 (1.23%) SP was detected on the anteromedial aspect of the right humerus (Fig. 3). The protrusion of SP from the surface was 35 mm, its base was vertically 6 mm long and 2.5 mm wide, the distance from the root of the protrusion to the upper end of the ME was 53 mm, and the distance of SP to the nutrient foramen was 30 mm. The direction of SP was anteriorly, inwardly, and distally oriented. The lengths of the proximal, midshaft, and distal medullary canal widths of the humerus with SP were determined as 14 mm, 12 mm, and 18 mm, respectively (Fig. 2).

The STF was detected in 13 (16.04%) bones in total. Of the humeri with STF, 4 (9.52%) were right, and 9 (23.07%) were left. In the present study, we found STF more on the left side. Most STF had an oval shape in 76.92%, which was followed by a round shape in 15.38% and a triangular shape in 7.69% (Table 1, Fig. 1). No statistically significant difference was found between the TD, VD, ME, and LE of STF of the right and left humeri (Table 2).

The narrower distal medullary canal widths of humeri with STF than the distal medullary canal widths of the control humeri were found to be statistically significant ($p = 0.045$). There was no statistically significant difference in terms of the proximal and midshaft medullary canal widths (Table 3, Fig. 2). The narrower distal medullary canal widths of the right humeri with STF than the distal medullary canal widths of the left humeri with STF were found to be statistically significant ($p = 0.006$). No statistically significant difference was found between the right and left humeri with STF in terms of proximal and midshaft medullary canal widths, the distance between the end of the medullary canal and STF, and the distance between the lower point of STF and the lower end of the bone (Table 4).

Table 2. The different measurements in supratrochlear foramen

Measurements	Right side [mm]		Left side [mm]		P
	Median	Min–Max	Median	Min–Max	
TD	5.75	3.00–12.00	4.10	2.00–10.00	0.439
VD	2.75	2.50–7.50	3.50	2.00–7.00	0.938
ME	24.50	21.00–26.50	24.00	20.00–31.50	0.877
LE	25.25	20.00–28.50	26.50	20.00–30.00	0.353

Min–Max — minimum–maximum; TD — transvers diameter; VD — vertical diameter; ME — the distance from the medial edge of the supratrochlear foramen to the medial epicondyle; LE — the distance from the lateral edge of the supratrochlear foramen to the lateral epicondyle

Table 3. Comparison of the proximal, midshaft, and distal medullary canal widths of humeri with the supratrochlear foramen and control humeri

Measurements	Supratrochlear foramen [mm]		Control humerus [mm]		P
	Median	Min–Max	Median	Min–Max	
PMCW	14.0	11.0–18.0	15.5	14.0–17.0	0.169
MMCW	9.0	6.0–15.0	12.5	12.0–14.0	0.068
DMCW	12.0	9.0–18.0	14.5	14.0–16.0	**0.045**

Min–Max — minimum–maximum; PMCW — proximal medullary canal width; MMKW — midshaft medullary canal width; DMKW — distal medullary canal width

Table 4. Comparison of medullary canal widths of right and left humerus with supratrochlear foramen

Measurements	Right side [mm]		Left side [mm]		P
	Median	Min–Max	Median	Min–Max	
PMCW	12.0	11.0–18.0	14.0	12.0–16.0	0.260
MMCW	9.5	7.0–13.0	9.0	6.0–15.0	0.825
DMCW	9.0	9.0–11.0	12.0	11.0–18.0	**0.006**
MSF	9.5	6.0–11.0	10.0	9.0–12.0	0.330
SFLEB	12.0	11.0–14.0	12.0	11.0–17.0	0.604

Min–Max — minimum–maximum; PMCW — proximal medullary canal width; MMCW — midshaft medullary canal width; DMCW — distal medullary canal width; MSF — the distance between the end of the medullary canal and the supratrochlear foramen; SFLEB — the distance between the lower point of the supratrochlear foramen and the lower end of the bone

Table 5. Measurements of supracondylar process (SP) as reported by different authors

Measurement of SP	Gupta and Mehta, 2008	Ravi and Patil, 2014	Uyaroglu et al., 2005	Present study Coskun et al., 2022
Length of spine	3 mm	8 mm	10.6 mm	3.5 mm
Breadth at the base of spine	11 mm	12 mm	–	2.5 mm
Distance of spine from medial epicondyle	65 mm	53 mm	37 mm	53 mm
Distance of spine from nutrient foramen	–	38 mm	–	30 mm

The translucent septum was detected in 37 (45.67%) humeri. The translucent septum was observed at similar rates on both sides (right 45.23%, left 46.15%) (Fig. 3).

DISCUSSION

The SP of the humerus has a very low incidence. The incidence of SP was found to be 1.3% in Caucasians [14], 2.5% in Nigerians [18], 0.7% in Japanese (Kyoto) [1], and 1.25% in Indians (Assam) [21]. Uyaroglu et al. [27] found the incidence of SP as 1.44% in their study on the Turkish population. This rate is very similar to our study.

Our study is compatible with the study by Gupta and Mehta [11] in terms of length of the spine and with the study by Ravi and Patil [22] in terms of distance of the spine from the ME and distance of the spine from the nutrient foramen. In their study, Uyaroglu et al. [27] found the length of SP to be longer than that in our study and the distance of SP to the ME shorter than that in our study (Table 5).

Studies on the proximal, midshaft, and distal medullary canals in the literature reviews have been conducted directly on the bone or conventional radiographs [16, 20]. However, no studies have been encountered on the 3D humerus models created from CT images by employing the digital transparentising method. The proximal and midshaft medullary canal width of the humerus with SP was found to be smaller than the mean medullary canal width of the control group humeri, whereas the distal medullary canal width was revealed to be more than the mean medullary canal width of the control group humeri. The mean proximal, midshaft, and distal medullary canal widths of the humeri in the control group were detected to be 15.5 mm, 12.7 mm, and 14.7 mm, respectively. Since the number of SP was 1, a statistical evaluation could not be carried out.

It is necessary to differentiate the SP from osteochondroma in pathological terms. The SP is distally oriented, toward the elbow without discontinuities in the cortex of the humerus. An osteochondroma points away from the joint. The X-ray of SP demonstrates that an underlying humeral cortex is intact, while the cortex of the tumour is continuous with the humeral cortex in an osteochondroma. A SP can also be mimicked by heterotopic bone, e.g. myositis ossificans [24].

The incidence of STF in people ranges from 0.3% to nearly 60% around the world. The incidence of STF was found to be 0.304% in Greeks [19], 57% in Libyans [13], 47.0% in Africans [9], 30.5% [4] and 31.3% [2] in Indians, 6.9% in Americans [3], and 6.0% in Europeans [9]. The two studies on the Turkish population found the incidence of STF as 10.8% [8] and 12.0% [7], respectively. In the current study, we found the incidence of STF as 16.04%. This rate we found is close to the incidence percentages determined in the Turkish population. Indians and Africans have been stated to have a higher prevalence of STF in comparison with Europeans and Turks.

In the current research, the prevalence of STF was determined to be higher on the left side compared to the right side. Our findings also support previous reports [2, 4]. On the contrary, Nayak et al. [15] found STF more frequently on the right side in their study. They detected 73 STF on the right side and 59 STF on the left side.

Studies have shown that STF is mostly oval-shaped [2, 4, 6]. In our study, the shape of STF was oval in 76.92%, round in 15.38%, and triangular in 7.69% of 13 samples (Table 1). Shivaleela et al. [23] encountered mostly round-shaped STF in their study, which was followed by round-shaped STF and oval-shaped STF. They revealed that 47.37% of STF had a round shape and 42.11% had an oval shape [23].

In our study, no statistically significant difference was revealed between the TD, VD, ME, and LE of STF of the right and left humeri (Table 2). In most studies, no statistical significance was determined between the transverse and VD of the right and left STF [6, 15, 23, 25]. Erdogmus et al. [8] found the TD of STF to be wider on the left side and STF to be closer to the ME on the left side.

The narrower distal medullary canal widths of the humeri with STF than distal medullary canal widths of the control humeri in our study were found to be statistically significant. No statistically significant difference was revealed in terms of the proximal and midshaft medullary canal widths (Table 3). Paraskevas et al. [20] found the width of the medullary canal narrower in the distal of humeri with STF. In our study, it was determined to be statistically significant that the distal medullary canal widths of the right humeri with STF were narrower than the distal medullary canal widths of the left humeri with STF ($p = 0.006$). No statistically significant difference was detected between the right and left humeri with STF in terms of proximal and midshaft medullary canal widths, the distance between the end of the medullary canal and STF, and the distance between the lower point of STF and the lower end of the bone (Table 4). Ndou et al. [16] found no significant difference in the distal medullary canal widths of bones with STF.

Since STF is directly related to the size of the intramedullary canal, it may play a key role in the preoperative planning of intramedullary nailing [6]. In humeral fractures of STF, surgeons should remember antegrade medullary nailing is better compared to retrograde nailing because a secondary fracture is more likely to occur since the canal at the distal portion of humeri with STF is extremely narrow [20].

In our study, the incidence of the translucent septum was 45.67%. In the studies by Nayak et al. [15] and Shivaleela et al. [23], the incidence of the translucent septum was 56.7% and 47.89%, respectively.

CONCLUSIONS

The incidence of the SP in the Turkish population was determined as 1.23%. The SP is often evaluated by mistake as a pathological condition of the bone instead of a normal anatomical variation. Knowing the mentioned variation and its prevalence may reduce misdiagnosis in radiographic images. We determined the incidence of STF in the Turkish population to be 16.04%, mostly on the left side. Having knowledge of the anatomy of STF may play a key role in the preoperative planning of intramedullary nailing since there may be variations in the width of the medullary canal of the humerus with STF. It is also essential for anatomists and radiologists to have knowledge of the anatomy of STF. We think that this study, in which we employed the 3D reconstruction method, will contribute to the literature.

Conflict of interest: None declared

REFERENCES

1. Adachi B. Das Arterien System Der Japaner. Verlag der Kaiserlich-Japanishcen Universitat, Kyoto 1928.
2. Ananthi K, Manickam S, Vaithianathan G, et al. Study of intercondyloid foramen of humerus. Rev Arg de Anat Clin. 2011; 3(1): 32–36.
3. Benfer RA, McKern TW. The correlation of bone robusticity with the perforation of the coronoid-olecranon septum in the humerus of man. Am J Phys Anthropol. 1966; 24(2): 247–252, doi: 10.1002/ajpa.1330240213, indexed in Pubmed: 5938202.
4. Bhanu PS, Sankar KD. Anatomical note of supratrochlear foramen of humerus in south costal population of Andhra Pradesh. NMJ. 1970; 1(2): 28–34.
5. Camerlinck M, Vanhoenacker FM, Kiekens G. Ultrasound demonstration of Struthers' ligament. J Clin Ultrasound. 2010; 38(9): 499–502, doi: 10.1002/jcu.20700, indexed in Pubmed: 20931650.
6. Chagas CAa, Gutfiten-Schlesinger G, Leite TF, et al. Anatomical and Radiological Aspects of the Supratrochlear Foramen in Brazilians. J Clin Diagn Res. 2016; 10(9): AC10–AC13, doi: 10.7860/JCDR/2016/21846.8503, indexed in Pubmed: 27790415.
7. Çimen M, Koşar Y, Sönmez M. Humerus'ta apertura septalis ile ilgili bir araştırma (A study on the aperture septalis in the humerus). Antropoloji. 2003; 14: 20–23.
8. Erdogmus S, Guler M, Eroglu S, et al. The importance of the supratrochlear foramen of the humerus in humans: an anatomical study. Med Sci Monit. 2014; 20: 2643–2650, doi: 10.12659/MSM.892074, indexed in Pubmed: 25515544.
9. Glanville EV. Perforation of the coronoid-olecranon septum. Humero-ulnar relationships in Netherlands and African populations. Am J Phys Anthropol. 1967; 26(1): 85–92, doi: 10.1002/ajpa.1330260111, indexed in Pubmed: 5633731.
10. Gray H, Williams PL, Bannister LH. Gray's anatomy: the anatomical basis of medicine and surgery. 38 ed. Churchill Livingstone, New York 1995.
11. Gupta RK, Mehta CD. A study of the incidence of supracondylar process of the humerus. J Anat Soc India. 2008; 57: 111–115.
12. Kate BR, Dubey PN. A note on the septal apertures in the humerus in the humerus of Central Indians. Eastern Anthropol. 1970; 33: 105–110.
13. Macalister A. Anatomical notes and quaries. Series II. 1. Perforate humeri in ancient Egyptian skeletons. J Anat Phys. 1990; 35: 121–122.
14. Natsis K. Supracondylar process of the humerus: study on 375 Caucasian subjects in Cologne, Germany. Clin Anat. 2008; 21(2): 138–141, doi: 10.1002/ca.20601, indexed in Pubmed: 18266286.
15. Nayak SR, Das S, Krishnamurthy A, et al. Supratrochlear foramen of the humerus: an anatomico-radiological study with clinical implications. Ups J Med Sci. 2009; 114(2): 90–94, doi: 10.1080/03009730802688819, indexed in Pubmed: 19396695.
16. Ndou R, Maharaj S, Schepartz LA. A radiographic investigation of the relationships between humeral cortical bone thickness, medullary canal width and the supratrochlear aperture (STA). Surg Radiol Anat. 2017; 39(1): 57–68, doi: 10.1007/s00276-016-1701-2, indexed in Pubmed: 27241519.
17. Ndou R, Smith P, Gemell R, et al. The supratrochlear foramen of the humerus in a South African dry bone sample. Clin Anat. 2013; 26(7): 870–874, doi: 10.1002/ca.22132, indexed in Pubmed: 22855439.
18. Oluyemi K, Okwuonu U, Adesanya O, et al. Supracondylar and infratubercular processes observed in the humeri of Nigerians. Afr J Biotechnol. 2007; 6(21): 2439–2441, doi: 10.5897/ajb2007.000-2384.
19. Papaloucas C, Papaloucas M, Stergioula A. Rare cases of humerus septal apertures in greeks. Trends Med Res. 2011; 6(3): 178–183, doi: 10.3923/tmr.2011.178.183.
20. Paraskevas GK, Papaziogas B, Tzaveas A, et al. The supratrochlear foramen of the humerus and its relation to the medullary canal: a potential surgical application. Med Sci Monit. 2010; 16(4): BR119–123.
21. Prabahita B, Pradipta RC, Talukdar KL. A study of supracondylar process of humerus. J Evol Med Dent Sci. 2012; 1(5): 817–822, doi: 10.14260/jemds/131.
22. Ravi V, Patil SP. Study of supracondylar process of humerus. Int J Health Allied Sci. 2014; 3(2): 134–136, doi: 10.4103/2278-344x.132708.
23. Shivaleela C, Afroze KH, Lakshmiprabha S. An osteological study of supratrochlear foramen of humerus of south Indian population with reference to anatomical and clinical implications. Anat Cell Biol. 2016; 49(4): 249–253, doi: 10.5115/acb.2016.49.4.249, indexed in Pubmed: 28127499.
24. Shivaleela C, Suresh B, Kumar G, et al. Morphological study of the supracondylar process of the humerus and its clinical implications. J Clin Diagn Res. 2014; 8(1): 1–3, doi: 10.7860/JCDR/2014/6743.3915, indexed in Pubmed: 24596708.
25. Silva FA, Silva TS, Souza P, et al. Morphological and morphometric study of the supratrochlear foramen. J Morphol Sci. 2018; 35(01): 54–57, doi: 10.1055/s-0038-1660487.
26. Symeonides PP. The humerus supracondylar process syndrome. Clin Orthop Relat Res. 1972; 82: 141–143, indexed in Pubmed: 4334694.
27. Uyaroglu FG, Kayalıoglu G, Erturk M. Processus supracondylaris humeri. Med J Goztepe Training Res Hospital. 2005; 20: 222–225.

VIA MEDICA

ORIGINAL ARTICLE

Folia Morphol.
Vol. 82, No. 4, pp. 875–884
DOI: 10.5603/fm.97440

ISSN 0015–5659
eISSN 1644–3284
journals.viamedica.pl

Topography of the infraorbital foramen in human skulls originating from different time periods

A. Gawlikowska-Sroka[1], Ł. Stocki[2], J. Szczurowski[3], W. Nowaczewska[4]

[1]*Department of Anatomy, Pomeranian Medical University, Szczecin, Poland*
[2]*Orion Dental Wawrzyniak and Stocki Dental Clinic, Szczecin, Poland*
[3]*Department of Anthropology, Wroclaw University of Environmental and Life Sciences, Wroclaw, Poland*
[4]*Department of Human Biology, University of Wroclaw, Poland*

[Received: 15 September 2023; Accepted: 18 October 2023; Early publication date: 30 October 2023]

Background: *The infraorbital foramen (IOF) is present on the maxilla under the infraorbital margin. Its identification is essential in various surgical procedures. The main aim of this study was the morphometric assessment of the position of the right and left infraorbital foramina in relation to specific structural elements of the facial skeleton, their width and direction, and also the determination of the location of these foramina above maxillary teeth in examined male skulls (belonging to European populations) dated to the beginning of the 20th century and the medieval and post-medieval period. This aim concerned also the assessment of the symmetry of the examined foramina (their location and size). An additional goal was to determine differences between the cranial samples concerning the analysed traits.*

Materials and methods: *The six metric and two non-metric traits concerning the IOF were collected from the male cranial samples including modern skulls (n = 87), the medieval and post-medieval skulls (from 13th centuries and 15–17th centuries, respectively; n = 47) obtained from archaeological excavations in Wroclaw, and the sample of the medieval skulls (11–13th centuries, n = 100) from Sypniewo. The sex and age of the specimens were determined using the standard methodology. The appropriate statistical analysis was performed.*

Results: *Significant differences were established for three traits (taken from the left and right side) in the case of modern skulls (diameter of IOF, its distance to the midline, and zygomaticomaxillary suture) and one in the case of medieval skulls from Sypniewo (distance to the midline). In all of the cranial samples IOF most frequently occurred above the first upper molar. The greater diameter of IOF and its shorter distance to the alveolar crest and nasal notch were observed in non-modern skulls compared to modern skulls.*

Conclusions: *The results of this study provide new additional data on the topography of IOF and its asymmetry, confirm the presence of both geographical and chronological differences between populations, and can be used in dental practice, and forensic odontology in the analysis of archaeological bone materials.* (Folia Morphol 2023; 82, 4: 875–884)

Key words: infraorbital foramen, palaeoanthropology, anatomy, asymmetry, maxillary nerve, trigeminal nerve, infraorbital nerve, infraorbital canal, forensic medicine

Address for correspondence: Dr. A. Gawlikowska-Sroka, Department of Anatomy, Pomeranian Medical University, Al. Powstańców Wlkp. 72, 70–111 Szczecin, Poland, e-mail: aleksandra.gawlikowska.sroka@pum.edu.pl

INTRODUCTION

The facial skin from the top of the forehead to the chin and laterally to the auricles receives sensory innervation from the branches of the trigeminal nerve. Branches of the fifth cranial nerve also provide sensory innervation of the mucous membranes in the nasal cavity and paranasal sinuses, oral cavity, eyelids, and the teeth [6, 13, 49]. On the anterior side of the facial skeleton there are three holes that transmit important branches of the trigeminal nerve: the supraorbital foramen, the infraorbital foramen (IOF), and the mental foramen. Differences in the location of the supraorbital, infraorbital and mental foramina, as well as the topography of the mandibular canal have important clinical implications in many medical disciplines, including maxillofacial surgery, dentistry, neurology, neurosurgery, radiology, and in anthropological and forensic research [39, 40, 59, 60, 62]. Maxillofacial surgeons consider these differences when planning complex resection procedures of neoplastic lesions in the craniofacial area, in orthognathic procedures, or in trauma surgery [40]. In ophthalmology the infraorbital and supraorbital foramina are topographic reference points important in high-precision eye surgeries [30, 33–35, 38, 42, 51]. The topography of these foramina also has clinical relevance when performing nerve blocks in dentistry, dermatology, plastic surgery and neurology. The accurate localization of these foramina reduces the risk of nerve damage [6, 49]. The IOF is located in the body of maxilla (*corpus maxillae*) under the infraorbital rim (IOR). The IOF is the terminal opening of the infraorbital canal (*canalis infraorbitalis*), which is an extension of the infraorbital sulcus (*sulcus infraorbitalis*) located on the orbital surface (*facies orbitalis*) of the body of maxilla. The infraorbital sulcus and canal transmit the homonymous (infraorbital) vessels and nerve. Studies have revealed variation in the shape and location of the IOF, as well as the presence of accessory foramina in different populations and ethnic groups [45, 56, 64]. The anatomical differences in the position of the IOF might be evidence of the evolution of the human skeletal system, or be an adaptation to the environment developed over many centuries in response to changing climatic conditions [44, 61, 63]. Studies have also demonstrated that ambient temperature can modify the morphology of the facial skeleton during development and growth [28, 50, 52]. Accessory infraorbital foramina have most often been identified in populations from cold climate zones, and least often in populations from the equatorial and tropical zones [64]. Both genetic and environmental factors [48] have a huge impact on the brachycephalisation and gracilisation of the facial skeleton [11, 19, 25]. Brachycephalisation is associated with reduction in the length of the skull, and thus also the length of the body of maxilla. The development of the neurocranium and the simultaneous shortening of its anteroposterior dimension are accompanied by an enlargement of the skull base, which might be manifested by a widening of the middle cranial fossa, and consequently changes in the topography of the IOF [19, 31, 43, 59]. Studies on the topography of the IOF have also identified asymmetry in the position of left and right foramina in different ethnic populations [56, 58, 64]. Due to the clinical relevance of the IOF and practical implications of findings in dentistry [4, 6, 26, 54], maxillofacial surgery, as well as in anthropological analyses of materials from archaeological excavations or in forensic analyses, the aim of this study was to assess anthropometric data on the location and symmetry of the IOF in modern and medieval skeletal material from Poland, and identify potential significant differences in the topography of the IOF in skulls from different time periods [19–24, 31, 39, 43, 48, 59].

MATERIALS AND METHODS

Study material was composed of:

- 87 modern human skulls dated to the beginning of the 20th century, kept in the museum collections of the Department of Anatomy of the Pomeranian Medical University in Szczecin, acquired during archaeological excavations in the cemetery near the church of St. Joseph in Szczecin in 1969–1970;
- 100 skulls from individuals living in the Middle Ages constituting a part of the collection kept at the Department of Human Biology, the University of Wroclaw, acquired during archaeological excavations carried out in 1959–1989 at the cemetery in Sypniewo (necropolis dated to the 11–13th centuries), and 47 skulls from individuals living in Wroclaw in the Medieval and the post-Middle Ages constituting a part of the collection kept at the Department of Anthropology, Wroclaw University of Environmental and Life Sciences, acquired during archaeological excavations in 2004 in the Church of St. Matthias (necropolis dated to the 13th century) and that carried out from 1974 and 1996–1991 in the Church of St.

Christopher in Wroclaw (necropolis dated to the 15–16th centuries).

All skulls belonged to male individuals classified as adultus (age at death 30–35 years) or maturus (50–55 years), and represented European populations in the region of present day Poland.

The age and sex of individuals were determined based on the morphology of the skull [9, 10, 17, 46, 47], the obliteration of cranial sutures [9, 10] and the degree of tooth wear according to the scoring system by Brothwell [9].

The criteria for inclusion in the study were as follows: adult age, male sex, good preservation of the bone material.

The exclusion criteria were as follows: damage to the bone material preventing all measurements, and developmental anomalies of the maxilla.

To define the topography of the IOF we took the following anthropometric measurements (Figs. 1, 2), also used by other researchers [1, 3, 12, 13, 15, 21, 24, 27, 53, 64]:

— distance between the IOF and infraorbital margin — *For.Inf.-Mar.Inf.*;
— distance between the medial margin of the IOF and the nasal notch at the level of the conchal crest — *For.Inf.-Inc.Nasalis*;
— distance between the medial margin of the IOF and the midline — *For.Inf.-L.M.*;
— location of the IOF in relation to dental alveolus — *loc.For.Inf.*;
— distance between the IOF and the zygomatico-maxillary suture — *For.Inf.-Sut.Zyg-Max.*;
— distance between the superior margin of the IOF and the superior margin of the alveolar process of maxilla located below the IOF — *For.inf.-Pr.alveolaris*;
— diameter of the IOF measured at the widest point — *diam.For.Inf.*;
— direction of opening of the IOF — *dir.For.Inf*.

Statistical analysis

The distribution of continuous variables was characterized by sample size (n), range (min–max), median (Me), arithmetic mean (M), and standard deviation (SD).

Continuous variables were verified for the normality of distribution using the Shapiro-Wilk test. Normally distributed variables were presented as the arithmetic mean (a measure of central tendency) and the standard deviation (a measure of spread). Non-normally distributed continuous variables were presented as the median (a measure of the central tendency) and the interquartile range.

Figure 1. Selected anthropometric parameters of the infraorbital foramen on the front of the skull; A — For.Inf-Mar.Inf; B — For.Inf.--Inc.Nasalis; C — For.Inf.-Pr.alveolaris; E — For.Inf.-Sut.Zyg.-Max.

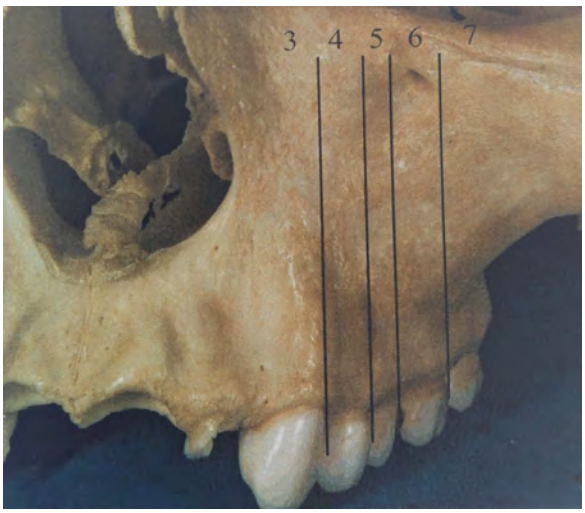

Figure 2. Location of the infraorbital foramen in relation to alveoli on the front of the skull; 3 — canine; 4 — 1st premolar; 5 — 2nd premolar; 6 — 1st molar; 7 — 2nd molar.

The qualitative variables for the studied samples, such as edentulism, opening directions of the IOF, were characterized by sample size (n), category (e.g. I — inferior, S — superior, A — anterior, P — posterior, and the observed combination of these categories), and the number and percentage of cases identified for each category.

Measurements were taken by one investigator. The error of measurement was estimated. The probability of type 1 error (level of statistical significance) was adopted at $p = 0.05$.

Two groups of independent variables were compared using Student's t-test or the Mann-Whitney

Table 1. The descriptive statistics of the measurements of the relative position of the infraorbital foramen and its diameter taken from the modern skulls (n = 87) and the results of the comparison between measurements concerning the right and left sides of the facial skeleton

Variable	P value Student's t test	Mean ± SD	Median	Minimum	Maximum
For.Inf.-Mar.Inf. R	> 0.98	7.02 ± 1.46	6.98	3.42	12.18
For.Inf.-Mar.Inf. L		7.02 ± 1.44	6.84	2.64	11.33
For.Inf.-Inc.Nasalis R	> 0.5	20.09 ± 1.88	20.21	16.20	24.77
For.Inf.-Inc.Nasalis L		20.18 ± 1.81	20.00	16.21	25.66
For.Inf.-L.M. R	**> 0.04**	28.00 ± 2.06	27.75	23.59	33.30
For.Inf.-L.M. L		27.62 ± 1.97	27.43	23.20	33.51
For.Inf.-Sut.Zyg-Max. R	**> 0.004**	23.47 ± 2.97	23.57	15.19	32.71
For.Inf.-Sut.Zyg-Max. L		22.96 ± 2.85	23.00	15.67	32.09
For.inf.-Pr.alveolaris R	> 0.95	33.74 ± 3.25	33.71	23.26	42.54
For.inf.-Pr.alveolaris L		33.72 ± 2.93	33.89	26.80	41.35
Diam.For.Inf. R	> **0.003**	3.11 ± 0.77	3.11	1.36	5.07
Diam.For.Inf. L		3.30 ± 0.69	3.33	1.63	5.16

The statistically significant differences were marked in bold. All measurements in millimetres. R — right side; L — left side; SD — standard deviation; rest abbreviations — see text

U test. Two groups of dependent variables were compared using Student's t-test or the Wilcoxon matched-pairs test.

The significance of differences between the frequencies of particular categories of the examined qualitative variables for two independent groups was assessed using Yates's chi-squared test.

Data were processed using STATISTICA PL version 7.1 software [57].

RESULTS

Table 1 presents the summary statistics of the measurements taken in modern skulls and the results of the analysis concerning the presence of the asymmetry in this sample. In the case of the problem of the asymmetry the significant differences were established between the means (right and left) of the following traits: the distance between the medial margin of the IOF and the midline of the skull (the mean value of this trait was higher for the right side of the facial skeleton than on the left side), the distance between the IOF and the zygomaticomaxillary suture (the mean value of this trait was also highest for the right side), and the diameter of the IOF measured at the widest point (the mean value of this trait was higher on the left side than on the right) (Table 1).

In most skulls the IOF was located above the first molar tooth alveolus: in 82.75% of skulls on the right side and in 73.56% of skulls on the left side (Table 2). In most skulls the opening of the infraorbital canal pointed in the anteroinferior direction (A/I) (Fig. 3).

Table 2. Location of the infraorbital foramen (IOF) in modern human skulls in relation to type of tooth (n = 87)

	Location of IOF in relation to type of tooth			
	Right		Left	
	N	%	N	%
4	0	0	0	0
4/5	0	0	0	0
5	13	14.94	17	19.54
5/6	1	1.14	6	6.89
6	72	82.75	64	73.56
6/7	0	0	0	0
7	1	1.14	0	0

4 — 1st premolar; 5 — 2nd premolar; 6 — 1st molar; 7 — 2nd molar; 8 — 3rd molar

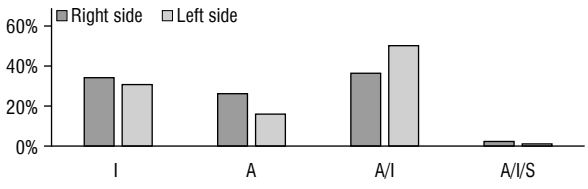

Figure 3. Direction of opening of the infraorbital foramen in modern skulls (n = 87); I — inferior; A — anterior; A/I — anteroinferior; A/I/S — anteroinferior-superior.

The summary statistics of the analysed metric traits of medieval skulls from the Church of St. Matthias and post-medieval skulls from the Church of

Table 3. The descriptive statistics of the measurements of the relative position of the infraorbital foramen and its diameter taken from the non-modern skulls (n = 47) from Church of St. Matthias (medieval skulls) and the Church of St. Christopher (post-medieval skulls) in Wroclaw, and the results of the comparison between measurements concerning the right and left sides of the facial skeleton

Variable	P value Student's t test	Mean ± SD	Median	Minimum	Maximum
For.Inf.-Mar.Inf. R	> 0.42	6.89 ± 1.41	6.76	4.18	10.14
For.Inf.-Mar.Inf. L		6.75 ± 1.65	6.70	3.59	10.25
For.Inf.-Inc.Nasalis R	> 0.34	19.49 ± 2.53	18.91	14.55	27.13
For.Inf.-Inc.Nasalis L		19.26 ± 2.29	18.71	15.41	27.25
For.Inf.-L.M. R	> 0.45	28.27 ± 2.33	27.89	23.59	35.01
For.Inf.-L.M. L		28.08 ± 2.54	27.61	23.04	36.38
For.Inf.-Sut.Zyg-Max. R	> 0.24	22.46 ± 2.74	22.81	17.07	27.66
For.Inf.-Sut.Zyg-Max. L		22.05 ± 3.09	22.26	10.04	29.42
For.inf.-Pr.alveolaris R	> 0.12	31.65 ± 4.14	31.59	23.90	40.97
For.inf.-Pr.alveolaris L		31.22 ± 4.14	30.49	24.53	41.33
Diam.For.Inf. R	> 0.81	3.48 ± 0.70	3.47	1.98	5.01
Diam.For.Inf. L		3.51 ± 0.68	3.48	2.22	5.13

All measurements in millimetres. R — right side; L — left side; SD — standard deviation; rest abbreviations — see text

Table 4. The descriptive statistics of the measurements of the relative position of the infraorbital foramen and its diameter taken from the medieval skulls from Sypniewo (n = 100), and the results of the comparison between measurements concerning the right and left sides of the facial skeleton.

Variable	P value Student's t test	Mean ± SD	Median	Minimum	Maximum
For.Inf.-Mar.Inf. R	< 0.39	7.18 ± 1.57	7.12	3.80	12.95
For.Inf.-Mar.Inf. L		7.08 ± 1.53	7.05	3.33	12.30
For.Inf.-Inc.Nasalis R	> 0.30	19.14 ± 2.10	19.04	12.87	26.37
For.Inf.-Inc.Nasalis L		18.97 ± 1.96	18.88	14.52	23.38
For.Inf.-L.M. R	**< 0.03**	28.03 ± 2.16	28.04	23.07	33.46
For.Inf.-L.M. L		27.63 ± 1.85	27.04	23.10	32.08
For.Inf.-Sut.Zyg-Max. R	> 0.21	23.54 ± 2.43	23.86	18.26	29.69
For.Inf.-Sut.Zyg-Max. L		23.35 ± 2.30	23.57	17.32	28.17
For.inf.-Pr.alveolaris R	> 0.24	31.76 ± 4.14	31.47	22.90	53.44
For.inf.-Pr.alveolaris L		31.46 ± 3.49	31.35	23.00	38.14
Diam.For.Inf. R	> 0.09	3.42 ± 0.69	3.38	2.10	5.54
Diam.For.Inf. L		3.54 ± 0.69	3.47	2.19	5.89

The statistically significant differences were marked in bold. All measurements in millimetres. R — right side; L — left side; SD — standard deviation; rest abbreviations — see text

St. Christopher (representing a historic population of Wroclaw) and skulls from Sypniewo (dated to the mediaeval period) are presented in Tables 3 and 4. Results of the analysis concerning the issue of the asymmetry are also presented in these Tables. There were no significant differences between analysed traits (between left and right sides) in the sample including these groups of the skulls (Table 3). In the case of the cranial sample from Sypniewo the significant difference was established only for the distance between the medial margin of the IOF and the midline of the facial skeleton (this distance was greater on the right side) (Table 4).

In both above-listed cranial samples, the most frequent location of the IOF (on the right and left side) was that above the first molar teeth alveolus (Tables 5, 6).

Thus there was no difference between the above-mentioned trait between modern and non-modern cranial samples.

Table 5. Location of the infraorbital foramen (IOF) in relation to the type of the tooth, non-modern skulls (n = 47) from the Church of St. Matthias (medieval) and the Church of St. Christopher (post-medieval)

	Location of IOF in relation to the type of the tooth			
	Right		Left	
	N	%	N	%
4	0	0	0	0
4/5	0	0	0	0
5	1	2.12	2	4.25
5/6	8	17.02	7	14.89
6	37	78.72	37	78.72
6/7	1	2.12	1	2.12
7	0	0	0	0

4 — 1st premolar; 5 — 2nd premolar; 6 — 1st molar; 7 — 2nd molar; 8 — 3rd molar

Table 6. Location of the infraorbital foramen (IOF) in relation to the type of the tooth; medieval skulls from Sypniewo (n = 100)

	Location of IOF in relation to the type of the tooth			
	Right		Left	
	N	%	N	%
4	0	0	0	0
4/5	0	0	0	0
5	6	6.00	5	5.00
5/6	24	24.00	26	26.00
6	70	70.00	69	69.00
6/7	0	0	0	0
7	0	0	0	0

4 — 1st premolar; 5 — 2nd premolar; 6 — 1st molar; 7 — 2nd molar; 8 — 3rd molar

The most frequent directions of opening of the IOF on the left and right sides were anteroinferior (A/I) in skulls from the Church of St. Christopher and St. Matthias (Fig. 4), and inferior (I) in skulls from Sypniewo, $p < 0.05$ (Fig. 4).

The comparison of modern skulls and non-modern skulls for the location of the IOF revealed a significantly greater distance from the IOF to the nasal notch in modern skulls on the right side ($p < 0.002$) and on the left side ($p < 0.001$), and a greater distance from the IOF to the top of the alveolar process of maxilla in modern skulls on both sides ($p < 0.001$). The diameter of the IOF was greater in medieval and post-medieval skulls (pooled sample): $p < 0.003$ for the right side, and $p < 0.02$ for the left side. There were no significant differences in the location of the

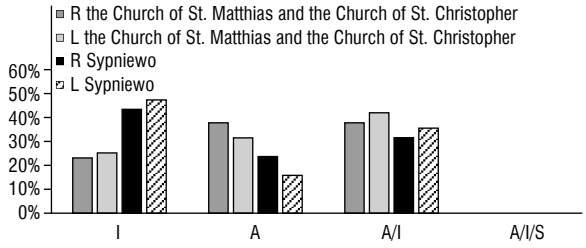

Figure 4. Direction of opening of the infraorbital foramen in non-modern skulls from the Church of St. Matthias and the Church of St. Christopher (n = 47) and in skulls from Sypniewo (n = 100); R — right side; L — left side; I — inferior; A — anterior; A/I — anteroinferior; A/I/S — anteroinferior-superior.

Table 7. Dominance of values of the analysed traits concerning the relative position and parameters of the infraorbital foramen on the left and right sides in modern and non-modern skulls

Variable	Modern skulls	Medieval/non-modern skulls
For.Inf.-Mar.Inf.	Right	Right
For.Inf.-Inc.Nasalis	Left	Right
For.Inf.-L.M.	Right	Right
For.Inf.-Sut.Zyg-Max.	Left	Right
For.inf.-Pr.alveolaris	Right	Right
Diam.For.Inf.	Left	Left

IOF in relation to the alveolar arch. In both samples, the most frequent location of the IOF was above the first molar alveolus. The most frequent directions of opening of the IOF were inferior in medieval skulls, and anteroinferior in modern skulls, but differences between these samples were not statistically significant.

The comparison of skulls for the symmetry of the IOF is presented in Table 7. Accessory infraorbital foramina were not identified in the analysed samples of skulls.

DISCUSSION

The knowledge of the topography of the infraorbital canal and its terminal opening is essential for clinicians, especially dentists and dental surgeons, neurologists and plastic surgeons [8, 30, 36, 37, 38, 40]. Some ethnic differences have been reported in the location of the infraorbital canal and its foramen, including the presence of the accessory IOF [8, 14, 15, 32, 58], and these variants should be considered when planning medical procedures, in anthropometric analyses of bone materials explored during archaeological research, and in the forensic assessment of human remains.

The knowledge of topographical variants and trends in the position of the IOF helps achieve therapeutic success in everyday clinical practice and prevents the risk of misdiagnosis, misinterpretation of X-ray images, reduces the rate of complications, and also improves the outcomes of certain medical procedures and the accuracy of anthropological assessments.

In the sample of the modern skulls the mean distance between the superior rim of the IOF and the IOR was 7.02 ± 1.46 mm for the right side and 7.02 ± 1.44 mm for the left side (Table 1). However, in this study the difference between these means was statistically insignificant. According to results obtained by Kazkayasi et al. [38], Cutright et al. [13], and Agthong et al. [2] in studies on modern human skulls the IOF was lower on the right side, while on the left side the IOF was closer to the orbital rim. In our study the distance between the IOF and midline of the facial skeleton was higher on the right side in two examined cranial samples (including modern skulls and medieval skulls from Sypniewo). The distance between this foramen and the zygomaticomaxillary suture was higher on the right side of the facial skeleton and the widest diameter of the IOF was present on the left side of the facial skeleton only in the sample of the examined modern skulls. No other significant differences (concerning the problem of asymmetry) occurred in the examined samples of human crania. A study by Agthong et al. [2] revealed that the distance from the IOF to the top of the alveolar process of maxilla was almost identical to that measured in our analysis (Table 1). Aziz et al. [5] reported the distance to the IOR about 1 mm greater, and the distance from the IOF to the midline almost identical to that found in our study. Similar parameters were reported by Chung et al. [12] and Cutrig et al. [13]. In studies by Kazkayasi et al. [38] and Rahman et al. [53] the distance between the IOF and the nasal notch was 17.23 ± 2.64 mm, while in the modern skulls analysed in our study it was 20.09 ± 1.88 mm (R) and 20.18 ± ± 1.81 mm (L). Distances from the IOF to the maxillary midline and the IOR reported by Gupta [27] were very similar to those measured in our study. Gupta [27] also provided information on the position of the IOF in relation to the dental alveoli of maxilla: in 56.50% (R) and 50.60% (L) of skulls the IOF was located above the second premolar, and in 32.90% (R) and 24.10% (L) of skulls it was above the line between the second premolar and the first molar. In our study the position of the IOF in relation to the dental alveoli of maxilla in modern skulls was assessed in the frontal view. In most skulls the IOF was located above the first molar alveolus. The second most frequent position of the IOF was above the second premolar (Table 2). Aziz et al. [5] reported the most frequent location of the IOF above the first premolar alveolus. A study by Apinhasmit et al. [3] revealed that in most skulls the IOF was found above the second premolar, and in 27.90% of skulls above the line between the first and second premolars.

In this study, in the case of the comparison between modern and non-modern cranial samples the significant differences concerned the distance of the IOF from the margin of the alveolar process (this distance was greater in modern skulls) and the distance of the IOF from nasal notch (which was also greater in modern skulls than in non-modern). The first of these differences may result from various types of edentulism in the region of measurement and, consequently, from progressive atrophy of the alveolar process of maxilla [4, 16, 53, 63]. Our study also demonstrated significant differences in the diameter of the IOF between the analysed samples of skulls. IOFs were much wider in non-modern skulls, and their diameter was similar to that reported by Gupta [27]. Chung et al. [12] found about 2 mm larger diameters of the IOF compared to values measured by us in medieval and post-medieval skulls, and 1.5 mm larger compared to modern skulls.

In most cases the location of the IOF in relation to the dental alveoli of maxilla in non-modern and modern skulls viewed from the front was above the first molar dental alveoli of maxilla. The second most frequent location of the IOF was between the second premolar and the first molar in medieval skulls and above the second premolar in modern skulls. In human skulls, the IOF analysed in the vertical plane was located above the line between the canine and the first molar [1, 37], but most frequently the IOF was found above and in line with the premolars. However, there is no consensus among researchers as to a higher frequency of the IOF above the first premolar [e.g. 5] or above the second maxillary premolar [e.g. 1, 3, 29].

No accessory infraorbital foramina were identified in our study, which also highlights ethnic differences. Hwang et al. [32] reported a higher frequency of accessory IOF in skulls from populations living above 60 degrees latitude, in cold zones, than in temper-

ate and tropical climates. Zhang et al. [64] found a higher frequency of accessory IOFs in a European population (21.7%) than in an African-American population (10%), while Sokhn [56] reported accessory IOFs in 8.6% of a sample representing a Lebanese population.

Studies on face and skull asymmetry are extremely important because of the need for detailed diagnostics in dental and orthodontic treatment, when planning local anaesthesia [6, 7, 41, 55, 65], or in paediatric surgery to repair cleft lip and palate [18, 33, 39, 42].

CONCLUSIONS

Our analysis revealed differences in the location of the IOF between modern and non-modern skulls, and also with findings reported in the literature, which confirms the presence of both geographical and chronological differences between populations. The comparison of examined populations revealed a greater distance of the IOF from the nasal notch and the margin of the alveolar process of maxilla in modern skulls.

Knowledge of differences in the position of the IOF between local populations is fundamental for the correct interpretation of findings from diagnostic radiological studies in dental practice, and for planning effective anaesthesia and implant placement. This knowledge is also necessary in forensic odontology or analysis of archaeological bone materials.

Acknowledgements

The authors would like to express their thanks to Prof. Barbara Kwiatkowska from the Department of Anthropology, Wroclaw University of Environmental and Life Sciences, and Prof. Bogusław Pawłowski from the Institute of Human Biology, University of Wroclaw for their help in leading the research.

Conflict of interest: None declared

REFERENCES

1. Aggarwal A, Kaur H, Gupta T, et al. Anatomical study of the infraorbital foramen: A basis for successful infraorbital nerve block. Clin Anat. 2015; 28(6): 753–760, doi: 10.1002/ca.22558, indexed in Pubmed: 26119635.
2. Agthong S, Huanmanop T, Chentanez V. Anatomical variations of the supraorbital, infraorbital, and mental foramina related to gender and side. J Oral Maxillofac Surg. 2005; 63(6): 800–804, doi: 10.1016/j.joms.2005.02.016, indexed in Pubmed: 15944977.
3. Apinhasmit W, Chompoopong S, Methathrathip D, et al. Supraorbital Notch/Foramen, Infraorbital Foramen and Mental Foramen in Thais: anthropometric measurements and surgical relevance. J Med Assoc Thai. 2006; 89(5): 675–682.
4. Atwood DA, Coy WA. Clinical, cephalometric, and densitometric study of reduction of residual ridges. J Prosthet Dent. 1971; 26(3): 280–295, doi: 10.1016/0022-3913(71)90070-9, indexed in Pubmed: 5284182.
5. Aziz SR, Marchena JM, Puran A. Anatomic characteristics of the infraorbital foramen: a cadaver study. J Oral Maxillofac Surg. 2000; 58(9): 992–996, doi: 10.1053/joms.2000.8742, indexed in Pubmed: 10981979.
6. Bahşi I, Orhan M, Kervancıoğlu P, et al. Morphometric evaluation and surgical implications of the infraorbital groove, canal and foramen on cone-beam computed tomography and a review of literature. Folia Morphol. 2019; 78(2): 331–343, doi: 10.5603/FM.a2018.0084, indexed in Pubmed: 30178457.
7. Bishara SE, Burkey PS, Kharouf JG. Dental and facial asymmetries: a review. Angle Orthod. 1994; 64(2): 89–98, doi: 10.1043/0003-3219(1994)064<0089:DAFAAR>2.0.CO;2, indexed in Pubmed: 8010527.
8. Bressan C, Geuna S, Malerba G, et al. Descriptive and topographic anatomy of the accessory infraorbital foramen. Clinical implications in maxillary surgery. Minerva Stomatol. 2004; 53(9): 495–505, indexed in Pubmed: 15499301.
9. Brothwell DR. Digging Up Bones. Natural History Museum Publications, London 1981.
10. Buikstra J, Ubelaker DH. Standards for data collection from human skeletal remains. Arkansas Archeological Survey Research, 1994, Series 44.
11. Charazińska Z. Obserwacje własne asymetrii twarzy uwarunkowanej zmianami w budowie czaszki i ustawienia kręgów szyjnych. Czas Stomat. 1973; 26(9): 1019–1026.
12. Chung MS, Kim HJ, Kang HS, et al. Locational relationship of the supraorbital notch or foramen and infraorbital and mental foramina in Koreans. Acta Anat (Basel). 1995; 154(2): 162–166, doi: 10.1159/000147763, indexed in Pubmed: 8722516.
13. Cutright B, Quillopa N, Schubert W. An anthropometric analysis of the key foramina for maxillofacial surgery. J Oral Maxillofac Surg. 2003; 61(3): 354–357, doi: 10.1053/joms.2003.50070, indexed in Pubmed: 12618976.
14. Czerwiński F, Sulisz T, Teul I, et al. Ocena morfologiczna zatok czołowych na podstawie zdjęć radiologicznych czaszek średniowiecznych łczesnych. Pol Przegl Radiol. 1996; 61(4): 363–366.
15. Dixit SG, Kaur J, Nayyar AK, et al. Morphometric analysis and anatomical variations of infraorbital foramen: a study in adult North Indian population. Morphologie. 2014; 98(323): 166–170, doi: 10.1016/j.morpho.2014.02.008, indexed in Pubmed: 24857562.
16. Fattore LD, Fine L, Edmonds DC. The hollow denture: an alternative treatment for atrophic maxillae. J Prosthet Dent. 1988; 59(4): 514–516, doi: 10.1016/0022-3913(88)90053-4, indexed in Pubmed: 3283333.
17. Ferembach D, Schwindezky M, Stoukal M. Recommendations for age and sex diagnoses of skeletons. J Hum Evol. 1980; 9(7): 517–549, doi: 10.1016/0047-2484(80)90061-5.

18. Fields SJ, Spiers M, Hershkovitz I, et al. Reliability of reliability coefficients in the estimation of asymmetry. Am J Phys Anthropol. 1995; 96(1): 83–87, doi: 10.1002/ajpa.1330960109, indexed in Pubmed: 7726299.
19. Florkowski A. Zmiany kierunkowe wybranych cech kraniometrycznych we wczesnośredniowiecznym Gruczynie. Człowiek w czasie i przestrzeni. Gdańsk. 1993: 313–317.
20. Gawlikowska A, Szczurowski J, Czerwiński F, et al. Analysis of skull asymmetry in different historical periods using radiological examinations. Pol J Radiol. 2007; 72(4): 35–43.
21. Gawlikowska A, Szczurowski J, Czerwiński F, et al. Analysis of skull asymmetry in different historical periods using radiological examinations. Pol J Radiol. 2007; 72(4): 35–43.
22. Gawlikowska-Sroka AK, Stocki L, Szczurowski J, et al. Topography of the mental foramen in human skulls originating from different time periods. Homo. 2013; 64(4): 286–295, doi: 10.1016/j.jchb.2013.03.009, indexed in Pubmed: 23726019.
23. Gawlikowska-Sroka A, Szczurowski J, Kwiatkowska B, et al. Concha Bullosa in Paleoanthropological Material. Adv Exp Med Biol. 2016; 952: 65–73, doi: 10.1007/5584_2016_62, indexed in Pubmed: 27614624.
24. Gawlikowska-Sroka A. [Methods for the assessment of skull asymmetry on radiograms]. Ann Acad Med Stetin. 2009; 55(3): 36–39, indexed in Pubmed: 20698176.
25. Golusik K, Sarul M, Rzeszut Ł, et al. Żuchwa ludzka w procesie ewolucji. Dent Med Probl. 2005; 42(1): 103–109.
26. Grayson BH, McCarthy JG, Bookstein F. Analysis of craniofacial asymmetry by multiplane cephalometry. Am J Orthod. 1983; 84(3): 217–224, doi: 10.1016/0002-9416(83)90129-x, indexed in Pubmed: 6577794.
27. Gupta T. Localization of important facial foramina encountered in maxillo-facial surgery. Clin Anat. 2008; 21(7): 633–640, doi: 10.1002/ca.20688, indexed in Pubmed: 18773483.
28. Harvati K, Weaver T. Human cranial anatomy and the differential preservation of population history and climate signatures. Anat Rec A Discov Mol Cell Evol Biol. 2006; 288A(12): 1225–1233, doi: 10.1002/ar.a.20395.
29. Hindy AM, Abdel-Raouf F. A study of infraorbital foramen, canal and nerve in adult Egyptians. Egypt Dent J. 1993; 39(4): 573–580, indexed in Pubmed: 9588126.
30. Huanmanop T, Agthong S, Chentanez V. Surgical anatomy of fissures and foramina in the orbits of Thai adults. J Med Assoc Thai. 2007; 90(11): 2383–2391, indexed in Pubmed: 18181324.
31. Hublin JJ, Ben-Ncer A, Bailey SE, et al. New fossils from Jebel Irhoud, Morocco and the pan-African origin of Homo sapiens. Nature. 2017; 546(7657): 289–292,, doi: 10.1038/nature22336, indexed in Pubmed: 28593953, Erratum in: Nature. 2018 Jun;558(7711):E6.
32. Hwang K, Lee SJ, Kim SY, et al. Frequency of existence, numbers, and location of the accessory infraorbital foramen. J Craniofac Surg. 2015; 26(1): 274–276, doi: 10.1097/SCS.0000000000001375, indexed in Pubmed: 25490578.
33. Kadanov D, Iordanov I, Aleksandrova N. [Symmetry and asymmetry of the orbital opening in Bulgarians]. Eksp Med Morfol. 1977; 16(1): 12–18, indexed in Pubmed: 880906.
34. Kamburoğlu K, Kiliç C, Ozen T, et al. Measurements of mandibular canal region obtained by cone-beam computed tomography: a cadaveric study. Oral Surg Oral Med Oral Pathol Oral Radiol Endod. 2009; 107(2): e34–e42, doi: 10.1016/j.tripleo.2008.10.012, indexed in Pubmed: 19138636.
35. Karakaş P, Bozkir MG, Oguz O. Morphometric measurements from various reference points in the orbit of male Caucasians. Surg Radiol Anat. 2003; 24(6): 358–362, doi: 10.1007/s00276-002-0071-0, indexed in Pubmed: 12652362.
36. Kazkayasi M, Batay F, Bademci G, et al. The morphometric and cephalometric study of anterior cranial landmarks for surgery. Minim Invasive Neurosurg. 2008; 51(1): 21–25, doi: 10.1055/s-2007-1022541, indexed in Pubmed: 18306127.
37. Kazkayasi M, Ergin A, Ersoy M, et al. Certain anatomical relations and the precise morphometry of the infraorbital foramen — canal and groove: an anatomical and cephalometric study. Laryngoscope. 2001; 111(4 Pt 1): 609–614, doi: 10.1097/00005537-200104000-00010, indexed in Pubmed: 11359128.
38. Kazkayasi M, Ergin A, Ersoy M, et al. Microscopic anatomy of the infraorbital canal, nerve, and foramen. Otolaryngol Head Neck Surg. 2003; 129(6): 692–697, doi: 10.1016/S0194-59980301575-4, indexed in Pubmed: 14663437.
39. Kercz TM, Kuroszczyk M. Powikłania znieczulenia miejscowego a zmienność anatomiczna twarzoczaszki. e-Dentico. 2007; 1: 28–32.
40. Koury ME, Epker BN. Maxillofacial esthetics: anthropometrics of the maxillofacial region. J Oral Maxillofac Surg. 1992; 50(8): 806–820, doi: 10.1016/0278-2391(92)90270-a, indexed in Pubmed: 1634972.
41. Lee UY, Nam SH, Han SH, et al. Morphological characteristics of the infraorbital foramen and infraorbital canal using three-dimensional models. Surg Radiol Anat. 2006; 28(2): 115–120, doi: 10.1007/s00276-005-0071-y, indexed in Pubmed: 16432643.
42. Leo JT, Cassell MD, Bergman RA. Variation in human infraorbital nerve, canal and foramen. Ann Anat. 1995; 177(1): 93–95, doi: 10.1016/S0940-9602(11)80139-1, indexed in Pubmed: 7872502.
43. Lieberman DE, McBratney BM, Krovitz G. The evolution and development of cranial form in Homosapiens. Proc Natl Acad Sci U S A. 2002; 99(3): 1134–1139, doi: 10.1073/pnas.022440799, indexed in Pubmed: 11805284.
44. Mackiewicz B, Prośba-Mackiewicz M, et al. Uwarunkowania kierunku rozwoju twarzoczaszkłczesnego człowieka. Człowiek w czasie i przestrzeni. Gdańsk. 1993: 112–115.
45. Mahajan A, Verma R, Razdan SK, et al. Morphological and morphometric relations of infraorbital foramen in north indian population. Cureus. 2023; 15(2): e34525, doi: 10.7759/cureus.34525, indexed in Pubmed: 36874344.
46. Malinowski A, Bożiłow W. Wskaźniki proporcji. In: Podstawy antropometrii. Metody, techniki, normy. Red. Gniazdowska J. Wydawnictwo Naukowe PWN, Warszawa 1997: 182–190.
47. Malinowski A, Strzałko J. Antropologia. Wydawnictwo Naukowe PWN, Warszawa 1985.
48. Malinowski A. Czynniki działające na rozwój i kształt czaszki. Auksologia a promocja zdrowia. Kielce. 1997: 89–96.
49. Nardi NM, Alvarado AC, Schaefer TJ. Infraorbital Nerve Block. 2023 Aug 8. In: StatPearls [Internet]. Treasure

Island (FL): StatPearls Publishing; 2023 Jan., indexed in Pubmed: 29763056.
50. Nowaczewska W, Dabrowski P, Kuźmiński Ł. Morphological adaptation to climate in modern Homo sapiens crania: the importance of basicranial breadth. Coll Antropol. 2011; 35(3): 625–636, indexed in Pubmed: 22053534.
51. Ozola B, Slaidina A, Laurina L, et al. The influence of bone mineral density and body mass index on resorption of edentulous jaws. Stomatologija. 2011; 13(1): 19–24, indexed in Pubmed: 21558787.
52. Rae TC, Vidarsdóttir US, Jeffery N, et al. Developmental response to cold stress in cranial morphology of Rattus: implications for the interpretation of climatic adaptation in fossil hominins. Proc Biol Sci. 2006; 273(1601): 2605–2610, doi: 10.1098/rspb.2006.3629, indexed in Pubmed: 17002945.
53. Rahman M, Richter EO, Osawa S, et al. Anatomic study of the infraorbital foramen for radiofrequency neurotomy of the infraorbital nerve. Neurosurgery. 2009; 64(5 Suppl 2): 423–427, doi: 10.1227/01.NEU.0000336327.10368.79, indexed in Pubmed: 19404120.
54. Rossi M, Ribeiro E, Smith R. Craniofacial asymmetry in development: an anatomical study. Angle Orthod. 2003; 73(4): 381–385, doi: 10.1043/0003-3219(2003)073<0381:CAIDAA>2.0.CO;2, indexed in Pubmed: 12940558.
55. Skvarilová B. Facial asymmetry: an X-ray study. Acta Chir Plast. 1994; 36(3): 89–91, indexed in Pubmed: 7618413.
56. Sokhn S, Challita R, Challita A, et al. The infraorbital foramen in a sample of the lebanese population: a radiographic study. Cureus. 2019; 11(12): e6381, doi: 10.7759/cureus.6381, indexed in Pubmed: 31938659.
57. Stanisz A. Przystępny kurs statystyki z zastosowaniem STATISTICA PL na przykładach z medycyny. Tom 1. Statystyki podstawowe. StatSofft Polska Sp. z o o. , Kraków 2006.
58. Suntiruamjairucksa J, Chentanez V. Localization of infraorbital foramen and accessory infraorbital foramen with reference to facial bony landmarks: predictive method and its accuracy. Anat Cell Biol. 2022; 55(1): 55–62, doi: 10.5115/acb.21.208, indexed in Pubmed: 35131950.
59. Szczurowski J. Cechy niemetryczne czaszek z Czeladzi Wielkiej. W: Studia Antropologiczne T 2 Wrocław. 1995; 127: 65–80.
60. Teul I, Czerwiński F, Gawlikowska A, et al. Asymmetry of the ovale and spinous foramina in mediaeval and contemporary skulls in radiological examinations. Folia Morphol. 2002; 61(3): 147–152, indexed in Pubmed: 12416930.
61. Tomaszewska A, Zelaźniewicz A. Morphology and morphometry of the meningo-orbital foramen as a result of plastic responses to the ambient temperature and its clinical relevance. J Craniofac Surg. 2014; 25(3): 1033–1037, doi: 10.1097/SCS.0000000000000552, indexed in Pubmed: 24699100.
62. Vasconcelos Jd, Avila GB, Ribeiro JC, et al. Inferior alveolar nerve transposition with involvement of the mental foramen for implant placement. Med Oral Patol Oral Cir Bucal. 2008; 13(11): E722–E725, indexed in Pubmed: 18978714.
63. Westerholm N. The determination by orthopantomographic measurement of bone resorption in the bone of the jaws (processus alveolaris). Odontol Tidskr. 1966; 74(1): 52–60, indexed in Pubmed: 5218663.
64. Zhang KR, Blandford AD, Hwang CJ, et al. Anatomic variations of the infraorbital foramen in caucasian versus african american skulls. Ophthalmic Plast Reconstr Surg. 2019; 35(1): 25–28, doi: 10.1097/IOP.0000000000001126, indexed in Pubmed: 29771753.
65. Żyszko A. Przyczynek zagadnienia zmian w narządzie żucia w przypadku asymetrii twarzo-czaszki. Czas Stomat. 1974; 27(5): 655–661.

VIA MEDICA

ORIGINAL ARTICLE

Folia Morphol.
Vol. 82, No. 4, pp. 885–891
DOI: 10.5603/FM.a2023.0001

ISSN 0015–5659
eISSN 1644–3284
journals.viamedica.pl

Prevalence of the Onodi cell in the Polish adult population: an anatomical computed tomography study

J. Jaworek-Troć[1], K. Ochwat[1], J.A. Walocha[1], I. Zamojska[1], M. Lipski[1], A. Żytkowski[2, 3], R. Chrzan[4], J. Zawiliński[1], S.K. Ghosh[5], M.P. Zarzecki[1]

[1]*Department of Anatomy, Jagiellonian University Medical College, Krakow, Poland*
[2]*Faculty of Philology, Department of Polish Dialectology and Logopaedics, University of Lodz, Poland*
[3]*Norbert Barlicki Memorial Teaching Hospital No. 1 of the Medical University of Lodz, Poland*
[4]*Department of Radiology, Jagiellonian University Medical College, Krakow, Poland*
[5]*Department of Anatomy, All India Institute of Medical Science, Patna, Bihar, India*

[Received: 17 September 2022; Accepted: 15 December 2022; Early publication date: 17 January 2023]

Background: *Onodi cell is a posterior ethmoid air cell with the optic canal bulging into it; the common position of the bulge is into the sphenoid sinus, usually immediately posterior to the posterior ethmoid air cells. Variable pneumatisation patterns lead to various structures of lamellae and sinuses occasionally exposing important nerves and vessels, such as the optic and vidian nerves, internal carotid artery and cavernous sinus. In clinical practice, special imaging techniques are used to navigate through the paranasal sinuses and hence avoid injury to these structures. This study is aimed to determine the prevalence of the Onodi cell in the Polish population and compare it with other reported occurrences.*

Materials and methods: *A retrospective analysis of 296 computed tomography (CT) scans of patients treated in Krakow, Poland, using a Siemens Somatom Sensation 16 spiral CT scanner. No contrast medium was administered.*

Results: *The Onodi cell was found in 31 out of the 296 patients, or approximately 10.5%, consistent with the majority of research reporting on Onodi variants. Additionally, there was one presentation of a bilateral Onodi cell in a male patient. No statistically significant difference was found between the male and female populations with a positive identification of the variant ($p = 0.095$, Chi^2 test).*

Conclusions: *This study helped approximate the Onodi variant prevalence of 10.47%, falling within a commonly reported range 8–14%. This gives clinicians and surgeons a better understanding of this variant's structure and significance, and therefore an opportunity to improve treatment outcomes and research.* (Folia Morphol 2023; 82, 4: 885–891)

Key words: Onodi cell, sphenoid sinus, anatomy, computed tomography

INTRODUCTION

The paranasal sinuses are air-filled cavities that communicate with and create a functional unit with the nasal cavity [27]. Ostia are the openings between the paranasal sinuses and nasal cavity that permit aeration and drainage, including a path for sinusitis

Address for correspondence: Dr. M.P. Zarzecki, MD, Department of Anatomy, Jagiellonian University Medical College, ul. Kopernika 12, 31–034 Kraków, Poland, tel/fax: +48 12 422 95 11, e-mail: michal.zarzecki96@gmail.com

infections and blockage [4]. Anatomical variations of bony structures within this region happen to be relatively common including subsequent clinical symptoms such as sinusitis, deviated septum, and various air cells [23].

The Onodi cell, or posterior sphenoethmoid cell, is an anatomical variant of the posterior-most ethmoidal air cells, pneumatised posteriorly to the extent that the optic canal is visible from within the cell [17]. It was first introduced by Onodi in 1904 [25]. Even though it is contraindicated to use eponyms in everyday clinical practice, they are still popular as they denote the same feature/condition in a much shorter, more appealing to medical professionals version [3]. It is also true in the case of the Onodi cell. A similar term, "posterior overriding ethmoid cell," has been reported by Ozturan et al. [26] which is defined as a posterior ethmoid cell that is pneumatised into the sphenoid bone and sinus, but is not characterised by an optic canal bulge. Since the internal carotid artery normally bulges into the sphenoid sinus, a patient with a positive identification of an Onodi cell will also, in most cases, present with a landmark often seen in transsphenoidal sinusoidal surgeries recess [32]. Other relevant structures mostly pertain to the lateral wall of the sphenoid sinus and ethmoid including the cavernous sinus and all its enclosed structures (cranial nerves III, IV, VI, V_1, and V_2) and the vidian nerve, as well as even the brain stem behind the clival part of the sphenoid bone. Anatomic variants of the paranasal sinuses and nasal cavity may be more common, and may even overlap leading to complicated structure and function [7–16].

The process of paranasal cavity expansion is called pneumatisation and its pattern of development can lead to abnormal sinus architecture. Pneumatisation of ethmoid air cells takes place bilaterally inside the ethmoid labyrinth, and can extend into surrounding paranasal sinuses creating the Haller cells, agger nasi cells, and Onodi cells [23].

The extent of pneumatisation of the ethmoid and sphenoid sinuses impacts the thickness of bone between the sinus and surrounding structures, and walls as thin as 0.5 mm separating the sphenoidal sinus from surrounding structures have been reported, sometimes even less [32]. During the pneumatisation of the sphenoid sinus, it will develop into one of three types of sinus: conchal, presellar, and sellar. Most common according to Lu et al. [21] is the sellar type which pneumatised posterior and inferior to the sella. The sphenoid sinus usually has bilateral cavities with an intersphenoid septum [14].

Modern imaging and surgical equipment such as computed tomography (CT) and endoscopes have improved visualisation and subsequently surgical procedures in the nasal and paranasal regions, even as far posteriorly as the petrous apex [21] and the hypophyseal fossa. It would be dangerous to assume a patient's anatomy to follow a standard textbook description, especially with so many variations in the paranasal architecture. Anatomical variants can be classified as normal since no human is the same and variation is inevitable [33]. That is why every variation must be studied and recorded, and identified before surgery takes place, or at least a surgeon ought to be prepared for variation and potential risks it bears.

To the best knowledge of the authors, there is a scarcity of information regarding the Onodi cells among the Polish adults. Henceforth, the main purpose for conducting this study was to determine more accurately the prevalence of Onodi cells in the Polish adult population. Moreover, a subgroup analysis based on the sex of the patients was planned in order to probe for any potential differences that might arise because of it.

MATERIALS AND METHODS

The following study was conducted as a retrospective analysis of CT scans of a total of 359 patients, derived from the Department of Medical Imaging, University Hospital in Krakow, Poland. For the patients to be included, they had to be over 18 years of age and had a CT scan involving the paranasal sinuses. The exclusion criteria comprised any visible pathology, trauma or surgical intervention involving either the nasal, orbital or cranial basis (63 patients). Ultimately, 296 patients (147 females, 149 males) were included in this analysis.

Medical imaging of the paranasal sinuses was obtained with the help of the Siemens Somatom Sensation 16 spiral CT scanner. Standard procedure applied, utilising Siemens CARE Dose 4D option. At no point in the present study was the contrast medium administered to any of the patients. Multiplanar reconstruction tool was used for better visualisation of the paranasal sinuses in frontal and sagittal planes, reconstructed from the original images in the transverse plane. The authors processed the obtained im-

aging data via the Siemens Volume Wizard diagnostic station.

The authors analysed the data by searching for the presence of the Onodi cell, as per the definition stated above. Whenever present, its laterality and sex of the patient was noted. Examples of the CT images presenting the Onodi cell were anonymised and attached in this work.

Ethical approval

All procedures performed in studies involving human participants were in accordance with the ethical standards of the institutional and/or national research committee and with the 1964 Helsinki declaration and its later amendments or comparable ethical standards.

Statistical analysis

The statistical analysis for the present study was performed with STATISTICA version 13.3 by TIBCO Software Inc®. Chi-squared and Fisher's exact tests applied, depending on the fulfilment of their criteria. P-value of < 0.05 was chosen to represent statistically significant results.

RESULTS

Presence of the Onodi cell was relatively frequently noted in the whole research material — it was found in 31 patients, more often in men (20 patients) than females (11 patients). There was no side predilection for this anatomical variation in the female group (5 were identified on the right side, whereas 6 on the left side). In the male group, the Onodi cell was prevalent more often on the left side (in 12 patients) than on the right side (7 patients). Bilateral Onodi cells were noted only in a single male patient.

No statistically significant differences were found between the presence and absence of the Onodi cell in the female and male groups ($p = 0.095$, Chi-squared test). In approximately 90% of men and women the Onodi cell was absent (Tables 1, 2).

Due to the fact that bilateral Onodi cells were noted only in a single case, the statistical analysis was not performed in this instance.

Within the group of patients with a unilateral Onodi cell, no statistically significant difference was found between the males and females which had right- or left-sided variants ($p = 0.712$, Fisher's exact test; Table 3).

For the female group with a unilateral Onodi cell, the variant was present on the right side in 45.5% and in 54.5% on the left side. In juxtaposition, a unilateral Onodi cell was found in males more often on the left side (63.2%) than on the right side (36.8%).

Table 1. Prevalence of the Onodi cell

The Onodi cell	F	F%	M	M%	F + M	F% + M%
Present	11	7.48%	20	13.42%	31	10.47%
Absent	136	92.52%	129	86.58%	265	89.53%

F — females; F% — the percentage of females; M — males; M% — the percentage of males

Table 2. Prevalence of the unilateral and bilateral Onodi cell in the total research group

The Onodi cell	F	F%	M	M%	F + M	F% + M%
Unilateral	11	7.48%	19	12.75%	30	10.14%
Bilateral	0	0%	1	0.67%	1	0.34%
Absent	136	92.52%	129	86.58%	265	89.52%

F — females; F% — the percentage of females; M — males; M% — the percentage of males

Table 3. Prevalence of the unilateral Onodi cell in the total research group

The Onodi cell	F	F%	M	M%	F + M	F% + M%
Right	5	3.4%	7	4.7%	12	4.05%
Left	6	4.08%	12	8.05%	18	6.08%

F — females; F% — the percentage of females; M — males; M% — the percentage of males

Figures 1–4 present examples of the identified Onodi cells in both transverse and frontal planes.

DISCUSSION

As shown in this study, the Onodi cell is a relatively frequent finding on the CT scans of paranasal sinuses of the Polish adult population. Its prevalence was found to be 10.5% for the whole research group. When present, it was noted more often on the left side in males (63.2%), whereas in females there was not a clear side predilection visible.

Concurrent results are given by Perez-Pinas et al. [27], assessing the presence of the Onodi cell at 10.9% (study of 110 CTs of the Spanish population), as well as Sethi et al. [30] — 13% (a dissection study of 30 Asian skulls).

A lower incidence of Onodi cells was reported by Elwany et al. [6] — 7.5%, determining the bilateral variant to be present in 5.3%. The reason for the discrepancies between the results may be attrib-

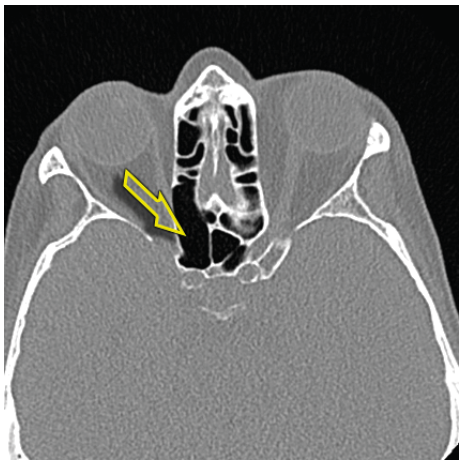

Figure 1. A computed tomography scan of the paranasal sinuses, transverse section. The Onodi cell is marked on the right side.

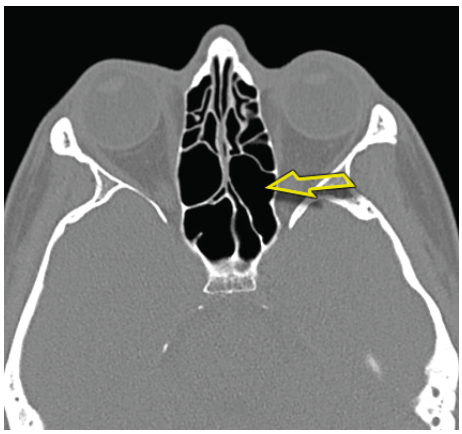

Figure 3. A computed tomography scan of the paranasal sinuses, transverse section. The Onodi cell is marked on the left side.

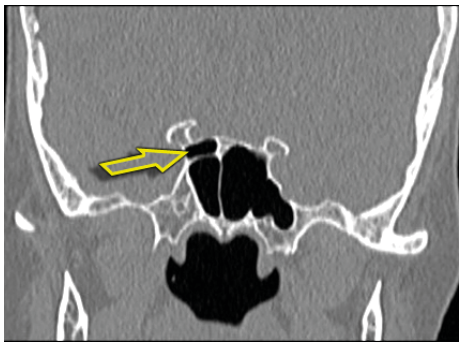

Figure 2. A computed tomography scan of the paranasal sinuses, frontal section. The Onodi cell is marked on the right side.

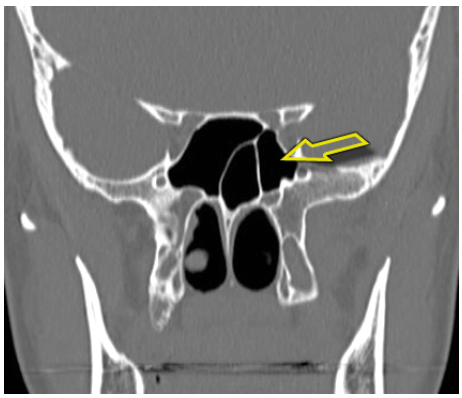

Figure 4. A computed tomography scan of the paranasal sinuses, frontal section. The Onodi cell is marked on the left side.

uted to the method of sinus evaluation (cadaveric endoscopic examination) and the number of sinuses examined (93 patients). A much lower prevalence of this variant was reported by Seddighi et al. [29] (1.56%), Kazkayasi et al. [19] (1.5%), and Daghighi and Daryani [4] (0.4%). In the case of the latter researchers, the study population (Iranian) and the age of the respondents (under 18) could have caused such different results.

Higher incidence of Onodi cells was reported by Ozturan et al. [26] — 16.6%, Tan and Ong [32] — 15%, Anusha et al. [2] — 14.3%, Lupascu et al. [22] — 18% (noting that the presence of the Onodi cell is associated with a smaller dimension of the sphenoid sinuses) and Earwaker [5] — 24%, of which bilateral cells were found in 9.36%. Similar results of the bilateral variant of the Onodi cell are presented by Kaplanoglu et al. [18] — 10.33%; however, giving a much higher incidence of unilateral incidence — 44%. The different results may possibly be related to the analysed ethnic group (Turkish).

Nitinavakarn et al. [24] reported the Onodi cell prevalence three times higher — 31.8% while investigating the adult Thai population (88 CT scans). A high frequency of this variant is also reported by Kainz and Stammberger [17] — 42%. It may be related to the number of examined heads (52) and the method of evaluation (cadaveric endoscopic examination). The highest incidence of Onodi cells was presented by Chinese researchers, Lu et al. [21], after endoscopic examination of 18 skulls — 61.1%, but the results refer to both sides of the skulls (i.e., 36).

Completely different results are presented by Sareen et al. [28], who did not find a single case of the Onodi cell, which could be due to the small number of sinuses (20 skulls) and the method of observations (autopsy).

Detailed comparison of the present work with the previously published data can be found in Table 4.

Table 4. Onodi cell prevalence in the previous studies

Author (materials and methods)	Present	Unilateral	Unilaterally on the right	Unilaterally on the left	Bilateral
Perenz-Pinas et al. (110 CT)			10.9%		
Sethi et al. (30 skulls, dissection study)	13%	10%	–	–	3%
Elwany et al. (93 skulls, endoscopic and dissection study)	7.5%	–	–	–	5.3%
Seddighi et al. (64 CT and MRI)			1.56%		
Kazkayasi et al. (267 CT)	1.5%	1.5%	–	–	0%
Daghighi and Daryani (292 CT)			0.4%		
Ozturan et al. (999 CT)			16.6%		
Tan and Ong (48 skulls, endoscopic and dissection study)			15%		
Anusha et al. (300 CT)	14.3%	72.1%	32.6%	39.5%	27.9%
Lupascu et al. (200 CT)	18%	–	–	–	–
Earwaker (800 CT)	24%	–	–	–	9.36%
Kaplanoglu et al. (300 CT)	54.33%	44%	22%	22%	10.33%
Nitinavakarn et al. (88 CT)	31.8%	13.6%	–	–	18.2%
Kainz and Stammberger (52 skulls, endoscopic study)			42%		
Lu et al. (18 skulls, endoscopic study)			61.1%		
Sareen et al. (20 skulls, dissection study)			0%		
Jaworek-Troć et al. (296 CT)	10.47%	10.14%	4.05%	6.08%	0.34%

CT — computed tomography; MRI — magnetic resonance imaging

Each paranasal sinus develops as an extension of the nasal cavity, through which they also drain and receive air. Furthermore, the sinuses develop differently and at points in life, leading to variable anatomy of the nasal and paranasal regions [23]. With an increased extent of pneumatisation, important anatomical entities (namely neurovascular) that pass around the paranasal sinuses may become dehiscent further increasing the risk of iatrogenic injury during surgery and trauma. Recesses in the sphenoid sinus have been found in 93.92% of the Polish adult patient population, in which case access is improved due to less need for bone drilling [10].

An Onodi cell develops when the posterior ethmoid cell's pneumatisation makes the optic canal visible from inside the cell [17]. Various patterns complicate both general anatomical terminology and surgical procedures; the paranasal sinuses are under constant review and research to discover and classify new variations and structures [23].

The sphenoid sinus is most commonly a sellar type sinus at the end of its development that usually occurs in the third decade of life. Next in order of frequency, are pre-sellar and conchal types [32]. Depending on the pattern of pneumatisation, the sphenoid sinus can have various anatomical variations e.g. accessory septae, deviated interspinous septae [32]. The ostia are found on the sphenoid bone's anterior aspect as a continuation of the sphenoethmoidal recess, and are closely associated with the posterior group of ethmoid air cells [11, 18].

The Onodi cell is important due to its relation to several vital structures such as the optic nerve, internal carotid artery, among others. Complications during surgery, trauma, and/or disease related to paranasal sinuses can affect these nerves and openings, and hence require special imaging to identify potential risks due to anatomy. Pneumatisation of the posterior ethmoid cell and subsequent bulging of the optic canal poses an increased risk due to increased exposure, e.g., during surgical excision of the inflammatory tissue from the ethmoid labyrinth. It is important to mention that the wall thickness and extent of protrusion of the optic canal is likewise variable from case to case. Injury to the optic nerve results in amaurosis. Studies have also shown that although the occurrence of Onodi cells are generally low, individuals with the Onodi variant have increased chances of bulging of other structures such as the internal carotid canal, creating a spheno-carotid recess, a landmark for otolaryngologists operating in the sphenoid sinus.

Limitations to studies searching for anatomical variations include sample size, equipment, and discrepancies in accepted terminology. Since the anatomy of the bony structures includes a considerable amount of variation, it is important to learn and understand each one to fully grasp the anatomy and importance of these structures. With the advent of modern imaging techniques, it has become much easier to visualise difficult to reach structures deep within the nasal cavity, such as the sphenoid sinus ostia. One of such techniques is utilising virtual dissection tables [31]. Endoscopic techniques have revolutionised procedures within this region and therefore continuing research into the structure will cooperatively develop surgical and other clinical procedures of the paranasal sinuses and associated structures [1].

In the future, focus can be shifted on the other air cells of the ethmoid and their invasion paths into the other paranasal sinuses. The Onodi cell is but one variant among many within the nasal and paranasal spaces, and therefore in many cases closely related to other anomalies. Additionally, CT may not be the only tool available in the near future; in development three-dimensional imaging and mixed reality (MR) technology may allow researchers and clinicians an even better approach to the paranasal structures, furthering this research [20]. The present study is limited by the sole use of two-dimensional imaging, however a comprehensive three-dimensional evaluation of the Onodi cell, as well as other paranasal sinuses and their variants could be of clinical interest to the surgeons having to operate in those oftentimes difficult to access regions. Finally, a wider sample size study could be carried out to quantify the prevalence of the cell in the polish population, as well as to identify other potential variations of paranasal anatomy.

CONCLUSIONS

Various studies have been done on the presence of anatomical variants of the paranasal sinuses that are helpful to the medical community in solidifying the terminology and specifications of anatomic variants, and determining their occurrence and clinical significance. Among the latter, of most importance, are surgical procedures involving endoscopic entry through the nasal cavity of anything in between that and the skull base. Imaging allows surgeons better preoperative planning and decreased chance of iatrogenic injury. In this study, we specifically determined the prevalence of the Onodi cell in the Polish population to be approximately 10% based on 296 CT scans.

This report, along with the studies conducted by the referred authors and many more, serves as continuing research into the anatomy of the paranasal structure; this then can be employed by surgeons, clinicians, and researches to further their expertise and treatment of individuals with normal and abnormal anatomical variants such as the Onodi cell. This study not only widens our knowledge of the prevalence of this variant in the Polish population, it also confirms a general trend of prevalence (8–14%), and contributes data required for understanding the paranasal architecture.

Acknowledgements

The authors would like to express their sincere gratitude to Mr. Jacenty Urbaniak for the technical support.

Conflict of interest: None declared

REFERENCES

1. Al-Zaidi HM, Badr HM. Unusual large central sphenoethmoidal cell separating the two sphenoid sinuses: a case report. Transl Res Anat. 2022; 28: 100212, doi: 10.1016/j.tria.2022.100212.
2. Anusha B, Baharudin A, Philip R, et al. Anatomical variants of surgically important landmarks in the sphenoid sinus: a radiologic study in Southeast Asian patients. Surg Radiol Anat. 2015; 37(10): 1183–1190, doi: 10.1007/s00276-015-1494-8, indexed in Pubmed: 25990686.
3. Burdan F, Dworzański W, Cendrowska-Pinkosz M, et al. Anatomical eponyms: unloved names in medical terminology. Folia Morphol. 2016; 75(4): 413–438, doi: 10.5603/FM.a2016.0012, indexed in Pubmed: 27830870.
4. Daghighi MH, Daryani A. Evaluation of anatomic variations of paranasal sinuses. Internet J Otorhinolaryngol. 2007; 7(1), doi: 10.5580/1a5d.
5. Earwaker J. Anatomic variants in sinonasal CT. RadioGraphics. 1993; 13(2): 381–415, doi: 10.1148/radiographics.13.2.8460226, indexed in Pubmed: 8460226.
6. Elwany S, Elsaeid I, Thabet H. Endoscopic anatomy of the sphenoid sinus. J Laryngol Otol. 1999; 113(2): 122–126, doi: 10.1017/s0022215100143361, indexed in Pubmed: 10396560.
7. Jaworek-Troć J, Iwanaga J, Chrzan R, et al. Anatomical variations of the main septum of the sphenoidal sinus and its importance during transsphenoidal approaches to the sella turcica. Transl Res Anat. 2020; 21: 100079, doi: 10.1016/j.tria.2020.100079.
8. Jaworek-Troć J, Walocha JA, Chrzan R, et al. Protrusion of the carotid canal into the sphenoid sinuses: evaluation before endonasal endoscopic sinus surgery. Folia Morphol. 2021; 80(3): 642–649, doi: 10.5603/FM.a2020.0086, indexed in Pubmed: 32789847.

9. Jaworek-Troć J, Walocha JA, Lipski M, et al. Agenesis of the sphenoid sinus and a single sphenoid sinus: a computed tomography anatomical evaluation. Folia Morphol. 2021; 80(4): 947–953, doi: 10.5603/FM.a2021.0092, indexed in Pubmed: 34545557.
10. Jaworek-Troć J, Walocha JA, Loukas M, et al. Extensive pneumatisation of the sphenoid bone: anatomical investigation of the recesses of the sphenoid sinuses and their clinical importance. Folia Morphol. 2021; 80(4): 935–946, doi: 10.5603/FM.a2020.0120, indexed in Pubmed: 33084012.
11. Jaworek-Troć J, Walocha JA, Skrzat J, et al. A computed tomography comprehensive evaluation of the ostium of the sphenoid sinus and its clinical significance. Folia Morphol. 2022; 81(3): 694–700, doi: 10.5603/FM.a2021.0063, indexed in Pubmed: 34219216.
12. Jaworek-Troć J, Zarzecki M, Bonczar A, et al. Sphenoid bone and its sinus — anatomo-clinical review of the literature including application to FESS. Folia Med Cracov. 2019; 59(2): 45–59, indexed in Pubmed: 31659348.
13. Jaworek-Troć J, Zarzecki M, Lusina D, et al. Incorporation of the sphenoid sinuses' septum / septa in the carotid canal - evaluation before the FESS. Folia Med Cracov. 2020; 60(4): 65–78, indexed in Pubmed: 33821852.
14. Jaworek-Troć J, Zarzecki M, Mróz I, et al. The total number of septa and antra in the sphenoid sinuses — evaluation before the FESS. Folia Med Cracov. 2018; 58(3): 67–81, doi: 10.24425/fmc.2018.125073, indexed in Pubmed: 30521512.
15. Jaworek-Troć J, Zarzecki M, Zamojska I, et al. The height and type of the main septum in the sphenoid sinuses — evaluation before the fess. Folia Med Crac. 2020; 60(3): 65–74, doi: 10.24425/fmc.2020.135796.
16. Jaworek-Troć J, Zarzecki M, Zamojska I, et al. The dimensions of the sphenoid sinuses: evaluation before the functional endoscopic sinus surgery. Folia Morphol. 2021; 80(2): 275–282, doi: 10.5603/FM.a2020.0059, indexed in Pubmed: 32488857.
17. Kainz J, Stammberger H. Danger areas of the posterior rhinobasis. Acta Otolaryngol. 1992; 112: 852–861.
18. Kaplanoglu H, Kaplanoglu V, Toprak U, et al. Surgical measurement of the sphenoid sinus on sagittal reformatted CT in the turkish population. Eurasian J Med. 2013; 45(1): 7–15, doi: 10.5152/eajm.2013.02, indexed in Pubmed: 25610242.
19. Kazkayasi M, Karadeniz Y, Arikan OK. Anatomic variations of the sphenoid sinus on computed tomography. Rhinology. 2005; 43(2): 109–114, indexed in Pubmed: 16008065.
20. Kolecki R, Pręgowska A, Dąbrowa J, et al. Assessment of the utility of mixed reality in medical education. Transl Res Anat. 2022; 28: 100214, doi: 10.1016/j.tria.2022.100214.
21. Lu Y, Pan J, Qi S, et al. Pneumatization of the sphenoid sinus in Chinese: the differences from Caucasian and its application in the extended transsphenoidal approach. J Anat. 2011; 219(2): 132–142, doi: 10.1111/j.1469-7580.2011.01380.x, indexed in Pubmed: 21517841.
22. Lupascu M, Comsa G, Zainea V. Anatomical variations of the sphenoid sinus: a study of 200 cases. ARS Medica Tomitana. 2014; 20(2): 57–62, doi: 10.2478/arsm-2014-0011.
23. Márquez S, Tessema B, Clement PAr, et al. Development of the ethmoid sinus and extramural migration: the anatomical basis of this paranasal sinus. Anat Rec (Hoboken). 2008; 291(11): 1535–1553, doi: 10.1002/ar.20775, indexed in Pubmed: 18951481.
24. Nitinavakarn B, Thanaviratananich S, Sangsilp N. Anatomical variation of the lateral nasal wall and paranasal sinuses: a CT study for endoscopic sinus surgery (ESS) in Thai patients. J Med Assoc Thai. 2005; 88(6): 763–768.
25. Onodi A. Die Sehstorungen und Erblindung nasalen Ursprunges, bedingt durch Erkrankungen der hinteren Nebenhohlen. Z Augenheilkd. 1904; 12: 23–46.
26. Ozturan O, Yenigun A, Degirmenci N, et al. Co-existence of the Onodi cell with the variation of perisphenoidal structures. Eur Arch Otorhinolaryngol. 2013; 270(7): 2057–2063, doi: 10.1007/s00405-012-2325-8, indexed in Pubmed: 23274877.
27. Pérez-Piñas I, Sabaté J, Carmona A, et al. Anatomical variations in the human paranasal sinus region studied by CT. J Anat. 2000; 197(Pt 2): 221–227, doi: 10.1046/j.1469-7580.2000.19720221.x, indexed in Pubmed: 11005714.
28. Sareen D, Agarwal AK, Kaul JM, et al. Study of sphenoid sinus anatomy in relation to endoscopic surgery. Int J Morphol. 2005; 23(3): 261–266, doi: 10.4067/s0717-95022005000300012.
29. Seddighi A, Seddighi AS, Mellati O, et al. Sphenoid sinus: anatomic variations and their importance in trans-sphenoid surgery. Int Clin Neurosci J. 2014; 1(1): 31–34.
30. Sethi DS, Stanley RE, Pillay PK. Endoscopic anatomy of the sphenoid sinus and sella turcica. J Laryngol Otol. 1995; 109(10): 951–955, doi: 10.1017/s0022215100131743, indexed in Pubmed: 7499947.
31. Stecco A, Boccafoschi F, Falaschi Z, et al. Virtual dissection table in diagnosis and classification of Le Fort fractures: A retrospective study of feasibility. Transl Res Anat. 2020; 18: 100060, doi: 10.1016/j.tria.2019.100060.
32. Tan HKK, Ong YK. Sphenoid sinus: an anatomic and endoscopic study in Asian cadavers. Clin Anat. 2007; 20(7): 745––750, doi: 10.1002/ca.20507, indexed in Pubmed: 17583590.
33. Żytkowski A, Tubbs R, Iwanaga J, et al. Anatomical normality and variability: Historical perspective and methodological considerations. Transl Res Anat. 2021; 23: 100105, doi: 10.1016/j.tria.2020.100105.

VIA MEDICA

ORIGINAL ARTICLE

Folia Morphol.
Vol. 82, No. 4, pp. 892–897
DOI: 10.5603/FM.a2022.0083

ISSN 0015–5659
eISSN 1644–3284
journals.viamedica.pl

Reference intervals of C2-C7 lateral spinous process deviation in Chinese adults

L.-Q. Liao[1], Z.-Y. Feng[1], H. Yang[1], Y.-K. Li[1], M.-X. Chen[2]

[1]*Department of TCM Orthopaedics and Traumatology, School of Traditional Chinese Medicine, Southern Medical University, Guangzhou, Guangdong, China*
[2]*Department of Orthopaedic, Hainan Traditional Chinese Medicine Hospital, Haikou, Hainan, China*

[Received: 22 July 2022; Accepted: 8 September 2022; Early publication date: 27 September 2022]

Background: *Lateral spinous process deviation (LSPD) is a commonly used morphological parameter in the anatomical study of the cervical spinous process. However, quantitative studies on this issue are still lacking. In this study we aimed to establish reference intervals of C2-C7 LSPD in the adult Chinese population and provide decision-making information for clinical practitioners.*

Materials and methods: *This was a retrospective study of 92 adult patients who received neck computed tomography scans, including 42 females and 50 males meeting the inclusion criteria. Three-dimensional reconstruction and anatomical measurements were performed using Mimics Research 19.0 and 3-Matic Research 11.0.*

Results: *The inter-observer reliability of LSPD measurement in this study was excellent (intraclass correlation coefficient value > 0.93). Only 2 cases of LSPD angles of 90 degrees were found, which means most cervical spinous process exist deviation. The reference interval for the C2-C7 LSPD angle was (85.11, 94.75) degrees. The C2 LSPD showed the different directions to C5 and C7 ($p < 0.05$). In the C4 vertebrae, the male tends to have greater LSPD angles than the female ($T = –2.013$, $p = 0.047$). In the C2 vertebrae, there was a statistically significant but weak correlation between age and LSPD angles ($r = 0.24$, $p = 0.029$). There was no statistically significant effect of sex or age on other levels of cervical vertebrae.*

Conclusions: *Cervical spinous process deviation of less than 5 degrees on either side is a common morphological manifestation in Chinese adults. Thus, LSPD may not be an indicator for clinical care. Moreover, the vertebrae may have opposite directions of LSPD in the upper levels (C2-C4) and lower levels (C5-C7).* (Folia Morphol 2023; 82, 4: 892–897)

Key words: morphology, cervical vertebra, lateral spinous process deviation, computerized tomography, retrospective analysis

INTRODUCTION

Neck pain is one of the most common musculoskeletal complaints, with an annual prevalence of more than 30% [2]. Spinal manipulation was proved an effective therapy for neck pain compared to no treatment or sham treatment [2, 3, 7]. Identifying bony landmarks by palpation is a prerequisite procedure for many kinds of manual therapy [12, 15]. One

Address for correspondence: Dr. Y.-K. Li, Department of TCM Orthopaedics and Traumatology, School of Traditional Chinese Medicine, Southern Medical University, Guangzhou, Guangdong, China, e-mail: ortho@smu.edu.cn; Dr. M.-X. Chen, Department of Orthopaedic, Hainan Traditional Chinese Medicine Hospital, Haikou, Hainan, China, e-mail: chenmeixiong64@126.com

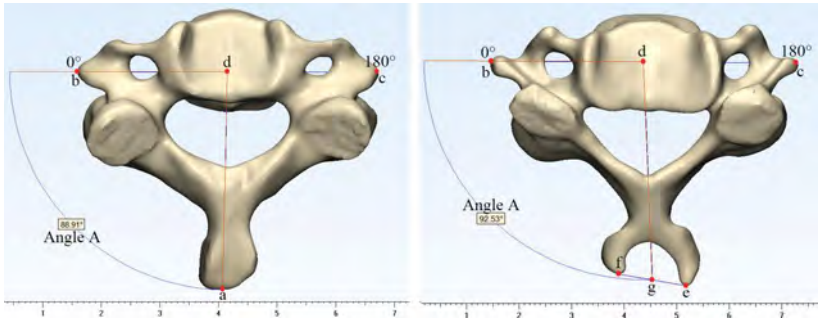

Figure 1. Measurement of lateral spinous process deviation (LSPD) in non-bifid spinous processes (SP) (left) and bifid SP (right). Anatomical landmarks: *a* — the most posterior tip of SP; *b* and *c* — the tip of the posterior tubercles of the transverse processes; *d* — the midpoint of line *bc*; *e and f* — the posterior tip of bifid SP branches; *g* — the midpoint of line *ef*. Angle *A* is the angle of LSPD.

of the most important bony landmarks in the cervical vertebra is the spinous processes (SPs) [12]. According to Mulligan's techniques, which was commonly used in musculoskeletal physical therapy, SPs are thrust points in many spinal manipulations [9, 12]. Likewise, before spinal manipulation, Maitland emphasized using the tip of the thumb to palpate the SPs for the assessment of bony outlines [14]. Theoretically, SPs of a spine should align in the posterior midline of the neck region [11, 15]. To date, the definition of the midline alignment of SPs still lacks quantitative study. According to previous research, lateral spinous process deviation (LSPD) angle is a commonly used morphological parameter in the anatomical study of the cervical spinous process, but its correlation with clinical symptoms remains doubtful [1, 4, 5]. In addition, it is still controversial regarding the static imaging measures of LSPD as indicators for clinical treatment [4, 13]. To fully understand the definition of the midline alignment of SPs, the cut-off values of LSPD in normal populations need to be determined. Also, previous studies of cervical spinous processes failed to acquire data of multiple segments of the same individuals. Therefore, in this research we aim to determine the reference intervals of C2-C7 LSPD in an adult Chinese population and provide decision-making information for clinicians and therapists.

MATERIALS AND METHODS

We collected 92 cases of patients who underwent cervical computed tomography (CT) scanning between January 2018 to December 2019 from Nanfang Hospital of Southern Medical University. The inclusion criteria were age 18 to 60 asymptomatic subjects. The exclusion criteria included vertebral malrotation, cervical deformity, chronic neck pain, tumours, infections, trauma, and any other pathological neck condition. This study had approval from the institutional review board and the requirement for informed patient consent was waived. This study also complies with current regulations in our country. Ethical approval for this study was obtained from the Chinese Ethics Committee of Registering Clinical Trials (Reference number: ChiECRCT20210191).

A US GE 16-slice spiral CT was used to perform CT scans. Mimics Research 19.0 was used for the reconstruction of all C2-C7 cervical vertebra. The 3-Matic Research 11.0 was used for anatomical measurement, performed by two independent observers. According to standard anthropometric measurements, measurements were taken using bony landmarks for reproducibility, as shown in Figure 1. The angle of LSPD was defined as the angle between line *bc* and line *ad* (angle *A*). Both examiners were blinded to the radiological data and patient data. The SP was defined as left deviation (LSPD $<$ 90 degrees), right deviation (LSPD $>$ 90 degrees), or no deviation (LSPD $=$ 90 degrees).

Statistical analysis

The SPSS statistical software package 20.0 (IBM, New York) was used for statistical analysis. Data were expressed as mean ± standard deviation (SD), using the mean value from the two examiners. The inter-and intra-observer reliability for LSPD measurement was evaluated using intraclass correlation coefficient (ICC) and reliability was classified as inferior (0–0.39), moderate (0.4–0.74), or excellent (0.75–1) according to ICC value. The reference intervals were established using the mean ± 2×SD. A single sample t-test was used to test whether LSPD differed from 90 degrees. The chi-square test was used to analyse the differenc-

Table 1. Inter- and intra-observer reliability for spinal process deviation angles (ICCs [95% confidence interval])

Levels	Inter-observer	P	Intra-observer	P
C2	0.934 (0.868–0.963)	< 0.01	0.983 (0.966–0.991)	< 0.01
C3	0.953 (0.929–0.969)	< 0.01	0.988 (0.982–0.992)	< 0.01
C4	0.960 (0.939–0.974)	< 0.01	0.990 (0.984–0.993)	< 0.01
C5	0.957 (0.935–0.972)	< 0.01	0.989 (0.984–0.993)	< 0.01
C6	0.969 (0.953–0.979)	< 0.01	0.992 (0.988–0.995)	< 0.01
C7	0.966 (0.948–0.977)	< 0.01	0.991 (0.987–0.994)	< 0.01

Inter- and intra-observer reliability in all cervical levels were excellent (intraclass correlation coefficient [ICC] > 0.93, p < 0.01)

es in deviating directions among C2-C7 levels. One--way repeated measure analysis of variance (ANOVA) was used to compare LSPD in different cervical levels (C2-C7), and post hoc used the Bonferroni test. The sex difference was analysed using independent-sample t-tests. The correlation of LSPD angles with age was analysed using the Pearson correlation coefficient. P < 0.05 was considered statistically significant.

RESULTS

The study subjects consisted of 92 CT scans of Chinese adults, including 42 (45.65%) women and 50 (54.35%) men, with a mean age of 40.99 ± 9.49 (range 19–59) years old. ICCs were used to evaluate the intra- and inter-observer reliability of LSPD angles. The results of ICCs were expressed as 95% confidence intervals (CI) in Table 1. The intra- and inter-observer ICCs were excellent in LSPD angles at each cervical level (ICC > 0.93, p < 0.01).

The frequencies of different ranges of LSPD at all cervical levels are presented in Table 2. In this study, only 2 cases showed precisely 90 degrees in the LSPD angle measured by 1 investigator, while the majority deviated to a different extent. All experimental results in this study are expressed as mean values of 2 independent investigators. According to our results, the range of LSPD angle in C2-C7 was approximately 85 to 95 degrees, and 95% CI was (89.74, 90.13) degrees. Thus, we evaluated the frequency of various ranges of LSPD angles from a larger range (85∼95 degrees) to a smaller range (89∼91 degrees). As shown in Table 2, 93.12% of vertebrae presented LSPD of (85∼95) degrees, while 32.97% presented LSPD of (89∼91) degrees. This indicated that most SPs showed a deviation of more than one degree. But, a single sample t-test showed no significant difference between the mean LSPD and 90 degrees (t = 0.249, p = 0.804), indicating that all SPs did not deviate significantly in statistics.

Table 2. The frequency of various lateral spinous process deviation (LSPD) ranges

The range of LSPD (degrees)	Frequency (%)
89∼91	182 (32.97%)
88∼92	361 (65.40%)
87∼93	424 (76.81%)
86∼94	483 (87.5%)
85∼95	514 (93.12%)

Table 3. Statistics of lateral spinous process deviation angles in C2-C7

Levels	Mean ± SD	Lower, upper limits	95% CI
C2	89.02 ± 1.97	85.16, 92.88	88.63–89.41
C3	89.75 ± 2.47	84.91, 94.59	89.25–90.24
C4	89.54 ± 2.43	84.78, 94.30	89.03–89.97
C5	90.51 ± 2.10	86.39, 94.63	90.09–90.93
C6	90.19 ± 2.49	85.31, 95.07	89.70–90.69
C7	90.56 ± 2.86	84.95, 96.17	89.97–91.12
Total	89.93 ± 2.46	85.11, 94.75	89.74–90.13

CI — confidence interval; SD — standard deviation

According to Table 3, the upper levels (C2-C4) displayed a mean LSPD angle of fewer than 90 degrees, whereas the lower levels (C5-C7) showed greater than 90 degrees. This result indicated that the LSPD presumably changed from left deviation to right deviation from C2 to C7 levels. In addition, the chi--square test showed that the LSPD direction among C2-C7 levels were different. As shown in Table 4, the pairwise comparison showed statistically significant differences in LSPD between C2 and C5, C2 and C7 (p < 0.05), while no statistical difference was found between other levels (Fig. 2). One-way repeated measures ANOVA showed significant differences between C2 and C5 (p < 0.001), C2 and C7 (p < 0.001), C4 and C5 (p < 0.05), and C4 and C7 (p < 0.05). No statistical differences were detected among other levels in post

Table 4. The frequency of lateral spinous process deviation directions among C2-C7 levels

Cervical levels C2-C7	Direction of spinous process deviation		Total
	Right	Left	
C2	28	64	92
C3	44	48	92
C4	44	48	92
C5	54	38	92
C6	47	45	92
C7	61	31	92
Total	278	274	552

A chi-square test ($\chi^2 = 26.487$, $p = 0.000$) indicated that the deviations of spinous processes (SPs) were different among C2-C7 levels. Pairwise comparison was statistically significant ($p < 0.05$) between the deviations of C2 SP and C5 SP, C2 SP and C7 SP.

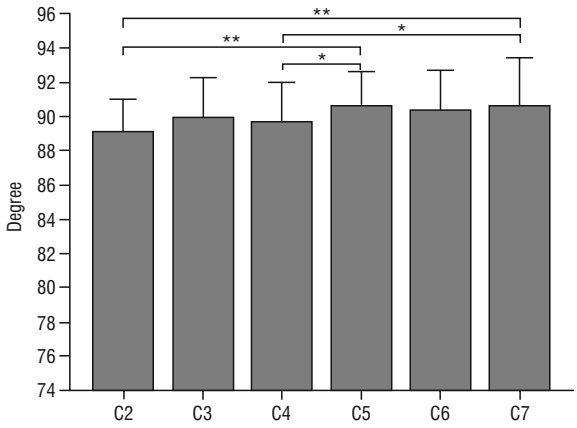

Figure 2. Statistical differences of C2-C7 lateral spinous process deviation angle; **p < 0.001, *p < 0.05.

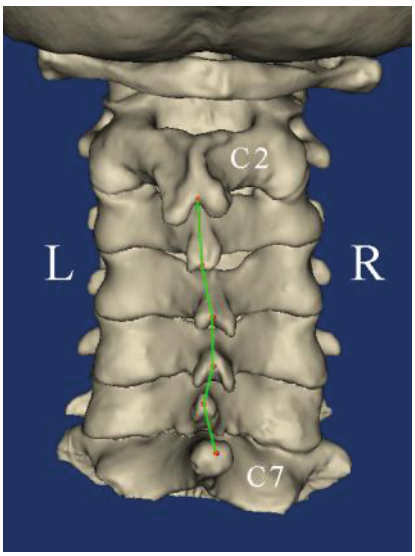

Figure 3. The posterior view of cervical vertebrae with spinal process deviation (SPD). The green line connects the tip of spinous processes, the SPD transformed from right deviation to left deviation in C7 to C2.

hoc tests. Therefore, the above results indicated that the C2 and C5, C2 and C7 have the opposite direction of LSPD (Fig. 3). Due to the opposite direction of LSPD, the overall deviation between C2 and C7 SP could be up to 1.54 degrees. Regarding sex difference, men tend to have greater LSPD angle than women at the C4 level in this study ($T = -2.013$, $p = 0.047$), while no statistically significant difference was found in other levels (Table 5). Additionally, a statistically weak correlation was found ($r = 0.24$, $p = 0.029$) between age and LSPD angles at the C2 level. When correlated with the other levels, age exhibited small correlations with LSPD ($p > 0.05$).

DISCUSSION

In this study, we introduced a method of LSPD quantification and analysed the C2-C7 LSPD in the Chinese adult population. In previous studies, there were different methods for LSPD measurements. Gradl et al. [5] defined LSPD as SPs that are not aligned with the midline of cervical anterior-posterior radiographs. Macpherson et al. [13] suggested that the LSPD is relative to the axis of the vertebral body and posterior arch. Tang et al. [16] defined the LSPD as the angle between the midsagittal line of the vertebral body and the longitudinal line of SP, using landmarks such as the centre of the vertebral body, the centre of spinolaminar junction, and the SP. Ji-Hong et al. [10] described LSPD as the midsagittal line through SP that was not coinciding with the bisector of the vertebral foramen in the horizontal plane. Liao et al. [12] performed an LSPD measurement using the angle between the line connecting two transverse processes tips and the midsagittal line through SP [12]. Zhang et al. [18] measured the LSPD with the angle between the long axis of SP and the median line of the vertebra in the superior aspect. The 6 methods mentioned above were common existing methods of LSPD measurement. We believe that quantification methods of LSPD should ensure the reliability and repeatability of measurement. Therefore, we chose the tips of transverse processes and spinous processes as reference landmarks for easy identification. In addition, previous methods often failed to address the issue of LSPD measurement in bifid SPs. We defined the midpoint of two tips of bifid branches as the end of the SP axis (*g* point), and the LSPD angle was defined as the angle between line *bc* and line *dg*. Repeated measurements with this method showed excellent reliability for two observers with ICCs. We hope this

Table 5. C2-C7 lateral spinous process deviation angles (degrees) of sex groups

Groups	C2	C3	C4	C5	C6	C7
Females	88.77 ± 2.01	90.07 ± 2.39	88.90 ± 2.42*	90.27 ± 2.33	90.26 ± 2.30	90.78 ± 2.52
Males	89.23 ± 1.94	89.48 ± 2.52	90.09 ± 2.32*	90.71 ± 1.88	90.13 ± 2.66	90.36 ± 3.14

*$P < 0.05$ for independent sample t-tests comparisons between the male and the female in the C4 level.

method may provide a reference for diagnosis and research in the future.

Spinous processes are often described in many works as aligned on the posterior midline but lack quantification of the midline alignment [14, 15]. Since LSPD is a common variation, the reference interval should be determined to realise the range of normal SP alignment. Although only 2 cases were found to be exact 90 degrees in the LSPD angle, our results showed no statistically significant difference between the overall LSPD angle and 90 degrees, indicating that all subjects in this study were considered to have SPs aligned in the posterior midline. Our results showed that the overall reference interval of LSPD was approximately within ± 5 degrees, which is 85∼95 degrees. This reference interval covers 93.12% of our samples, approximately 95% of the subjects. This observation may support the hypothesis that 85∼95 degrees were the appropriate reference interval of LSPD angle as normal variation in the asymptomatic population.

As we all know, there has been literature arguing about the reliability of LSPD measurement in static imaging as an indicator of vertebral rotation [4, 13]. According to Gradl et al. [5], in a radiograph, the SP tip deviates 1 mm from the posterior midline indicating a vertebral rotation of 1.62 degrees. However, according to our results, the reference intervals of LSPD have a difference of 5 degrees on each side, which is about 3 mm deviation on the radiograph. Thus, we recommend that researchers take into account the reference intervals of LSPD when studying the vertebral rotation in the static radiograph. The LSPD may also had an influence on the reliability of static palpation of SP in vertebral alignment assessment. Nevertheless, some researchers have already doubted the reliability of static palpation in manual therapy [8, 17]. As a matter of fact, a small deviation of SP was commonly seen in asymptomatic subjects. To study the relationship between pathological SP deviation and clinical symptoms, researchers should exclude subjects within the reference interval of 85–95 degrees LSPD to truly analyse the connection between SP deviation and clinical symptoms. We also noticed that our results of LSPD angle were slightly different from other studies, possibly due to the differences between measuring methods [5, 10, 12, 18]. Nevertheless, our results are consistent with the conclusion of other studies that LSPD is common in the asymptomatic population [10, 12, 14, 15].

Another important finding of normal cervical spinal alignment often neglected by researchers is the different directions of LSPD between the upper and lower cervical vertebra. The C2 and C7 SPs are two prominent bony landmarks in the cervical vertebra that are palpable through the surface [14, 15]. In our study, we found that C2 LSPD usually deviated in the opposite direction of C7 LSPD in a small magnitude. Based on this finding, the maximum angle between the deviation of C2 and C7 SPs could be up to 1.54 degrees. Nevertheless, such a small range of differences may not be identified through palpation, as muscles and soft tissues cover SP in the posterior neck region. Previous studies have already noted that the upper and lower cervical SPs commonly have an opposite direction of deviation [6]. Our findings echoed Greiner's research [6], that the SPs tend to deviate to the left in the C2-C4 cervical levels, whereas tend to deviate to the right side in the C5-C7 levels. Unfortunately, Greiner [6] only investigated the SPs of C3-C7. One possible explanation for such findings is that at some point in early age, muscle contractions may have had an influence on the development of SP. Most studied subjects were right-handed, resulting in the special directions of LPSD in the upper and lower cervical levels [6]. In addition, we found that age and sex have little impact on LSPD. The male consistently had greater LSPD angles in the C4 levels when compared to the female. There was a statistically weak correlation ($r = 0.24$, $p = 0.029$) between age and LSPD angles at the C2 level. No statistical difference in sex and age was found at other levels.

Limitations of the study

There are some limitations that need to be acknowledged. The study population is not strictly a normal population. The reasons for ordering the CT

scans might have some unknown effects on the alignment of cervical vertebrae. Most importantly, there is no known relationship between small LSPD and current or future clinical conditions of the cervical spine that may warrant treatment for small LSPD. No palpation of the cervical spine was conducted, so the relationship between CT findings and palpation findings is unknown. It is not known to what extent a clinician can feel such small deviations of the SP.

CONCLUSIONS

Clinical practitioners should be aware of normal reference intervals for LSPD. LSPD have a weak association with age and small gender differences in the cervical spine. LSPD of small magnitude may be a normal variant without clinical implications. Further work is required to determine if LSPD has concurrent or predictive validity for identifying the need and site of spinal manipulation.

Acknowledgements

We would like to thank the 92 Chinese adults for their support during this project.

Funding

The study was supported by Sanming Project of Medicine in Shenzhen (No. SZZYSM202108013) and The Innovation Team and Talents Cultivation Programme of National Administration of Traditional Chinese Medicine (No: ZYYCXTD-C-202003).

Conflict of interest: None declared

REFERENCES

1. Amevo B, Aprill C, Bogduk N. Abnormal instantaneous axes of rotation in patients with neck pain. Spine (Phila Pa 1976). 1992; 17(7): 748–756, doi: 10.1097/00007632-199207000-00004, indexed in Pubmed: 1502637.
2. Cohen SP. Epidemiology, diagnosis, and treatment of neck pain. Mayo Clin Proc. 2015; 90(2): 284–299, doi: 10.1016/j.mayocp.2014.09.008, indexed in Pubmed: 25659245.
3. Corum M, Aydin T, Medin Ceylan C, et al. The comparative effects of spinal manipulation, myofascial release and exercise in tension-type headache patients with neck pain: a randomized controlled trial. Complement Ther Clin Pract. 2021; 43: 101319, doi: 10.1016/j.ctcp.2021.101319, indexed in Pubmed: 33517104.
4. Farmer PK, Snodgrass SJ, Buxton AJ, et al. An investigation of cervical spinal posture in cervicogenic headache. Phys Ther. 2015; 95(2): 212–222, doi: 10.2522/ptj.20140073, indexed in Pubmed: 25301967.
5. Gradl G, Maier-Bosse T, Penning R, et al. Quantification of C2 cervical spine rotatory fixation by X-ray, MRI and CT. Eur Radiol. 2005; 15(2): 376–382, doi: 10.1007/s00330-004-2498-7, indexed in Pubmed: 15449004.
6. Greiner TM. Shape analysis of the cervical spinous process. Clin Anat. 2017; 30(7): 894–900, doi: 10.1002/ca.22948, indexed in Pubmed: 28646520.
7. Gross A, Langevin P, Burnie SJ, et al. Manipulation and mobilisation for neck pain contrasted against an inactive control or another active treatment. Cochrane Database Syst Rev. 2015(9): CD004249, doi: 10.1002/14651858.CD004249.pub4, indexed in Pubmed: 26397370.
8. Haneline MT, Young M. A review of intraexaminer and interexaminer reliability of static spinal palpation: a literature synthesis. J Manipulative Physiol Ther. 2009; 32(5): 379–386, doi: 10.1016/j.jmpt.2009.04.010, indexed in Pubmed: 19539121.
9. Hing W, Hall T, Mulligan B. The Mulligan Concept of Manual Therapy. 2E. Elsevier, Australia 2015: 21–324.
10. Ji-Hong F, Li-Ping Wu, Yi-Kai Li, et al. Variable morphology of the axis vertebrae in 100 specimens: implications for clinical palpation and diagnostic imaging. J Manipulative Physiol Ther. 2010; 33(2): 125–131, doi: 10.1016/j.jmpt.2009.12.002, indexed in Pubmed: 20170778.
11. Joseph E. The muscle and bone palpation manual: with trigger points, referral patterns and stretching. Elsevier, Mosby 2015: 102.
12. Liao LQ, Li YK, Yuan F, et al. Morphological characteristics of the spinous process of axis: clinical implications for cervical spine manipulation. J Manipulative Physiol Ther. 2019; 42(1): 82–88, doi: 10.1016/j.jmpt.2018.05.002, indexed in Pubmed: 31054597.
13. Macpherson BC, Campbell C. C2 rotation and spinous process deviation in migraine: cause or effect or coincidence? Neuroradiology. 1991; 33(6): 475–477, doi: 10.1007/BF00588037, indexed in Pubmed: 1780047.
14. Maitland GD, Hengeveld E, Banks K. Maitland's Vertebral Manipulation. 7th ed. Elsevier, Oxford 2005: 65–261.
15. Maitland GD, Hengeveld E, Banks K. Maitland's Vertebral Manipulation. 8th ed. Elsevier, Philadelphia, PA 2014: 7–256.
16. Tang S, Liu H, Zhang Y. Spinous process deviation and disc degeneration in lumbosacral segment. J Surg Res. 2015; 193(2): 713–717, doi: 10.1016/j.jss.2014.10.039, indexed in Pubmed: 25466517.
17. Triano JJ, Budgell B, Bagnulo A, et al. Review of methods used by chiropractors to determine the site for applying manipulation. Chiropr Man Therap. 2013; 21(1): 36, doi: 10.1186/2045-709X-21-36, indexed in Pubmed: 24499598.
18. Zhang L, Luo Z, Wang H, et al. An anatomical study of the spinous process of the seventh cervical vertebrae based on the three-dimensional computed tomography reconstruction. Exp Ther Med. 2018; 16(2): 511–516, doi: 10.3892/etm.2018.6245, indexed in Pubmed: 30116309.

VIA MEDICA

ORIGINAL ARTICLE

Folia Morphol.
Vol. 82, No. 4, pp. 898–908
DOI: 10.5603/FM.a2022.0094

ISSN 0015–5659
eISSN 1644–3284
journals.viamedica.pl

A micro-computed tomography study of the sinus tympani variation in humans

J. Skrzat[1], M. Kozerska[1], M. Zarzecki[1], S. Wroński[2], J. Tarasiuk[2]

[1]*Department of Anatomy, Jagiellonian University Medical College, Krakow, Poland*
[2]*Department of Condensed Matter Physics, AGH-UST University of Science and Technology, Krakow, Poland*

[Received: 29 August 2022; Accepted: 16 October 2022; Early publication date: 28 October 2022]

Background: *The posterior part of the tympanic cavity comprises a depression called the sinus tympani (ST). The said structure is of outmost importance, e.g. in surgical procedures involving the middle ear, as a pathology (microbial biofilm or cholesteatoma) present in this difficult to access location might hinder its effective treatment. The aim of the study was to evaluate anatomical variants of the ST in human adult petrous bones. For this purpose, three-dimensional (3D) models of the ST were recreated from micro-computed tomography (CT) scans of 44 dry petrous bone samples (19 female, 25 male), applying 3D Slicer, Meshmixer and MeshLab software.*

Materials and methods: *Anatomical variants of the ST were classified in terms of both shape and surface configuration. The internal configuration of the ST was classified as heterogeneous — containing small bony trabeculae and crests up to 1.0 mm in size, contrasting to homogeneous ST that characterizes a relatively smooth interior, or mere presence of minor depressions and mild folds. Female STs were more bowl-shaped (57.9%) than saccular (42.1%), and had heterogeneous surface configuration (52.6%) compared to homogeneous (47.4%). On the contrary, male STs were more saccular (52.0%) rather than bowl-shaped (48.0%), and predominantly had a heterogeneous surface (84.0%) over homogeneous (16.0%).*

Results and Conclusions: *A complex combination of ST features comprised of a saccular shape and heterogeneous surface occurred in 52.0% of males and in 15.8% of females (a statistically significant difference; $p = 0.0254$, Fisher's exact test) seems to be clinically important because of its potential negative implication on health outcomes after surgery in the case of, for example, cholesteatoma, and it may also favour chronic pathological processes.* (Folia Morphol 2023; 82, 4: 898–908)

Key words: sinus tympani, retrotympanum, middle ear, micro-computed tomography

INTRODUCTION

The sinus tympani (ST) is a depression localized in the retrotympanum (the posterior area of the tympanic cavity) and forms its medial portion. The mean depth of the ST in adults was estimated to be 2.6–2.7 mm, but there are also reports stating that it can reach even up to 10 mm [8, 16, 41]. The ST lies below and posteriorly to the promontory, posteriorly to the round window, extends medially to the pyramidal eminence, stapedial muscle, and facial canal

Address for correspondence: M. Kozerska, PhD, Department of Anatomy, Jagiellonian University Medical College, ul. Kopernika 12, 31–034 Kraków, Poland, e-mail: magdalena.kozerska@uj.edu.pl

(its mastoid segment) and laterally to the posterior semicircular canal [19]. The superior boundary of the ST forms the ponticulus, whereas the subiculum is the inferior boundary. The subiculum is the posterior extension of the promontory that separates the ST from the round window [34].

Many studies have emphasized the clinical importance of the ST because of pathological processes which may occur inside, and highlight difficulties in surgical approaches and endoscopic explorations of this region of the middle ear [5, 7]. One of such pathologies is cholesteatoma that is an abnormal accumulation of keratinized squamous epithelium inside the ear. It has a destructive effect on the auditory structures causing their inflammation that might eventually lead to erosion of the bone. Therefore, a timely treatment is required, involving surgical removal of the cholesteatoma [48].

Epidemiological data revealed that cholesteatomas occur more often in Caucasian than African or Asian populations. The cholesteatoma affects all age groups. The annual incidence of cholesteatoma is estimated to be about 3 per 100,000 in children and about 9 to 12 per 100,000 in adults, with a male predominance (1.4:1) [39]. However, its occurrence has changed over time, and varies across countries showing different annual trends [27, 47]. Moreover, this disease can manifest unilaterally or bilaterally. The bilateral occurrence of cholesteatomas has been found in 10–20% of cases, male children and adolescents are affected more often than females [47].

Although cholesteatoma has been recognised for more than three centuries [20], the nature of this disorder has yet not been fully determined, particularly the factors regulating its progression [28]. Some studies revealed that sex predilection for cholesteatoma might be dependent on the expression of female sex hormone receptors in the middle ear that act as an auditory protectant [43]. It has also been noted that various expression of genes may control pathogenesis of cholesteatomas [3, 29, 40].

Pathophysiological and epidemiological data encourage undertaking various studies aimed at identifying factors that favour implantation of cholesteatoma, and those that restrict its complete removal from the middle ear. It is particularly true for its excision from the ST which is regarded as the so-called "hidden structure in the ear," and endoscopic and surgical access to its interior can be troublesome. Therefore, detailed three-dimensional (3D) presentation of the ST topography and anatomy may enhance perspectives in treating cholesteatoma, which often invades this part of the middle ear.

In the recent years, high-resolution computed tomography (CT) and endoscopic examinations have been used to show the internal anatomy of the ear [14, 15]. These imaging techniques allow to perceive morphological changes related to the ear pathologies or structural malformations important from the clinical point of view. Notwithstanding, some anatomical details can be omitted in visual assessment or hardly recognised due to limited spatial imaging attained in clinical tomography or due to limited field of view during an endoscopic inspection.

In pre-clinical studies such technical limitations of viewing anatomical structures in detail can hinder appropriate evaluation of the morphological variants, especially if their dimensions are in range of a millimetre or even less. Formerly, only manual sectioning of the ear could reveal the entire spectrum of its morphological details and varieties [25]. Nowadays, this tedious and time consuming procedure has been substituted by the micro-computed tomography (micro-CT) which delivers images with microscopic precision. Hence, series of the micro-CT scans allows to perform 3D reconstructions of the studied samples and to section them virtually in order to display their internal morphology [18, 44].

Therefore, in the present study the authors applied micro-CT imaging of the ST, so as to display its anatomy in the 3D mode. The said approach facilitated multidirectional viewing and comparison of its morphological features, allowing for their subsequent assessment and classification of possible variations.

MATERIALS AND METHODS

Three-dimensional imaging of the ST was performed on 44 adult temporal bones (25 male and 19 female of Caucasian origin) whose age at death ranged from 30 to 70 years. The examined bones have been dated back to the XVIIth century. In order to obtain the temporal bones, we used fragmented human skulls found during archaeological excavations conducted in the Southern Poland that were deposited in the Department of Anatomy of the Jagiellonian University Medical College. Henceforth, no skulls were neither deliberately damaged nor destroyed in order to conduct the present study. The specimens were well preserved and did not show any pathological

changes, nor deformations that would exclude them from the present study.

The petrous part was cut off from each temporal bone and scanned with micro-CT using a Nanotom 180N equipped with 180 kV/15 W ultra-high performance nanofocus X-ray tube, with set parameters: I = 250 μA and V = 70 kV (GE Sensing & Inspection Technologies Phoenix X-ray Gmbh). The tomograms were registered on a Hamamatsu 2300 × 2300 pixel detector.

The reconstructions of the scanned specimens were created with the aid of the GE software datosX ver. 2.1.0 using the Feldkamp algorithm [22]. The obtained micro-CT scans had dimensions of 1796 × × 2284 × 1100 pixels, whereas the image pixel size was 18.6 μm. The post-reconstruction data processing included: denoising, cropping and 16 to 8 bit conversion, performed by the means of the VGStudio Max 2.1 software (https://www.volumegraphics.com).

In order to obtain stand alone 3D models of the ST, serial micro-CT scans of the petrous bone images representing the retrotympanum were segmented with the help of the thresholding algorithm. This procedure was performed with the aid of the 3D Slicer software (https://www.slicer.org) which is a free, open source package dedicated for medical and biomedical applications [21].

In the next step, the Autodesk Meshmixer free software (https://www.meshmixer.com) was used for virtual extraction of the ST from the retrotympanum and other anatomical structures included in the initial 3D model of the petrous bone. Such pre-prepared 3D models of the retrotympanum with the ST were displayed on the computer screen and processed interchangeably by the means of Meshlab and Meshmixer software to obtain isolated 3D models of the ST. Using clipping planes and tools dedicated for virtual cutting of the 3D models, the authors removed these parts of the model which occluded the ST. The MeshLab software (https://www.meshlab.net) was indispensable for accomplishing the 3D model of the ST represented by the mesh of triangles, stored in the STL file format [17].

With the aid of the MeshLab software, the authors decimated and smoothed the original mesh of triangles representing the retrotympanum which was further used for creating the final 3D model of the ST. Mesh decimation reduces the number of vertices, edges, and triangles in a mesh, thus the file including 3D model attains smaller size and can be processed quicker by the computer software [6]. Decimation was necessary because the original meshes approximating geometrical configuration of the entire retrotympanum consisted of a huge number of triangles (in the order of 10 million) which tremendously effected the size of the STL files. In our material, the size of the original STL files ranged approximately from 300 Mb to 500 Mb, whereas decimated meshes by half yielded twice smaller files but still preserved the mesh's topology. To simplify the initial mesh of the triangles we applied quadratic edge collapse decimation strategy implemented in the MeshLab software [24]. Thus, the target meshes representing standalone 3D models of the ST usually comprised 20,000–100,000 triangles, depending on the volume of the ST.

The mesh smoothing reduced noise in the model surface and resulted in a more user friendly visual perception. For this purpose, the authors applied the Laplacian smoothing algorithm which creates a new mesh according to local information on the position of the vertexes in the mesh [32]. However, this operation was taken with the outmost precaution, because the smoothing algorithm may inadvertently alter the surface properties of the object and shrink the mesh. To prevent the unwanted changes of the mesh geometry, the authors experimentally adjusted the smoothing force at each iteration applied for mesh processing and compared the changes with reference to the original mesh topology. This was a crucial step in the present study in order to obtain reliable results of visual observations of the ST's interior. Overly smoothened model may erroneously reflect geometrical and morphological properties of the anatomical structures due to extreme elimination of tiny elements like spikes, folds or depressions which naturally exist on the ST's surface.

The process of creating 3D models used for evaluation ST's morphology has been visualized in the flowchart (Fig. 1).

By rotating the 3D models and viewing the ST at different angles on the computer screen, the authors evaluated resemblance of their shapes to geometrical figures. In truth, the shapes reflected by the 3D models should be considered to be virtual endocasts of the STs.

Surface configuration of the ST's interior was evaluated visually with reference to the material texture (smooth — homogeneous, rough — heterogeneous). Outstanding features characteristic for the ST configuration were measured on the 3D models by means of the ruler tool available in the MeshLab software.

The occurrence of each anatomical variant of the ST was estimated as the percentage of the defined

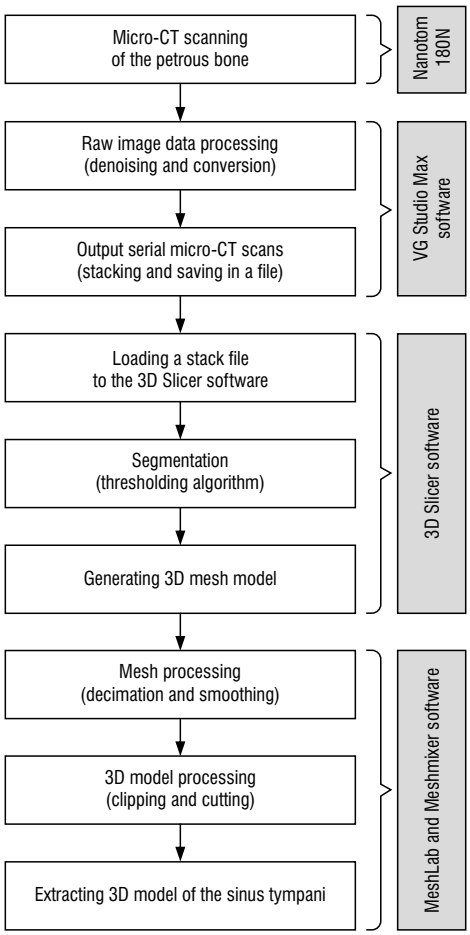

Figure 1. The flowchart of the three-dimensional (3D) model generation from micro-computed tomography (CT) scans.

types in the whole data set, determined separately for the female and male temporal bones. Statistical analysis was completed using a Fisher's exact test processed with the Statistica package ver. 13 (https://www.statsoft.pl). The level of statistical significance for the results was set at $p < 0.05$.

Ethical consideration

The study was conducted with approval (KBET/198/B/2014) of the Bioethics Committee of the Jagiellonian University.

RESULTS

For better orientation in the ST topography, the authors present a representative 3D model showing the location of the ST in relation to the surrounding osseous structures of both the middle and inner ear (Fig. 2).

Regarding the shape of the ST, the authors distinguished two basic morphological forms that were regarded as saccular or bowl. The saccular shaped ST characterizes postero-inferior elongation. This means that one of its diameters is considerably bigger than the other two. In turn, the bowl shaped ST resembles an irregular ovoid, in which three dimensions are similar (Fig. 3). The authors also found that the bowl shaped STs were usually wide and relatively shallow compared to the saccular types of the STs which were sitted deeply in the retrotympanum. The saccular STs

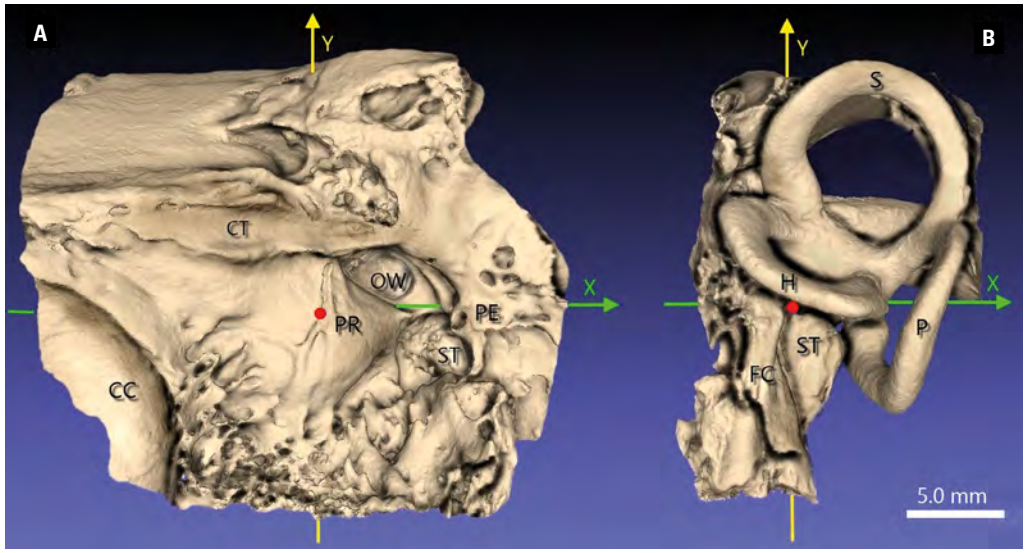

Figure 2. A. A three-dimensional model of the retrotympanum showing the location of the sinus tympani (ST) seen in the medial projection; CC — carotid canal; CT — canal of tensor tympani muscle; PR — promontory; OW — oval window; PE — pyramidal eminence; **B.** The same model rotated clockwise along the Y-axis; wall of the ST bulges posteriorly in the close proximity to the facial canal (FC) and semicircular canals: horizontal (H), posterior (P), superior (S). Orientation of the XYZ coordinate system follows as: the X-axis runs between the lower edge of the OW and the superior edge of the opening to the ST, the Y-axis corresponds to the descending portion of the FC, the Z-axis passes through the promontory (red point), perpendicularly to the X-Y axis.

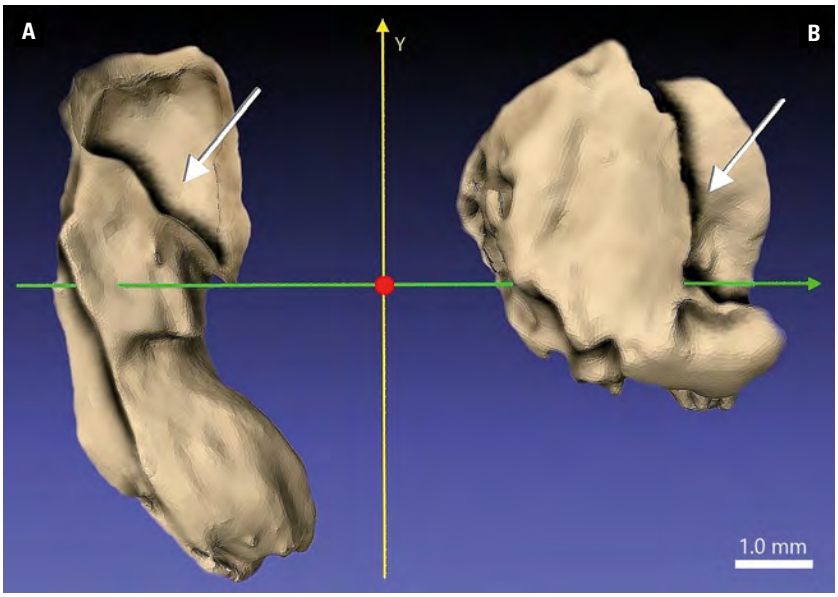

Figure 3. Three-dimensional models of the sinus tympani being of distinct shape: the saccular (**A**) and the bowl (**B**); the arrows indicate the entry to the interior of the sinus tympani.

were usually cylindrical in shape, except for a singular case in which a form, reseambling triangular pyramids (tetrahedra) of variable size, was noted (Fig. 4).

Regardless of the shapes of the STs, their interior structure revealed variable configuration which was defined as homogeneous or heterogeneous, depending on the presence or absence of tiny bony structures located in their walls (Fig. 5). The irregular bony structures found in the heterogeneous STs looked like: trabeculae, crests or laminae with diameters of around 1.0 mm. It should be noted that some of the heterogeneous STs were characterised by the presence of recesses or diverticula emerging from their walls. Such structural modifications were chiefly found in the saccular type of the STs. However, their existence was not included in the STs classification because their size and configuration did not affect the overall shape of the ST.

In turn, homogeneous configuration was attributed to these STs in which their interior was relatively smooth. Their walls were characterized by the lack of bony protrusions. Nonetheless, in some of them mild folds and depressions or pits were observed.

The present study demonstrated that both the saccular and bowl-shaped STs had a similar prevalence (47.7% and 52.3%, respectively) in the combined sex analysis. Furthermore, the authors did not find significant differences between the occurrence of these shapes in the male and female subgroups (Fisher's exact test, $p = 0.557$). As for the internal characteristics of the ST, the heterogeneous surface was typical for the entire sample (70.5%), whereas homogeneous surface was less common with respect to all the samples (29.5%); however, almost half of the female subgroup (47.4%) was characterized with the latter type of the ST. Although male STs were largely heterogeneous (84.0%), their prevalence just about predominated in females (52.6%). The differences in prevalence of the homogeneous and heterogeneous surfaces of the STs in male and female subgroups were statistically significant (Fisher's exact test, $p = 0.044$). The percentage of all observed morphological variants of the ST in male and female subgroups are graphed in Figure 6 and presented in Table 1.

Finally, the authors estimated the number of cases in which the ST revealed a combination of the following morphological features: saccular shape and heterogeneous surface. Such a complex anatomy may hinder surgical operations and lead to pathological processes by facilitating the harbouring of pathogens. Among all the examined sinuses, 36.4% involved this specific anatomy (Table 2). However, the said combination occurred in 13 out of 25 male samples (52.0%), whereas only 3 out of 19 (15.8%) female samples had this composition, a statistically significant difference (Fisher's exact test, $p = 0.025$).

DISCUSSION

So far, morphological variation of the ST has been evaluated utilising either CT or endoscopic images, or dissected temporal bones. Therefore, its evaluation

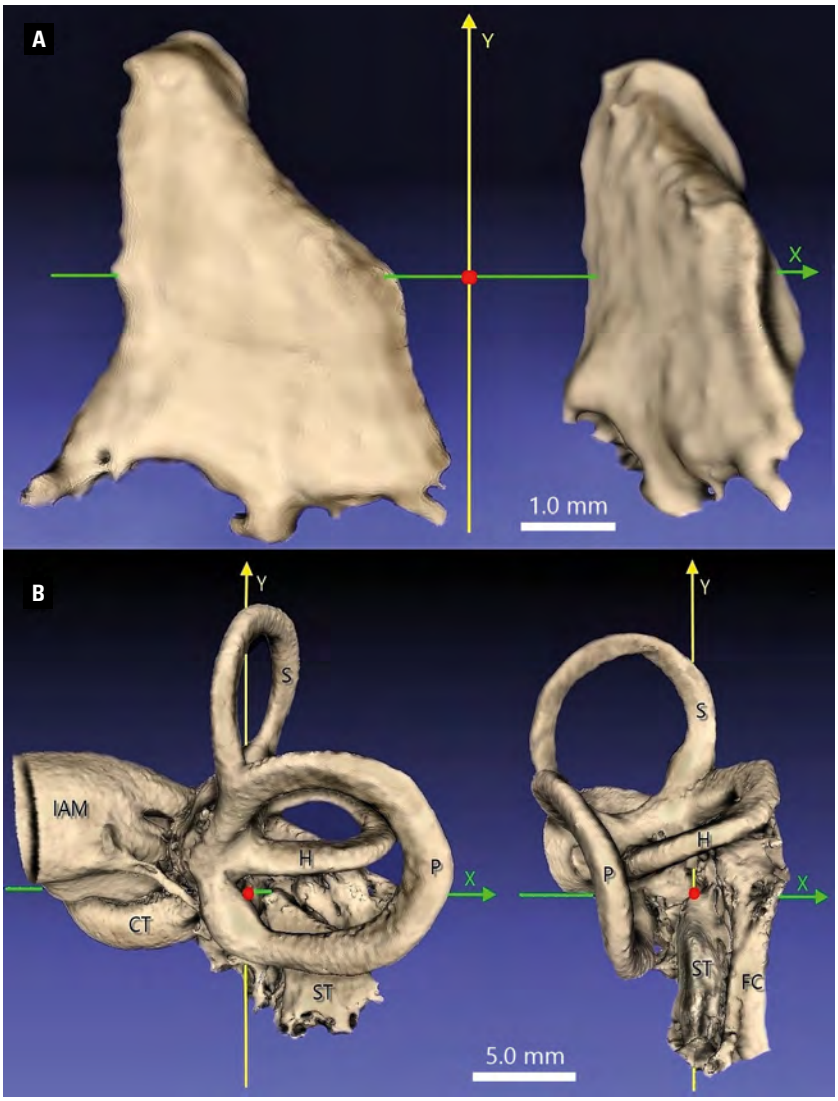

Figure 4. A. The three-dimensional (3D) model of the specific saccular type of sinus tympani (ST) resembling a tetrahedron in shape, seen in both lateral and posterior projection; **B.** A 3D model displaying topography of the ST in reference to the semicircular canals: posterior (P) — horizontal (H), superior (S) and the facial canal (FC); the cochlear turn (CT) and the internal acoustic meatus (IAM) were also identified.

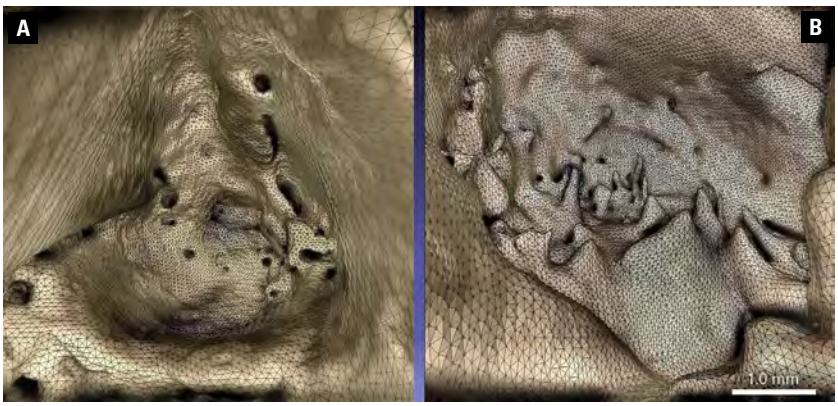

Figure 5. Three-dimensional models showing different internal characteristics of the sinus tympani (ST), approximated by the mesh of triangles; **A.** Homogeneous configuration of the ST. The inner surface is relativly smooth. It is possible to notice tiny pits and small pockets; **B.** Heterogeneous configuration of the ST. The inner surface is rough and irregular; bony spikes, protuberances and creases protrude from the wall of the ST into its lumen, therefore resemble small hillocks and valleys.

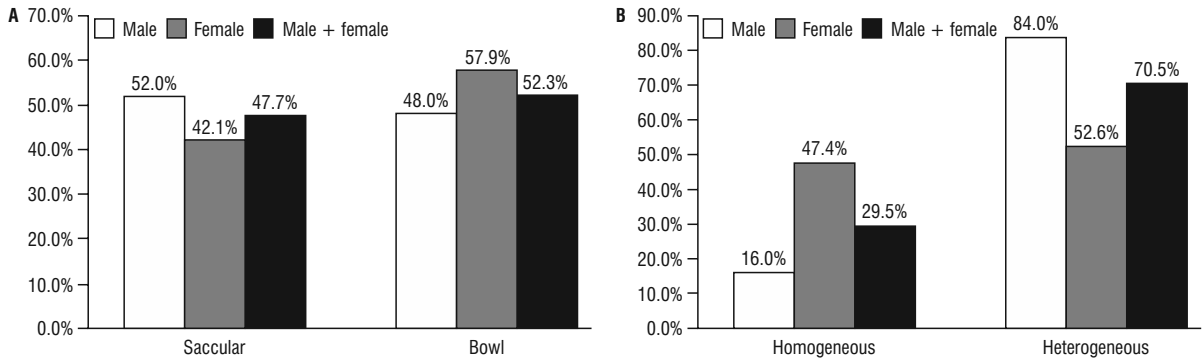

Figure 6. Percentage values of the morphological variants of the sinus tympani, classified according to shape (**A**) and surface (**B**) configuration in male and female temporal bones, respectively.

Table 1. Percentage of the morphological variants of the sinus tympani

Sex	Shape				Surface configuration			
	Saccular		Bowl		Homogeneous		Heterogeneous	
	N	%	N	%	N	%	N	%
Male (n = 25)	13	52.0	12	48.0	4	16.0	21	84.0
Female (n = 19)	8	42.1	11	57.9	9	47.4	10	52.6
Male + female (n = 44)	21	47.7	23	52.3	13	29.5	31	70.5

Table 2. Percentage of the combined variants (shape and surface configuration) of the sinus tympani

Sex	Saccular and homogeneous		Saccular and heterogeneous		Bowl and homogeneous		Bowl and heterogeneous	
	N	%	N	%	N	%	N	%
Male (n = 25)	0	0	13	52.0	4	16.0	8	32.0
Female (n = 19))	5	26.3	3	15.8	4	21.1	7	36.8
Male + female (n = 44)	5	11.4	16	36.4	8	18.2	15	34.1

was actually limited to the description of only the shape of the ST's orifice visible on the dry specimens, or the ST was assessed in the cross-sectional CT scans, or its interior was viewed by the means of endoscope [8, 10, 11, 15, 30, 35, 41].

Each of these techniques have some technical limitations which may hinder detailed evaluation of the STs' shapes, especially in the 3D way, as neither are capable of simultaneous display of the topographical relationships. Actually, this can be attained in volume renderings obtained from CT scans. Nevertheless clinical CT data are not accurate enough to create 3D reconstructions which could reveal ST anatomy and topography in great details. Therefore, the authors applied micro-CT for exploration of the ST anatomy because this modality offers extremely high spatial resolution for imaging objects which dimensions range on a millimetre scale.

The present study revealed that both the shape of the ST and its interior surface configuration vary considerably amongst human adults. The factors affecting the shape and volume of the ST still remain unclear; however, degree of the temporal bone pneumatisation is regarded as one of the physiological reasons that can affect the retrotympanum, as well as the ST itself [10, 26].

Bekci et al. [10] noticed that the volume of the ST has been greater in patients with pneumatised petrous apex. In turn, Baklaci et al. [9] found that a well-pneumatised mastoid process is associated with a deep ST. The effect of pneumatisation on the ST's shape and size has also been noticed by Abou-Bieh and Haberkamp [1]. The aforementioned authors recognised a few types of the ST from CT scans of adult temporal bones, classified as: shallow (15.8%), deep (33.8%), and intermediate (50.5%).

Detailed descriptions of small cavities within the retrotympanum, including: the sinus subtympanicus, lateral tympanic sinus, and posterior tympanic sinus were presented by Cheiță et al. [16] and Marchioni et al. [33]; however, their studies did not include a description of the ST interior.

Up-to-date internal morphological features of the ST have only been briefly mentioned by Nitek et al. [37]. The said authors noticed presence of bony trabeculae within 3 of 30 examined samples, but they did not analyse their size and sex in which these structures occurred. Bonali et al. [13] reported on the rare existence (6%) of bony crests as part of a description of anatomical variants of the ST.

In principle, there is scanty information in the anatomical literature describing the internal morphology of the ST; therefore, this issue was raised in the present study. Our classification of the ST differs from those presented in literature, because it combines shape of the ST with its internal configuration. It is based on the anatomical features which seem to be clinically very important, hence explored in 3D space thanks to the virtual models which can be viewed from any direction. A huge number of triangles comprised in the mesh that approximated surface geometry of the ST and other structural components of the temporal bone provided accurate exhibit of their anatomical features.

Previous reports yield information about morphological features of the ST obtained usually from CT images or direct visual observations of the ST using endoscopes or operative microscopes. Thus, Cheiță et al. [16] performed endoscopic examinations and classified the ST as oval, rectangular, round, trapezoidal or rhomboidal. Nitek et al. [37] recognised the ST as either vertically oval, horizontally oval, round or polygonal. Wang et al. [49] used a CT analysis of the ST in patients with congenital aural atresia, and distinguished three types of the ST shape: cup, pear and boot-shaped. The boot-shaped ST was an unusual variant characterized by a large cavity, and appeared only in patients affected by congenital aural atresia. As part of an endoscopic study of the retrotympanum, Nogueira et al. [38] identified the ST to have the following shapes: classical, confluent, partitioned or restricted.

Our classification of the ST was simplified to two basic morphological types defined as: saccular or bowl. We assume that both saccular and bowl form of the ST results from individual developmental pattern of the retrotympanum, which might be slightly differentiated in females and males regarding the overall size of the temporal bone. The proposed division of the STs into two basic forms: saccular or bowl corresponds with the data presented by Niemczyk et al. [36] who recognized two main developmental forms of the ST — deep and shallow. In our classification, the saccular form of the ST has always been deep, due to its inferior elongation, whereas the bowl shaped ST were shallow and wide, in contrast to the saccular one.

Bilińska et al. [12] compared the ST shape to a trough. This seems to be a very general approximation of the variety of shapes the STs present, especially if magnified in the 3D space. Nevertheless, from the practical point of view classifications of the ST should be based on the morphological features which can impact surgical access to its interior (peculiar shape and size) or may promote progression of the pathological processes (configuration of the internal surface).

Therefore, explored here internal morphology of the ST by means of micro-CT expands knowledge about variation of bony structures that may exist inside the ST. Furthermore some of them may render clinical implications if they are extensively developed. Besides the bony trabeculae, the ST may contain spikes, crests, small depressions and recesses. The presence of the abovementioned structures was predominant in male STs (84.0%), significantly higher than their occurrence in females (52.6%), as confirmed by Fisher's exact test ($p = 0.044$). Accessory bony structures within the ST, such as secondary recesses emerging from its wall, complicate the anatomy of the ST — particularly in the case of the saccular shape. The possible implications of such a configuration include increased bacterial biofilm adherence to the irregular surface which may lead to middle ear inflammation [46].

It has been estimated that over 20 million people worldwide are afflicted with middle ear infection (otitis media), whereas approximately one-fourth of them have cholesteatoma [4].

According to Saunders et al. [45], bacterial biofilms are common in suppurative otitis media and infected cholesteatomas. The biofilm is most often produced by *Staphylococcus aureus* and *Pseudomonas aeruginosa*. Such biofilms have been found in 75–85% samples taken from patients with chronic middle ear infection associated with cholesteatoma [23, 45].

The rough surface of the ST may also favour the formation of cholesteatoma (abnormal skin growth),

and may prove to be an obstacle in irrigating it from the small cavities and recesses.

Effectively, complete removal may not be possible, due to the difficulties of reaching this region for endoscopic observation or surgery [7, 42, 48]. The literature suggests that the prevalence of cholesteatoma is 1.4 times greater in males than in females [31, 39]. In addition, epidemiological studies performed by Aquino et al. [4] showed that the incidence of cholesteatoma in males is predominant (64.7%) over females (35.3%). Very similar results concerning the prevalence of cholesteatoma were reported by Ajallouеyan [2] (64.0% male vs. 36.0% female).

In an attempt to find possible correlations, the present study included an investigation on the occurrence of a complex ST anatomy comprised of a saccular shape and heterogeneous surface. This combination of morphological features may constitute complications during surgical treatments, as they are the difficult to access. Furthermore, the irregularities of the ST wall favour pathological processes ongoing inside the ST. It was demonstrated that such type of the ST is more common in males (52.0%) than in females (15.8%), being statistically significant ($p = 0.025$). This morphological feature of the ST may explain the reason for the higher prevalence of cholesteatoma in males in juxtaposition to females. Thereby, a detailed anatomical demonstration of the ST may be beneficial for better understanding the interactions between ear structures and diseases, as well helpful for simulating the route for surgical access to the ST by presenting its potential anatomical variants and local variation of the inner surface configuration.

Limitations of the study

Nevertheless, we perceive some limitations of the performed study. Firstly, micro-CT imaging of the ST is only applicable for the specimens which have been removed from the human body; therefore, the proposed classification of the STs may be rather of cognitive meaning than serve directly in the clinical practice supported by the CT imaging of lower spatial resolution. Secondly, the assessed configuration of the ST interior reflects details of bony wall morphology without the inclusion of the mucosae, which is routinely observed during endoscopic examination. Lastly, the sample size used in the current study is too small in number in order to conclude objectively that only such types of the ST as have been recognized may exist in the general population.

Thereby, it would be valuable to perform similar studies on cadaveric temporal bones which preserve structures composed of soft tissues, and are numerous enough to be representative for each gender subset taken from the general population.

CONCLUSIONS

Micro-CT of the petrous bones yielded image data that allowed to build accurate 3D models of the ST and compare their shapes in 3D space.

Upon visual assessment, the STs typically revealed two distinct morphological forms classified as saccular and bowl, regarding their shapes. Hence, internal inspection of the ST allowed to recognise variable configuration of their walls, and define them as homogeneous or heterogeneous, depending on the presence or lack of tiny extensions or depressions localised on the walls of the ST.

A statistically significant difference was found between males and females for internal surface configuration, but not for the shape of ST. A complex combination of ST features composed of a saccular shape and heterogeneous surface seems to be clinically important. This may rise negative impact on health outcomes after surgery in the case of cholesteatoma, and may favour chronic pathological processes.

Acknowledgements

The authors would like to thank Andrzej Stanisz, M.Sc. from the Department of Bioinformatics and Telemedicine of the Jagiellonian University Medical College for his help with statistical analysis.

Funding

This study has been funded using Jagiellonian University Medical College statutory funds N41/ /DBS/000151.

Conflict of interest: None declared

REFERENCES

1. Abou-Bieh A, Haberkamp T. Sinus tympani: a practical classification. Otolaryngol Head Neck Surg. 2014; 151(S1), doi: 10.1177/0194599814541629a285.
2. Ajalloueyan M. Surgery in cholesteatoma: Ten years follow-up. Iran J Med Sci. 2006; 31(1): 37–40.
3. Albino AP, Reed JA, Bogdany JK, et al. Expression of p53 protein in human middle ear cholesteatomas: pathogenetic implications. Am J Otol. 1998; 19(1): 30–36, indexed in Pubmed: 9455944.
4. Aquino JE, Cruz Filho NA, de Aquino JN. Epidemiology of middle ear and mastoid cholesteatomas: study of 1146

cases. Braz J Otorhinolaryngol. 2011; 77(3): 341–347, doi: 10.1590/s1808-86942011000300012, indexed in Pubmed: 21739009.
5. Aslan A, Guclu G, Tekdemir I, et al. Anatomic limitations of posterior exposure of the sinus tympani. Otolaryngol Head Neck Surg. 2004; 131(4): 457–460, doi: 10.1016/j.otohns.2004.03.028, indexed in Pubmed: 15467617.
6. Attene M, Campen M, Kobbelt L. Polygon mesh repairing: an application perspective. ACM Comput. Surv. 2013; 45(2): 1–33, doi: 10.1145/2431211.2431214.
7. Badr-El-Dine MM. Surgery of sinus tympani cholesteatoma: endoscopic necessity. Int Adv Otol. 2009; 5(2): 158–165.
8. Baki F, Dine M, Saiid I, et al. Sinus tympani endoscopic anatomy. Otolaryngol Head Neck Surg. 2016; 127(3): 158–162, doi: 10.1067/mhn.2002.127588, indexed in Pubmed: 12297804.
9. Baklaci D, Kuzucu I, Guler I, et al. Effect of mastoid bone pneumatization on the conformation and depth of the sinus tympani, a high-resolution computed tomography study. Surg Radiol Anat. 2019; 41(8): 921–926, doi: 10.1007/s00276-019-02246-3, indexed in Pubmed: 31037347.
10. Bekci T, Hizli O, Ozturk M, et al. Quantitative three-dimensional computed tomography analysis of sinus tympani volume in temporal bones with petrous apex pneumatization. Auris Nasus Larynx. 2020; 47(4): 587–592, doi: 10.1016/j.anl.2020.01.009, indexed in Pubmed: 32057525.
11. Bennett ML, Zhang D, Labadie RF, et al. Comparison of middle ear visualization with endoscopy and microscopy. Otol Neurotol. 2016; 37(4): 362–366, doi: 10.1097/MAO.0000000000000988, indexed in Pubmed: 26945313.
12. Bilińska M, Wojciechowski T, Sokołowski J, et al. Analysis of tympanic sinus shape for purposes of intraoperative hearing monitoring: a microCT study. Surg Radiol Anat. 2022; 44(2): 323–331, doi: 10.1007/s00276-021-02859-7, indexed in Pubmed: 34817623.
13. Bonali M, Anschuetz L, Fermi M, et al. The variants of the retro- and hypotympanum: an endoscopic anatomical study. Eur Arch Otorhinolaryngol. 2017; 274(5): 2141–2148, doi: 10.1007/s00405-017-4492-0, indexed in Pubmed: 28243781.
14. Bonali M, Fermi M, Alicandri-Ciufelli M, et al. Correlation of radiologic versus endoscopic visualization of the middle ear: implications for endoscopic ear surgery. Otol Neurotol. 2020; 41(9): e1122–e1127, doi: 10.1097/MAO.0000000000002787, indexed in Pubmed: 32925849.
15. Burd C, Pai I, Connor S. Imaging anatomy of the retrotympanum: variants and their surgical implications. Br J Radiol. 2020; 93(1105): 20190677, doi: 10.1259/bjr.20190677, indexed in Pubmed: 31593485.
16. Cheiță AC, Măru N, Mogoantă CA, et al. The recesses of the retro-tympanum. Rom J Morphol Embryol. 2010; 51(1): 61–68, indexed in Pubmed: 20191121.
17. Cignoni P, Callieri M, Corsini M, et al. MeshLab: an open-source mesh processing tool. Proceedings of the Eurographics Italian Chapter Conference. The Eurographics Association. 2008: 129–136, doi: 10.2312/LocalChapterEvents/ItalChap/ItalianChapConf2008/129-136.
18. Dalchow CV, Weber AL, Yanagihara N, et al. Digital volume tomography: radiologic examinations of the temporal bone. Am J Roentgenol. 2006; 186(2): 416–423, doi: 10.2214/AJR.04.1353, indexed in Pubmed: 16423947.
19. Donaldson JA, Anson BJ, Warpeha RL, et al. The surgical anatomy of the sinus tympani. Arch Otolaryngol. 1970; 91(3): 219–227, doi: 10.1001/archotol.1970.00770040325003, indexed in Pubmed: 5414075.
20. Du Verney JG. Traité de l'Organe de l'Ouie. E Michaillet, Paris, France 1683.
21. Fedorov A, Beichel R, Kalpathy-Cramer J, et al. 3D Slicer as an image computing platform for the Quantitative Imaging Network. Magn Reson Imaging. 2012; 30(9): 1323–1341, doi: 10.1016/j.mri.2012.05.001, indexed in Pubmed: 22770690.
22. Feldkamp LA, Davis LC, Kress JW. Practical cone-beam algorithm. J Opt Soc Am. 1984; 1(6): 612, doi: 10.1364/josaa.1.000612.
23. Galli J, Calò L, Giuliani M, et al. Biofilm's role in chronic cholesteatomatous otitis media: a pilot study. Otolaryngol Head Neck Surg. 2016; 154(5): 914–916, doi: 10.1177/0194599816630548, indexed in Pubmed: 26932953.
24. Garland M, Heckbert P. Surface simplification using quadric error metrics. Proceedings of the 24th annual conference on Computer graphics and interactive techniques. SIGGRAPH '97. ACM Press/Addison-Wesley Publishing Co. 1997: 209–216, doi: 10.1145/258734.258849.
25. Harada T, Ishii S, Tayama N. Three-dimensional reconstruction of the temporal bone from histologic sections. Arch Otolaryngol Head Neck Surg. 1988; 114(10): 1139–1142, doi: 10.1001/archotol.1988.01860220073027, indexed in Pubmed: 3415822.
26. Hool SL, Beckmann S, Hakim A, et al. Variability of the retrotympanum and its association with mastoid pneumatization in cholesteatoma patients. Eur Arch Otorhinolaryngol. 2023; 280(1): 131–136, doi: 10.1007/s00405-022-07465-w, indexed in Pubmed: 35695918.
27. Im GiJ, do Han K, Park KHo, et al. Rate of chronic otitis media operations and cholesteatoma surgeries in South Korea: a nationwide population-based study (2006-2018). Sci Rep. 2020; 10(1): 11356, doi: 10.1038/s41598-020-67799-5, indexed in Pubmed: 32647201.
28. Jovanovic I, Zivkovic M, Jesic S, et al. Non-coding RNA and cholesteatoma. Laryngoscope Investig Otolaryngol. 2022; 7(1): 60–66, doi: 10.1002/lio2.728, indexed in Pubmed: 35155784.
29. Jung MH, Lee JH, Cho JG, et al. Expressions of caspase-14 in human middle ear cholesteatoma. Laryngoscope. 2008; 118(6): 1047–1050, doi: 10.1097/MLG.0b013e3181671b4d, indexed in Pubmed: 18520823.
30. Karchier EB, Niemczyk K, Orłowski A. Comparison of visualization of the middle ear by microscope and endoscopes of 30° and 45° through posterior tympanotomy. Wideochir Inne Tech Maloinwazyjne. 2014; 9(2): 276–281, doi: 10.5114/wiitm.2014.41618, indexed in Pubmed: 25097700.
31. Kemppainen HO, Puhakka HJ, Laippala PJ, et al. Epidemiology and aetiology of middle ear cholesteatoma. Acta Otolaryngol. 1999; 119(5): 568–572, doi: 10.1080/00016489950180801, indexed in Pubmed: 10478597.
32. Lipman Y, Sorkine O, Alexa M, et al. Laplacian framework for interactive mesh editing. Int J Shape Model. 2005; 11(01): 43–61, doi: 10.1142/s0218654305000724.
33. Marchioni D, Alicandri-Ciufelli M, Piccinini A, et al. Inferior retrotympanum revisited: an endoscopic anatomic study.

Laryngoscope. 2010; 120(9): 1880–1886, doi: 10.1002/lary.20995, indexed in Pubmed: 20715093.
34. Marchioni D, Alicandri-Ciufelli M, Pothier DD, et al. The round window region and contiguous areas: endoscopic anatomy and surgical implications. Eur Arch Otorhinolaryngol. 2015; 272(5): 1103–1112, doi: 10.1007/s00405-014-2923-8, indexed in Pubmed: 24510236.
35. Marchioni D, Valerini S, Mattioli F, et al. Radiological assessment of the sinus tympani: temporal bone HRCT analyses and surgically related findings. Surg Radiol Anat. 2015; 37(4): 385–392, doi: 10.1007/s00276-014-1366-7, indexed in Pubmed: 25173355.
36. Niemczyk K, Nitek S, Wysocki J, et al. [Anatomy of sinus tympani]. Otolaryngol Pol. 2003; 57(3): 389–393, indexed in Pubmed: 14524183.
37. Nitek S, Wysocki J, Niemczyk K, et al. The anatomy of the tympanic sinus. Folia Morphol. 2006; 65(3): 195–199, indexed in Pubmed: 16988915.
38. Nogueira JF, Mattioli F, Presutti L, et al. Endoscopic anatomy of the retrotympanum. Otolaryngol Clin North Am. 2013; 46(2): 179–188, doi: 10.1016/j.otc.2012.10.003, indexed in Pubmed: 23566904.
39. Olszewska E, Wagner M, Bernal-Sprekelsen M, et al. Etiopathogenesis of cholesteatoma. Eur Arch Otorhinolaryngol. 2004; 261(1): 6–24, doi: 10.1007/s00405-003-0623-x, indexed in Pubmed: 12835944.
40. Park K, Moon SK, Choung YH, et al. Expression of beta-defensins in human middle ear cholesteatoma. Acta Otolaryngol. 2003; 123(2): 236–240, doi: 10.1080/0036554021000028102, indexed in Pubmed: 12701748.
41. Parlier-Cuau C, Champsaur P, Perrin E, et al. High-resolution computed tomographic study of the retrotympanum. Anatomic correlations. Surg Radiol Anat. 1998; 20(3): 215–220, doi: 10.1007/BF01628898, indexed in Pubmed: 9706682.
42. Pulec J. Sinus tympani: retrofacial approach for the removal of cholesteatomas. Ear Nose Throat J. 1996; 75(2): 77–88, doi: 10.1177/014556139607500207.
43. Raynov AM, Choung YH, Moon SK, et al. Expression of female sex hormone receptors in human middle-ear cholesteatomas. J Laryngol Otol. 2005; 119(12): 941–945, doi: 10.1258/002221505775010878, indexed in Pubmed: 16354354.
44. Ritman EL. Current status of developments and applications of micro-CT. Ann Rev Biomed Eng. 2011; 13: 531–552, doi: 10.1146/annurev-bioeng-071910-124717, indexed in Pubmed: 21756145.
45. Saunders J, Murray M, Alleman A. Biofilms in chronic suppurative otitis media and cholesteatoma: scanning electron microscopy findings. Am J Otolaryngol. 2011; 32(1): 32–37, doi: 10.1016/j.amjoto.2009.09.010, indexed in Pubmed: 20036033.
46. Scheuerman TR, Camper AK, Hamilton MA. Effects of substratum topography on bacterial adhesion. J Colloid Interface Sci. 1998; 208(1): 23–33, doi: 10.1006/jcis.1998.5717, indexed in Pubmed: 9820746.
47. Thomas JP, Volkenstein S, Minovi A, et al. [Current aspects of paediatric cholesteatomas]. HNO. 2013; 61(5): 380–387, doi: 10.1007/s00106-012-2641-8, indexed in Pubmed: 23463409.
48. Toran KC, Shrestha S, Kafle P, et al. Surgical management of sinus tympani cholesteatoma. Kathmandu Univ Med J (KUMJ). 2004; 2(4): 297–300, indexed in Pubmed: 16388240.
49. Wang Z, Hou Q, Wang Pu, et al. The image variations in mastoid segment of facial nerve and sinus tympani in congenital aural atresia by HRCT and 3D VR CT. Int J Pediatr Otorhinolaryngol. 2015; 79(9): 1412–1417, doi: 10.1016/j.ijporl.2015.06.014, indexed in Pubmed: 26164212.

VIA MEDICA

ORIGINAL ARTICLE

Folia Morphol.
Vol. 82, No. 4, pp. 909–920
DOI: 10.5603/FM.a2022.0093

ISSN 0015–5659
eISSN 1644–3284
journals.viamedica.pl

Air spaces of the temporal bone: a morphometric analysis with clinical implications

E. Szczepanek[1, 2, 3], P. Ostrowski[1], D. Rams[1], M. Bonczar[1], J. Batko[1], W. Wojciechowski[4], K. Niemczyk[2], J. Walocha[1], M. Koziej[1]

[1]*Department of Anatomy, Jagiellonian University Medical College, Krakow, Poland*
[2]*Department of Ortholaryngology and Head and Neck Surgery, Medical University of Warsaw, Poland*
[3]*Doctoral School in Medical Sciences and Health Sciences, Jagiellonian University Medical College, Krakow, Poland*
[4]*Department of Radiology, Jagiellonian University Medical College, Krakow, Poland*

[Received: 31 July 2022; Accepted: 5 October 2022; Early publication date: 28 October 2022]

Background: *The main objective of the present study was to analyse the morphological variations of the air spaces of the temporal bone, that is, the pneumatized and air-filled spaces of the temporal bone cavities.*

Materials and methods: *A total of 99 sides were analysed. Temporal bone pneumatic spaces (TBPS) were defined as the free spaces inside the cavities of the temporal bone filled with air, excluding the volume of the structures present in the investigated region. Total volumes of TBPS were calculated as the sum of total volumes of mastoid air cells (MAC), tympanic cavity (TC), and external auditory canal (EAC). Analyses were performed considering the general population and the female and male subgroups.*

Results: *The overall results obtained on Polish population were set as follows: the median total volume of TBPS was demonstrated at 7882.58 mm³ (lower quartile [LQ]: 6200.56 mm³; higher quartile [HQ]: 10393.16 mm³). The median volume of MAC was set at 5813.05 mm³ (LQ: 4224.94 mm³; HQ: 8181.81 mm³). The median of the total volume of the EAC was demonstrated at 1294.36 mm³ (LQ: 1099.68 mm³; HQ: 1627.84 mm³).*

Conclusions: *In the present study, the morphometric properties of the temporal bone cavities were analysed. The results showed that the total volume of the MAC was, on average, lower in women than in men. This should be taken into account when performing procedures on the mastoid, such as mastoidectomies. It is hoped that the results of this study can help reduce potential surgical complications associated with otological procedures.* (Folia Morphol 2023; 82, 4: 909–920)

Key words: temporal bone, temporal bone trauma, laryngeal anatomy and physiology, external ear

INTRODUCTION

The temporal bone is a complex structure that contains a network of pneumatic spaces and typically consists of four parts: squamous, petromastoid, tympanic, and styloid processes [40]. Pneumatization refers to the development of air-filled cavities in the bone, where the epithelium infiltrates the developing bone, resulting in the formation of air cell cavities [18]. The air cells are typically lined by a single layer of epithelium divided from bone by subepithelial

Address for correspondence: Dr. M. Koziej, Department of Anatomy, Jagiellonian University Medical College, ul. Mikołaja Kopernika 12, 33–332 Kraków, Poland, tel: +48 888 202 628, e-mail: mateusz.koziej@gmail.com

connective tissue [33]. In 1969, Allam [2] was the first to; propose the classification of temporal bone pneumatization (TBP). He divided this system into: 1) mastoid pneumatization, 2) petrous pneumatization, and 3) accessory pneumatization (extending beyond the limits of the mastoid and petrous regions). Another classification of TBP was presented by Han et al. [17], which consisted of four groups according to the degree of pneumatization in relation to the sigmoid sinus: group 1 (hypopneumatization), group 2 (moderate pneumatization); group 3 (good pneumatization), and group 4 (hyperpneumatization). TBP begins prenatally, typically around 24 weeks of gestation [4, 33]. The process consists of three stages, which are the infantile, transitional, and adult stages. The development is usually completed at the age of 10 years in women and 15 years in men [13, 19].

The aeration of the temporal bone has many functions, such as reception of sound, preventing negative pressures, and avoiding changes in the middle ear mucosa, among others [23, 38, 44]. The extent to which pneumatization occurs in the temporal bone varies considerably, and numerous studies on TBP have been presented in the literature [10]. Gibelli et al. [16] conducted a study in which the degree of TBP was analysed. They emphasized that there are significant variations in the degree of pneumatization in some areas of the temporal bone, such as the petrous apex or the infralabyrinthine portion. In general, the squamous, petromastoid and tympanic parts are the most frequently pneumatized parts, but pneumatization may also be extended to the articular eminence of the zygomatic process [15]. These variations must be taken into account clinically, especially when planning surgical procedures in this area.

Air cavities of the temporal bone are areas of minimal resistance that allow the spreading of the pathologies within the temporal bone, e.g. cholesteatoma, cholesterol granuloma, and otitis media, among others [21, 37, 45]. Air cells can form connections with the surrounding cavities, such as mastoid air cells (MAC) connecting to the tympanic cavity (TC). However, this connection can be a pathway for infection to spread in cases of otitis media, resulting in possible mastoiditis [28]. On the other hand, increased TBP has been associated with fewer and less severe complications associated with temporal bone fractures [24, 28].

Having a good understanding of the variations in the morphometric properties of temporal bone cavities can help to choose the right surgical approach for various otorhinolaryngological procedures. Surgeons can apply this knowledge when performing procedures directly on the external acoustic canal (EAC) or on the tympanic membrane, such as myringoplasty [7]. There are different surgical approaches to choose from when performing this procedure. Similarly, knowledge of the morphometric characteristics of the mastoid cavity is necessary to perform mastoidectomies properly. Mastoidectomy is a common surgical procedure with multiple indications, and each mastoidectomy is unique due to variations in the TBP patterns [27].

Although many studies have investigated the degree of TBP, there is still a lack of data regarding the total volumes and morphometric properties of the different temporal bone cavities. Therefore, the main objective of the present retrospective study was to analyse the morphological variations of the air spaces of the temporal bone, i.e. the pneumatized and air-filled spaces of the temporal bone cavities. Additionally, the objective was to establish possible alliances and correlations between parameters, as well as to assess sexual dimorphism.

MATERIALS AND METHODS

A retrospective observational study was performed on 55 randomly selected computed tomography (CT) angiographies (CTA) of the head and neck region that were analysed in the Department of Radiology of Jagiellonian University Medical College, Krakow, Poland, in April 2022. In this study, CTAs were evaluated instead of CTs due to the greater availability of these results. All participants consciously agreed to the examination. The research protocol was submitted for evaluation and approved by the Bioethical Committee of Jagiellonian University, Krakow, Poland. Further stages of the study were carried out in accordance with the approved guidelines. The structure of the study group consisted of 99 temporal bones, of which 42 were from women and 57 from men, with a median age of 49.7. All patients were Polish. Each study was analysed bilaterally (110 cases). Exclusion criteria were established as follows: (1) head trauma affecting the air spaces of the ear and/or the surrounding anatomical area, (2) significant artifacts that prevented accurate and precise imaging and/or measurement (3) low quality and illegible images. Defects that met the exclusion criteria but included only one side of the CT, without interference with

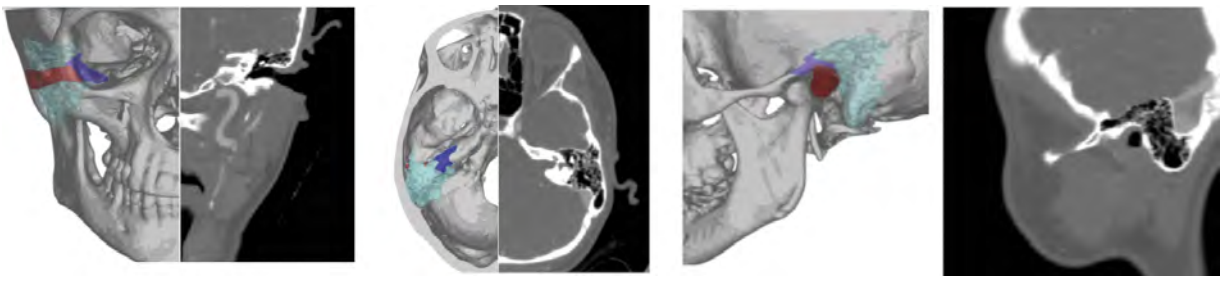

Figure 1. Three-dimensional representation of the studied region with computed tomography cross-section; red — external auditory canal; violet — tympanic cavity; turquoise — mastoid air cells.

the contralateral side, did not disqualify the entire CT, but only the affected side. Finally, a total of 99 sides were analysed.

Ethical approval

The research protocol was submitted for evaluation and approved by the Bioethical Committee of Jagiellonian University, Krakow, Poland.

CTA

The CTAs were performed on a 128-slice scanner CT (Philips Ingenuity CT, Philips Healthcare). The main CT imaging parameters were as follows: collimation/increment: 0.625/0.3 mm; tube current: 120 mAs; field of view: 210 mm; matrix size: 512 × × 512. All groups of patients received intravenous administration of contrast material at a dose of 1 mL/kg (standard dose). A non-ionic contrast medium (CM) containing 350 mg of iodine per mL was used (Jowersol 741 mg/mL, Optiray®, Guerbet, France). CT data acquisition was triggered using a real-time bolus-tracking technique (Philips Healthcare) with the region of interest placed in the ascending aorta. The CM was intravenously injected using a power injector at a flow rate of 5 mL/s. This was immediately followed by the injection of 40 mL of saline solution at the same flow rate. Following the injection of CM and saline, image acquisition was started automatically with a 2-s delay when the attenuation trigger value reached a threshold of 120 Hounsfield units (HU). Scanning was performed in the caudocranial direction.

Image processing

Biomedical data was processed by two experienced and independent investigators and a qualified senior radiologist was also consulted. Anonymised source files in DICOM format were imported into specialised software (Mimics Innovation Suite 22; Materialise, Plymouth, MI, USA). Individual multilayer graphic masks in the region of corresponding anatomical structures were created with built-in semiautomatic algorithms using technique of the maximum intensity projection based on the corresponding HU range. Additionally, in each study, a three-dimensional reconstruction was performed to obtain a better volume match. Any distortions that could have caused an error were manually removed.

Measurements

The exact representation of the measurements is illustrated in Figures 1 and 2. Each measurement was performed twice, with an accuracy to the second decimal place, and a mean result was established afterwards. In further statistics, the mean values were taken into account. In the present study, temporal bone pneumatic spaces (TBPS) were defined as the free spaces within the temporal bone cavities filled with air, excluding the volume of the structures presented in the investigated region. The total volumes of the TBPS were calculated as the sum of the total volumes of MAC, TC, and EAC. Then the percentage value of each component was calculated. MAC were designated as the enclosed spaces within the mastoid process of the temporal bone along with the canal leading to the entrance to the tympanic antrum, just above the epitympanic recess. Porous spaces that originated mainly from the MAC and extend beyond the mastoid process were also included. The TC was bounded by six entities: the medial labyrinthic wall, the lateral wall with the tympanic membrane taking into account its angle of inclination, the roof bounded by the tegmen tympani, the floor demarcating the TC from the jugular fossa, the posterior wall with a cutoff point just above the epitympanic recess, and the anterior wall including the bony portion of the Eustachian tube. All EAC parameters were determined in the normal sagittal plane. A point inside

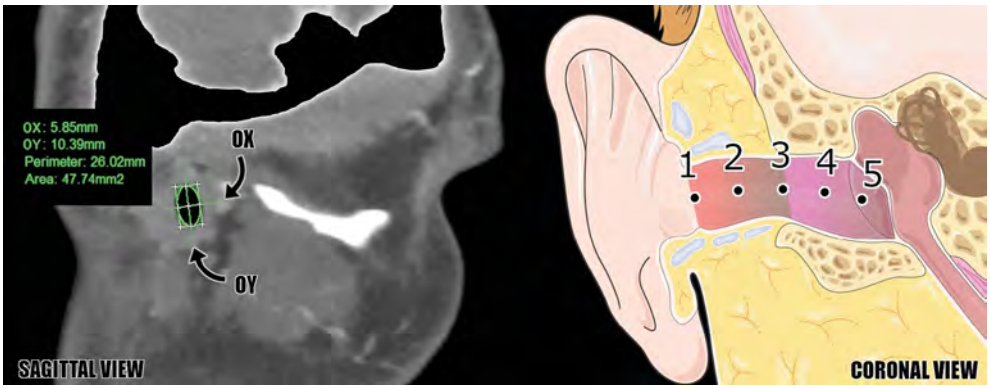

Figure 2. Location of measurement points for the external auditory canal (EAC) along with the evaluation method. 0X and 0Y denote the horizontal and vertical axes. Point 1 corresponds to the distal end of the EAC. Point 3 corresponds to the transition from the bone (bEAC) to the cartilage (cEAC). Point 5 is at the proximal end of the EAC and indicates the origin of the bEAC itself, not the dimensions of the eardrum itself. Points 2 and 4 are placed halfway between points 1–3 and 3–5. The evaluation in the sagittal section on the left side of the figure is shown at measurement point 1; pink gradient — bEAC; reddish gradient — cEAC.

the canal, just behind the tragus, inside the concha cavity, where the section of the canal takes a constant elliptical, oval, or round shape, was chosen as the lateral border. The tympanic membrane was chosen as the medial border, taking into account its angle of inclination. Furthermore, the EAC was divided into two parts corresponding to cartilage (cEAC) and bone (bEAC). The point of transition from cartilage to bone was determined as complete closure of the perimeter of the visible round contour in the proper section. The volume and surface area corresponding to the epithelium lining the EAC was determined with cEAC and bEAC. Compared to volume, the surfaces did not encase the included ends of the EAC. The length of the EAC was provided as the centre line to the canal wall, taking into account its curvature. The EAC also defines five locations where selected morphological parameters were assessed. Taking into account the measurements in the sagittal plane, the X-plane measurements corresponded to a range of +45 to –45 degrees with respect to the horizontal line, while the Y-plane measurements corresponded to the same range in the vertical plane. X1/Y1 corresponds to the site of the lateral border of the EAC, X3/Y3 corresponds to the site corresponding to the cartilaginous-bone transition, and X5/Y5 corresponds to the site just distal to the appearance of the tympanic membrane where the bEAC perimeter visible in cross section opens. X2/Y2 was determined in the cEAC halfway between X1/Y1 and X3/Y3, while X4/Y4 was determined in the bEAC halfway between X3/Y3 and X5/Y5. Furthermore, the cross-sectional area and perimeter were labelled for each point.

Statistical analysis

Statistical analysis was performed with SATISTICA v13.1 (StatSoft Inc., Tulsa, OK, USA). The frequencies and percentages presented qualitative features. The Shapiro-Wilk test was used to assess the normal distribution. Quantitative features were presented by medians and higher and lower quartiles (HQ, LQ). Statistical significance was defined as $p < 0.05$. The Spearman rank correlation coefficient was used to determine possible correlations between parameters. U Mann-Whitney and Wilcoxon signed-rank tests were used to establish potential differences between two groups. To detect a simple correlation ($r = 0.3$) with 80% power and a 5% significance level (two-tailed; $\alpha = 0.05$; $\beta = 0.2$), the minimal sample size was set at 85 cases.

RESULTS

Baseline characteristics

Analysis was carried out from every side in a total of 99 TBPS of 49 patients, between 15 and 82 years of age (mean age: 50 years old; standard deviation: 19.3), of which 42 TBPS (42.4%) were from women and 57 (57.6%) from men. The left sides were analysed in 50 (50.5%) cases and the right sides in 49 (49.5%) cases. All further descriptions, which refer to the names of the categories mentioned in the materials and methods section, are illustrated in Figure 3.

EAC results

Data on EAC were collected in 30 categories. For each category, analyses were performed considering the general population and the female and male

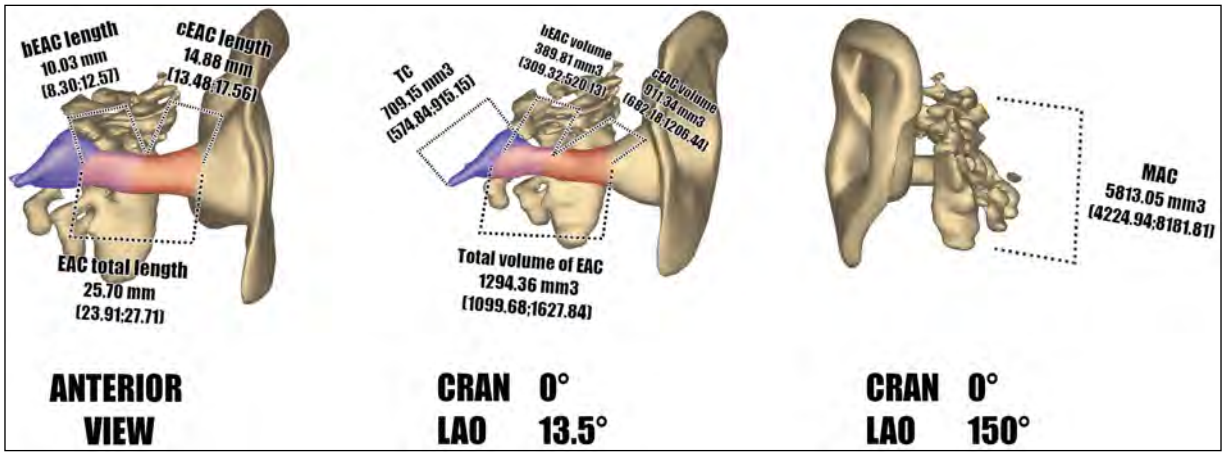

Figure 3. Results presented as a form of median with lower and higher quartile on a three-dimensional model. Pinna along with colours were added to emphasize the view; violet — tympanic cavity; pink gradient — bone external auditory canal; reddish gradient — cartilage external auditory canal; CRAN — cranial view; LAO — left anterior oblique view; rest abbreviations — see Table 1.

Table 1. Results of the measurements

Category	Median	LQ	HQ	Minimum	Maximum	Mean	SD
Total volume of TBPS [mm^3]	7882.58	6200.56	10393.16	2111.74	22589.79	8606.67	3595.39
MAC [mm^3]	5813.05	4224.94	8181.81	414.17	19528.21	6470.97	3442.69
TC [mm^3]	709.15	574.84	915.15	345.95	1342.18	750.12	221.16
Total volume of EAC [mm^3]	1294.36	1099.68	1627.84	658.12	2605.12	1385.59	403.76
EAC surface [mm^2]	711.24	626.40	815.11	425.88	1247.51	735.60	154.33
cEAC volume [mm^3]	911.34	682.18	1206.44	339.72	1962.02	960.87	342.50
cEAC surface [mm^2]	448.88	370.53	550.72	218.82	823.29	464.82	123.32
cEAC-to-EAC volume ratio	0.70	0.62	0.76	0.43	0.88	0.69	0.11
bEAC volume [mm^3]	389.81	309.32	520.13	150.14	1078.53	424.72	168.18
bEAC surface [mm^2]	264.52	206.12	332.61	112.19	520.10	270.78	86.68
EAC total length [mm]	25.70	23.91	27.71	19.87	34.80	25.98	3.05
cEAC length [mm]	14.88	13.48	17.56	9.22	21.86	15.45	2.80
bEAC length [mm]	10.03	8.30	12.57	4.97	18.18	10.53	2.95

LQ — lower quartile; HQ — higher quartile; SD — standard deviation; TBPS — temporal bone pneumatic spaces; MAC — mastoid air cells; TC — tympanic cavity; EAC — external acoustic canal; cEAC — cartilage part of the external acoustic canal; bEAC — bony part of the external acoustic canal

subgroups. For the general population, the median total volume of EAC was determined at 1294.36 mm^3 (LQ: 1099.68; HQ: 1627.84). The median surface of the EAC was set at 711.24 mm^2 (LQ: 626.40; HQ: 815.11). The median volume of cEAC was determined at 911.34 mm^3 (LQ: 682.18; HQ: 1206.44). The median surface of the cEAC was set at 448.88 mm^2 (LQ: 370.53; HQ: 550.72). The median length of the cEAC was demonstrated at 14.88 mm (LQ: 13.48; HQ: 17.56). The median volume of bEAC was set at 389.81 mm^3 (LQ: 309.32; HQ: 520.13). The median surface of the bEAC was demonstrated at 264.52 mm^2 (LQ: 206.12; HQ: 332.61). The median length of the bEAC was set to 10.03 mm (LQ: 8.30; HQ: 12.57). The of the EAC of the cartilage part surface was demonstrated at 64.00% of the EAC (LQ: 56.00%; HQ: 70.00%). The surface of the bone part of EAC was set at 36.00% of EAC (LQ: 30.00%; HQ: 44.00%). All the results mentioned above and more detailed values are presented in Table 1.

The median surface of the EAC was set at 75.75 mm^2 (LQ: 57.07; HQ: 89.94) at the site of its lateral border (X1/Y1); 44.82 mm^2 (LQ: 37.85; HQ: 53.97) in the cartilaginous-bone transition (X3/Y3); and 30.84 mm^2 (LQ: 26.59; HQ: 36.57) at the site just distal to the appearance of the tympanic membrane (X5/ /Y5). All mentioned above and more detailed results regarding all parameters are illustrated in Table 2.

Table 2. Results of the measurements

Category	Median	LQ	HQ	Minimum	Maximum	Mean	SD
EAC X1 [mm]	8.35	7.38	9.52	4.33	13.84	8.45	1.74
EAC Y1 [mm]	10.88	9.48	12.57	3.96	15.66	10.88	2.22
EAC P1 [mm^2]	31.13	27.94	34.16	15.78	39.44	30.63	4.61
EAC Area1 [mm^2]	75.75	57.07	86.94	19.28	119.77	72.46	20.44
EAC X2 [mm]	7.27	6.26	8.24	3.90	64.00	7.95	5.96
EAC Y2 [mm]	9.69	8.61	11.17	6.30	13.22	9.79	1.56
EAC P2 [mm^2]	26.51	24.40	29.68	2.03	37.41	27.02	4.63
EAC Area2 [mm^2]	53.27	43.79	65.47	25.84	109.30	56.91	17.45
EAC X3 [mm]	6.17	5.46	7.05	4.41	14.93	6.37	1.50
EAC Y3 [mm]	9.60	8.19	10.57	5.27	14.49	9.42	1.75
EAC P3 [mm^2]	25.08	22.53	27.18	16.07	37.36	25.16	3.84
EAC Area3 [mm^2]	44.82	37.85	53.97	20.00	98.43	47.31	14.44
EAC X4 [mm]	5.29	4.76	5.97	3.76	10.75	5.53	1.30
EAC Y4 [mm]	7.90	7.07	8.68	4.04	11.09	7.95	1.37
EAC P4 [mm^2]	20.88	19.52	23.08	14.87	32.31	21.44	2.82
EAC Area4 [mm^2]	32.43	27.68	39.88	16.86	82.25	34.33	9.84
EAC X5 [mm]	5.15	4.48	6.64	3.29	9.67	5.61	1.44
EAC Y5 [mm]	7.63	7.05	7.98	2.64	10.93	7.34	1.31
EAC P5 [mm^2]	20.40	19.17	21.90	14.91	29.03	20.58	2.56
EAC Area5 [mm^2]	30.84	26.59	36.57	14.51	66.79	31.97	9.46

LQ — lower quartile; HQ — higher quartile; SD — standard deviation; EAC — external auditory canal; Point 1 corresponds to the distal end of the EAC; Point 3 corresponds to the transition from the bEAC to cEAC part; Point 5 is located at the proximal end of the EAC; Points 2 and 4 were placed halfway between points 1-3 and 3-5; For detailed description of the points 1-5, please see the Materials and Methods section

Regarding all categories mentioned in Table 1, potential differences in EAC between men and women were analysed. The measurement results obtained from male cases were significantly higher in 8 of 10 categories ($p < 0.05$): (1) total volume of EAC, (2) surface of EAC, (3) volume of cEAC, (4) surface of cEAC, (5) volume of bEAC, (6) surface of bEAC, (7) total length of EAC, (8) length of cEAC. All results mentioned above and detailed values regarding sex differences are presented in Table 3.

Furthermore, potential correlations were established with respect to the EAC results between each of the categories. None of the EAC results correlated with age. However, some categories corresponded to each other. The correlations between the categories are summarized in Table 4.

Air spaces results

Data on the air spaces were collected in three categories. For each category, analyses were performed considering the general population and the female and male subgroups. For the general population, the median total volume of the TBPS was demonstrated at 7882.52 mm^3 (LQ: 6200.56; HQ: 10393.16). The median MAC volume was set to 5813 mm^3 (LQ: 4224.94; HQ: 8181.81). The medial TC volume was set at 709.15 mm^3 (LQ: 574.84; HQ: 915.15). All the results mentioned above and more detailed values are collected in Table 1.

Regarding the results of the measurements of the air spaces of the ear, potential differences between men and women were analysed. The measurement results obtained from male cases were significantly higher in 2 of 3 categories ($p < 0.05$): (1) total volume of TBPS and (2) volume of TC. All the aforementioned results and detailed values regarding sex differences are presented in Table 3.

Furthermore, potential correlations with the results of measurements of the airspaces of the ear were established between each of the categories. The total volume of TBPS was significantly inversely correlated with age ($R = –0.26$; $p < 0.05$). Furthermore, MAC volume was significantly inversely correlated with age ($R = –0.31$; $p < 0.05$). The correlations between the categories are summarized in Table 4.

Table 3. Results of measurements according to the sex of the patients. Highlighted in red are those parameters which were statistically significant ($p \leq 0.05$)

Category	Sex	Median	LQ	HQ	Minimum	Maximum	Mean	SD	P
Total volume of TBPS [mm^3]	Female	7262.26	6200.56	8869.95	3649.67	14291.01	7644.75	2307.27	0.04
	Male	8628.54	6340.25	11767.53	2111.74	22589.79	9315.45	4185.58	
MAC [mm^3]	Female	5646.36	4281.17	7007.97	1606.27	11752.44	5810.50	2174.48	0.22
	Male	6015.76	4224.94	9100.49	414.17	19528.21	6957.62	4087.92	
TC [mm^3]	Female	648.89	543.62	851.14	345.95	1342.18	705.17	231.57	0.05
	Male	745.42	619.30	915.15	439.09	1254.85	783.24	209.05	
Total volume of EAC [mm^3]	Female	1102.73	999.85	1253.41	658.12	1627.84	1129.08	220.13	0.00
	Male	1515.85	1290.45	1791.14	917.20	2605.12	1574.59	405.09	
EAC surface [mm^2]	Female	632.07	583.63	708.10	425.88	833.96	641.09	90.82	0.00
	Male	790.83	697.06	896.44	508.57	1247.51	805.24	154.95	
cEAC volume [mm^3]	Female	731.04	616.82	911.34	339.72	1401.31	767.36	238.29	0.00
	Male	1105.43	843.52	1356.76	499.86	1962.02	1103.46	339.01	
cEAC surface [mm^2]	Female	402.24	330.94	460.44	218.82	605.52	400.09	93.95	0.00
	Male	497.04	430.66	615.55	274.97	823.29	512.52	121.22	
cEAC-to-EAC surface ratio	Female	0.61	0.56	0.70	0.42	0.80	0.62	0.10	0.16
	Male	0.64	0.58	0.71	0.41	0.82	0.64	0.09	
bEAC volume [mm^3]	Female	367.57	276.82	425.72	150.14	636.59	361.73	111.45	0.00
	Male	430.10	318.20	584.28	198.75	1078.53	471.13	187.71	
bEAC surface [mm^2]	Female	258.55	196.04	282.63	112.19	382.16	241.00	64.99	0.01
	Male	272.88	216.06	360.77	139.76	520.10	292.72	94.34	
EAC total length [mm]	Female	24.05	22.50	26.10	19.87	30.00	24.36	2.51	0.00
	Male	26.98	25.18	28.79	20.72	34.80	27.17	2.87	
cEAC length [mm]	Female	14.25	12.44	16.01	9.22	18.70	14.06	2.32	0.00
	Male	16.38	14.45	18.74	9.86	21.86	16.47	2.69	
bEAC length [mm]	Female	9.64	8.38	11.93	4.97	16.65	10.30	2.87	0.50
	Male	10.21	8.21	12.77	5.91	18.18	10.70	3.02	

LQ — lower quartile; HQ — higher quartile; SD — standard deviation; TBPS — temporal bone pneumatic spaces; MAC — mastoid air cells; TC — tympanic cavity; EAC — external acoustic canal; cEAC — cartilage part of the external acoustic canal; bEAC — bony part of the external acoustic canal

DISCUSSION

Numerous studies have reported on the degree of pneumatization patterns of the temporal bone using CT. Dexian Tan et al. [12] conducted a study in which a classification of TBP was made on high-resolution CT. In the study, they concluded that the degree of TBP varies among the different compartments. They also indicated the existing significant association between age and sex with the degree of pneumatization of the petrous apex and the infralabyrinthine compartment. Another type of classification of TBP using CT was carried out by Han et al. [17]. However, the aforementioned study contained a classification that was based on the sigmoid sinus. In the study, they explained that when the sigmoid sinus at the level of the malleoincudal complex was used in the classification, there were statistically significant variations between the groups that correlated with the entire volume of the temporal bone. These results match what was found in the present study, that is, that variations in the morphology of the air spaces of the temporal bone are associated with sex and age.

Many imaging techniques for the evaluation of temporal bone cavities have been presented in the literature [35]. CT is the most common modality for assessing the bony anatomy of the temporal bone. In our study, CTAs were used to analyse the air spaces of the temporal bone. Although CT is a good option for conducting analyses of air-filled spaces of the temporal bone, comparable evaluation of the osseous components of the skull base and sinonasal anatomy is possible at a lower cost and radiation dose with cone-beam computed tomography (CBCT) [22]. Therefore, numerous studies have been conducted on

Table 4. Table gathers the R values obtained in the correlation analysis between categories. Highlighted in red are those in which the p value was smaller than 0.05

Category	Age	Total volume of TBPS [mm³]	MAC [mm³]	TC [mm³]	Total volume of EAC [mm³]	EAC surface [mm²]	cEAC volume [mm³]	cEAC surface [mm²]	cEAC-to-EAC surface ratio [%]	bEAC volume [mm³]	bEAC surface [mm²]	EAC total length [mm]	cEAC length [mm]	bEAC length [mm]
Age	1.00	–0.26	–0.31	–0.06	0.15	0.17	0.12	0.10	–0.09	0.14	0.17	0.18	0.05	0.17
Total volume of TBPS [mm³]	–0.26	1.00	0.98	0.58	0.07	0.17	–0.03	0.02	–0.13	0.18	0.21	0.26	0.05	0.19
MAC [mm³]	–0.31	0.98	1.00	0.50	–0.07	0.03	–0.16	–0.10	–0.15	0.11	0.14	0.17	–0.02	0.15
TC [mm³]	–0.06	0.58	0.50	1.00	0.30	0.39	0.15	0.19	–0.12	0.33	0.32	0.37	0.08	0.27
Total volume of EAC [mm³]	0.15	0.07	–0.07	0.30	1.00	0.92	0.90	0.86	0.29	0.40	0.32	0.60	0.59	0.08
EAC surface [mm²]	0.17	0.17	0.03	0.39	0.92	1.00	0.75	0.79	0.10	0.55	0.52	0.71	0.50	0.25
cEAC volume [mm³]	0.12	–0.03	–0.16	0.15	0.90	0.75	1.00	0.96	0.61	0.03	–0.04	0.39	0.71	–0.22
cEAC surface [mm²]	0.10	0.02	–0.10	0.19	0.86	0.79	0.96	1.00	0.65	0.02	–0.05	0.41	0.77	–0.26
cEAC-to-EAC surface ratio	–0.09	–0.13	–0.15	–0.12	0.29	0.10	0.61	0.65	1.00	–0.69	–0.77	–0.19	0.62	–0.76
bEAC volume [mm³]	0.14	0.18	0.11	0.33	0.40	0.55	0.03	0.02	–0.69	1.00	0.95	0.58	–0.12	0.70
bEAC surface [mm²]	0.17	0.21	0.14	0.32	0.32	0.52	–0.04	–0.05	–0.77	0.95	1.00	0.61	–0.20	0.80
EAC total length [mm]	0.18	0.26	0.17	0.37	0.60	0.71	0.39	0.41	–0.19	0.58	0.61	1.00	0.43	0.57
cEAC length [mm]	0.05	0.05	–0.02	0.08	0.59	0.50	0.71	0.77	0.62	–0.12	–0.20	0.43	1.00	–0.45
bEAC length [mm]	0.17	0.19	0.15	0.27	0.08	0.25	–0.22	–0.26	–0.76	0.70	0.80	0.57	–0.45	1.00

TBPS — temporal bone pneumatic spaces; MAC — mastoid air cells; TC — tympanic cavity; EAC — external acoustic canal; cEAC — cartilage part of the external acoustic canal; bEAC — bony part of the external acoustic canal

the TBP patterns with the use of CBCT [11, 14]. The image quality of the CBCT has also been described as superior to that of multiple-slice CT scans [36].

Knowledge about the morphology of the EAC is of great importance when performing procedures in that area, e.g. when performing myringoplasty. Myringoplasty is the term used for surgical repairs of minor perforations of the tympanic membrane. These perforations are most often caused by trauma, infections, or iatrogenic causes. Up to 80% of them are said to close spontaneously [1]. However, in some cases, myringoplasty is required. To access the tympanic membrane for myringoplasty, there are three recognised surgical approaches: permeatal, endaural, and postaural. Sharma et al. [39] conducted a prospective study on the different surgical approaches used when performing myringoplasty. In the study, they presented different results of myringoplasty when using these approaches. The highest success rate was found to be associated with the postaural approach (86.66%) and the lowest with the permeatal approach (73.33%). It was also stated that an issue with the permeatal approach was that it was only suitable in cases where the EAC was wide enough to allow complete visualisation of the tympanic membrane. Other studies have also stated the same [31]. The current study showed that there is sexual dimorphism in the morphometric properties of the EAC. Women, on average, had lower volumes, smaller total surface area, and shorter length of EAC. These results show that the permeatal approach might be less favourable in women than in men and that a different approach should be considered. Extensive knowledge of the morphology of the EAC is also important when treating squamous cell carcinoma (SCC) in that area. SCC is the most common primary type of cancer that affects the temporal bone, including the EAC [3]. The main form of therapy for cancers of the EAC and temporal bone is surgery. Nakagawa et al. [32] presented a study on the treatment of a SCC in the EAC. In the study, they performed a lateral bone resection of the tumour, not beyond the tympanic membrane. They concluded that radical surgery with preoperative chemoradiotherapy was effective in improving the estimated survival of patients with an advanced stage of SCC of the temporal bone. EAC cholesteatoma is an inflammatory process associated with ectopic proliferation of squamous tissue that results in osteolysis. It is a rare form of cholesteatoma first described by Toynbee in 1850 [42]. The typical

location of this disease is the middle ear cavity, and the treatment modalities for EAC cholesteatomas vary and depend on the extent of the involvement. For smaller lesions localized to the EAC, debridement is suggested and for greater lesions, surgery is recommended [6].

Tympanosclerosis (TS) represents the deposition of hyalinised collagen in the TC and has been reported to be associated with chronic otitis media [30]. Deposition can occur in the tympanic membrane, the mucosa lining of the TC, the ossicular chain, and occasionally the mastoid [5]. However, in most cases, TS affects mainly the tympanic membrane. Intratympanic TS most commonly involves silent areas in the middle ear, with ossicular involvement seen in 30–40% of cases of intratympanic TS [29]. The severity of the impact of TS on hearing is determined primarily by the location and extent of TS plaques [5]. When TS plaques affect the mobility of the tympanic membrane, they have to be surgically removed. Larem et al. [29] presented a high success rate of tympanoplasty in the myringosclerosis ears with a postoperative air-bone gap $\leq$ 20 dB in 96.5% of cases. As mentioned above, the ossicle chain can also be affected by TS. This can lead to fixation of the incudo-malleal complex or fixation of stapes. Tympanoplasty has been generally accepted as the choice of procedure for hearing restoration in cases where TS involves the ossicular chain. This involves the removal of TS mass, followed by a reconstruction of the middle ear sound conductive mechanism [43]. In cases of fixation of the incudo-malleal complex, possible treatment may be the removal of the incus and the head of the malleus and the insertion of a partial ossicular replacement prosthesis [29]. Surgical interventions when the stapes is fixed are a manner of great controversy. Some authors state that stapedectomy is the more reliable treatment for stapes fixation [9, 46]. However, others report that this procedure carries an unacceptable risk of postoperative sensorineural hearing loss and that mobilisation of stapes could be a better option [41]. Knowledge of the morphology of the TC is crucial when performing procedures in this area. The results of the present study show that there is a sexual dimorphism in the morphometric properties of the TC. TC was shown to have, on average, a smaller total volume in women than in men. Kavakli et al. [26] investigated the differences in the volume of the TC between men and women. In the results study, the presented were similar to those in the present analysis. Therefore, surgeons should consider this when performing operations in this area.

The morphometric properties of the MAC are of great importance in order to understand their physiology and pathogenesis. These properties are mainly studied from a volumetric point of view because the mastoid cavity has been regarded as an air reservoir [34]. Colhoun et al. [10] conducted a CT-based study in which the area and volume measurements of the mastoid air spaces of 26 normal temporal bones of cadavers were analysed. In the study, the mean value of mastoid volume was measured at 8.4 $\pm$ 3.6 cm^3. Similarly, Park et al. [34] studied these properties in 24 normal ears, where the mean value of mastoid volume was 10.43 $\pm$ 6.66 cm^3. In the present study, the mean volume of MAC was measured to be 6.47 $\pm$ 3.44 cm^3, which is relatively lower than the two values mentioned above. Both of the cited studies were performed on cadavers, compared to the subjects used in this paper, which consisted of living patients. An explanation for this discrepancy may be that the extent of the contrast window was defined differently. This suggests that the boundary layers corresponding to the epithelium, for example, were chosen too restrictively, resulting in an underestimation of the measurement. Studies about the morphometric properties of the MAC based on CT have also been published in the literature. Karakas et al. [25] presented a morphometric examination of the MAC using CT. In the study, the mean value of the mastoid volume was 14.05 $\pm$ 7.24 cm^3, which is more than double the volume recorded in the present analysis. However, the results of the current study are very similar to those presented by Isono et al. [20], which were measured to be 6.3 cm^3 (no standard deviation was reported). The differences between the values might be due to many different factors, such as measuring techniques, the number of subjects used, or racially based differences.

Understanding the anatomy of the temporal bone is crucial when performing mastoid surgery. Mastoidectomy is a surgical procedure of the temporal bone in which postauricular air cells are opened by removing the bone that separates them. There are many indications for mastoidectomy to be performed, which can include cholesteatoma, acute mastoiditis, and chronic mastoiditis [8]. Mastoidectomy is also performed as a surgical approach for numerous otological procedures, such as facial nerve surgery, coch-

lear implantation, and labyrinthectomy [27]. In the present study, measurements and statistical analysis of MAC volume were performed. The sexual dimorphism was shown to occur in the total volume of the mastoid cavity. Women had, on average, smaller volumes of MAC than men. Additionally, a statistically significant correlation was found between mastoid cavity volume and age, where the volume of the mastoid cavity was shown to become lower with age. Therefore, these results should be taken into consideration when performing mastoidectomies or other procedures concerning the mastoid. The patients' age should be taken into account when performing these procedures, especially in older patients, since their mastoid cavity volumes might be lower.

Limitations of the study

However, this study is not without limitations. The authors of the current study did not have access to clinical data about the patients from whom the CTs were analysed. Despite statistically significant results, a study in a larger study group is still warranted to minimise potential bias and establish the most accurate parameters. Furthermore, this study is also burdened with a possible measurement error, as the results are only as good as the quality of the images analysed and the numerical accuracy of the software used.

CONCLUSIONS

The present study is the first to analyse the degree of pneumatization and the morphology of temporal bone cavities, with respect to different compartments, sides, sex, and age. The results showed that the total volume of the mastoid air cells was, on average, lower in women than in men. This should be taken into consideration when performing procedures on the mastoid, such as mastoidectomies. Furthermore, sexual dimorphism in the morphometric properties of the external auditory canal was found. Women, on average, had lower volumes, smaller total surface areas, and shorter external auditory canals. This study provides surgeons with crucial data that can surely be useful when performing otological procedures — which should be taken into consideration to avoid any unexpected complications.

Conflict of interest: None declared

REFERENCES

1. Aggarwal R, Saeed SR, Green KJM. Myringoplasty. J Laryngol Otol. 2006; 120(6): 429–432, doi: 10.1017/S0022215106000697, indexed in Pubmed: 16772050.
2. Allam AF. Pneumatization of the temporal bone. Ann Otol Rhinol Laryngol. 1969; 78(1): 49–64, doi: 10.1177/000348946907800105, indexed in Pubmed: 5763190.
3. Allanson BM, Low TH, Clark JR, et al. Squamous cell carcinoma of the external auditory canal and temporal bone: an update. Head Neck Pathol. 2018; 12(3): 407–418, doi: 10.1007/s12105-018-0908-4, indexed in Pubmed: 30069837.
4. Anson B, Donaldson J. Surgical anatomy of the temporal bone. 3d ed. Saunders, Philadelphia 1981.
5. Asiri S, Hasham A, al Anazy F, et al. Tympanosclerosis: review of literature and incidence among patients with middle-ear infection. J Laryngol Otol. 1999; 113(12): 1076–1080, doi: 10.1017/s0022215100157937, indexed in Pubmed: 10767919.
6. Aswani Y, Varma R, Achuthan G. Spontaneous external auditory canal cholesteatoma in a young male: Imaging findings and differential diagnoses. Indian J Radiol Imaging. 2016; 26(2): 237–240, doi: 10.4103/0971-3026.184419, indexed in Pubmed: 27413272.
7. Ayache S, Beltran M, Guevara N. Endoscopic transcanal myringoplasty for anterior tympanic membrane perforation. Eur Ann Otorhinolaryngol Head Neck Dis. 2019; 136(5): 413–415, doi: 10.1016/j.anorl.2019.05.001, indexed in Pubmed: 31126894.
8. Bennett M, Warren F, Haynes D. Indications and technique in mastoidectomy. Otolaryngol Clin North Am. 2006; 39(6): 1095–1113, doi: 10.1016/j.otc.2006.08.012, indexed in Pubmed: 17097435.
9. Celik H, Aslan Felek S, Islam A, et al. Analysis of long-term hearing after tympanosclerosis with total/partial stapedectomy and prosthesis used. Acta Otolaryngol. 2008; 128(12): 1308–1313, doi: 10.1080/00016480801953056, indexed in Pubmed: 18607937.
10. Colhoun EN, O'Neill G, Francis KR, et al. A comparison between area and volume measurements of the mastoid air spaces in normal temporal bones. Clin Otolaryngol Allied Sci. 1988; 13(1): 59–63, doi: 10.1111/j.1365-2273.1988.tb00282.x, indexed in Pubmed: 3370855.
11. Delilbasi C, Orhan K, Icen M, et al. Evaluation of articular eminence pneumatization using cone beam computed tomography. Minerva Stomatol. 2013; 62(10): 349–354, indexed in Pubmed: 24217683.
12. Dexian Tan A, Ng JH, Lim SuA, et al. Classification of temporal bone pneumatization on high-resolution computed tomography: prevalence patterns and implications. Otolaryngol Head Neck Surg. 2018; 159(4): 743–749, doi: 10.1177/0194599818778268, indexed in Pubmed: 29807479.
13. Diamant M. Otitis and pneumatization of the mastoid bone. Acta Otolaryngol. 1940; 41: 1–149.
14. Erovic BM, Chan HHL, Daly MJ, et al. Intraoperative cone-beam computed tomography and multi-slice computed tomography in temporal bone imaging for surgical

treatment. Otolaryngol Head Neck Surg. 2014; 150(1): 107–114, doi: 10.1177/0194599813510862, indexed in Pubmed: 24170658.
15. Friedrich RE, Viezens L, Grzyska U. Pneumatization of the zygomatic process of temporal bone on computed tomograms. GMS Interdiscip Plast Reconstr Surg DGPW. 2016; 5: Doc16, doi: 10.3205/iprs000095, indexed in Pubmed: 27347473.
16. Gibelli D, Cellina M, Gibelli S, et al. Temporal bone pneumatization: relationship with sex and variants of the ethmoid and sphenoid bone. J Craniofac Surg. 2021; 32(8): 2888–2891, doi: 10.1097/SCS.0000000000007809, indexed in Pubmed: 34231515.
17. Han SJ, Song MH, Kim J, et al. Classification of temporal bone pneumatization based on sigmoid sinus using computed tomography. Clin Radiol. 2007; 62(11): 1110–1118, doi: 10.1016/j.crad.2007.04.019, indexed in Pubmed: 17920872.
18. Hill CA. Ontogenetic change in temporal bone pneumatization in humans. Anat Rec (Hoboken). 2011; 294(7): 1103–1115, doi: 10.1002/ar.21404, indexed in Pubmed: 21618436.
19. Hindi K, Alazzawi S, Raman R, et al. Pneumatization of mastoid air cells, temporal bone, ethmoid and sphenoid sinuses. Any correlation? Indian J Otolaryngol Head Neck Surg. 2014; 66(4): 429–436, doi: 10.1007/s12070-014-0745-z, indexed in Pubmed: 26396957.
20. Isono M, Murata K, Azuma H, et al. Computerized assessment of the mastoid air cell system. Auris Nasus Larynx. 1999; 26(2): 139–145, doi: 10.1016/s0385-8146(98)00055-8, indexed in Pubmed: 10214891.
21. Jackler RK, Cho M. A new theory to explain the genesis of petrous apex cholesterol granuloma. Otol Neurotol. 2003; 24(1): 96–106, doi: 10.1097/00129492-200301000-00020, indexed in Pubmed: 12544037.
22. Jadhav AB, Fellows D, Hand AR, et al. Classification and volumetric analysis of temporal bone pneumatization using cone beam computed tomography. Oral Surg Oral Med Oral Pathol Oral Radiol. 2014; 117(3): 376–384, doi: 10.1016/j.oooo.2013.12.398, indexed in Pubmed: 24528795.
23. Jen A, Sanelli PC, Banthia V, et al. Relationship of petrous temporal bone pneumatization to the eustachian tube lumen. Laryngoscope. 2004; 114(4): 656–660, doi: 10.1097/00005537-200404000-00011, indexed in Pubmed: 15064619.
24. Kang TK, Ha R, Oh JH, et al. The potential protective effects of temporal bone pneumatization: A shock absorber in temporal bone fracture. PLoS One. 2019; 14(5): e0217682, doi: 10.1371/journal.pone.0217682, indexed in Pubmed: 31150482.
25. Karakas S, Kavakli A. Morphometric examination of the paranasal sinuses and mastoid air cells using computed tomography. Ann Saudi Med. 2005; 25(1): 41–45, doi: 10.5144/0256-4947.2005.41, indexed in Pubmed: 15822493.
26. Kavakli A, Ogeturk M, Yildirim H, et al. Volume assessment of age-related conversion of the tympanic cavity by helical computerized tomography scanning. Saudi Med J. 2004; 25(10): 1378–1381, indexed in Pubmed: 15494806.
27. Kenneth LK, Jerry WL. Mastoidectomy. StatPearls Publishing, Treasure Island 2021.
28. Klein J. Otitis externa, otitis media, and mastoiditis. Mandell, Douglas, and Bennett's Principles and Practice of Infectious Diseases. 2015: 767–773.e1, doi: 10.1016/b978-1-4557-4801-3.00062-x.
29. Larem A, Abu Rajab Altamimi Z, Aljariri AA, et al. Reliability of high-resolution CT scan in diagnosis of ossicular tympanosclerosis. Laryngoscope Investig Otolaryngol. 2021; 6(3): 540–548, doi: 10.1002/lio2.594, indexed in Pubmed: 34195376.
30. Mahajan SB, Kochhar L. Surgical management of tympanosclerosis-our experience. Med J Armed Forces India. 2000; 56(3): 198–200, doi: 10.1016/S0377-1237(17)30165-X, indexed in Pubmed: 28790706.
31. Man SC, Nunez DA. Tympanoplasty — conchal cavum approach. J Otolaryngol Head Neck Surg. 2016; 45: 1, doi: 10.1186/s40463-015-0113-3, indexed in Pubmed: 26739478.
32. Nakagawa T, Kumamoto Y, Natori Y, et al. Squamous cell carcinoma of the external auditory canal and middle ear: an operation combined with preoperative chemoradiotherapy and a free surgical margin. Otol Neurotol. 2006; 27(2): 242–249, doi: 10.1097/01.mao.0000190463.88873.3d, indexed in Pubmed: 16436996.
33. Palva T, Palva A. Size of the human mastoid air cell system. Acta Otolaryngol. 1966; 62(3): 237–251, doi: 10.3109/00016486609119570, indexed in Pubmed: 5970742.
34. Park MS, Yoo SH, Lee DH. Measurement of surface area in human mastoid air cell system. J Laryngol Otol. 2000; 114(2): 93–96, doi: 10.1258/0022215001904969, indexed in Pubmed: 10748822.
35. Pyykkö I, Zou J, Gürkov R, et al. Imaging of temporal bone. Adv Otorhinolaryngol. 2019; 82: 12–31, doi: 10.1159/000490268, indexed in Pubmed: 30947168.
36. Saati S, Kaveh F, Yarmohammadi S. Comparison of cone beam computed tomography and multi slice computed tomography image quality of human dried mandible using 10 anatomical landmarks. J Clin Diagn Res. 2017; 11(2): ZC13–ZC16, doi: 10.7860/JCDR/2017/20637.9253, indexed in Pubmed: 28384972.
37. Sadé J. Treatment of cholesteatoma and retraction pockets. Eur Arch Otorhinolaryngol. 1993; 250(4): 193–199, doi: 10.1007/BF00171523, indexed in Pubmed: 8369113.
38. Seibert JW, Danner CJ. Eustachian tube function and the middle ear. Otolaryngol Clin North Am. 2006; 39(6): 1221–1235, doi: 10.1016/j.otc.2006.08.011, indexed in Pubmed: 17097443.
39. Sharma DK, Singh S, Sohal BS, et al. Prospective study of myringoplasty using different approaches. Indian J Otolaryngol Head Neck Surg. 2009; 61(4): 297–300, doi: 10.1007/s12070-009-0086-5, indexed in Pubmed: 23120654.
40. Standring S, Borley NR, Gray H. Gray's anatomy: the anatomical basis of clinical practice. 40th ed., anniversary ed. Elsevier, Churchill Livingstone 2008.
41. Tos M, Lau T, Arndal H, et al. Tympanosclerosis of the middle ear: late results of surgical treatment.

J Laryngol Otol. 1990; 104(9): 685–689, doi: 10.1017/s0022215100113623, indexed in Pubmed: 2230573.
42. Toynbee J. A specimen of molluscum contagiosum developed in the external auditory meatus. London Medical Gazette. 1850; 46: 809–811.
43. Tsuzuki K, Yanagihara N, Hinohira Y, et al. Tympanosclerosis involving the ossicular chain: mobility of the stapes in association with hearing results. Acta Otolaryngol. 2006; 126(10): 1046–1052, doi: 10.1080/00016480600672634, indexed in Pubmed: 16923708.
44. Tumarkin A. On the nature and vicissitudes of the accessory air spaces of the middle ear. J Laryngol Otol. 1957; 71(2): 65–99, doi: 10.1017/s0022215100051598, indexed in Pubmed: 13406420.
45. Turgut S, Tos M. Correlation between temporal bone pneumatization, location of lateral sinus and length of the mastoid process. J Laryngol Otol. 1992; 106(6): 485–489, doi: 10.1017/s0022215100119942, indexed in Pubmed: 1624879.
46. Vincent R, Oates J, Sperling NM. Stapedotomy for tympanosclerotic stapes fixation: is it safe and efficient? A review of 68 cases. Otol Neurotol. 2002; 23(6): 866–872, doi: 10.1097/00129492-200211000-00010, indexed in Pubmed: 12438848.

VIA MEDICA

ORIGINAL ARTICLE

Folia Morphol.
Vol. 82, No. 4, pp. 921–931
DOI: 10.5603/FM.a2023.0025

ISSN 0015–5659
eISSN 1644–3284
journals.viamedica.pl

Would you donate your body? Attitudes of students of nursing and physiotherapy towards body donation for educational and scientific purposes

W. Likus[1], P. Janiszewska[2]

[1]*Department of Anatomy, Faculty of Health Sciences in Katowice, Medical University of Silesia, Katowice, Poland*
[2]*Department of Reproductive Health and Sexology, Department of Women's Health, Faculty of Health Sciences in Katowice, Medical University of Silesia, Katowice, Poland*

[Received: 4 March 2023; Accepted: 12 March 2023; Early publication date: 3 April 2023]

Background: *Human body is the most perfect atlas of human anatomy. Body donation after death is, next to donation of organs for the purpose of transplantation, another most altruistic act, which significantly influences the future of medicine, as regards teaching of anatomy and clinical disciplines. Because students are mainly the beneficiaries of corpse donations, it appears important to learn about their attitudes to this altruistic act. The purpose was to assess the awareness and attitudes of students of nursing and physiotherapy towards body donation for educational and scientific purposes.*

Materials and methods: *A total of 128 Polish students (110 women and 18 men) from the faculties of nursing and physiotherapy of the Medical University of Silesia in Katowice, Poland took part in the questionnaire study. The average age in respective groups was 19.94 ± 0.34 years of age in case of nursing and 19.93 ± 0.25 years of age in case of physiotherapy. The first part of the proprietary questionnaire concerned classes in body dissection conducted in prosectorium and their significance for teaching anatomy. The second part applied to the programme of Conscious Body Donation, attitudes towards the body in prosectorium and the approach to body donation for educational and scientific purposes.*

Results: *The results of the study indicate that students from both faculties are in favour of body donation after death for educational and scientific purposes. Unfortunately, only a small percentage of them expressed the willingness to become body donators. The main reasons for the reluctance to do so included psychological barrier and concern for the family.*

Conclusions: *Most of students who responded to the questionnaire support the idea of body donation for educational and scientific purposes after death, yet they appear to be more willing to donate their organs for transplantation than their bodies for educational or scientific purposes after death. There are numerous factors which influence students' attitude to body donation. More emphasis should be put on educating students, which could contribute to changing their attitude toward that altruistic act, and in consequence may increase the number of donors in the future.* (Folia Morphol 2023; 82, 4: 921–931)

Key words: whole body donation, students, physiotherapy, nursing, cadaver, anatomy

Address for correspondence: Dr hab. n. med. Wirginia Likus, prof. SUM, Department of Anatomy, Faculty of Health Sciences in Katowice, Medical University of Silesia in Katowice, ul. Medyków 18, 40–752 Katowice, Poland, e-mail: wirginia.likus@gmail.com

INTRODUCTION

Anatomy is a specific course in the curriculum, as it allows to gain thorough knowledge of human body structures. It provides the basis without which it is not possible to fathom many fields of clinical medicine, in particular those related to conducting medical procedures [9, 14, 17, 46]. Human body is the most perfect atlas of human anatomy. Donation of organs and of the entire body constitute two most significant altruistic acts, which significantly influence the future of medicine [12]. Cadaver dissection classes in prosectorium constitute the first part of encounters of students with medical sciences. In many countries, voluntary body donation is the primary act, without which it is not possible to teach anatomy in lawful manner [26]. The authors who conducted studies on body donation emphasize that encounters with the donor's body are of utmost importance for the student. Body donors are even referred to as first patients or silent teachers [18, 28]. An important role in the entire process of education and in the attitude to donors' bodies is attributed to the ceremonial burials, in the course of which students have the possibility to personally meet the families of donors [20, 23, 27].

Analysing the literature that focused on body donation, one can note that a substantial portion of such studies is devoted to the attitude of students, from both medical and non-medical faculties, to the act of donating organs for transplantation [10, 12, 15, 25, 29, 32, 33, 35, 36, 39, 43, 44, 48], to the cadaver dissection for teaching anatomy [2, 6, 24] as well as to the attitude towards body donation among university staff [4, 5, 13, 38, 47], or among the elderly [31]. There are but a few studies that deal with the attitude to whole body donation after death, particularly among the students who do not plan to become medical doctors.

In Poland, cadavers for student and post-graduate training in medical universities are obtained from donors registered in cadaver donation programmes. Those donors, when still alive, decided to make body donation for educational and scientific purposes to a specific medical university [9]. Taking a decision about body donation after death for educational and scientific purposes is extremely difficult and is influenced by numerous factors.

Among the main beneficiaries of conscious body donation are students of medical universities, not only those from medical departments but also students of disciplines that belong under faculties of health sciences, such as nursing, obstetrics, physiotherapy, or electrocardiology. Anatomy classes in prosectorium are important as, unlike a living body, cadavers "do not punish for mistakes made" [30]. Experience and knowledge gained through necropsy and body dissection are more thorough than what can be gained by means of three-dimensional atlases, models, or virtual reality. As bodies of the "first patients" are so important, it is also relevant to find out about the attitude of those who are beneficiaries of the altruistic act of body donation for educational and scientific purposes. While the students of medical departments of Polish universities have classes in anatomy only in prosectorium environment, students of other medical sciences either do not have classes in prosectorium at all, or have such classes in a limited scope. Thus, for our questionnaire study we selected students who do not plan to become medical doctors, and who, when studying medical sciences, have a limited contact with the prosectorium environment, in order to learn their opinions concerning body donation.

As has been underlined above, because students are the main beneficiaries of body donation acts, it appears substantial to learn about their attitudes to body donation. Our study is the first one of such type in Poland, and the results obtained may contribute to extending the knowledge and attitude of young people towards dead human body. Students, as future employees of the medical sector, may have an important role to play in raising social awareness as concerns body donation.

MATERIALS AND METHODS

The study comprised students of medical sciences who do not plan to become medical doctors and who are students of the Faculty of Health Sciences in Katowice, Medical University of Silesia in Katowice, Poland. For the purposes of the study reported here, two fields of study have been selected, which differ as to the amount of hours to be spent in dissecting room during classes: nursing with the total of 35 hours of anatomy classes, including 4 classes in the dissecting room, and physiotherapy, with 60 hours of such classes, including 50 hours of anatomy lessons in the prosectorium with cadavers.

A proprietary questionnaire was used for the purpose of the study, it was voluntary to fill the questionnaire which was anonymous. The questionnaire contained questions in two parts: the first one referred to classes in the dissecting room and their

Table 1. Do you know where the cadavers used in body dissection classes come from? — opinions of students of nursing (n = 67) and physiotherapy (n = 61)[#]

Origin of cadavers used in body dissection classes in prosectorium	Number of respondents selecting a given response		P*
	Nursing	Physiotherapy	
They come from those who consciously donated their bodies to the university, when still alive	54 (80.6%)	57 (93.44%)	0.0164
They are provided by family members after a person's death	19 (28.36%)	9 (14.75%)	0.0314
They are bodies of unidentified persons (NN)	10 (14.92%)	9 (14.75%)	NS
They are bodies of homeless people who do not have families	8 (11.94%)	9 (14.75%)	NS
The cadavers are bodies of prisoners who died in prisons	6 (8.96%)	3 (4.91%)	< 0.001
The bodies come from social care homes	4 (5.97%)	1 (1.64%)	< 0.001

[#]A multiple choice question; *Chi square test; NS — no statistical significance

importance in learning anatomy, the second one referred to the programme of Conscious Body Donation, attitudes towards the body in prosectorium and the approach to body donation for educational and scientific purposes. The link to the questionnaire was sent to the total of 365 students of the first year, in the abovementioned fields of study, who completed the entire course in anatomy and who were about to take the exam in this subject.

The study received approval of the bioethics committee of the Medical University of Silesia in Katowice (No. KNW/0022/KB/53/18).

Statistical analysis

The results obtained with the use of questionnaire were statistically analysed with the application of TIBCO Statistica® 13.3 software. Descriptive statistics' calculations were made. The statistical difference among groups was accessed using chi-square tests. The threshold assumed for statistical significance was $p < 0.05$.

RESULTS

The study group comprised 128 students, 67 of them studied nursing (67 females) whereas 61 studied physiotherapy (43 females and 18 males), which equals to 52.34% and 47.66% in percentage terms, respectively. Women constituted the majority of respondents, due to the female gender predominance in those fields of studies. The average age in respective groups was 19.94 ± 0.34 years of age in case of nursing and 19.93 ± 0.25 years of age in case of physiotherapy.

In both groups, the most often declared religion was the Roman Catholicism, in case of 80.6% students of nursing and 68.5% students of physiotherapy, respectively. As regards religion, the second most popular response was "not religious" (nonbeliever/atheist/agnostic), with 17.91% and 18.03% declaring it, respectively. In answering the question "What or who do you consider human body to be after death?" students from both fields of study frequently selected the answer "A being that lived once" — 53.73% and 49.18%. Physiotherapy students statistically significantly more often indicated "inanimate object" — 6.56% or "container for soul" — 11.48% ($p = 0.01$, $p = 0.05$). Sadly, it has to be stated that as many as 5 ladies studying nursing selected the response in which the cadaver was labelled as "organic waste". Students agree that classes in the prosectorium are really needed in the course of anatomy. Such a response was provided by as many as 88.06% of the students of nursing and 95.08% of students of physiotherapy. The remaining students expressed no opinion in that matter. It needs to be stressed that none of the students in both fields of study responded as "definitely not needed". As in case of anatomical preparations, as many as 73.13% of the students of nursing and 73.38% of the students of physiotherapy considered them very useful in learning.

Students, when asked "where do the cadavers used in body dissection classes come from?" in the majority of cases (80.6% of nursing students and 93.44% of physiotherapy students) selected the response "they come from those who consciously donated their bodies to the university, when still alive". Unfortunately, students of nursing provided incorrect answers above the threshold of statistical significance, indicating that the cadavers are those of prisoners who died in prisons ($p < 0.001$; Table 1). Among the respondents, 83.58% of nursing students and 73.77% of physiotherapy students replied that

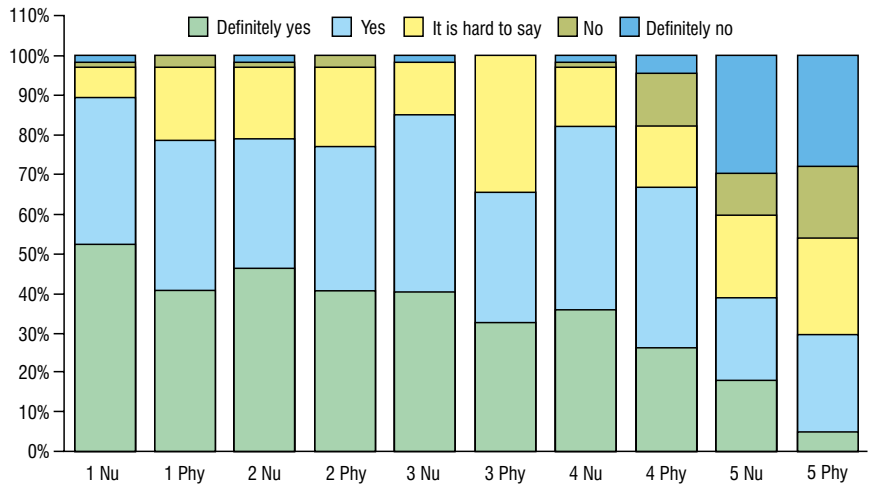

Figure 1. Opinions (%) of students of nursing (Nu; n = 67) and physiotherapy (Phy; n = 61) concerning treatment of donors' bodies in departments of anatomy. Explanatory notes: 1. "Donors' bodies are treated properly in departments of anatomy"; 2. "In the course of dissection the cadavers are treated with due respect"; 3. "The dissected parts and remains of corpses are not properly protected after dissection"; 4. "Donors' bodies are treated with due respect by the students"; 5. "Donors' bodies may be destroyed by students in the course of anatomy classes".

they were aware of the body donation programme. The most frequently indicated sources of information about body donation in both cases were university staff members (69.64% and 62.22%, respectively). The students of nursing more often indicated, with statistical significance, that also the Internet was their source of information in that respect (48.21%) while in case of students of physiotherapy such sources of information included "other students" (44.4%), friends (17.7%) or television (11.11%). In case of physiotherapy students, the least frequently selected option in responding to this question was "other", e.g. a "radio documentary". Students agree that the most efficient way to convince people about making body donation for educational and scientific purposes is the testimony of a person who has already made the decision about body donation (68.66% and 55.74%, respectively). Future physiotherapists more frequently, with statistical significance, indicated medical personnel (64.18%) as the influencers here, while students of nursing pointed out to clergymen (44.26%) and celebrities (21.31%) as those who could convince them about making a whole body donation. When asked about the remuneration for donors or their families for making body donation for educational and scientific purposes, a majority of respondents selected the option "they do not get remuneration" with 28% selecting the response "I do not know". In the question concerning ethical assessment of the Conscious Body Donation Programme, students from both fields of studies provided a positive response, in the majority of cases. With statistical significance, students of nursing (80.36%) more often selected a positive response ($p = 0.0143$), whereas students of physiotherapy indicated the unethical nature of that program (31.11%, $p = 0.05$). Yet another question concerned the opinion of students regarding the way donors' bodies are treated in departments of anatomy and the way those cadavers are treated by students themselves. The respondents were requested to assess, using a five point Likert scale, the veracity of the following statements: 1. "Donors' bodies are treated properly in departments of anatomy"; 2. "In the course of dissection the cadavers are treated with due respect"; 3. "The dissected parts and remains of corpses are not properly protected after dissection"; 4. "Donors' bodies are treated with due respect by the students"; 5. "Donors' bodies may be destroyed by students in the course of anatomy classes". The results are presented in the Figure 1. The statistical analysis performed for most of the statements revealed no significant differences in responses between the represented fields of study. Only in case of statement 1, which concerns proper treatment of cadavers, and in statement 3, referring to protection of corpses, students of physiotherapy selected the response "it is hard to say" more often, with statistical significance ($p = 0.035$; $p = 0.025$, respectively). In case of statements 4 and 5, about treating cadavers with due respect and about destroying donors' bodies by

students, physiotherapy students selected the "no" and "definitely not" responses statistically significantly more often ($p = 0.007$, $p = 0.035$), in comparison with nursing students, which — in case of the statement concerning due respect for the body — poses a substantial problem that needs to be thought over.

A clear majority of students from both fields of study (58.21% of those studying nursing and 54.1% of those studying physiotherapy) believe in life after death; however, a statistically significantly higher percentage of nursing students, 28.36%, deny the existence of life after death ($p = 0.006$), while 27.7% of physiotherapy students admit they have not given that question a thought ($p = 0.021$). Students, although young, have been wondering about the fate of their bodies after death (73.13% of future nurses and 68.85% of future physiotherapists pondered upon that).

The question: "Do you support body donation for educational/scientific purposes after death?" received a positive answer from nursing students (79.11%) statistically significantly more often ($p = 0.006$), whereas physiotherapy students statistically significantly more frequently selected the response indicating they had no opinion regarding this issue (24.59%) ($p = 0.0043$) or have not given it a thought yet (16.39%) ($p = 0.0028$). The respondents were also inquired about their awareness concerning whether their creed approves the body donation act. 56.72% of future nurses and 42.62% of future physiotherapists responded selecting the "I don't know" answer ($p = 0.055$). A very small percentage of responses from nursing students (4.48%) as well as physiotherapy students (8.2%) selected the negative response ("no"). When inquired about body donation and organ donation after death, the respondents provided divergent answers. Students of both fields were more willing to donate their organs for transplantation (65.67% and 52.46%, respectively) than to donate the entire body for educational/ /scientific purposes after death (11.94% and 24.59%, respectively). In general, most of the nursing students (44.78%) have not pondered upon donating their bodies so far. Physiotherapy students, who have more hours at the dissecting table, selected a similar answer less frequently (19.67%, $p = 0.013$). The students who indicated they were not willing to make a body donation for educational/scientific purposes after death were requested to provide their reasons. In the specific question asked in the questionnaire, they could select more than one response. Students of nursing ($n = 27$) most frequently selected the response: "So that the family would not suffer again" (37.04%), or indicated fear of necropsy (37.04%) and fear that the cadaver may be destroyed by students (33.33%). In case of students of physiotherapy ($n = 33$) the most frequently selected response was "psychological barrier" (36.36% of respondents). Students of nursing more often indicated, with statistical significance, the "fear of losing the chance for eternal life" ($p = 0.004$), whereas students of physiotherapy selected the response option of "wasting the body" risk and absence of detailed knowledge concerning donation ($p < 0.001$) (Table 2). Also, those persons who declared their willingness to become body donors after death were inquired about the reasons for making such choice. Students of both fields most often selected the response which stated the "Awareness of the need for developing medical sciences" (Table 3). That response was the option most often selected in case of the question asked to all respondents, namely "Why, in your opinion, people decide to donate the body for educational/scientific purposes after death?" (Table 4). Students of nursing selected twice as often the response indicating willingness to help in scientific research, and in enhancing education of doctors and medical personnel ($p = 0.028$), whereas in case of physiotherapy students, 13% of them selected the response "to avoid costs connected with the funeral" and "to avoid the funeral ceremony". When inquired about who can be most efficient in convincing people to make a body donation for educational/scientific purposes after death, the most frequently selected response option was: "People who have already consented to make body donation" (68.66% of nursing students and 55.74% of physiotherapy students). In response to the question: "Does, in your opinion, the attitude of the student towards the cadaver during classes in prosectorium reflect the future approach of such student to the patient?" most of the students from both fields provided an affirmative answer (73.11% and 62.3%, respectively). No statistically significant differences were observed between the fields of study. Students asked the question: "Have body dissection classes made you change your opinion concerning making a body donation for educational/scientific purposes after death?" provided a negative answer in case of a majority of nursing students (73.13%) ($p = 0.046$), whereas most of physiotherapy students (48.19%) selected a response stating that classes in prosectorium influenced the way they perceive the body donation act ($p = 0.006$).

Table 2. Why you do not want to donate the body for scientific purposes after death? — opinions of students of nursing (n = 27) and physiotherapy (n = 33)[#]

Reasons why you do not want to donate the body for educational/scientific purposes after death	Number of respondents selecting a given response		P*
	Nursing	Physiotherapy	
Concern for the family, so that they would not suffer again	10 (37.04%)	10 (30.30%)	NS
I do not want to be dissected (I do not want my body to be cut)	10 (37.04%)	6 (18.18%)	0.0491
Fear that my body will be destroyed by students	9 (33.33%)	7 (21.21%)	NS
Psychological barrier	8 (29.63%)	12 (36.36%)	NS
Fear that my body will not be treated with due respect	8 (29.63%)	10 (30.30%)	NS
Fear that my body will not be property used after death	7 (25.93%)	10 (30.30%)	NS
I am not able to state the reason	5 (18.52%)	5 (15.15%)	NS
Because I love my body	4 (14.82%)	6 (18.18%)	NS
Reluctance of family members	3 (11.11%)	5 (15.15%)	NS
I am afraid	3 (11.11%)	7 (21.21%)	0.0148
I believe in life after death	3 (11.11%)	3 (9.09%)	NS
Fear of losing the chance for eternal life	2 (7.41%)	1 (3.03%)	0.004
My body can be wasted	2 (7.41%)	4 (12.12%)	< 0.001
Lack of thorough knowledge concerning body donation	2 (7.41%)	4 (12.12%)	< 0.001
Others:			
"I don't want people to look at my body and put their fingers in me"	1 (3.71%)		
"I want my body to be buried shortly after I die"	1 (3.71%)		
"I am not dying yet, so I do not think about it"	1 (3.71%)		
"The cadavers are destroyed sometimes, so structures are not visible, perhaps it also depends on the topics which are discussed during class"	1 (3.71%)		
"I just do not want to"		1 (3.03%)	
"It's my body and I want it to stay that way forever"		1 (3.03%)	

[#]A multiple choice question; *Chi square test; NS — no statistical significance

Table 3. Why do you want to donate the body for educational/scientific purposes after death? — opinions of students of nursing (n = 8) and physiotherapy (n = 15)[#]

Reasons why you want to donate the body for educational/scientific purposes after death	Number of respondents selecting a given response		P*
	Nursing	Physiotherapy	
Awareness of the need for developing medical sciences	7 (87.5%)	12 (80%)	NS
I want to feel useful, even after death	7 (87.5%)	9 (60%)	0.0286
To help in developing education of future doctors and medical personnel	7 (87.5%)	9 (60%)	0.0286
To prevent the shortage of body donors for scientific purposes	3 (37.5%)	7 (46.67%)	NS
To help in medical research, knowledge improvement, science	7 (87.5%)	6 (40%)	NS
To express gratitude towards doctors for life and health	1 (12.5%)	4 (26.67%)	NS
Not to burden others with the costs of funeral	1 (12.5%)	4 (26.67%)	NS
Body donation is the only rational decision for me, and a moral choice	1 (12.5%)	4 (26.67%)	NS
To avoid costs connected with the funeral	0 (0%)	2 (13.13%)	
To avoid the funeral ceremony	0 (0%)	2 (13.13%)	
Because they do not have relatives	0 (0%)	1 (6.67%)	
Others	1 (87.5%)	1 (6.67%)	

[#]A multiple choice question; *Chi square test; NS — no statistical significance

Table 4. Why, in your opinion, people decide to donate the body for educational/scientific purposes after death? — opinions of students of nursing (n = 67) and physiotherapy (n = 61)[#]

Reasons why people decide to donate the body for educational/scientific purposes after death	Number of respondents selecting a given response		P*
	Nursing	Physiotherapy	
Awareness of the need for developing medical sciences	57 (85.07%)	44 (72.13%)	< 0.001
Willingness to help in medical research, knowledge improvement, science	52 (77.61%)	20 (32.79%)	0.018
They want to feel useful, even after death	47 (70.15%)	37 (60.66%)	0.004
To help in developing education of future doctors and medical personnel	46 (68.66%)	25 (40.98%)	0.016
Body donation is the only rational decision for them, and a moral choice	17 (25.37%)	8 (13.12%)	0.040
To prevent the shortage of body donors for scientific purposes	16 (23.88%)	13 (21.31%)	NS
Because they do not have relatives	12 (17.91%)	9 (14.75%)	NS
To express gratitude towards doctors for life and health	8 (11.94%)	7 (11.48%)	NS
To avoid the funeral ceremony	7 (10.45%)	3 (4.91%)	NS
Not to burden others with the costs of funeral	4 (5.97%)	7 (11.48%)	NS
To avoid costs connected with the funeral	1 (1.49%)	5 (8.20%)	0.036
Others:			
"I did not think about it"			< 0.001
"Everyone can have different reasons"		1 (1.64%)	
"They want money for it"		1 (1.64%)	

[#]A multiple choice question; *Chi square test; NS — no statistical significance

DISCUSSION

The results of our questionnaire study involving first year undergraduate students of nursing and physiotherapy at the Medical University of Silesia in Katowice, Poland make it possible to extend the knowledge concerning awareness and attitudes of students towards body donation for educational/scientific purposes. No other studies of that kind have been conducted in Poland so far. The latest research study related to the topic of body donation conducted in Poland had the aim of examining donors' profile [8].

In our study, as in other similar studies, women constituted the dominating group [1, 11, 19, 41]. It is due to the fact that the fields of study we dealt with women dominate. Other authors conducted research on groups of students composed mainly of men [40, 45]. The age of respondents in our research did not exceed 21 years of age, as in case of research performed by other authors [7, 19]. Perry and Ettarh [40], in their paper reported a much higher percentage of respondents 21 years of age.

The analysis of questionnaires reveals that Catholicism was the dominating religion among students in Poland, which reflects the cross-section of Polish society in terms of religious beliefs. According to the research of other authors, the majority of respondents were also Christians, with Catholics prevailing [19, 41]. There are also studies conducted on students of other creeds [1, 3, 21, 37, 42].

Analysing the responses of students, which referred to the importance of classes in prosectorium, it has been found that a clear majority of them considered such classes to be undoubtedly needed in the course of studies at medical universities. It has been also found in other studies, in which most students considered cadaveric dissections, and thus classes at dissection table, to be a significant element of studies in normal anatomy [11, 19, 34].

Students of both nursing and physiotherapy positively assessed the usefulness of various sources of knowledge concerning human anatomy. In their opinion, anatomical preparations were the most useful ones. The study of Vertemati et al. [49] resulted in somewhat different responses, which entailed that artificial anatomical models are the most useful aids for learning anatomy. Azer and Eizenberg [7] inquired first year students of medical faculties about the same. The answers no doubts, the future medical doctors were of the opinion that cadavers prepared for learning human anatomy were the most useful teaching aids [7].

The knowledge concerning body donation for educational and scientific purposes was sufficient among Medical University of Silesia students of both

nursing and physiotherapy. Most respondents were aware of the Conscious Body Donation Programme, their main source of information was the University staff. Abbasi Asl et al. [1] obtained similar results in their study. Mwachaka et al. [37] conducted a study involving first year medical students from the University of Nairobi, Kenya, which revealed that the majority of study subjects have not heard about any local programme of body donation after death. In another study, conducted in Nigeria, the researchers asked medical students about their knowledge concerning body donation after death. The research conclusion was the most of them had no knowledge about it [22].

Body donation for educational and scientific purposes after death plays a significant role in educating the future representatives of the health care sector. The analysis of results obtained via questionnaire studies demonstrated that quite a low percentage of students declared willingness to become body donors after death. It can also be concluded from the responses of both groups that almost twice as many students of physiotherapy (24.59%) in comparison with the students of nursing (11.94%) declared readiness to become body donors. Similar results were obtained by researchers from other countries. This may have resulted from more hours devoted to teaching anatomy at the dissecting table. Two studies have been conducted in Nigeria. In the first, 13% of subjects supported body donation after death, with only 4.1% declaring the same in the other [3]. In the study involving students of medical university in Kenya, those who opted for making a body donation amounted to 22.2% of subjects [37]. Research by De Gamma et al. [21] among South African students indicated that a mere 14.7% of students there would agree to make a body donation after death. Biljana et al. [11] published a paper which reports that only 20% of students from the Serbian University of Novi Sad would be willing to be body donors. In the study performed in Iran, only 25.4% of students would agree to make a body donation after death [1]. There were also studies reporting quite different results. In India, a study was published which reported that a majority of students would agree to become body donors [45], a likewise declaration was made by 78% of Spanish students of nursing [32]. Quiroga-Garza et al. [41] conducted their research using students of a Mexican medical university as subjects, they also received similar results, with as many as 63.5% of students declaring to make body donation for educational and scientific purposes after death. In the study performed by Jenkin et al. [29], 82.5% of Australian students declared support for organ donation, with only 26.5% being positive about body donation. Similar results have been obtained by Parsa et al. [39].

We compared students' attitudes towards body donation after death with the attitude towards donation of organs for transplantation. The results demonstrated that the majority of students, both from the field of nursing (65.67%) and physiotherapy (52.46%) have the preference for being donors of organs for transplantation, rather than making body donation for educational and scientific purposes. Those result appear to confirm that in Polish society body donation for the purpose of organ transplantation is more publicized and popularized. Researchers from other countries obtained similar results [3, 41, 45].

The main reason in case of reluctance to make body donation for educational and scientific purposes that was provided by physiotherapy students was the psychological barrier, whereas the most often cause of reluctance among physiotherapy students was the concern regarding family; students do not want family members to suffer anew. Students' responses given in other studies differed from those provided in the study reported here. Saha et al. [45] reported the condition of cadaveric dissections as the main course of reluctance. De Gama et al. [21] published a study which points out to religious beliefs as the main reason for reluctance in making body donation for educational use after death among South African students. Serbs, in the results of their studies, noted that most students would not decide to make a body donation due to possible lack of respect for the cadaver [11].

Students of nursing who were ready to make body donation after death would be willing to do so mainly because of their awareness of the need for development of medical sciences, their willingness to help in advancing medical research, knowledge, science, as well as fostering the education of future doctors and medical personnel. What motivated the students of physiotherapy was the awareness that medical sciences need to develop. In other studies published on that topic, responses were pretty similar. De Gama et al. [21] noted that in case of most students the decision of becoming a body donor is motivated by the eagerness to help in teaching anatomy and conducting research. Biljana et al. [11]

published quite comparable results, where most people provided being of assistance in medical research as the main reason, along with being of use after death, and helping others.

In our study, the majority (73.13%) of nursing students expressed the opinion that classes held in prosectorium have not influenced their attitude towards making body donation for educational or scientific purposes after death. The responses of physiotherapy students were different, with more than half of them (50.82%) stating that those classes influenced their attitude towards body donation. The reason for differences in the attitude between students from those two fields may be connected with the amount of classes at dissecting table, planned in their curricula. Future physiotherapists definitely have more numerous opportunities to use cadaveric dissections than future nurses.

Research that has been published worldwide also suggests that classes at dissecting table may influence the attitude of students towards making body donation for educational or scientific purposes after death. Perry and Ettarh [40] as well as Cahill and Ettarh [16] conducted studies involving students of medical universities using three questionnaires: the first one was distributed before students began their classes in prosectorium, the second one after the first class, and the third one after the second class. The results of both studies occurred to be similar. Cahill and Ettarh [15, 16] noted that before the class was held in prosectorium environment, 23.4% of subjects were reluctant to become donors, 7.1% definitely did not want to be donors, while 31.5% opted for becoming body donors after death. Ultimately, in the third questionnaire, the results changed significantly: reluctance towards making the donation increased from 23.4% to 40.2%, definite refusal percentage went up from 7.1% to 18.6%. The percentage of respondents who would agree to make the donation dropped from 31.5% to 19.6% [16]. Perry and Ettarh [40] also reported a similar decrease. The willingness of persons who before classes at dissection table wanted to become cadaver donors (35.1%) ultimately dropped to 24.3%, whereas the reluctance to make body donation after death increased, from initial 16.25% to 27% [40]. Martinez-Alarcon et al. [32] analysed the attitude of Spanish students of nursing towards cremation, burial, and autopsy. They have analysed a total of 750 students as regards responses given. 71% accept cremations, mainly those who are not afraid of body mutilation, 86% of them accept autopsies [32]. Singh et al. [48] assessed the attitude to body donation among students of nursing coming from Nepal. Forty-three per cent of those students are prepared to donate their bodies. In the opinion of those students, the motivators for donating the corpse after death include celebrities, family members, as well as lecturers [48].

CONCLUSIONS

In summary, it can be stated that numerous factors influence the attitude of students to body donation for scientific purposes. More stress on educating students is required, which could contribute to changing their attitude towards that altruistic act, thus increasing the number of donors in the future.

Founding

The study was financed from contract for statutory purposes of the Medical University of Silesia, No. KNW-1-025/N/8/P.

Conflict of interest: None declared

REFERENCES

1. Abbasi Asl J, Nikzad H, Taherian A, et al. Cultural acceptability and personal willingness of Iranian students toward cadaveric donation. Anat Sci Educ. 2017; 10(2): 120–126, doi: 10.1002/ase.1634, indexed in Pubmed: 27517382.
2. Alamneh Y. Knowledge and attitude towards ethical cadaver dissection among medical and health sciences students, 1997–2020: A systematic review and meta-analysis. Transl Res Anat. 2021; 25: 100149, doi: 10.1016/j.tria.2021.100149.
3. Anyanwu EG, Obikili EN, Agu AU. The dissection room experience: A factor in the choice of organ and whole body donation: a Nigerian survey. Anat Sci Educ. 2014; 7(1): 56–63, doi: 10.1002/ase.1370, indexed in Pubmed: 23650046.
4. Arráez-Aybar LA, Biasutto S, Amer MAR, et al. Latin American Anatomists' views on human body dissection and donation. Ann Anat. 2023; 246: 152037, doi: 10.1016/j.aanat.2022.152037, indexed in Pubmed: 36436719.
5. Arráez-Aybar LA, Bueno-López JL, Moxham BJ. Anatomists' views on human body dissection and donation: an international survey. Ann Anat. 2014; 196(6): 376–386, doi: 10.1016/j.aanat.2014.06.004, indexed in Pubmed: 25048843.
6. Asante EA, Maalman RS, Ali MA, et al. Perception and attitude of medical students towards cadaveric dissection in anatomical science education. Ethiop J Health Sci. 2021; 31(4): 867–874, doi: 10.4314/ejhs.v31i4.22, indexed in Pubmed: 34703187.
7. Azer SA, Eizenberg N. Do we need dissection in an integrated problem-based learning medical course? Perceptions of first- and second-year students. Surg Radiol Anat.

2007; 29(2): 173–180, doi: 10.1007/s00276-007-0180-x, indexed in Pubmed: 17318286.
8. Bajor G, Likus W, Kuszewski P, et al. "Mortui vivos docent" or who gives his body to science? The analysis of the personal questionnaires of Polish donors in the Conscious Body Donation Program. PLoS One. 2015; 10(3): e0121061, doi: 10.1371/journal.pone.0121061, indexed in Pubmed: 25790303.
9. Barcik J, Pilarz Ł. Wykorzystanie zwłok i szczątków ludzkich przez studentów do celów dydaktycznych a przestępstwo znieważenia zwłok z art. 262 § 1 k.k. Czasopismo Prawa Karnego i Badań Prenatalnych. 2016: 1–31.
10. Batista EL, Nascimento MM, Castro AR, et al. Perception of Brazilian medical students toward organ donation. Rev Assoc Med Bras (1992). 2022; 68(12): 1675–1680, doi: 10.1590/1806-9282.20220695, indexed in Pubmed: 36449792.
11. Biljana S, Zorka D, Goran Š. Attitudes of medical and allied medical students from Serbia toward whole body donation. Bioscience J. 2016; 32(5): 1388–1402, doi: 10.14393/bj-v32n1a2016-34414.
12. Boduç E, Allahverdi TD. Medical students' views on cadaver and organ donation. Transplant Proc. 2022; 54(8): 2057–2062, doi: 10.1016/j.transproceed.2022.08.021, indexed in Pubmed: 36207151.
13. Bolt S, Venbrux E, Eisinga R, et al. Anatomist on the dissecting table? Dutch anatomical professionals' views on body donation. Clin Anat. 2012; 25(2): 168–175, doi: 10.1002/ca.21215, indexed in Pubmed: 21748808.
14. Boulware LE, Ratner LE, Cooper LA, et al. Whole body donation for medical science: a population-based study. Clin Anat. 2004; 17(7): 570–577, doi: 10.1002/ca.10225, indexed in Pubmed: 15376295.
15. Cahill KC, Ettarh RR. Attitudes to cadaveric organ donation in Irish preclinical medical students. Anat Sci Educ. 2011; 4(4): 195–199, doi: 10.1002/ase.236, indexed in Pubmed: 21656917.
16. Cahill KC, Ettarh RR. Student attitudes to whole body donation are influenced by dissection. Anat Sci Educ. 2008; 1(5): 212–216, doi: 10.1002/ase.42, indexed in Pubmed: 19177413.
17. Champney TH. A bioethos for bodies: respecting a priceless resource. Anat Sci Educ. 2019; 12(4): 432–434, doi: 10.1002/ase.1855, indexed in Pubmed: 30589510.
18. Chu SY, Tseng TC, Ho YC, et al. The impact of a gross anatomy curriculum with donor family interaction: thematic analysis of student letters to silent mentors. Acad Med. 2022; 97(7): 1065–1070, doi: 10.1097/ACM.0000000000004678, indexed in Pubmed: 35320128.
19. Ciliberti R, Gulino M, Gazzaniga V, et al. A survey on the knowledge and attitudes of italian medical students toward body donation: ethical and scientific considerations. J Clin Med. 2018; 7(7), doi: 10.3390/jcm7070168, indexed in Pubmed: 29987216.
20. da Rocha AO, Maués JL, Chies GA, et al. Assessing the impact of a ceremony in honor of the body donors in the development of ethical and humanistic attitudes among medical students. Anat Sci Educ. 2020; 13(4): 467–474, doi: 10.1002/ase.1920, indexed in Pubmed: 31515966.
21. De Gama BZ, Bhengu TT, Satyapal KS. Attitudes of undergraduate South African students towards body donation. Int J Morphol. 2018; 36(1): 130–134, doi: 10.4067/s0717-95022018000100130.
22. Ebeye A, Ojebor C, Alabi A. Perception of organ and corpse donation among students of basic medical sciences. Int J Foren Med Inv. 2016; 2(1): 8, doi: 10.21816/ijfmi.v2i1.10.
23. El-Haddad J, Prvan T, Štrkalj G. Attitudes of anatomy students toward commemorations for body donors: a multicultural perspective. Anat Sci Educ. 2021; 14(1): 89–98, doi: 10.1002/ase.1994, indexed in Pubmed: 32539194.
24. Ergano M, Gerbi A, Hamba N, et al. Assessment of the determinants of Knowledge, Attitude and Practice (KAP) of Ethiopian Medical Students towards ethical Cadaver Dissection. Transl Res Anat. 2020; 19: 100067, doi: 10.1016/j.tria.2020.100067.
25. Gerbi A, Bekele M, Tesfaye S, et al. Knowledge, attitude, and willingness towards cadaveric organ donation among Jimma University medical centre health care professionals. Transl Res Anat. 2020; 18: 100056, doi: 10.1016/j.tria.2019.100056.
26. Habicht JL, Kiessling C, Winkelmann A. Bodies for anatomy education in medical schools: an overview of the sources of cadavers worldwide. Acad Med. 2018; 93(9): 1293–1300, doi: 10.1097/ACM.0000000000002227, indexed in Pubmed: 29561275.
27. Halliday NL, Moon MB, O'Donoghue DL, et al. Transformation and closure for anatomical donor families that meet medical students. Anat Sci Educ. 2019; 12(4): 399–406, doi: 10.1002/ase.1888, indexed in Pubmed: 31038285.
28. Hasselblatt F, Messerer DAC, Keis O, et al. Anonymous body or first patient? A status report and needs assessment regarding the personalization of donors in dissection courses in German, Austrian, and Swiss Medical Schools. Anat Sci Educ. 2018; 11(3): 282–293, doi: 10.1002/ase.1744, indexed in Pubmed: 29742328.
29. Jenkin RA, Garrett SA, Keay KA. Altruism in death: Attitudes to body and organ donation in Australian students. Anat Sci Educ. 2023; 16(1): 27–46, doi: 10.1002/ase.2180, indexed in Pubmed: 35344291.
30. Korf HW, Wicht H, Snipes RL, et al. The dissection course: necessary and indispensable for teaching anatomy to medical students. Ann Anat. 2008; 190(1): 16–22, doi: 10.1016/j.aanat.2007.10.001, indexed in Pubmed: 18342138.
31. Kostorrizos A, Koukakis A, Samolis A, et al. Body donation for research and teaching purposes: the contribution of blood donation units in the progress of anatomical science. Folia Morphol. 2019; 78(3): 575–581, doi: 10.5603/FM.a2018.0103, indexed in Pubmed: 30371929.
32. Martínez-Alarcón L, Balaguer A, Santainés-Borredá E, et al. Nursing students faced with organ donation: Multicenter stratified national study. Nurse Educ Pract. 2022; 63: 103394, doi: 10.1016/j.nepr.2022.103394, indexed in Pubmed: 35797831.
33. Martínez-Alarcón L, Ríos A, López-Navas AI, et al. Attitude toward organ donation related to personal preferences for the final disposition of the dead body in nursing students in Southeast Spain. Transplant Proc. 2018; 50(2): 358–361, doi: 10.1016/j.transproceed.2017.11.065, indexed in Pubmed: 29579803.
34. McMenamin PG, McLachlan J, Wilson A, et al. Do we really need cadavers anymore to learn anatomy in undergraduate medicine? Med Teach. 2018; 40(10): 1020–1029, doi:

10.1080/0142159X.2018.1485884, indexed in Pubmed: 30265177.
35. Mikla M, Rios A, Lopez-Navas A, et al. Factors affecting attitude toward organ donation among nursing students in Warsaw, Poland. Transplant Proc. 2015; 47(9): 2590–2592, doi: 10.1016/j.transproceed.2015.09.031, indexed in Pubmed: 26680044.
36. Mikla M, Rios A, Lopez-Navas A, et al. Organ donation: what are the opinions of nursing students at the University of Bialystok in Poland? Transplant Proc. 2016; 48(7): 2482–2484, doi: 10.1016/j.transproceed.2016.08.024, indexed in Pubmed: 27742329.
37. Mwachaka PM, Mandela P, Saidi H. Repeated exposure to dissection does not influence students' attitudes towards human body donation for anatomy teaching. Anat Res Int. 2016; 2016: 9251049, doi: 10.1155/2016/9251049, indexed in Pubmed: 27190650.
38. Oktem H, Pelin C, Kurkcuoglu A, et al. Attitudes of Turkish university employees and their relatives towards whole body and organ donation. Ann Anat. 2020; 229: 151426, doi: 10.1016/j.aanat.2019.151426, indexed in Pubmed: 31676348.
39. Parsa P, Taheri M, Rezapur-Shahkolai F, et al. Attitudes of Iranian students about organ donation: a qualitative study. BMC Med Ethics. 2019; 20(1): 36, doi: 10.1186/s12910-019-0372-z, indexed in Pubmed: 31138188.
40. Perry GF, Ettarh RR. Age modulates attitudes to whole body donation among medical students. Anat Sci Educ. 2009; 2(4): 167–172, doi: 10.1002/ase.86, indexed in Pubmed: 19459206.
41. Quiroga-Garza A, Reyes-Hernández CG, Zarate-Garza PP, et al. Willingness toward organ and body donation among anatomy professors and students in Mexico. Anat Sci Educ. 2017; 10(6): 589–597, doi: 10.1002/ase.1705, indexed in Pubmed: 28575538.
42. Rajeh NA, Badroun LE, Alqarni AK, et al. Cadaver dissection: a positive experience among Saudi female medical students. J Taibah Univ Med Sci. 2017; 12(3): 268–272, doi: 10.1016/j.jtumed.2016.07.005, indexed in Pubmed: 31435250.
43. Riley K, Evans MM, Hupcey J, et al. Impact of an educational intervention on organ donation attitudes in college-aged students. Omega (Westport). 2021; 84(1): 116–125, doi: 10.1177/0030222819880708, indexed in Pubmed: 31594464.
44. Ríos A, López-Navas A, López-López A, et al. A multicentre and stratified study of the attitude of medical students towards organ donation in Spain. Ethn Health. 2019; 24(4): 443–461, doi: 10.1080/13557858.2017.1346183, indexed in Pubmed: 28665141.
45. Saha A, Sarkar A, Mandal S. Body donation after death: the mental setup of educated people. J Clin Diagn Res. 2015; 9(6): AC05–AC09, doi: 10.7860/JCDR/2015/12246.6011, indexed in Pubmed: 26266106.
46. Saritha S, Rao MV, Supriya G, et al. Voluntary body donation: the gift that lives on forever. Int J Adv Res Technol. 2012; 1: 273–280.
47. Sehirli US, Saka E, Sarikaya O. Attitudes of Turkish anatomists toward cadaver donation. Clin Anat. 2004; 17(8): 677–681, doi: 10.1002/ca.20056, indexed in Pubmed: 15495167.
48. Singh P, Phuyal N, Khadka S, et al. Knowledge of medical students and faculties of a medical college towards human body and organ donation: a descriptive cross-sectional study. J Nepal Med Assoc. 2021; 59(234): 141–145, doi: 10.31729/jnma.6200, indexed in Pubmed: 34506450.
49. Vertemati M, Rizzetto F, Vezzulli F, et al. Teaching anatomy in a modern medical course: an integrated approach at Vialba Medical School in Milan. MedEdPublish. 2018; 7: 19, doi: 10.15694/mep.2018.0000019.1.

VIA MEDICA

CASE REPORT

Folia Morphol.
Vol. 82, No. 4, pp. 932–935
DOI: 10.5603/FM.a2022.0092

ISSN 0015–5659
eISSN 1644–3284
journals.viamedica.pl

Variant origin of three main coronary ostia from the right sinus of Valsalva: report of a rare case

I.N. Dimitrova[1], L. Gaydarski[2], B. Landzhov[2], Ł. Olewnik[3], N. Zielinska[3], R.S. Tubbs[4–8], G.P. Georgiev[9]

[1]*Department of Cardiology, University Hospital "Al. Tschirkov", Medical University of Sofia, Bulgaria*
[2]*Department of Anatomy, Histology and Embryology, Medical University of Sofia, Bulgaria*
[3]*Department of Anatomical Dissection and Donation, Chair of Anatomy and Histology, Medical University of Lodz, Poland*
[4]*Department of Anatomical Sciences, St. George's University, Grenada, West Indies*
[5]*Department of Neurosurgery, Tulane University School of Medicine, New Orleans, Louisiana, United States*
[6]*Department of Neurology, Tulane University School of Medicine, New Orleans, Louisiana, United States*
[7]*Department of Structural and Cellular Biology, Tulane University School of Medicine, New Orleans, Louisiana, United States*
[8]*Department of Surgery, Tulane University School of Medicine, New Orleans, Louisiana, United States*
[9]*Department of Orthopaedics and Traumatology, University Hospital Queen Giovanna – ISUL, Medical University of Sofia, Bulgaria*

[Received: 6 October 2022; Accepted: 14 October 2022; Early publication date: 28 October 2022]

Observing anomalies in the origin of the coronary arteries is a rare but recognised scenario during coronarography. All the major coronary arteries originating from the right sinus of Valsalva is an extremely rare anomaly, its reported incidence being 0.008% in angiographic studies. Most coronary artery variations are benign and are therefore found accidentally or postmortem. However, some anomalies in the origin of the coronary arteries are associated with myocardial ischaemia and a higher risk of sudden cardiac death.

Herein, we report a sporadic case of anomalous origin of the coronary arteries, in which the right coronary artery, anterior interventricular artery and left circumflex artery arise separately from the right sinus of Valsalva, each originating from a separate ostium.

Regardless of their low incidence rate, coronary artery anomalies can cause serious technical challenges during coronary angiography and percutaneous interventions because of the unusual location and course of the artery. Echocardiography, computed tomography, and magnetic resonance imaging can be useful in such cases. (Folia Morphol 2023; 82, 4: 932–935)

Key words: coronary arteries, ostia, variation, coronarography, angiogram

INTRODUCTION

The heart's blood supply is usually carried via the coronary arteries (CAs). Normally, there are two of these, the right (RCA) and left (LCA) coronary arteries. The LCA further separates into the left anterior descending (LAD) (anterior interventricular artery) and left circumflex coronary (LCx) artery. The RCA normally originates from the right sinus of Valsalva (RSV), and the LCA from the left sinus of Valsalva (LSV) [10]. Coronary artery anomalies (CAAs) arise from

Address for correspondence: G.P. Georgiev, MD, PhD, DSc, Department of Orthopaedics and Traumatology, University Hospital Queen Giovanna – ISUL, Medical University of Sofia, 8 Bialo More St., BG1527 Sofia, Bulgaria, tel: +359884 493523, e-mail: georgievgp@yahoo.com

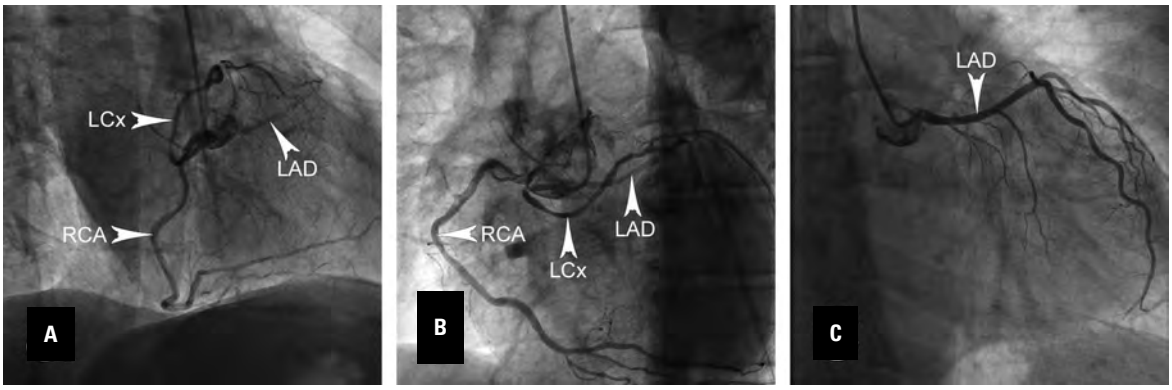

Figure 1. A–C. Coronary angiographic views showing three variant arteries: right coronary artery (RCA), left interventricular (LAD) (anterior interventricular artery) and left circumflex artery (LCx) as separate arteries arising from the right sinus of Valsalva.

a wide diversity of congenital variations in the origin, course and branches of the CA [2]. Such variations are rare, their incidence rate ranging between 0.3% [1] and 3.06% [9]. The vast majority of CAAs are benign and pose no increase in cardiovascular risk, but some rarer CAAs are associated with myocardial ischaemia, congestive heart failure, and sudden cardiac death. Angina can occur because of obstructive coronary artery disease, abnormal origin angulation of the CA, or compression between the aorta and the pulmonary artery. Detailed knowledge of any possible variation of the CA is paramount for all invasive cardiologists and cardiac surgeons to ensure the correct diagnosis and treatment of CA pathology [11].

The aim of the present report is to describe a rare CAA discovered during selective coronary angiography and to highlight the immense importance of recognising such possibilities to preclude complications and unfavourable diagnostic and therapeutic results.

CASE REPORT

A rare anomaly was registered when a 57-year-old male presented with stable angina pectoris for 2 years and no history of syncope. His risk factors were arterial hypertension, dyslipidaemia and smoking. The resting electrocardiography revealed sinus rhythm, left anterior hemiblock and negative T-waves in leads V5–V6. Echocardiography revealed mild symmetric left ventricular hypertrophy, ejection fraction –60%, and no valvular heart disease. The laboratory tests were normal. We considered that the patient had a high clinical likelihood for obstructive coronary artery disease because of typical angina at a low level of exercise that did not affect from optimal medical therapy, and coronary angiography was performed. Initially, the RCA was relatively easily engaged with a 5F JR3.5 diagnostic catheter, and no significant stenosis was visible. Catheterisation of the LCA was then attempted with a 5F JL3.5 diagnostic catheter. After several unsuccessful attempts, and no vessels originating from the left sinus of Valsalva visible, the contrast medium was ejected non-selectively into the RSV, leading to the visualisation of three separate vessels. No left main coronary artery (LCA) was demonstrated. Multiple attempts were made to cannulate the LAD (anterior interventricular artery) and LCX selectively, and we succeeded by using a JR catheter for the LAD (anterior interventricular artery) and an AR1 for the LCx. After thorough and careful catheterisation of each of the three vessels, one of them was found to course to the right margin of the heart and to supply blood to the right atrium and right ventricle; thus, this vessel was named the RCA (Fig. 1A, B). The second vessel descended into the middle of the heart toward the apex, supplying blood to the anterior portion of the interventricular septum; therefore, this vessel was labelled the LAD (anterior interventricular artery) (Fig. 1A–C). The third vessel curved left and posteriorly, surrounding the heart, and was deemed the LCx (Fig. 1A, B). The RCA was dominant and had no stenosis, the LAD (anterior interventricular artery) had moderate stenosis on the distal segment, and the LCx had non-significant stenosis proximally. The patient was discharged with medical therapy and planned for further investigations after 3 months.

DISCUSSION

Anomalies in the origin of the CA are rarely reported. Alexander and Griffith [1], in an autopsy study,

reported a 0.3% mean incidence of CAAs. Lipsett et al. [8], in another multicentred autopsy study, found a 0.5% incidence rate. In an angiographic study of 126,595 patients, Yamanaka and Hobbs [12] reported a 1.3% rate. Yildiz et al. [13] reported a 1% incidence rate in an angiographic study of 12,457 patients. According to the angiographic study by Sidhu et al. [9], the incidence rate of CAAs is 3.06%. Among the various CAAs described, the most common are anomalies in the origin of the LCx and LCA [8, 12, 13]. In contrast, CAAs involving multiple vessels arising from the RSV via separate ostia have been described in only a few case reports [4]. Yildiz et al. [13] reported all the major CAs arising from the RSV in 0.008% of the population. Origins of all three coronaries from the RSV, as in our case, were reported by Asciutto et al. [3] and Chan et al. [5]. Suspicion for this during angiography is based on the detection of an "avascular area" in the anatomical zone of the LCA and the absence of collaterals [3]. In some cases, this extraordinary origin of all three main arteries cannot be detected by angiography, and multidetector computed tomography can be used for correct evaluation of the coronary anatomy [3, 5].

Coronary artery anomalies are most commonly asymptomatic and are discovered by chance or during an autopsy postmortem [1, 6]. Nevertheless, they are clinically important owing to their association with higher cardiovascular risk and the threat of sudden cardiac death [11]. According to Yamanaka and Hobbs [12], CAAs can be separated into two groups according to their origin and course: benign, and potentially serious. An LCx originating from the RSV is classed as a benign variation. However, a LAD (anterior interventricular artery) originating from the RSV is deemed potentially serious [12], especially if it courses between the aorta and the pulmonary trunk, when it is associated with exercise-induced sudden cardiac death [11]. Serious complications could be provoked in such cases if angiography is conducted by an inexperienced interventional cardiologist; it is a technically and logistically demanding procedure. Moreover, the management of patients with such an anomaly is not clear because guidelines are lacking and cases are extremely rare.

Through the literature, several different types of classification have been proposed to provide a detailed and precise depiction of CAAs. Angelini et al. [2] proposed a thorough and sophisticated approach that categorised CAAs on the basis of their origin, course, intrinsic anatomy, termination site and anastomoses. According to this classification, our anomaly should be classified as A4b2c1 [2]. Another classification, more limited and nowhere near as complex, was proposed by Dollar and Roberts [7]. This classification considers only the number of ostia in the coronary sinuses. It has three categories, for one to three ostia in the coronary sinus [7].

CONCLUSIONS

Despite their rarity, anomalies in the origin of the coronary arteries can pose severe diagnostic, technical and therapeutic problems during coronary angiographies. Therefore, detailed knowledge of these variations is essential for the correct diagnosis and treatment of any pathology regarding the coronary arteries.

Conflict of interest: None declared

REFERENCES

1. Alexander RW, Griffith GC. Anomalies of the coronary arteries and their clinical significance. Circulation. 1956; 14(5): 800–805, doi: 10.1161/01.cir.14.5.800, indexed in Pubmed: 13374855.
2. Angelini P, Velasco JA, Flamm S. Coronary anomalies: incidence, pathophysiology, and clinical relevance. Circulation. 2002; 105(20): 2449–2454, doi: 10.1161/01.cir.0000016175.49835.57, indexed in Pubmed: 12021235.
3. Asciutto S, La Franca E, Cirrincione G, et al. Anomalous origin of all three coronary arteries from right sinus of Valsalva. Indian Heart J. 2016; 68(Suppl 2): S85–S87, doi: 10.1016/j.ihj.2016.08.005, indexed in Pubmed: 27751340.
4. Bartorelli AL, Capacchione V, Ravagnani P, et al. Anomalous origin of the left anterior descending and circumflex coronary arteries by two separate ostia from the right sinus of Valsalva. Int J Cardiol. 1994; 44(3): 294–298, doi: 10.1016/0167-5273(94)90295-x, indexed in Pubmed: 8077077.
5. Chan NH, Alama M, Swarbrick D. Anomalous origin of the three coronary arteries with separate ostia from right sinus of Valsalva in a young patient presenting with myocarditis: a very rare congenital anomaly. Eur Heart J Case Rep. 2019; 3(4): 1–2, doi: 10.1093/ehjcr/ytz186, indexed in Pubmed: 32123790.
6. de Oliveira DM, Gomes V, Caramori P. Intravascular ultrasound and pharmacological stress test to evaluate the anomalous origin of the right coronary artery. J Invasive Cardiol. 2012; 24(6): E131–E134, indexed in Pubmed: 22684396.
7. Dollar AL, Roberts WC. Retroaortic epicardial course of the left circumflex coronary artery and anteroaortic intramyocardial (ventricular septum) course of the left anterior descending coronary artery: an unusual coronary anomaly and a proposed classification based on the number of coronary ostia in the aorta. Am J Cardiol. 1989; 64(12): 828–829, doi: 10.1016/0002-9149(89)90780-7, indexed in Pubmed: 2801543.

8. Lipsett J, Cohle SD, Berry PJ, et al. Anomalous coronary arteries: a multicenter pediatric autopsy study. Pediatr Pathol. 1994; 14(2): 287–300, doi: 10.3109/15513819409024261, indexed in Pubmed: 8008691.
9. Sidhu NS, Wander GS, Monga A, et al. Incidence, characteristics and atherosclerotic involvement of coronary artery anomalies in adult population undergoing catheter coronary angiography. Cardiol Res. 2019; 10(6): 358–368, doi: 10.14740/cr941, indexed in Pubmed: 31803334.
10. Standring S, Borley NR, Gray H. Gray's anatomy: the anatomical basis of clinical practice. Churchill Livingstone/ Elsevier, Edinburg 2008.
11. Taylor A, Virmani R. Coronary artery anomalies in adults: which are high risk? ACC Curr J Rev. 2001; 10(5): 92–95, doi: 10.1016/s1062-1458(01)00426-3.
12. Yamanaka O, Hobbs RE. Coronary artery anomalies in 126,595 patients undergoing coronary arteriography. Cathet Cardiovasc Diagn. 1990; 21(1): 28–40, doi: 10.1002/ccd.1810210110, indexed in Pubmed: 2208265.
13. Yildiz A, Okcun B, Peker T, et al. Prevalence of coronary artery anomalies in 12,457 adult patients who underwent coronary angiography. Clin Cardiol. 2010; 33(12): E60–E64, doi: 10.1002/clc.20588, indexed in Pubmed: 21184546.

VIA MEDICA

CASE REPORT

Folia Morphol.
Vol. 82, No. 4, pp. 936–942
DOI: 10.5603/fm.97261

ISSN 0015–5659
eISSN 1644–3284
journals.viamedica.pl

Superficial brachioulnar artery in man

P. Flisiński[1], M. Badura[1], M. Szpinda[1, 2]

[1]*Department of Anatomy, Ludwik Rydygier Collegium Medicum in Bydgoszcz, Nicolaus Copernicus University in Torun, Bydgoszcz, Poland*
[2]*Medical Faculty, Academy of Applied Medical and Social Sciences, Elblag, Poland*

[Received: 4 September 2023; Accepted: 26 September 2023; Early publication date: 29 September 2023]

The individual arterial pattern of the upper limb is considerably variable (11–24%) and relevant for intraarterial interventions performed by cardiologists, plastic and vascular surgeons, radiologists, anaesthesiologists, transplant specialists, orthopaedists and neurosurgeons. Arterial variants in the upper limb result from modifications in the maintenance and regression of the initial capillary plexus, which forms dominant arterial channels and gradually expands into the growing upper limb bud between stages 12 and 21. In this case report we present the superficial brachioulnar artery with its external diameter of 3 mm and length of 525 mm, and of relevant course in the left upper limb of a 78-year-old male Caucasian formalin-fixed cadaver. The superficial brachioulnar artery unusually started with the superior part of axillary artery, presented the following five parts: axillary, brachial, cubital, antebrachial and palmar, and was finally continuous with the superficial palmar arch. The typical ulnar artery was somewhat hypoplastic and limited to the forearm. To the best of our knowledge, this is the first report in the professional literature to describe the start of the superficial brachioulnar artery with the superior part of axillary artery. We conclude the individual arterial pattern of the upper limb to be indispensably recognised preoperatively, so as to circumvent any unwanted injuries to the superficial brachioulnar artery that is considerably large, overlies the antebrachial fascia and supplies the superficial palmar arch. (Folia Morphol 2023; 82, 4: 936–942)

Key words: superficial brachioulnar artery, superficial ulnar artery, axial artery, arterial variants, variant origin of ulnar artery, upper limb, Rodriguez-Niedenführ classification

INTRODUCTION

The arterial supply to the upper limb is derived from the subclavian artery and consecutively comprises the following arteries: the axillary artery in the axillary cavity, the brachial artery in the arm that bifurcates in the cubital fossa into the ulnar and radial arteries. Both the ulnar and radial arteries traverse the forearm and enter the hand to end in the superficial and deep palmar arches, respectively. The boundaries between the subclavian and axillary arteries, the axillary and brachial arteries, and the brachial and both antebrachial arteries refer to the following levels: the outer border of rib I, the inferior border of teres major muscle and the neck of radius, respectively [1–4, 6, 22–25, 29].

Rodriguez-Niedenführ et al. [22–25] proposed the comprehensive terminology for arterial variants in the upper limb. An atypical origin of the radial artery from either the axillary artery in the axillary cavity or the

Address for correspondence: Prof. M. Szpinda, Department of Anatomy, Ludwik Rydygier Collegium Medicum in Bydgoszcz, Nicolaus Copernicus University in Torun, ul. Łukasiewicza 1, 85–821 Bydgoszcz, Poland, e-mail: michal.szpinda@cm.umk.pl

brachial artery in the arm used to be called a "high origin of the radial artery" or "high bifurcation of the brachial artery", and now is referred to as the brachioradial artery, with the reported incidence of 4.67% to 15.6% [4, 22–25]. On the other hand, an ulnar artery with a high origin that courses over the superficial forearm flexor muscles and displays a kind of relevant aberrant artery in the arm and forearm is defined as the superficial brachioulnar artery (SBUA) [22–25]. The incidence of the SBUA ranges from 0.67% to 9.38%, with only 0.17% to 2% starting with the axillary artery [19]. It may originate from either the axillary artery [6, 10, 11, 14, 16, 18, 19, 22–25, 30, 31] or the brachial artery [3, 17, 28, 30, 31], passes deeply in the arm, mostly traverses subcutaneously in the forearm or rarely underlies the antebrachial fascia, and finally ends in the superficial palmar arch.

The arterial arrangement of the upper limb is undoubtedly relevant for intraarterial interventions performed by cardiologists, plastic and vascular surgeons, radiologists, anaesthesiologists, transplant specialists, orthopaedists and neurosurgeons [1–8, 11, 12, 17, 18, 21, 26, 27]. The incidence of anatomic variations of the major arteries of the upper limb ranges from 11% to 24% [19]. Failure to recognize or appropriately manage the SBUA may result in a compromised surgical outcome [8]. Since the SBUA usually arches and overlies the antebrachial fascia it may inadvertently be mistaken for either a superficial antebrachial vein or superficial phlebitis, and so be injured by presumptive venipuncture [9, 11, 15, 25, 26, 30]. Such a large subcutaneous artery in the forearm is prone to unwanted injury and brings an elevated risk of bleeding complications in unexpected situations [3, 5, 6, 9, 11, 13, 14].

In the present case report we have described the unique SBUA — with its external diameter of 3 mm and length of 525 mm — which unusually originated from the superior part of axillary artery, in the arm passed superficially to the median nerve, overlay the antebrachial fascia, reached the distal one-fourth of the ulnar antebrachial groove, and finally ended in the superficial palmar arch. To the best of our knowledge, this is the first report in the professional literature to describe the origin of the SBUA from the superior part of axillary artery.

CASE REPORT

We report on the SBUA, arising from the superior part of axillary artery, which was encountered in the left upper limb of a 78-year-old male Caucasian embalmed cadaver during a routine didactic dissection at Department of Normal Anatomy of Ludwik Rydygier Collegium Medicum in Bydgoszcz of Nicolaus Copernicus University in Torun in the academic year 2021/2022. The consecutive course of SBUA was then carefully dissected and documented (Fig. 1A–E).

The SBUA passed transitionally throughout its course in the arm and forearm, without giving off any branches. In the hand it was continuous with the superficial palmar arch. In terms of topography, the SBUA presented the following five parts: axillary, brachial, cubital, antebrachial and palmar. The external diameter of the SBUA was 3 mm throughout its course.

The axillary part of SBUA with its length of 73 mm stemmed anteriorly from the superior part of axillary artery, some 35 mm proximally to the pectoralis minor muscle, just between the medial and lateral roots of median nerve. It passed deeply in the axillary cavity, as an anterolateral relation of the median nerve. On exiting the axilla, the SBUA entered the medial bicipital groove.

The brachial part of SBUA with its length of 121 mm traversed the medial bicipital groove subjacent to the brachial fascia and was positioned both superficial to the brachial artery and lateral to the median nerve. While descending in the arm, the SBUA gradually deviated laterally from the brachial artery.

The cubital part of SBUA with its length of 79 mm assumed the most lateral and superficial position in the cubital fossa. It was crossed anteriorly by the hypoplastic cephalic vein; the latter together with the basilic vein formed the brachial vein.

The antebrachial part of SBUA with its length of 192 mm proceeded superficially since it overlay the antebrachial fascia, and followed from radial to ulnar, without any concomitant structures. Before approaching the ulnar nerve in the distal one-fourth of the ulnar antebrachial groove, the SBUA through the antebrachial fascia crossed anteriorly the three antebrachial flexors: pronator teres muscle, flexor carpi radialis muscle and palmaris longus muscle. After reaching the end of ulnar antebrachial groove the SBUA adopted the course of a typical ulnar artery.

The palmar part of SBUA with its length of 73 mm overlay the carpal tunnel, by passing through the ulnar canal of Guyon, along the radial side of the pisiform bone. After crossing the ulnar side of the hook of hamate bone it directed radially, so as to be continuous with the superficial palmar arch.

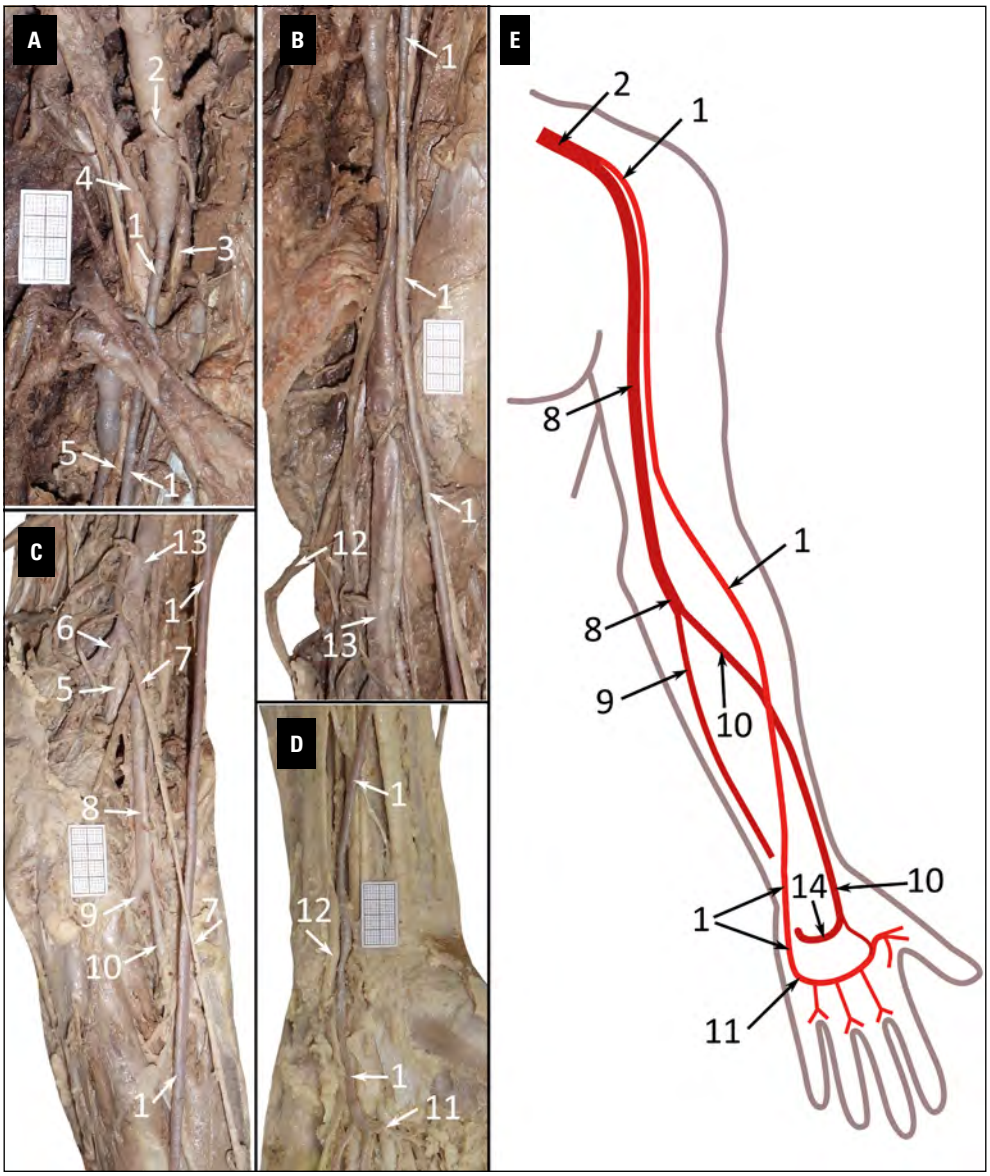

Figure 1. A–E. The consecutive course of the superficial brachioulnar artery through the axillary cavity, arm, cubital fossa, forearm and palm: 1 — superficial brachioulnar artery; 2 — axillary artery; 3 — lateral root of median nerve; 4 — medial root of median nerve; 5 — median nerve; 6 — basilic vein; 7 — hypoplastic cephalic vein; 8 — brachial artery; 9 — ulnar artery; 10 — radial artery; 11 — superficial palmar arch; 12 — ulnar nerve; 13 — brachial vein; 14 — deep palmar arch.

It is noteworthy that in the present case both the ulnar and radial arteries started typically at the brachial artery bifurcation, but the former was somewhat hypoplastic. The course of the hypoplastic ulnar artery was limited to the forearm alone. Consequently, the ulnar artery did not reach the hand, being completely excluded from the formation of the superficial palmar arch.

DISCUSSION

In order to comprehensively discuss the SBUA its following three aspects will successfully be emphasized: the embryology, variability and clinical aspects.

Embryology of the SBUA

In terms of embryology, at stage 12 the upper limb bud is solely supplied by an initial capillary plexus, which is a derivative of the dorsal aorta. The maturation, enlargement and remodelling of this initial capillary plexus extends in a proximal to distal sequence as the bud of upper limb grows, finally resulting in formation of a single vessel, called the axial artery [2–4, 23, 29]. The axial artery consecutively differentiates into its following four segments: subclavian and axillary arteries by stage 15, the brachial artery extending until the elbow by

stage 17 and the anterior interosseous artery by stage 18 [23, 27].

Formation of the subclavian artery indicates bilateral differences: the left subclavian artery is wholly derived from the left seventh intersegmental artery, while the right subclavian artery is a derivative of three arteries: the right fourth aortic arch, a segment of the right dorsal aorta and the right seventh intersegmental artery [27, 30]. The axillary, brachial and anterior interosseous arteries traverse the shoulder, the arm and the forearm, respectively. The anterior interosseous artery ends in the palmar plexus, i.e. the primitive deep palmar arch. Due to both an angiogenic sprouting mechanism and remodelling of the initial capillary plexus by stage 18 develop the proximal part of the radial artery arising from the brachial artery, and antebrachial arteries: the median and posterior interosseous arteries, followed by the ulnar artery. The posterior interosseous artery is destined for the extensor compartment of forearm, while the median artery accompanies the median nerve and ends in the primitive superficial palmar arch. It should be emphasized that the radial artery is "youngest", being definitively formed as late as stage 21.

Regression of the distal part of the median artery results in its disconnection from the primitive superficial palmar arch, which by stage 18 is joined by the ulnar artery, a branch of the primary anterior interosseous artery. Afterwards, regression of the distal part of the anterior interosseous artery results in its disconnection from the primitive deep palmar arch, which is soon joined by the distal part of the primitive radial artery, arising in the middle of the brachial artery. After the proximal part of the primitive radial artery — referring to the inferior half of arm — atrophies, the brachial artery somewhat above the ulnar artery origin gives off a short stem of the radial artery, which joins the primitive radial artery in the cubital fossa and together form the radial artery by stage 21. The proximal segment of the primary anterior interosseous artery between origins of the radial and ulnar arteries is finally involved into the ulnar artery. It is noteworthy that the ulnar artery was primarily a branch of the anterior interosseous artery, but after the proximal segment of the anterior interosseous artery was incorporated in the ulnar artery, the anterior interosseous artery became a branch of the ulnar artery. The definitive arterial pattern of the upper limb is organized by stage 21.

Unlike the modified sprouting theory developed by Poteat [20], according to Rodriguez-Niedenführ et al. [23], certain capillary vessels maintain, enlarge and differentiate into arteries, while the others regress, resulting in dominant arterial channels, which form the final individual arterial pattern, including anomalous arteries. The SBUA results from the embryological abnormality, called the superficial brachial artery [2, 18, 23]. The superficial brachial artery probably develops from branches of the sixth and seventh cervical intersegmental arteries, finally stems from either the axillary artery or the brachial artery, passes deeply in the arm — but superficial to the median nerve — and superficially in the forearm. Its superficial course with relation to the median nerve may result in its entrapment neuropathy [2]. In the forearm the superficial brachial artery may end in a four-fold manner. Firstly, it may substitute for the hypoplastic ulnar artery and adopts its distal course as the SBUA [11, 14, 16–19, 22–25, 30, 31], described in the present case report. Secondly, the superficial brachial artery adopts a typical radial artery as the superficial brachioradial artery [13]. Thirdly, the superficial brachial artery may bifurcate and contribute to the superficial brachioulnoradial artery [23]. Fourthly, the superficial brachial artery adopts the superficial brachiomedian artery [23].

Variability of the SBUA

The variability of the arterial tree in the upper limb was unequivocally unified by the Rodriguez-Niedenführ classification [23]. Anomalous arteries are named after a combination of their topography and ending, and their deep or superficial position as superficial brachial, superficial brachioradial, superficial brachioulnar, superficial brachioulnoradial and superficial brachiomedian arteries. All these anomalous arteries are formed as late as the arrangement of the brachial artery is definitively achieved, i.e. stage 17 onwards [4, 23].

In the professional literature, the SBUA was precisely described in human cadavers by anatomical dissection [3, 5, 6, 16, 17, 22, 24] and in a minority in embryos by three-dimensional reconstruction [23, 25] and in living subjects by angiography [30], Doppler ultrasound [16] and raising of antebrachial flaps [5, 21]. Typically, the SBUA originates from either the inferior part of axillary artery just below the subscapular artery [9, 11, 14, 16, 18, 19, 22–25, 30, 31] or from the proximal half of brachial artery [3, 10, 17, 31].

Sporadically, the SBUA may stem from the middle part of axillary artery [7, 10, 19]. After reviewing the professional literature, we failed to find the SBUA arising from the superior part of axillary artery, as presented in this case report. Thus, to the best of our knowledge, this is the first report in the professional literature to present the SBUA, which originates from the superior part of axillary artery.

After originating from the axillary artery, the SBUA underlies the brachial fascia, crosses in front the medial and lateral roots of median nerve, and afterwards descends superficially to the median nerve, as does the SBUA originating from the brachial artery [25]. It is usually subjacent to the bicipital aponeurosis, less commonly overlies it, and sporadically perforates it to assume an epifascial position in the forearm [25]. The SBUA crosses superficially the common flexor tendon, usually overlies the antebrachial fascia and sporadically underlies it to eventually adopt its typical position in the inferior half of ulnar antebrachial groove [25].

Because the SBUA is of great variability, its blood supply territory may consequently be highly variable [3]. The reported overall incidence of the SBUA ranges from 1% [30] to 9.38% [5]. As emphasized by Rodriguez-Niedenführ et al. [25], the SBUA more commonly originated from the brachial artery when compared to the axillary artery. The origin of SBUA from the axillary artery changed from 0.17% to 2% [11, 18, 22–25, 30, 31], while from the brachial artery was found in 4.2% [25]. The combination of bilateral SBUA originating from the axillary arteries appears to be extremely rare [6, 10, 11]. Gupta et al. [10] found the bilateral SBUA, in both upper limbs originating from the middle part of axillary artery. The left SBUA unusually underlay the antebrachial fascia and sent off a few muscular branches to superficial antebrachial flexors, while the right one overlay the antebrachial fascia; bilateral arteries were continuous with the superficial palmar arch.

Clinical aspects of the SBUA

Vascular anomalies in the arm and forearm tend to increase the likelihood of damaging the superficial anomalous arteries during surgery [21]. Thus, awareness of numerous arterial variations in the upper limb is of great interest to clinicians of different specialties: cardiologists, plastic and vascular surgeons, and radiologists for successful interventional and surgical procedures — including native arteriovenous fistulae for dialysis — anaesthesiologists for monitoring vital signs during invasive procedures and in the intensive care unit, orthopaedists and neurosurgeons while performing surgery in the carpal tunnel or the ulnar canal of Guyon. The use of antebrachial arteries for coronary artery bypass grafting indispensably requires accurate knowledge of the pattern and extent of anomalous vessels, including the SBUA [10]. As a pulsatile vessel, the SBUA may easily be diagnosed preoperatively by careful palpation, and its course may precisely be confirmed by vascular Doppler ultrasound [3, 5]. The SBUA in the forearm gives off several adequate fasciocutaneous branches, on which a fasciocutaneous flap, similar to a radial forearm flap, may be raised with safety [5, 9, 11, 21]. Otherwise, when raising forearm flaps in reconstructive surgery any accidental damage to the SBUA can seriously jeopardize hand circulation [5]. The usefulness of the flap with the SBUA lies in it uncomplicated dissection, preservation of both antebrachial arteries, and thus circumventing any vascular compromise to the upper limb [22]. An understanding of anomalous antebrachial arteries prerequisites the creation of autogenous fistulae in patients undergoing haemodialysis [10, 12]. During the surgical creation of another arteriovenous fistula from a transposed basilic vein in a patient with the radial artery occluded due to thrombosis of a previously performed radiocephalic fistula Frunze et al. [7] found the SBUA to be closely related to the course of the basilic vein. Had these authors ligated the SBUA during preparation of the basilic vein, a blood flow to the palmar arches would have been stopped completely, causing hand ischaemia. The presence of the SBUA may lead to accidental intraarterial injection or misinterpretation of angiographic images during surgical procedures in the upper limb [10].

CONCLUSIONS

While surgery in the upper limb is required, the individual arterial pattern should indispensably be recognised, so as to circumvent any unwanted injuries to the main supplying artery of unusual course like the SBUA.

The SBUA is a transitional vessel in the arm and forearm that substitutes for the distal part of the typical ulnar artery and is continuous with the superficial palmar arch.

Conflict of interest: None declared

REFERENCES

1. Aharinejad S, Nourani F, Hollensteiner H. Rare case of high origin of the ulnar artery from the brachial artery. Clin Anat. 1997; 10(4): 253–258, doi: 10.1002/(sici)1098-2353(1997)10:4<253::aid-ca7>3.0.co;2-t.
2. Clarke E, Mazurek A, Radek M, et al. Superficial brachial artery – a case report with commentaries on the classification. Trans Res Anat. 2021; 23: 100112, doi: 10.1016/j.tria.2021.100112.
3. Clarke E, Skrzat J, Mazur M, et al. Anatomical variations of the superficial ulnar artery: case series observed on historical specimens prepared by Ludwik Karol Teichmann. Folia Morphol. 2022; 81(1): 227–233, doi: 10.5603/FM.a2021.0014, indexed in Pubmed: 33577075.
4. Clarke E, Skrzat J, Tubbs RS, et al. Rare origin of the brachioradial artery – a case found on a historical specimen prepared by Ludwik Karol Teichmann. Trans Res Anat. 2021; 23: 100109, doi: 10.1016/j.tria.2020.100109.
5. Devansh. Superficial ulnar artery flap. Plast Reconstr Surg. 1996; 97(2): 420–426, doi: 10.1097/00006534-199602000-00022, indexed in Pubmed: 8559826.
6. Fadel RA, Amonoo-Kuofi HS. The superficial ulnar artery: development and surgical significance. Clin Anat. 1996; 9(2): 128–132, doi: 10.1002/(sici)1098-2353(1996)9:2<128::aid-ca5>3.0.co;2-d.
7. Frunze S, Grochowiecki T, Ciąćka T, et al. The importance of the superficial brachioulnar artery during surgical creation of an arteriovenous fistula for dialysis from a transposed basilic vein – potential implications for hand ischemia in case of a previously thrombosed radiocephalic arteriovenous fistula. Polish Surgery. 2011; 13(2): 166–170, doi: 10.5603/chp.28774.
8. Funk GF, Valentino J, McCulloch TM, et al. Anomalies of forearm vascular anatomy encountered during elevation of the radial forearm flap. Head Neck. 1995; 17(4): 284–292, doi: 10.1002/hed.2880170403, indexed in Pubmed: 7672968.
9. Görmüs G, Özçelik M, Çelik H, et al. Variant origin of the ulnar artery. Clin Anat. 1998; 11(1): 62–64, doi: 10.1002/(sici)1098-2353(1998)11:1<62::aid-ca11>3.0.co;2-l.
10. Gupta G, Singh K, Chhabra S, et al. Bilateral superficial ulnar artery with high origin from the axillary artery: its anatomy and clinical significance. Folia Morphol. 2012; 71(1): 48–51, indexed in Pubmed: 22532186.
11. Jacquemin G, Lemaire V, Medot M, et al. Bilateral case of superficial ulnar artery originating from axillary artery. Surg Radiol Anat. 2001; 23(2): 139–143, doi: 10.1007/s00276-001-0139-2, indexed in Pubmed: 11462864.
12. Kinnaert P. Relevance of the ulnaris fistula as a dialysis shunt. Nephrol Dial Transplant. 1995; 10(12): 2379, doi: 10.1093/ndt/10.12.2379a, indexed in Pubmed: 8808256.
13. Konarik M, Knize J, Baca V, et al. Superficial brachioradial artery (radial artery originating from the axillary artery): a case-report and Its embryological background. Folia Morphol. 2009; 68(3): 174–178, indexed in Pubmed: 19722162.
14. Mannan A, Sarikcioglu L, Ghani S, et al. Superficial ulnar artery terminating in a normal ulnar artery. Clin Anat. 2005; 18(8): 602–605, doi: 10.1002/ca.20150, indexed in Pubmed: 16187323.
15. McWilliams RG, Sodha I. Doppler ultrasound diagnosis of a superficial ulnar artery. Eur J Ultrasound. 2000; 12(2): 155–157, doi: 10.1016/s0929-8266(00)00106-3, indexed in Pubmed: 11118923.
16. Nakatani T, Tanaka S, Mizukami S, et al. The superficial ulnar artery originating from the axillary artery. Ann Anat. 1996; 178(3): 277–279, doi: 10.1016/S0940-9602(96)80068-9, indexed in Pubmed: 8712378.
17. Nakatani T, Tanaka S, Mizukami S. Superficial ulnar artery originating from the brachial artery and its clinical importance. Surg Radiol Anat. 1998; 20(5): 383–385, doi: 10.1007/BF01630626, indexed in Pubmed: 9894322.
18. Natsis K, Papadopoulou AL, Paraskevas G, et al. High origin of a superficial ulnar artery arising from the axillary artery: anatomy, embryology, clinical significance and a review of the literature. Folia Morphol. 2006; 65(4): 400–405, indexed in Pubmed: 17171623.
19. Panagouli E, Tsaraklis A, Gazouli I, et al. A rare variation of the axillary artery combined contralaterally with an unusual high origin of a superficial ulnar artery: description, review of the literature and embryological analysis. Ital J Anat Embryol. 2009; 114(4): 145–156, indexed in Pubmed: 20578671.
20. Poteat WL. Report of a rare human variation: absence of the radial artery. Anat Rec. 1986; 214(1): 89–95, doi: 10.1002/ar.1092140115, indexed in Pubmed: 3954062.
21. Ramani CV, Kundagulwar GK, Prabha YS, et al. Anomalous superficial ulnar artery based flap. Indian J Plast Surg. 2014; 47(1): 124–126, doi: 10.4103/0970-0358.129643, indexed in Pubmed: 24987217.
22. Rodriguez-Baeza A, Nebot J, Ferreira B, et al. An anatomical study and ontogenic explanation of 23 cases with variations in the main pattern of the human brachio-antebrachial arteries. J Anat. 1995; 187(Pt 2): 473–479, indexed in Pubmed: 7592009.
23. Rodríguez-Niedenführ M, Burton GJ, Deu J, et al. Development of the arterial pattern in the upper limb of staged human embryos: normal development and anatomic variations. J Anat. 2001; 199(Pt 4): 407–417, doi: 10.1046/j.1469-7580.2001.19940407.x, indexed in Pubmed: 11693301.
24. Rodríguez-Niedenführ M, Sañudo JR, Vázquez T, et al. Anastomosis at the level of the elbow joint connecting the deep, or normal, brachial artery with major arterial variations of the upper limb. J Anat. 2000; 196(Pt 1): 115–119, doi: 10.1046/j.1469-7580.2000.19610115.x, indexed in Pubmed: 10697294.
25. Rodríguez-Niedenführ M, Vázquez T, Nearn L, et al. Variations of the arterial pattern in the upper limb revisited: a morphological and statistical study, with a review of the literature. J Anat. 2001; 199(Pt 5): 547–566, doi: 10.1046/j.1469-7580.2001.19950547.x, indexed in Pubmed: 11760886.
26. Sañudo JR, Mirapeix RM, Garcia R, et al. A superficial ulnar artery anastomosing with a larger anterior interosseous artery to supply the wrist and hand. J Anat. 1998; 192(Pt 3): 439–441, doi: 10.1046/j.1469-7580.1998.19230439.x, indexed in Pubmed: 9688511.
27. Sieger J, Patel L, Sheikh K, et al. Superficial brachioulnar artery and its clinical significance. Anat Cell Biol. 2019;

52(3): 333–336, doi: 10.5115/acb.19.008, indexed in Pubmed: 31598363.
28. Solan S. Accessory superficial ulnar artery: a case report. J Clin Diagn Res. 2013; 7(12): 2943–2944, doi: 10.7860/JCDR/2013/6688.3799, indexed in Pubmed: 24551682.
29. Szpinda M. Anatomia prawidłowa człowieka. 1th ed. Vol. 1. Wydawnictwo Medyczne Edra Urban & Partner, Wrocław 2022.
30. Uglietta JP, Kadir S. Arteriographic study of variant arterial anatomy of the upper extremities. Cardiovasc Intervent Radiol. 1989; 12(3): 145–148, doi: 10.1007/BF02577379, indexed in Pubmed: 2507150.
31. Yazar F, Kirici Y, Ozan H, et al. An unusual variation of the superficial ulnar artery. Surg Radiol Anat. 1999; 21(2): 155–157, doi: 10.1007/s00276-999-0155-1, indexed in Pubmed: 10399219.

VIA MEDICA

CASE REPORT

Folia Morphol.
Vol. 82, No. 4, pp. 943–947
DOI: 10.5603/FM.a2022.0111

ISSN 0015–5659
eISSN 1644–3284
journals.viamedica.pl

Branching pattern of the internal iliac artery accompanied by a venous anastomosis: rare vascular variations

M. Kula[1], Ł. Olewnik[1], K. Ruzik[1], R.S. Tubbs[2–7], A. Balcerzak[1], N. Zielinska[1]

[1]*Department of Anatomical Dissection and Donation, Medical University of Lodz, Poland*
[2]*Department of Anatomical Sciences, St. George's University, Grenada, West Indies*
[3]*Department of Neurosurgery, Tulane University School of Medicine, New Orleans, Louisiana, United States*
[4]*Department of Neurology, Tulane University School of Medicine, New Orleans, Louisiana, United States*
[5]*Department of Structural and Cellular Biology, Tulane University School of Medicine, New Orleans, Louisiana, United States*
[6]*Department of Surgery, Tulane University School of Medicine, New Orleans, Louisiana, United States*
[7]*Department of Neurosurgery, Ochsner Medical Centre, New Orleans, Louisiana, United States*

[Received: 10 July 2022; Accepted: 21 August 2022; Early publication date: 23 December 2022]

The ability to navigate the complex and often deceptive branching patterns of the internal iliac artery can be decisive in planning and performing surgeries within the lesser pelvis. The following case report presents a peculiar quadruple division of the internal iliac artery, accompanied by a venous anastomotic structure. Apart from the posterior and anterior trunks, the superior vesicle and iliolumbar arteries arose independently from the internal iliac artery. The division was surrounded by a venous oval, compressing certain branches and potentially complicating surgical access. Due to the uncommon course of the internal iliac artery and the presence of the anastomosis, a possible nerve root compression has been identified. Both clinical significance and classification method of the case are discussed. Knowledge of this anatomical variation is valuable for both diagnosis and surgery, especially within the specialties of urology, gynaecology and general surgery. (Folia Morphol 2023; 82, 4: 943–947)

Key words: anatomical variations, internal iliac artery, case report

INTRODUCTION

The internal iliac artery (IIA), also known as the hypogastric artery, is the main blood vessel supplying the walls and organs of the pelvis, the reproductive organs, buttocks, muscles of the lumbar region and the medial section of the thigh. About 3–4 cm long, it is significantly smaller than the external iliac artery [7]. The IIA arises at the bifurcation of the common iliac artery, anterior to the pelvic brim, at the level of the L5-S1 intervertebral disc [16]. It descends posteriorly to the upper margin of the sciatic foramen, where it divides into two branches, the posterior and anterior trunks (AT).

The posterior trunk (PT) bends posteriorly and passes towards the greater sciatic foramen, exiting the pelvis above the piriformis muscle. It most commonly gives off three parietal branches, the iliolumbar, lateral sacral and superior gluteal arteries, the last-named being its termination. The AT passes proximally to the piriformis muscle and the sacral plexus until it reaches the lower section of the sciatic foramen. It gives rise to six visceral branches: the umbilical, superior vesi-

Address for correspondence: Ł. Olewnik, MD, PhD, Department of Anatomical Dissection and Donation, Chair of Anatomy and Histology, Medical University of Lodz, ul. Żeligowskiego 7/9, 90–410 Łódź, Poland, e-mail: lukasz.olewnik@umed.lodz.pl

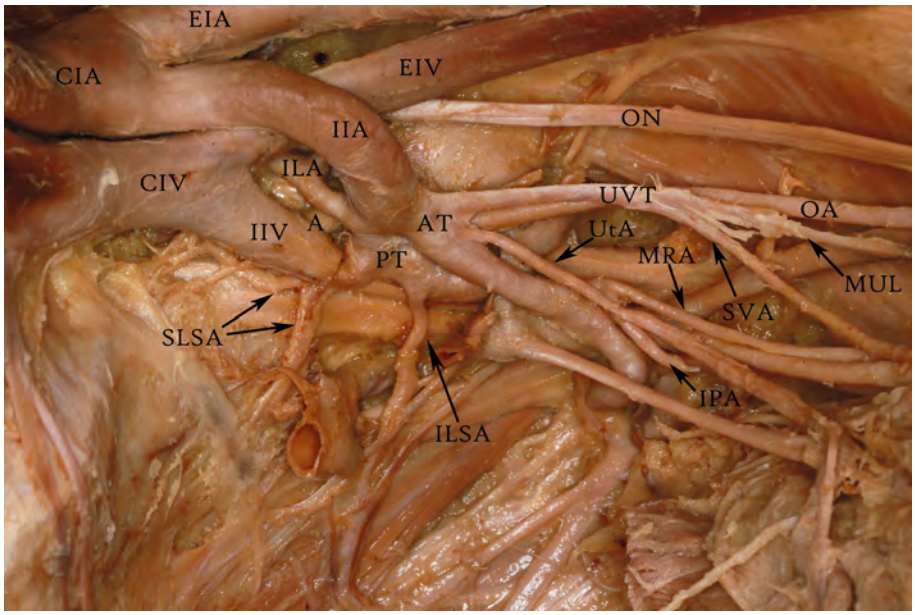

Figure 1. Branching point of a left internal iliac artery seen from the medial perspective. Section of a left internal iliac vein has been resected for better exposure; A — point of anastomosis of the EIV (beginning of the venous circle); AT — anterior trunk of internal iliac artery; CIA — common iliac artery; CIV — common iliac vein; EIA — external iliac artery; EIV — external iliac vein; IIA — internal iliac artery; IIV — internal iliac vein; ILA — iliolumbar artery; ILSA — inferior lateral sacral artery; IPA — interior pudendal artery; MRA — medial rectal artery; MUL — median umbilical ligament; OA — obturator artery; ON — obturator nerve; PT — posterior trunk of internal iliac artery; SLSA — superior lateral sacral artery; SVA — superior vesical artery; UtA — uterine artery; UVT — umbilico-vesical trunk.

cal, inferior vesical and middle rectal arteries and, in females, the vaginal and uterine arteries. It also gives off two parietal branches, the obturator and inferior gluteal arteries, the latter being its termination.

The following case study describes an unusual branching pattern of the IIA. Instead of giving rise to two main trunks that further divided into its terminations, the IIA divided into four lower calibre branches, the iliolumbar and superior vesical arteries arised directly from its main trunk. The division was encircled by a venous anastomotic structure derived from the internal iliac vein. The anastomosis passed between the posterior and AT of the IIA, surrounding the artery's division and coming back beneath the iliolumbar artery (ILA) before ending its course, reaching the external iliac artery.

Understanding the elusive branching pattern of the IIA is invaluable for clinicians, especially gynaecologists [9]. This knowledge is likely to prove essential during surgical procedures in which a certain part of the artery needs to be ligated in order to control pelvic haemorrhage.

CASE REPORT

A female cadaver 75 years old at death was subjected to routine anatomical dissection for research and educational purposes at the Department of Anatomical Dissection and Donation, Medical University of Lodz, Poland. During a routine assessment of the lumbosacral plexus, an anomaly of IIA branching was identified (Fig. 1).

The lengths and widths of the branches were measured using a digital calliper. A detailed analysis of the branching pattern revealed an unusual division, which has not previously been described to our knowledge. Additionally, a venous anastomotic structure surrounding the division was exposed (Fig. 2).

The IIA begins its course at the bifurcation of the common iliac artery. It is 38.6 mm long and its diameter is 7.21 mm. After branching out of the common iliac artery, it descends medially alongside the posterior pelvic wall towards the external iliac vein (EIV). Upon passing the EIV it descends towards the pelvic floor for approximately 16 mm before giving rise to its 5 branches: the ILA, the superior lateral sacral artery, the PT, the AT, and the superior vesical artery (SVA) from which the medial umbilical ligament arises. Immediately after branching from the IIA, the ILA (7.94 mm) bends upwards and runs on top of the anastomosis of the internal iliac vein, then passes beneath the EIV and divides into its terminations, the iliac and lumbar branches. The uterine artery (UtA) begins at the AT 3.12 mm below the origin

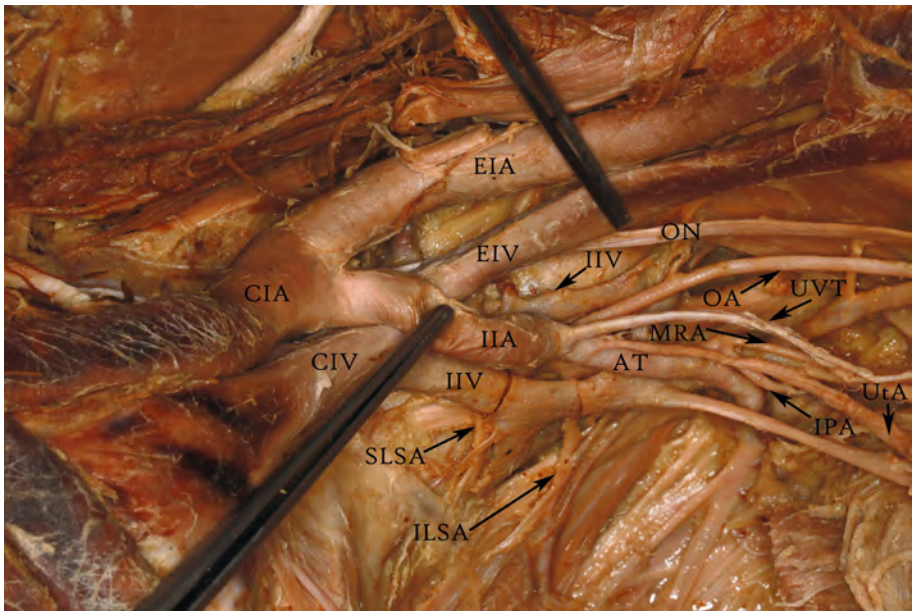

Figure 2. Branching of the internal iliac artery surrounded by a venous anastomosis originating from the internal iliac vein. Top-down perspective; AT — anterior trunk of internal iliac artery; CIA — common iliac artery; CIV — common iliac vein; EIA — external iliac artery; EIV — external iliac vein; IIA — internal iliac artery; IIV — internal iliac vein; ILA — iliolumbar artery; ILSA — inferior lateral sacral artery; IPA — interior pudendal artery; MRA — medial rectal artery; OA — obturator artery; ON — obturator nerve; SLSA — superior lateral sacral artery; UtA — uterine artery; UVT — umbilico-vesical trunk.

of the umbilico-vesical trunk and descends towards the uterus. The internal pudendal artery and the middle rectal artery share a short (6.09 mm) common trunk, which begins at the AT 20 mm below the beginning of the UtA and almost immediately bifurcates, creating points of origin for the aforementioned vessels. After giving off the internal pudendal artery and the middle rectal artery, the AT passes anteriorly for 18 mm and then bends posteriorly, exiting the lesser pelvic cavity between the L5 and S1 spinal nerves and below the piriformis muscle to become the inferior gluteal artery. Further dissection and assessment of the inferior gluteal artery ruled out the presence of a sciatic artery. The PT arises from the IIA below the AT and descends anteriorly. Before exiting the pelvic cavity above the piriformis muscle and becoming the superior gluteal artery, it gives off the inferior lateral sacral artery 7 mm below the superior lateral sacral artery, and the obturator artery, which arises from the PT directly opposite the inferior lateral sacral artery. Further dissection and analysis of the obturator artery and the inferior epigastric artery ruled out the presence of a "corona mortis" anastomosis [2]. The PT is 4.43 mm in diameter.

The venous anastomotic structure originates from the internal iliac vein and is oval. The anastomosis is 9.48 mm wide and 19.76 mm long and encircles the division of the IIA. The PT of the IIA passes through the venous circle and descends towards the pelvic floor, whereas the AT runs anteriorly, resting on top of the anastomosis, pressing it down against the PT. Applied pressure forces the PT down, causing it to rest on the L5 root of the sciatic nerve (Table 1).

Table 1. Measurements of the structures of interest

Structure	Length [mm]	Width [mm]
Internal iliac artery	38.6	7.21
Anterior trunk	41.97	3.97
Posterior trunk	22	4.43
Iliolumbar artery	7.94	3.12
Uterine artery	84.41	2.22
Umbilico-vesical trunk	27	2
Umbilical ligament	90	1.34
Vesical artery	79.4	1.47
Obturator artery	47.3	1.67
Middle rectal artery	29	1.22
Internal pudendal artery	19.4	1.25
Internal iliac vein anastomosis	19.76	9.48

Ethical approval

The cadavers belonged to the Department of Anatomical Dissection and Donation, Medical University of Lodz, Poland.

DISCUSSION

Since the pelvic vascularisation is intricate, it is essential for a wide range of specialists such as gynaecologists, urologists, proctologists and general surgeons to understand the possible anatomical variations of the IIA to maximise the efficiency of certain procedures [3, 5, 11, 14]. Especially in laparoscopic surgery, there is a huge demand for precise descriptions of pelvic vascularisation to help preclude iatrogenic injuries [10, 13, 18].

The branching pattern described here resembles type III in the Balcerzak classification [1] because three main branches (AT, PT, ILA) exit the common trunk. However, certain nuances such as a SVA arising directly from the IIA instead of the AT, and two sacral lateral arteries, distinguish it significantly since none of them are considered in Balcerzak's system [1]. The artery described in the present article has a further uncommon anatomical variation: the obturator artery branches out of the posterior division of the IIA. Pai et al. [15] estimated the prevalence of a similar variant at 8–10%. This has some clinical value: during procedures such as embolization or ligation of the obturator artery, it is vital for the operator to be aware of the possible points of origins of the vessel. Such knowledge can reduce the duration of the procedure and thereby minimise potential complications [20].

Since the IIA provides the main blood supply to the uterus, it is also crucial in the development of a range of uterine pathologies such as adenomyosis [17] and uterine fibroids [12]. Both those conditions are exacerbated by an excessive blood supply from the UtA, which is why UtA embolisation provides effective treatment. During this procedure, a catheter is inserted through the femoral or radial artery into the IIA and then into the UtA. It is therefore important for the surgeon to have a good understanding of the highly variable branching pattern of IIA in order to avoid dire complications. For instance, in the case presented here, the procedure could prove difficult because of the close proximity (3.12 mm) of the UtA to the SVA and the difference in vessel diameters: UtA: 1.72 mm, SVA: 2.2 mm. This could lead to accidental insertion of the catheter into the SVA; or puncture of the AT, inevitably causing profuse haemorrhage.

Because the IIA follows a sinuous course and is close to major nerves, anatomical variations often correlate directly with compression syndromes. Conditions such as aneurysms involving a drastic increase of the artery's diameter are the most common causes of such pathologies. In a recent case study, de Bruijn et al. [6] described a type IA (Balcerzak, 2021) IIA containing an aneurysm located between the L5 and S1 nerve roots. The location of the aneurysm combined with the artery's branching pattern elicited buttock ischaemia and neurological symptoms such as impairment of active knee and plantar foot flexion, absent dorsal flexion, and sensitivity disorders below the knee, all caused by nerve root compression [6]. In the case presented here, owing to the venous anastomosis, the PT of the IIA applied considerable pressure on the L5 nerve, causing it to deform. It is unclear whether this caused any discomfort during life, but it certainly aggravated or increased the risk of closely-related conditions such as wallet neuritis, lotus neuropathy or piriformis syndrome.

Rupture of the IIA and its branches is a rare but potentially lethal complication that can occur during pregnancy [4, 19]. In a case report describing three instances of utero-ovarian ruptures, Ginsburg et al. [8] estimate the initial overall mortality at up to 49%. However, owing to the rapid development of intensive intraoperative and postoperative treatments, a decline to 3.6% has been noted (Table 2) [8].

Table 2. The 2021 Balcerzak classification. "Main vessels" include the superior gluteal, inferior gluteal, internal pudendal and sciatic arteries (in group V)

Type	Description
Group I	Main vessels have two points of origin: the first is a single branch, the second a common trunk
Subgroup A: Common trunk divides inside the pelvic cavity Subgroup B: Common trunk divides outside the pelvic cavity	
Group II	Main vessels have two points of origin: the first is a common trunk, the second a single branch
Subgroup A: Common trunk divides inside the pelvic cavity Subgroup B: Common trunk divides outside the pelvic cavity	
Group III	Main vessels have three points of origin; order of origin is irrelevant
Group IV	Main vessels have one point of origin; order of origin is irrelevant
Group V	Main vessels have four points of origin; additionally includes the sciatic artery

CONCLUSIONS

In conclusion, variations of the IIA are common and it is nearly impossible to classify them comprehensively. This underlines the importance of supplementing existing classifications with case studies like the present one. Preoperative knowledge of anatom-

ical variants and their relationships to neighbouring structures is crucial in planning and performing surgical procedures on the IIA and in its vicinity.

Conflict of interest: None declared

REFERENCES

1. Balcerzak A, Hajdys J, Shane Tubbs R, et al. Clinical importance of variability in the branching pattern of the internal iliac artery: an updated and comprehensive review with a new classification proposal. Ann Anat. 2022; 239: 151837, doi: 10.1016/j.aanat.2021.151837, indexed in Pubmed: 34601060.
2. Boutefnouchet T, Bassett J, Patil S. Anatomy and clinical relevance of the 'corona mortis': a review of the literature and current aspects of management. J Orthopedics Rheumatol. 2016; 3(2): 5, doi: 10.13188/2334-2846.1000026.
3. Chayen D, Copeliovitch L, Itzhakov Z, et al. An original external iliac artery reconstruction with internal iliac artery translocation in a blunt injury of the pelvic vessels in a 4-year-old child: A 12-year follow-up study. J Vasc Surg Cases Innov Tech. 2019; 5(4): 492–496, doi: 10.1016/j.jvscit.2019.09.003, indexed in Pubmed: 31763506.
4. Cole M, Elton C, Bosio P, et al. Spontaneous rupture of utero-ovarian vessels in labour: a rare case of obstetric haemoperitoneum. J Obstet Gynaecol. 2005; 25(3): 301–303, doi: 10.1080/01443610500105811, indexed in Pubmed: 16147745.
5. Das BN, Biswas AK. Ligation of internal iliac arteries in pelvic haemorrhage. J Obstet Gynaecol Res. 1998; 24(4): 251–254, doi: 10.1111/j.1447-0756.1998.tb00085.x, indexed in Pubmed: 9798353.
6. De Bruijn MT, Verbelen T, Kralt CP, et al. An internal iliac artery aneurysm causing sudden buttock ischemia and nerve root compression. J Vasc Surg Cases. 2015; 1(2): 151–153, doi: 10.1016/j.jvsc.2015.04.015, indexed in Pubmed: 31724591.
7. Fătu C, Puişoru M, Fătu IC. Morphometry of the internal iliac artery in different ethnic groups. Ann Anat. 2006; 188(6): 541–546, doi: 10.1016/j.aanat.2006.05.016, indexed in Pubmed: 17140147.
8. Ginsburg KA, Valdes C, Schnider G. Spontaneous utero-ovarian vessel rupture during pregnancy: Three case reports and a review of the literature. Obstetrics Gynecol. 1987; 69: 474–476, indexed in Pubmed: 3808529.
9. Giordano G, Meo D, Magnano San Lio V. Internal iliac artery aneurysm embolization with direct percutaneous puncture and thrombin injection. Radiol Case Rep. 2020; 15(3): 210–213, doi: 10.1016/j.radcr.2019.11.018, indexed in Pubmed: 31890070.
10. Jeon SH, Lee SH, Choi WC. Iliac artery perforation following lumbar discectomy with microsurgical carbon dioxide laser: a report of a rare case and discussion on the treatment. Spine (Phila Pa 1976). 2007; 32(3): E124–E125, doi: 10.1097/01.brs.0000254078.88358.33, indexed in Pubmed: 17268256.
11. Kemmochi R, Matsumoto M, Kubo Y, et al. Hypogastric and lumbar artery bypasses to restore gluteal perfusion after open aortoiliac aneurysm repair. J Vasc Surg. 2013; 58(4): 1073–1075, doi: 10.1016/j.jvs.2012.12.079, indexed in Pubmed: 23561432.
12. Levy BS. Modern management of uterine fibroids. Acta Obstet Gynecol Scand. 2008; 87(8): 812–823, doi: 10.1080/00016340802146912, indexed in Pubmed: 18607823.
13. Lu Gao J, Lortie K, Singh SS. Laparoscopic internal iliac artery ligation for postpartum spontaneous hemoperitoneum. J Obstet Gynaecol Can. 2010; 32(12): 1172–1175, doi: 10.1016/S1701-2163(16)34742-9, indexed in Pubmed: 21176330.
14. O'Brien MC, Schell BA, Lands H, et al. Massive gluteal muscle necrosis after iliac arterial embolization in pelvic trauma: a literature review and illustrative case report. J Orthop Case Rep. 2018; 8(3): 23–27, doi: 10.13107/jocr.2250-0685.1092, indexed in Pubmed: 30584510.
15. Pai MM, Krishnamurthy A, Prabhu LV, et al. Variability in the origin of the obturator artery. Clinics (Sao Paulo). 2009; 64(9): 897–901, doi: 10.1590/S1807-59322009000900011, indexed in Pubmed: 19759884.
16. Sakthivelavan S, Aristotle S, Sivanandan A, et al. Variability in the branching pattern of the internal iliac artery in Indian population and its clinical importance. Anat Res Int. 2014; 2014: 597103, doi: 10.1155/2014/597103, indexed in Pubmed: 25580296.
17. Sharara FI, Kheil MH, Feki A, et al. Current and prospective treatment of adenomyosis. J Clin Med. 2021; 10(15), doi: 10.3390/jcm10153410, indexed in Pubmed: 34362193.
18. Siedhoff MT, Gubernick L, Ronen I, et al. Internal iliac artery ligation in laparoscopic myomectomy. J Min Inv Gynecol. 2019; 26(7): S1, doi: 10.1016/j.jmig.2019.09.007.
19. Vellekoop J, de Leeuw JP, Neijenhuis PA. Spontaneous rupture of a utero-ovarian vein during pregnancy. Am J Obstet Gynecol. 2001; 184(2): 241–242, doi: 10.1067/mob.2001.110310, indexed in Pubmed: 11174514.
20. Wojciechowski J, Znaniecki L, Brzeziński M. Obturator artery aneurysm. EJVES Extra. 2005; 9(6): 129–130, doi: 10.1016/j.ejvsextra.2005.04.002.

VIA MEDICA

CASE REPORT

Folia Morphol.
Vol. 82, No. 4, pp. 948–952
DOI: 10.5603/FM.a2023.0026

ISSN 0015–5659
eISSN 1644–3284
journals.viamedica.pl

Bilateral absence of the deep brachial artery

W. Przybycień[1], M. Bonczar[1, 2], P. Ostrowski[1, 2], K. Możdżeń[1], A. Murawska[1], A. Gil[1], K. Balawender[3], J. Walocha[1, 2], M. Koziej[1, 2]

[1]*Department of Anatomy, Jagiellonian University Medical College, Krakow, Poland*
[2]*Youthoria, Youth Research Organization, Krakow, Poland*
[3]*Department of Normal and Clinical Anatomy, Institute of Medical Sciences, Medical College of Rzeszow University, Rzeszow, Poland*

[Received: 8 February 2022; Accepted: 12 March 2022; Early publication date: 3 April 2022]

The aim of the following study was to present and comprehensively describe a case of a bilateral absence of the deep brachial artery (DBA). Furthermore, its embryology and clinical significance will also be discussed.

During routine dissection, a 71-year-old male cadaver with a bilateral abnormality in the DBA and its branches was found. The first branch of the brachial artery (BA) was found to be the radial collateral artery, which passed behind the radial nerve. Furthermore, the middle collateral artery originated distal to the radial collateral artery and gave off first a singular, minor muscular branch and then the superior ulnar collateral artery. Later, the preceding nutrient arteries of the humerus and the deltoid branch consecutively branched off from the middle collateral artery. Subsequently, the middle ulnar collateral artery, the inferior ulnar collateral artery, the deltoid artery, the radial artery, and the ulnar artery branched off from the BA, as adapted in the current knowledge regarding the anatomy of the upper extremity. Furthermore, detailed measurements of the distances between the mentioned arteries were carried out.

In the present study, a bilateral absence of the DBA was demonstrated. Meta-analysis focusing on the anatomy of this artery has shown how variable its characteristics are. However, our case report is the first in the literature to present this extremely rare variation. Having adequate knowledge regarding the anatomy of the arteries of the proximal arm is of immense importance when performing orthopaedic and reconstructive surgeries in this area. (Folia Morphol 2023; 82, 4: 948–952)

Key words: deep brachial artery, arm, upper limb, anatomy, embryology

INTRODUCTION

The deep brachial artery (DBA), according to the literature, is considered the largest branch of the brachial artery (BA) in the arm. The DBA arises in the upper part of the arm on the posteromedial side of the BA and then runs in a downward direction, spiralling around the posterior surface of the humerus. During its course, the DBA accompanies the radial nerve and runs parallel to it along the radial groove. It assists in supplying the deltoid, triceps brachii, and anconeus muscles. The DBA divides into two branches as it reaches either the lateral interosseous septum or anterior to this septum. One of these branches is the radial collateral artery which, together with the radial nerve, passes through the lateral intermuscular septum and terminates by anastomosing with the

Address for correspondence: Dr. M. Koziej, Department of Anatomy, Jagiellonian University Medical College, ul. Mikołaja Kopernika 12, 33–332 Kraków, Poland, e-mail: mateusz.koziej@gmail.com

radial recurrent artery. The second branch arising from the DBA is the middle collateral artery which anastomoses with the recurrent interosseous artery [11, 12, 14]. The DBA is involved in periarticular arterial anastomosis, which is located around the elbow joint.

As previously mentioned, the DBA is a branch of the BA, which is a continuation of the axillary artery (AA). During embryological development, the developing limb buds are supplied by the intersegmental arteries. The primary axial artery develops from the lateral branch of the seventh intersegmental artery and becomes the BA, which the DBA originates from [1].

Numerous anatomical variations of the DBA have been presented in the literature. As early as 1931, Charles et al. [2] created a classification based on the origin of the DBA. It consisted of origins such as a common origin with the superior ulnar collateral artery or the subscapular artery, amongst others. Furthermore, reports of double and triple DBAs and the complete absence of this artery have also been reported [2–5, 13, 17].

Variations of the arterial system are frequently observed by medical professionals of many distinct specialties worldwide and oftentimes influence the daily clinical practice in the form of treatment options [18]. Having appropriate knowledge concerning the variable anatomy of the DBA is of immense importance when performing procedures such as the lateral forearm flap, cerclage wiring of the humeral diaphysis, and open subpectoral biceps tenodesis, amongst others [12, 14, 15]. Therefore, the aim of the following study was to present and comprehensively describe a case of a bilateral absence of the DBA. Furthermore, its embryology and clinical significance will also be discussed.

CASE REPORT

During routine dissection, a 71-year-old male cadaver with a bilateral abnormality in the DBA and its branches was found. Despite the currently adapted normal anatomy of the DBA [12, 14], the said vessel was absent.

On the left upper extremity

The first branch of the BA was found to be the radial collateral artery, which passed behind the radial nerve. Furthermore, the middle collateral artery originated distal to the radial collateral artery and gave off first a singular, minor muscular branch and then the superior ulnar collateral artery. Later, the preceding nutrient arteries of the humerus and the deltoid branch consecutively branched off from the middle collateral artery. Subsequently, the middle ulnar collateral artery, the inferior ulnar collateral artery, the deltoid artery, the radial artery, and the ulnar artery branched off from the BA, as adapted in the current knowledge regarding the anatomy of the upper extremity. Furthermore, detailed measurements of the distances between the mentioned arteries were carried out. All measurements were taken three times by three independent researchers (W.P., P.O., and M.B.), and a mean value was established, taking all measurements into account.

The distance between the origin of the radial collateral artery and the origin of the middle collateral artery was found to be 9.22 mm. The said distance was measured over the surface of the BA.

The distance, measured over the surface of the radial collateral artery, between the origin of the said artery and the origin of the first minor muscular artery was found to be 10.28 mm.

The distance, measured over the surface of the middle collateral artery, between the origin of the said artery and the origin of the minor muscular branch was found to be 8.10 mm.

The distance, measured over the surface of the middle collateral artery, between the origin of the minor muscular branch to the origin of the superior ulnar collateral artery was found to be 5.38 mm.

The distance between the origin of the middle collateral artery and the origin of the middle ulnar collateral artery, measured over the surface of the BA, was found to be 15.36 mm.

On the right upper extremity

The branching pattern the aforementioned branches was the same as in the left upper limb.

The distance between the origin of the radial collateral artery and the origin of the middle collateral artery was found to be 16.76 mm. The said distance was measured over the surface of the BA.

The distance, measured over the surface of the radial collateral artery, between the origin of the said artery and the origin of the first minor muscular artery was found to be 11.11 mm.

The distance, measured over the surface of the middle collateral artery, between the origin of the said artery and the origin of the minor muscular branch was found to be 14.91 mm.

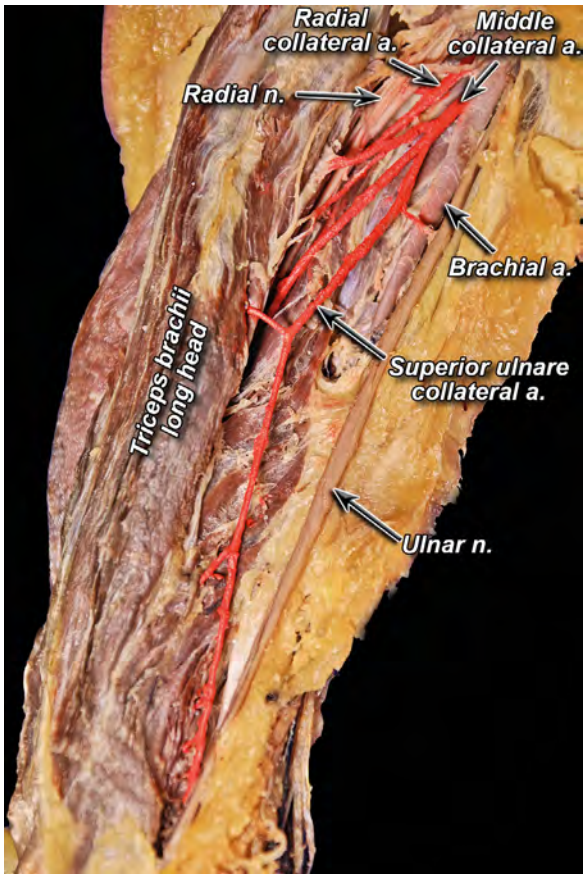

Figure 1. Left upper limb of the said cadaver.

The distance, measured over the surface of the middle collateral artery, between the origin of the minor muscular branch to the origin of the superior ulnar collateral artery was found to be 13.51 mm.

The distance between the origin of the middle collateral artery and the origin of the middle ulnar collateral artery, measured over the surface of the BA, was found to be 32.64 mm.

The mentioned abnormalities are presented in Figures 1 and 2.

DISCUSSION

Multiple studies have discussed the origin of the DBA. However, in a meta-analysis conducted by Przybycien et al. [12], it was stated that the said artery originated most frequently (92.87%) directly from the AA or from the BA. Variations included in this cohort were also cases of multiple DBAs (double, triple, etc.). The pooled prevalence of DBAs originating indirectly from the AA or BA was found to be 7.13%, where common origins with the subscapular artery, the superior ulnar collateral artery, and the posterior circumflex humeral artery were included. However, a total absence of the DBA is one of the rarest variations of the said vessel, especially a bilateral absence, such as the one demonstrated in the present case report. As mentioned earlier, Charles et al. [2] presented a classification system of the various origins of the DBA consisting of seven types. Type I is the DBA branching out of the BA as a single branch, Type Ia is the DBA branching out as a double branch, and type Ib is a triple branch. The DBA may also share a common origin with the superior ulnar collateral artery (type II). The DBA originating at the teres major muscle between axillary and brachial arteries has been classified as type III. Type IV means the DBA branching of the AA. The DBA may also branch off as a common trunk with the posterior circumflex humeral artery (type V). The DBA can originate off the subscapular artery from the axillary artery (type VI). The last variation described is type VII with the complete absence of the DBA. This rare variation was also described by Ciervo in 2001 [3]. The DBA was absent and replaced by an unnamed tortuous branch running between the coracobrachialis and the triceps brachii muscle and then rejoining to the classic BA, next divided into the ulnar and radial. In this case, the ulnar collateral artery was also absent [3, 17]. The present case report demonstrates the variation type VII (the DBA is absent). However, to the best knowledge of the authors, the present study is the first to present a case of a bilateral absence of the DBA in the available literature.

The embryology of the arterial system is incredibly complex; however, understanding it is essential in order to explain the variant anatomy of the upper limb. During the 12th stage of the embryological period, blood vessels course into the developing limb bud. The capillary plexus infiltrates the limb primordium forming the axial artery and marginal veins. The said vessel are responsible for the blood supply of the developing limb and terminal plexus of the future hand. Subsequently, the brachial, axillary, and anterior interosseous arteries develop from the axial artery [12, 14, 15]. The axillary and brachial arteries develop during the 16th and 17th stage of the embryological development [16]. Hence, the variations of the arterial network of the upper limb demonstrated in the present case study, occurred in that period.

Due to the absence of the DBA in the subject described in our study, the radial collateral artery and the middle collateral artery had an abnormal anatomy. The said arteries, both on the left and right upper limb,

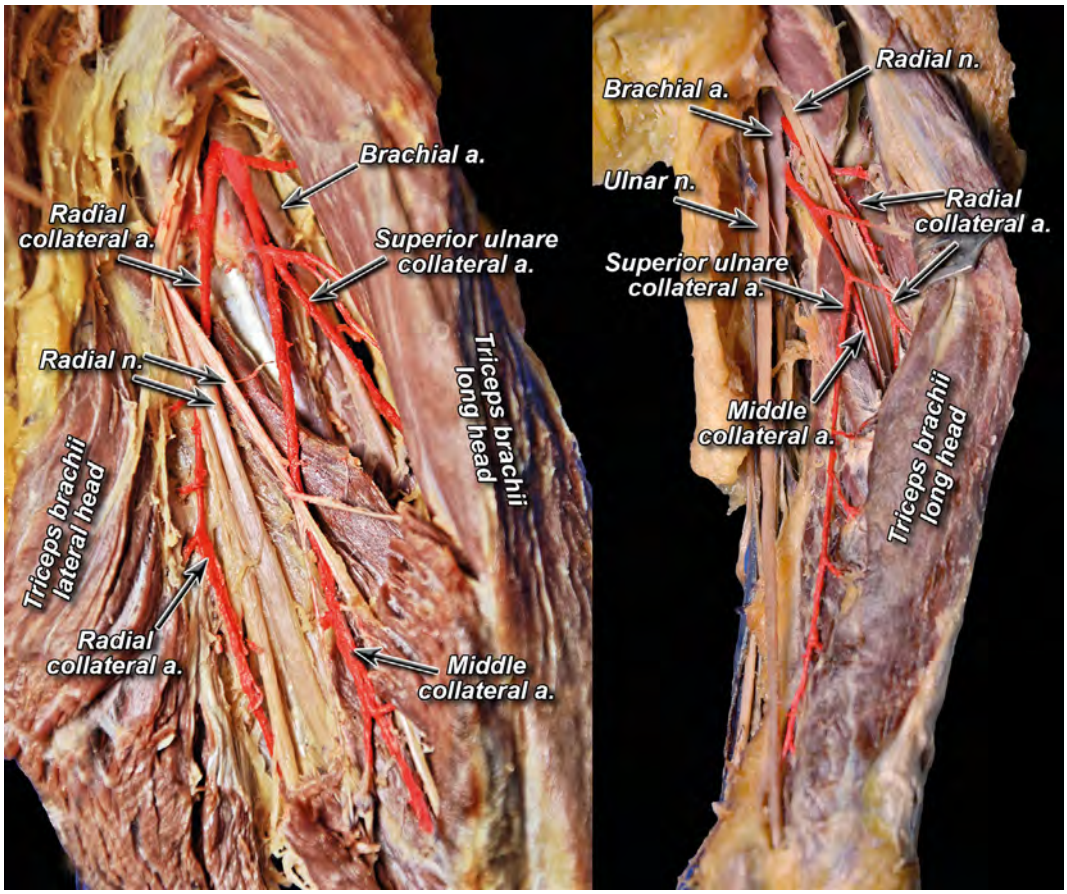

Figure 2. Right upper limb of the said cadaver.

originated directly off the BA. Furthermore, the superior ulnar artery originated from the middle collateral arteries, rather than from its usual origin, which is the BA. This variability of the arterial anatomy of the upper limbs might pose problems when performing numerous surgical procedures in that area. The lateral forearm flap has increased in popularity and is commonly used for covering minor-to-moderate-sized defects for which thin and soft skin is needed [10]. The main artery supplying this reconstructive flap is the radial collateral artery, which is one of the terminating branches of the DBA. The present variation demonstrated in our study can pose problems for surgeons performing this flap, especially if they attempt to locate the radial collateral artery from its origin, which should normally be from the DBA. Furthermore, the close proximity of the radial collateral artery to the radial nerve, as presented in our case report, may put the radial nerve at risk of injury.

The DBA is also important to take into consideration concerning vascular injuries of the BA. The BA has been stated to be the most commonly injured artery of the upper limb, accounting for 28% of all vascular injuries [1, 6]. When evaluating a vascular injury to the BA, it is crucial to analyse whether the injury is proximal or distal to the DBA as this correlates with ischaemia [9]. It is said that if the BA is damaged distal to the origin of the DBA at the inferior border of the teres major muscle, the DBA will act as the primary source of collateral circulation to the distal extremity. Despite the variable arterial anatomy of the proximal upper limbs presented in the current case report, the branches of the DBA still had a relatively proximal origin, approximately at the same level of which a normal DBA would have (being the first branch of the brachial artery).

The cerclage wire technique is generally used as a fixation mechanism for a fracture, to stabilise fractures around the prosthetic stem in the presence of osteoporosis, to prevent intraoperative propagation of a fracture, and as an indirect reduction tool, amongst others [7]. When inserting cerclage wires into the proximal arm, great care must be taken due to the risk of damaging the DBA and the accompanying radial nerve [12]. In our case report, the DBA was

absent bilaterally, and its terminating branches (radial and middle collateral arteries), originated directly off the BA at the same level at which a usual DBA would have. The radial collateral artery, in both upper limbs, coursed beneath the radial nerve, constantly being in a very close proximity to it. Therefore, even though the DBA is absent in our subject, the risk of damaging its terminating arteries would still be as high when performing the cerclage wire technique in the proximal part of the upper limb.

CONCLUSIONS

In the present study, a bilateral absence of the DBA was demonstrated. Meta-analysis focusing on the anatomy of this artery has shown how variable its characteristics are [12]. However, our case report is the first in the literature to present this extremely rare variation. Having adequate knowledge regarding the anatomy of the arteries of the proximal arm is of immense importance when performing orthopaedic and reconstructive surgeries in this area.

Acknowledgements

The authors are deeply beholden to Mr Jacenty Urbaniak for the technical support and graphical depiction. The authors wish to sincerely thank those who donated their bodies to science so that anatomical research could be performed. Results from such research can potentially improve patient care and increase mankind's overall knowledge. Therefore, these donors and their families deserve our highest gratitude [8].

Funding

The author(s) received no financial support for the research, authorship, and/or publication of this article. Dr. Mateusz Koziej was supported by the Foundation for Polish Science (FNP). The funders had no role in the study's design, data collection and analysis, decision to publish, or preparation of the manuscript.

Conflict of interest: None declared

REFERENCES

1. Breeland G, Alshuqayfi HA. Anatomy, Shoulder and Upper Limb, Profunda Brachii Artery. 2022.
2. Charles CM, Penn L, Holden HF, et al. The origin of the deep brachial artery in American white and in American negro males. Anat Rec. 1931; 50(3): 299–302, doi: 10.1002/ar.1090500307.
3. Ciervo A, Kahn M, Pangilinan AJ, et al. Absence of the brachial artery: report of a rare human variation and review of upper extremity arterial anomalies. J Vasc Surg. 2001; 33(1): 191–194, doi: 10.1067/mva.2001.112212, indexed in Pubmed: 11137944.
4. Clarke E, Mazurek A, Radek M, et al. Superficial brachial artery: a case report with commentaries on the classification. Transl Res Anat. 2021; 23: 100112, doi: 10.1016/j.tria.2021.100112.
5. Clarke E, Olszewska A, Zarzecki M, et al. Case report of the brachial artery trifurcation: an anatomical study and concise literature review. Transl Res Anat. 2022; 27: 100198, doi: 10.1016/j.tria.2022.100198.
6. Ekim H, Tuncer M. Management of traumatic brachial artery injuries: a report on 49 patients. Ann Saudi Med. 2009; 29(2): 105–109, doi: 10.4103/0256-4947.51797, indexed in Pubmed: 19318753.
7. Grechenig S, Hohenberger G, Bakota B, et al. Humeral shaft cerclage wiring: a safe technique to prevent radial nerve injury. Injury. 2017; 48 (Suppl 5): S12–S14, doi: 10.1016/S0020-1383(17)30732-5, indexed in Pubmed: 29122115.
8. Iwanaga J, Singh V, Takeda S, et al. Acknowledging the use of human cadaveric tissues in research papers: Recommendations from anatomical journal editors. Clin Anat. 2021; 34(1): 2–4, doi: 10.1002/ca.23671, indexed in Pubmed: 32808702.
9. McCready RA. Upper-extremity vascular injuries. Surg Clin North Am. 1988; 68(4): 725–740, doi: 10.1016/s0039-6109(16)44582-2, indexed in Pubmed: 3046002.
10. Meirer R, Schrank C, Putz R. Posterior radial collateral artery as the basis of the lateral forearm flap. J Reconstr Microsurg. 2000; 16(1): 21–24, doi: 10.1055/s-2000-7537, indexed in Pubmed: 10668750.
11. Moore KL, Dalley AF, Agur A. Clinically oriented anatomy. 8th ed. Lippincott Williams and Wilkins 2017.
12. Przybycień W, Bonczar M, Ostrowski P, et al. The deep brachial artery-A meta-analysis of its origin and diameter with a review of the literature. Clin Anat. 2022; 35(7): 838–846, doi: 10.1002/ca.23853, indexed in Pubmed: 35313051.
13. Przybycień W, Wysiadecki G, Olszewska A, et al. Diverse variants of the profunda brachii artery: a series of three cases. Transl Res Anat. 2022; 27: 100196, doi: 10.1016/j.tria.2022.100196.
14. Przybycień W, Zarzecki M, Musiał A, et al. Anatomy of the deep brachial artery - general overview (cadaveric study) — discussion on terminology. Folia Med Cracov. 2021; 61(3): 85–93, doi: 10.24425/fmc.2021.138953, indexed in Pubmed: 34882666.
15. Rodríguez-Baeza A, Nebot J, Ferreira B, et al. An anatomical study and ontogenetic explanation of 23 cases with variations in the main pattern of the human brachio-antebrachial arteries. J Anat. 1995; 187(Pt 2): 473–479, indexed in Pubmed: 7592009.
16. Rodríguez-Niedenführ M, Burton GJ, Deu J, et al. Development of the arterial pattern in the upper limb of staged human embryos: normal development and anatomic variations. J Anat. 2001; 199(Pt 4): 407–417, doi: 10.1046/j.1469-7580.2001.19940407.x, indexed in Pubmed: 11693301.
17. Tubbs RS, Shoja MM, Loukas M. Bergman's Comprehensive Encyclopedia of Human Anatomic Variation. Wiley 2016.
18. Żytkowski A, Tubbs R, Iwanaga J, et al. Anatomical normality and variability: Historical perspective and methodological considerations. Transl Res Anat. 2021; 23: 100105, doi: 10.1016/j.tria.2020.100105.

VIA MEDICA

CASE REPORT

Folia Morphol.
Vol. 82, No. 4, pp. 953–956
DOI: 10.5603/FM.a2022.0105

ISSN 0015–5659
eISSN 1644–3284
journals.viamedica.pl

A rare occurrence of persistent hypoglossal artery and its clinical significance

S. Yasin[1], R. Tasdemir[2], O.F. Cihan[3]

[1]Department of Neurology, Faculty of Medicine, Gaziantep University, Gaziantep, Turkey
[2]Department of Anatomy, Faculty of Medicine, Gaziantep Islam, Science and Technology University, Gaziantep, Turkey
[3]Department of Anatomy, Faculty of Medicine, Gaziantep University, Gaziantep, Turkey

[Received: 16 September 2022; Accepted: 6 December 2022; Early publication date: 22 December 2022]

Persistent hypoglossal artery (PHA) is an embryological vascular variation mostly originating from the internal carotid artery. The presence of PHA has been associated with the incidence of some diseases such as cerebral ischaemia, atherosclerosis, and aneurysm. Here, a very rare case of PHA that was discovered incidentally by digital subtraction angiography in Turkey is reported. Endovascular stenting was not performed for this patient. Also, its clinical importance is discussed. (Folia Morphol 2023; 82, 4: 953–956)

Key words: persistent hypoglossal artery, digital subtraction angiography, rare variation, vertebrobasilar insufficiency

INTRODUCTION

Presegmental arteries are the carotid-vertebrobasilar anastomoses that supply blood from the internal carotid artery (ICA) to the vertebrobasilar system in the embryonic period. Four pairs of presegmental arteries, which are named for neighbouring structures, arise from the primitive ICA: the trigeminal, otic, hypoglossal, and proatlantal intersegmental arteries (Fig. 1). After the posterior communicating arteries develop and the vertebral and basilar arteries join, these temporary collateral vessels disappear at approximately 5 weeks of gestation [8]. The first to regress is the otic artery, followed by the hypoglossal artery, the trigeminal artery, and then the proatlantal intersegmental arteries [7]. Rarely, primitive carotid-vertebrobasilar anastomoses do not disappear and they persist into adult life. Persistent hypoglossal artery (PHA) is the second most common anastomosis with an incidence of 0.03–0.09% [9]. It has been reported that PHA is more common in females and on the left side [3]. PHA usually originates from the ICA at the C1–C3 level and rarely from the external carotid artery.

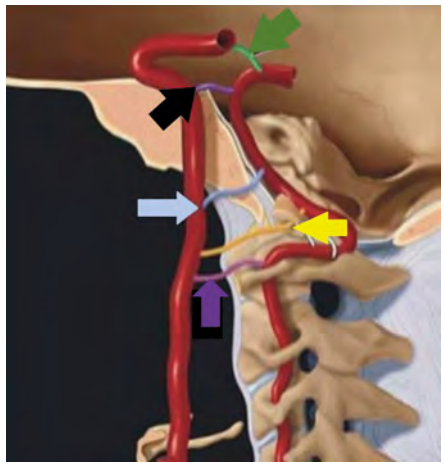

Figure 1. Persistent carotid vertebro-basilar anastomoses. Black and green arrows show trigeminal artery, blue arrow otic artery, yellow arrow hypoglossal artery and purple arrow indicates proatlantal artery. Srinivas et al. (2016) [9] adapted from his work.

CASE REPORT

A 57-year-old male patient presented to our clinic with complaints of numbness of the left arm and left leg, impaired balance, and severe dizziness. On neurological

Address for correspondence: Dr. R. Tasdemir, Department of Anatomy, Faculty of Medicine, Gaziantep Islam, Science and Technology University, Gaziantep, Turkey, tel: +90 505 854 8754, e-mail: rabiatsdmr@gmail.com

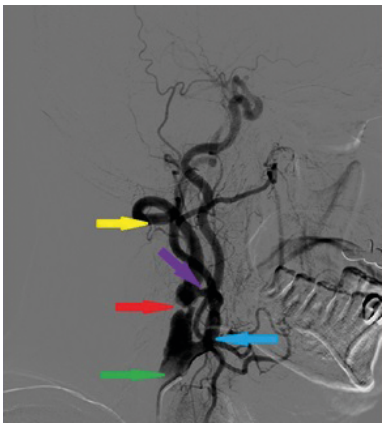

Figure 2. Red arrow shows severe stenosis of the persistent hypoglossal artery (PHA), proximal to the right internal carotid artery, and distal to the bulb on the right side of the patient on digital subtraction angiography imaging; yellow arrow indicates PHA. Green arrow shows common carotid artery, blue arrow external carotid artery and purple arrow proximal right internal carotid artery.

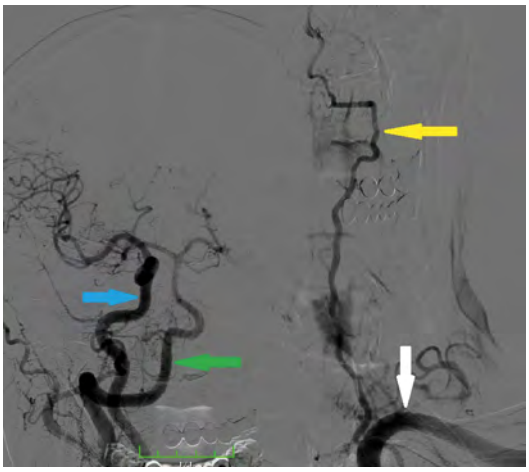

Figure 4. Left vertebral artery appears hypoplastic compared to right side persistent hypoglossal artery (PHA). Yellow arrow indicates left vertebral artery, green arrow PHA, blue arrow right internal carotid artery and white arrow left subclavian artery.

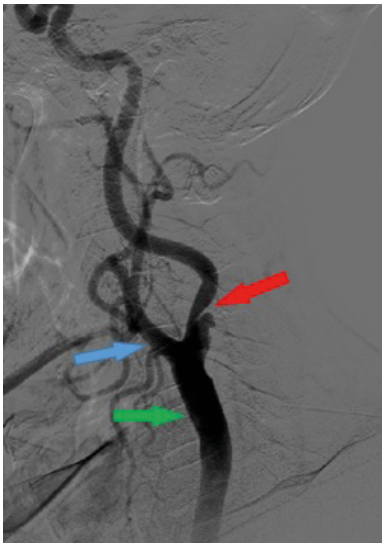

Figure 3. Red arrow shows stenosis of the left internal carotid artery on digital subtraction angiography imaging. Green arrow shows common carotid artery and blue arrow external carotid artery.

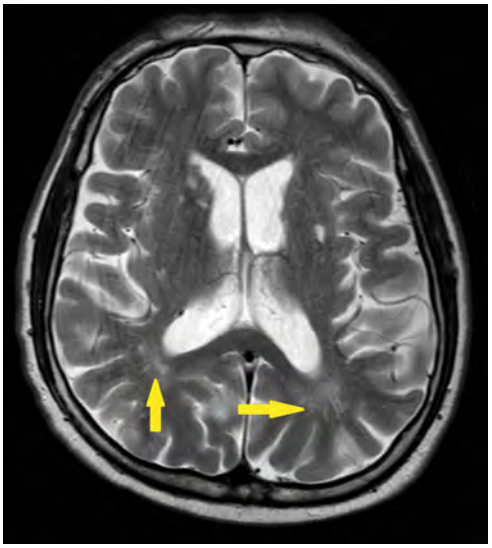

Figure 5. Yellow arrows show diffuse hyperintense millimetric ischaemic gliotic foci in the supratentorial white matter on brain magnetic resonance imaging T2-FLAIR sequence.

examination, the patient showed no motor function loss and his cerebellar tests were normal. The patient reported that dizziness increased when standing up and partially improved after lying down. Doppler ultrasonography of the carotid vertebral artery showed the presence of PHA on the right side. Upon detecting 70–99% stenosis of the proximal right ICA and 70% stenosis of the proximal left ICA along with PHA, imaging with digital subtraction angiography (DSA) was planned. DSA revealed PHA on the right side and 95% stenosis of the PHA, proximal to the right ICA and distal to the bulb (Fig. 2). The patient also had atherosclerotic stenosis causing 75% stenosis in the proximal left ICA (Fig. 3, Suppl. Video 1). The left vertebral artery appeared hypoplastic compared to the right-sided PHA (Fig. 4). In addition, widespread ischaemic gliotic foci were observed in the supratentorial white matter on magnetic resonance images of the patient (Fig. 5). Endarterectomy was planned for 95% stenosis on the right side of the patient because of anatomical incompatibility. Elective endovascular stenting for 70% stenosis proximal to the left ICA was scheduled following endarterectomy at our centre.

DISCUSSION

Four criteria have been determined for the diagnosis of PHA: 1) the hypoglossal artery originates from the ICA as a robust branch at the C1–C3 level, 2) enters the posterior cranial fossa through the hypoglossal canal, 3) joins the basilar artery just beyond its origin near the pontomedullary junction, 4) the posterior communicating artery is either absent or not visible on angiography [1]. Vertebral arteries may be hypoplastic or aplastic [7]. It was reported that the diameter of the anterior condylar foramen is normally 6–7 mm, which can increase up to 8 mm in the presence of PHA [4].

Begg (1961) [see 4] first demonstrated the presence of PHA on angiographic imaging. PHA is usually detected incidentally on imaging studies and is often asymptomatic. However, considering the fact that anterior and posterior cerebral circulation depends on the blood supplied by the ICA, it is crucial to identify such a variation before deciding how to perform surgical or endovascular interventions [6].

Although PHA is considered an anatomical variation of embryological origin, cerebral pathologies should also be considered because any aneurysm may be accompanied by vascular diseases or atherosclerosis [7]. Presence of PHA may be associated with abnormal vessel wall structure. Accordingly, as reported by former studies, exposure of the basilar artery to excessive haemodynamic stress may cause the development of aneurysms and arteriovenous malformations. Cases associated with ruptured aneurysms and arteriovenous malformations have been reported in the literature [6].

Persistent hypoglossal artery has also been associated with atherosclerotic cerebrovascular disease. Atherosclerotic plaque may develop because PHA originates from the ICA, causing haemodynamics similar to that of the carotid bulb. The presence of a plaque in this region is extremely important in patients with carotid and vertebrobasilar ischaemia because PHA generally supplies most of the posterior circulation [6]. Additionally, there are studies in the literature showing the presence of posterior cerebral artery fenestrations and cerebral infarction with PHA [7, 10, 11]. As a matter of fact, areas of atherosclerosis and cerebral infarction were observed in the present study, which is consistent with the literature data.

Angiography is required before performing carotid endarterectomy and surgical procedures to the skull base region. This is even more important in the absence of the vertebral artery, since in that case the ICA will be the sole source of cerebral blood supply and it will be difficult to maintain cerebral perfusion during surgery to this region.

Although the incidence of PHA varies in different parts of the world, only 7 cases were reported in Turkey based on our literature search [2, 4, 5, 7, 8, 11, 12]. The fact that so few cases were reported in Turkey makes the present case report even more noteworthy.

CONCLUSIONS

While dizziness has many possible causes, it should be borne in mind that a rare variation such as PHA and vertebrobasilar insufficiency as well as carotid artery stenosis, as emerges in this case, may also cause dizziness. DSA may be considered for the diagnosis of PHA in patients with unexplained dizziness and impaired balance. We believe that this case is representative of a very rare variation and will make a valuable contribution to the literature since there are few cases reported from Turkey.

Acknowledgements

This study was conducted in accordance with the ethical standards and the 1964 Declaration of Helsinki and its later amendments. Written informed consent was obtained from the patient.

All authors certify that they have no affiliations with or involvement in any organization or entity with any financial interest or non-financial interest in the subject matter or materials discussed in this case report.

Conflict of interest: None declared

REFERENCES

1. Albay S, Kastamoni Y, Koyuncu E. Embriyonal Kalıntı Arterler. SDÜ Tıp Fakültesi Dergisi. 2012; 19: 62–67.
2. Aysel T, Tülay Ö, Turhan C, et al. Multidetector CT angiography of the persistent primitive hypoglossal artery. Eur J Radiol Extra. 2008; 68(2): e63–e66, doi: 10.1016/j.ejrex.2008.06.013.
3. Coulier B. Persistent hypoglossal artery. J Belg Soc Radiol. 2018; 102(1): 28, doi: 10.5334/jbsr.1481, indexed in Pubmed: 30039040.
4. Memiş A, Güney B. Persistan hipoglossal arterin MR anjiyografi ile görüntülenmesi. Turk J Diagn Iintervent Radiol. 2001; 7: 248–251.
5. Numan F. A successful treatment with carotid arterial stenting for symptomatic severe internal carotid artery stenosis with ipsilateral persistent primitive hypoglossal artery and aplasia of the A1 segment of anterior cerebral artery: a case report. Turkish J Thoracic Cardiovasc Surg. 2013; 21(2): 440–444, doi: 10.5606/tgkdc.dergisi.2013.5162.

6. Paraskevas GK, Tsitsopoulos PPh, Papaziogas B, et al. Persistent primitive hypoglossal artery: an incidental autopsy finding and its significance in clinical practice. Folia Morphol. 2007; 66(2): 143–147, indexed in Pubmed: 17594674.
7. Pasaoglu L, Hatipoglu HG, Vural M, et al. Persistent primitive hypoglossal artery and fenestration of posterior cerebral artery: CT and MR angiography. Neurocirugia (Astur). 2009; 20(6): 563–566, doi: 10.1016/s1130-1473(09)70137-x, indexed in Pubmed: 19967323.
8. Petik B, Colak D, Sirik M, et al. Rare variants of carotid-vertebrobasilar anastomoses. J Belg Soc Radiol. 2016; 100(1): 74, doi: 10.5334/jbr-btr.1167, indexed in Pubmed: 30151473.
9. Srinivas MR, Vedaraju KS, Manjappa BH, et al. Persistent primitive hypoglossal artery (PPHA): a rare anomaly with literature review. J Clin Diagn Res. 2016; 10(1): TD13–TD14, doi: 10.7860/JCDR/2016/15556.7116, indexed in Pubmed: 26894148.
10. Tse GH, Martin A, Dyde RA, et al. Persistent hypoglossal artery aneurysm: case report and qualitative systematic review. Interv Neuroradiol. 2019; 25(2): 164–171, doi: 10.1177/1591019918809087, indexed in Pubmed: 30394836.
11. Uysal E, Velioglu M, Kara E, et al. Persistent hypoglossal artery associated with a ruptured ipsilateral posterior inferior cerebellar artery aneurysm. A case report. Neuroradiol J. 2007; 20(5): 570–573, doi: 10.1177/197140090702000516, indexed in Pubmed: 24299948.
12. Yilmaz E, Ilgit E, Taner D. Primitive persistent carotid-basilar and carotid-vertebral anastomoses: a report of seven cases and a review of the literature. Clin Anat. 1995; 8(1): 36–43, doi: 10.1002/ca.980080107, indexed in Pubmed: 7697511.

VIA MEDICA

CASE REPORT

Folia Morphol.
Vol. 82, No. 4, pp. 957–962
DOI: 10.5603/FM.a2022.0109

ISSN 0015–5659
eISSN 1644–3284
journals.viamedica.pl

Variations of accessory thoracic muscles identified in the ethnically diverse whole-body donation population in Northern California

H. Anderson, J.A. Weil, R.P. Tucker

Department of Cell Biology and Human Anatomy, University of California, School of Medicine, Davis, California, United States

[Received: 21 July 2022; Accepted: 7 October 2022; Early publication date: 23 December 2022]

Accessory thoracic muscles in humans are relatively common and it is important to draw awareness to their variable presentations and potential clinical implications owing to their close association with the axilla. Here we report four cases of accessory thoracic muscle variations identified in the ethnically diverse whole--body donation population in Northern California (4 out of 48 donors, 8.3%). Of these, combined presentations of thoracic accessory muscles were observed in two of the donors, one involving bilateral axillary arches and a pectoralis quartus on the left and the other a unilateral axillary arch on the left and bilateral pairs of pectoral fascicles. In the former, the proximal ends of the left axillary arch and pectoralis quartus joined to form a common aponeurosis which inserted onto the deep tendon of the pectoralis major; in the latter, the pectoral fascicles originated from the surface of the ribs and inserted into the deep surface of the pectoralis major muscle. In the other two donors, unilateral axillary arches were observed. Our observations illustrate that accessory thoracic muscles, in isolated as well as combined forms, are commonplace in the general population. We also describe the proposed embryonic origins of these accessory muscles, which may reflect their frequent occurrence, and potential clinical implications of these muscles, as discussed in literature. (Folia Morphol 2023; 82, 4: 957–962)

Key words: accessory thoracic muscle, axillary arch, pectoralis quartus, latissimus dorsi, pectoralis major, cadaver, gross anatomy laboratory

INTRODUCTION

Muscles demarcating the axilla are used as critical landmarks of the region. An understanding of accessory muscles located in this region allows more accurate decision making during surgical procedures involving lymph nodes in the breast [10, 17, 21]. One of the well-known accessory thoracic muscles of this class is the axillary arch (AA). The AA, also referred to as Langer's AA [24] or Achselbogen muscle [3], is a musculotendinous slip that crosses the axilla anteriorly [9]. Typically, the AA originates from the anterior boarder of the latissimus dorsi near the base of the axilla and inserts onto the deep tendon of the pectoralis major. In some cases it inserts onto the coracoid process of the scapula, or onto musculotendinous structures near the proximal humerus [9]. The AA is one of the more common variations of accessory thoracic muscles. In a recent meta-analysis report, the prevalence of the AA has been reported as 5.3% [23], though it varies among populations [4, 14]. An-

Address for correspondence: Dr. H. Anderson, Department of Cell Biology and Human Anatomy, University of California, 1 Shields Avenue, Davis, CA 95616 United States, tel: 530 752 0389, e-mail: hnanderson@ucdavis.edu

other frequently reported accessory thoracic muscle associated with the axilla is the pectoralis quartus. The pectoralis quartus is defined as a muscular slip typically originating in the thorax lateral to, or at the lateral border of, the pectoralis major, and inserting onto the deep pectoralis major tendon, or onto the aforementioned insertion sites of the AA [3, 4, 8].

Because of their common occurrence and implied clinical relevance, accessory thoracic muscles associated with the axilla warrant close attention. Although the AA itself is common, occurrence of bilateral AAs as well as additional thoracic accessory muscle variations accompanying the AA are less common [4, 23]. In the current study we report 4 cases of AA variations identified among 48 donors (4/48 = 8.3%) of an ethnically diverse whole-body donation population. In one case, bilateral AAs were accompanied with a left pectoralis quartus, and in another a left AA was accompanied with bilateral pairs of pectoral fascicles, originating from the surface of the ribs and inserting onto the deep surface of the pectoralis major. We summarise these cases and briefly discuss their proposed origins based on the theories described in literature.

CASE REPORT

All 4 cases of AA variations described below were identified in the gross anatomy laboratory for first-year medical students at the University of California, Davis, School of Medicine over a 2-year period (2020 and 2021).

Case 1

Bilateral AAs and a left pectoralis quartus were identified in an 80-year-old male donor diagnosed with cerebral atherosclerosis and vascular dementia. The left pectoralis quartus was first noted during the dissection of the thoracic region as a slender muscle slip embedded within the sub-cutaneous fat. This muscle slip attached distally to the superior border of the 6th rib superficial to the external oblique, and then ran along the inferolateral boarder of the pectoralis major, which covered the proximal half of the pectoralis quartus slip (Fig. 1A). In its entirety, the pectoralis quartus travelled laterally to the pectoralis minor and inserted onto the deep fascia of the pectoralis major and measured 12 cm long and 1.2 cm wide near its distal attachment. Based on the relative location to the pectoralis major and its distal and proximal attachments, we classified this accessory thoracic muscle as a pectoralis quartus [22]. Its insertion site at the pectoralis major was encased in a thick fascia to which the proximal end of another muscle slip, a left AA, joined (Fig. 1B). Further dissection of this fascia revealed that the pectoralis quartus and AA were linked via an aponeurosis (Fig. 1C). The source of innervation to the pectoralis quartus was found to be the medial pectoral nerve, which branched where it penetrated the pectoralis minor and extended to the pectoralis quartus (Fig. 1C). We did not find clear innervation to the AA as seen for the pectoralis quartus.

The origin of the left AA was found at the anteroinferior margin of the tendinous part of the latissimus dorsi. The striation of the AA was perpendicular to that of the latissimus dorsi, with a defining tendinous ridge located between the two (Fig. 1D). The left AA measured 8 cm long and 0.6 cm wide at its midpoint. In addition, this donor had a right AA. Like the left AA, the right AA originated from the anteroinferior margin of the tendinous part of the latissimus dorsi and inserted onto the fascia deep to the pectoralis major (Fig. 1E). Its dimension was 7 cm long and 0.6 cm wide at its midpoint. Both AAs traversed across the axilla anterior to the brachial plexus (Fig. 1B, E).

Case 2

A left AA and bilateral pairs of thoracic fascicles deep to the pectoralis major were identified in an 83-year-old male donor diagnosed with vascular dementia. The AA was 8 cm long and 0.5 cm wide at its midpoint. Like the AAs described in Case 1, this AA originated from the anterior margin of the tendinous part of the latissimus dorsi, and it inserted onto the deep fascia of the pectoralis major (Fig. 2A). In addition to the AA, pairs of pectoral fascicles were observed, on both the left and right sides, anterior to the pectoralis minor (Fig. 2B). These fascicles originated from the anterior surface of the ribs and eventually merged into the deep fascia of the pectoralis major. The fascicle pair on the right originated at the level of the 4th rib and ran closely parallel to each other, between which the medial pectoral nerve traversed from the pectoralis minor to the pectoralis major (Fig. 2C). Both fascicles measured 11.5 cm in length. The superior fascicle was 0.8 cm wide and the inferior fascicle was 0.6 cm wide. The fascicles on the left were more distant from each other, with the superior fascicle originating at the level of the 1st rib and the inferior fascicle at the level of the 3rd rib (Fig. 2D). The superior fascicle measured 6.5 cm in length and 1.0 cm in width, and the inferior fascicle was 11 cm in length and 0.7 cm in width.

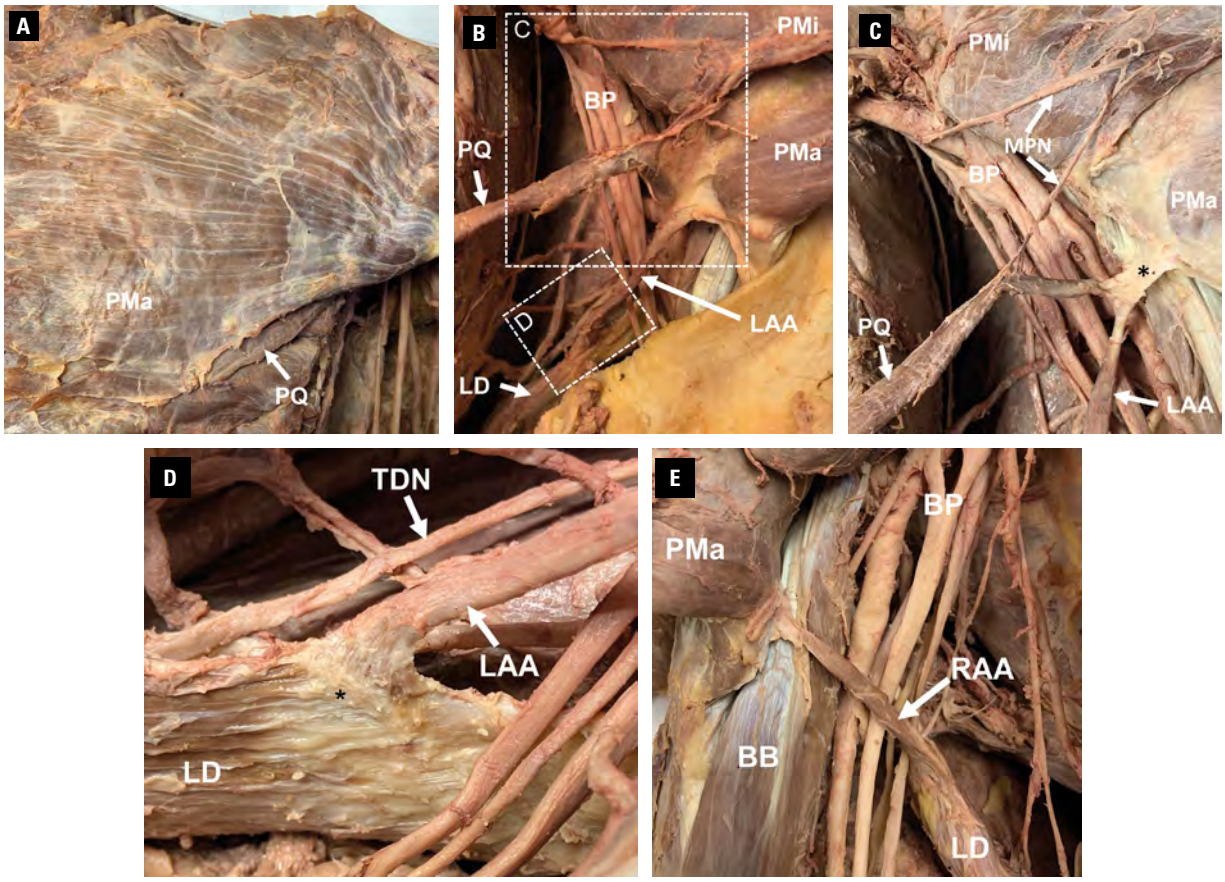

Figure 1. Case 1: 80-year-old male donor presenting bilateral axillary arches and a left pectoral quartus muscle; **A.** The left pectoralis quartus at the inferolateral boarder of the left pectoralis major; **B.** A thick fascia encasing the insertion sites of the pectoralis quartus and the axillary arch that insert onto the deep fascia of the pectoralis major; **C.** A closer look of box C demarcated in panel B. An aponeurosis (*) linking the pectoralis quartus and the left axillary arch. A branch of the medial pectoral nerve innervates the pectoralis quartus; **D.** A closer look of box D demarcated in panel B. A tendinous ridge (*) is formed where the striation of the axillary arch perpendicularly meets that of the latissimus dorsi; **E.** The right axillary arch; BB — biceps brachii; BP — brachial plexus; LAA — left axillary arch; LD — latissimus dorsi; MPN — medial pectoral nerve; PMa — pectoralis major; PMi — pectoralis minor; PQ — pectoralis quartus; RAA — right axillary arch; TDN — thoracodorsal nerve.

Case 3

A right AA was identified in an 82-year-old female donor diagnosed with Alzheimer's disease (Fig. 3A). The arch originated from the anteroinferior margin of the tendinous part of the latissimus dorsi. Unlike the left AA in Case 1, the muscle fibres of this AA ran in parallel and were continuous with those of the latissimus dorsi. The arch traversed across the axilla anterior to the brachial plexus and inserted onto the deep fascia of the pectoralis major.

Case 4

A right AA crossing anterior to the intercostobrachial nerve in addition to the proximal terminal branches of the brachial plexus was identified in a 71-year-old male donor diagnosed with gastroesophageal adenocarcinoma (Fig. 3B). The AA arose from the anteroinferior border of the latissimus dorsi tendon, perpendicular to its striation, and inserted onto the deep fascia of the pectoralis major near its lateral border.

DISCUSSION

Accessory thoracic muscles in humans have been reported in the literature for over 200 years [20]. The embryonic origins of the AA and pectoralis quartus have been discussed by multiple authors based on their source of innervation as well as their phylogenetic relationships with thoracic muscles found in non-human mammalian species [3, 8, 11, 14, 26, 28]. One of the frequently cited views is that these accessory thoracic muscles are remnants of the panniculus carnosus [2, 8, 11, 16], the cutaneous skeletal muscle sheets found in mammals such as cats, dogs, rodents, horses and to a certain extent in some primate species [11, 12]. Rostrally, the panniculus carnosus attaches

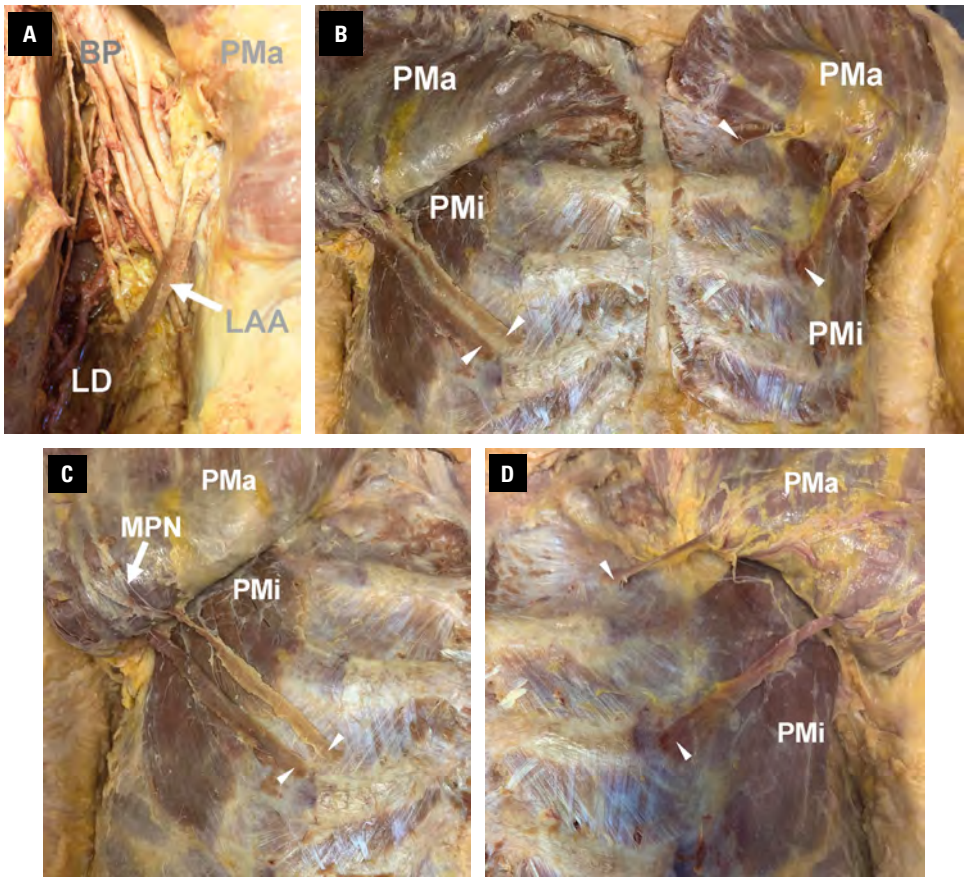

Figure 2. Case 2: 83-year-old male donor presenting a left axillary arch and bilateral pairs of thoracic fascicles deep to the pectoralis major; **A.** The left axillary arch; **B.** Bilateral thoracic fascicles; **C.** A closer look of the right pectoral fascicles. The medial pectoral nerve travels between the fascicles to traverse from the pectoralis minor to the pectoralis major; **D.** A closer look of the left pectoral fascicles; white arrowheads indicate pectoral fascicles; BP — brachial plexus; LD — latissimus dorsi; LAA — left axillary arch; MPN — medial pectoral nerve; PMa — pectoralis major; PMi — pectoralis minor.

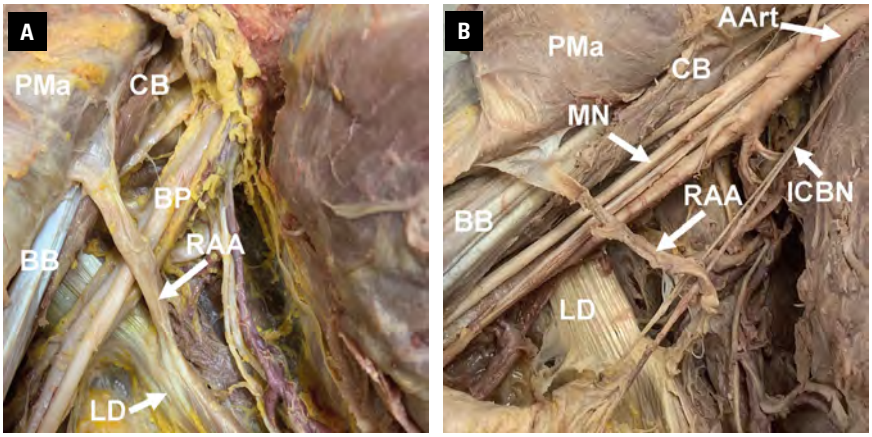

Figure 3. Case 3 and Case 4: 82-year-old female and 71-year-old male donor presenting a right axillary arch; **A.** The right axillary arch traversing the axilla; **B.** The right axillary arch traversing anterior to the intercostobrachial nerve; AArt — axillary artery; BB — biceps brachii; BP — brachial plexus; CB — coracobrachialis; ICBN — intercostobrachial nerve; LD — latissimus dorsi; MN — median nerve; PMa — pectoralis major; RAA — right axillary arch.

to the humerus via the fascia deep to the pectoralis muscles, and caudally inserts beneath the dermis of the back and flank regions [11, 12, 25]. The observations that accessory thoracic muscles such as the

sternalis, pectoralis quartus, and AA, are often found physically connected to each other [1, 4, 7, 8] may reflect the close phylogenetic relationship proposed between the panniculus carnosus and pectoral muscles [8, 11, 16].

An alternative origin of the pectoralis quartus has been also proposed in literature. Based on comparative anatomical studies that show concurrent presence of the pectoralis quartus and the panniculus carnosus in several mammalian species, the view that the pectoralis quartus is a segmented portion of the lower part of the pectoralis major, not a vestigial rudiment of the panniculus carnosus, has been described [3]. In this view, the pectoralis quartus is considered as a variation of the pectoralis major, to a certain extent similar to the pectoral fascicles found deep to the pectoralis major, which were identified in Case 2 of the current report. Deep accessory pectoral fascicles have been reported in primates such as chimpanzees and bonobos as a common occurrence [18]. In the same report, the authors also identified similar accessory pectoral fascicles in two human cadavers [18]. Independently, an accessory head of the pectoralis major muscle has been reported [13]. The bilateral paired accessory pectoral fascicles reported in Case 2 of the current report appears to be a rarer presentation of these muscles since the reports cited above described only unilateral accessory pectoral fascicles.

The source of the relatively common occurrence of accessory muscles of the pectoralis major and the latissimus dorsi may lie in the complex migration pattern taken by their myogenic precursor cells. Recent investigation on embryonic origins of the pectoral and latissimus dorsi muscles revealed that these superficial shoulder girdle muscles arise through the two-step process, referred to as the "in-out" mechanism, in which the myogenic precursors first migrate into the forelimb bud from the thoracic somites and then return to the trunk region to complete the muscle development [19, 27]. This complex developmental process may possibly lead to varied migration paths among the precursors, giving rise to accessory pectoral muscles associated with the pectoral and latissimus dorsi muscles.

Because the accessory thoracic muscles discussed above are common in the general population and closely associated with clinically important structures such as the neurovascular bundles and lymph nodes in the axillary region, awareness of their implications to medical procedures such as surgery and potential chronic conditions is warranted [6, 23]. For instance, potential interference of the AA and the pectoralis quartus with sentinel lymph node biopsy and axillary lymphadenectomy have been discussed [10, 17, 21]. Also, compression on the neurovasculature in the axilla by the AA may be involved in conditions such as a thoracic outlet syndrome [5] and can cause deep vein thrombosis [15]. The accessory pectoral muscles closely associated with axilla, therefore, have significant implications for regularly performed surgical procedures in the axillary region and chronic conditions affecting the axillary neurovasculature.

CONCLUSIONS

In this report, we examined 48 donors and found 4 cases of AA (8.3%) in an ethnically diverse donor population. Additional thoracic accessory muscles were identified, a pectoralis quartus associated with bilateral AAs and bilateral paired pectoral fascicles associated with a unilateral AA. Since these thoracic accessory muscles are in close proximity to the axillary lymph nodes and neurovasculature, the relatively common occurrence of these variations merits awareness.

Acknowledgements

The authors are grateful to the staff of the UC Davis Body Donation Programme for their support and wish to express gratitude to the individuals who donated the bodies for the advancement of medical education and research.

Conflict of interest: None declared

REFERENCES

1. Bergman RA. Doubled pectoralis quartus, axillary arch, chondroepitrochlearis, and the twist of the tendon of pectoralis major. Anat Anz. 1991; 173(1): 23–26, indexed in Pubmed: 1952092.
2. Besana-Ciani I, Greenall MJ. Langer's axillary arch: anatomy, embryological features and surgical implications. Surgeon. 2005; 3(5): 325–327, doi: 10.1016/s1479-666x(05)80111-8, indexed in Pubmed: 16245651.
3. Birmingham A. Homology and innervation of the achselbogen and pectoralis quartus, and the nature of the lateral cutaneous nerve of the thorax. J Anat Physiol. 1889; 23(Pt 2): 206–223, indexed in Pubmed: 17231782.
4. Bonastre V, Rodríguez-Niedenführ M, Choi D, et al. Coexistence of a pectoralis quartus muscle and an unusual axillary arch: case report and review. Clin Anat. 2002; 15(5): 366–370, doi: 10.1002/ca.10053, indexed in Pubmed: 12203382.
5. Clarys JP, Barbaix E, Van Rompaey H, et al. The muscular arch of the axilla revisited: its possible role in the thoracic

outlet and shoulder instability syndromes. Man Ther. 1996; 1(3): 133–139, doi: 10.1054/math.1996.0261, indexed in Pubmed: 11440500.
6. Douvetzemis S, Natsis K, Piagkou M, et al. Accessory muscles of the anterior thoracic wall and axilla. Cadaveric, surgical and radiological incidence and clinical significance during breast and axillary surgery. Folia Morphol. 2019; 78(3): 606–616, doi: 10.5603/FM.a2019.0005, indexed in Pubmed: 30664230.
7. Humphry GM. Lectures on human myology. Br Med J. 1872; 2(601): 4–5, doi: 10.1136/bmj.2.601.4, indexed in Pubmed: 20746690.
8. Huntington GS. The derivation and significance of certain supernumerary muscles of the pectoral region. J Anat Physiol. 1904; 39(Pt 1): 1–54.27, indexed in Pubmed: 17232622.
9. Jelev L, Georgiev GP, Surchev L. Axillary arch in human: common morphology and variety. Definition of "clinical" axillary arch and its classification. Ann Anat. 2007; 189(5): 473–481, doi: 10.1016/j.aanat.2006.11.011, indexed in Pubmed: 17910401.
10. Karanlik H, Fathalizadeh A, Ilhan B, et al. Axillary arch may affect axillary lymphadenectomy. Breast Care. 2013; 8(6): 424–427, doi: 10.1159/000357307, indexed in Pubmed: 24550750.
11. Langworthy O. The panniculus carnosus in cat and dog and its genetical relation to the pectoral musculature. J Mammal. 1924; 5(1): 49–63, doi: 10.2307/1373485.
12. Langworthy O. A morphological study of the panniculus carnosus and its genetical relationship to the pectoral musculature in rodents. Am J Anat. 1925; 35(2): 283–302, doi: 10.1002/aja.1000350207.
13. Loukas M, South G, Louis RG, et al. Jr, A case of an anomalous pectoralis major muscle. Folia Morphol. 2006; 65(1): 100–103, indexed in Pubmed: 16783751.
14. Lhuaire M, Wehbe K, Garrido I, et al. Anatomy of the axillary arch: from its incidence in human to an embryologic and a phylogenetic explanation of its origins. Surg Radiol Anat. 2021; 43(5): 619–630, doi: 10.1007/s00276-020-02605-5, indexed in Pubmed: 33136183.
15. Magee C, Jones C, McIntosh S, et al. Upper limb deep vein thrombosis due to Langer's axillary arch. J Vasc Surg. 2012; 55(1): 234–236, doi: 10.1016/j.jvs.2011.07.002, indexed in Pubmed: 21924577.
16. Naldaiz-Gastesi N, Bahri OA, López de Munain A, et al. The panniculus carnosus muscle: an evolutionary enigma at the intersection of distinct research fields. J Anat. 2018 [Epub ahead of print]; 233(3): 275–288, doi: 10.1111/joa.12840, indexed in Pubmed: 29893024.
17. Natsis K, Vlasis K, Totlis T, et al. Abnormal muscles that may affect axillary lymphadenectomy: surgical anatomy. Breast Cancer Res Treat. 2010; 120(1): 77–82, doi: 10.1007/s10549-009-0374-5, indexed in Pubmed: 19306056.
18. Potau JM, Arias-Martorell J, Bello-Hellegouarch G, et al. Inter- and intraspecific variations in the pectoral muscles of common chimpanzees, bonobos, and humans . Biomed Res Int. 2018; 2018: 9404508, doi: 10.1155/2018/9404508, indexed in Pubmed: 29581990.
19. Pu Q, Huang R, Brand-Saberi B. Development of the shoulder girdle musculature. Dev Dyn. 2016; 245(3): 342–350, doi: 10.1002/dvdy.24378, indexed in Pubmed: 26676088.
20. Ramsay A. Account of unusual conformations of some muscles and vessels. Edinb Med Surg J. 1812; 8(31): 281–283, indexed in Pubmed: 30329503.
21. Scrimgeour GE, St John ER, Leff DR. Langer's arch: A rare but important consideration for axillary surgery with implications for training. Breast J. 2020; 26(11): 2226–2228, doi: 10.1111/tbj.14082, indexed in Pubmed: 33049796.
22. Snosek M, Loukas M. Thoracic wall muscles. In: Bergman's comprehensive encyclopedia of human anatomic variation. John Wiley & Sons, Ltd 2016: 335–368.
23. Taterra D, Henry BM, Zarzecki MP, et al. Prevalence and anatomy of the axillary arch and its implications in surgical practice: A meta-analysis. Surgeon. 2019; 17(1): 43–51, doi: 10.1016/j.surge.2018.04.003, indexed in Pubmed: 29801707.
24. Testut L. Les anomalies musculaires chez l'homme expliquées par l'anatomie comparée, leur importance en anthropologie par L. Testut: Précédé d'une préface par M. le professeur Mathias Duval. G. Masson 1884: 107–116.
25. Theriault E, Diamond J. Nociceptive cutaneous stimuli evoke localized contractions in a skeletal muscle. J Neurophysiol. 1988; 60(2): 446–462, doi: 10.1152/jn.1988.60.2.446, indexed in Pubmed: 3171637.
26. Turner WM. On the Musculus Sternalis. J Anat Physiol. 1867; 1(2): 246–378.25, indexed in Pubmed: 17230716.
27. Valasek P, Theis S, DeLaurier A, et al. Cellular and molecular investigations into the development of the pectoral girdle. Dev Biol. 2011; 357(1): 108–116, doi: 10.1016/j.ydbio.2011.06.031, indexed in Pubmed: 21741963.
28. Wilson JT. The innervation of the Achselbogen muscle. J Anat Physiol. 1912; 47(Pt 1): 8–17, indexed in Pubmed: 17232944.

VIA MEDICA

CASE REPORT

Folia Morphol.
Vol. 82, No. 4, pp. 963–968
DOI: 10.5603/FM.a2022.0107

ISSN 0015–5659
eISSN 1644–3284
journals.viamedica.pl

A fully capable pianist with a congenital bilateral agenesis of extensor pollicis brevis muscle

K.P. Dąbrowski[1], P. Palczewski[2], H. Stankiewicz-Jóźwicka[3], A. Kowalczyk[1], J. Wróblewski[3], B. Ciszek[1, 4]

[1]*Department of Descriptive and Clinical Anatomy, Centre for Biostructure Research, Medical University of Warsaw, Poland*
[2]*First Department of Clinical Radiology, Medical University of Warsaw, Poland*
[3]*Department of Instrumental Studies, The Fryderyk Chopin University of Music, Warsaw, Poland*
[4]*Department of Neurosurgery in Bogdanowicz Children's Hospital, Warsaw, Poland*

[Received: 1 October 2022; Accepted: 6 November 2022; Early publication date: 22 December 2022]

A 28-year-old male musical student has been presented with visible inability of active abduction and extension of the thumbs in both hands beyond the neutral position. The student has not been previously diagnosed and claimed no history of trauma or surgical procedures in the area of hands and no family history of such disabilities. The student remained capable of playing on keyboard instruments on high level due to compensation by hyperextension of the interphalangeal joint of both thumbs and showed no increased frequency of the injuries or playing-related disorders. The ultrasound and magnetic resonance imaging showed complete bilateral agenesis of extensor pollicis brevis muscles and was classified as isolated congenital clasped thumb syndrome. Due to the age of the student and the agenesis of the muscles the conservative treatment was deemed inadequate and due to high functionality of the student as a musician and unforeseeable results it might have on a musician's career, surgical treatment has been disadvised. (Folia Morphol 2023; 82, 4: 963–968)

Key words: extensor pollicis brevis, hand, musician, agenesis, clasped thumb

INTRODUCTION

Extensor pollicis brevis muscle (EPB) is one of the newest — from an evolutionary point of view — structures in the upper extremity. As a separate, independent muscle it seems to only exist in humans and gorillas [9], which might be one of the reasons behind its substantial morphological variability, so much so it can have significant differences even between the two hands of the same individual [5]. In its standard description EPB has its origin on the posterior surface of the radius and the adjacent part of the interosseous membrane of forearm, dorsally to the origin of abductor pollicis longus muscle (APL). The tendon of the EPB passes through the first compartment of the extensor retinaculum and has its insertion at the posterior surface of the base of the proximal phalanx of the thumb [5, 7, 9].

Among most common variations of EPB there are differences in size of the belly of the muscle, including significant reduction, size and shape of the tendon including splitting into multiple collagenous bands, separation of the tendon of EPB from the tendon of

Address for correspondence: K.P. Dąbrowski, PhD, Department of Descriptive and Clinical Anatomy, Centre for Biostructure Research, Medical University of Warsaw, ul. Indiri Gandhi 35/15, 02–776 Warszawa, Poland, e-mail: krzysztof.dabrowski@wum.edu.pl

APL within the compartment of the Extensor Retinaculum, varying degree of fusion with the APL and changes in exact location of the insertions [4, 6, 7, 9]. Singular authors include also complete duplication of the muscle [4], or complete agenesis of the muscle [9]; however, those statements do not seem to be reflected in other authors' work, or sometimes even in those same authors studies.

The matter of function of the EPB proves to be a little more complicated than it could be assumed. Although it is described to be an extensor of the first metacarpophalangeal joint, as the name would suggest, the EPB seems to play an important part in the abduction of the thumb, function and structure of the extensor hood of the thumb and extension of the interphalangeal joint of the thumb [5, 10]. And yet, at the same time there are authors arguing that EPB's contribution to the mobility of the thumb is so limited that its reduction or even full absence should not cause significant limitation in function of the hand [6] It depends, however, on what can be considered a „significant" limitation, especially when it comes to a profession depending on quick, repetitive and precise movements of the hand, thumb included.

CASE REPORT

During data gathering for a different study a 28-year-old male student of musical university has been brought to authors' attention. The student has been complaining about straining of the thumbs, especially during exercises and repertoire requiring wide spreading of the hand and the teacher of the instrument have noticed unusual shape and function of the student's hands (Fig. 1).

A general examination, a face to face semi-structured interview and an observation of the work with the instrument were arranged. Upon general examination thumbs of both hands showed symmetrical limitation of the extension and abduction in active movement with inability to surpass the neutral position in which the long axis of the proximal phalanx of the thumb is more or less parallel to the forearm, which the student compensated with near 90 degrees overextension in the interphalangeal joints and a very strong ulnar adduction of the hand and abduction of the fifth finger. Examination of passive movement shown a full range of motion without resistance of the tissues. Patient denied any history of substantial trauma or surgical procedures in the area of the hands and wrists and claimed that aforementioned limitation was present for as long as he could remember. Family history showed absence of similar limitations in close family members, although due to personal reasons gathering information on the extended family was impossible.

Interestingly, according to the student, despite going through full musical education from the early years of the childhood, the teacher at the University level was the first one to notice and question the described limitation of the hands' function.

According to the teacher, the examined student does not show any decrease in ability to play compared to his peers and does not show increased frequency of strain or misuse related trauma.

Following general examination and history the student has been examined via ultrasound (LOGIQF8 GE with L6-12, 6–13 MHz probe). The examination showed bilaterally a single tendon in the first compartment of the Extensor Retinaculum which was recognized as belonging to APL. Neither a tendon nor a belly of the EPB were found.

For the sake of confirmation a magnetic resonance imaging (MRI) was performed with a 1.5T scanner (Ingenia, Philips, Eindhoven, the Netherlands) using a body coil and a dedicated 8-channel phased-array wrist coil (ds Wrist). Three-millimetre thick T1-weighted FSE images without fat suppression of both forearms and wrists were acquired in coronal and axial planes (Table 1).

Magnetic resonance imaging showed bilaterally sole tendons of APL in the first compartments of extensor retinaculum. The muscle bellies of the EPBs were absent, their anatomic locations were filled by the APL bellies. The remaining forearm muscles were unremarkable (Figs. 2, 3).

DISCUSSION

The matter of morphological variability is one of the key aspects of anatomical studies, and not without a reason. Throughout the world medical practitioners learn human anatomy based of textbooks and atlases showing standardised, idealised versions of each structure and each organ and only some of them describe a few most common variations, which is often considered an extracurricular material. At the same time research shows that substantial proportion, in not majority, of clinical malpractice claims within surgical specialties is a direct result of operator's

Table 1. Magnetic resonance imaging protocol

	TE [ms]	TR [ms]	NA	ST [mm]	IG [mm]	AT [min]
Forearm coronal	15	280	2	3.5	0.4	1:16
Forearm axial	15	609	2	3	0.3	3:50
Wrist coronal	22	500	3	3	0.3	3:21
Wrist axial	24	540	2	3	0.3	3:41

TE — echo time; TR — repetition time; NA — number of averages; ST — slice thickness; IG — interslice gap; AT — acquisition time

Figure 1. Hands of the student on the keyboard. Despite a position close to neutral a substantial abduction of the first metacarpal bones and limited extension of the first metacarpophalangeal joints can be observed.

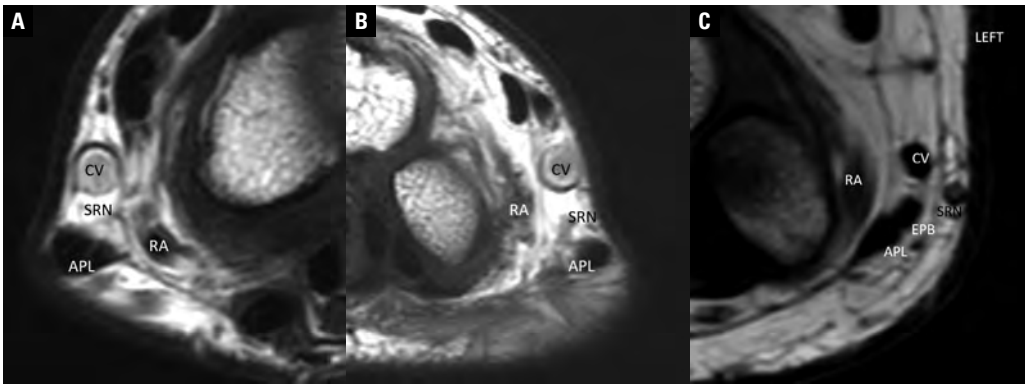

Figure 2. Magnetic resonance imaging sections at the level of radiocarpal articulation of the right limb (**A**) and the left limb (**B**) show bilaterally a sole tendon of abductor pollicis longus (APL) in the first extensor compartments. A corresponding section through a normal left wrist of another patient is shown for the reference (**C**); EPB — extensor pollicis brevis; CV — cephalic vein; SRN — superficial branch of the radial nerve; RA — radial artery.

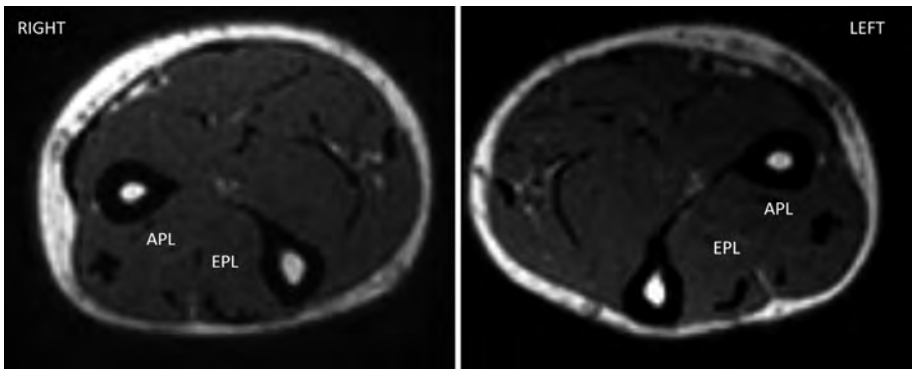

Figure 3. Magnetic resonance imaging sections through distal forearms. Absent bellies of extensor pollicis brevis muscles; APL — abductor pollicis longus; EPL — extensor pollicis longus.

ignorance regarding morphological variability [6]. It is safe to assume that situation is similar when it comes to conservative treatment as well.

The clinical image observed in the examined student seems to fall within a category of a "congenital clasped thumb syndrome" (CCTS) which is defined as a congenital flexed and adducted thumb caused by deformity or agenesis of the muscles of the thumb, usually the extensors. In most cases it is diagnosed after third month of life, due to natural for infants to this age position of thumb within the hand but it can also be diagnosed via radiological imaging or the autopsy [8, 11, 13]. It is usually observed as an accompanying syndrome in serious genetic dysfunctions. Subasioglu Uzak et al. [11] observed that in 88% of cases CCTS is associated with serious deformities related to genetic disorders and mentions 27 genetic disorders that consistently feature CCTS, for example Taee et al. [12] describes a case of CCTS in a newborn with sirenomelia.

Weckesser et al. [14] theorizes that to maintain such frequent symmetry CCTS would have to be associated with a genetic defect within the zygote before first division and suggests its origin in a recessive, sex-linked gene since, according to his observation supported later by Ghani et al. [2], majority of cases are observed in males.

In cases when CCTS is an isolated deformity, or patient's condition is good enough for CCTS to be considered a priority there are treatment options to be considered. Most common and most effective treatment is a surgical tendon transfer of either EPB if possible, or extensor indicis muscle. It is considered to have satisfactory results allowing for regaining full range of motion and ability to perform everyday tasks, and small chance of post-surgery complications. There is also an option of conservative treatment of splinting followed by manual therapy. Unfortunately, it is considered applicable only in very mild cases and with the youngest of patients — Al Smail et al. [1] in his case report described a 5 year old girl as too old for conservative treatment — it is also considered ineffective in cases of complete agenesis of EPB [1, 8].

Regarding the case described in this paper, it needs to be said that it is a very unique occurrence, beginning with full bilateral agenesis of EPB without any confirmed family history. Ghani et al. [2] and Soubhagya Nayak et al. [9] in their writing acknowledge possibility of complete agenesis of EPB, but also state that they have not observed such occurrence in their studies. Rousset et al. [7] describes only one case when EPB was replaced by a ligamentous band from the radial styloid process to the proximal phalanx of the thumb [2, 7, 9]. Most described cases of CCTS have confirmed family tendency [8, 14], yet that is not the case. Another matter is lack of any other visible anomalies. As it was stated before, CCTS is usually considered a symptom accompanying other genetic dysfunctions. According to Ghani et al. [2], in 78% of cases of CCTS other dysfunctions are clearly noticeable during general examination and considering existing research it would not be unreasonable to expect the isolated CCTS cases to be related to reduction or weakening of EPB rather than full agenesis. That being said, Al Smail et al. [1] describes a case of a 5-year-old girl with full agenesis of both extensors of the right thumb with full stability of the carpometacarpal joint of the thumb and lack of any other malformations or anomalies. Hong et al. [4] on the other hand describes a case of a 10-year-old girl with full agenesis of abductor pollicis longus, abductor pollicis brevis, opponens pollicis and extensor pollicis brevis in her right hand and a surprisingly efficient compensation by extensor pollicis longus thanks to unusual placement of the insertion on the distal phalanx, which allowed the abduction and extension movements to reach the neutral position. Hong et al. [4] describes function the thumb as "satisfactory". In this report, however, there is a 28-year-old keyboard musician that despite visible limitations in movement is capable of performing at consistently high level and up to that point remained undiagnosed due to efficient compensation mechanisms which, arguably, qualifies for a much better mark than "satisfactory".

Another surprising factor was the student being undiagnosed throughout the primary and secondary musical education despite being tutored by multiple teachers of multiple instrument, including piano, trumpet and church organs which might suggest that many teachers on the primary and secondary level do not have the basic anatomical knowledge that could be helpful in taking care for their students health, nor do they give enough attention to their technique and biomechanics of their hands as long as the score is being played adequately. It was only at the level of higher musical education that a teacher has noticed irregularities. It could be due to a very effective compensation mechanism of the student, including near 90 degrees overextension in the interphalangeal

joints and a very strong ulnar adduction of the hand and abduction of the fifth finger resulting in a hand-span of 21 cm in the left hand and 19.5 cm in the right between the tips of the first and fifth finger in maximal active stretch. Although it is a modest span compared to the size of the student's hands, it does not stand out much among his peers. Thanks to that the student has been able to consistently perform on a high level.

A question can be posed "what can modern medicine do in that case". Considering that the examined student's thumbs were capable of a full range of movement when moved passively, it would fall under type 1 both in Weckesser's [14] and Tsuyuguchi's [13] classification, which can be considered a mild case of CCTS. Yet both the age of the student and the fact of complete agenesis of EPB disqualify the idea of treatment through splinting and therapy, especially since such proceedings would ban the student from playing for a prolonged period of time with little to no reward in sight [1, 8]. It is not possible to strengthen an absent muscle. An intervention via orthesis or therapy on the present muscles were discussed and the authors decided against it, seeing as it would carry a risk of disrupting the compensation mechanism. The authors of this paper would also like to make an argument against surgical treatment due to foreseeable risks. Although in most cases the surgery is safe and brings good results, it is important to consider that most patients undergoing such procedure are children and the criteria for a successful operation fall within the spectrum of ability to write and perform everyday tasks, not performing piano recitals. The authors find no reasons to believe that an invasive procedure requiring long convalescence and therapy by design could improve a quality of life and career longevity of the discussed musician.

Nevertheless, there are certain risks that need to be taken under consideration regarding the student's further career. The full scope of occupational risks and diseases of musicians is not yet known and increase of these risks in case of such an unusual case is hard to estimate. Henry describes a tendency for osteoarthritis to affect the carpometacarpal joint of thumb, causing adduction contracture of the thumb and — when forced against in everyday use — resulting in hyperextension instability and significant deficits in function [3]. It is something to be wary of in future management of the examined student since described mechanism shares many similarities with the student's compensation mechanism.

CONCLUSIONS

Considering the brought up arguments, it seems reasonable to suggest a close observation and care of a trusted medical professional to facilitate early treatment and management of any disorder that might occur in the future career and continuous work with an instrument teacher in order to choose a repertoire that causes the least possible amount of strain.

Conflict of interest: None declared

REFERENCES

1. Al Smail MH, Aloulou M, Zrek A. A rare case of neglected clasped thumb of 5-year-old girl treated with simple z-plasty, two tendons transplantation, and followed up for 17 years. J Surg Case Rep. 2020; 2020(2): rjz398, doi: 10.1093/jscr/rjz398, indexed in Pubmed: 32104564.
2. Ghani HA, El-Naggar A, Hegazy M, et al. Characteristics of patients with congenital clasped thumb: a prospective study of 40 patients with the results of treatment. J Child Orthop. 2007; 1(5): 313–322, doi: 10.1007/s11832-007-0057-x, indexed in Pubmed: 19308526.
3. Henry M. Extensor pollicis brevis spiral tenodesis for combined metacarpophalangeal instability and trapeziometacarpal arthritis. Hand (NY). 2018; 13(2): 190–193, doi: 10.1177/1558944717695753, indexed in Pubmed: 28720007.
4. Hong J, Kim DK, Kang S, et al. Anomalous course of the extensor pollicis longus with multiple absences of thumb muscles. Ann Rehabil Med. 2013; 37(1): 151, doi: 10.5535/arm.2013.37.1.151.
5. Jabir S, Lyall H, Iwuagwu F. The extensor pollicis brevis: a review of its anatomy and variations. Eplasty. 2013; 13(e35): 267–277, indexed in Pubmed: 23882301.
6. Ogeng'o J. Clinical significance of anatomical variations. Anat J Africa. 2013; 2(1): 57–60.
7. Rousset P, Vuillemin-Bodaghi V, Laredo JD, et al. Anatomic variations in the first extensor compartment of the wrist: accuracy of US. Radiology. 2010; 257(2): 427–433, doi: 10.1148/radiol.10092265.
8. Serbest S, Tosun H, Tiftikci U, et al. Congenital clasped thumb that is forgetten a syndrome in clinical practice. Medicine. 2015; 94(38): e1630, doi: 10.1097/md.0000000000001630.
9. Soubhagya Nayak R, Hussein M, Krishnamurthy A, et al. Variation and clinical significance of extensor pollicis brevis: a study in south indian cadavers. Chang Gung Med J. 2009; 32(6): 600–604, indexed in Pubmed: 20035638.
10. Strauch RJ, Strauch CB. Extensor pollicis brevis tendon can hyperextend thumb interphalangeal joint in absence of extensor pollicis longus: Case report and review of the literature. World J Orthop. 2016; 7(7): 448–451, doi: 10.5312/wjo.v7.i7.448, indexed in Pubmed: 27458556.

11. Subasioglu Uzak A, Fryns JP, Dundar M. Syndromes presenting adducted thumb with/without clubfoot and Dundar syndrome. Genetic Counseling. 2014; 25(2): 159–168, indexed in Pubmed: 25059014.
12. Taee N, Tarhani F, Goodarzi MF, et al. Mermaid syndrome: a case report of a rare congenital anomaly in full-term neonate with thumb deformity. AJP Rep. 2018; 8(4): e328–e331, doi: 10.1055/s-0038-1669943, indexed in Pubmed: 30443435.
13. Tsuyuguchi Y, Masada K, Kawabata H, et al. Congenital clasped thumb: A review of forty-three cases. J Hand Surg. 1985; 10(5): 613–618, doi: 10.1016/s0363-5023(85)80193-3.
14. Weckesser EC, Reed JR, Heiple KG. Congenital clasped thumb (congenital flexion-adduction deformity of the thumb). J Bone Joint Surg. 1968; 50: 1417–1428, doi: 10.2106/00004623-196850070-00011, indexed in Pubmed: 5677295.

VIA MEDICA

CASE REPORT

Folia Morphol.
Vol. 82, No. 4, pp. 969–974
DOI: 10.5603/FM.a2022.0108

ISSN 0015–5659
eISSN 1644–3284
journals.viamedica.pl

A three-headed piriformis muscle: an anatomical case study and narrative review of literature

T. Kozioł[1]*, W. Chaba[1]*, P. Janda[1], K. Ochwat[1], P. Pękala[1], K. Balawender[2], J.A. Walocha[1], M.P. Zarzecki[1]

[1]*Department of Anatomy, Jagiellonian University Medical College, Krakow, Poland*
[2]*Department of Normal and Clinical Anatomy, Institute of Medical Sciences, Medical College of Rzeszow University, Rzeszow, Poland*

[Received: 4 October 2022; Accepted: 29 November 2022; Early publication date: 22 December 2022]

The piriformis muscle (PM) is found in the gluteal region, exiting the pelvis through the greater sciatic foramen and dividing it into the suprapiriform and infrapiriform foramina. The piriformis works as part of the hip external rotator muscle group, and is responsible for rotation of the femur upon hip extension and abduction of the femur during flexion of the hip joint. The aim of the present report is to describe a very rare case of the primary three-headed PM. To the best knowledge of the authors, the said variant has not yet been described in the existing literature.

The 71-year-old male formalin-fixed cadaver was subjected to routine dissection. After careful removal of the connecting tissue, three separate, primary heads of the PM were identified. The lower head of the PM arose from the middle part of the sacral bone; 87.56 mm long and 9.73 mm wide. The medial head was attached to the internal part of the posterior inferior iliac spine; 121.6 mm long and 20.97 mm wide. The upper head was attached to the external part of the posterior inferior iliac spine; 78.89 mm long and 23.94 mm wide. All heads converged into a common tendon which inserted onto the greater trochanter.

The clinical importance of this work comes down to the fact that the aberrant PM may be the reason behind the piriformis syndrome and its associated symptoms. Moreover, knowledge regarding the variant anatomy of the PM is of immense importance to, e.g. anaesthesiologists performing computed tomography- or ultrasound-guided sciatic nerve injection for local anaesthesia, radiologists interpreting imaging studies, and surgeons, especially during posterior approaches to the hip and pelvis. (Folia Morphol 2023; 82, 4: 969–974)

Key words: piriformis muscle, piriformis syndrome, sciatic nerve, anatomy

INTRODUCTION

The piriformis muscle (PM) is located in the gluteal region of the pelvis, posteriorly from the hip joint, passes through the greater sciatic foramen thus dividing it into two topographic areas: the suprapiriform and infrapiriform foramina [5, 7]. The muscle is a part

Address for correspondence: Dr. M.P. Zarzecki, MD, Department of Anatomy, Jagiellonian University Medical College, ul. Kopernika 12, 31–034 Kraków, Poland, tel/fax: +48 12 422 95 11, e-mail: michal.zarzecki96@gmail.com

*Equal contribution

of the hip external rotator muscle group, consisting namely of: the piriformis, quadratus femoris, obturator internus, obturator externus, gemellus inferior and superior. The piriformis is responsible for rotation of the femur upon hip extension and abduction of the femur during flexion of the hip joint.

The possible proximal attachment points for the PM are: the anterior surface of the lateral process of the sacral bone, the spinal region of the gluteal muscles, the gluteal surface of the iliac bone, the capsule of the sacroiliac joint or sacrotuberous ligament [5]. The distal attachment of the piriformis is the superomedial surface of the greater trochanter of the femur [23]. The piriformis muscle is innervated by the nerve to piriformis which can originate from the L5-S2 ventral rami, S1-S2 ventral rami or S1-S3 ventral rami [9].

The term "piriformis syndrome" was first introduced by Robinson in 1947 [18]. The condition was defined as a type of sciatica caused by an abnormal state of PM and probably resulted from a trauma to this region. According to Hopayian and Danielyan [8], the leading symptoms of the said condition involve: pain radiating to the ipsilateral leg (70%), external tenderness found close to the greater sciatic notch (61%), pain located in the gluteal region (56%), and aggravation of pain while sitting (40%). Noteworthy, the piriformis syndrome may be confused with sciatica, what in turn may lead to inappropriate treatment [6]. Moreover, the female-to-male ratio regarding the piriformis syndrome was 75:61 and the mean age of patients was 43 years [8].

The piriformis syndrome may exist in correlation with the abnormal structure of the PM or its spatial relation with the sciatic nerve (SN), whereby the SN is compressed by the PM [12]. The variants of this muscle need to be taken into account while performing procedures such as computed tomography- or ultrasound-guided SN injection for local anaesthesia, interpreting medical imaging studies by radiologists, and in surgical posterior approaches to the hip and pelvis.

The aim of the present report is to describe a very rare case of the previously unreported primary (i.e. undivided by a nerve or a vessel) three-headed piriformis muscle. Measurements of the width and length of each head were taken and included in the following article.

CASE REPORT

The 71-year-old male formalin-fixed cadaver was subjected to routine dissection at the Department of Anatomy, Jagiellonian University Medical College. The donor's height was 180 cm, and weight 107 kg. The process was performed by 3 authors (T.K., W.C., P.J.), under close supervision of more senior prosectors (M.P.Z., J.A.W.). The skin, adipose tissue and fascia were removed from the gluteal region on the right lower extremity. As the next step, the gluteus maximus was gently sectioned and after careful removal of the connecting tissue, three separate, primary heads of the PM were identified. Every measurement of the described muscle was made 3 times, using an electronic calliper and then the average was calculated (Fig. 1).

The lower head of the PM arised from the middle part of the sacral bone. It was 87.56 mm long and 9.73 mm wide. The medial head, which was the longest, was attached to the internal part of the posterior inferior iliac spine. It was 121.6 mm long and 20.97 mm wide. The upper head, which was the widest head, was attached to the external part of the posterior inferior iliac spine. It was 78.89 mm long and 23.94 mm wide. All heads converged into a common tendon which inserted onto the greater trochanter as classically depicted in anatomical textbooks. Unfortunately, the authors were not able to identify neither the nerve branches nor blood vessels supplying the heads. To the best of our understanding, they arose from the inferior gluteal vessels and nerves, though they were inadvertently not preserved with the transposition of the gluteus maximus to uncover the subgluteal space.

Undivided SN, posterior femoral cutaneous nerve, inferior gluteal nerve with inferior gluteal artery and vein were visible leaving the lesser pelvis underneath the lower head of the PM. The superior gluteal nerve, artery and vein exited through the suprapiriform foramen over the upper head of the PM. The authors have observed neither signs of potential nerve entrapment nor nerve or vascular compression in the dissected area. The contralateral subgluteal space did not exhibit any anatomical variants. No visible pathology was observed on either lower extremity. Regrettably, the donor's medical records indicating any possible clinical involvement were not available to the authors.

Ethical concern

All procedures performed in studies involving human participants were in accordance with the ethical standards of the institutional and/or national research committee and with the 1964 Helsinki declaration and

Figure 1. Posterior view of the gluteal region, following removal of the gluteus maximus muscle; 1 — lower head of the piriformis muscle; 2 — medial head of the piriformis muscle; 3 — upper head of the piriformis muscle; 4 — gluteus maximus muscle; 5 — sciatic nerve.

its later amendments or comparable ethical standards. The material used for this research was obtained from a body donation programme.

DISCUSSION

Anatomical aberrances in the gluteal region are a frequent finding. The present study aimed to introduce the primary three-headed PM and discuss its embryological basis, as well as, emphasize the clinical significance of this finding. To the best knowledge of the authors, the said variant has not yet been described in the literature. Overall, the PM and the SN tend to be aberrant in 16.9% of cases [20].

Embryological considerations

When it comes to the prenatal development, the PM is situated close to the coccygeus muscle, gluteus maximus and pudendal nerve at approximately 9 weeks of gestation. The SN runs between the PM and the obturator internus. Moreover, an aponeurosis is visible between the coccygeus muscle and the PM or gluteus maximus at the 20th gestational week [16]. The PM tendon resembles a condensation of fibres between the 6th and 15th week of gestation. About the 15th week, the PM tendon merges with the gluteus medius tendon. Additionally, the PM tendon forms its final insertion in the later development (after the 15th week) [14].

Sulak et al. [21] characterised the relationship between the PM and the SN in fetuses. Two hundred SNs of 200 human fetuses (between 9th and 40th gestational weeks) were included in the study. Based on gestational ages, the fetuses were categorised into four groups: 9–12 weeks, 13–25 weeks, 26–37 weeks, and 38–40 weeks. Then, some measurements were made, three of them regarded the distance between the SN and intergluteal sulcus, greater trochanter and ischial tuberosity. All of the distances rose with gestational age. There was a statistically significant difference between the age groups ($p < 0.05$) [21].

Another measurement involved the connection between the bifurcation levels of the SN and the popliteal fossa (PF) [21]. The SN was separated: into the tibial nerve (TN) and common peroneal nerve (CPN) in the PF, into the terminal branch of SN above the PF, or at the level of PM in 88.5%, 9.5% and 2%, respectively. Furthermore, the SN exited the lesser pelvis underneath the PM in 98% of the cases, while the remaining variants included the CPN piercing the PM and the CPN exiting above the PM [21]. The data suggests that the bifurcation levels of SN in fetuses are lower than in adults. In the latter group, that division happens most often when the SN is located in the posterior compartment of the thigh [1].

Similarly to the aforementioned case, Kurtoglu et al. [11] reported that the level of the SN splitting

in fetuses is found in 97.5% of cases in the PF. The bifurcation was located above the upper border of the PF only in one leg from 40 dissected. The fetuses incorporated in the said study were between 20th and 36th gestational weeks [11].

PM variations described in the literature

Żytkowski et al. [26] highlighted that the concept of norm regarding the human body has evolved throughout history. The anatomical norm and abnormality do not have strict boundaries and thus determining whether a certain feature is a variant or not can pose a challenge. With almost every established anatomical structure comes its variation, which does not necessarily impair body functions [26]. The most frequent variants of the PM and its surrounding structures are described hereafter.

The PM is inherently associated with the SN. Tomaszewski et al. [23] presented a modified system of classification of the PM and SN, which regarded the relationship between the SN and PM and the way the SN exited the pelvis. According to that system, the PM described in the present study appears to be type A, which is also the most common type, with a pooled prevalence estimate of 85.2% [23].

Nevertheless, PM comprising primarily three heads has never been reported in the literature before. Natsis et al. [15] described a case with three muscle bellies of the PM that were formed due to the passage of the CPN and the TN through between the bellies. However, the case described herein points towards a three-headed PM that was not divided by the neurovascular entities passing right through it. Arifoglu et al. [2] reported a case of double PM existing alongside double superior gemellus muscle. The SN divided within the pelvis and the CPN was present between the lower and upper PM, while the tibial nerve was located under the lower PM.

What is more, a fusion between the PM and gluteus maximus muscle is also a possibility. Arora et al. [3] encountered a muscle merging proximally with the gluteus maximus muscle and distally with the PM. That particular anomaly may impinge on the SN and present clinically in the form of pain in the gluteal region.

Bifid PM is another variation, classified as type B, D, or E, depending on the SN bifurcation [23]. Thompson and Visagie [22] described a case where a 12-year-old girl had a bifid PM identified 4 months after surgery. The surgical procedure was performed due to osteoid osteoma located in the acetabular roof of the right leg. In this instance, two heads of PM were pierced by the CPN and the TN passed below the PM, which corresponds to type B of PM [22]. Such an anomaly resulted in the iatrogenic injury of the CPN, therefore, taking those variations into account while operating on a patient is undoubtedly of utmost importance.

Similar to the above-mentioned case, Wun-Schen [25] depicted a bipartite PM. Notwithstanding, it was the SN that came between the two heads of the PM. Moreover, the entrapment of the SN gave symptoms such as sciatica, and numbness in the area innervated by the CPN. Having corrected the position of the PM, the pain was relieved [25].

Last but not least, the PM may also be absent altogether in the gluteal region. Brenner et al. [4] reported such a case of unilateral absence of PM, the inferior gluteal artery was also missing ipsilaterally. Possibilities of the disappearance included fusion with another muscle, involution due to medical intervention, and true aplasia, with the latter being indicated by the authors as the most probable cause.

Clinical significance of the PM

In addition to the aforementioned clinical information regarding the piriformis syndrome, the said condition may be treated by a novel method, introduced by Tubbs et al. [24], which proved to be attainable in a cadaveric study thus far. The technique was performed on 5 adult cadavers and included the exposure of the PM in the proximity of the greater sciatic foramen. What is more, in order to achieve that an incision was performed near the pubic tubercle and then underlying adductor muscles, as well as deeper obturator muscles, were split. Subsequently, a laparoscope was inserted into the emergent canal and the SN was identified. As a result, the PM was cut which relieved the compression of the SN. Neither the SN nor neuromuscular bundles were damaged during the procedure [24].

The PM is also involved in certain invasive procedures. Ozisik et al. [17] described a computed tomography-guided injection into the PM. The group which received that form of treatment consisted of 10 patients. What is more, one of the patients had right PM hypertrophy found on the magnetic resonance imaging. When it comes to the technique, an 18G needle was placed in the PM and the insertion was confirmed with the computed tomography. The

methylprednisolone (Depo-Medrol 40 mg/1 vial) and bupivacaine (Marcaine 1 amp) were applied to the muscular tissue [17]. Concerning the PM features, such a precise diagnostic process resulted in the good recovery of 9 patients.

Thorough knowledge regarding the PM's anatomical variations is also essential in ultrasound-guided injection. Santamato et al. [19] illustrated the usage of botulinum toxin in the treatment of the piriformis syndrome. The injection process comprises three stages: placing the linear transducer on the line connecting the projections of the greater trochanter and the ischial tuberosity, then identifying the PM by using the probe and consequently, inserting the needle underneath the close ultrasound surveillance. As a result, the patient's symptoms were alleviated [19].

Furthermore, McLawhorn et al. [13] reported anatomical outcomes of direct anterior approach total hip arthroplasty, for instance, the violation of the PM. During the direct anterior approach an incision on the front of the hip is made, and then muscles are moved instead of detaching the tendons so as to replace the joint. Promptly after the procedure, 75% (24 out of 32) of the PM tendons were found to be intact, whereas a 1-year follow-up showed that only 1 patient out of 32 had PM tendon damaged. In addition, 22% of hips manifested moderate atrophy of the PM [13].

Limitations of the study

The principal limitation of the present study is lack of patient's medical records. Without those, it is impossible to determine whether the patient felt any discomfort or pain due to the existence of the three-headed PM. Furthermore, the anatomical variant of the PM should be taken into consideration in a differential diagnosis concerning pain localized in the gluteal region of unknown origin.

CONCLUSIONS

This study presented a case of the primary three-headed PM with discussion of its possible embryological basis. To the best knowledge of the authors, the said variant has not yet been described in the literature. The clinical importance of this work comes down to the fact that the aberrant PM may be the reason behind the piriformis syndrome and its associated symptoms. Moreover, knowledge regarding the variant anatomy of the PM is of immense importance to, e.g. anaesthesiologists, performing computed tomography- or ultrasound-guided SN injection for local anaesthesia.

Acknowledgements

The authors are indebted to Mr Jacenty Urbaniak for the technical support. "The authors sincerely thank those who donated their bodies to science so that anatomical research could be performed. Results from such research can potentially increase mankind's overall knowledge that can then improve patient care. Therefore, these donors and their families deserve our highest gratitude" [10].

Conflict of interest: None declared

REFERENCES

1. Apaydin N, Tunstall R. Pelvic girdle and lower limb: overview and surface anatomy. In: Standring S (ed.) Gray's Anatomy 41st ed. Elsevier Ltd., London 2016: 1323.
2. Arifoglu Y, Sürücü HS, Sargon MF, et al. Double superior gemellus together with double piriformis and high division of the sciatic nerve. Surg Radiol Anat. 1997; 19(6): 407–408, doi: 10.1007/BF01628510, indexed in Pubmed: 9479716.
3. Arora J, Mehta V, Kumar H, et al. A rare bimuscular conglomeration gluteopiriformis case report. Morphologie. 2010; 94(305): 40–43, doi: 10.1016/j.morpho.2009.12.001, indexed in Pubmed: 20149708.
4. Brenner E, Tripoli M, Scavo E, et al. Case report: absence of the right piriformis muscle in a woman. Surg Radiol Anat. 2019; 41(7): 845–848, doi: 10.1007/s00276-018-02176-6, indexed in Pubmed: 30758526.
5. Chang C, Jeno SH, Varacallo M. Anatomy, bony pelvis and lower limb, piriformis muscle. [Updated 2021 Oct 11]. In: StatPearls [Internet]. Treasure Island (FL): StatPearls Publishing. https://www.ncbi.nlm.nih.gov/books/NBK519497/?fbclid=IwAR3hEMtHgQqHD_sB_SdNciw42dkO1ZJuObub9d8d8Me9eGMcXkJhq3hMMso (2022 Jan).
6. Fishman LM, Schaefer MP. The piriformis syndrome is underdiagnosed. Muscle Nerve. 2003; 28(5): 646–649, doi: 10.1002/mus.10482, indexed in Pubmed: 14571472.
7. Haładaj R, Pingot M, Polguj M, et al. Anthropometric study of the piriformis muscle and sciatic nerve: a morphological analysis in a Polish population. Med Sci Monit. 2015; 21: 3760–3768, doi: 10.12659/msm.894353, indexed in Pubmed: 26629744.
8. Hopayian K, Danielyan A. Four symptoms define the piriformis syndrome: an updated systematic review of its clinical features. Eur J Orthop Surg Traumatol. 2018; 28(2): 155–164, doi: 10.1007/s00590-017-2031-8, indexed in Pubmed: 28836092.
9. Iwanaga J, Eid S, Simonds E, et al. The majority of piriformis muscles are innervated by the superior gluteal nerve. Clin Anat. 2019; 32(2): 282–286, doi: 10.1002/ca.23311, indexed in Pubmed: 30408241.

10. Iwanaga J, Singh V, Takeda S, et al. Acknowledging the use of human cadaveric tissues in research papers: Recommendations from anatomical journal editors. Clin Anat. 2021; 34(1): 2–4, doi: 10.1002/ca.23671, indexed in Pubmed: 32808702.
11. Kurtoglu Z, Aktekin M, Uluutku MH. Branching patterns of the common and superficial fibular nerves in fetus. Clin Anat. 2006; 19(7): 621–626, doi: 10.1002/ca.20235, indexed in Pubmed: 16302233.
12. Lewis S, Jurak J, Lee C, et al. Anatomical variations of the sciatic nerve, in relation to the piriformis muscle. Transl Res Anat. 2016; 5: 15–19, doi: 10.1016/j.tria.2016.11.001.
13. McLawhorn AS, Christ AB, Morgenstern R, et al. Prospective evaluation of the posterior tissue envelope and anterior capsule after anterior total hip arthroplasty. J Arthroplasty. 2020; 35(3): 767–773, doi: 10.1016/j.arth.2019.09.045, indexed in Pubmed: 31679976.
14. Naito M, Suzuki R, Abe H, et al. Fetal development of the human obturator internus muscle with special reference to the tendon and pulley. Anat Rec (Hoboken). 2015; 298(7): 1282–1293, doi: 10.1002/ar.23121, indexed in Pubmed: 25683268.
15. Natsis K, Totlis T, Konstantinidis GA, et al. Anatomical variations between the sciatic nerve and the piriformis muscle: a contribution to surgical anatomy in piriformis syndrome. Surg Radiol Anat. 2014; 36(3): 273–280, doi: 10.1007/s00276-013-1180-7, indexed in Pubmed: 23900507.
16. Niikura H, Jin ZWu, Cho BH, et al. Human fetal anatomy of the coccygeal attachments of the levator ani muscle. Clin Anat. 2010; 23(5): 566–574, doi: 10.1002/ca.20983, indexed in Pubmed: 20544951.
17. Ozisik PA, Toru M, Denk CC, et al. CT-guided piriformis muscle injection for the treatment of piriformis syndrome. Turk Neurosurg. 2014; 24(4): 471–477, doi: 10.5137/1019-5149.JTN.8038-13.1, indexed in Pubmed: 25050669.
18. Robinson DR. Pyriformis syndrome in relation to sciatic pain. Am J Surg. 1947; 73(3): 355–358, doi: 10.1016/0002-9610(47)90345-0, indexed in Pubmed: 20289074.
19. Santamato A, Micello MF, Valeno G, et al. Ultrasound-guided injection of botulinum toxin type a for piriformis muscle syndrome: a case report and review of the literature. Toxins (Basel). 2015; 7(8): 3045–3056, doi: 10.3390/toxins7083045, indexed in Pubmed: 26266421.
20. Smoll NR. Variations of the piriformis and sciatic nerve with clinical consequence: a review. Clin Anat. 2010; 23(1): 8–17, doi: 10.1002/ca.20893, indexed in Pubmed: 19998490.
21. Sulak O, Sakalli B, Ozguner G, et al. Anatomical relation between sciatic nerve and piriformis muscle and its bifurcation level during fetal period in human. Surg Radiol Anat. 2014; 36(3): 265–272, doi: 10.1007/s00276-013-1179-0, indexed in Pubmed: 23892789.
22. Thompson G, Visagie R. Type II sciatic nerve variant: an unexpected interventional hazard. Skeletal Radiol. 2017; 46(10): 1453–1458, doi: 10.1007/s00256-017-2712-8, indexed in Pubmed: 28748363.
23. Tomaszewski KA, Graves MJ, Henry BM, et al. Surgical anatomy of the sciatic nerve: a meta-analysis. J Orthop Res. 2016; 34(10): 1820–1827, doi: 10.1002/jor.23186, indexed in Pubmed: 26856540.
24. Tubbs R, Barton J, Watson C, et al. A novel method for sciatic nerve decompression: cadaveric feasibility study with potential application to patients with piriformis syndrome. Transl Res Anat. 2015; 1: 40–43, doi: 10.1016/j.tria.2015.10.006.
25. Wun-Schen C. Bipartite piriformis muscle: an unusual cause of sciatic nerve entrapment. Pain. 1994; 58(2): 269–272, doi: 10.1016/0304-3959(94)90208-9, indexed in Pubmed: 7816495.
26. Żytkowski A, Tubbs R, Iwanaga J, et al. Anatomical normality and variability: historical perspective and methodological considerations. Transl Res Anat. 2021; 23: 100105, doi: 10.1016/j.tria.2020.100105.

VIA MEDICA

CASE REPORT

Folia Morphol.
Vol. 82, No. 4, pp. 975–979
DOI: 10.5603/FM.a2022.0091

ISSN 0015–5659
eISSN 1644–3284
journals.viamedica.pl

Five-headed superior omohyoid

K. Maślanka[1], N. Zielinska[1], R.S. Tubbs[2–7], B. Gonera[1], K. Ruzik[1], Ł. Olewnik[1]

[1]*Department of Anatomical Dissection and Donation, Medical University of Lodz, Poland*
[2]*Department of Anatomical Sciences, St. George's University, Grenada, West Indies*
[3]*Department of Neurosurgery, Tulane University School of Medicine, New Orleans, Louisiana, United States*
[4]*Department of Neurology, Tulane University School of Medicine, New Orleans, Louisiana, United States*
[5]*Department of Structural and Cellular Biology, Tulane University School of Medicine, New Orleans, Louisiana, United States*
[6]*Department of Surgery, Tulane University School of Medicine, New Orleans, Louisiana, United States*
[7]*Department of Neurosurgery, Ochsner Medical Centre, New Orleans, Louisiana, United States*

[Received: 10 July 2022; Accepted: 27 July 2022; Early publication date: 28 October 2022]

The omohyoid is an infrahyoid muscle with two bellies. It is responsible for lowering and positioning of the hyoid bone. It is morphologically variable in the origin, insertion and morphology of its bellies. Quantitative variations of the superior belly of the omohyoid muscle are not common. We present a case of a five-headed superior omohyoid, and a short clinical review related to this muscle. All the bellies had their origin in an intermediate tendon and were attached to the hyoid bone. The volume of its superior part was greater than usual. Knowledge of the anatomy of this muscle is important, especially for surgeons operating in the anterolateral neck region. (Folia Morphol 2023; 82, 4: 975–979)

Key words: omohyoid muscle, compression, additional head, clinical implications, myofascial pain syndrome, plastic surgery, reconstructive surgery

INTRODUCTION

The omohyoid muscle (OH) is the long thin muscle that runs obliquely in the lateral cervical region [9, 22]. Traditionally, it has two bellies, superior (OMS) and inferior (OMI), which are united by an intermediate tendon connected to the clavicle by a fascial sling [22]. The inferior belly arises and shifts to the intermediate tendon from the superior margin of the scapula, medial to the scapular notch [14]. The superior belly begins in the intermediate tendon and is inserted to the inferior border of the hyoid bone. It is positioned superficial to the phrenic nerve and brachial plexus and lies superficial to the internal jugular vein [19, 29, 30]. The OMS is innervated by terminal branches of the ansa cervicalis, but no direct branches to the OMI have been found to date [15]. The blood supply to the omohyoid comes from the superior and inferior thyroid arteries [8, 16]. This article pays particular attention to the upper part of this muscle.

The OMS has many anatomical variations in its insertion, course and number of bellies [3, 17, 34]. A one-sided lack of it has been reported, but this is very rare [6, 32, 33]. Sukekawa and Ito [29] proposed a classification into several types of superior belly. Their type III included an OMS that can consist of three to five bellies, but as they admitted, their cases of four or five-headed OMs were unclear and were speculative [29].

The following case describes the separate and clear appearance of a five-headed OMS.

Address for correspondence: Ł. Olewnik, MD, PhD, Department of Anatomical Dissection and Donation, Chair of Anatomy and Histology, Medical University of Lodz, ul. Żeligowskiego 7/9, 90–410 Łódź, Poland, e-mail: lukasz.olewnik@umed.lodz.pl

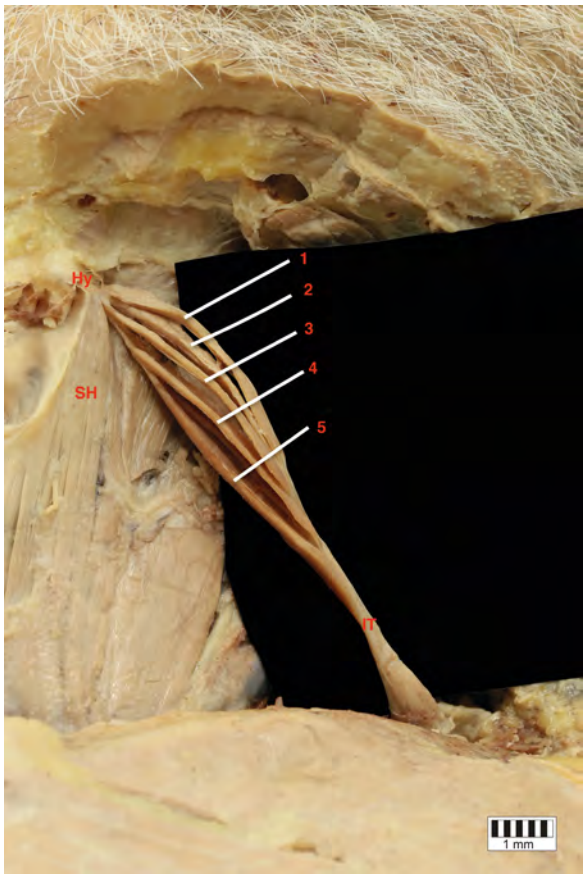

Figure 1. Five-headed omohyoid muscle. Neck. Hy — hyoid bone; SH — sterno-hyoideus; IT — intermediate tendon of omohyoideus; 1 — first head of the omohyoideus; 2 — the second head of the omohyoideus; 3 — the third head of the omohyoid muscle; 4 — the fourth head of the omohyoid muscle; 5 — the fifth head of the omohyoideus.

CASE REPORT

During a dissection performed for research and didactic purposes at the Department of Anatomical Dissection and Donation, Medical University of Lodz, we noticed supernumerary heads of the OM. The subject of investigation was the neck of a 76-year-old male cadaver. The donor had no surgeries in the neck area. The dissection was performed by the traditional anatomical method [20, 25]. Each belly of the OM was thoroughly dissected to visualise its origin and insertion.

In the present case, the OMS was represented by five separate heads (Fig. 1), which had origin in the intermediate tendon that unites the superior and inferior bellies. At this point, the muscle was 8.19 mm wide and 3.96 mm thick.

All the distinct heads had a distal attachment on the inferior border of the hyoid bone. The first head was shortest (38.6 mm long). Its width and thickness were 2.96 mm and 0.61 mm, respectively, at the point of transition to the tendon, which was 2.82 long.

The second head was little longer than the first (39.19 mm). The proximal end of the belly was 4.53 mm wide (the widest of all five) and 0.69 mm thick. The tendon was 2.28 mm long.

The third head was 46.6 mm long. In the point of origin, its width was 2.74 mm and its thickness was 0.18 mm (the thinnest of all). Its tendon, which was attached to the intermediate tendon, was just 1.70 mm long.

The width of the fourth head in its proximal part was 1.82 mm; its thickness here was 0.26 mm. This head was 51.02 mm long and the tendon was 3.48 mm. The fifth, final head was the longest of all (59.8 mm). Its tendon is also the longest of all (10.99 mm). The point of the belly arising from the tendon was 3.12 mm wide and 0.56 mm thick.

The inferior belly of the omohyoid was also measured. Its dimensions were greater than those of the OMS. In its distal part the width was 7.68 mm and the thickness was 3.89 mm. Its length could be as much as 84.16 mm, more than twice as long as the first and second bellies. The third head of the OMS was 55.4% of the length of the OMI, the fourth head was 60.6% and the fifth 71%.

Importantly, we noticed a vague division into two main layers of the hyoid muscle, superficial and deep. The superficial layer contained the first, second and third bellies, while the deep layer was formed by the fourth and fifth bellies. We believe that this could be an interesting point of departure for researchers in future studies on the omohyoid muscle.

An electronic calliper (Mitutoyo Corporation, Kawasaki-shi, Kanagawa, Japan) was used for measurements. Each measurement was obtained twice by different researchers with an accuracy of up to 0.1 mm (Table 1).

DISCUSSION

The omohyoideus is formed by myoblasts from the cervical myotomes and is the fastest growing infrahyoid muscle during fetal life [11]. The extent of development of the infrahyoid muscles is very diverse [2, 22]. Anderson's hypothesis was that only the superior belly is the true infrahyoid muscle, while inferior belly shares its embryology with the subclavian muscle. This hypothesis is corroborated by the case of clavicular attachment of the OM [28]. This muscle has the same primordium as the sterno-

Table 1. Measurements of individual heads of the omohyoid muscle

	1st head	2nd head	3rd head	4th head	5th head
Length	38.6 mm	39.19 mm	46.6 mm	51.02 mm	59.8 mm
Tendon					
Length	2.82 mm	2.28 mm	1.70 mm	3.48 mm	10.99 mm
Insertion	Inferior border of the hyoid bone				
Width	8.19 mm				
Thickness	3.96 mm				
Origin	Intermediate tendon of the omohyoid muscle				
Width	2.96 mm	4.53 mm	2.74 mm	1.82 mm	3.12 mm
Thickness	0.61 mm	0.69 mm	0.18 mm	0.26 mm	0.56 mm

hyoid muscle, which is probably why they frequently merge [18].

The upper part of this muscle is highly variable, but the additional heads described are unusual and very rare [26, 29]. Some of them have significant clinical relevance in many areas, which makes it an important and at the same time interesting object of research [22].

One of the most common abnormalities of the OM is the junction of the OMS with the sternohyoid muscle, mentioned earlier [22]. Also, a large part of it is cleido-hyoideus, by which the inferior belly is attached to the lateral part of the clavicle while the superior belly is attached to the lateral part of the body of the hyoid bone [3, 14, 22]. These two types are part of the classification of variability proposed by Kasapoglu and Dokuzlar [12] in 2007 and constitute types III and II respectively. Type IV has a superior normal belly with fibres received from the sternum. Previously, anomalies of this muscle were classified into six types by Miura et al. [17], and more than a century ago into five types by Loth [see 5]. Sukekawa and Ito [29] in 2005 classified the OMS into four types. Our case corresponds to the third type in their classification.

Duplication of this muscle is also not uncommon and has been described several times [1, 17, 35]. Also interesting is its total absence, which has been described by Tamega et al. [32], Bergman et al. [2], and Thangarajan et al. [33]. It should be noted that this muscle is the most frequently absent of all the infrahyoid group [2]. An OMS consisting of several heads has probably only been presented previously by Sukekawa and Itoh [29].

As mentioned earlier, this muscle often undergoes fusion for reasons of embryology [2]. A classical illustration is a combined OM and sternohyoid muscle — a sternoomohyoideus [17]. The connections between them are very different, as described by Miura et al. [12]. The cleidohyoideus originates from the cledoidomastoid part of the sternocleidomastoideus [2]. However, from a clinician's point of view, the connection with the cervical fascia seems most important [2, 22]. The cleidofascialis and hyofascialis are examples of variations that can impose more tension on the cervical fascia, increasing internal jugular vein (IJV) compression, thereby impairing blood flow in this vessel. Moreover, this variability presumably affects the occurrence of omohyoideus myofascial pain syndrome [23].

The omohyoideus is of great interest because of its clinical importance [22]. First, it divides the posterior and anterior cervical triangles into smaller ones. These muscles are the surgical landmark for the IJV, brachial plexus, and levels 3 and 4 lymph node metastases [12, 13, 24]. Because of this, lack of or a highly variant course of the OM can be particularly dangerous during surgery in the anterolateral neck region. Also, because of this close correlation with the IJV, the course or contraction of the muscle affects the vessel lumen and its haemodynamics [21, 38]. The variability of its length is key to this aspect, as a short OM markedly increases the compression force on the IJV [21]. As noted previously, the area of the OM also contains the brachial plexus, which can be irritated by a hypertrophied OM [7]. Fibrosis of the OM in specific cases can cause torticollis, according to Shih and Chuang [27]. Tubbs et al. [34] presented an unusual origin of the OM that could significantly affect not only omohyoideus function but also cervical spine biomechanics.

The omohyoid muscle, especially its upper belly, is often used in reconstructive and plastic surgery [37]. In laryngeal paralysis, surgeons use the OM to restore normal function [4]. When a small patch is needed for reconstruction, for example in facial reanimation surgery, vocal reconstruction, sphincters or blink restoration surgery the OMS could be used, but more anatomical research on it is needed to optimise this process [19]. Surek and Girod [31] described the use of the OMS to repair cervical oesophageal perforation. The course of the omohyoid muscle is also extremely useful during vagus nerve stimulator implantation [36].

CONCLUSIONS

We report a case of a five-headed omohyoid muscle. Owing to its embryology, the omohyoideus

is highly variable. Its location makes it extremely important during surgical procedures within the anterolateral neck and for the haemodynamics of the head and neck veins. Recently, its potential has been recognised in plastic and reconstructive surgery, but further anatomical and functional studies are necessary to realize its full potential in this area of medicine.

Ethical approval and consent to participate

The study protocol was accepted by the Bioethics Committee of the Medical University of Lodz. The cadavers were the property of the Department of Anatomical Dissection and Donation, Medical University of Lodz, and of the Donors and Dissecting Rooms Centre, Universidad Complutense de Madrid, Spain. Informed consents were obtained from all participants before they died.

Acknowledgements

The authors sincerely thank those who donated their bodies to science so that anatomical research could be performed. Results from such research can potentially increase mankind's overall knowledge that can then improve patient care. Therefore, these donors and their families deserve our highest gratitude [10].

Conflict of interest: None declared

REFERENCES

1. Anderson RJ. The morphology of the omohyoid muscle. Dublin J Med Sci. 1881; 10: 1–17.
2. Bergman RA, Afifi AK, Miyauchi R. Illustrated Encyclopedia of Human Anatomic Variation: Muscular System: Omohyoideus, Sternohyoideus, Thyrohyoideus, Sternothyroideus. 1996.
3. Bolla S, Nayak S, Vollala V, et al. Cleidohyoideus – a case report. Indian J Pract Dr. 2007; 3: 1–2.
4. Crumley RL. Muscle transfer for laryngeal paralysis. Restoration of inspiratory vocal cord abduction by phrenic-omohyoid transfer. Arch Otolaryngol Head Neck Surg. 1991; 117(10): 1113–1117, doi: 10.1001/archotol.1991.01870220061010, indexed in Pubmed: 1910695.
5. des Halses LEM. In: Beitrage zur Anthropologie der Negerweichteile. Streker and Schroder, Stuttgart 1912: 58–73.
6. Ezer H, Banerjee AD, Thakur JD, et al. Dorello's canal for laymen: a lego-like presentation. J Neurol Surg B Skull Base. 2012; 73(3): 183–189, doi: 10.1055/s-0032-1311753, indexed in Pubmed: 23730547.
7. Fiske LG. Brachial plexus irritation due to hypertrophied omohyoid muscle; a case report. J Am Med Assoc. 1952; 149(8): 758–759, doi: 10.1001/jama.1952.72930250002013a, indexed in Pubmed: 14927441.
8. Görmüs G, Bayramoğlu A, Aldur MM, et al. Vascular pedicles of infrahyoid muscles: an anatomical study. Clin Anat. 2004; 17(3): 214–217, doi: 10.1002/ca.10178, indexed in Pubmed: 15042569.
9. Hatipoğlu ES, Kervancioğlu P, Tuncer MC. An unusual variation of the omohyoid muscle and review of literature. Ann Anat. 2006; 188(5): 469–472, doi: 10.1016/j.aanat.2006.03.004, indexed in Pubmed: 16999212.
10. Iwanaga J, Singh V, Takeda S, et al. Acknowledging the use of human cadaveric tissues in research papers: Recommendations from anatomical journal editors. Clin Anat. 2021; 34(1): 2–4, doi: 10.1002/ca.23671, indexed in Pubmed: 32808702.
11. Jakubowicz M, Radziemski A, Kedzia A. Histological and quantitative studies of the muscle spindles in human fetal infrahyoid muscles. Folia Morphol. 1992; 51(1): 55–59, indexed in Pubmed: 1478563.
12. Kasapoglu F, Dokuzlar U. An unknown anatomical variation of omohyoid muscle. Clin Anat. 2007; 20(8): 964–965, doi: 10.1002/ca.20554, indexed in Pubmed: 17948298.
13. Krishnan KG, Pinzer T, Reber F, et al. Endoscopic exploration of the brachial plexus: technique and topographic anatomy: a study in fresh human cadavers. Neurosurgery. 2004; 54(2): 401–408, doi: 10.1227/01.neu.0000103423.08860.a9, indexed in Pubmed: 14744288.
14. Kumar R, Borthakur D, Rani N, et al. Anatomical diversity of inferior belly of the omohyoid muscle - anatomical, physiological and surgical paradigm. Morphologie. 2023; 107(356): 142–146, doi: 10.1016/j.morpho.2022.01.003, indexed in Pubmed: 35148950.
15. Loukas M, Thorsell A, Tubbs RS, et al. The ansa cervicalis revisited. Folia Morphol. 2007; 66(2): 120–125, indexed in Pubmed: 17594670.
16. Meguid EA, Agawany AE. An anatomical study of the arterial and nerve supply of the infrahyoid muscles. Folia Morphol. 2009; 68(4): 233–243.
17. Miura M, Kato S, Itonaga I, et al. The double omohyoid muscle in humans: report of one case and review of the literature. Okajimas Folia Anat Jpn. 1995; 72(2-3): 81–97, doi: 10.2535/ofaj1936.72.2-3_81, indexed in Pubmed: 8559563.
18. Moore KL. The developing human. WB Saunders Co, Philadelphia 1988: 350.
19. Muñoz-Jimenez G, Telich-Tarriba J, Palafox-Vidal D, et al. A novel highly specialized functional flap: omohyoid inferior belly muscle. Plastic Aesthetic Res. 2018; 5(4): 14, doi: 10.20517/2347-9264.2018.04.
20. Olewnik Ł, Tubbs R, Ruzik K, et al. Quadriceps or multiceps femoris? — Cadaveric study. Clin Anat. 2021; 34(1): 71–81, doi: 10.1002/ca.23646, indexed in Pubmed: 32644202.
21. Patra P, Gunness TK, Robert R, et al. Physiologic variations of the internal jugular vein surface, role of the omohyoid muscle, a preliminary echographic study. Surg Radiol Anat. 1988; 10(2): 107–112, doi: 10.1007/BF02307818, indexed in Pubmed: 3135615.
22. Rai R, Ranade A, Nayak S, et al. A study of anatomical variability of the omohyoid muscle and its clinical relevance. Clinics (Sao Paulo). 2008; 63(4): 521–524, doi: 10.1590/s1807-59322008000400018, indexed in Pubmed: 18719765.
23. Rask MR. The omohyoideus myofascial pain syndrome: report of four patients. J Craniomandibular Pract. 1984;

2(3): 256–262, doi: 10.1080/07345410.1984.11677872, indexed in Pubmed: 6206170.
24. Robbins KT, Medina JE, Wolfe GT, et al. Standardizing neck dissection terminology. Official report of the Academy's Committee for Head and Neck Surgery and Oncology. Arch Otolaryngol Head Neck Surg. 1991; 117(6): 601–605, doi: 10.1001/archotol.1991.01870180037007, indexed in Pubmed: 2036180.
25. Ruzik K, Waśniewska A, Olewnik Ł, et al. Unusual case report of seven-headed quadriceps femoris muscle. Surg Radiol Anat. 2020; 42(10): 1225–1229, doi: 10.1007/s00276-020-02472-0, indexed in Pubmed: 32318799.
26. Sasagawa KKI, Takahashi K, Igarashi A, et al. A case of an abnormal bundle from the anterior margin of the right and left trapezius and the abnormality in the right omohyoid appeared in a cadaver. Shigaku. 1982; 70: 439–448.
27. Shih TY, Chuang JH. Fibrosis of the omohyoid muscle — an unusual cause of torticollis. J Pediatr Surg. 1998; 33(5): 741–742, doi: 10.1016/s0022-3468(98)90204-4, indexed in Pubmed: 9607485.
28. Singh N, Kathole M, Kaur J, et al. Bilateral clavicular attachment of omohyoid muscle. Morphologie. 2018; 102(337): 87–90, doi: 10.1016/j.morpho.2017.08.001, indexed in Pubmed: 28890314.
29. Sukekawa R, Itoh I. Anatomical study of the human omohyoid muscle: regarding intermediate morphologies between normal and anomalous morphologies of the superior belly. Anat Sci Int. 2006; 81(2): 107–114, doi: 10.1111/j.1447-073X.2006.00138.x, indexed in Pubmed: 16800295.
30. Sulek M. Otolaryngology–head and neck surgery. 2nd ed. Vols. 1, 2, 3, 4. Cummings C, Fredrickson JM, Harker LA, Krause CJ, Schuller DE. (ed.) . Mosby Year Book, St. Louis, Missouri 1993.
31. Surek CC, Girod DA. Superior omohyoid muscle flap repair of cervical esophageal perforation induced by spinal hardware. Ear Nose Throat J. 2014; 93(12): E38–E42, doi: 10.1177/014556131409301203, indexed in Pubmed: 25531854.
32. Tamega OJ, Garcia J, Soares JC, et al. About a case of absence of the superior belly of the omohyoid muscle. Anat Anz. 1983; 154(1): 39–42, indexed in Pubmed: 6625183.
33. Thangarajan R, Shetty P, Sirasanagnadla SR, et al. Unusual morphology of the superior belly of omohyoid muscle. Anat Cell Biol. 2014; 47(4): 271–273, doi: 10.5115/acb.2014.47.4.271, indexed in Pubmed: 25548726.
34. Tubbs RS, Salter EG, Oakes WJ. Unusual origin of the omohyoid muscle. Clin Anat. 2004; 17(7): 578–582, doi: 10.1002/ca.20039, indexed in Pubmed: 15376287.
35. Wood J. Additional varieties in human myology. Proc R Soc Lond. 1865; 14: 379–392.
36. Yowtak J, Jenkins P, Giller C. Transection of omohyoid muscle as an aid during vagus nerve stimulator implantation. World Neurosurg. 2017; 99: 118–121, doi: 10.1016/j.wneu.2016.11.146, indexed in Pubmed: 27931947.
37. Zhao W, Liu J, Xu Ji, et al. Duplicated posterior belly of digastric muscle and absence of omohyoid muscle: a case report and review of literature. Surg Radiol Anat. 2015; 37(5): 547–550, doi: 10.1007/s00276-014-1374-7, indexed in Pubmed: 25218516.
38. Ziolkowski M, Marek J, Oficjalska-Młyńczak J. The omohyoid muscle during the fetal period in man. Folia Morphol. 1983; 42(1): 21–30, indexed in Pubmed: 6603393.

VIA MEDICA

CASE REPORT

Folia Morphol.
Vol. 82, No. 4, pp. 980–987
DOI: 10.5603/FM.a2022.0098

ISSN 0015–5659
eISSN 1644–3284
journals.viamedica.pl

Hypogenetic right lung with partial anomalous pulmonary venous return and accessory diaphragm: a case of "scimitar lung"

C. Melovitz-Vasan[1], A. White[1], S. Huff[2], N. Vasan[1]

[1]*Department of Biomedical Sciences, Cooper Medical School of Rowan University, Camden, New Jersey, United States*
[2]*Rowan University, Glassboro, New Jersey, United States*

[Received: 21 August 2022; Accepted: 14 October 2022; Early publication date: 29 November 2022]

Partial anomalous pulmonary venous return (PAPVR) is a rare congenital cardiovascular condition in which some of the pulmonary veins drain into the systemic circulation. We report on the cadaveric dissection of a 71-year-old Caucasian male donor who died of chronic obstructive pulmonary disease with hypertension. We noted a faint incisional scar on the thorax extending from the parasternal region at the 4th intercostal level to the midaxillary line. Since the straight-line incision followed the ribs and the scar was quite faint, surgery probably occurred when the donor was young. We also observed numerous surgical interventions of the heart, lungs, and vasculature to correct various defects.

The morphology of the heart was normal, but was shifted more to the right side. An atrial septal defect (ASD) was closed with sutures. The right superior pulmonary vein that drained into the superior vena cava (SVC) was ligated close to the SVC and the right inferior, left superior, and inferior pulmonary veins all drained directly into the left atrium. We noticed a dilated coronary sinus entering the right atrium adjacent to the ASD; the ostium of the coronary sinus noticeably lacked the normal valve-like structure. We initially thought the right lung was a "horseshoe" lung, but realised that it was a "hypogenetic" lung with PAPVR and an accessory diaphragm. Compared to the left, the right secondary bronchi were much narrower and branched uncharacteristically, as seen in hypogenetic lung syndrome. The inferior lobe was highly disorganised, severely hypoplastic, and exhibited uncharacteristic morphology. The superior bronchopulmonary segment was markedly hypoplastic. The posterior and medial basal segments were not only hypoplastic and slender, but also extended like a tail to the left pulmonary cavity behind the heart/pericardium and in front of the oesophagus and aorta. The right lung, though hypoplastic, demonstrated patent bronchi and the lobes were inflatable. Based on the hypogenetic lung and PAPVR, we conclude that the donor exhibited 'scimitar' lung. (Folia Morphol 2023; 82, 4: 980–987)

Key words: scimitar lung, congenital cardiovascular anomaly, partial anomalous pulmonary venous return (PAPVR), partial anomalous pulmonary venous connection (PAPVC)

Address for correspondence: Prof. N. Vasan, DVM, MVSc, PhD, Department of Biomedical Sciences, Cooper Medical School of Rowan University, 401 South Broadway, Camden, New Jersey 08103, United States, tel: +1 (856) 361-2889, e-mail: vasan@rowan.edu

INTRODUCTION

Partial anomalous pulmonary venous return (PAPVR), additionally recognised as partial anomalous pulmonary venous connection (PAPVC), is an inherited cardiac circulatory condition; it occurs infrequently and results in few, but not all of the pulmonary veins emptying into the general circulation, instead of the left atrium [19]. Present at birth, PAPVC is a multifaceted cardiac defect; it has no known cause, though there is a possibly multifactorial origin that includes genetic component [31]. Numerous variations of this vascular anomaly have appeared in the literature. The first description of scimitar syndrome, a variant of partial anomalous pulmonary venous drainage (PAPVD), appeared in 1836 [3, 4]. This rare, complex, congenital anomaly is characterised by abnormal pulmonic venous blood flow from the right lung shunted into the inferior vena cava (IVC) or right atrium via superior vena cava (SVC), thus a left-to-right shunt. Hypoplasia of the right lung, dextrocardia, malformations of the right pulmonary artery and bronchial tree, and abnormal arterial supply of the right lung (the so-called pulmonary sequestration) are associated anomalies that manifest frequently. Atrial septal defect happens in approximately 40% of cases with right-sided PAPVR [21]. Classic scimitar syndrome consists of hypoplasia of the right lung and right pulmonary artery, dextroposition of the heart, an abnormal pulmonary vein draining into the IVC, and a systemic collateral supply to the lung [3, 4].

In the complete form of the infrequently occurring, inherited abnormality called scimitar (hypogenetic) lung, systemic arterial blood flow supplies the right lung and its inferior lobe and empties partially or totally to the general veinous circulation. Hypoplasia of the pulmonary arteries and uncharacteristic bronchial branching accompany this disorder [23, 24]. The aberrant pulmonary venous return typically includes the right side [5]. A rare variation called horseshoe lung is often accompanied by vascular abnormalities of the hypogenetic lung [10, 17, 33].

The blending of posterior basilar segments of the right and left inferior lobes involving an incomplete parietal pleural deficiency constitutes horseshoe lung, which has a frequency that varies from 0.4% to 0.7% [11]. Most horseshoe lung cases are associated with right lung hypoplasia; approximately 80% are associated with PAPVR from the right lung to the IVC or right atrium (scimitar syndrome) [20, 37]. In PAPVR, one of the abnormal veins from the lung drains into general venous circulation, creating a left-to-right diversion, rather than normally occurring emptying of venous blood from the lung into the left atrium. In right-sided PAPVR, an anomalous pulmonary vein drains into either the SVC [18], right atrium [13], coronary sinus [22], or IVC [9]. Right upper lobe flow most commonly drains into the SVC and the condition is often associated with a high sinus venosus atrial septal defect near the orifice of the SVC [18]. An accessory diaphragm seen in the case reported here is a rare congenital anomaly associated with an atrial septal defect described in paediatric patients [28, 34] that occurs mostly on the right side [5] and is composed of fibromuscular tissue with a serosal lining [8]. In all the described cases, aplasia or certain extent of pulmonary hypoplasia was obvious on the involved side [5].

Embryology of lung development

As normal embryonic development occurs in the first 2 months, venous blood from the lungs empties into the systemic veins [9] and the common initial pulmonary vein develops from a bulge in the dorsal wall of the early stage left atrium [9, 11]. As development continues, the early-stage lungs attach to the common pulmonary vein and the connections that allow pulmonary venous return to the systemic veins disappear [9, 11]. Thus, the shared pulmonary vein integrates into the left atrium and four well-separated pulmonary veins arise, two from each lung [9, 11]. Abnormal resorption of the developing structures can bring about (1) changes in the size or the number of pulmonary veins or (2) atypical emptying into the general veins or right atrium.

MATERIALS AND METHODS

The cadaveric specimen was obtained from the willed body programme intended for the purpose of dissection by medical students. This study is based on the cadaveric dissection of a 71-year-old Caucasian male donor who died of chronic obstructive pulmonary disease/hypertension. We observed a number of what appeared to be surgical interventions of the heart, lung, and vasculatures, possibly due to malformations and anomalous venous drainage. In the dissection procedure, the anterior thoracic wall was removed, as guided by the faculty, and the thoracic viscera were dissected and studied. The students' dissection protocol called for opening the thoracic cage and studying in detail first the heart, followed by the respiratory system. Since the major

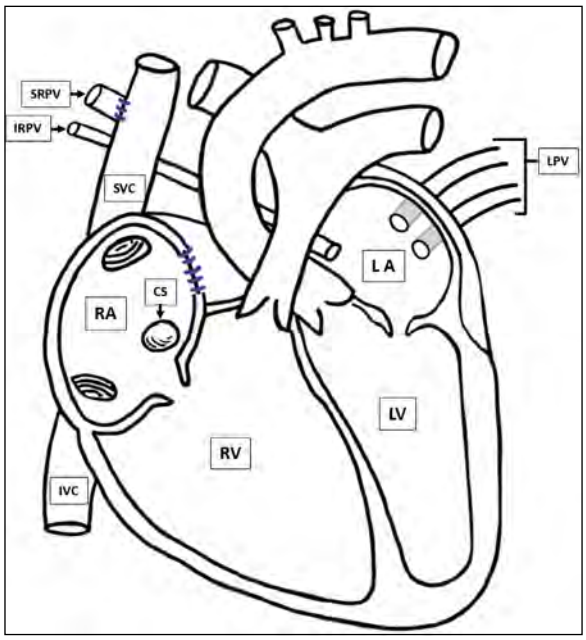

Figure 1. Schematic representation of the heart the students dissected and studied. The defects are corrected by surgical sutures as indicated by zig-zag suture lines, including right superior pulmonary vein that drained into the superior vena cava (SVC), which was ligated close to the SVC and atrial septal defect; RA — right atrium; LA — left atrium; LV — left ventricle; RV — right ventricle; CS — coronary sinus; IVC — inferior vena cava; SRPV — superior right pulmonary vein; IRPV — inferior right pulmonary vein; LPV — left pulmonary veins.

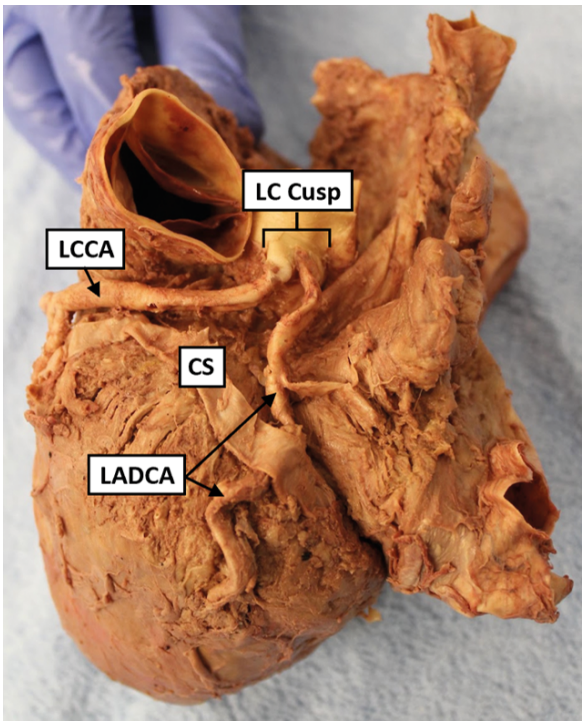

Figure 2. Actual cadaveric heart specimen with independent origins of the left anterior descending and circumflex coronary arteries from the left coronary cusps thus showing the lack of normal left coronary artery. Also shown is the dilated coronary sinus entering the right atrium; LC Cusp — left coronary cusp; LADCA — left anterior descending coronary artery; C-S — coronary sinus; LCCA — left circumflex coronary artery.

part of the dissection was performed by the students, some of the vascular and other structures were not optimally preserved. Additionally, the surgical corrective procedures disturbed the natural architecture of the gross morphology.

OBSERVATIONS AND RESULTS

On the right side of the thoracic wall, we observed an incision extending from the parasternal region at the 4th intercostal level to the midaxillary line, apparently to surgically address anomalies. Considering the straight line (not curved) incision following the ribs on the thorax, we believed that the surgery was performed during the donor's childhood, since the ribs are more horizontal in young age. An experienced in-house pathologist who examined the cadaver described the incision scar as faint and very old, suggestive of surgical intervention in childhood to correct problems in the thoracic viscera.

Heart, vasculatures, and surgical interventions

The morphology of the heart was normal in both size and shape. However, as reported in an earlier study, the heart and mediastinum were shifted more toward the right side [37]. We observed evidence of surgical procedures performed on the heart, likely to correct congenital defects. We found that the atrial septal defect (ASD) was corrected by closure with sutures (Fig. 1). The right superior pulmonary vein that drained into the SVC was ligated close to the SVC (Fig. 1). While the right coronary artery originated normally from the right coronary cusp, the left coronary circumflex and the left anterior descending arteries arose independently from the left coronary cusp, thus lacking the typical left coronary artery (Fig. 2). Additionally, we recognised a dilated coronary sinus entering the right atrium adjacent to the ASD (Fig. 2) and the ostium of coronary sinus noticeably lacked the normal valve-like structure.

Respiratory system: right lung

We initially thought the right lung was a typical 'horseshoe' lung, as described in the literature [21, 37]. Upon closer examination of all the thoracic viscera, vasculatures, and surgical interventions, we

realised that what we encountered was a hypogenetic right lung with PAPVR and accessory diaphragm (Fig. 3). The trachea was normal in size and location, bifurcated at the level of 4th thoracic vertebra; the carina was situated normally at the bifurcation. Upon division from the trachea, the right and left primary bronchi were of normal size. However, the right secondary bronchi were much narrower compared to the left and branched uncharacteristically, as seen in hypogenetic lung syndrome (Fig. 3) [24].

In the hypoplastic right lung, the oblique fissure separated the superior lobe from the inferior lobe and a horizontal fissure defining the small middle lobe was also observed. The inferior lobe was highly disorganised and severely hypoplastic and exhibited uncharacteristic morphology. The superior bronchopulmonary segment was markedly hypoplastic; the posterior basilar and medial basal segments were not only hypoplastic and fused, but also formed a slender "tail" that extended to the left pulmonary cavity behind the heart/pericardium and in front of oesophagus and aorta. However, the fused, tail-like right segments did not fuse with the similar segments of the left lung, as seen in "scimitar" lung. Notably, we also observed an accessory diaphragm separating the fused anterior and lateral basal segments (Fig. 3). Furthermore, the fused anterior and lateral basal segments that were wedged between the true diaphragm and the accessory diaphragm were inflatable. Though hypoplastic, the bronchi were patent; using an air pump, we were able to inflate the superior and middle lung segments. Importantly, we were also able to inflate all the lower lobe bronchopulmonary segments and pass a soft probe (pipe cleaner) into the pulmonary arterial branches of the lower lobe bronchopulmonary segments.

Respiratory system: left lung

Both lobes of the left lung were normal in size and exhibited typical gross morphology. An oblique fissure separated the upper and lower lobes and surface visceral impressions appeared normal (Fig. 3). The left lung shifted more towards the right, causing the observed mediastinal shift, and no pathology was noted. The left lung was inflatable by air pump, showing a normal patency of the bronchi and their functional ability. We were able to pass a soft probe (pipe cleaner) into the pulmonary arterial branches of all bronchopulmonary segments.

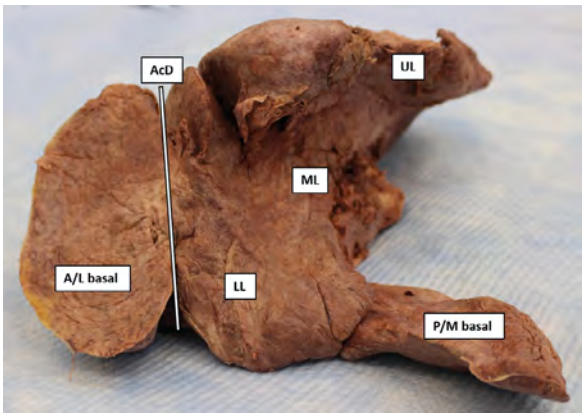

Figure 3. The cadaveric lungs showing normal left lung and the hypogenetic right lung with aberrant morphology. The inferior lobe was highly disorganized and severely hypoplastic and exhibited uncharacteristic morphology. The right superior bronchopulmonary segment was markedly hypoplastic; the posterior basilar and medial basal segments were not only hypoplastic and fused, but also formed a slender "tail" like morphology. We also observed an accessory diaphragm (indicated by a line) separating the fused anterior and lateral basal segments. The fused anterior and lateral basal segments that were wedged between the true diaphragm and the accessory diaphragm were inflatable; UL — upper lobe; LL — lower lobe; ML — middle lobe; AcD — accessory diaphragm; A/L basal — anterior and lateral basal fused segments; P/M basal: — posterior basilar and medial basal fused segments.

Figure 4. Splenomegaly with greatly enlarged and coiled vasculatures.

Pulmonary veins

The right superior pulmonary vein drained directly into the SVC; the inferior right pulmonary vein from the lower lobe drained into the left atrium. The left superior and inferior pulmonary veins drained directly into the left atrium. In this case, the anomalous pulmonary vein that drained from the right lung into the SVC was corrected by ligation close to the SVC (Fig. 1).

Apart from the cardiopulmonary changes, we also observed hitherto unreported splenomegaly (Fig. 4) and greatly enlarged and coiled splenic vasculatures. The spleen was 28 cm long, 16 cm wide, 6 cm in thickness, and weighed 1,856 g. The liver, pancreas, and kidneys were normal in size without any pathology such as liver cirrhosis, pancreatic cancer, or others.

DISCUSSION

In the following paragraphs, we compare the findings of this case, highlighting relevance with similar cases described in the literature. We have included pertinent embryology related to the case. Oftentimes, in childhood, infants with scimitar syndrome or PAPVR are asymptomatic and this condition goes unnoticed; in adults, it is incidentally observed during imaging studies. However, the person (donor) in this report had surgical interventions at a young age to correct anomalous venous return and cardiac anomaly such as ASD. In addition, we also observed other cardiovascular anomalies, such as a widened coronary sinus and the left anterior descending and left circumflex arteries arising independently from the left coronary cusp.

Congenital pulmonary venolobar syndrome

Felson [12] coined the term congenital pulmonary venolobar syndrome (CPVS) in 1973; it incorporates a mixed group of unusual anomalies that may occur alone or in combination; abnormal unions of the lung parenchyma, the lung and general vasculature, and, infrequently, the digestive system may be seen [12]. Components of CPVS are hypogenetic lung, such as lobar agenesis, aplasia or hypoplasia, PAPVR, lack of pulmonic artery and/or IVC, pulmonic impounding, general pulmonic arterialization, and secondary diaphragm [25].

In scimitar syndrome, a type of PAPVR, venous blood from the hypoplastic lung flows through an abnormal pulmonic vein and drains into the general venous system. This is one of the rare inherited variations of developmental pulmonic venolobar syndrome that almost always occur on the right side [5]. The two most constant features of this syndrome are anomalous pulmonary venous return into systemic circulation and lung hypoplasia [1, 15, 16].

In the case of PAPVR, inconsequential right upper lobe venous drainage into SVC is frequently observed [18]. Most patients live symptom free; some with coexisting cardiac anomalies or dangerous forms of lung atresia or hypoplasia may have medical signs early in life that require surgical intervention. In the case reported (Fig. 1), the hypoplasia of the right lung and cardiovascular anomalies, as well as evidence of surgical interventions, confirm that the donor was symptomatic as an infant. The CPVS is displayed when one or additional, but not all, of the pulmonic veins empty into a general vein, causing a left-to-right bypass. The wide range of clinical presentations of this syndrome comprises hypogenetic lung (including lobar agenesis, aplasia, or hypoplasia), PAPVR, lack of pulmonic artery and/or IVC, pulmonic impounding, general pulmonic arterialisation, and extra diaphragm [12].

A small component of CPVS includes horseshoe lung, wherein a basal segment herniation of the right pulmonary lobe may cause a bridge of lung parenchyma to extend from the right lung bottom through the midline backside of the pericardium/heart to join the posterobasal segments of the left lung: a true horseshoe lung [14]. The herniated portion may be attached or may be separated by pleural membranes. Pleural separation of pulmonary lobes distinguishes pseudo-horseshoe appearance from a true horseshoe lung [35]. In the case reported here, the fusion of the right and left posterobasal segments were not observed, thus establishing the presence of a pseudo-horseshoe lung (Fig. 3). The herniated right posterobasal segment was a functional unit, as it could be aerated using an air pump.

Development of pulmonary vein and related anomaly

The pulmonary vein develops early in embryonic life and the blood from the lung buds empties into the visceral plexus, which connects with paired central veins and umbilicovitelline veins. The right central vein develops into the SVC, while the left cardinal vein mostly disappears. The umbilicovitelline veins develop into the IVC, portal venous system, and ductus venosus. During the 4th fetal week, a shared pulmonic vein arises from the wall behind the left atrium and joins the general pulmonic vein that empties blood flow from the lung buds. Thus, the common pulmonary vein becomes incorporated into the dorsal wall of the left atrium, eventually giving rise to four separate pulmonary veins. If the common pulmonic vein fails to join the visceral plexus and a visceral plexus connection with a principal or umbilicovitelline vein perseveres, some type of full abnormal pulmonic venous link (TAPVC) or limited pulmonic venous link/return PAPVR will occur [11]. An earlier report on

TAPVC described four types of cardiovascular anomalies: supracardiac, infracardiac, cardiac, and mixed types [6]. A recent case of PAPVR describes multiple congenital anomalies, such as annular pancreas and patent umbilical vein with connection to left portal vein, in addition to cardiovascular anomalies [32].

Hypogenetic lung

Though infrequent, inherited underdevelopment of one or more pulmonic lobes is found in patients with CPVS [12]. Reports describe pulmonic agenesis, pulmonary aplasia, and pulmonary hypoplasia, wherein the air sac and bronchial tube are present, but the involved section is undersized [12]. Collectively, these three abnormalities are mentioned as hypogenetic pulmonic disorder [12, 26]. In the case reported here, we observed that the right lung was present, but the three lobes were extremely hypoplastic; as in most cases of hypogenetic lung, the trachea was normal. The case presented here is the form with pulmonary hypoplasia: air sac and bronchial tube are present, but the involved part is small, as described. Hypogenetic lung is much more common on the right side [5] and involvement of multiple lobes frequently occurs [26]. The large percentage of patients with lone hypogenetic lung exhibit no signs or symptoms [17, 19]; nevertheless, when other cardiac and vascular structures are affected, as in the case reported here, surgical intervention is warranted.

Partial anomalous pulmonary venous return can roughly be typed into two forms: one that occurs in association with ASD and the other in association with hypogenetic lung [7]. The second form of PAPVR is a part of CPVS. In PAPVR, an atypical vein empties a portion or the whole hypogenetic lung [5, 12, 26]. The configuration of the anomalous vein (right pulmonary vein draining into the IVC) on anterior-posterior thoracic radiograms has been equated to a Turkish sword or scimitar [2] and so "scimitar syndrome" describes hypogenetic lung and PAPVR presenting together [2]. While hypogenetic lung might occur on the left, scimitar syndrome occurs nearly exclusively on the right-side [2, 5, 30]. In virtually all occurrences, the anomalous vein is a pulmonic vein [2, 5, 12].

In scimitar syndrome, the abnormal pulmonic vein most often empties into the IVC inferior to the right hemidiaphragm [2, 12]; rarely, PAPVR empties into the suprahepatic segment of the IVC [5, 13, 29]. When PAPVR empties into a general vein or to the right atrium, there is a left-to-right bypass; in general, patients experience no symptoms unless the shunt is 2:1 or larger [13]. In the case presented here, the right superior pulmonary vein drained into the SVC. Because the donor had both hypogenetic lung and PAPVR, we concluded that the person experienced a "scimitar" lung.

Accessory diaphragm

An accessory diaphragm is a thin fibromuscular membrane perhaps associated with partial descent of the septum transversum [8]. This anomaly is predominantly a right-sided condition. Why this occurs is unclear, but it was acceptably explained that the timing difference in growth of the two lung buds is probably involved [8]. In other reports, aplasia or a certain amount of pulmonic hypoplasia was apparent on the involved side; this also occurred in the case presented here (Fig. 3). The accessory diaphragm thus separates the pleural cavity on the right side into a part that traps part or all of the right middle or a part that traps the lower lobes beneath it [5]; this is also seen in the case we present (Fig. 3). If the lung trapped beneath the accessory diaphragm is aerated, as seen in the case presented here, it will move with respiration [12]. Most interestingly, we observed an accessory diaphragm separating the fused anterior and lateral basal segments that could be aerated using a pump, thus providing evidence that it was functional. Furthermore, the 'sequestered' segments were supplied by a branch of the pulmonary artery.

In the case reported here, we identified a dilated coronary sinus entering the right atrium adjacent to the ASD and the ostium of coronary sinus noticeably lacked the typical valve-like structure. Widening of the coronary sinus resulted from an increased volume of flow of blood into the right atrium through anomalous communication of the right pulmonary vein with SVC (PAPVR) and the presence of left-to-right shunt through the ASD. We speculate that the excessive volume of blood shunted into the right atrium and an increase in intra-atrial pressure associated altered haemodynamics caused the observed widened coronary sinus. In 2017, the coexistence of ASD and 'unroofed coronary sinus' with TAPVC in a 16-year-old female was reported [27]. It seems that dilated coronary sinus is seen in association with ASD [27].

Aetiology

Partial anomalous pulmonary venous return is a congenital cardiac defect with no known cause; it

may have a multifactorial origin, including a genetic component. No evidence has implicated common teratogens (e.g., drugs, infections) in the genesis of PAPVC. No evidence for a genetic predisposition has been reported [31], though it is reportedly seen with Turner syndrome [36].

In addition to the cardiopulmonary changes, we also observed splenomegaly (the spleen was 28 cm long, 16 cm wide, 6 cm in thickness, and weighed 1,856 g) and greatly enlarged and coiled splenic vasculatures, probably due to vascular or macrophage sequestration (Fig. 4). The size of a normal, healthy spleen can vary considerably from person to person. Women tend to have smaller spleens than men and taller people tend to have larger spleens than shorter people. In general, an adult spleen is about 12.7 cm long, 7.6 cm wide, 3.8 cm thick, and weighs about 6 ounces. It is hard to even speculate a cause for the splenomegaly, since the portal system, liver and pancreas were normal.

CONCLUSIONS

In conclusion, we present a case of hypogenetic right lung with other unusual features such as partial anomalous pulmonary venous return, pseudo horseshoe lung, atrial septal defect, and accessory diaphragm. The right superior pulmonary vein returned blood to the SVC instead of the left atrium. Considering the fact that the donor has both hypogenetic lung and PAPVR, we conclude that this represents a "scimitar" lung. To sustain life, some of these defects were corrected in childhood, which allowed the donor to live for 71 years.

Acknowledgements

The authors sincerely thank the donor and his family for their generosity, which made this study possible and facilitated scientific and medical innovations in patient care.

Funding

This study was supported by the Cooper Medical School of Rowan University research and innovation grant.

Conflict of interest: None declared

REFERENCES

1. Ahamed MF, Al Hameed F. Hypogenetic lung syndrome in an adolescent: imaging findings with short review. Ann Thorac Med. 2008; 3(2): 60–63, doi: 10.4103/1817-1737.39639, indexed in Pubmed: 19561908.
2. Canter C, Martin T, Spray T, et al. Scimitar syndrome in childhood. Am J Cardiol. 1986; 58(7): 652–654, doi: 10.1016/0002-9149(86)90296-1.
3. Chassinat R. Observation d'anomalies anatomiques remarquables de l'appareil circulatoire, aved hépatocèle congénitale, n'ayant donné lieu pendant la vie à aucun symptôme particulier: suivie de réflexions. II. Archives générales de médecine, Paris 1836: 80–91.
4. Cooper G. Case of malformation of the thoracic viscera consisting of imperfect development of the right lung and transposition of the heart. London Medical Gazette. 1836; 18: 600–602.
5. Currarino G, Williams B. Causes of congenital unilateral pulmonary hypoplasia: a study of 33 cases. Pediatr Radiol. 1985; 15(1): 15–24, doi: 10.1007/BF02387847, indexed in Pubmed: 3969292.
6. Darling RC, Craig JM, Rothney WB. Total pulmonary venous drainage into the right side of the heart; report of 17 autopsied cases not associated with other major cardiovascular anomalies. Lab Invest. 1957; 6(1): 44–64, indexed in Pubmed: 13386206.
7. Daves ML. Cardiac roentgenology: shadows of the heart. Year-Book, Chicago, Ill 1981: 274–281.
8. Davis WS, Allen RP. Accessory diaphragm. Duplication of the diaphragm. Radiol Clin North Am. 1968; 6(2): 253–263, indexed in Pubmed: 5667501.
9. Demos TC, Posniak HV, Pierce KL, et al. Venous anomalies of the thorax. AJR Am J Roentgenol. 2004; 182(5): 1139–1150, doi: 10.2214/ajr.182.5.1821139, indexed in Pubmed: 15100109.
10. Dikensoy O, Kervancioglu R, Bayram NG, et al. Horseshoe lung associated with scimitar syndrome and pleural lipoma. J Thorac Imaging. 2006; 21(1): 73–75, doi: 10.1097/01.rti.0000203635.36135.0d, indexed in Pubmed: 16538166.
11. Dillman JR, Yarram SG, Hernandez RJ. Imaging of pulmonary venous developmental anomalies. AJR Am J Roentgenol. 2009; 192(5): 1272–1285, doi: 10.2214/AJR.08.1526, indexed in Pubmed: 19380552.
12. Felson B. Chest roentgenology. Philadelphia, Saunders 1973: 81–92.
13. Folger GM. The scimitar syndrome. Anatomic, physiologic, developmental and therapeutic considerations. Angiology. 1976; 27(6): 373–407, doi: 10.1177/000331977602700605, indexed in Pubmed: 1053480.
14. Frank JL, Poole CA, Rosas G. Horseshoe lung: clinical, pathologic, and radiologic features and a new plain film finding. AJR Am J Roentgenol. 1986; 146(2): 217–226, doi: 10.2214/ajr.146.2.217, indexed in Pubmed: 3484566.
15. Frydrychowicz A, Landgraf B, Wieben O, et al. Images in Cardiovascular Medicine. Scimitar syndrome: added value by isotropic flow-sensitive four-dimensional magnetic resonance imaging with PC-VIPR (phase-contrast vastly undersampled isotropic projection reconstruction). Circulation. 2010; 121(23): e434–e436, doi: 10.1161/CIRCULATIONAHA.109.931857, indexed in Pubmed: 20547935.
16. Gaillard F, Weerakkody Y. Scimitar syndrome (lungs). Reference article, Radiopaedia.org. https://radiopaedia.org/articles/2027 (accessed on 21 Apr 2022).

17. Goo HW, Kim YH, Ko JK, et al. Horseshoe lung: useful angiographic and bronchographic images using multidetector-row spiral CT in two infants. Pediatr Radiol. 2002; 32(7): 529–532, doi: 10.1007/s00247-002-0705-8, indexed in Pubmed: 12107588.
18. Gustafson R, Warden H, Murray G, et al. Partial anomalous pulmonary venous connection to the right side of the heart. J Thorac Cardiovasc Surg. 1989; 98(5): 861–868, doi: 10.1016/s0022-5223(19)34264-3.
19. Halasz NA, Halloran KH, Liebow AA. Bronchial and arterial anomalies with drainage of the right lung into the inferior vena cava. Circulation. 1956; 14(5): 826–846, doi: 10.1161/01.cir.14.5.826, indexed in Pubmed: 13374858.
20. Hartman T. Case 9 - Horseshoe lung. In: Hartman T (ed.). Pearls and Pitfalls in Thoracic Imaging: Variants and Other Difficult Diagnoses. Cambridge University Press, Cambridge 2011: 22–23.
21. Ho ML, Bhalla S, Bierhals A, et al. MDCT of partial anomalous pulmonary venous return (PAPVR) in adults. J Thorac Imaging. 2009; 24(2): 89–95, doi: 10.1097/RTI.0b013e318194c942, indexed in Pubmed: 19465830.
22. Ibrahim M, Burwash IG, Morton B, et al. Direct drainage of the right pulmonary veins into the coronary sinus with intact interatrial septum: a case report. Can J Cardiol. 2001; 17(7): 807–809, indexed in Pubmed: 11468647.
23. Kabbani M, Haider N, Abu-Sulaiman R. Bilateral scimitar syndrome. Cardiol Young. 2004; 14(4): 447–449, doi: 10.1017/S1047951104004160, indexed in Pubmed: 15680054.
24. Kamijoh M, Itoh M, Kijimoto C, et al. Horseshoe lung with bilateral vascular anomalies: a rare variant of hypogenetic lung syndrome (scimitar syndrome). Pediatr Int. 2002; 44(4): 443–445, doi: 10.1046/j.1442-200x.2002.01566.x, indexed in Pubmed: 12139574.
25. Konen E, Raviv-Zilka L, Cohen R, et al. Congenital pulmonary venolobar syndrome: spectrum of helical CT findings with emphasis on computerized reformatting. RadioGraphics. 2003; 23(5): 1175–1184, doi: 10.1148/rg.235035004.
26. Mata JM, Cáceres J, Lucaya X, et al. CT of congenital malformations of the lung. Radiographics. 1990; 10(4): 651–674, doi: 10.1148/radiographics.10.4.2377765, indexed in Pubmed: 2377765.
27. Muthiah R. Coronary sinus atrial septal defect (unroofed coronary sinus) with total anomalous pulmonary venous connection: a case report. Case Rep Clin Med. 2017; 06(01): 1–18, doi: 10.4236/crcm.2017.61001.
28. Nazarian M, Currarino G, Webb WR, et al. Accessory diaphragm. Report of a case with complete physiological evaluation and surgical correction. J Thorac Cardiovasc Surg. 1971; 61(2): 293–299, indexed in Pubmed: 5549287.
29. Olson MA, Becker GJ. The Scimitar syndrome: CT findings in partial anomalous pulmonary venous return. Radiology. 1986; 159(1): 25–26, doi: 10.1148/radiology.159.1.3952313, indexed in Pubmed: 3952313.
30. Partridge JB, Osborne JM, Slaughter RE. Scimitar etcetera: the dysmorphic right lung. Clin Radiol. 1988; 39(1): 11–19, doi: 10.1016/s0009-9260(88)80329-5, indexed in Pubmed: 3338237.
31. Petullà M, Comito L, Settino V, et al. Scimitar syndrome (or Halasz Syndrome): description of a case originating in adulthood. J Radiol Rev. 2020; 7(6), doi: 10.23736/s2723-9284.20.00081-5.
32. Silawal S, Essing T, Schaupp C, et al. Rare malformations associated with partial anomalous pulmonary venous return: a cadaveric case report. Folia Morphol. 2022; 81(2): 526–531, doi: 10.5603/FM.a2021.0026, indexed in Pubmed: 33749806.
33. Takahashi M, Murata K, Yamori M, et al. Horseshoe lung: demonstration by electron-beam CT. Br J Radiol. 1997; 70(837): 964–966, doi: 10.1259/bjr.70.837.9486078, indexed in Pubmed: 9486078.
34. Tomisawa M, Goto M, Kimpara K, et al. Accessory diaphragm: report of a case associated with atrial septal defect. J Pediatr Surg. 1974; 9(2): 223–226, doi: 10.1016/s0022-3468(74)80126-0, indexed in Pubmed: 4825795.
35. Tosun A, Leblebisatan S. Congenital pseudohorseshoe lung associated with scimitar syndrome. Iran J Radiol. 2012; 9(2): 99–102, doi: 10.5812/iranjradiol.7808, indexed in Pubmed: 23329972.
36. van den Hoven AT, Chelu RG, Duijnhouwer AL, et al. Partial anomalous pulmonary venous return in Turner syndrome. Eur J Radiol. 2017; 95: 141–146, doi: 10.1016/j.ejrad.2017.07.024, indexed in Pubmed: 28987660.
37. Woodring JH, Howard TA, Kanga JF. Congenital pulmonary venolobar syndrome revisited. Radiographics. 1994; 14(2): 349–369, doi: 10.1148/radiographics.14.2.8190958, indexed in Pubmed: 8190958.

VIA MEDICA

CASE REPORT

Folia Morphol.
Vol. 82, No. 4, pp. 988–996
DOI: 10.5603/FM.a2022.0079

ISSN 0015–5659
eISSN 1644–3284
journals.viamedica.pl

Metopic skull with occipitalisation of the atlas

S.Y. Nikolova, D.H. Toneva

Department of Anthropology and Anatomy, Institute of Experimental Morphology, Pathology and Anthropology with Museum, Bulgarian Academy of Sciences, Sofia, Bulgaria

[Received: 10 June 2022; Accepted: 16 August 2022; Early publication date: 25 August 2022]

In this study we report a combination of anatomic variations in the neurocranium of an adult male skull. The skull is scanned using an industrial µCT system Nikon XT H 225. The cranial vault shows a persistent metopic suture, a remnant from the mendosal suture and supernumerary bones. Cranial base inspection reveals atlas occipitalisation (AO), basilar kyphosis, unusually shaped dorsum sellae and bilateral interclinoid bridging. AO is extensive without signs of atlantooccipital articulation. The anterior and posterior arches of the atlas and the right transverse process are fussed to the occipital bone above. The complete fusion of the posterior arch causes a formation of bone canals for the vertebral arteries passage into the cranium. AO in this case is not related to a reduction of the foramen magnum dimensions and clivus length. (Folia Morphol 2023; 82, 4: 988–996)

Key words: persistent metopic suture, atlas assimilation, supernumerary calvarial bones, wormian bones, intraclinoid bridging, caroticoclinoid foramen, posterior interclinoid foramen

INTRODUCTION

Anatomic variations in the skull also called discrete, non-metric, discontinuous or epigenetic traits have been considered intrinsically innocuous minor skeletal variants [10, 14]. The boundaries between variations and anomalies, however, are not so clear. Fluctuation of size, form and position within a commonly experienced range has been considered as "normal variation", whereas "anomaly" has been accepted as synonymous to structural abnormality caused by aberrant developmental processes. Unlike anomalies, variations have no impact on the function of a particular structure under normal circumstances, even though sometimes harmless variations could have a negative effect [33] and could indicate generalized disorders [6, 17]. Persistent sutures and supernumerary bones are variations in the cranial configuration causing an abnormal partition of the vault.

Metopism arises when the metopic suture, which forms between the growing halves of the frontal bone after the 16th fetal week [8] and normally closes before the end of the first postnatal year [38], fails to fuse. Persistent metopic suture is found to occur with varying frequency in different population groups from being absent to exceeding 15% [9, 20, 39]. It has been observed that metopic crania differ from non-metopic ones in many aspects. Metopic crania have distinctive cranial morphology [26, 27, 29] with frequently manifested supernumerary calvarial bones, remnants from embryonic sutures [9, 21, 26, 35] and underdeveloped frontal sinus [23, 24]. They demonstrate a general delay in calvarial sutures closure [28] and a wide array of midline closure defects [37]. Moreover, persisting MS is a common finding in some congenital disorders related to impaired bone formation [6, 17, 19]. Supernumerary bones could arise due to non-fusion

Address for correspondence: S.Y. Nikolova, PhD, Department of Anthropology and Anatomy, Institute of Experimental Morphology, Pathology and Anthropology with Museum, Bulgarian Academy of Sciences, Acad. G. Bonchev Str., Bl. 25, BG-1113 Sofia, Bulgaria, tel: +359-2-9792318, e-mail: sil_nikolova@abv.bg

of normally present ossification centres or they may appear from additional ossification centres. The squamous part of the occipital bone is an intricate site where different variations arise due to faulty fusion between the ossification centres of the interparietal part of the occipital squama and a frequent occurrence of wormian bones [17, 18].

Atlas occipitalisation (AO), also known as atlas assimilation, atlanto-occipital fusion, occipitocervical synostosis and atlantooccipital joint ankylosis is a spinal anomaly of cranial base characterised by a partial or complete fusion of the first cervical vertebra (C1, atlas) to the occipital bone. AO is a congenital osseous abnormality in the craniovertebral junction, which arises during the early embryonic period (4th fetal week) as a result of maldevelopment due to an incomplete segmentation of the first cervical sclerotome into cranial and caudal components. Then, the caudal portion of the fourth occipital somite fusses with the entire first cervical sclerotome and the cranial portion of the second cervical sclerotome, resulting in an assimilation of the atlas into the occipital region [4]. Incomplete incorporation or failure of segmentation of the last occipital and C1 sclerotomes leads to a spectrum of fusion-related anomalies and accessory structures, many of which are asymptomatic. The occipitovertebral border is an embryologically unstable area and the phenomenon of cranial–caudal border shifting is still not entirely understood. A caudal shift in the position of the atlanto-occipital demarcation is more common than a cranial shift. A caudal shift causes an assimilation of the atlas into the occipital bone as well as a basilar impression/platybasia and presence of paracondylar and epitransverse processes. A cranial shift results in an occipital vertebra (proatlas) expressed by precondylar tubercle or process at the anterior border of foramen magnum, transverse basilar clefts, bipartite condylar facets and divided hypoglossal canals [7]. Paracondylar process has also been considered to be a manifestation of parts of the proatlas transverse process [12].

Atlas occipitalisation is normally congenital, but in rare cases it may be a result of diseases such as osteomyelitis, arthritis, syphilis, tuberculosis and other infections or traumatic injuries of the cervical vertebrae [31, 36]. Factors such as malnutrition or disease-related disturbances during development or genetic anomalies may also predispose a fetus toward developing AO [31]. It has been reported that AO could be associated with Pfeiffer, Crouzon and Apert syndromes involving craniosynostosis, as well as with Goldenhar, Klippel-Feil and Pierre-Robin syndromes [5, 16]. The fusion between the occipital bone and the atlas varies as it could be localised or extensive, uni- or bilateral. In majority of the cases, the fusion is localised to the region of the atlantooccipital articulations and the complete bone union is rare [4, 7]. Since AO and the related abnormalities could be asymptomatic they often go undetected and AO is commonly diagnosed incidentally in radiographs, intraoperatively or during autopsy. The reported AO frequency ranges between 0.03% and 3.6% in the contemporary populations [12, 16, 31].

In this study, we report a case of an adult male cranium showing a rare combination of different anatomical variations in the *neurocranium* including persistent metopic suture and AO. We also discuss the origin and possible clinical complications of these variations.

CASE REPORT

The investigated cranium (Fig. 1) is part of the osteological material stored in the Ossuary at the National Museum of Military History (Bulgaria). The cranium belonged to an adult Bulgarian soldier who died in the wars at the beginning of the 20th century. The cranium was scanned using an industrial μCT system Nikon XT H 225 following the previously established optimal scanning protocol for dry skulls [25]. The sagittal suture closure was assessed on cross-sectional tomograms and regression models for age-at-death prediction, elaborated on the same population [25], were applied. Based on the sagittal suture closure degree, the age-at-death of the individual was assessed to be 34 years.

Variations in the calvarial morphology. The crania had a persistent metopic suture lying between *nasion* and *bregma* (Fig. 2A). Supernumerary calvarial bones and remnants from embryological sutures were observed. A rounded preinterparietal bone [18] along with a few separate bones of different size occupied the upper triangular portion of the occipital squama (Fig. 2B). A remnant from the mendosal suture was visible on the left side of the occipital squama (Fig. 2B). An epipteric ossicle was found at the right pterion (Fig. 1C), which could be classified as "false" or "incomplete" epipteric bone (*os epiptericum spurium totum peritemporale*) according to the classification of Kadanoff and Mutafov [12].

Variations in the cranial base. The atlas was fused to the occipital bone (Fig. 2D). The posterior

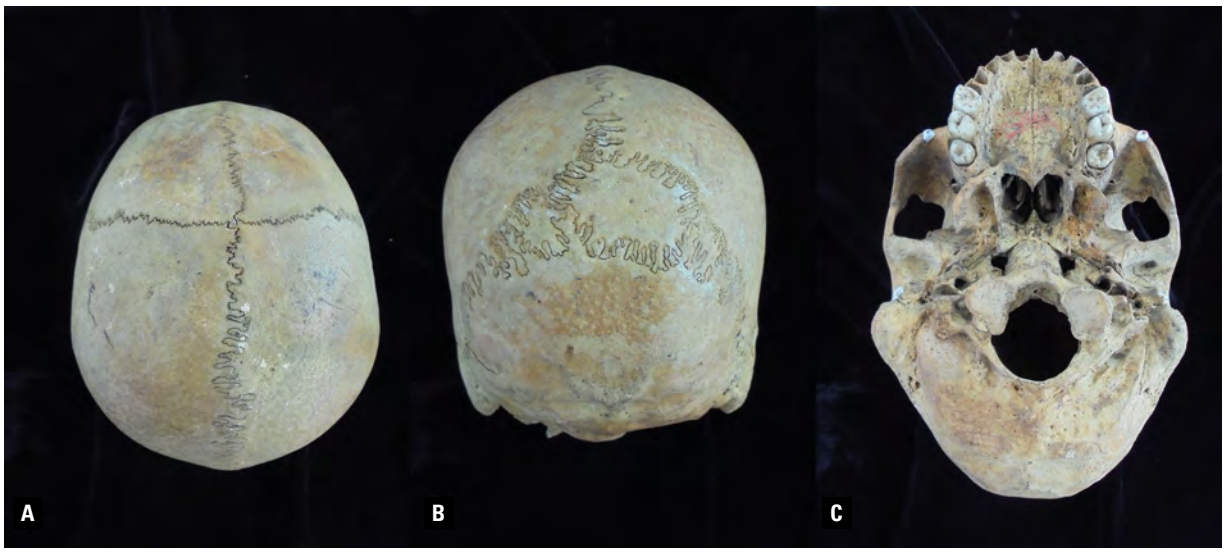

Figure 1. An adult male skull; **A.** Parietal view; **B.** Occipital view; **C.** Basilar view.

vertebral arch was complete and entirely fused to the occipital squama, whereas a small aperture (width 9.2 mm; height 4.1 mm) between the anterior arch and the anterior margin of foramen magnum was observed (Fig. 3A). Both lateral masses were ossified to the occipital condyles without any signs of atlantooccipital articulation between them. The inferior articular facets were asymmetrical. The transverse processes were normally developed, enclosing the transverse foramina. The left transverse process was free, while the right one was fused directly to the inferior surface of the jugular process of the occipital bone (Fig. 3B). This way, an additional transversal foramen was formed, enclosed by the fussed occipital bone and the transverse process of the atlas (Fig. 3B). At the level of the fused margins of the posterior arch and the occipital bone, right behind the fused lateral masses, were bilaterally formed bone canals for the vertebral arteries passage (Fig. 3B). Behind the right canal, there was a small vertical bony bridge between the occipital bone and the fused posterior arch forming a foramen (Fig. 3B). The hypoglossal canals on both sides were of normal appearance and position. The atlas midsagittal axis was slightly rotated to the left side. The atlas was also inclined from the transversal plane and its right side (the fused C1 transverse process) was in an upper position compared to the free left side (Figs. 2D, 3A).

The intracranial inspection revealed an unusually shaped dorsum sellae along with erosion of its base and top (Fig. 4A). There was also a bilateral interclinoid bridging. According to the classification of Archana et al. [3], it was an interclinoid bridging type II, mixed type on the right side (Fig. 4B). The bridge was formed between the anterior, middle and posterior clinoid processes. The ossified ligaments enclosed an anterior interclinoid foramen (caroticoclinoid foramen) between anterior and middle clinoid processes, and a posterior interclinoid foramen between the middle and posterior clinoid processes (Fig. 4B). On the left side, there was an interclinoid bridging type I, contact type [3] representing a bone bridge between the anterior and middle clinoid processes, enclosing an anterior interclinoid foramen (Fig. 4C). The cranial base angle (CBA) was constructed and measured in the midsagittal plane between the landmarks *nasion*, *sellae* and *basion* (Fig. 5). The borderline values of CBA delimiting a normal from flexed and extended base angle were used after Koenigsberg et al. [13]: basilar kyphosis, an extensive flexion of the skull base, CBA < 125°; normal angulation, CBA between 125° and 143°; platybasia, an abnormal flattening of the skull base, CBA > 143°. The measured cranial base angle in this case indicated basilar kyphosis (119.52°).

Linear measurements. Cranial length (g-op): 174 mm; cranial width (eu-eu): 135 mm; cranial height (ba-b): 130 mm; maximum foramen magnum anteroposterior diameter (H): 39.5 mm; maximum foramen magnum width (W): 35.6 mm; *clivus* length: 47.7 mm

Calculated indices. Cranial index (eu-eu/g-op): 77.6, *mesocran*; height-length index; (ba-b/g-op): 74.7, *orthocran*; height-breadth index (ba-b/eu-eu): 96.3, *metriocran*.

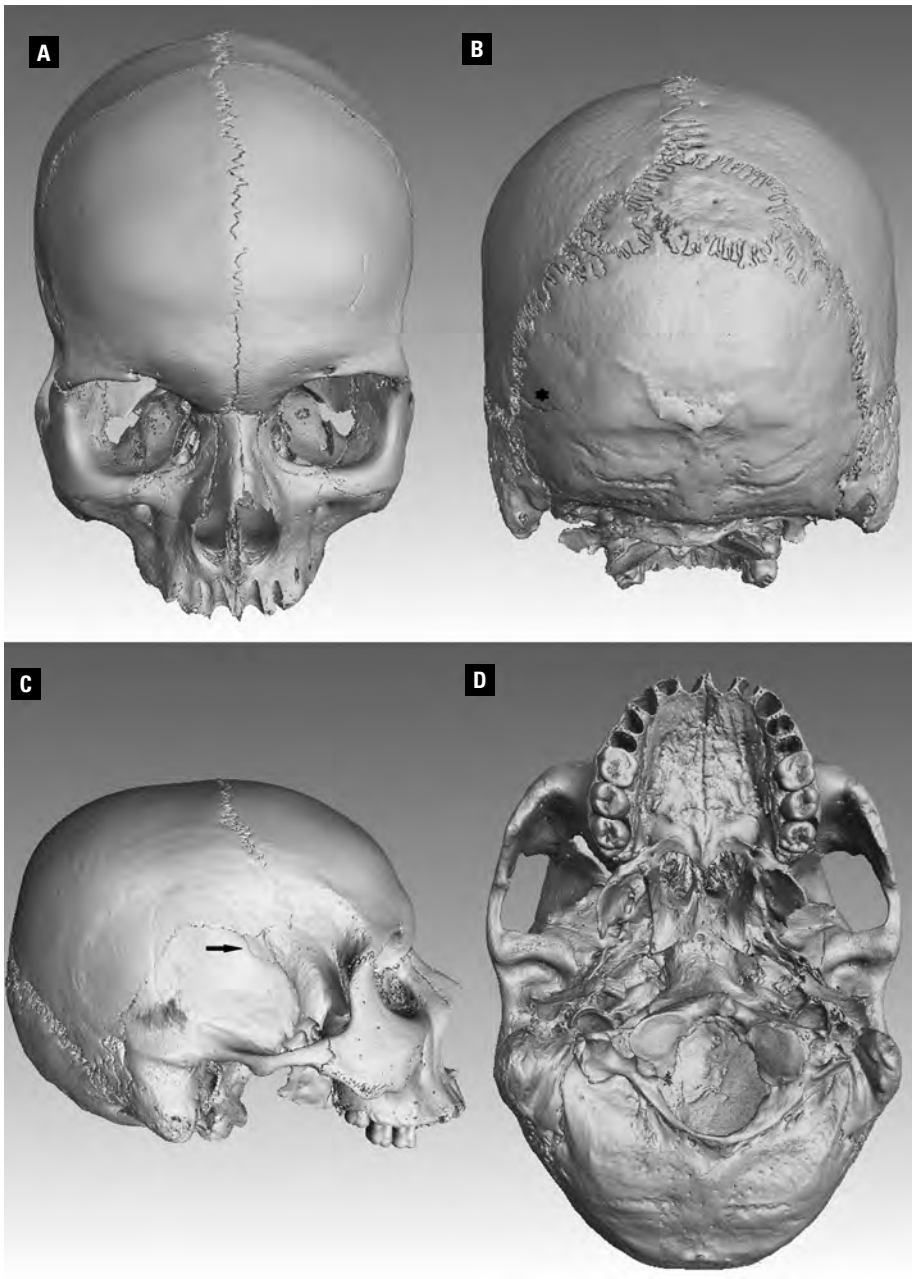

Figure 2. Volumetric rendering of the skull; **A.** Frontal view: an entirely preserved metopic suture; **B.** Occipital view: supernumerary calvarial bones at the interparietal portion of the occipital bone, a remnant from the mendosal suture (asterisk); **C.** Right lateral view: an incomplete epipteric bone; **D.** Basilar view: atlas occipitalisation.

The actual area of the foramen magnum was calculated according to the formula of Radinsky [32]: **Area = π × 1/4 × W × H**, where W is the maximum foramen magnum width and H is its maximum antero-posterior diameter in the midsagittal plane. Foramen magnum area — 1103.9 mm^2.

DISCUSSION

The causes for non-fusion of the frontal bone halves are widely discussed but still not fully understood. *Metopism* has been attributed to various conditions and causes such as increased intracranial pressure, mechanical stress, endocrine dysfunction, growth retardation, mental defects, heredity and heredo-specific factors as well as to specific cranial deformations such as plagiocephaly, stenocrotaphy, brachycephaly, scapho-cephaly and hydrocephaly [1, 35]. In this case, the cranium is of medium size without any obvious deformations in its shape and size. *Metopism* is frequently associated with under-

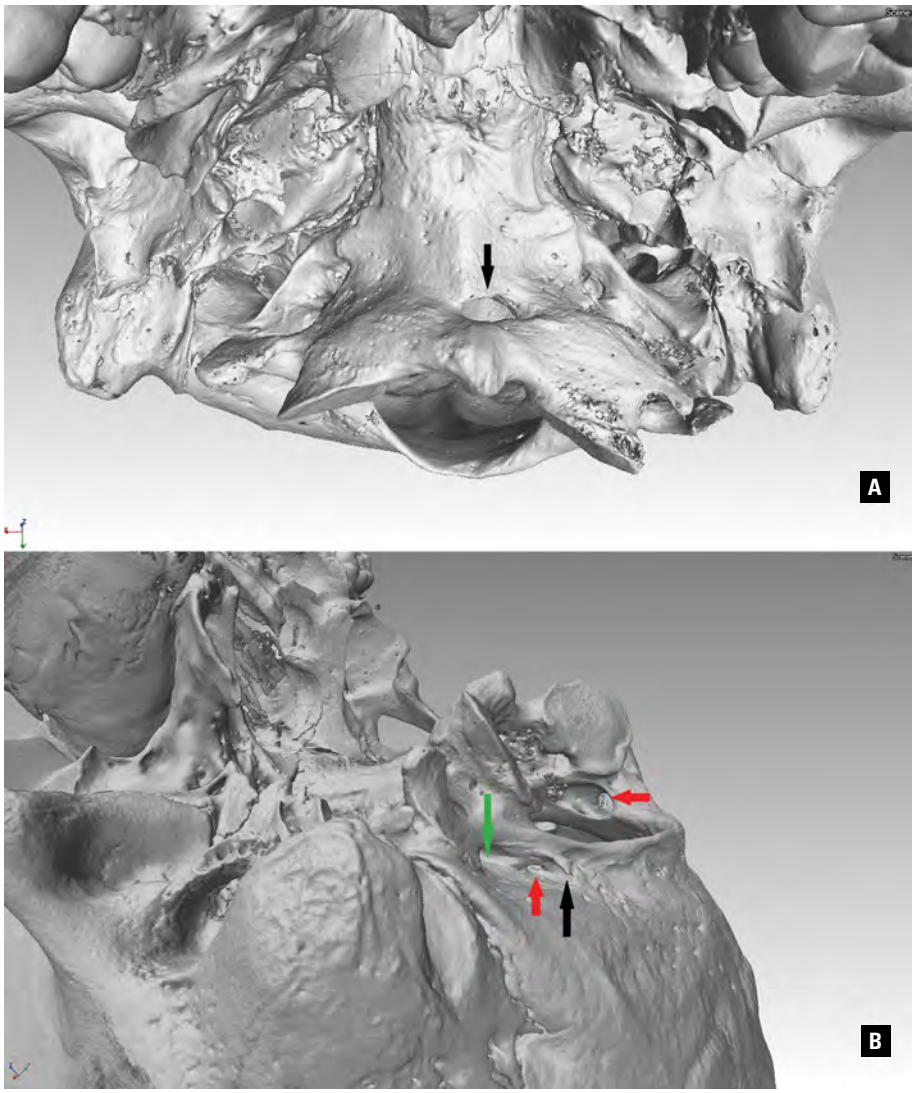

Figure 3. A close up view of the fused atlas; **A.** Anterior view: an aperture between the fused foramen magnum margin and the anterior arch of the atlas (arrow); **B.** Bilateral canals for the vertebral arteries passage (red arrows); a foramen formed between the fused transverse process of the atlas and the occipital bone (green arrow); a small vertical bony bridge between the occipital bone and the fused posterior arch of the atlas (black arrow).

development of the frontal sinus [17, 19, 20, 23, 24]. However, in the reported case all paranasal sinuses are well-developed.

Atlas occipitalisation and the supernumerary bones in the occipital squama could be explained by developmental anomalies, which occur during the occipital bone formation and seem to be unrelated due to the different timetables and ossification patterns of the occipital bone partition in which they evolve. AO arises around the 4th week of gestation as a result of maldevelopment of the intrasegmental fissure of the C1 sclerotome segment, with a consequent lack of recombination of the C1 somite [4]. The interparietal part of the occipital squama is a triangular space situated between the highest nuchal line and both parietal bones, which undergoes an intramembranous ossification (after the 8th fetal week) from a variable number of ossification centres giving rise to numerous variations in cases of non-fusion. The presence of a true preinterparietal bone is still questionable, but we use this term to designate a single bone or a group of bones (bipartite, tripartite or multipartite preinterparietal bone) of different size forming a triangular territory in the central lambda region, and separated by a transverse suture located higher than the midline between the *lambda* and the highest nuchal line [18]. In the reported case, it is observed a relatively large rounded bone occupying the upper portion of the occipital squama. This bone together with a few smaller irregular bones delineates

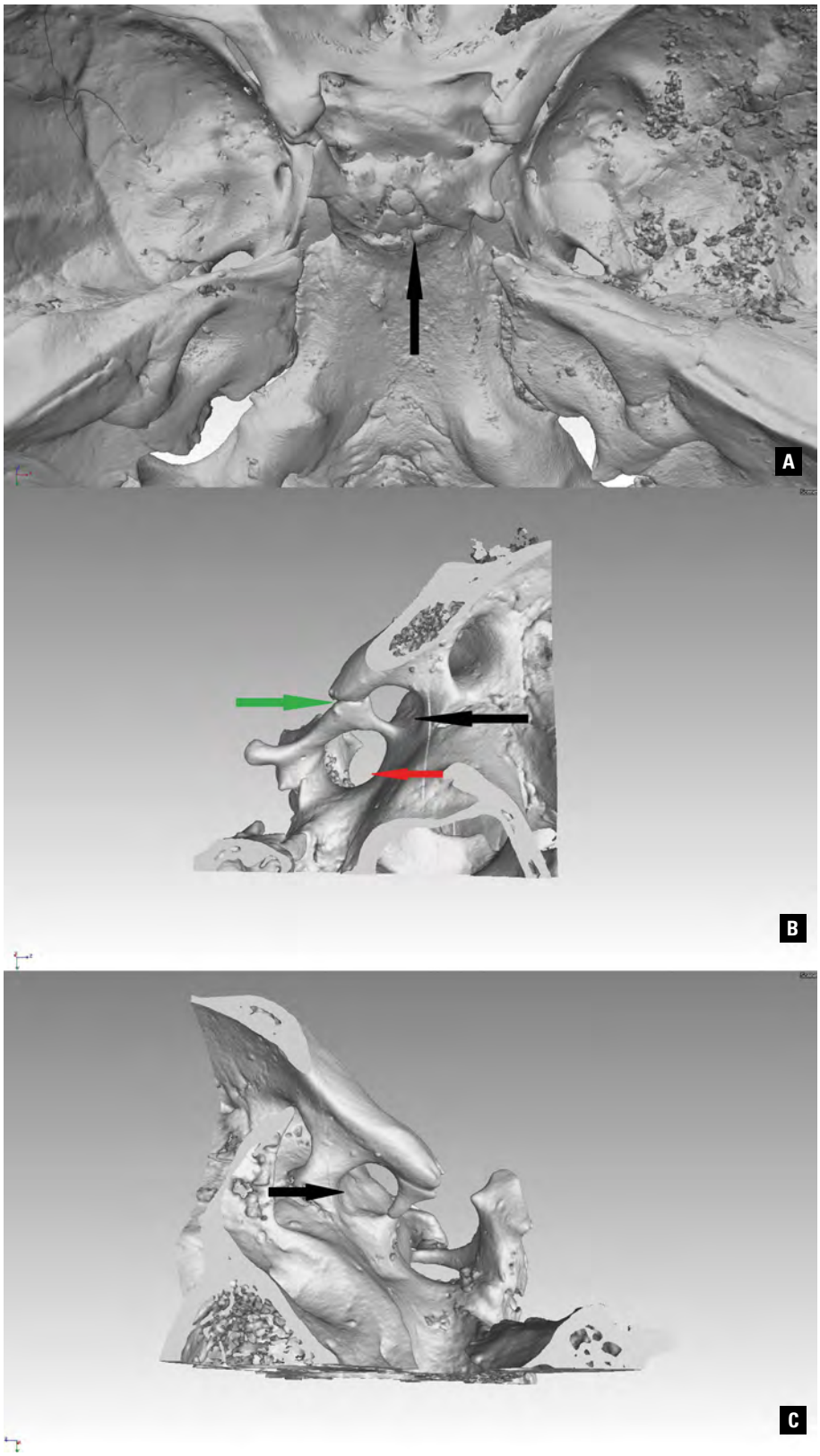

Figure 4. Middle cranial fossa: **A.** Dorsum sellae; **B.** An interclinoid bridging type II, mixed type (green arrow) on the right side enclosing an anterior interclinoid foramen (caroticoclinoid foramen) between the anterior and middle clinoid processes (black arrow), and a posterior interclinoid foramen between the middle and posterior clinoid processes (red arrow); **C.** Interclinoid bridging type I, contact type representing a bone bridging between the anterior and middle clinoid processes, enclosing an anterior interclinoid foramen on the left side.

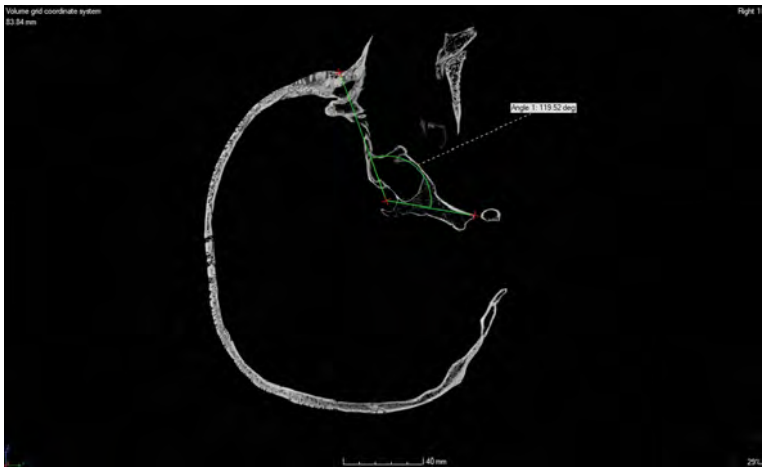

Figure 5. Cranial base angle constructed and measured in the midsagittal plane between the landmarks *nasion*, *sellae* and *basion*.

a triangular space below *lambda*. Supernumerary bones may arise from a fragmentation in the primary ossification centres or they may develop from additional centres [17]. Besides the supernumerary bones in the upper portion of the occipital squama, there is a remnant from the mendosal suture on the left side, which lies at the level of the highest nuchal line, i.e. on the demarcation line between the primary and secondary ossification centres. Thus, considering the occipital bone development, the mechanisms causing these variations seem unrelated since AO occurs much earlier in embryogenesis than the non-fusion of the ossification centres of the intramembranous portion of the occipital squama and the emergence of wormian bones in the lambda region after the sixth fetal month [15]. It is interesting, however, that *metopism* is frequently accompanied by supernumerary bones and remnants from other embryonic sutures [9, 21, 26, 35] as in this case. In view of the calvarial bone morphogenesis, these variations are closely interrelated and their accumulation and overexpression are typical of some congenital disorders linked to impaired intramembranous bone formation.

In AO, a slight rotation of the midsagittal axis of the atlas, similar to that in the reported case, has been previously noted [2, 4, 5]. Unilateral paracondylar process, also called paramastoid process [12] is a common finding in AO [4, 12]. Paracondylar process could be connected to an epitransverse process of the transverse process of the atlas by a paracondylar-epitransverse articulation [11, 12]. In the here described case the right transverse process of the atlas is fused directly to the jugular process of the occipital bone, without formation of a paracondylar process (Fig. 3B). This additionally shortens the distance between the occipital bone and the atlas on the right side compared to the contralateral left side, where the transverse process is unfused. This results in an inclination of the atlas from the horizontal plane (Fig. 3A). According to Kadanoff and Mutafov [12], AO leads to formation of a new lower foramen magnum, called foramen occipitale (atlantooccipitale) magnum. It has been reported that AO is related to an abnormal shape of foramen magnum and a reduction of its dimensions, which may lead to neurological complications due to compression of the spinal cord and other nerves [2, 16]. In this case, the foramen magnum dimensions and the calculated area are slightly enlarged compared to the mean values (length: 36.63 mm; breadth: 31.47 mm; area: 906.17 mm^2) reported for contemporary Bulgarian males [34], which is unusual. Similar to our case, it has been reported an irregular anterior atlantooccipital foramen formed between the superior aspect of the anterior arch of the atlas and the anterior margin of the foramen magnum with dimensions of 2–4 mm vertically and 18 mm horizontally [5]. Thus, the aperture is of similar height, but two times wider than the aperture in our case.

Atlas occipitalisation could impair the passage of either the vertebral arteries or C1 spinal nerves, which pass over the most anterior part of the posterior arch of the atlas. AO is frequently related to abnormalities in the vertebral artery and its route into the skull through accessory foramina and canals [2, 5, 16, 36]. If the posterior arch or hemiarch of the atlas is fused to the occipital bone, one should expect to find an anomalous osseous pathway for the vertebral artery

to enter the cranium [36], canalis atlantooocipitalis a. vertebralis [12], as it is in the reported case. The abnormal passage may clamp on the arterial wall, thus narrowing the lumen of the vessel and decreasing the velocity of blood flow into the vertebral artery. The compression may result to ischaemic symptoms, vertebro-basilar insufficiency and brainstem anoxia, while the artery entrapment in a bony canal may cause dizziness, seizures, mental deterioration, syncope and rarely sudden death [16].

Atlas occipitalisation has also been linked to a reduction of the clivus length, inadequate or no formation of the atlantooccipital joint and flattening of the skull base [2, 16]. The measured *clivus* length in this case does not indicate such a reduction, and what is more interesting, the CBA expresses an extensive flexion of the skull base instead of platybasia. It has been established that *metopism* is not related to a significant alteration in the CBA [22], so the basilar kyphosis in this case is quite unusual.

Demineralisation at the base of the dorsum sella is a valuable indicator of intracranial pathology. This appearance may be due to increased intracranial hypertension; it may also be secondary to a local mass lesion such as craniopharyngioma, optic chiasm glioma, or meningioma. An eroded posterior clinoid has also been reported with suprasellar aneurysm, histiocytosis X, and dilated third ventricle [30].

The interclinoid ligament joins the anterior and posterior clinoid processes while the caroticoclinoid ligament connects the anterior and middle clinoid processes. Sellar bridging has been recognised as an age-related phenomenon. Since the clinoid bars have been commonly reported in fetuses and infants, it seems more likely the interclinoid bridging to reflect an abnormality at a much earlier stage in the *chondrocranium* development [7]. Interclinoid bridging is not pathological, but could cause many complications during surgical procedures in this area [3, 40]. Sellar bridging type I results in the formation of anterior interclinoid foramen also known as caroticoclinoid foramen or arterial foramen through which the internal carotid artery passes. Bridging type II gives rise to two separate foramina: caroticoclinoid foramen, and posterior interclinoid foramen, called as venous foramen which transmits the lateral part of circular sinus [3].

CONCLUSIONS

In the reported case, the observed variations in the *neurocranium* represent deviations from the normal developmental process arising at different stages during embryogenesis. The variations of the cranial base occur at an earlier developmental stage compared to that of the *calvaria*. The observed variations most commonly are asymptomatic and of little clinical significance, although they could be involved and/or cause serious health issues in some cases. In the described case, there is no evident sign of a generalized disorder, which could cause the unusual co-occurrence of all this variations in the morphology of the *neurocranium*. Furthermore, bearing in mind that the individual was fit for military service, we can conclude that the man did not suffer from any severe complications.

Funding

This study was supported by the Bulgarian National Science Fund, Grant DN11/9-15.12.2017.

Conflict of interest: None declared

REFERENCES

1. Ashley-Montagu MF. The medio-frontal suture and the problem of metopism in the primates. J Roy Anthrop Inst Great Britain Ireland. 1937; 67: 157–201, doi: 10.2307/2844176.
2. Al-Motabagani MA, Surendra M. Total occipitalization of the atlas. Anat Sci Int. 2006; 81(3): 173–180, doi: 10.1111/j.1447-073X.2006.00129.x, indexed in Pubmed: 16955668.
3. Archana R, Anita R, Jyoti C, et al. Incidence of osseous interclinoid bars in Indian population. Surg Radiol Anat. 2010; 32(4): 383–387, doi: 10.1007/s00276-009-0582-z, indexed in Pubmed: 19862467.
4. Black S, Scheuer L. Occipitalization of the atlas with reference to its embryological development. Int J Osteoarchaeol. 1996; 6(2): 189–194, doi: 10.1002/(sici)1099-1212(199603)6:2<189::aid-oa259>3.0.co;2-d.
5. Bodon G, Glasz T, Olerud C. Anatomical changes in occipitalization: is there an increased risk during the standard posterior approach? Eur Spine J. 2013; 22 Suppl 3(Suppl 3): S512–S516, doi: 10.1007/s00586-013-2768-7, indexed in Pubmed: 23575658.
6. Castriota-Scanderbeg A, Dallapiccola B. Abnormal skeletal phenotypes. Springer-Verlag, Berlin, Heidelberg 2005.
7. Cunningham C, Scheuer L, Black S. Developmental Juvenile Osteology. Academic Press, London 2016.
8. Faro C, Benoit B, Wegrzyn P, et al. Three-dimensional sonographic description of the fetal frontal bones and metopic suture. Ultrasound Obstet Gynecol. 2005; 26(6): 618–621, doi: 10.1002/uog.1997, indexed in Pubmed: 16193520.
9. Hanihara T, Ishida H. Frequency variations of discrete cranial traits in major human populations. II. Hypostotic variations. J Anat. 2002; 198(6): 707–725, doi: 10.1046/j.1469-7580.2001.19860707.x.
10. Hauser G, DeStefano GF. Epigenetic variants of the human skull. Schweizerbartsche Verlagsbuchandlung, Stuttgart 1989.
11. Janssen N, Mebis W, Gielen J. Unilateral paracondylar-epitransverse neo-articulation with secondary atlas-axis

rotation anomaly: teaching point: variants of the craniovertebral junction can be depicted and characterized on CT. J Belg Soc Radiol. 2019; 103(1): 42, doi: 10.5334/jbsr.1844, indexed in Pubmed: 31276096.
12. Kadanoff D, Mutafov S. The human skull in a medico-anthropological aspect: form, dimensions and variability. Prof. Marin Drinov Academic Publishing House, Sofia 1984.
13. Koenigsberg RA, Vakil N, Hong TA, et al. Evaluation of platybasia with MR imaging. AJNR Am J Neuroradiol. 2005; 26(1): 89–92, indexed in Pubmed: 15661707.
14. Mann RW, Hunt DR, Lozanoff S. Photographic Regional Atlas Of Non-Metric Traits And Anatomical Variants In The Human Skeleton. Charles C Thomas Publisher, Springfield, IL, 2016.
15. Matsumura G, Uchiumi T, Kida K, et al. Developmental studies on the interparietal part of the human occipital squama. J Anat. 1993; 182(Pt 2): 197–204, indexed in Pubmed: 8376194.
16. Natsis K, Lyrtzis C, Totlis T, et al. A morphometric study of the atlas occipitalization and coexisted congenital anomalies of the vertebrae and posterior cranial fossa with neurological importance. Surg Radiol Anat. 2017; 39(1): 39–49, doi: 10.1007/s00276-016-1687-9, indexed in Pubmed: 27192980.
17. Nikolova SY, Toneva DH, Yordanov YA, et al. Multiple Wormian bones and their relation with definite pathological conditions in a case of an adult cranium. Anthropol Anz. 2014; 71(3): 169–190, doi: 10.1127/0003-5548/2014/0355, indexed in Pubmed: 25065115.
18. Nikolova S, Toneva D, Yordanov Y, et al. Variations in the squamous part of the occipital bone in medieval and contemporary cranial series from Bulgaria. Folia Morphol. 2014; 73(4): 429–438, doi: 10.5603/FM.2014.0055, indexed in Pubmed: 25448900.
19. Nikolova S, Toneva D, Georgiev I. A case of skeletal dysplasia in bone remains from a contemporary male individual. Acta Morphologica et Anthropologica. 2015; 22: 97–107.
20. Nikolova S, Toneva D, Georgiev IA. persistent metopic suture – Incidence and influence on the frontal sinus development (preliminary data). Acta Morphologica et Anthropologica. 2016; 23: 83–90.
21. Nikolova S, Toneva D, Georgiev I, et al. Two cases of large bregmatic bone along with a persistent metopic suture from necropoles on the northern Black Sea coast of Bulgaria. Anthropol Sci. 2016; 124(2): 145–153, doi: 10.1537/ase.160530.
22. Nikolova S, Toneva D, Georgiev I. Cranial Base angulation in metopic and non-metopic cranial series. Acta Morphologica et Anthropologica. 2017; 24: 45–49.
23. Nikolova S, Toneva D, Georgiev I, et al. Digital radiomorphometric analysis of the frontal sinus and assessment of the relation between persistent metopic suture and frontal sinus development. Am J Phys Anthropol. 2018; 165(3): 492–506, doi: 10.1002/ajpa.23375, indexed in Pubmed: 29266191.
24. Nikolova S, Toneva D, Georgiev I, et al. Relation between metopic suture persistence and frontal sinus development. Challenging Issues on Paranasal Sinuses. 2019, doi: 10.5772/intechopen.79376.
25. Nikolova S, Toneva D, Georgiev I, et al. Sagittal suture maturation: Morphological reorganization, relation to aging, and reliability as an age-at-death indicator. Am J Phys Anthropol. 2019; 169(1): 78–92, doi: 10.1002/ajpa.23810, indexed in Pubmed: 30848843.
26. Nikolova S, Toneva D, Agre G, et al. Data mining for peculiarities in the configuration of neurocranium when the metopic suture persists. Anthropol Anz. 2020; 77(2): 89–107, doi: 10.1127/anthranz/2019/1051, indexed in Pubmed: 31851204.
27. Nikolova S, Toneva D, Lazarov N. A comparative digital morphometric study of nasofrontal region in metopic and non-metopic cranial series. Anthropol Anz. 2021; 78(4): 347–358, doi: 10.1127/anthranz/2021/1388, indexed in Pubmed: 34160545.
28. Nikolova S, Toneva D, Agre G, et al. Influence of persistent metopic suture on sagittal suture closure. Ann Anat. 2022; 239: 151811, doi: 10.1016/j.aanat.2021.151811, indexed in Pubmed: 34384857.
29. Nikolova S, Toneva D, Tasheva-Terzieva E, et al. Cranial morphology in metopism: A comparative geometric morphometric study. Ann Anat. 2022; 243: 151951, doi: 10.1016/j.aanat.2022.151951, indexed in Pubmed: 35523397.
30. Penkrot RJ, Bures C. The "apparently" eroded dorsum sella: a new anomaly. AJR Am J Roentgenol. 1979; 132(6): 1005–1006, doi: 10.2214/ajr.132.6.1005, indexed in Pubmed: 108949.
31. Pott LN, Austin RM, Eller AR, et al. Population-level assessment of atlas occipitalization in artificially modified crania from pre-Hispanic Peru. PLoS One. 2020; 15(9): e0239600, doi: 10.1371/journal.pone.0239600, indexed in Pubmed: 32970756.
32. Radinsky L. Relative brain size: a new measure. Science. 1967; 155(3764): 836–838, doi: 10.1126/science.155.3764.836, indexed in Pubmed: 4959814.
33. Sañudo JR, Vázquez R, Puerta J. Meaning and clinical interest of the anatomical variations in the 21st century. Eur J Anat. 2003; 7(S1): 1–3.
34. Toneva D, Nikolova S, Harizanov S, et al. Sex estimation by size and shape of foramen magnum based on CT imaging. Leg Med. 2018; 35: 50–60, doi: 10.1016/j.legalmed.2018.09.009.
35. Torgersen J. A roentgenological study of the metopic suture. Acta Radiol. 2013; Original Series, Volume 33(1): 1–11, doi: 10.1177/028418515003300101.
36. Tubbs RS, Salter EG, Oakes WJ. The intracranial entrance of the atlantal segment of the vertebral artery in crania with occipitalization of the atlas. J Neurosurg Spine. 2006; 4(4): 319–322, doi: 10.3171/spi.2006.4.4.319, indexed in Pubmed: 16619679.
37. Vinchon M. The metopic suture: Natural history. Neurochirurgie. 2019; 65(5): 239–245, doi: 10.1016/j.neuchi.2019.09.006, indexed in Pubmed: 31562880.
38. Weinzweig J, Kirschner RE, Farley A, et al. Metopic synostosis: Defining the temporal sequence of normal suture fusion and differentiating it from synostosis on the basis of computed tomography images. Plast Reconstr Surg. 2003; 112(5): 1211–1218, doi: 10.1097/01.PRS.0000080729.28749.A3, indexed in Pubmed: 14504503.
39. Zdilla MJ, Russell ML, Koons AW, et al. Metopism: a study of the persistent metopic suture. J Craniofac Surg. 2018; 29(1): 204–208, doi: 10.1097/SCS.0000000000004030, indexed in Pubmed: 29049140.
40. Żytkowski A, Skrzat J, Mazurek A, et al. Clinical relevance of the caroticoclinoid foramen: a case report and concise literature review. Transl Res Anat. 2021; 25: 100153, doi: 10.1016/j.tria.2021.100153.

FOLIA MORPHOLOGICA

Folia Morphol. Vol. 82, No. 4, November 2023

CONTENTS

←

Folia Morphologica is currently indexed by: Arianta, CAS, CINAHL, CrossRef, Dental Abstracts, EBSCO, Elsevier Biobase (CABS), EmBiology, FMJ, Google Scholar, Index Copernicus, Index Scholar, Medline, Polish Medical Bibliography, Polish Ministry of Education and Science, Proquest, Scopus, SJR (*Scimago Journal & Country Rank*), Ulrich's Periodicals Directory, Veterinary Bulletin, Web of Science (SCIE, *Science Citation Index Expanded*, Biological Abstracts, BIOSIS Previews, ESI, *Essential Science Indicators*, Zoological Record) and WorldCat.

Cover picture: Posterior view of the gluteal region, following removal of the gluteus maximus muscle; 1 — lower head of the piriformis muscle; 2 — medial head of the piriformis muscle; 3 — upper head of the piriformis muscle; 4 — gluteus maximus muscle; 5 — sciatic nerve. For details see: T. Kozioł et al., Folia Morphol 2023; 82, 4: 969–974.